ICIMOD

UNDP

Landslide Hazard Mitigation

in the Hindu Kush-Himalayas

Editors

Li Tianchi

Suresh Raj Chalise

Bishal Nath Upreti

about the ICIMOD

The International Centre for Integrated Mountain Development (ICIMOD)is an international organisation devoted to development of the Hindu Kush-Himalayan region covering all or parts of eight sovereign states, Afghanistan, Bangladesh, Bhutan, China, India, Myanmar, Nepal, and Pakistan. The Centre is located in Kathmandu, Nepal. The primary objective of the Centre is to promote the development of an economically and environmentally sound mountain ecosystem and to improve the living standards of mountain populations.

ICIMOD

UNDP

Landslide Hazard Mitigation
in the Hindu Kush-Himalayas

Editors
Li Tianchi
Suresh Raj Chalise
Bishal Nath Upreti

Cover Plate
Landslide on the left bank of the Sunkoshi, Nepal (Li Tianchi)
Landslide control and measures on the roadside at Sindhuli-Bardibas, Nepal (Li Tianchi)
Debris flow in Dongchuan, Yunnan, China (Li Tianchi)

ISBN: 92 9115 328 1

Published by
International Centre for Integrated Mountain Development
GPO Box 3226, Kathmandu, Nepal

Editorial Team
Greta Rana (Senior Editor)
A. Beatrice Murray Shrestha (Editor)
Asha Kaji Thaku (Cartographer)
Sushil Man Joshi (Technical Support and Layout)

Preface

The Hindu Kush-Himalayan (HKH) Region is the most dominating physiographic feature on our planet. Constituting the youngest mountain system in the world and with unstable geologic conditions, the terrain is fragile, giving rise to unstable slope-land systems. Characterised by a monsoon climate, the region commonly experiences extreme weather events and intense seasonal precipitation which commonly trigger natural hazards such as debris flows and landslides. The peoples of the HKH region suffer greatly from these disasters. Every year, landslides and related hazards cause several billion US$ in economic losses and thousands of deaths are suffered in the region, accounting for about 50 per cent of the total deaths from such hazards in the world. Apart from natural conditions, large-scale deforestation, unplanned human settlement, extension of agriculture on to landslide prone areas, and badly-engineered mountain roads have rapidly increased the number of landslides in the HKH. As the population of this region increases, the frequency and intensity of landslides is also bound to increase. Institutional capacity to deal with these problems on a systematic basis needs to be strengthened substantially in the regional countries through generation of awareness and dissemination of appropriate technology and skills.

In the last few decades, studies and management of landslides have significantly increased in scope. Dissemination of this knowledge can help mitigate landslide hazards in the region. The knowledge needs to be disseminated both to the grass roots as well as to higher technical levels. A multidisciplinary approach and bringing together of professionals of different disciplines such as engineering geologists, geotechnical engineers, hydrologists, meteorologists, geomorphologists, foresters, agricultural scientists, and civil engineers are the keys to effective mitigation of landslide hazards.

Landslide studies and management requires input from professionals from diverse fields as well as very close interaction among them. Publications dealing with the problems of landslides by pooling together diverse subjects, such as geology, engineering geology, geophysics, geotechnical engineering, civil engineering, hydrology, meteorology, and bioengineering, in one volume are not common, and they are particularly rare for use on the HKH region. The present publication is an attempt to fill this gap.

The resource materials contained presented in this volume are from China, India, Japan, Nepal, and the UK. All the papers that appear in the volume were reviewed and edited before the publication. The first part of the volume has 14 papers that deal with the principles and investigation of landslides and debris flows and the second part has 4 papers dealing with mitigation and management based on case studies in Nepal and China. An attempt has been made to include related topics such as the physical aspects of the HKH region (geology, physiography, seismicity, climate, and rainfall) and their bearing on landslide problems and techniques of investigation and mitigation methods. While preparing this volume care has been taken to keep the articles as simple as possible and understandable by a diverse group of professionals.

These days specialists as disparate as foresters, civil engineers, development workers, tourist guides, and agricultural advisors may be confronted directly or indirectly with landslide risk assessment and hazard mitigation. However, few have any formal training in the subject, and there are few resource books that can be used by the technically able non-specialist, and even less that are specifically concerned with the HKH region. This book, which is the final product of materials prepared for a series of regional training programmes organised by ICIMOD, is designed to fill this gap. It is a comprehensive reference manual, with information about a wide range of topics related to landslide development and mitigation and assessment of risk. It is hoped that the chapters will provide useful reference material both for field engineers and for the many other experts engaged at the field level in landslide hazard management and control in the HKH countries. It can also be used as course material for academic and professional training on landslide management and control as well as for students of civil engineering and the geosciences.

The first draft of the resource materials for training in landslide hazard management and control was tested during a 4-week pilot training course from May/June, 1996, in collaboration with the Water Induced Disaster Prevention Technical Centre (DPTC) of the Ministry of Water Resources, His Majesty's Government of Nepal. Altogether 18 professionals, mainly engineers and geologists from Bangladesh, China, India, Nepal, and Pakistan, participated in this pilot course. Subsequently the training materials were sent to experts for review, and then a revised version was received from the respective authors based on the comments and suggestions from the reviewers. The revised training materials were tested again during the second training course conducted by ICIMOD during September/October, 1999, which was attended by 16 participants from Bangladesh, Bhutan, China, India, Myanmar, Nepal, and Pakistan. Fourteen trainers and resource persons from Austria, China, Germany, India, and Nepal provided the training. In order to improve the capacities of the relevant partner institutions in the countries of the Hindu Kush-Himalayan region in training and applied research for disaster mitigation, with particular reference to landslide hazards, some training materials were selected for publication in this volume.

It is hoped that the materials in this volume are useful to experts as well as middle-level technical manpower in the related fields. The materials might also be useful for academic institutions for courses in civil engineering, geotechnical engineering, engineering geology, geomorphology and other related subjects with particular reference to the HKH.

Foreword

One of the goals set by ICIMOD in its Mountain Natural Resources' Programme is "to improve the conditions of mountain resources and environments in the Hindu Kush-Himalayan (HKH) region by reducing and eventually reversing their degradation." The programme activities include the identification of measures to mitigate different types of natural hazards which result in the loss of natural resources; promotion of skills and methodologies for natural hazard assessment; and improvement of public awareness for better disaster preparedness in mountain areas.

ICIMOD has developed and implemented different activities in landslide hazard management and control since 1994 with financial support from the Government of Japan. These have included training and capacity building, research, documentation, and information sharing — with a major focus on training people involved at different levels in the field of landslide hazard mitigation and management. The common theme in all these activities is improved landslide hazard management based on a better understanding of the different natural and manmade processes and, through this, improved planning of infrastructure, settlements, and sloping agricultural land management. With the increase in construction and development activities on sloping lands across the HKH region, it has become essential to have a better understanding of geo-environmental, hydro-climatic, biophysical, bioengineering, and socio-institutional processes in order to avoid an increase in disasters.

I would like to express my sincere appreciation and thanks to the Government of Japan and the United Nations Development Programme (UNDP) for their generous support to ICIMOD's Landslide Hazard Management Programme and hazard mapping and risk assessment activities (2000-2002), which are part of the Participatory Disaster Management Programme (NEP/99/014) implemented by UNDP/Nepal. Professor S. R. Chalise and Professor Li Tianchi from ICIMOD were the coordinators of the programme at various phases. Professor B. N. Upreti of the Department of Geology,Tribhuvan University, and Mr. M.N. Sharma, TAEC Consult (P) Ltd., assisted with the technical editing. Many thanks are also due to the experts and resource persons who shared their knowledge and experience during the training events and also spent valuable time preparing and revising the training materials.

ICIMOD would welcome any comments and suggestions that will help us prepare an improved future edition of the publication.

Binayak Bhadra
Director of Programmes
ICIMOD

Acknowledgements

These resource materials are the outcome of the contributions of many people. The editors are thankful to all the authors for contributing their papers to this publication and for their unfailing cooperation and support. As most of the papers were originally in a different format and were not intended for formal publication, the authors had to do a great deal of rewriting. This and other necessary work consumed a lot of time and, therefore, preparation of this document took longer than planned.

The authors and the publisher have made every effort to obtain permission to reproduce copyright materials throughout this book. If any proper acknowledgement has not been made, or permission not received, we invite any copyright holder to inform us of this oversight, which will be corrected in subsequent editions.

This publication would not have been possible without the support of all the staff from ICIMOD, in particular, we would like to record our appreciation and thanks to the former Director General of ICIMOD, Mr. Egbert Pelinck, for his encouragement and untiring support for the landslide hazard management programme and for the publication of this document. We are equally thankful to the present Director General, Dr. J. Gabriel Campbell, and Dr. Binayak Bhadra, Director of Programmes, ICIMOD, for their keen interest and support for this publication. Special thanks are due to Ms. Greta Rana, Senior Editor, and Dr. A. Beatrice Murray Shrestha, Editor, of ICOD, ICIMOD, for all their work in bringing the document and its contents into its current shape. Ms. Reeta Rana, Senior Secretary, Mountain Natural Resources Division, deserves special thanks for her secretarial support Thanks are also due to Dr. S.M. Rai for computer drafting most of the figures included in this volume and to Mr. Asha Kaji Thaku and Mr. Sushil Man Joshi for the long hours spent on the graphics and layout.

Li Tianchi
S.R. Chalise
B.N. Upreti

Acronyms and Abbreviations

BIS	Bureau of Indian Standards
BP	bank protection
BT	Basement Thrust
CD	Check Dam
CDP	common depth point (technique)
CMP	common midpoint (technique)
cumec	cubic metres per sec (stream/river discharge)
DCPT	Dynamic Cone Penetration Test
DEM	Discrete Element Method
DPTC	(Water-induced) Disaster Prevention Technical Centre
DoR	Department of Roads
EDM	Electronic Distance Meters
EP	Electrical Profiling
ERT	Electrical Resistivity Tomography
FOS	Factor of Safety
GLOF	Glacial Lake Outburst Flood
GPR	ground penetrating radar
GRM	Generalised Reciprocal Method
ITT	Indus-Tsangpo Thrust
ITS	Indus-Tsangpo Suture Zone
HDP	high damage potential
HFT	Himalayan Frontal Thrust
HH	high hazard
HHZ	High Himalayan Zone
HMGN	His Majesty's Government of Nepal
HP	hazard probability
HR	high risk
IDA	International Development Agency
IMHE	Institute of Mountain Hazards and Environment
JICA	Japanese International Cooperation Agency

LDP	low damage potential
LH	low hazard
LHEF	Landslide Hazard Evaluation Factor
LHM	landslide hazard management
LRA	landslide risk assessment
LR	low risk
LZE	Lesser Himalayan Zone
M	Magnitude (of earthquake)
masl	metres above sea level
MB	Mahabharat Thrust
MBT	Main Boundary Thrust
MCT	Main Central Thrust
MDP	Moderate Damage Potential
MFT	Main Frontal Thrust
MHT	Main Himalayan Thrust
MH	moderate hazard
MM	Modified Mercalli Scale
MR	moderate risk
MRE	Mountain Risk Engineering
NEA	Nepal Electricity Authority
OCR	Over Consolidate Ratio
RA	risk assessment
RAM	Risk Assessment Matrix
RFRP	Road Flood Rehabilitation Project
RMR	rock mass rating
RQD	rock quality designation
SDC	Swiss Development Co-operation
SMR	slope mass rating
SN	State-of-Nature
SPT	Standard Penetration Test
SRC	soil, rock, and concrete
SSI	Sub Surface Imaging
STD	South Tibetan Detachment
TEHD	Total Estimated Hazard
THZ	Tethys Himalayan Zone
TRZ	Trans Himalayan Zone
VES	vertical electrical sounding
VHDP	very high damage potential
VHR	very high risk
VLDP	very low damage potential
VLR	very low risk
WERDP	Water and Energy Resources Development Project

Glossary

adit	nearly horizontal tunnel used for exploration; excavation of a main tunnel; or access, drainage, or ventilation of a mine or other structure
base-flow	flow in a river from groundwater sources rather than from precipitation events
bedload	the amount of solid material (like sand, gravel, and boulders) carried along a river-bed by rolling pushing or bouncing (in contrast to the sediment load which is carried in suspension); the material can result from landslides, debris flows, and GLOFs as well as coming from the river-bed
berm	a horizontal ledge cut between the foot and top of an embankment (or other slope) to stabilise the slope by intercepting sliding earth
break of slope	an abrupt change of slope resulting from differences in erosional history of the terrain or from lithological contrasts; the change of slope in the long-profile of a river bed is termed a knickpoint (nickpoint) or rejuvenation head
catchment area	in British usage, the total area drained by a single stream or river with all its tributaries; in the USA, the intake area and all areas that contribute surface water to the intake area of an aquifer (see also river basin, watershed)
cumec	a measurement unit relating to the rate of discharge of a stream; refers to the volume of water passing through a particular section of the stream and is obtained by multiplying the cross-section of the channel at the position of the measuring station by the velocity of the flow
damage potential	a measure of the damage that could be caused by a disaster like a landslide in the form of loss or damage to life and property
debris	a superficial collection of broken rocks, earth, and other inorganic material (usually that has been removed from an original site by streams of water or ice and redeposited)
debris avalanche	a very to extremely rapid debris flow

debris flow	a rapid mass movement of loose soil, rocks, and organic material along with entrapped air and water to form a slurry that flows downslope
debris slide	a slide of coarse-grained soil usually containing angular rock fragments, typically made up of debris from glaciers or from colluvium resulting from the disintegration of rocks in situ
decollement	deformation of superficial rocks or sedimentary beds by folding or faulting without the rocks at depth being affected; usually accomplished by sliding over the underlying rock
dip direction	the direction of a discontinuity perpendicular to the strike of the rock strata given in terms of the points of the compass
dip	the maximum inclination of a structural discontinuity to the horizontal plane measured in a direction perpendicular to the strike of the rock strata
dislocation	the displacement of rocks on opposite sides of a fault; area of a fault along which a slip has occurred
earth flow	a flow with a characteristic bowl-like depression at the head where the slope material becomes liquefied and flows out; the flow is usually channelised on the slope and spreads out at the toe; such flows generally occur in fine-grained materials or clayey rocks under saturated conditions
electrical resistivity	the electrical resistance that a unit volume of a particular material offers to the flow of current at 0°C; it is the reciprocal of conductivity and is measured in ohm metres
epicentre	point on the earth's surface that is directly above the focus of an earthquake
factor of safety (F)	for a rock slope, the ratio of the total force resisting sliding to the total force tending to induce sliding
falls	an abrupt movement of materials that become detached from steep slopes or cliffs and drop down by free fall or a series of leaps and bounds
fault	a rupture or fracture of rock strata due to strain, in which displacement is observable
fault plane solution	the results of calculations of the type or nature of movement of an earthquake
fault zone	(fracture zone) an area in the vicinity of the fault where the rocks are normally highly crushed or sheared
first motion data	direction of motion of earliest seismic wave from an earthquake
flash flood	a short-lived but rapid rise of water in a river due to heavy rainfall or the collapse of a dam (natural or artificial)
flashy river	a river often subject to flash floods
flat	low lying, or lacks any curvature

focal mechanism	the direction of slip in an earthquake and the orientation of the fault on which it occurs, represented by a 'beach-ball' diagram
focus	the point source of an earthquake
geomorphological hazard	a perceived event, natural or human-induced, which causes a fluctuation or malfunction in the normal operation of a geomorphological process sufficient to pose a threat to life and property. Realisation of the hazard usually leads to an extreme event (e.g., avalanche, earth-flow, landslide, flood) which may or may not culminate in disaster
geomorphological map	a map depicting selected terrain features which assists in understanding the evolutionary history of the landforms of an area
geomorphological processes	the physical and chemical interactions between the earth's surface and the natural forces acting upon it to produce landforms (gravity, ice, rivers, waves, wind and so on)
geomorphological unit	part of a landform, like a mountain range or plateau on a large scale, or slope or stream bed on a small scale
geomorphology	the scientific study of the origin of landforms based on a cause-and-effect relationship, especially the genesis, evolution, and processes involved in the formation of the surface forms of the earth
geophone	a receiver or detector for seismic waves that converts ground motion into electrical energy, the output of a geophone is further filtered, amplified, and recorded on a seismograph. The record of each geophone is called a trace and a group of traces makes a seismogram (i.e., the record produced by a seismograph).
glacial lake outburst flood (GLOF)	a debris torrent resulting from the sudden and catastrophic release of water from a lake of glacial origin; such lakes are usually impounded by glacial ice or a moraine
hazard	the probability that a particular danger occurs in a particular area within a given period of time
highland-lowland interactions	the impact of upland activities and events on lowland areas
inclination	see 'dip'
insolation	quantity of solar radiation per unit area falling on a surface
island arc	a lengthy chain of oceanic islands which frequently exhibit an ocean trench on the convex side; many are volcanic and generally the location of severe seismic activity
landslide hazard	a measure of the probability of a landslide occurring at a particular location within a particular time
landslide hazard zonation	a macro approach that categorises an area into various zones from very stable to very unstable based on the hazard associated with separate slope facets

landslide risk	refers to the probable extent of damage if a landslide occurs and is a function of the hazard probability and the damage potential
landslide	commonly used to denote the downward and outward movements of slope-forming materials along surfaces of separation by falling, sliding, or flowing at a faster rate, a type of mass wasting; sometimes used specifically to refer to 'slides' (see below)
landslide-dam	a natural river dam formed by the rock, earth, debris, and or mud transported by a landslide; easily formed in the steep, narrow valleys of high rugged mountains, and can fail catastrophically, causing major downstream flooding and loss of life
lithology	the study of rock characteristics (e.g., particle size, physical and chemical character) and rock types
macrobasin	a complete river basin or a large part thereof
mass wasting	the general term for a variety of processes by which large masses of earth materials are moved under gravity, either slowly or quickly, from one place to another (see 'mass movement')
mass movement	(gravitational mass movement) the downhill movement of surface materials under the influence of gravity but assisted by buoyancy due to rainfall or snow melt, see also landslide
microbasin	the area drained by a stream or small river
microtopography	surface features with dimensions from a few centimetres to one metre (see topography)
mid-oceanic ridge	a large scale linear elevation rising from the ocean floor approximately in the middle of the N and S Atlantic and the Indian Oceans; it marks the boundary of adjoining plate margins
Modified Mercalli Scale	a subjective measure that describes the intensity of an earthquake shock felt at a particular place
Moho	(Mohorovicic discontinuity) boundary surface or sharp seismic discontinuity that separates the earth's crust from the subadjacent mantle
mud flow	a type of earth flow containing about 50% of sand, silt, and clay-sized particles that are well saturated and flow rapidly
mud slide	a landslide of essentially homogeneous clay-silt material, but with a lower water content and without the velocity or linear extent of a mud flow
nickpoint	see 'break of slope'
nodal plane	fault plane along which rupture takes place
normal fault	a dipping fault plane with the top dropping down; this arises from extension when two blocks of rock diverge
ocean trench	(ocean deep or foredeep) a deep trench (>5,500m) of the ocean floor, often associated with the subduction zone at the margins of two tectonic plates

orogenic belt	a linear region that has undergone folding or other deformation during an orogenic (geotectonic) cycle
orography	the study of mountain systems and depiction (mapping) of their relief; the terrestrial relief form of mountains
penstock	the water conduit from the intake to the turbines in a hydroelectric plant
piping	the presence of sloping tube-like features in rock, often marked by seepage
precipitation threshold	the level of precipitation (rainfall duration and intensity) needed to initiate a landslide, debris flow, or similar event; the threshold is specific for a particular slope and hazard as it depends on a large number of factors like slope angle, soil type, vegetation cover, and soil saturation, not just on rainfall, however, generalisations can be made for different types of slope in different areas
ramp	steep inclined segment of a thrust fault or steep inclined plane
rheology	the branch of physics concerned with the flow and change of shape of matter
Richter Scale	a logarithmic scale used to express the magnitude of an earthquake
risk	the probability that a potential hazard will be realised and the probability of the harm itself; risk is the combined effect of the probability of occurrence of an undesirable event and the magnitude of the event
river basin	(drainage basin) the area drained by a river and all its tributaries, usually large-scale (see watershed, catchment area)
rock material/rock matrix	the intact material in rock between discontinuities, for example, a hard piece of rock taken from a drill core
rock or rock mass,	the total in situ medium of rock including all discontinuities like joints, fractures, faults, etc
rupture zone	overall geological area affected by an earthquake where the stresses produced exceeded the ultimate strength of the rocks, as shown by crushing and fracturing
sediment load	the amount of material carried down by a river in suspension, solution or as bed load
seismic activity	earthquake activity
seismograph	instrument for detecting and recording earthquakes
seismogram	the record produced by a seismograph illustrating the magnitude, frequency, and duration of seismic waves
shotcreting	a process of conveying mortar or concrete through a hose at high velocity on to a surface, the material bonds tenaciously to a properly prepared concrete surface and to a number of other materials

slickenside	a polished and scratched planar surface at a fault plane produced by friction between the opposing sides of a fault, the surface only feels smooth when rubbed in the same direction as the former movement
slides	(sometimes 'landslide') mass movements with a distinct surface of rupture separating the slide material from more stable underlying material (slope failure); the downward sliding material is usually relatively dry.
slope facet	a part of a hill slope that has more or less homogeneous characteristics showing consistent slope direction and inclination; facets are mostly bounded by ridges, spurs, gullies, or rivers; local within a facet may be called sub-facets.
slope morphometry	the features of a slope including shape, angle, and aspect
strike slip fault	a fault in which the movement is parallel to the fault strike, there is no vertical motion (see also transform fault)
strike	the angular direction with respect to north (compass bearing) of the line of intersection of a bedding plane, fault plane (then called fault strike), or other planar structural feature (e.g., discontinuity plane) with a horizontal plane
subduction zone	the linear areas that represent the zones where crustal plates are overridden by other plates and are forced down into the underlying mantle along an oblique plane of thrusting; they mark plate collision zones
teleseismic phase data	data from a distant earthquake
thrust fault	a dipping fault plane with the top riding over the bottom; arises from compression, when two blocks of rocks converge (also known as a reverse fault)
topography	the surface features of the earth's surface including the relief, the terrain, and all the features in the landscape created by human endeavour; i.e., the shape and form of the earth's surface
transcurrent fault	a type of strike-slip fault
transform fault	a special type of strike-slip fault forming the boundary between two moving plates, usually along an offset segment of the oceanic ridge
water balance	in hydrology used to mean the input/output/storage relationship of water in a given area (includes calculations of precipitation, overland flow, throughflow, evapotranspiration, storage and others)
watershed	formerly used to mean a divide, the water-heading from which headstreams flow to different rivers; now generally used to mean the area drained by a particular river or stream with all its tributaries (the catchment area of a single drainage basin) — most commonly a smallish river. Although river (drainage) basin and watershed are more or less synonymous, river basin is usually used for the large scale (regional), watershed for the small scale (local)

About the Authors

T.L. Adhikari is a Technical Director of ITECO Nepal (P) Ltd, a Swiss-Nepal joint venture engineering consulting company based in Kathmandu, Nepal. He received his first degree in civil engineering from the University of Roorkee, India in 1984 and a Masters in Soil Engineering from the Asian Institute of Technology, Thailand in 1998. Most of his professional career has been devoted to the solution of geotechnical problems in landslides and gully erosions related to highways and hydropower facilities in the mountainous regions of Nepal and Bhutan. He was the responsible civil cum geotechnical engineer in the design and construction of the Salleri-Chalsa small hydropower (1984-87), Charnawati rehabilitation (1988-90), Arniko Highway rehabilitation (1992-93), Thankot-Naubise rehabilitation (1991), and Bhainse river training (1994) projects in Nepal and the Road Bank Stabilization project in Bhutan (1993). He is also involved in the training of engineers and geologists in landslide management work in Nepal and Bhutan.

R. Anbalagan is an Assistant Professor of Engineering Geology at the University of Roorkee, India. After serving for 11 years in the Geological Survey of India, he joined Roorkee University in 1988. He has contributed to the field of Landslide Hazard Zonation and Landslide Risk Assessment mapping. Dr. Anbagalan has aobut 45 research papers to his credit published in international and national journals and conferences. He has supervised 4 PhD theses in engineering geology. In addition, Dr. Anbalagan has supervised 30 M.tech. and 7 M.E. dissertations. He has also contributed chapters to the Mountain Risk Engineering Handbook published by ICIMOD and edited a book on "Design Practices in Enrthquake Geotechnical Engineering. He has been a Professor in the University of Asmara, Eritrea, since 1999.

R.K. Bhandari has a PhD in Soil Mechanics from the Imperial College of Science & Technology, University of London. After serving the Central Building Research Institute of India until 1989 as its Director, from 1990-1995 he was chief of a major programme on Landslide Hazard Mapping in Sri Lanka for the United Nations Centre for Human Settlements (Habitat). He is currently the Head of the International Science & Technology Affairs Directorate of the Council of Scientific & Industrial Research of India.

The main professional contributions of Dr. Bhandari lie in the areas of natural disaster reduction; multi hazard mapping; geo-technical instrumentation of landslides and other mass movements and early warning; hazard, risk, and environmental impact assessment; and sustainable development of hilly areas in hazardous zones. He was the first to enunciate undrained loading as a fundamental mechanism for occurrence of low angled mudslides, jointly with Professor J N Hutchinson of Imperial College, London.

D. Bhattarai is a Senior Divisional Engineer at the Department of Water Induced Disaster Prevention (DWIDP), Ministry of Water Resources, His Majesty's Government of Nepal. He received a BSc. from Tribhuvan University in 1970, a BSc in Civil Engineering degree from Middlesex Polytechnic, U.K., in 1975, and a P.G. Diploma in Sanitary Engineering from IHE, Delft, Netherlands in

1986. He has worked for various government departments spanning a service period of about 24 years. At present, he is involved in training engineers and geologists in the field of water induced disaster prevention.

B.B. Deoja earned an undergraduate degree in civil engineering from the University of Peshawar, Pakistan, in 1967 and a graduate degree from the University of Washington, Seattle, in 1986. He has served in the public sector of Nepal in various capacities: Deputy Director General of Department of Roads, Director General of Civil Aviation, Board Member of the Royal Nepal Airlines Corporation and Joint Secretary in the Ministry of Works and Transport. Currently Mr. Deoja is Joint Secretary in the Ministry of Physical Planning and Works.

Mr. Deoja was involved in design, construction, and maintenance of mountain roads in Nepal from 1967 to 1985. He developed Mountain Risk Engineering (MRE) at ICIMOD from 1988 to 1990 as a Programme Coordinator. He also co-authored the MRE Handbook and authored an ICIMOD occasional paper on Sustainable Management of Mountain Roads and Other Infrastructure in the Hindu Kush-Himalayas.

Mr. Deoja has played an instrumental role in the formulation of policy and acts in the transportation and public infrastructure sector in Nepal since 1992.

J. Howell is a British professional soil scientist who has specialised in the use of vegetation for slope stabilisation (bio-engineering) in South Asian countries, as well as in environmental assessment and other technical fields. He has worked in Nepal periodically for fourteen years, as well as in other parts of the Himalayas, on a series of natural resources and road development projects. He is a director of Living Resources Limited, a UK-based consulting company.

N.R. Khanal is an Associate Professor in the Central Department of Geography, Tribhuvan University, Kathmandu Nepal. His main field of research is mountain geography with a focus on landscape and resource dynamics. He has studied the extreme geohydrological events that recently occurred in Nepal, such as the debris flow at Larcha and landslides and floods caused by extreme precipitation events in the Kulekhani area in 1993, Lele watershed in 1981, and Syangja and Butwal in 1998. Similarly, he has also studied floods and their impacts in the lowland Terai, in Mahuli Khola in the Eastern Terai, and Karnali River in the Western Terai.

Mr. Khanal is also actively involved in organising the training programme on landslide hazard control and management. From its inception, he has been actively involved in the Mountain Risk Engineering Unit of Tribhuvan University, which is involved in organising training and developing a training curriculum in the field of Mountain Risk Engineering. Mr. Khanal has a number of research publications to his credit in national and international journals.

S. Miyajima obtained his degree in Bachelor of Agriculture form the Tokyo University of Agriculture and Technology, Japan, in 1984. He is presently working as Deputy Director of the River Planning Division at Hokkaido Development Bureau, Japan. Mr. Miyajima joined the Hokkaido Development Agency in 1984 and worked in different capacities as the Chief Officer of Sabo Planning, River Planning and Sea Coast Planning, Deputy Director of the River Improvement Division, and Director of Sanru-dam. He also worked as the Deputy Director of River Planning Division of the Ministry of Construction, Government of Japan from 1994 to 1996 and was assigned to work in Nepal as a Sabo expert through the Japan International Cooperation Agency (JICA).

During his assignment in Nepal he worked as a Sabo expert in the Water Induced Disaster Prevention Technical Centre (DPTC), His Majesty's Government of Nepal. Mr. Miyajima is a member of the Japanese Society of Erosion Control Engineering.

S.R. Pant received his MSc with Honours from the Faculty of Geophysics, St. Petersburg State Mining Institute, Russia in 1987 and is now Lecturer in Applied Geophysics in the Department of Geology, Tribhuvan University, Kathmandu, Nepal. His research work has focused on the application of geophysics in engineering and environmental studies, mainly using electrical, electromagnetic, and seismic methods, with current research interests in the field of correlation of electrical resistivity with hydraulic parameters and rock mass quality. Mr. Pant has supervised many MSc students and has worked in a variety of projects to provide geophysical services related to hydropower development, glacier lake study, groundwater exploration, mineral exploration, and road construction and maintenance. He has published many papers related to the application of geophysical methods in landslide studies.

M. Paudel is a civil engineer. He received his civil engineering degree in 1976 from the University of Roorkee, India, and a Master's in Engineering in Geotechnical and Transportation Engineering in 1985 from the Asian Institute of Technology, Bangkok, Thailand.

Mr. Paudel has worked as an engineer for nearly 25 years in various government departments of His Majesty's Government of Nepal and has been with the Department of Irrigation for the last fifteen years. He was the coordinator of the Irrigation Sector Project funded by the Asian Development Bank and Irrigation Line of Credit Project funded by the World Bank. He also worked as a Project Director at the Water Induced Disaster Prevention Technical Centre, a project funded by the Japan International Cooperation Agency (JICA). He was the Project Manager of the Bagmati Irrigation Project funded by Saudi Arabia, one of the biggest irrigation projects in Nepal. Mr. Paudel has presented many papers on disaster management at different international seminars and symposiums.

G.S. Pokharel is a Geological Engineer with the Nepal Electricity Authority, Kathmandu, Nepal, and presently heads its Geotechnical Division. He received his MSc degree in Engineering Geology in 1978 from the Leningrad Mining Institute in the former USSR. He has a wide experience in the field of engineering geological and geotechnical investigations in a number of hydropower projects in Nepal. Mr. Pokharel was involved in the pre-feasibility and pre-design stage investigation of Arun-III Hydro power project, feasibility study of Karnali (Chisapani) hydroelectric project, engineering geological study, supervision and design of cement grouting and foundation works in the Kulekhani hydroelectric project. In addition to these large projects, he was also involved in the geotechnical investigations of a number of small and medium hydropower projects in Nepal. Mr. Pokharel has also worked in many projects related to debris torrent control and landslide stabilization work.

K.K. Purohit obtained his MSc degree in Applied Geology from the University of Delhi in 1977 and PhD from Garhwal University, India, specialising in geochemistry of migmatites. He was a Research Scholar at the University of Delhi (1977-1979) and Wadia Institute of Himalayan Geology, India (1979-1981). Dr. Purohit joined the Wadia Institute in 1981 as a Scientist and continues to work there.

Dr. Purohit has done extensive geological work in the Himachal and Uttaranchal Himalaya, and also investigated the environmental aspects of Doon Valley soils using the multipurpose and multi-

element geochemical mapping technique. Encouraged by the success of the technique, he has extended the work now to the upper reaches of the Himalayan belt. Dr. Purohit has published 17 research papers in national and international journals.

A.B. Singh is Professor of Civil Engineering at the Institute of Engineering (IOE), Tribhuvan University, Nepal, which he joined in 1971. He received an MSc from Moscow Automobile Highway Engineering Institute, USSR, in 1969, and a PhD in Rock Mechanics from the University of New South Wales, Australia, in 1980. As well as teaching, he has served on various technical committees such as the Working Committee of the Royal Commission for Higher Education, 1984; Review Committee on the Design of the Approach Road to the Arun-III Hydropower Project in 1990; Committee for the Investigation of the Bagmati River flood, 1993; and the Technical Committee of the Nepal Bureau of Standards. He has published a number of research papers in national and international journals and has been associated with the design and construction of some important road and dam projects in Nepal. Professor Singh was an Associate Member of the Royal Nepal Academy of Science and Technology for two terms and is currently on the Executive Board of the International Commission on Large Dams, Nepal.

B. Singh is a Professor of Civil Engineering at the Civil Engineering Department, University of Roorkee, India. He obtained his PhD degree from the University of Rookee in 1960. Prof. Singh has published 150 research papers, mainly related to rock mechanics and geotechnical engineering, in addition to 80 consultancy reports. He has guided 13 PhD theses and 40 M.E. dissertations. He is the recipient of 8 national awards. Professor Singh is also the Chairman of the Sectional Committee on Rock Mechanics of the Bureau of Indian Standards as well as the Chairman of the Editorial Board of the Commission on the International Society of Rock Mechanics.

V.C. Thakur is former Director of the Wadia Institute of Himalayan Geology, Dehradun, India and currently CSIR Emeritus Scientist at the same Institute. He received an MSc in geology from the Punjab University, India, and PhD and DIC from Imperial College, London. He has done research work in the Scottish Highlands and Swiss Alps, and has worked extensively in the Himalaya for the past 28 years on regional geology, tectonics, and seismotectonics, with the current focus on seismotectonics and earthquake hazard assessment in the Western Himalaya. Dr. Thakur has published over 100 research papers in national and international journals. He was Chairman of the Himalaya Coordinating Committee of the International Lithosphere Programme from 1992 to 1996, and Convener of the Symposium on Himalayan Tectonics in the International Geological Congress (IGC) in 2000, 1996, and 1989. He has served on various editorial boards and is a Founder Editor of the Journal on Geology of the Western Himalaya. Dr. Thakur was awarded the National Mineral Award of the Government of India and is a Fellow of the Indian Academy of Sciences.

K.B. Thapa, has been associated with Tribhuvan University, Kathmandu, Nepal, since 1974, where he is now Professor in the Central Department of Hydrology and Meteorology. He has carried out many field studies in Nepal related to snow hydrology and floods and has been a consultant for various hydrometeorological projects. Professor Thapa has many research papers to his credit on a wide range of topics related to geomorphology, rainfall runoff and flood studies, and snow hydrology.

B. Tiwari is a graduate in civil engineering from Tribhuvan University, Nepal. He has also obtained a Master's degree in Geo and Biosphere Science from Niigata University, Japan, with specialisation in landslide mechanisms. Mr. Tiwari started his career in 1992 as a civil engineer at the Department

of Roads, His Majesty's Government of Nepal. Later he was deputed to the Water Induced Disaster Prevention Technical Centre (DPTC) as a landslide engineer and worked there from 1993 to 1997. During his stay in the DPTC, he was responsible for surveying, investigating, monitoring, and planning and implementating countermeasures for landslides in Nepal. Mr. Tiwari was also involved in providing training on 'landslide mitigation' to government officers through various organisations. He was involved in various preliminary investigation works of disaster events in Nepal as a landslide expert.

Mr. Tiwari was the editor of ' Disaster Review', an annual publication of DPTC and various landslide manuals and reports. He has presented many papers on landslide and geo-techniques in national and international seminars and has published research papers on landslides, on aspects like the residual shear strength of soil. Presently Mr. Tiwari is a research fellow at the Research Institute of Hazards, Niigata University, Niigata, Japan.

N.S. Virdi has been associated with the Wadia Institute of Himalayan Geology (WIHG), Dehradun, India since 1977, where he has been Director since February 2000. From 1975 to 1979, he taught at the Punjab University, Chandigarh, and Indian Photointerpretation Institute (now Indian Institute of Remote Sensing), Dehradun, India, and has been Courtesy Professor at the University of Oregon, U.S.A. since 1997. He was awarded a Commonwealth Scholarship to study in Britain and received his PhD from the University of Leeds in 1973. Dr. Virdi has done extensive geological work in the Indian states of Ladakh, Jammu & Kashmir, Himanchal Pradesh, and Uttaranchal. His work on geological hazards and their management has included geotechnical feasibility surveys for hydel projects, ropeways, tubewells, and building complexes, and control of landslides. In 1985, Dr Virdi was awarded the National Mineral Award by the Ministry of Steel and Mines, Government of India, for outstanding contributions to the fundamental aspects of earth sciences and in 1996 an MSc by Punjab University, India.

Wu Jishan is a Professor in the Institute of Mountain Hazards and Environment, Chinese Academy of Sciences, Chengdu, China. He was the Director of this Institute from 1983 to 1995. Currently he is Chairman of the Mountain Research Committee of the Geographic Society of China. He graduated from Nanjing University in 1962 and received his MSc. from the Geography Institute of the Chinese Academy of Sciences in 1966.

Professor Wu has done extensive research on mountain hazard mitigation in China. His main field of research has been on formation, dynamics, investigation, and mitigation of debris flow hazard. He has supervised many MSc dissertations and some students have completed PhDs under his co-supervision. Professor Wu also coordinated the Integrated Training on Mountain Risk Engineering project in China from 1995-1998 with support from ICIMOD. Over the past 35 years, he was coordinated 12 national and international projects on debris flow and landslide hazard mitigation. He has published over 30 research papers on debris flow studies in national and international journals, and he is the author or co-author of 7 books. Professor Wu is also the recipient of 6 scientific and technical awards from the state and provinces.

H. Yagi is an Associate Professor of Geomorpholoy at the Yamagata University, Japan. He obtained his Doctor of Science degree from Tohoku University, Japan, in 1986. Dr. Yagi also worked as a Lecturer in the National Defense Academy, Japan, from 1986 to 1996. His main interests are in the field of Neotectonics, Quaternary Geology, and landslide and regional study of Nepal. His field of research has spanned from northwestern Japan to Nepal and the adjacent Himalayan region. Dr

Yagi was also in charge of the Landslide Hazard Management Control Project at ICIMOD in 1995, a position to which he was deputed by the Japan International Cooperation Agency (JICA). Dr. Yagi has many publications to his credit in the field of geomorphology, hazard mapping and landslide studies.

Yin Chongqin is a senior engineer of the Institute of Debris Flow Prevention of Dongchuan city, Yunnan Province, China. He graduated from Kunming College of Water Conservation in 1963. Since then, he has worked as an engineer for 15 years in the Bureau of Water Conservation of Dongchuan city and remained with the Institute of Debris Flow Prevention.

After serving for more than 30 years in the fields of water conservation, soil erosion, and debris flow control, he has wide experience in the field of debris flow hazard mitigation and control. He was engineer in charge of 12 debris flow control projects in Yunnan Province, China. He was also involved in a study on the relationship between debris flow and precipitation in the Dongchuan area. Mr. Yin has published a number of research papers in national and international journals. He was recognised for his outstanding contribution by the Yunnan Provincial Government in 1989, and he also received a certificate for making an outstanding contribution to the development of engineering from the State Council in 1997.

Table of Contents

Principles and Management

Section 1

1 Regional Geology and Geological Evolution of the Himalaya

V. C. Thakur
Wadia Institute of Himalayan Geology,
33, Gen. Mahadeo Singh Road, Dehra Dun-248001, India
Email : bindu@nde.vsnl.net.in

The Himalaya is divided longitudinally into five tectonic zones, known as (from south to north) the Siwalik Zone (or Sub or Outer Himalaya), the Lesser (Lower) Himalaya, the Higher (Great) Himalaya, the Tethys (or Tibetan-Tethys) Himalaya, and the Trans Himalaya. These tectonic zones are separated from each other by major intracrustal thrusts: the Main (or Himalayan) Frontal Thrust (MFT or HFT), the Main Boundary Thrust (MBT), the Main Central Thrust (MCT), the South Tibetan Detachment (STD), and the Indus-Tsangpo Thrust (ITT). The Himalaya originated as a result of the closing of the Tethys ocean and the subsequent continent-continent collision of the Indian and Asian (Karakoram-Tibet block) plates. The Ladakh-Gangdes granitic-volcanic arc of Cretaceous to early Eocene (100 to 40 million years) age resulted from the subduction of oceanic lithosphere of the Indian plate under the Asian continent. The rock assemblages found in the Indus-Tsangpo Suture region today, represent both the Tethys oceanic crust and the subduction zone complex. Prior to the collision, the Mesozoic sequence of the Tethys Himalaya represented the north-facing passive margin of the Indian plate. The collision between India and Asia took place between 55 and 40 million years ago. The collision and continued northward convergence of India produced the main intracrustal thrust faults, accommodating more than 500 km of crustal shortening. Crustal shortening generated metamorphism and leucogranites at the mid-crustal level (15-20 km), with the metamorphic and granitic rocks being brought to the surface along the MCT as Higher Himalaya crystalline. The principal phase of metamorphism, the main phase of activity of the MCT and of northward displacement along the South Tibetan Detachment, took place 18-22 million years ago. The thrusts grow progressively younger as one moves from north to south; the MCT was initiated 22 million years ago, the MBT 10 million years ago, and the MFT around 0.5 million years ago.

Introduction

The Himalayan mountain range extends from east to west in a massive arc for about 2,500 km with a width of 230 to 350 km. The Himalaya is the highest mountain range in the world, containing 10 of the world's 14 peaks over 8,000 masl, and more than 40 peaks over 7,000m. The Himalaya occupies a unique physiographic and geological setting: it lies between the Indian subcontinent with normal crustal thickness (35 km) to the south, and the highest plateau in the world, the Tibetan plateau with a double crustal thickness (70 km), to the north.

The Himalaya originated as a result of continent-continent collision between India and Asia (Dewey and Bird 1970; Powell and Conagan 1973). The collision took place 55-40 million years (Searle et al. 1987; Dewey et al. 1989). Penetration of India under Asia (Karakoram-Tibet) produced crustal shortening and slicing of the northern margin of the Indian continent into slivers along three principal thrusts: the Main Central Thrust (MCT), the Main Boundary Thrust (MBT), and the Main (or Himalayan) Frontal Thrust (MFT or HFT). The continental slivers were stacked one over the other, propagating southward and building the architecture of the Himalaya (Molnar 1984). The load of the crustal stacks flexed the Indian plate to the south giving rise to a foreland depression in

which sediments of the Muree/Dharamsala and Siwalik groups, 18 million years old and younger, were deposited in the basin.

One of the striking features of the Himalaya is the extreme altitudinal variation from almost sea level on the Indo-Gangetic plains to an average elevation of 8,000m in the Higher Himalaya, all within a direct distance of less than 150 km. The perennial rivers of the range are fed by more than 5,000 glaciers, meltwater from accumulated snow, and monsoon rain. The combination of these agents with the young topography and altitudinal variation leads to the erosion of a vast amount of rock material, which is deposited from the Indo-Gangetic and Brahmaputra plains to as far away as the Bay of Bengal and Arabian sea, where the deposits form the very large Bengal and Indus fans.

Hillside stability and mass movement, including landslides, are controlled by several factors, including geology, climate, and topography. In the Himalaya geology plays an important role, but the geology is also very diverse as a result of the great variation in the composition of geological materials and the framework while traversing from south to north. The major zones are described below in the section on tectonic zonation. Fault and fracture zones are sites of structural weakness, to understand them and predict their effects we must understand the nature and origin of the Himalayan structures. Geodynamically, the Himalaya is an active tectonic belt, as evidenced by the changing mountain morphology and frequent earthquake activity. The effect of climate also varies across the region. South of the Higher Himalaya, in the region with a monsoon climate, rainfall is the dominant factor; whereas in and to the north of the Higher Himalaya, in the monsoon rain shadow zone, snow and temperature variation are the dominant factors. Topography is another factor showing great variation; both the topography and the drainage pattern of the Siwaliks, for example, are different from those of the Lesser and Higher Himalaya. Thus there is a very complex matrix of geology, climate, topography, hydrology, and seismic activity - each of which can play a vital role in destabilising slopes in different tectonic zones. Thus it is always difficult to assign failure of a hill slope to any one parameter.

Tectonic Zonation

According to Gansser's (1974) widely-accepted classification, the Himalaya can be divided longitudinally into five tectonic zones on the basis of geological evolution. The tectonic zones correspond broadly with the physiographic and climatic zones. From south to north, the tectonic zones are the Siwaliks (also known as the Outer or Sub Himalaya), the Lesser (Lower) Himalaya, the Higher (Great) Himalaya, the Tethys (Tibetan) Himalaya, and the Trans Himalaya (Figures 1.1 and 1.2). The northern edge of the Indo-Gangetic Plain, or Terai, is sometimes included as the southernmost zone of the Himalaya. The Trans Himalaya is further subdivided into the Indus-Tsangpo Suture and the Lhasa-Karakoram block. These tectonic zones are separated from each other by the principal Himalayan thrust faults (Thakur 1981, 1992). The southernmost fault, the Main (or Himalayan) Frontal Thrust (HFT) separates the Siwaliks from the alluvial plains (the northern edge of the Indo-Gangetic Plain). The Main Boundary Thrust (MBT) separates the Lesser Himalaya from the Siwaliks. The Main Central Thrust (MCT) lifts the middle-level crustal rocks of the Higher Himalaya over those of the Lesser Himalaya. The South Tibetan Detachment (STD) marks the boundary between the Higher Himalaya and the overlying fossiliferous sequence of the Tethys Himalaya along a low angle normal fault. The Indus-Tsangpo Thrust (ITT) separates the rocks of the Indus-Tsangpo Suture in the Trans Himalaya from the Tethys Himalaya. These zones are described in more detail below.

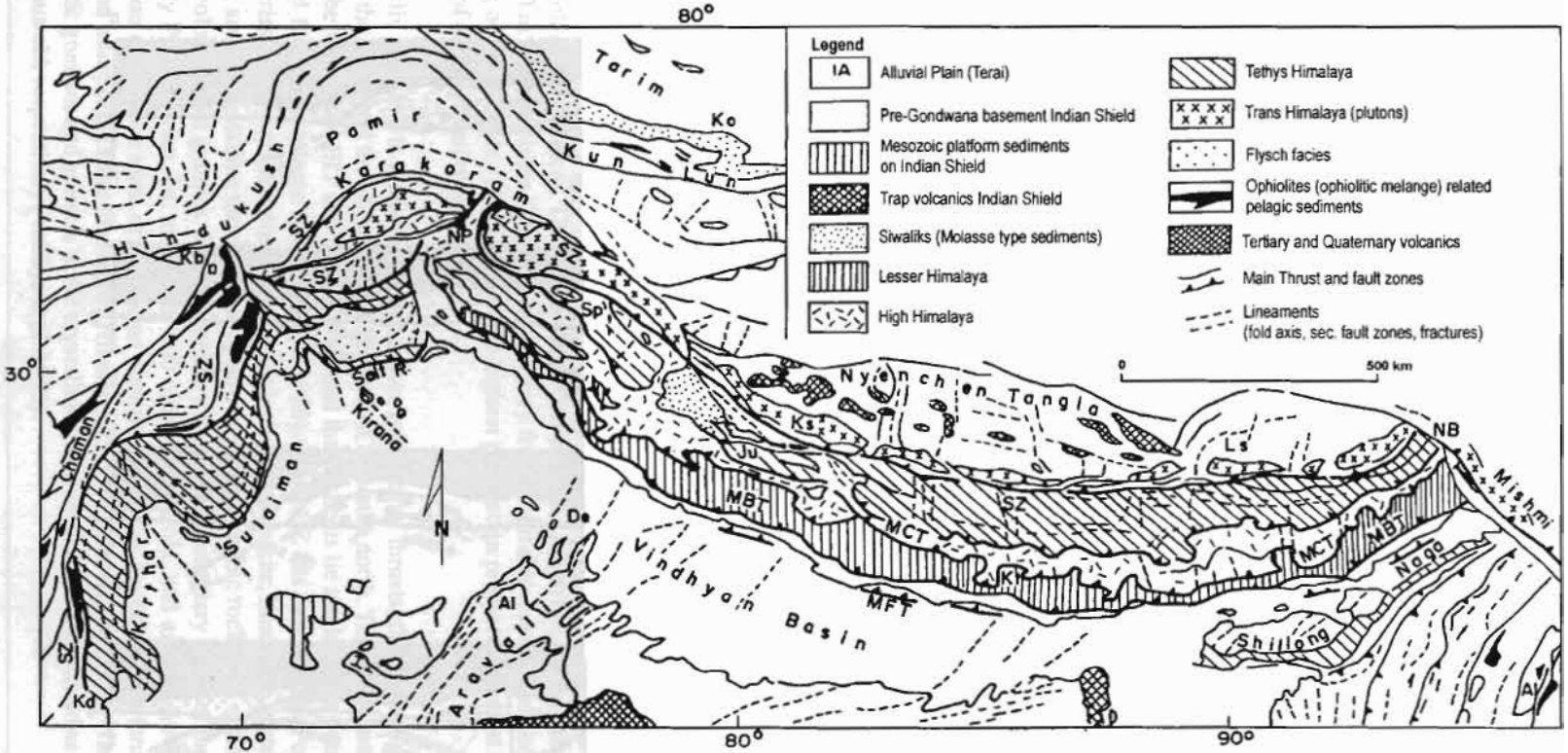

Figure 1.1: **Tectonic zonation of the Himalaya** (after Gansser 1974)

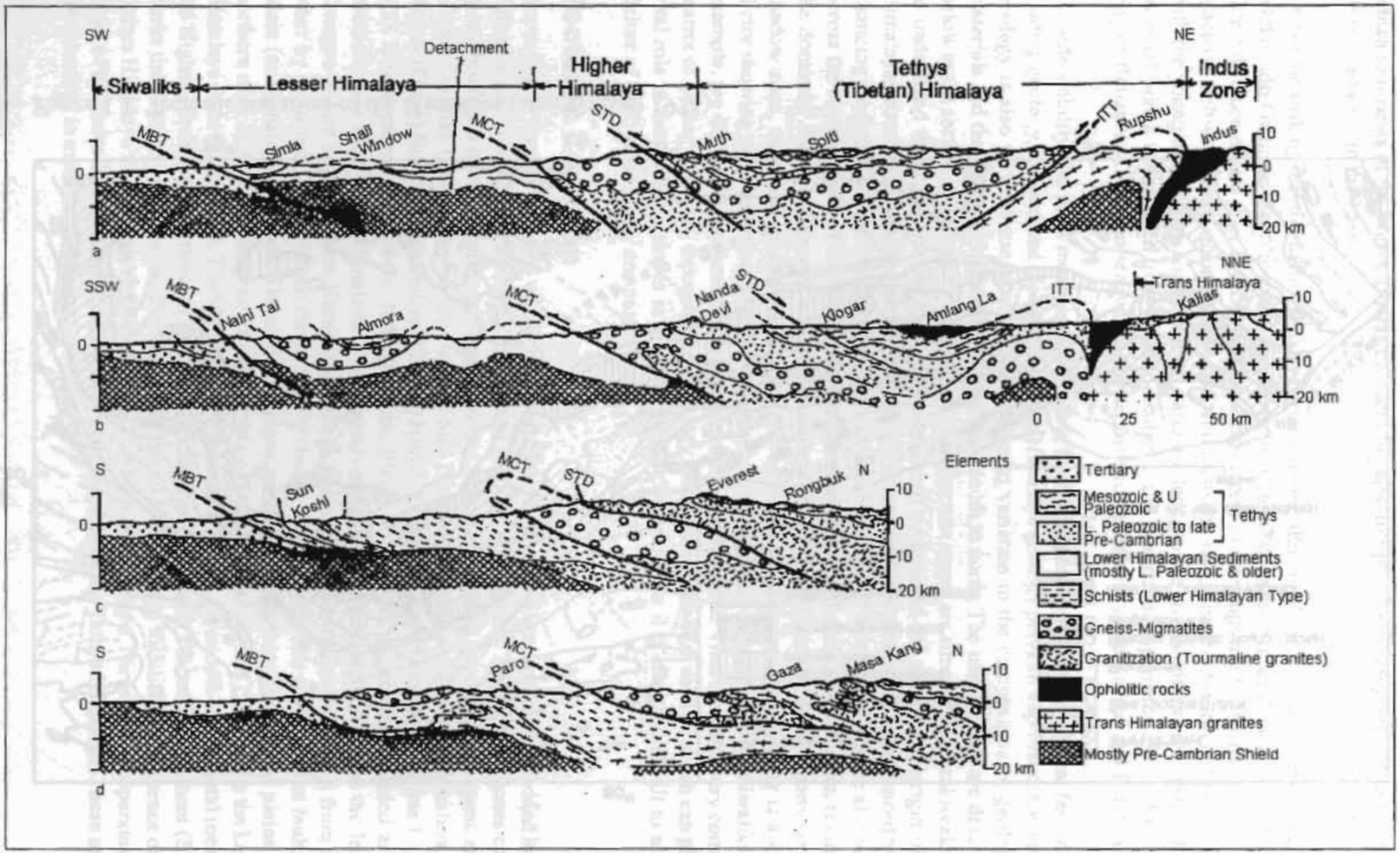

Figure 1.2: Cross-section across the Himalaya: (a) across Western Himalaya, (b) across Kumaun, (c) across Nepal, (d) across Bhutan (after Gansser 1974)

The Siwaliks or Outer Himalayan Zone

The foothill ranges of the Himalaya are called the Siwaliks and comprise the southernmost tectonic zone, which is also called the Outer or Sub Himalayan Zone. The altitude ranges from almost sea level to more than 800m, with an average of 500m. The climate is tropical with a great variation of temperature between summer and winter. Erosion is faster than in other zones of the Himalaya, especially during the monsoon. The Siwaliks consist of an 8,000-10,000m thick pile of sedimentary rocks ranging in age from Paleocene (50 million years ago) to Upper Pleistocene (0.2 million years ago) (Burbank et al. 1997).

The Siwaliks are bounded to the south by the Main (or Himalayan) Frontal Thrust (MFT), which separates them from the alluvial plains. To the north, they are separated from the older rock formations of the Lesser Himalaya by a fault called the Main Boundary Thrust (MBT). The Siwalik Zone is further differentiated into the Rawalpindi Group, which includes Paleocene-Lower Eocene-marine and Murree/Dharamsala Group fluvial sequences, and the Siwalik Group (Burbank et al. 1997). The rock formations of the Siwalik Group include thick bedded sandstone, mudstone, and shale in the lower and middle parts, and conglomerate in the upper part. These rocks are of fluvial origin, that is they were deposited by rivers in a situation similar to that of the present day Indo-Gangetic plains (Raiverman et al. 1983). The Siwalik strata have yielded rich assemblages of vertebrate fossils of elephant, hippopotamus, giraffe, horse, bovines, tortoise and many others similar to those of the present day, and of their ancestral fauna (Barry et al. 1982). These fossils were used in earlier times to assign ages to the rock formations. In recent years a more precise method, magnetostratigraphic dating, has been used and has shown the base of the Lower Siwalik to be 18.3 million years old, the Middle Siwalik to be 6 to 8million years old, and the Upper Siwalik to be 5.44 to 0.22 million years old (Johnson et al. 1983; Thakur 1992). Paleoenvironmental reconstruction of the Siwaliks based on plant and vertebrate fossils, rock types, and sedimentary structures, indicates that 15 million years ago the climate was warm and humid with active monsoons, that the area had dense forests inhabited by large mammals, and that it was drained by rivers and contained swamps and lakes.

Lesser Himalayan Zone (LHZ)

The mountain ranges lying between the Siwalik foothills and the Higher Himalaya comprise the Lesser Himalayan Zone (LHZ). This zone is characterised by V-shaped valleys and ridges with several levels of river terraces. The average height varies from 1,500m to 2,000m, with a maximum of up to 3000 m in some places. The climate can vary from tropical to subtropical and subtemperate depending on the altitude. This zone has the highest population pressure and most anthropogenic activities of all the Himalayan Zones.

Geologically the LHZ is bounded by two major intracrustal thrusts, the Main Boundary Thrust (MBT) to the south and the Main Central Thrust (MCT) to the north. The LHZ is structurally very complex; between the MBT and the MCT several thrust sheets lie stacked one over the other and folded and faulted on a large scale (Valdiya 1980). The LHZ has two principal components: a) sedimentaries and low grade metasedimentaries including quartzite, limestone, slate, siltstone, and volcanics; and b) crystalline thrust sheets comprising metamorphic rocks like schist, gneiss, marble, metavolcanic, and granites. The sedimentary and metasedimentary rocks of the LHZ are predominantly PreCambrian, i.e. more than 600 million years old, and are believed to represent a continuation of the rock units of the Indian continent; whereas the crystalline thrust sheets were derived and transported from the Higher Himalaya Zone to override the Lesser Himalayan rocks. The granitic gneisses and granites in the crystalline thrust sheets have been dated as 1,800 and 500 million years old, respectively (Valdiya et al. 1988).

Higher Himalayan Zone (HHZ)

The mountain ranges of the Higher Himalayan Zone (HHZ) appear as a rampart wall when viewed from the south. They constitute the highest uplifts in the Himalaya with an average height of over 6000m. The altitudinal variation is extreme. The Higher Himalaya acts as a great barrier to the South Asian monsoon causing it to precipitate most of its rain to the south; it also prevents the cold northern winds from Tibet and the Karakoram reaching the Indian plains. The climate is temperate alpine with a snowline at 5,500m. There are more than 5,000 glaciers, and large parts are covered by snow during winter. The topography is characterised by deep narrow gorges with narrow valleys and steeply rising mountains

The HHZ is composed of a 15-20 km thick slab of crystalline rocks comprising metamorphics like gneiss, schist, quartzite, marble, and amphibolite, together with granites (Pecher 1989; Hodges et al. 1996). These rocks are of Proterozoic age, 1,800-2,000 million years old, and were buried at mid-crustal level at a depth of 15-20 km. Originally, they constituted the northern part of the Indian continent. The southern boundary of the HHZ is demarcated by the Main Central Thrust (MCT). The MCT forms a broad (1-5 km) shear zone, which has brought the rocks of the HHZ from mid-crustal to their present level. The MCT is a structurally weak zone where there are frequent mass movements. A belt of moderate earthquakes lies close by (Yeats and Lillie 1991; Khatri 1987); some scientists think that this zone is neotectonically active. A pressure-temperature (PT) estimate of the metamorphic rocks of the HHZ indicates that they were buried at a depth of up to 20 km at temperatures ranging from 500 to 700°C and pressure of from 5,000 bar to 12,000 bar[1]. Two types of granites are associated with the metamorphics, older granites from 500 and 1,800 million years ago, and the younger leucogranites from 15 to 20 million years ago (LeFort 1981).

The Tethys Himalayan Zone (THZ)

The Tethys (or Tibetan) Himalaya (THZ) occupies a 30-40 km wide belt north of the Higher Himalaya. This zone has an average altitude of over 3,000m and lies in the rain shadow zone of the Higher Himalaya. It receives scant rainfall (less than 30 cm per year) and the climate is cold arid.

This THZ is characterised by a 10 km (maximum) thick, well-bedded sedimentary sequence made of limestone, marl, shale, quartzite, and sandstone. This sequence is richly fossiliferous and a paradise for fossil hunters (Gaetani and Garzanti 1991; Gardstein et al. 1991). The fossils of bivalves, molluscs, ammonoids, and others have helped scientists to assign ages to the different rock formations and construct biostratigraphic zones in the sequence. The Tethys Himalaya sequence of rocks range in age from Cambrian (500 million years old) to Lower Eocene (60 million years old). The THZ rocks are essentially composed of marine facies deposited in the shelf and slope region of a continental margin of the ancient Tethys sea (Gaetani and Garzanti 1991). A record of the marine life of the past is preserved in the rocks in the form of fossils, which have been extensively studied in Spiti and Malla Johar in India and in Nepal (Hayden1904; Sinha 1989; Gardstein et al. 1991). The Tethys sedimentary sequence overlies the crystalline rocks of the HHZ along a low angle, north dipping normal fault, the South Tibetan Detachment, and is separated from the rocks of the Trans Himalaya Zone to the north by the Indus-Tsangpo Thrust fault (ITT).

Trans Himalayan Zone (TRZ)

The Trans Himalaya Zone (TRZ) lies to the north of the Tethys Himalaya. Monsoon precipitation is very low, with an average annual rainfall of less than 30 cm. The climate is cold and dry. The base level erosion and valley floors lie at a height of 3,000m.

[1] 1 bar = 10^5 Pa

The TRZ can be further divided into the Indus-Tsangpo Suture (ITS), and the Karakoram-Lhasa block. The Indus and Tsangpo rivers flow in opposite directions, towards west and east respectively, parallel to the mountain range. The Indus-Tsangpo Suture (ITS) represents the collision boundary between the Indian and Asia plates, and it is the site along which the vast Tethys ocean gap was closed (Searle et al. 1987). The ITS is mainly composed of ultramafic rocks (like peridotite and dunite), gabbro, and volcanics representing the oceanic crust of the Tethys ocean (Nicolas et al. 1981). The other components are granites, tonalites, and volcanics of magmatic arc, and sedimentary rocks of fore-arc, oceanic trench, and intramontane basin (Thakur and Misra 1984). These varied lithologies of rocks ranging from sedimentary to plutonic and volcanic have ages of 130 to 40 million years. The different hues in the suture zone rocks result in a dramatic panoramic landscape.

The Karakoram-Lhasa block to the north of the ITS comprises the Karakoram mountains and southern Tibet and belongs to the northern Asia plate. This is a region of high mountains and high plateaus with a minimum elevation of more than 4,000m. Rainfall is scanty and most of the precipitation is in the form of snow. The Karakoram-Lhasa block has three main components, a sedimentary sequence, granite, and metamorphics (Allegre et al. 1984; Searle 1991). The sedimentary sequence comprises limestone, marl, siltstone, sandstone, shale, quartzite, and subordinate volcanics. The rocks of this sequence are fossiliferous with an age ranging from Middle Paleozoic to Cretaceous (250 to 65 million years ago) (Yin et al. 1988; Gaetani et al. 1990; Bagati et al. 1994). The metamorphics predominantly comprise schist, gneiss, and phyllite and constitute a narrow belt underlying the sedimentaries. The granites form large bodies with areas of ten to a hundred sq km. and intrude the sedimentary and metamorphic rock sequences. The granites have been dated as around 95 million and 25 million years old (Scharer et al. 1984 a,b).

Geological Evolution

Approximately 200 million years ago before the Himalayas were formed, India formed part of a southern supercontinent called Gondwanaland. The other members of this assembly were South America, Africa, Australia, and Antarctica together with smaller fragments of Arabia, Madagascar, and New Zealand. The northern large landmass, Laurasia, included North America, Greenland, Europe, and most of Asia. A vast ocean called the Tethys lay between these two continental masses. Between 200 and 130 million years ago, a northern fringe separated from Gondwana into a number of small continental fragments which drifted north and were plastered against the southern margin of Asia, eventually forming Iran, Afghanistan, northern Pakistan and southern Tibet (Smith et al. 1981; Molnar 1986).

Closing of the Tethys Ocean

By 100 million years ago India had separated from the other southern continents; the 3,000-4,000 km wide Tethys ocean lay between India and Asia (which included the Karakoram and Southern Tibet). India continued its northward journey at a rate of some 10-15cm per year; the Tethys ocean gap closed and the Indian ocean opened (Figure 1.3). The closing of the Tethys ocean was accomplished by a downward movement, or subduction, of the oceanic lithosphere of the Indian plate under the southern Tibet and Karakoram part of the Asia plate (Figure 1.4).

The best present day example of subduction is that of the Pacific oceanic plate beneath the Japan and Aleutian islands, a process manifested in the generation of island arc volcanoes. The large sized granite bodies, exposed as a result of erosion in the Peruvian Andes and Western Cordillera of the USA, were produced as a result of subduction of the Pacific oceanic plate underneath the western continental coast of North and South America.

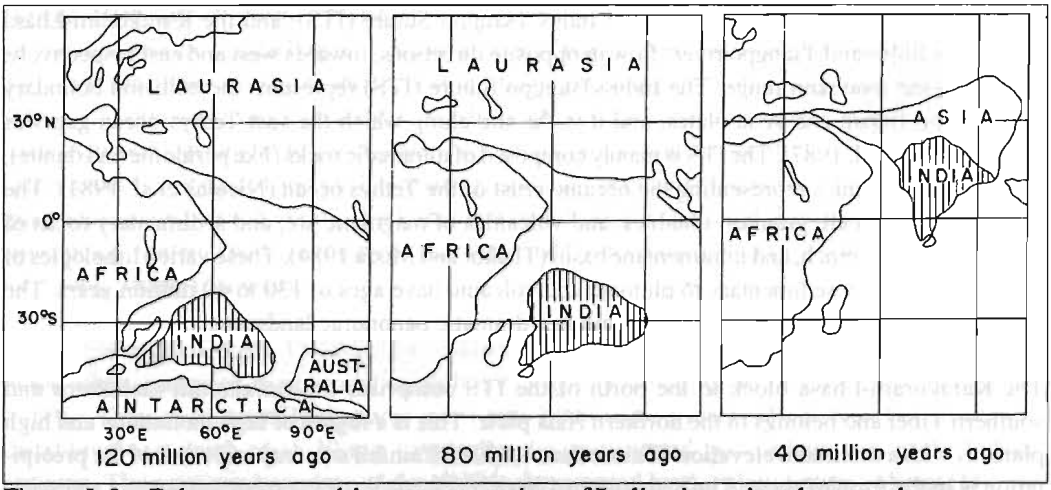

Figure 1.3: **Palaeogreographic reconstruction of India vis-a-vis other southern continents 120 million years ago. Separation of India and its northward movement in closing the Tethys ocean through subduction process 80 million years ago. Collision of Indian continent against Asia (Tibet-Karakoram) and formation of Himalaya and high plateau of Tibet 40 million years ago** (Smith et al 1981, Molnar 1986)

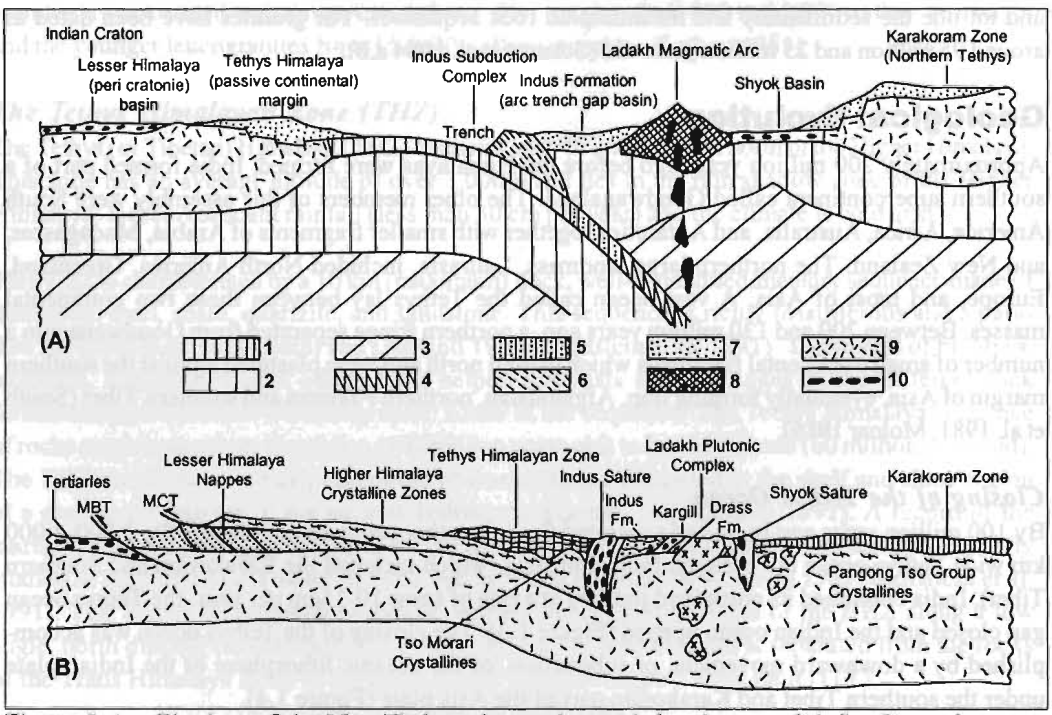

Figure 1.4: **Closing of the Neo Tethys shown in a subduction model, 1 - Oceanic crust, 2-Bottom of the lithosphere, 3-Asthenosphere, 4-Eclogite layer, 5-Transitional zone from eclogite to basalt, 6-subduction complex (melanges, trench sediments), 7-Arc-trench gap (fore-arc) sediments, 8-Crust of magmatic arc, 9-Continental crust, 10-Magma. (b) Suturing of India with Asia, showing principal tectonic elements of Himalaya** (Thakur 1989)

Geological mapping, geochemical analysis of the rocks, and geochronological dating have proven the existence of island arc volcanoes in Ladakh in India (Robertson and Degnan 1994), Kohistan in Pakistan (Asif Khan et al. 1993), and around Lhasa in southern Tibet (Allegre et al. 1984). These volcanics have ages ranging from 130 to 40 million years, the time of subduction of the Indian oceanic plate. Large granite bodies, hundreds of kilometres long, and associated igneous rocks occupy a belt extending from Deosai in Pakistan through Ladakh in India to the Gangdese mountains in southern Tibet. These granite bodies, 100 to 40 million years old, were generated as a result of subduction of the Indian oceanic plate under the Karakoram and southern Tibet (Honegger et al. 1982; Ahmad et al. 1998). Other evidence of the subduction process is provided by the ophiolitic melanges (scrapped-off oceanic crust rocks like serpentinite mixed with deep sea sediments) and very high pressure (> 8 kb) blue schist rocks recorded along the entire length of the Indus-Tsangpo Suture zone (Jan 1990). The remainder of the Tethys oceanic crust rocks, called ophiolite, are exposed as dismembered fragments along the suture zone both in Ladakh (Thakur and Misra 1984) and in southern Tibet (Nicolas et al. 1981). Thus the Indus-Tsangpo suture zone exposes rock assemblages that are typical products of the geological processes involved in the closing of the Tethys ocean by northward subduction of the Indian plate beneath Asia (Searle et al. 1987).

Continent-Continent Collision

By 55 million years ago, the Tethys ocean gap was completely closed, the oceanic lithosphere of the Indian plate lay beneath the Asian continent, and the continental lithosphere of the Indian plate was juxtaposed against the Asian continent. (The Indian plate has two types of lithosphere: continental, rich in silicates which have have a lower density, and oceanic, rich in Fe and Mg minerals which have a higher density).

Around 50 million years ago the Indian continent was completely lodged against the Asian continent resulting in collision tectonics (Coward et al. 1986). By that time the last remains of the marine condition of the Tethys had disappeared. As the continental crust of India could not sink to the great depths needed (>100 km) to be consumed (unlike oceanic crust), resistance developed against the northward movement of India. The rate of northward movement of India decreased from 15 cm to 5 cm per year. This decrease in rate and disappearance of marine condition are interpreted as representing the time of collision between the continents of India and Asia. After collision, as a result of the ongoing northward convergence of India against Asia (Tibet), the Indian crust thickened, producing metamorphism and transforming the deep-seated rocks of the Higher Himalayan Zone at temperatures ranging from 500 to 700°C and at pressures of 5 kb to 12 kb (Pecher 1989). Around 20-23 million years ago, the northern margin of the Indian continent was sliced at mid-crustal level (~15-20 km) along the fault called the Main Central Thrust (MCT). The rock sequences above the MCT were detached and moved south up to 100 km overriding the rock formations that now constitute the Lesser Himalayan zone (Figures 1.4 and 1.5). The MCT (Hubbard and Harrison 1989) originated at a depth of 15-20 km some 20-23 million years ago and brought the deep-seated rocks, metamorphics, and granites upward to be exposed to erosion as rocks of the Higher Himalaya. This upward thrust movement and erosion initiated the uplift of the Higher Himalaya.

Around 10 million years ago, the fault called the Main Boundary Thrust (MBT) developed south of the Lesser Himalaya as a result of continued northward convergence and slowdown of activity along the MCT (Meigs et al. 1995) (Figures 1.4 and 1.5). This thrust detached the top sedimentary layer of the Indian continent (now constituting the Lesser Himalayan Zone) and brought them up to override the younger rocks of the Siwalik (Outer Himalayan) Zone. Finally the Siwalik strata were uplifted as a result of the development of the Main (Himalayan) Frontal Thrust in Upper Pleistocene

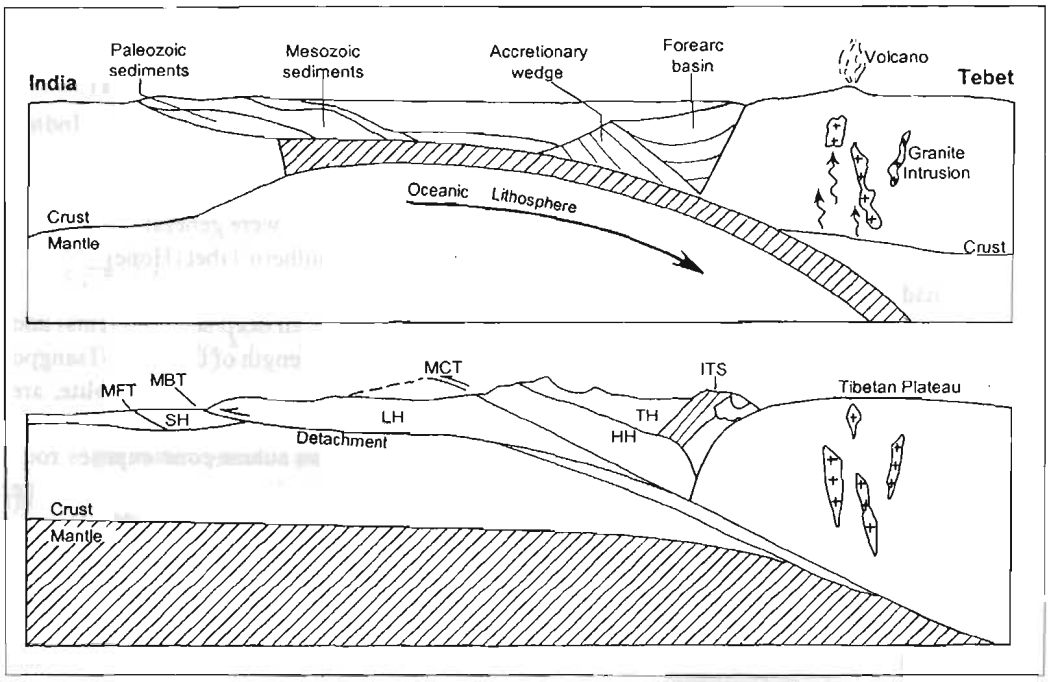

Figure 1.5: **Upper figure: closing of Tethys ocean by subduction of oceanic lithosphre of Indian plate under Tibet (Asia), producing island arc volcanoes, granite intrustions, accretionary wedge and fore-arc basin, some 80 million year ago. Lower figure: continent-continent collision between Indian crust and Tibetan crust at 50 million years ago. Slicing of Indian margin crust along MCT, MBT and MFT and stacking of crustal slabs** (after Molnar 1986, Valdiya 2988)

age (0.5 to 0.2 million years ago), producing a sharp topographic break between the Siwaliks and the alluvial plains (Nakata 1989). Thus the architecture of the Himalaya developed from the stacking up of slivers of the northern margin of India on top of one another (like a pack of cards) over the Indian plate (Molnar 1984). During this process, the crust thickened, and shortening of more than 500 km has been accommodated (Figure 1.5).

The stacking of thrust slabs (slivers) exerted a load on the Indian plate causing flexure (bending) of the plate (Lyon Chen and Molnar 1983). The flexed part of the plate in front of the uplifted Himalaya produced a depression (foredeep), called the foreland basin of the Siwalik and Indus-Ganga. The rocks that were eroded from the uplifted northern tectonic zones of the Himalaya were deposited as the sediments of the Siwalik Group and the Indus-Ganga basin. Dating of the Siwalik Group strata indicates that deposition of sediments started as early as 18 million years ago and has continued to the present. A considerable part of the eroded sediments from the mountains were taken to the sea and deposited to form the Bengal fan and Indus fan. Ocean bed drilling in these fans has yielded rocks at their base with a provenance from Himalayan rocks that are as much as 16 million yearsold.

It The deformation front in the Himalaya appears to have migrated southward. The thrusts grow progressively younger from north to south; the MCT was initiated 22 million years ago, the MBT 10 million years ago, and the MFT around 0.5 million years ago.

For the last 60 million years, the Indian continent has been penetrating deeper and deeper into the rest of Asia (Molnar 1986). In the process it has uplifted the Himalaya and Tibetan plateau. This penetration (convergence) continues to the present, making the Himalaya tectonically and seismically active. This neotectonic activity, together with the climatic factors of rain and temperature variation, and compounded by human intervention, make the Himalaya vulnerable to mass movement and other forms of environmental degradation.

REFERENCES

Ahmad, T.; Thakur, V.C.; Islam, R.; Khanna, P.P.; Mukherjee, P.K. (1998) 'Geochemistry and Geodynamic Implication of Magmatic Rocks from the Trans Himalayan Magmatic Arc'. In *Geochemical Journal*, 32(6): 383-404

Allegre, C.J.; Courtillot, V.; Tapponnier, P.; Hirn, A.; Mattauer, M.; Coulon, C.; Jager, J.J.; Achache, J.; Scharer, U.; Marcoux, J.; Burg, J.P.; Girardeau, J.; Armijo, R.; Gariepy, G.; (1984) 'Structure and Evolution of the Himalaya-Tibet Orogenic Belt'. In *Nature*, 307:17-22

Asif Khan, M.; Qasim Jan, M.; Weaver, B.L. (1993) 'Evolution of the Lower Arc Crust in Kohistan, N. Pakistan: Temporal Arc Magmatism through Early, Mature and Intra-arc Rift Stages'. In Treloar, P.J. and Searle, M.P. (eds) *Himalayan Tectonics,* Geol. Soc. London, 74: 123-138 (Special Publication)

Bagati, T.N.; Rai, H.; Kumar, R.; Juyal, K.P. (1994) 'Expedition Report on the Geology of Eastern Karakoram, India'. In *Jour. Him. Geol.*, 5(1): 65-92

Barry, J.L.; Lindsay, C.N.; Jacobs, L.I. (1982) 'A Biostratigraphic Zonation of the Middle and Upper Siwaliks of the Potwar Plateau of Northern Pakistan'. In *Paleogeogr. Paleoclim. Paleoecol.*, 37: 95-150

Burbank, D.W.; Beek, R.A.; Mulder, T. (1997) 'The Himalayan Foreland Basin'. In Yin, A. and Harrison, M. (eds.) *The Tectonic Evolution of Asia*, pp 149-188. Cambridge: Cambridge University Press

Coward, M.P.; Windley, B.F.; Broughton, R.D.; Luff, I.W.; Petterson, M.G.; Pudsey, C.J.; Rex, D.C.; Khan, M. A. (1986) 'Collision Tectonics in the NW Himalayas'. In Coward, M.P. and Ries, A.C. (eds) *Collision Tectonics,* Geological Society Special Publication No. 19, pp 203-219. Oxford: Blackwell

Dewey, J.F.; Bird, J.M. (1970) 'Mountain Belts and Its New Global Tectonics'. In *Jour. Geophys. Res.*, 75: 2625-2647

Dewey, J.F.; Cande, S.; Pitman, W.C. (1989) 'Tectonic Evolution of the India/Eurasia Collision Zone'. In *Eclogae Geol. Helv.*, 82: 717-734

Gaetani, M.; Garzanti, E.; Jadoul, F.; Nicora, A.; Tintori, A.; Pasini, M.; Khan, K.S.A. (1990) 'The North Karakoram Side of the Central Asia Geopuzzle'. In *Geol. Soc. Amer. Bull.*, 102: 54-62

Gaetani, M.; Garzanti, E. (1991) 'Multicyclic History of the Northern India Continental Margin (NW Himalaya)'. In *Amer. Assoc. Petrol. Geologists Bull.*, 15(9): 1427-1446

Gansser, A. (1974) 'Himalaya'. In Spencer, A.M. (ed) *Mesozoic Cenozoic Orogenic Belts: Data for Orogenic Studies,* The Geological Society Special Publication No. 4, pp 267-278

Gardstein, F.M.; Gibling, M.R.; (1991) 'Mesozoic Tethyan Strata of Thakola, Nepal: Evidence for the Drift and Break up of Gondwana'. In *Paleogeography Paleoclimate, Paleoecology*, 81: 193-218

Hayden, H.H. (1904) 'The Geology of Spiti and Parts of Bushar and Rupshu'. In *Geol. Surv. India Mem.*, 34: 121

Hodges, K.V.; Parrish, R.; Searle, M.P. (1996) 'Tectonic Evolution of the Central Annapurna Range'. In *Nepalese Himalaya Tectonics*, 15: 1264-1291

Honegger, K.; Dietrich, V.; Frank, W.; Gansser, A.; Thoni, M.; Trommsdorff, V. (1982) 'Magmatism and Metamorphism in the Ladakh Himalayas (the Indus-Tsangpo Suture Zone)'. In *Earth Planet. Sci. Lett.*, 60: 253-292

Hubbard, M.; Harrison, T.M. (1989) '40Ar/39Ar Age Constraints on Deformation and Metamorphism in the Main Central Thrust Zone and Tibetan Slab, Eastern Nepal Himalaya'. In *Tectonics*, 8: 865-880

Jan, Q.M. (1990) 'High-P Metamorphic Rocks from Himalaya and Their Tectonic Implication - A Review. In *Physics and Chemistry of the Earth*, 18: 329-343

Johnson, G.D.; Opdyke, Tandon, S.K.; Nanda, A.C. (1983) 'The Magnetic Polarity Stratigraphy of the Siwalik Group at Haritalyangar (India) and a New Appearance Datum for Ramapithecus and Sivapithecus in Asia'. In *Paleogeogr. Paleoclimat. and Paleoecol.*, 44: 223-249

Khattri, K.N. (1987) 'Great Earthquakes, Seismicity Gaps and Potential for Earthquake Disaster along the Himalaya Plate Boundary'. In *Tectonophysics*, 138: 79-92

LeFort, P. (1981) 'Manaslu Leucogranite : A Collision Signature of the Himalaya. A Model for Its Genesis and Emplacement'. In *Journal of Geophysical Research,* 86: 10545-10568

Lyon-Chen, H.; Molnar, P. (1983) 'Constraints on the Structure of the Himalaya from an Analysis of Gravity Anamolies and a Flexural Model of the Lithosphere'. In *Jour. Geophysical Research*, 88: 8171-8191

Meigs, A.J.; Burbank, D.W; Beck, R.A. (1995) 'Middle-Late Miocene (>10 Ma) formation of the Main Boundary Thrust in the Western Himalaya'. In *Geology*, 23: 423-426

Molnar, P. (1986) 'The Geologic History and Stracture of the Himalaya'. In *American Scientist*, 74: 144-154

Molnar, P. (1984) 'Structure and Tectonics of the Himalaya : Constraints and Implications of Geophysical Data'. In *Annu. Rev. Earth Planet. Sci.*, 12: 489-518

Nakata, T. (1989) 'Active Faults of the Himalaya of India and Nepal'. In Maliconico, I.I., Lillie, R.J. (eds) *Tectonics of the Western Himalayas, Geol. Soc. America*, 232: 243-264

Nicolas, A.; Girardeau, J.; Marcoux, J.; Dupre, B.; Wang, X.B.; Zhang, H.X.; Zhao, Y.G.; Xiao, X.C. (1981) 'The Nature of Xigaze Ophiolite: A Peculiar Oceanic Lithosphere'. In *Nature*, 294: 414-417

Pecher, A. (1989) 'The Metamorphism in Central Himalaya'. In *Jour. of Metamorphic Geology*, 7: 31-41

Powell, C.McA.; Conagan, P.J. (1973) 'Plate Tectonics and the Himalayas'. In *Earth Planet. Sci.Lett.*, 20: 1-12

Raiverman, V.; Kunte, S.V.; Mukherjee, A. (1983) 'Basin Geometry, Cenozoic Sedimentation and Hydrocarbon in Northwestern Himalaya and Indo-Gangetic Plains. In *Petroleum Asia Journal,* 67-92

Robertson, A.; Degnan, P. (1994) 'The Dras Complex: Lithofacies and Reconstruction of a Late Cretaceous Oceanic Volcanic Arc in the Indus Suture Zone'. In *Sedimentary Geology*, 92: 117-145

Scharer, U.; Hamet, J.; Allegre, C.J. (1984a) 'The Transhimalaya (Gangdese) Plutonism in the Ladakh Region: A U-Pb and Rb-Sr Study'. In *Earth Planet. Sci. Lett.*, 67: 327-339

Scharer, U.; Xu, R.H.; Allegre, C.J. (1984b) 'U-Pb Geochronology of Gangdese (Transhimalaya) Plutonisum in the Lhasa-Xigase Region, Tibet'. In *Earth Planet'. Sci. Lett.*, 69: 311-320

Searle, M.P.; Windley, B.P.; Coward, M.P.; Cooper, D.J.W.; Rex, A.J.; Red, D.; Li Tinh-Dong; Xiao Xu-Chang; Jan, M.Q.; Thakur, V.C.; Surendar K. (1987) 'The Closing of Tethys and the Tectonics of Himalaya'. In *Geol. Soc. Amer. Bull.*, 98(6): 678-701

Searle, M.P.; Cooper, D.J.W.; Rex, A.J. (1988) 'Collision Tectonics of the Ladakh-Zanskar Himalaya'. In *Philosophical Transactions of the Royal Society, London*, 326A: 117-150

Searle, M.P. (1991) *Geology and Tectonics of the Karakoram Mountains*. Chichester (England): John Wiley and Sons

Sinha, A.K. (1989) *Geology of Higher Central Himalaya*. Chichester: John Wiley & Sons

Smith, A.G.; Hurley, A.M.; Briden, J.C. (1981) *Phanerozoic Paleocontinental World Maps*. Combridge: Cambridge University Press

Thakur, V.C. (1981) 'Regional Framework and Geodynamic Evolution of the Indus-Tsangpo Suture Zone in the Ladakh Himalayas'. In *Transactions of the Royal Society of Edinburgh: Earth Sciences*, 72: 89-97

Thakur, V.C.; Misra, D.K. (1984) 'Tectonic Framework of the Indus and Shyok Suture Zones in Eastern Ladakh, Northwest Himalaya'. In *Tectonophysics*, 101: 207-220

Thakur, V.C. (1992) *Geology of Western Himalaya*. Oxford: Pergamon Press

Valdiya, K.S. (1980) *Geology of the Kumaun Lesser Himalaya*. Dehradun (India): Wadia Institute of Himalayan Geology

Valdiya, K.S. (1988) 'Tectonics and Evolution of the Central Sector of the Himalaya'. In *Philosphical Transection,* A326, 151-175. London: Royal Society

Yeats, R.S.; Lillie, R.J. (1991) 'Contemporary Tectonics of the Himalayan Frontal Fault System: Folds, Blind Thrusts and the 1905 Kangra Earthquake'. In *Jour. Structural Geology*, 13: 215-225

Yin, J.; Xu, J.; Liu, C.; Li, H. (1988) 'The Tibetan Plateau: Regional Stratigraphic Context and Previous Work'. In Chang, C., Shackleton, R.M., Dewey, J.F. and Yin, J. (eds) *The Geological Evolution of Tibet. Royal Society of London Phiolosphical Transections*, 327: 379-413

2 A Note on Himalayan Seismicity

V.C. Thakur, N.S. Virdi, K.K. Purohit
Wadia Institute of Himalayan Geology
33, Gen. Mahadeo Singh Road, Dehra Dun-248001, India

The Himalaya has been the locus of some of the world's great earthquakes during the last 100 years. The region is a typical example of a collision type orogenic belt — a linear region that has undergone folding or other deformation during an orogenic (geotectonic) cycle. Himalayan seismicity is similar in nature to that of regions of oceanic subduction, being the result of the northward movement of the Indian plate. The absence of surface or primary ground rupture accompanying the region's great earthquakes indicates that its seismicity is related to a rupture along the Himalayan arc on a shallow north-dipping (3-5°) decollement that coincides with the top surface of the Indian shield and is encountered at a depth of 15-20 km beneath the Lesser and Higher Himalaya. This is also reflected by a belt of seismic activity in the 6-7 magnitude (M) range with a focal depth ranging from 15 to 20 km. This belt also follows the Main Central Thrust (MCT) and runs along the region of greatest uplift and a line of more than 3500m altitude. This is interpreted as the surface expression of a basement ramp where the dip of decollement changes from 5-6 degrees to 15 degrees. The region's four great (M 8+) recorded earthquakes – in 1897 (Assam), 1905 (Kangra), 1934 (Bihar-Nepal), and 1950 (Assam) – were confined to the frontal belt along the Main Boundary Thrust (MBT). These earthquakes ruptured 200-300 km of fault zone each; between these ruptures are seismic gaps, or seismically quiet zones, which are regarded as future potential sites of such great earthquakes. In addition, there have been over 650 other events of M 5-7 during the same period, which have typically occurred along transverse structures or other major thrusts or normal faults.

Introduction

Non-specialists will find introductory information on earthquakes in the appendix at the end of this paper; some definitions are provided in the glossary. The following is concerned specifically with seismicity in the Himalaya.

The Himalaya were formed by the collision of two continental plates, the Asian and the Indian. The region is a typical example of a collision type orogenic belt — a linear region that has undergone folding or other deformation during an orogenic (geotectonic) cycle. Accompanying the mountain range is a major global seismic belt where earthquakes of magnitude 4.5 to 5.5 occur every year; over 600 earthquakes of magnitude 5 (M 5) or above were recorded during the period 1950-1990. To date, four very major ('great') earthquakes of M 8 or greater have been recorded in the Himalaya or adjacent regions: the Great Assam earthquake of 1897, the 1905 Kangra earthquake, the 1934 quake near the Bihar-Nepal border, and the 1950 Assam earthquake (Figure 2.1). These earthquakes collectively killed well over 30,000 people. Other events of M 6-7, such as the Kinnaur earthquake of 1975 and the Uttarkashi earthquake of 1991, have also caused extensive damage to life and property.

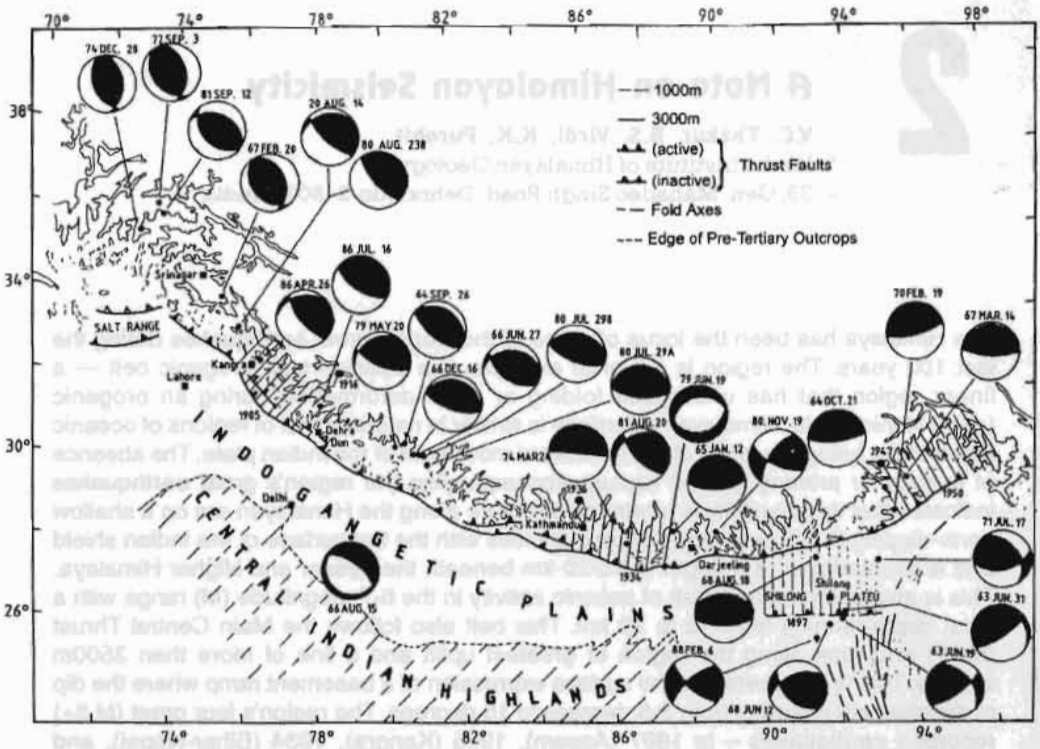

Figure 2.1: **Distribution of moderate and great earthquakes in the Himalaya and adjoining area, showing focal mechanisms ('beach ball' shapes) of moderate earthquakes (5.5≤M≤7) and rupture zones (hatched lines) of four great earthquakes: Assam, 1897; Kangra, 1905; Bihar,1934; Assam,1950** (modified after Molnar 1990). **The black area in each beach ball shape represents the fault plane of the earthquake in stereographic projection**

Most of the earthquakes that could be clearly located in the Himalaya were found to occur within a band roughly 60-100 km north or northeast of the southern margin of the range, and 10-50 km south or southwest of the crest of the Higher Himalaya (Molnar 1990). Thus along most of the chain, the earthquakes occur south of the surface trace of the Main Central Thrust.

Fault plane solutions of most moderate earthquakes in the Himalaya (M 5-7) indicate thrust faulting, with one nodal plane dipping gently northwards or northeastwards and the other dipping steeply southward or southeastwards (Figure 2.1) (Rastogi 1974; Baranowski et al. 1984; Ni and Barazangi 1984). Nearly all measured focal depths of earthquakes in the Himalaya lie between 12 and 18 km below the earth's surface. Most of the moderately sized earthquakes occur on the top surface of the Indian plate where it slides beneath the overriding crystalline nappes comprising the Lesser Himalaya (Baranowski et al. 1984; Ni and Barazangi 1984).

The Himalaya is the locus of the world's greatest intracontinental earthquakes. Three great earthquakes – Kangra (1905), Bihar-Nepal (1934), and Assam (1950) – occurred within a 50-year span, and the seismic moments of these great earthquakes appear to have been the largest among intracontinental earthquakes in the 20th century. The rupture zone of the 1905 Kangra earthquake is estimated at 120 km long and 100 km wide, and the average displacement was 5m (Molnar 1990).

The rupture zone of the 1934 Bihar-Nepal earthquake was 200 km by 100 km and its calculated average displacement was 6.2m, while the rupture zone of the 1950 Assam earthquake was estimated to be some 400 km long and 100 km wide with an average slip of 9m on thrust faults. (For a better understanding of seismicity, general aspects concerning earthquakes are described in the appendix to this paper.)

Seismological aspects

The seismic network being managed by various organisations has provided useful data on the intensity and magnitude of Himalayan earthquakes, but focal depth estimates still differ for many events. The record of past activity shows that various sections of the Himalaya have witnessed different intensities and frequencies of earthquakes. In the Lesser and Higher Himalaya, the density of tremors is relatively high and follows a linear pattern parallel to the Himalayan arc. Moreover, there are some pockets of more concentrated activity. The seismicity north of the Higher Himalaya is rather diffuse, without any discernible linear trends.

The western sector of the Himalayan arc – the region from Kangra through Tehri-Garhwal to Kumaon – shows a linear trend of seismic activity paralleling the Himalayan arc, with pockets of high concentration around Kangra and north of Tehri (Figure 2.2). The central sector, from the Garhwal-Kumaon Himalaya in the west through Nepal to Sikkim in the east, also shows trends paralleling the Himalayan arc and pockets of concentrated activity in the Garhwal-Kumaon and Nepal area. The activity in the region east of Kathmandu is also quite high. The activity is also very high in the eastern Himalayan sector, from Darjeeling through Itanagar (not shown in Figure 2.2) up to the site of the great earthquake of 1950 in the extreme northeast. The earthquakes in this sector follow the NE-SW trend of the arc.

The earthquake parameters determined from distant recordings made at globally distributed seismological observatories (teleseismic phase data) are reasonably accurate with regard to epicentre locations, but the depth of foci are not well determined. Some broad patterns of depth-wise distribution of earthquakes have nevertheless emerged. The main Himalayan arc region comprising the three sectors (western, central, and eastern) is marked by an occurrence of shallow earthquakes (focal depths of less than 50 km). In contrast, the India-Myanmar border region is the site of a very high density of shallow to intermediate depth earthquakes.

The spatial disposition of earthquake epicentres can help to delineate the lateral extension of faults. A study of earthquake foci in depth sections can reveal the subsurface nature of these faults. The linear patterns seen on an epicentral map of the Himalayan region broadly reflect the trends of active tectonic features. These trends parallel the trends of the Main Boundary Thrust (MBT) and the Main Central Thrust (MCT). Some transverse trends are also discernible. The data on depth distribution, however, do not reflect well-defined trends.

Major seismo-tectonic features

The evolution of the Himalaya is attributed to the continent-continent collision of the Indian plate with the Eurasian plate. The major tectonic features in the region are the outcome of this phenomenon. Four major tectonic features running almost the entire length of Himalaya are recognised and widely described in the literature. From north to south, these features are the Indus-Tsangpo Suture Zone (ITS), the Main Central Thrust (MCT), the Main Boundary Thrust (MBT), and the Main Frontal Thrust (MFT). Along a north-south section, these features divide

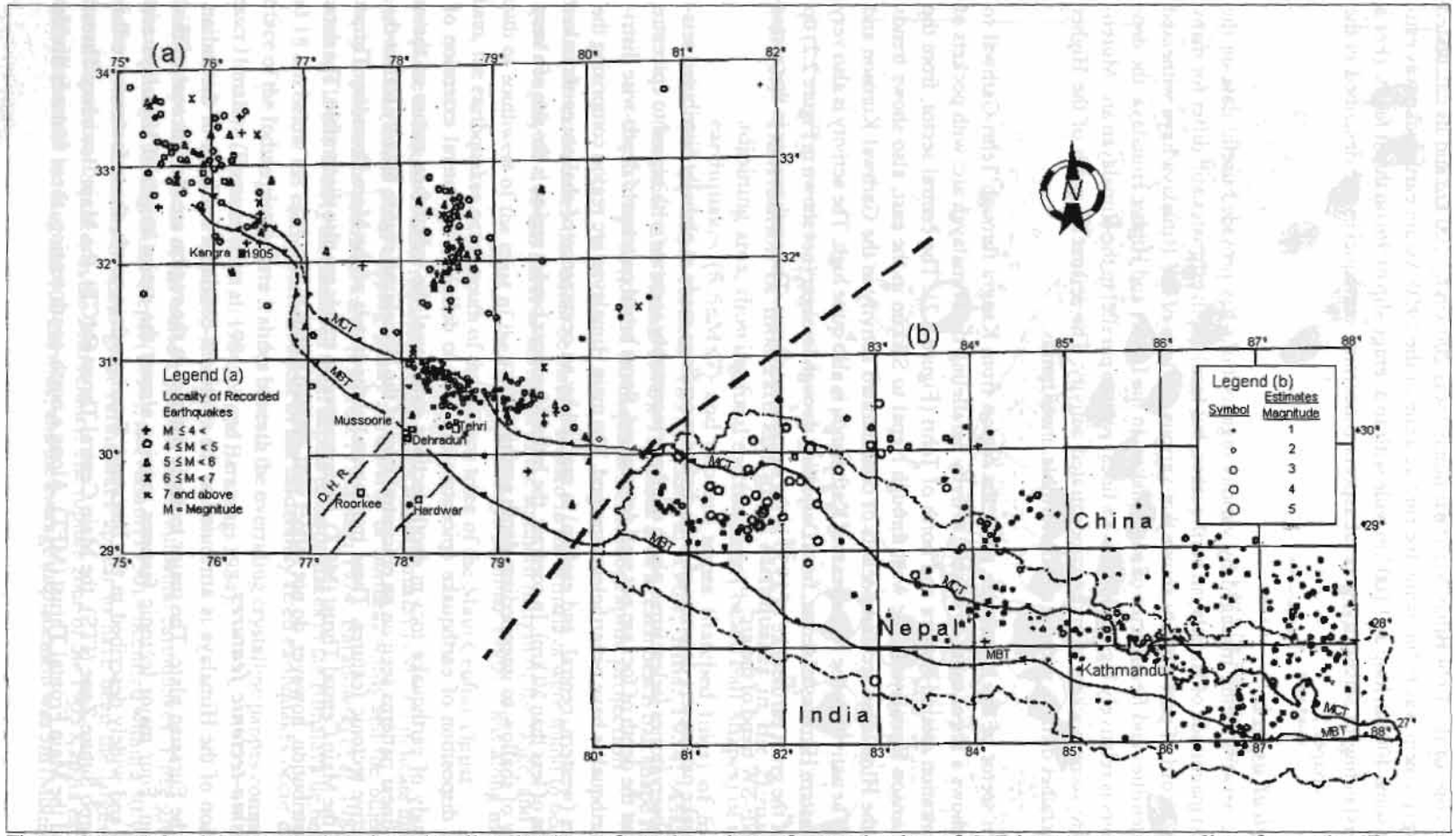

Figure 2.2: Seismicity map showing the distribution of earthquakes of magnitudes of 2-7 in an area extending from the Kangra-Chamba region to eastern Nepal in two blocks: a) Kangra-Chamba region to the Kumaon Himalaya in India, and b) the Nepal Himalaya. (a) shows earthquakes with a magngitudes of 4-7 between 1979 and 1982; (b) shows earthquakes with magnitudes of 2-5 between 1982 and 1985

the Himalaya into three geologically and tectonically distinct sectors. In addition to these, there are some localised tectonic elements either parallel to or transverse to the three major elements. Transverse features like the Delhi-Hardwar ridge or Monghyr-Sahgrsa ridge are regarded as a continuation of the tectonic fabric of the Indian Peninsular shield into the Himalayan arc (Sastri et al. 1971).

The ITS marks the northern boundary of the Indian plate following the closure of the Tethys ocean in the late Cretaceous-early Tertiary period (around 55-50 million years ago). The MCT, which separates the Higher Himalaya from the Lesser Himalaya, is regarded as the base slab of the Higher Himalayan Crystalline rocks and dips 30-40 degrees northwards; it appears to have developed in the mid-Miocene (20 million years ago). The MBT and the MFT were initiated around 10 and 0.2 million years ago, respectively. There has been a progressive shifting of planes of underthrusting from north to south: the MFT, which separates the foothills from the plains, is the youngest and presently tectonically active thrust.

Seeber et al. (1981) postulated that there was a detachment surface (fault) underlying the entire Himalaya and representing the upper surface of the underthrusting Indian plate (Figure 2.3). This fault was thought to be a decollement, an area with folding or faulting of sedimentary beds as a result of sliding over underlying rock. The fault was thought to dip north at a shallow angle below the Sub-Himalaya (Siwalik zone) at a depth of 2 to 7 km, and then continue into a steeper dipping Basement Thrust (BT) under the Higher Himalaya and Tethys Himalaya. The Himalayan rock formations appear in the form of thrust wedges overlying the detachment; as the Indian plate moves northward (at a rate of 1.5 to 5 cm per year depending on the location), the thrust wedges are pushed southward relative to the northward movement like a pack of cards.

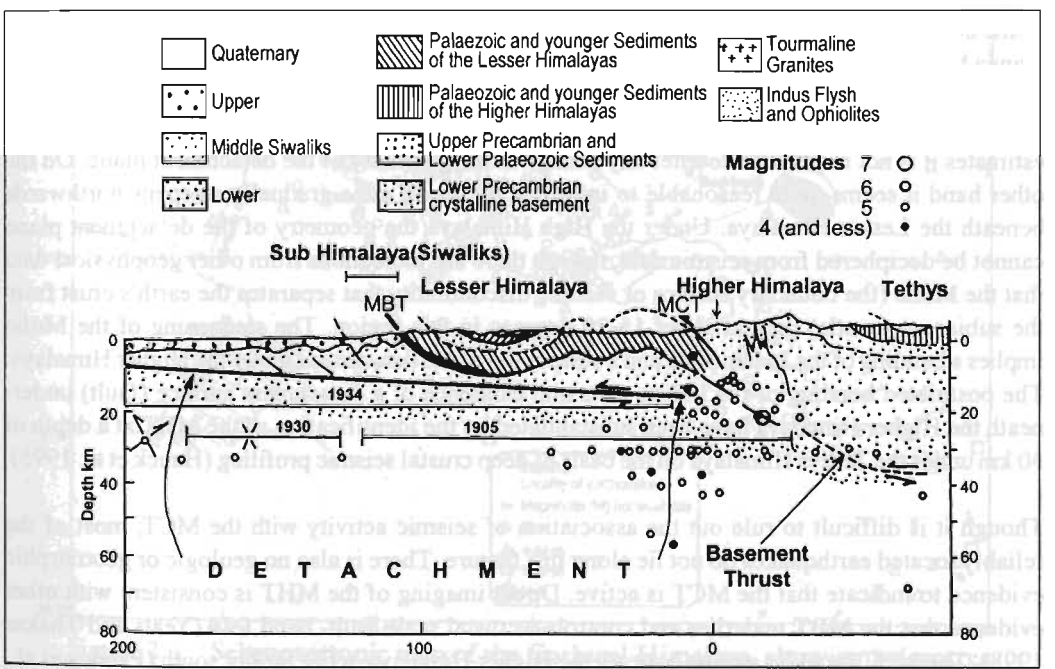

Figure 2.3: **Seismotectonic model of the Himalaya showing rupture zone of the great earthquake of 1905, 1930 and 1934, which were associated with slip along the detachment** (modified after Seeber et al. 1981)

The detachment fault was identified in the form of a deep crustal seismic profile beneath the Tethys Himalaya in southern Tibet (Hauck et al. 1995), designated the Main Himalayan Thrust (MHT) by Zhao et al. (1993). It has also been located in a seismic profile image in the Siwalik zone in the Dehradun region (Power et al. 1998), where it was found to dip at a shallow angle (5-10°C) at a depth ranging from 2 to 7 km, as postulated by Seeber et al. (1981). Seismic data indicate that in the Garhwal Himalaya the detachment fault lies at a depth of 15-20 km under the Lesser and Higher Himalaya (Khattri et al. 1988). The MCT, MBT, and MFT are splays of thrusts emerging from the detachment fault.

Most of the earthquakes in the Himalayan region are confined to shallow depths and are concentrated in a 50-100 km wide zone between the MBT and MCT. Most of the earthquakes with thrust-type focal mechanisms (i.e., resulting from compression when plates or areas of plates converge) lie within this belt. Focal mechanisms of the moderate-sized earthquakes suggest underthrusting of the Indian plate along the Himalayan arc. Some earthquakes located further south, in the Indo-Gangetic alluvial region and the Sub Himalaya, show normal fault plane solutions (arising from extension). The normal fault-type events can be considered to be of the same type as observed in oceanic trenches associated with island arcs and are perhaps due to flexing of the Indian plate as it bends and underthrusts beneath the Himalaya.

Seeber et al. (1981) interpreted the available seismological data to determine that most of the medium-sized thrust-type earthquakes occur either along the BT or along the down-dip projection of the MCT (Figure 2.3). Molnar and Chen (1983) proposed that the medium-sized thrust events occur along the part of the detachment beneath the northern Lesser Himalaya and perhaps along the down-dip projection of the MCT and nearby subsidiary faults. The great (magnitude 8 or higher) Himalayan earthquakes, however, are believed to occur along the master detachment surface between the Sub Himalaya and the Lesser Himalaya.

Some borehole data suggest that the upper surface of the Indian plate dips 2-3 degrees beneath the Ganga basin. Most of the focal mechanisms show fault plane dipping of the order of 5-30 degrees due NW or NE (with uncertainties of 5-15 degrees). While estimated dips in the western sector are generally higher than those in the eastern sector, owing to the higher uncertainties in the western estimates it is not reasonable to infer any change in the geometry of the detachment plane. On the other hand it seems quite reasonable to infer that the thrust zone gradually steepens northwards beneath the Lesser Himalaya. Under the High Himalaya the geometry of the detachment plane cannot be deciphered from seismic data, though there are indications from other geophysical data that the Moho (the boundary surface or seismic discontinuity that separates the earth's crust from the subjacent mantle) dips at about 15-20 degrees in this region. The steepening of the Moho implies a bending of the Indian plate and a steeper dip of the detachment under the Higher Himalaya. The postulated bending of the Indian plate and existence of a detachment surface (fault) underneath the Higher Himalaya have been substantiated by the identification of the MHT at a depth of 30 km under the Tethys Himalaya on the basis of deep crustal seismic profiling (Hauck et al. 1995).

Though it is difficult to rule out the association of seismic activity with the MCT, most of the reliably located earthquakes do not lie along this feature. There is also no geologic or geomorphic evidence to indicate that the MCT is active. Direct imaging of the MHT is consistent with other evidence that the MBT underlies and controls a crustal scale fault- band fold (Yeats and Thakur 1998). The MHT includes a ramp beneath the Higher Himalaya, a flat farther south (Pandey et al., 1995), and another ramp at the Himalayan front (Power et al. 1998). The down-dipping ramp under the Higher Himalaya is characterised by a zone of earthquakes of moderate magnitude. On rare

occasions, earthquakes on the down-dipping ramp have trigerred rupture across the flat to the front of the range. This has led to at least three great earthquakes on the flat in this century.

Steeply dipping faults transverse to the Himalayan arc are widely distributed in the Sub Himalaya (Siwaliks) and Lesser Himalaya. These transverse faults represent lateral ramps and have a strike-slip component, i.e. with movement parallel to the fault strike. The fault plane solution of one reliably located earthquake in the Darjeeling region (19 November 1980) shows a predominantly strike-slip mechanism. The event was located within the overthrusting Lesser Himalaya block and is representative of transverse faulting in this block. The fault plane solutions in the Tethys Himalayan region show that active tectonics are dominated by north-south-trending normal faults.

Local seismicity in the Garhwal Himalaya

During the years 1984-88, the Department of Earth Sciences, University of Roorkee operated a short-aperture local network of seismological stations in the Garhwal Himalaya in the vicinity of Tehri-Garhwal and the Uttarkashi region (Khattri et al. 1988). This has provided additional data on earthquakes of magnitudes less than 4.5. The location of these events is considered to be correct to within a few kilometres. These stations' recordings, which were done in analogue form, have led to a greater understanding of the region's tectonic features. A seismotectonic map showing seismicity and tectonic features of the Garhwal and Kumaon region is shown in Figure 2.4.

No reliable focal mechanism based on teleseismic (distant) observations for the Garhwal Himalaya. The nearest available focal mechanism indicates thrust-type solutions. The dip of the composite

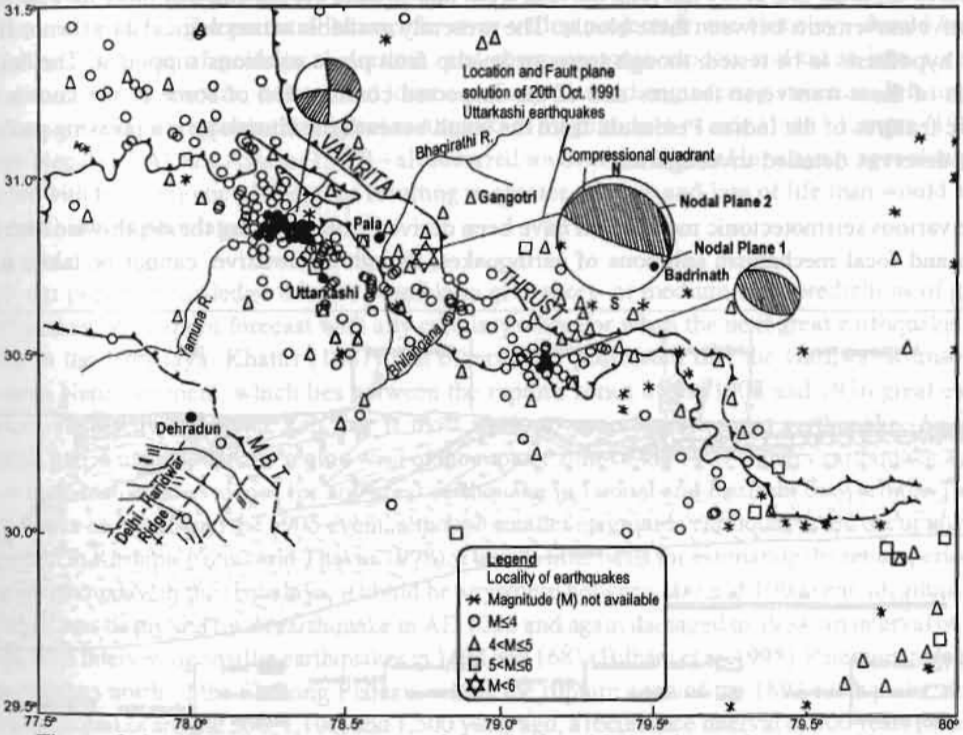

Figure 2.4: **Seismotectonic map of the Garhwal Himalaya, showing epicentres of earthquakes with magnitudes of 4-6** (modified after Thakur and Kumar 1994). **The shaded area in the beach ball shapes represents the fault plane of the earthquake in stereographic projection**

fault plane solutions referred to earlier are of the order of 60 degrees, which conforms with the geological observation that the thrust faults in the Himalaya have steeper dips at shallow depths

Local seismicity in the Nepal Himalaya

Geoscientists from His Majesty's Government of Nepal and a team of geophysicists from France have been monitoring microseismicity in Nepal for more than 10 years. Out of the 4,000 local events recorded between 1985 and 1992, 1,200 occurred within the Kathmandu network. Most of these microseismic events were shallow with local magnitudes of less than 4 (one notable exception was a tremor of magnitude 6.5 on 21 August 1988). Pandey et al. (1995) noted a clustering of microseismic events in an east-west belt along the front of the Higher Himalaya and following the trace of the Main Central Thrust (MCT). Most of the seismic events were clustered at a shallow depth of 5-20 km in the vicinity of the midcrustal ramp beneath the Higher Himalaya (Figure 2.5). Based on this model, Pandey and his co-workers proposed that the microseismicity recorded at the front of the Higher Himalaya over the last decade has resulted from stress accumulation over the midcrustal ramp.

Some significant problems of Himalayan seismicity

The present seismological data do not enable an understanding of the seismic nature of features transverse to the Himalayan arc, nor of strike-slip movements. The gaps in fault plane solution data are quite prominent over wide spans. In the framework of plate tectonics, the entire Himalayan arc is considered to be the result of the northeasterly-moving Indian plate and its underthrusting beneath the Tibetan plateau. However, it would appear most probable that there are transverse features dividing this 2,400 km long moving front into smaller blocks and that there may be some relative movements between these blocks. The presently available seismological data do not allow this hypothesis to be tested, though some strike-slip fault plane solutions support it. The delineation of these transverse features and of the suspected continuation of some of the known tectonic features of the Indian Peninsula from the south beneath the Himalaya is a pressing problem that deserves detailed investigation.

The various seismotectonic models that have been derived from studying the depth-wise distribution and focal mechanism solutions of earthquakes, though informative, cannot be taken to be

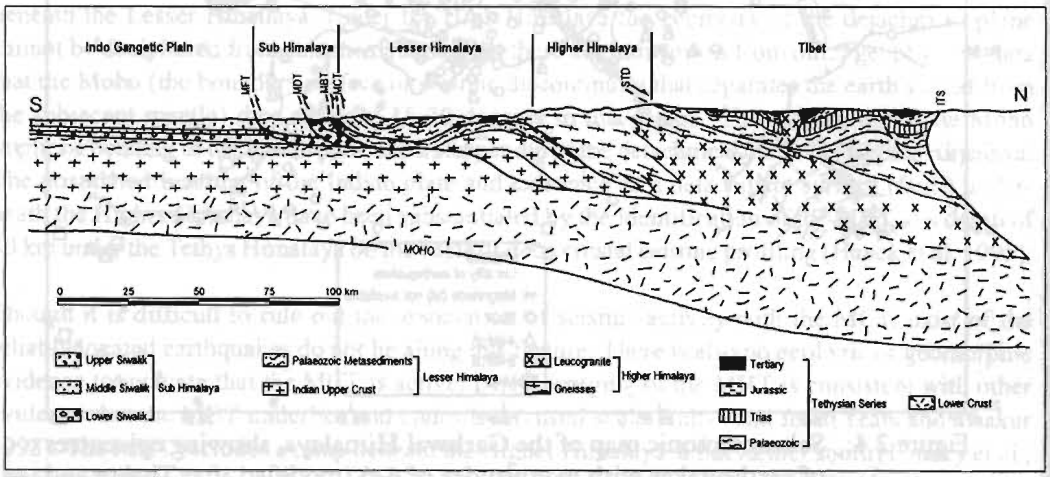

Figure 2.5: **Seismotectonic model of the Central Nepal Himalaya, showing detachment and ramp structures** (modified after Pandey et al. 1995)

conclusive, as they are based on preliminary and inadequate data. Because of a paucity of data, depth sections are often prepared by projecting events lying in a rather wide zone of a few hundred kilometres onto a single vertical plane, without regard to changes in tectonic and seismic trends. Such sections have resulted in potentially questionable features.

Since the Himalayan belt is very large in its lateral extent, any attempt to acquire data of the type mentioned above would have to be carried out at a few key locations where tectonic elements are well mapped on the surface. These locations then should be covered with a network of seismological observatories that enable the acquisition of earthquake data in digital form. The network might be operated in one location for about a year and then shifted to another key area. One could plan to have five such networks operating simultaneously, each covering an area of 100 km radius. To start with, these five locations could be the Kangra area, Tehri-Garhwal, the Kumaon Himalaya, the Nepal-Bihar border (site of major earthquakes in1934 and 1988), and the area centred at 27°N and 93°E in the eastern Himalaya.

In addition to seismological experiments, it would also be very useful to launch simultaneously other geophysical experiments, such as detailed gravity and magnetic and geodetic investigation, in these selected key areas. Such an approach would also permit tomographic modelling of subsurface features and boundaries, which in turn would help in delineating the continuity of tectonic features at depth.

Seismic hazards

Earthquakes pose great hazards to all major developmental activities, including dams, canals, roads, and bridges. The potential hazard for river-valley projects in the Himalaya should be assessed on the basis of geological, seismic, and seismotectonic aspects and taken into account when determining the size, design, and location of any planned engineering structure. It is important to note that the region's three great earthquakes (magnitude>8) since 1900 – Kangra (1905), Bihar-Nepal (1934), and Assam (1950) – all occurred south of the Higher Himalaya ranges along the border with the Gangetic plains, thus resulting in greater damage and loss of life than would have occurred in less populated regions.

With our present knowledge it is not possible to give short- or medium-term predictions of great earthquakes. We cannot forecast with any certainty where or when the next great earthquake will strike in the Himalaya. Khattri (1987) and others have postulated that the Garhwal-Kumaon—Western Nepal segment, which lies between the rupture zones of the 1905 and 1936 great earthquakes, represents a seismic gap that is most likely to experience a great earthquake. Another seismic gap is indicated in the region west of the rupture zone of the 1905 Kangra earthquake, since there is no historical evidence for any great earthquake in Jammu and Kashmir between the Taxila earthquake of AD 25 and the 1905 event, although smaller magnitude earthquakes did occur in 1828 and 1885 in Kashmir (Yeats and Thakur 1998). There is little basis for estimating the return period of great earthquakes in the Himalaya, it could be anywhere between 100 and 1000 years. Kathmandu in Nepal was destroyed by an earthquake in AD 1255 and again damaged in 1934, an interval of 679 years, with intervening smaller earthquakes in 1408 and 1681 (Bilham et al. 1995). Paleoseismological observations north of the Shillong Plateau, within the rupture zone of the 1897 earthquake, document earthquakes around 500, 1,100, and 1,500 years ago, a recurrence interval of 500 years (Sukhija et al. 1996). But much more needs to be done

References

Baranowski, J.; Armbruster,J.; Seeber,L.; Molnar, P. (1984) 'Focal Depths and Fault Plane Solutions of Earthquakes and Tectonics of the Himalaya'. In *Jour. Geophy. Res.*, 89: 6918-6928

Bilham, R.; Bodin, P.; Jackson, M. (1995) 'Entertaining a Great Earthquake in Western Nepal : Historical Inactivity and Geodetic Tests for Development of Strain'. In *Journal Nepal Geological Society*, 11: 73-88

Hauck, M.L.; Nelson, K.D.; Wu, C.; Cogan, M.J.; Brown, L.D.; Kidd, W.S.F.; Edwards, M.E.; Kuo, J.T.; Zhao, W. (1995) 'Ramping of the Main Himalayan Thrust and Development of the South Tibetan Detachment and Kangmar Basement Dome: In Depth Reflection Profiles in Southern Tibet'. In *Geol. Soc. Am. Abstract Programms*, 27, A-336

Khattri, K.N. (1987) 'Great Earthquakes, Seismicity Gaps and Potential for Earthquake Disaster along the Himalayan Plate Boundary'. In *Tectonophysics*, 138: 79-82

Khattri, K.N.; Gaur, V.K.; Chander, R.; Moharir, P.S.; Singh, V.N.; Sarkar, I.; Mukhopadhyay, S.; Kumar, Sriram,V.; Khannal,K.N.; Chauhan,P.K.S. (1988) *Seismological Studies in Garhwal Himalaya and North Eastern Region, India,* pp. 132, Technical Report submitted to DST, New Delhi

Molnar, P.; Chen, W.P. (1983) 'Focal Depth and Fault Plane Solutions of Earthquakes under the Tibetan Plateau'. In *Jour. Geophy. Res.*, 88: 1180-1196

Molnar, P. (1990) 'A Review of the Rates of Active Underthrusting and Deformation at the Himalaya'. In *Jour. Him. Geol.,* 1:131-154

Ni, J.; Barazangi, M. (1984) 'Seismotectonics of the Himalayan Collision Zone: Geometry of Underthrusting Indian Plate beneath the Himalaya'. In *Jour. Geophy. Res.*, 89: 1147-1163

Pandey, M.R.; Tandukar, R.P.; Avouac, J.P.; Lave, J.; Massot, J.P. (1995) 'Interseismic Strain Accumulation on the Himalayan Crustal Ramp (Nepal)'. In *Geophysical Research Letters*, 22: 751-754

Power, P.M.; Lillie, R.J.; Yeats, R.S. (1998) 'Structure and Shortening of the Kangra and Dehradun, SubHimalaya, India'. In *Geol. Soc. Amer. Bull.* 110: 1010-1027

Rastogi, B.K. (1974) 'Earthquake Mechanism and Plate Tectonics in the Himalayan Region'. In *Tectonophysics*, 21:47-56

Sastri, V.V.; Bhandari, L.L.; Raju, A.T.R.; Datta, A.K. (1971) 'Tectonic Framework and Sub-surface Tratigraphy of the Ganga Basin'. In *Jour. Geol. Soc. India*, 12:22-23

Seeber, L.; Armbruster, J.G.; Ouittmeyer, R.C. (1981) 'Seismicity and Continental Sub-duction in the Himalayan Arc'. In Gupta, H.K. and Elany, F.M.(eds) *Zagros-Hindu Kush-Himalaya Geodynamic Evolution,* American Geophysical Union Geodynamics Series no. 3, pp215-242. USA: American Geophysical Union

Sukhija, E.S.; Rao, M.N.; Reddy, D.V.; Nagabhushanam, Hussain, S; Chadha, R.K. Gupta, H.K. (1996) 'Evidence of Prehistoric Major Seismic Events in Shillong Plateau, Northeast India'. In *Geophysical Research Letters*

Thakur, V.C.; Kumar, Sushil. (1994) 'Seismotectonics of the 20th October 1981 Uttarkashi Earthquake, North India'. In *Terra Nova*, 6:90-94

Yeats, R.S.; Thakur, V.C. (1988) 'Reassessment of Earthquake Hazard Based on a Fault Bend Fold Model of the Himalayan Plate-boundary Fault'. In *Current Science*, 74(3): 230-233

Zhao, W; Nelson, K.D.; Che, J.; Lu, D. Wu,C.; Liu, X, Brown, L.D.; Hauck, M.L.; Kuo, J.T.; Klemper, S. and Makovsky, Y. (1993) 'Deep Seismic Reflection Evidence for Continental under Thrusting beneath Southern Tibet'. In *Nature*, 366(6455): 557-559

Appendix

Earthquakes - some general aspects

An earthquake is the oscillatory, sometimes violent movement of the earth's surface that follows a release of energy in the earth's crust. The energy can be generated by a sudden displacement and dislocation of segments of the crust, volcanic eruptions, or even manmade explosions. Most of the destructive earthquakes in the world are caused by dislocations in the earth's crust.

Seismology (from the Greek word 'seismos', meaning earthquake) is the science and study of earthquakes and seismic waves. **Seismographs** are instruments for detecting and recording earthquakes, while seismograms are records produced by these instruments. The seismicity of a region is the degree of susceptibility of a region to earthquake activity

The outer shell of the earth (the **crust**) consists of a several pieces called **plates**, which move relative to each other and to the interior of the earth (the **mantle**). These plates bump into, pull away from, or move past each other, creating strains. The plate movement also leads to the development of so-called **faults**, cracks in the earth that develop because sections of a plate, or two plates, are moving in different directions. Faults are more common, but not confined to, areas near the edges of plates.

The common types of faults are

- **normal fault**: a dipping fault plane with the top dropping down. This arises from extension when two plates diverge
- **thrust fault** (or **reverse fault**): dipping fault plane with the top riding over the bottom. This arises from compression, when two plates converge
- **strike slip** (or **transform fault**): no vertical motion, one side sliding horizontally relative to the other.

The plate movement (tectonic forces) causes blocks of rock on both sides of a fault or plate boundary to move past each other, but the movement isn't smooth. The rocks 'catch' on each other — they are still pushing against each other but not moving. After a while the rocks break because of the pressure that has built up – and an earthquake occurs.

Earthquake locations, when worked out with enough precision, are almost always along active faults. At the global scale, they define the plate boundaries. At the regional scale, the distribution of earthquakes defines the multiple faults that frequently characterise a plate boundary. In other words, plate boundaries and faults are major seismic zones. In general, major mountain belts, mid-oceanic ridges, faults, and trenches are zones of high seismicity; major shield regions are less seismic. However, no part of the earth's surface can be regarded as aseismic (free from earthquakes).

Origin and description

The most widely accepted theory of the origin of earthquakes postulates a process known as elastic rebound (the elastic rebound theory). According to this theory, when subjected to deep-seated forces (whose origins and natures are largely unknown), the crust may first bend but then, when the stress exceeds the strength of the rocks, it breaks and 'snaps' back to a new position. In the process of breaking, vibrations, or waves of energy, called **seismic waves** are generated. These waves travel from the source of the earthquake (referred to as the **focus**, or hypocentre) and travel through the earth and along its surface at varying speeds depending

upon the media through which they travel. The point on the surface of the earth directly above the focus is called the **epicentre**. The location of an earthquake is commonly described by the geographic position of its epicentre and its focal depth. Seismologists refer to the direction of slip in an earthquake and the orientation of the fault on which it occurs as the **focal mechanism**. The focal mechanism can be calculated from measurements of the radiation pattern (direction of seismic waves) from an earthquake made at a number of distant seismic stations (**teleseismic phase data**; the results of the calculation may be called the '**fault plane solution**'). This pattern may be represented by a '**beach ball**' diagram, the '**focal sphere**', which shows both the orientation of the fault and the sense of motion on it. The area of the fault along which a slip occurs is called the **dislocation**. A dislocation can measure from a few to more than 100 km, whereas the actual slip is more likely to be in the range of a few centimetres to a few metres. The overall geological area affected by the earthquake, where the stresses produced exceeded the ultimate strength of the rocks, as shown by crushing and fracturing, is called the **rupture zone**.

Earthquakes with a focal depth of less than 60 km are termed shallow. Those with depths of 60-300 km are referred to as intermediate, while those with focal depths greater than 300 km are termed deep. The foci of deep earthquakes may reach depths of 700 km. Most earthquakes occur in the brittle rock of the lithosphere, (the uppermost 80-100 km of the crust and upper mantle), and shallow earthquakes are responsible for most seismic-related destruction on the earth's surface.

Elastic Rebound theory explains shallow earthquakes. But for intermediate and deep focal earthquakes, the earth is too 'fluid like' for elastic rebound theory to work. The best explanation for deep earthquakes is a sudden change in phase from one crystal form to another.

Most of the earthquakes with thrust-type focal mechanisms (i.e., resulting from compression when plates converge) are shallow. Focal mechanisms of moderate-sized earthquakes in the Himalayan region suggest underthrusting of the Indian plate along the Himalayan arc. Some earthquakes located further south, in the Indo-Gangetic alluvial region and the Sub Himalaya, show normal fault plane solutions, in other words they are the result of parts of the plate moving away from each other, not of pushing together.

Magnitude and destructiveness

The **magnitude** of an earthquake is usually expressed in terms of the **Richter Scale**. This is a measure of the amplitude of seismic waves and is related to the amount of energy released, an amount that can be estimated from seismographic recordings. The Richter scale, named after Charles Richter of the California Institute of Technology, is logarithmic: thus a recording of 7 indicates disturbance with ground motion 10 times larger than a recording of 6. An earthquake of magnitude 2 is the smallest that can be felt by humans. Earthquakes with Richter values of 6 or more are commonly considered major earthquakes.

The **Modified Mercalli Scale** (MM scale) is a subjective measure that describes the intensity of a shock felt at a particular place. It is based on the extent of damage to property and loss of life by an earthquake, and ultimately gives the measure of an earthquake's effects in a given locality in values ranging from I to XII. The evaluation of intensity is made from intensive ground surveys, eyewitness records, and the like.

The destructiveness of an earthquake depends on many factors. In addition to magnitude, these include focal depth distance from the epicentre, local geological conditions, and the design of

buildings and other man-made structures, population density, and construction patterns in the affected area.

Earthquakes of large magnitude do not necessarily cause the most intense surface effects. The effects in a given region depend on local surface and sub-surface geological conditions. An area underlain by unstable ground (sand, clay, or other unconsolidated material) is likely to experience more noticeable effects than an area equally distant from an earthquake's epicentre but underlain by firm ground such as granite.

Prediction

The prediction of earthquakes is a subject that has occupied the minds of men since ancient times. Modern methods require large inputs of instrumentation and observations over long stretches of time. These include the following.

- Study and analysis of past activity, or palaeoseismology, which can help in estimating the repeat times of major earthquakes. However, such estimates can only be approximate.
- Frequent measurement of ground-elevation changes (geodetic measurements) in areas of known seismicity can be used to forecast seismicity.
- Emission of radon gas along weak zones, and water-level changes in wells and springs, can also be used as precursors.

However, the most reliable indicators of future seismicity are the results of a close network of sensitive seismographs that continuously record tremors. These measurements provide the basis for identifying seismically active areas and evaluating the depth, intensity, and magnitude of earthquakes. Seismologists can further analyse these data to estimate the extent of the rupture zone and determine the type or nature of movement (**focal mechanisms** or **fault plane solutions**).

Despite the creation of a global network of seismic stations, to date only a few earthquakes have been successfully predicted. Long-term predictions, made by analysing historic seismic gaps – extended periods of seismic quiescence – to estimate the repeat times of large earthquakes, can provide general guidance on probabilities and risks. However, short-term predictions (within a few hours or days of an event) have proved to be more challenging as a result of difficulties in establishing the magnitude and timing of fore-shocks or precursor events.

3 The Physiography and Geology of Nepal and Their Bearing on the Landslide Problem

B.N. Upreti
Department of Geology, Tri-Chandra Campus, Tribhuvan University, Ghantaghar, Kathmandu, Nepal

Nepal can be divided into eight distinct physiographic units: the Terai, the Siwalik (Churia) Range, the Dun Valleys, the Mahabharat Range, the Midlands, the Fore Himalaya, the Higher Himalaya, and the Inner and Trans Himalayan Valleys. Each of these units has distinct altitude, topographical, climatic, and vegetational characteristics.

Geologically, Nepal can be divided into five major tectonic zones: the Terai, the Siwaliks, the Lesser Himalaya, the Higher Himalaya, and the Tibetan-Tethys Himalaya. These zones are separated by major thrusts and faults; two of these, the Main Central Thrust (MCT) and the Main Boundary Thrust (MBT), bring fundamentally different tectonic zones against each other. Each of the tectonic zones is characterised by its rock types, age, metamorphism, structures, and geological history.

The Himalaya is said to be the most active and fragile mountain range in the world: it is a 'live mountain' with active tectonics. The Himalaya is still rising and its rocks are under constant stress as the northward-moving Indian Plate pushes against the more stable Tibetan block. This pressure forces the Himalaya to rise and move horizontally southward along major thrusts. The active nature of the range is also manifested in frequent earthquakes. Moreover, the inherently weak geological characteristics of the rocks make the Himalaya fundamentally very fragile. Triggering factors such as rainfall and earthquakes make the mountains highly vulnerable to landslides and other mass-wasting processes. The combination of weak geology and a monsoonal climate makes each physiographic zone of Nepal unique in its vulnerability to landslides; at present the most active parts of the Himalaya are the Siwalik and the Mahabharat ranges.

A better understanding of the geological nature of the terrain and the interplay of various triggering factors will greatly help in the development of safer infrastructures, mitigation of natural hazards, and control of environmental degradation in the Himalaya.

Introduction

Physiography

Nepal can be divided into eight well-defined physiographic units running roughly east-west (Table 3.1, Figure 3.1). This classification has been adopted from Hagen (1969), with some modifications. It encompasses the important and characteristic physiographic features of Nepal better than does the currently used fivefold classification (Terai, Siwalik (or Churia), Middle Mountain, High Mountain, and High Himalaya).

Terai

The Terai is the northern continuation of the Indo-Gangetic Plain, ranging in elevation from 100 to 200 masl and having a subtropical climate. It extends from the Nepal-India border in the south to the base of the Siwalik Hills in the north. Varying in width between 10 and 50 km, the Terai forms a nearly continuous belt from east to west, exceptions being along the Chitwan and Rapti valleys where the

Table 3.1: **Physiographic units of Nepal**

Physiographic unit	Width (km)	Altitude range (masl)	Main rock types	Age
1. Terai (northern edge of the Indo-Gangetic Plain)	10-50	100-200	Alluvium: coarse gravels in the north near the foot of the mountains, gradually becoming finer southward; foreland basin deposits	Recent
2. Siwalik (Churia) Range	10-50	200-1300	Mollase deposits of the Himalaya: sandstone, mudstone, shale, and conglomerate	Mid-Miocene to Pleistocene
3. Dun Valleys	5-30	200-300	Valleys within the Siwalik Hills filled up by coarse to fine alluvial sediments	Recent
4. Mahabharat Range	10-35	1000-3000	Schist, phyllite, gneiss, quartzite, granite, and limestone belonging geologically to the Lesser Himalayan Zone	Precambrian and Paleozoic, occasionally also Cenozoic
5. Midlands	40-60	200-2000	Schist, phyllite, gneiss, quartzite, granite, and limestone belonging geologically to the Lesser Himalayan Zone	Precambrian and Paleozoic to Mesozoic
6. Fore Himalaya	20-150	2000-5000	Gneisses, schists, phyllites, and marbles mostly belonging to the northern edge of the Lesser Himalayan Zone	Precambrian
7. Higher Himalaya	10-60	>5000	Gneisses, schists, migmatites, and marbles belonging to the Higher Himalayan Zone	Precambrian
8. Inner and Trans Himalayan Valleys		2500-4300	Gneisses, schists, and marbles of the Higher Himalayan Zone and Tethyan sediments (limestones, shale, sandstone, etc.) belonging to the Tibetan-Tethys Zone	Precambrian and Cambrian to Cretaceous

Nepal-India border coincides with the foot of the Siwalik Range for about 70 km and 80 km respectively. The Terai can be further subdivided into northern (Bhabar), middle, and southern zones.

Siwalik Range (Churia)

The frontal, or southernmost, hill ranges of the Himalaya are generally called the Siwaliks. In Nepal this range is often referred to as the Churia, and in other parts of the Himalaya they are sometimes known as the Outer Himalayan Zone, or Sub-Himalayan Zone. Generally they rise abruptly from the plains of the Terai (Figure 3.2). Running the length of Nepal, the Siwalik hills typically range in elevation from 200 to 1,000m, and rise to 1,300m in many places. They have an arc type face with conspicuously north-dipping beds, forming a steep escarpment towards the Terai. Geomorphologically, the Siwalik hills exhibit a very immature topography with highly rugged terrain dissected by numerous gullies (Figure 3.3). Though most parts of the range are covered by thick forest, it is very dry from December to early June. Due to the fragile character of the rocks, during the monsoon a great amount of sediment is washed from the Siwalik hills into the rivers originating within or to the north of the range. Most of the Siwalik rivers carry water only during the peak monsoon period. These hill ranges fall under the subtropical climatic zone.

Dun Valleys

Where the Siwalik hills bifurcate into two parallel ranges, wide valleys are formed, which are generally called the Dun valleys. The altitude of these valleys varies from 200 to 300m. They are

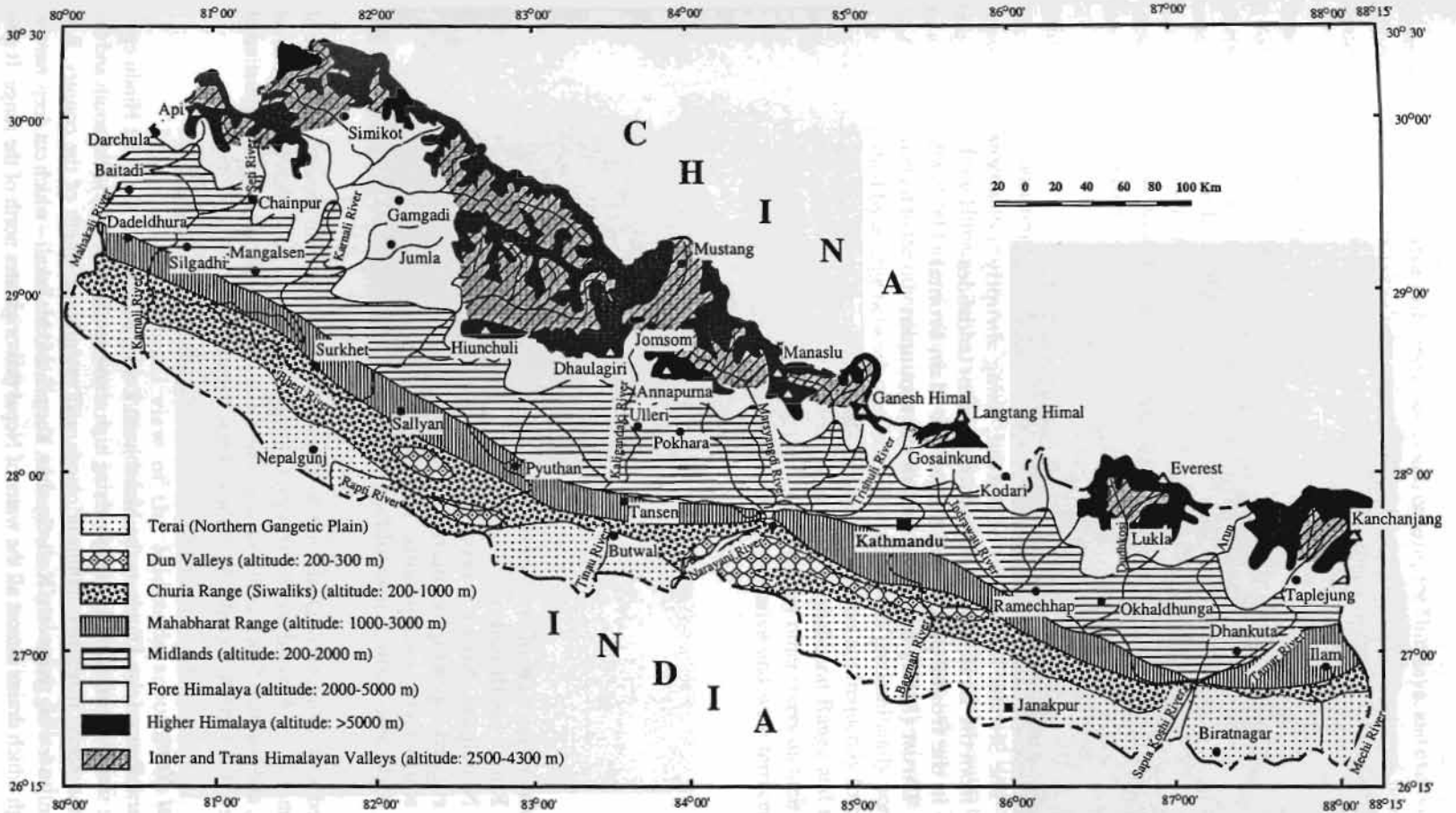

Figure 3.1: **Physiographic subdivisions of Nepal (reprinted from Journal of Asian Earth Sciences, Vol 17, Upreti et al., 'An overview of the stratigraphy and tectonics ....., p579 (1999), with permission from Elsevier Science)**

Figure 3.2: The Siwalik Range east of Butwal, rising abruptly from the Terai. Note the evidence of recent landslides in the frontal part of the range. The Main Frontal Thrust (MFT) lies at the foot of the mountain

Figure 3.3: An aerial view of the Siwalik Range north-east of Nepalgunj. Note the very rugged topography and the south-facing escarpments. The rocks also show gentle folding

normally filled with sediments of Quaternary to Recent (1.8 million years to present) age. Some of the larger Dun valleys of Nepal are the Trijuga, Chitwan (east Rapti), Nawalpur, Deokhuri (west Rapti), Dang, and Surkhet. Whereas the Siwalik hills remain sparsely populated, the population of the Dun valleys has increased markedly in the last few decades.

Mahabharat Range

The Mahabharat Range (also known as the Mahabharat Lekh), named after the great Hindu epic, dominates the southern part of the Himalaya, rising high above the Siwalik hills to the south and the Midlands to the north. It reaches 3000m in places, and extends the length of the country. It is breached by only a few big rivers – the Kosi, Gandaki, Karnali, and Mahakali – which cut deep, narrow gorges through which drains almost all the water of Nepal that originates north of the range. It also

forms the first effective barrier to the monsoon clouds entering the Himalaya, and exerts considerable influence on the country's rainfall distribution. The Mahabharat Range continues beyond Nepal's western border through the Indian hill ranges of Nainital, Mussouri, Simla, and beyond.

Topographically, the Mahabharat Range is markedly higher than the Siwalik hills and the Midlands. It forms rugged terrain with sharp crests and steep slopes. The southern slopes are generally steeper than the northern ones. In spite of its inhospitable terrain, the range is well populated, especially on its northern slopes. From the crest of the Mahabharat Range one commands a comprehensive view to the north of the low-lying Midland hills and the bright, snow-covered Himalayan ranges beyond; to the south, beyond the Siwalik hills, the vast Gangetic Plain seems to merge with the horizon.

Midlands

The Midlands, consisting of subdued hills, wide river valleys, and tectonic basins, form the most important physiographic province of Nepal. Bounded by the towering snow-clad Higher Himalayan ranges and the Fore Himalaya to the north and the Mahabharat Range to the south, this zone has an average width of 60 km and ranges in elevation from 200m (in river valleys) to 2,000m. The Midlands, in contrast to the other physiographic divisions, exhibit a mature landscape (Figure 3.4). The area is drained by a large network of rivers and streams with predominantly north-south and east-west valleys. The larger, predominantly south-flowing, rivers are frequently forced to deflect at right angles when they reach the northern slopes of the Mahabharat Range and subsequently flow east-west for long distances, collecting the waters of many other rivers on their way (Figure 3.1). Midland rivers have very low gradients and form extensive and wide terraces along their courses.

Figure 3.4: **A general view of the Midlands around the Panchkhal Valley, looking north. The mountains with snow cover in the background are part of the Higher Himalaya. Note the gentle topography of the Midlands with gradually sloping hills and wide valleys.**

Within the Midlands are the tectonic valleys of Panchkhal, Banepa, and Kathmandu in central Nepal, and Pokhara and Mariphant in western Nepal.

Due to the gentle topography and mild temperate climate, this zone is very densely populated, accounting for nearly 52% of the total population of Nepal. Every possible hill slope has been terraced and cultivated. Deforestation is a serious problem, and as a result this belt of the Nepal Himalaya is also faced with a high rate of soil erosion.

Fore Himalaya

All along the Nepal Himalaya, a transitional zone can be recognised between the Midlands and the Higher Himalaya. Named the Fore Himalaya by Hagen (1969), this zone ranges in altitude from 2,000 to 5,000m. It is best developed in the Chainpur-Humla-Mugu-Jumla area of western Nepal, where it is over 150 km wide, and in the Solu-Khumbu area (north of Okhaldhunga) in the east (Figure 3.1). Elsewhere it occupies a narrower strip, typically 20-30 km wide, lying directly to the south of the Higher Himalayan Ranges. This unit's physiography, climate, and vegetation are distinct from those of the Midlands and the Higher Himalaya. The topography is much more rugged and the slopes steeper than in the Midlands (Figure 3.5); the altitude is higher and temperatures much colder, with snowfall in winter, although summers are quite warm. Surprisingly, in some places, such as Jumla, rice is widely cultivated.

In the Fore Himalaya, the taller plant species are confined below 4,000m; shrubs and algae predominate from that elevation up to the permanent snow-covered area. The lack of good agricultural land and the cold climate have deterred human settlement, with the result that there is a comparatively low population density in this unit.

Higher Himalaya

The hills of the Fore Himalaya give way to the snow-capped peaks of the Higher Himalaya to the north. Nepal not only contains the highest peak of the world (Mt. Everest or Sagarmatha, 8,850m) but also the greatest number of peaks over 8,000m altitude. Unlike other physiographic zones, the Higher Himalaya is not a single range but rather a discontinuous echelon of parallel ranges variously

Figure 3.5: **A general view of the Fore Himalaya in far western Nepal, looking north.**

running east to west, north-west to south-east, and north-east to south-west. A few major rivers originating north of the Higher Himalaya dissect these ranges, forming some of the deepest gorges in the world. These antecedent rivers have been flowing along their courses since long before the rise of these formidable mountains; their continuous downcutting has kept pace with the mountains' rise.

Topographically, this mountain range shows extremely rugged terrain with very steep slopes and deeply cut valleys (Figures 3.6 and 3.7). Generally, all terrain above 5,000m (roughly corresponding to the permanent snow line in Nepal) may be considered the Higher Himalaya. The southern faces of the Higher Himalaya and the Fore Himalaya receive heavy precipitation: 2,000 mm on average, and as much as nearly 5,000 mm south of the Annapurna Range (Chalise et al. 1996; Upreti and Dhital 1996) (Figure 3.8).

Figure 3.6: **The Ganesh Himal (seen from the south), illustrating the very rugged topography and steep slopes of the Higher Himalaya**

Figure 3.7: **The Dudh Khosi north-east of Namche Bazaar in eastern Nepal, which forms a typically deep, steep-sloped valley of the Higher Himalaya. View to the west**

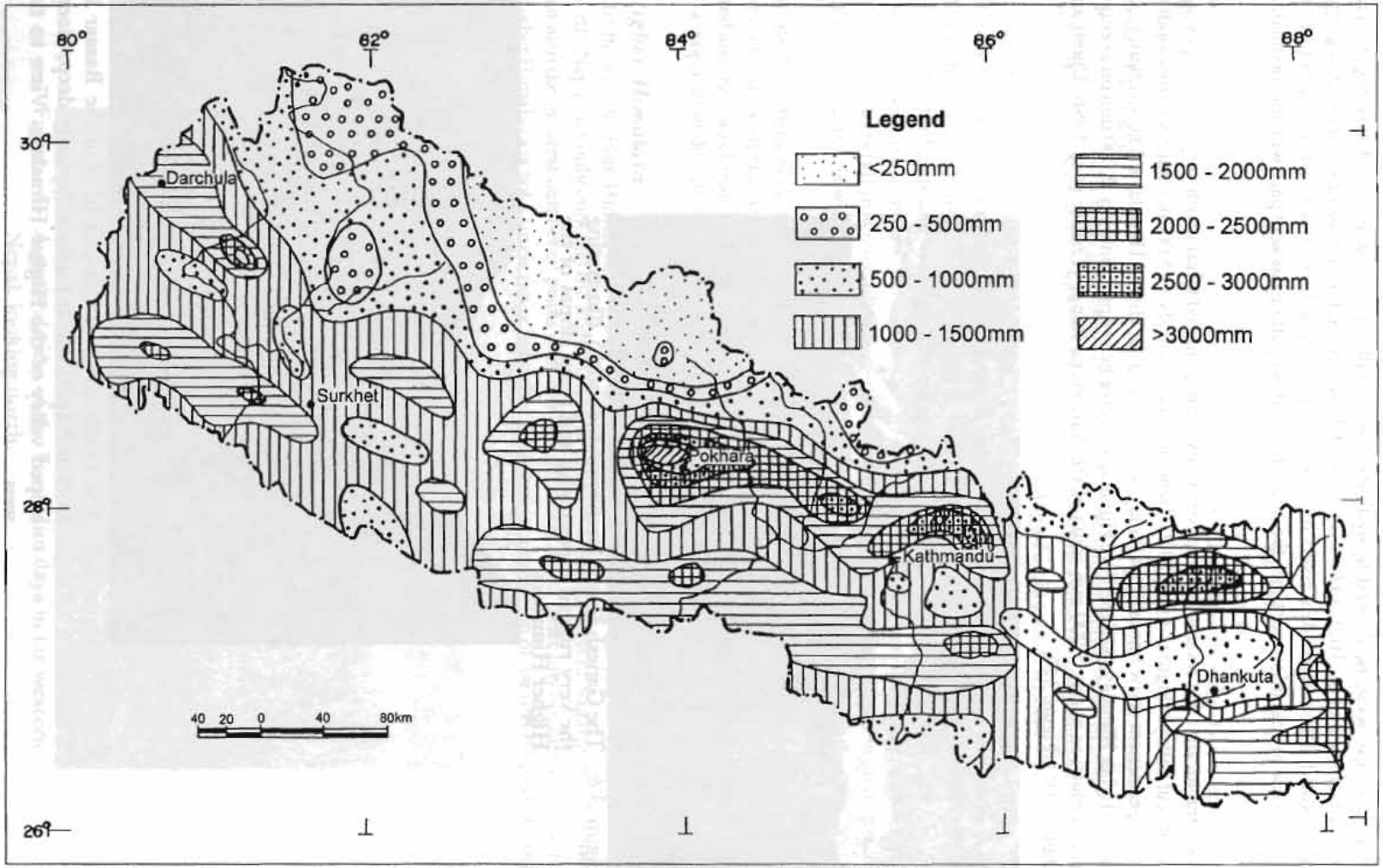

Figure 3.8: **Mean annual precipitation in Nepal 1971-85** (source: Upreti and Dhital 1996)

Inner and Trans Himalayan Valleys

A number of valleys in northern Nepal run north-south and east-west. Some, known as Trans Himalayan Valleys, are situated to the north of the Higher Himalayan ranges; these include Dolpa (north of the Hiunchuli and Dhaulagiri ranges), Mugu (north of the Kanjiroba range), Mustang (also known as the Thak Khola valley, north of Dhaulagiri and Annapurna), and Manang (north of Annapurna). Others, known as Inner Himalayan Valleys, lie south of the highest ranges but still within the Higher Himalaya. These include the Langtang Valley (south of Langtang Himal), Khumbu Valley (south of Everest), and Ghunsa (west of Kangchenjunga). The length and width of these valleys varies.

These Inner and Trans Himalayan Valleys are unique in their climate and vegetation. Lying within the rain shadow zone, they remain very dry throughout the year. However, rain-bearing clouds do reach these valleys through the deep river gorges between the Higher Himalayan ranges, bringing some precipitation (around 250 mm on average) and supporting some vegetation and fairly large populations. In this unit, human settlements can be found up to 4,000m and above (as high as 4,300m at Phopagaon in the Langtang area).

Figure 3.9: **The Thak Khola, a Trans Himalayan valley in western Nepal. Note the absence of vegetation on the hill slopes, indicating a dry climate. Where irrigation facilities are maintained, agriculture creates green oases.**

Major Geologic Zones of Nepal

Nepal can be divided, from south to north into the following five major tectonic zones separated by major thrusts and faults.

Terai Zone
Main Frontal Thrust (MFT) (sometimes called the Himalayan Frontal Thrust (HFT)
Siwalik Zone
(also known as the Churia, Outer Himalayan, or Sub Himalayan Zone)
Main Boundary Thrust (MBT)

Lesser Himalayan Zone
Main Central Thrust (MCT)
Higher Himalayan Zone
South Tibetan Detachment (STD)
Tethys Himalayan Zone
(in Nepal generally called the Tibetan-Tethys Himalayan Zone)

There are a number of other thrusts and faults, such as the Mahabharat Thrust (MT), but none that runs the length of the country.

Each zone is characterised by its own lithology, tectonics, structure, and geologic history. These features are summarised in the form of a generalised geological map in Figure 3.10. many of the names used in the physiographic divisions are also used for the geologic zones. However, the boundaries of the physiographic divisions are based arbitrarily on altitudes, whereas the geologic zones have clear and well-defined boundaries marked by thrusts or normal faults. The correspondence between the physiographic and geologic zones is shown in Table 3.2. Figure 3.5 in the previous paper shows a generalised cross-section through the meridian of Kathmandu showing the major tectonic features of the Himalaya.

Table 3.2: Geologic and physiographic units of Nepal

Geologic unit (south to north)	Physiographic unit (south to north)
Terai	Terai
Siwalik Zone	Siwalik Hill Range and Dun Valleys
Lesser Himalayan Zone	Midlands, Mahabharat Range, parts of Fore Himalaya
Higher Himalayan Zone	Higher Himalaya and parts of Inner Himalayan Valleys
Tibetan-Tethys Himalayan Zone	Some parts of the Higher Himalaya, and Inner and Trans Himalayan Valleys

Terai Zone

The southernmost tectonic division of Nepal, the Terai, represents the northern edge of the Indo-Gangetic alluvial basin. In the north it is bounded by the Main Frontal Thrust (MFT), whose outcrops are exposed at many places along the southern front of the Siwalik Range. The Terai plain is made up of alluvium of Pleistocene to Recent age (1.8 million years to the present) with an average thickness of about 1,500m. These sediments rest on the Siwalik Group (Middle Miocene-Pliocene), which in turn rests on rocks of still older ages belonging to the Indian Peninsular.

The Terai Zone shares a significant proportion of current Himalayan stress accumulation, which is manifested in the development of thrusts and thrust-propagated folds beneath the sediments. The northern part of the zone represents a mountain in the making: the Himalayan mountain front is continuously propagating to the south through this zone.

Siwalik Zone

The Siwalik Zone (in Nepal often called the Churia) consists of fluvial sedimentary rocks of Neogene to Quaternary age (14-1 million years ago). The zone is bounded to the north by the Main Boundary Thrust (MBT) and to the south by the Main Frontal Thrust (MFT). The outcrop of the MBT is very well exposed in the field and can be very well mapped even from aerial photos (Figure 3.11). Lesser Himalayan metasedimentary rocks have been thrust southward over the Siwalik rocks along this

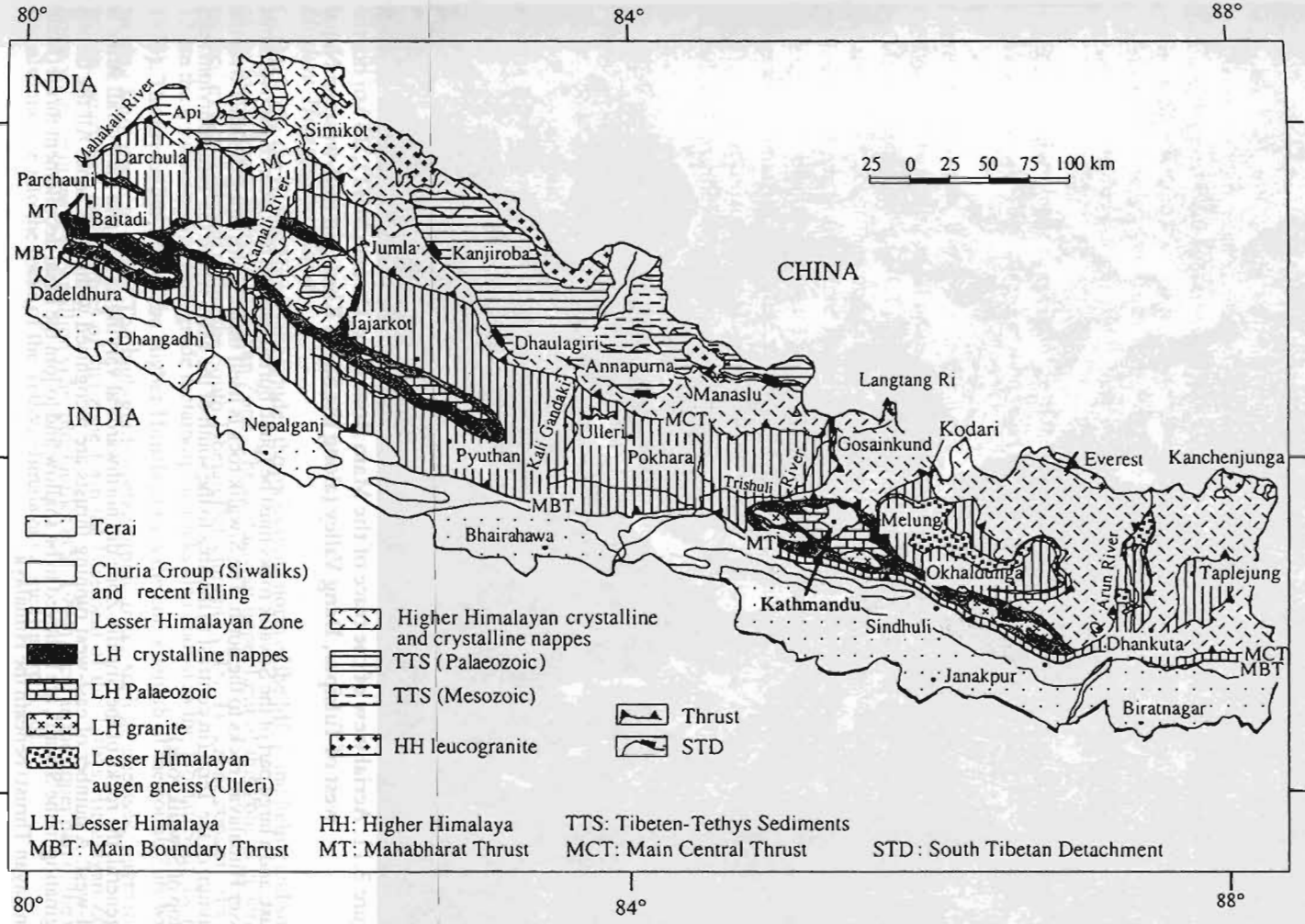

Figure 3.10: **Geological map of Nepal** (modified from Upreti and Le Fort 1999)

Figure 3.11: **Aerial view of the trace of the Main Boundary Thrust (MBT), 25 km north-west of Tulsipur, Dang Valley (along the Sarda Khola) in mid-western Nepal**

thrust, and a large part of the Siwalik rocks must be found buried beneath the cover of the overthrust Lesser Himalayan rocks to the north. The Siwalik rock is itself thrust south along the MFT over the alluvium of the Terai (in contrast to the area to the south of the MFT where the Terai alluvium rests on top of Siwalik rock).

In general, the rocks of the Siwalik Zone dip northwards at varying angles and the overall strike is east-west. A number of east-west running thrusts are recognised within this zone. All the thrusts originating in the Siwalik are believed to be shallow and to join the basal decollement thrust (Main Himalayan Thrust) beneath the Himalaya.

Rocks of this zone are divided stratigraphically into three parts. The deepest stratum, the Lower Siwalik, is essentially composed of alternations of fine-grained sediments such as various-coloured

mudstone, siltstone, and shale with subordinate amounts of fine-grained sandstone. The Middle Siwalik is marked by the first appearance of thick multistoried sandstone beds, measuring several metres to tens of metres in thickness and alternating with subordinate beds of mudstone. Because of the abundance of biotite and the presence of light-coloured quartzes and feldspars, these sandstones have acquired the nickname 'pepper-and-salt sandstones'. Cycles of fining-upward sequences are commonly observed, in which a bed begins with a coarse sandstone, gradually fines upward and ends up in thin clay layers or paleosols. The clay layers normally preserve good fossils of plants and (locally) freshwater molluscs. The Upper Siwalik is characterised by very coarse-grained rocks such as boulder conglomerates with minor proportions of mudstone intercalations.

Based on palaeomagnetic studies, the age of the exposed Siwalik Group in Nepal ranges from around 14 million years ago to less than 2 million years ago (Tokuoka et al. 1986; DeCelles et al. 1998).

Lesser Himalayan Zone

The Lesser Himalayan Zone (Figure 3.10) is bordered to the south by the MBT and to the north by the Main Central Thrust (MCT). The MBT is a low-angle fault that has brought very old Lesser Himalayan rocks over the younger Siwalik Group. Three physiographic units – the Mahabharat, Midlands, and parts of the Fore Himalaya – belong to the Lesser Himalayan Zone. The zone is made up mostly of unfossiliferous sedimentary, and metasedimentary rocks such as shale, sandstone, limestone, dolomite, slate, phyllite, schist, and quartzite, ranging in age from Precambrian (as old as 1, 800 million years) to Eocene (about 40 million years). The rocks in this zone are highly folded and faulted, and have developed complicated structures.

The Lesser Himalaya of Nepal shows much variation in stratigraphy, structures, and magmatism. In the east it is characterised by the development of extensive thrust sheets of crystalline rocks of the Higher Himalaya (gneisses and schists) that have travelled southward from their root zone in the north. Large tectonic windows – notably the Taplejung, Arun, and Chautara-Okhaldhunga – expose low-grade metamorphic rocks of the Lesser Himalaya below the cover of these crystalline thrust sheets. In central Nepal, a large thrust sheet called the Kathmandu Nappe covers a wide area around the Kathmandu region. West of Kathmandu, between the Burhi Gandaki and Bheri Rivers, the crystalline rocks are restricted to the region north of the MCT. Between the Bheri River and the western border of Nepal, crystalline nappes reappear and cover much of the Lesser Himalayan terrain (Figure 3.10).

Higher Himalayan Zone

Geologically, the Higher Himalaya includes the rocks lying north of the MCT and below and south of the fossiliferous Tethys Himalayan Zone. The northern or upper limit of this zone is generally marked by a normal fault called the South Tibetan Detachment (STD). This zone consists of a 10-12 km thick succession of high-grade metamorphic rocks also known as the Tibetan Slab (Le Fort 1975). The crystalline unit of the Higher Himalaya runs the entire length of the country, its width varying from place to place. The high-grade metamorphic rocks such as gneisses, migmatites, schists, quartzites, and marbles of this zone form the basement of the Tethys Himalayan Zone. Some young granites (24-19 million years old, Guillot et al. 1994) occur in the upper part of the unit and also intrude into the rocks of the Tethys Himalayan Zone (Figure 3.10).

Tethys Himalayan Zone

The Tethys Himalayan Zone, also known as the Tibetan-Tethys Himalayan Zone or Tibetan Tethys Zone, adjoins the Higher Himalayan Zone with a normal fault contact (the STD) and extends to the

north into Tibet. This zone is composed of sedimentary rocks such as shale, limestones, and sandstones, ranging in age from Cambrian (570 million years ago) to Cretaceous (70 million years ago). In Nepal, the fossiliferous rocks of the Tethys Himalayan Zone are well developed in the Thak Khola (Mustang), Manang, and Dolpa areas. Most of the High Himalayan peaks of Nepal, including Everest, Manaslu, Annapurna, and Dhaulagiri, are made up of these Tethys Himalayan rocks and of young granites intruding into them (Figure 3.10).

The Restless Mountain

The Indian plate is moving northward into the Eurasian plate at an average rate of about 1.5 to 5 cm per year (depending on the location), with nearly half of this horizontal slip being accommodated within the Himalaya (Bilham et al. 1998). This constant compression makes the Himalaya one of the world's most active and fragile mountain ranges. The rocks of the Himalaya are moving upward as well as horizontally southwards along the major thrusts discussed above. The range is presently rising at a rate of about a few millimetres per year depending on the location, reaching nearly one cm in the Fore Himalaya south of the MCT (Jackson and Bilham 1994).

Different parts of the range have moved at different rates in the past. Between approximately 25 and 19 million years ago, the Main Central Thrust (MCT) was very active and the northern part of the Himalaya (areas occupied by the present-day Higher Himalaya) rose very quickly, attaining nearly their present height; deformation and partial melting within the MCT hanging wall occurred around 22 million years ago (Copeland et al. 1991; Hodges et al. 1996). The movement along the MCT caused the Higher Himalayan rocks to move southward, sliding over the Lesser Himalaya, eventually travelling horizontally more than 100 km. Higher Himalayan crystallines must once have covered the Lesser Himalaya like a blanket, but most have by now been eroded away. After a period of inactivity, the MCT was reactivated 6-8 million years ago (Harrison et al. 1997), rejuvenating the Higher Himalaya.

Around 10-11 million years ago, the movement that had been occurring along the MCT shifted to a new location, the Main Boundary Thrust, essentially creating the Mahabharat Range (Meigs et al. 1995). This movement also forced the Lesser Himalayan rocks over the Siwalik rocks; a large contingent of Siwalik rocks is presumably buried under the Lesser Himalaya. The MBT remains very active, with the result that the frontal part of the Lesser Himalaya is rising comparatively fast.

As the MBT gradually became inefficient in accommodating the northward displacement of India, new thrusts formed to the south. They include the Main Frontal Thrust (MFT), along the southern front of the Siwalik Hills, as well as others further south in the plains. The latter are covered by the alluvium of the Ganges and Indus river systems (Figure 3.12) and therefore cannot be seen directly, but thrusting and uplifting can be inferred from folded and tilted river terraces and domal uplifts as much as tens of kilometres south of the mountain front. The still-active MFT continues to press the Siwalik Range higher and its rocks southwards.

All the above-mentioned thrusts run east-west the length of the Himalaya. The compression resulting from the northward movement of the Indian Plate against the rigid Asian landmass has also given rise to many other faults and folds, large and small, active and inactive, and of various orientations. In Nepal there are large east-west-running folds, an anticline (a fold in which layered strata are inclined down and away from the axes) within the northern part of the Lesser Himalaya, and a syncline (a concave upward fold with younger material in its core) in the front occupying the Mahabharat Range. The Himalayan rocks in general are also highly criss-crossed by joints (fractures without discernible displacement) as a result of the tectonic forces prevailing in the Himalaya.

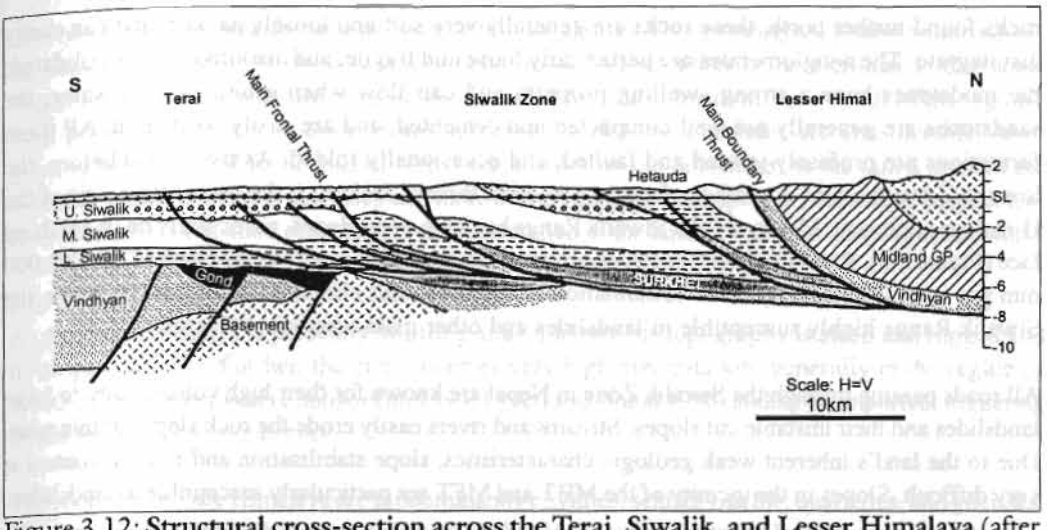

Figure 3.12: **Structural cross-section across the Terai, Siwalik, and Lesser Himalaya** (after Bashyal 1998, with permission from the Nepal on ecological society)

In general, the presence of so many thrusts, faults, folds, and joints makes any rock of the Himalaya physically weak. Rocks adjacent to faults and thrusts, those along the axis of folds, and those that are jointed are particularly weak.

A final factor in the dynamism of the Himalaya is its continual battle between weathering and uplift. Both mechanical and chemical weathering processes are quite intense in the region. The Himalaya, which is generally agreed to have attained nearly its present height by 17 million years ago (France-Lanord et al. 1993), would have been reduced to a plain if it had not constantly offset the weathering and erosion processes by further uplift. An area with a high uplift rate will maintain steep slopes and rugged features as it outpaces weathering and erosion; a slowly rising or stable area will over time become more smooth and rounded and will have thick soil development. Thus the parts of the Himalaya that are rising faster – the Higher Himalaya, Mahabharat, and Siwalik Ranges – are steeper and more rugged than the Lesser Himalaya. The latter has remained comparatively stable for a long time, geologically speaking, and therefore the effects of weathering and erosion can be seen in its rounded hills, less steep slopes, lower heights, and thick soil layers. This has resulted in the development of a more hospitable region for human settlement in an otherwise inhospitable Himalayan terrain.

Landslide Problems in Nepal

The predisposing factors for landslide occurrence and other slope instabilities are the inherent geological condition and the high angle of slope of the terrain. Factors such as raised groundwater level, undercutting by rivers, and loss of vegetation, may facilitate landslide occurrence. The actual triggering agents can be any of a variety of factors such as excessive rainfall, earthquakes or artificial vibrations, and various anthropogenic activities. Conditions predisposing to the occurrence of landslides on a wide scale are found in all the geomorphic and geological zones of the Himalaya.

Siwalik Range

As discussed above, the Siwalik Range is made up of geologically very young sedimentary rocks such as mudstones, shale, sandstones, siltstones, and conglomerates. Unlike the metamorphic

rocks found further north, these rocks are generally very soft and loosely packed, and can easily disintegrate. The conglomerates are particularly loose and fragile, and are almost unconsolidated; the mudstones have a strong swelling property and can flow when saturated with water; the sandstones are generally not well compacted and cemented, and are easily weathered. All these formations are profusely jointed and faulted, and occasionally folded. As mentioned before, the Siwalik Zone contains a number of major east-west thrusts, making it the most active part of the Himalaya at present. Moreover, the Siwalik Range has very steep slopes, particularly on its southern face (Figure 3.3). Rainfall in the Nepalese portion of this zone is normally in the range of 1,500-2,000 mm per year (Figure 3.8). This combination of geologic and climatic conditions has made the Siwalik Range highly susceptible to landslides and other mass-wasting processes.

All roads passing through the Siwalik Zone in Nepal are known for their high vulnerability to large landslides and their unstable cut slopes. Streams and rivers easily erode the rock slopes of this zone. Due to the land's inherent weak geologic characteristics, slope stabilisation and erosion control is very difficult. Slopes in the vicinity of the MBT and MFT are particularly susceptible to landslides.

Mahabharat Range

As the first effective mountain barrier to the monsoon clouds, the Mahabharat Range greatly influences the distribution of rainfall in Nepal. In some places, such as the Dhankuta-Okhaldhunga area, it even forms a kind of rain shadow to its north (Figure 3. 8) (Chalise et al. 1996). Where the range is relatively higher – as in (from east to west) Ilam, Ramechap-Udaipur Garhi, the southern and south-eastern rim of the Kathmandu Valley, Tansen, and Dadeldhura – rainfall amounts also tend to be higher (Chalise et al. 1996; Upreti and Dhital 1996). The frequency of high-intensity rainfall (cloudbursts) is also high in these areas (Upreti and Dhital 1996).

The climatic factors in combination with the very steep slopes and inherently weak geologic conditions, make the Mahabharat Range highly susceptible to landslides. The presence of phyllites, slates, and thinly bedded interlayered sequences of phyllites and quartzites add to the instability; intense weathering makes the rocks still weaker. Only where the Mahabharat Range is made up of rocks such as limestone, dolomite, marble, and granite are the slopes more stable. The region is dotted with prominent landslide paths: Ramechap, the east-flowing sector of the Sun Khosi River, and the Salyan-Pyuthan area are well known for their landslide activity. Roads passing through or crossing the Mahabharat Range are highly hazardous: the Dang-Salyan road, the Kanti Highway (Tikabhairab-Hetauda road), the newly constructed Katari-Okhaldhunga road, and the Dharan-Dhankuta road illustrate how hazardous and difficult it is to build – and maintain – roads in such terrain.

Better monitoring of rainfall data and the installation of more meteorological stations might help to give advance warning of disasters, floods and debris flows as well as landslides) and help save lives and property in the region.

Midlands

The Midlands have a more subdued topography than the other zones. However, the rocks in the Midlands are deeply weathered, and thick soil formations are found on most hill slopes; these soils are generally prone to landslides, especially in areas of intense deforestation. Most parts of the Midlands receive an annual rainfall of between 1,000 and 2,000 mm, with some exceptionally high precipitation pockets This rainfall intensity is enough to trigger widespread landslides in the Midlands. The bottoms of major valleys are particularly prone to landslides as a result of undercutting by rivers.

The Midlands are home to most of Nepal's hill population. This physiographic unit is intensively cultivated, with even the steepest slopes being used. Deforestation is most critical in this zone. Wherever possible, slopes are terraced and irrigated for rice cultivation. As a result of the region's high population density, anthropogenic influences in causing landslides are considerable. Most good agricultural land in the hills of Nepal actually lies on old landslides, as the failed mass of the landslide makes the terrain less steep and more moist. In such areas improper methods of irrigation or road or canal construction often trigger the reactivation of the landslide, threatening the entire slope.

Fore Himalaya

As the Fore Himalaya is presently uplifting at a rapid rate, its topography is steep and rugged and its slopes unstable. Further, the zone receives very high precipitation, generally in the region of 2,000-3,000 mm per year (Chalise et al. 1996; Upreti and Dhital 1996) adding an important triggering factor for landslide occurrence.

The rocks of the Fore Himalaya are predominantly phyllites, schists, marble, quartzites, and gneisses. The slopes are commonly covered with thick, bouldery soils, generally known as colluvium, that are prone to large and unmanageable landslides. A number of such landslides can be found along the Arniko Highway (Kathmandu-Kodari Highway), at Charnabati near Charikot, and north of Dolakha. Similar soils and associated landslides can be found along most of the major north-south flowing rivers of Nepal. In some narrow valleys, large parts of the hills have collapsed towards the centre of the valley, producing larger-scale landslides. These features can be seen along the Kodari Highway opposite Sakhua, north of Barhabise.

Higher Himalaya

The Higher Himalaya is the most rugged of Nepal's physiographic units. The gneisses, migmatites, schists, marbles, and quartzites of this zone have undergone metamorphism at very high temperatures and pressures, and so are comparatively strong and can support very steep slopes. Near-vertical pitches of 3,000m or more are not uncommon. The southern slopes of the Higher Himalaya generally receive high precipitation. Physical weathering is dramatic in this unit, but very little soil cover can remain on its very steep slopes.

Despite their geologic strength, the rocks of the Higher Himalaya are subject to landslides of various sizes. Most are rockslides, but exceptionally large landslides have also been reported: the Tsergo Ri mega-landslide in the Langtang Valley had a displaced volume of rock estimated at 10 cu. km (Weidinger and Schramm 1995). As the Higher Himalaya is practically unpopulated (except in some valley bottoms), these landslides generally have little socio-economic impact. However, construction of roads and other infrastructure in this zone is a formidable task.

Inner and Trans Himalayan Valleys

Lying in the rain shadow of the Himalaya, with an average annual rainfall of less than 250 mm, these valleys experience less frequent landslides than other areas. The most common cause of landslides here is the failure of colluvial and moranic materials on steep valley slopes.

Conclusion

Landslide occurrence in Nepal is a function of the inherently weak geology and physiography of slopes, combined with triggering factors such as heavy monsoon rainfall, cloudbursts, and earthquakes. These factors vary in different physiographic, geologic, and climatic zones. It is likely to be inappropriate to use a uniform approach to the study and mitigation of landslide hazards in

every zone of the Himalaya: the landslide problem in the Siwalik hills is unique and entirely different from that of the Higher Himalaya and vice versa. A better understanding of the geologic, physiographic, and climatic zones and their combined overall effects on the terrain is a prerequisite for any successful project of landslide study and mitigation in Nepal. Obtaining more reliable data through a better network of meteorological stations will greatly help correct assessment of the extent of rainfall and its role in landslide occurrence.

References

Bashyal, R.P. (1998) 'Petroleum Exploration in Nepal'. In *Journal of Nepal Geological Society*, 18: 19-24

Bilham, R.; Blume, F.; Bendick R.; Gaur, V.K. (1998) 'Geodetic Constraints on the Translation and Deformation of India: Implications for Future Great Himalayan Earthquakes'. In *Current Science*, 74 (3): 213-229

Chalise, S.R.; Shrestha, M.L.; Thapa, K.B.; Shrestha, B.R.; Bajracharya, B. (1996) *Climatic and Hydrological Atlas of Nepal.* Kathmandu: ICIMOD

Copeland, P.; Harrison, T.M.; Hodges, K.V.; Mareujol, P.; Le Fort; P.; Pecher, A. (1991) 'An Early Pliocene Thermal Perturbation of the Main Central Thrust, Central Nepal'. In *Implications for Himalayan Tectonics. J. Geophys. Res.*, 96: 8475-8500

DeCelles, P.G.; Gehrels, G.E.; Quade, J.; Ojha, T.P. (1998) 'Eocene-early Miocene Foreland Basin Development and the History of Himalayan Thrusting, Western and Central Nepal'. In *Tectonics*, 15: 741-765

France-Lanord, C.; Derry, L.A.; Michard, A. (1993) 'Evolution of the Himalaya Since Miocene Time: Isotopic and Sedimentologic Evidence from the Bengal Fan'. In Trelor, P.J., and Searle, M. (eds) *Himalayan Tectonics,* Special Publication, pp 603-621. London: Geological Society

Guillot, S.; Hodges, K.P.; Le Fort, P.; Pêcher, A. (1994) 'New Constraints on the Age of the Manaslu Leucogranite: Evidence for Episodic Tectonic Denudation in the Central Himalaya'. In *Geology*, 22: 559-562

Hagen, T. (1969) *Report on the Geological Survey of Nepal Preliminary Reconnaissance.* Zürich: Mémoires de la Soc. Helvétique des Sci. Naturelles.

Harrison, T.M.; Ryerson, F.J.; Le Fort.; P.; Yin, A.; Lovera, O.M. (1997) 'A Late Miocene-Pliocene Origin for the Central Himalayan Inverted Metamorphism'. In *Earth and Planetary Science Letters*, 146:E1-E8.

Hodges, K.V.; Parrish, R.R.; Searle, M.P. (1996) 'Tectonic Evolution of the Central Annapurna Range, Nepalese Himalaya'. In *Tectonics*, 15:1264-1291

Jackson, M.; Bilham, R. (1994) 'Constraints on Himalayan Deformation Inferred from Vertical Velocity Fields in Nepal and Tibet'. In *Journal of Geophysical Research*, 99: 13897-13912

Le Fort, P. (1975) 'Himalaya: The Collided Range: Present Knowledge of the Continental Arc'. In *American Journal of Science*, 275A: 1-44

Meigs A.J.; Burbank, D.W.; Beck, R.A. (1995) 'Middle-Late Miocene (>10 Ma) Formation of the Main Boundary Thrust in the Western Himalaya'. In *Geology*, 23(5): 423-426

Tokuoka, T.; Takayasu, K.; Yoshida, M.; Hisatomi, K. (1986) *The Churia (Siwalik) Group of the Arun Khola Area, West Central Nepal,* Vol. 20, pp 135-210. Matsue: Shimane University, Memoirs of the Faculty of Science

Upreti, B.N. (1999) 'An Overview of the Stratigraphy and Tectonics of the Nepal Himalaya.' In Upreti, B.N.; LeFort P. (eds) *Geology of the Nepal Himalaya: Recent Advances, Journal of Asian Earth Sciences,* 17(5-6): 577-606

Upreti, B.N.; Le Fort, P. (1999) 'Lesser Himalayan Crystalline Nappes of Nepal: Problem of Their Origin'. In Macfarlane, A., Quade, J., and Sorkhabi, R. (eds) *Himalaya and Tibet: Mountain Roots to Mountain Tops,* Vol. 328, Special Paper. USA: Geological Society of America

Upreti, B.N.; Dhital, M.R. (1996) *Landslide Studies and Management in Nepal.* Kathmandu: ICIMOD

Weidinger, J.T.; Schramm, J.M. (1995) 'A Short Note on the Tsergo Ri Landslide, Langtang Himal, Nepal'. In Upreti, B.N. and Dhital, M.R. (eds) *9th Himalaya-Karakorum-Tibet Workshop,* Vol 11, pp 257-272 Kathmandu: Journal of Nepal Geological Society

4 An Introduction to Climate, Hydrology, and Landslide Hazards in the Hindu Kush-Himalayan Region

S.R. Chalise
Mountain Natural Resources Division
ICIMOD, G.P.O. Box 3226, Kathmandu, Nepal

Extending some 3,500 km from Afghanistan to Myanmar, the Hindu Kush-Himalaya (HKH) is inherently fragile and susceptible to natural hazards as a result of its extremely weak geology, intense seasonal precipitation, and highly rugged topography. The climate at the macro scale is dominated by the summer monsoon. There is a general decrease in rainfall from east to west and south to north, with monsoon rains being less dominant in the west, and the Siwalik Zone (or Outer Himalaya) receiving more precipitation than the Trans Himalaya. The meso-scale climate is dominated by topography, with valleys being drier than the slopes and ridges, and southern slopes receiving more precipitation than northern ones. Microclimates are dominated by landforms, soil, vegetation, and other land-use practices, and are very complex and difficult to predict. Isolated heavy showers associated with afternoon convective heating, accompanied by lighting and intense precipitation, are characteristic of microclimatic effects in the region.

The HKH and the adjoining Tibetan Plateau together form the largest global storehouse of fresh water in the lower latitudes and are the source of several major rivers and their tributaries. The discharges of water and sediments in these rivers are determined by geology, topography, climate, and vegetation; they are dominated by monsoon characteristics, with high flows in summer and low flows in winter, and with the duration of the high-flow season increasing from west to the east. Suspended sediment discharge in these rivers is very high. The rivers of the Central Himalaya are of three distinct types: comparatively dry rivers originating from the Tibetan Plateau, perennial rivers originating from the Higher Himalaya, and rivers with flash flows originating from the Mahabharat and Siwalik (Churia) ranges. River flows are affected by many factors including extreme precipitation events, outbursts of glacial lakes, and development and failure of landslide-dams.

Inherent local factors, such as geology, topography, hydrology, land cover, and human activities relating to the use and management of land and water have triggered landslides, debris flows, and other forms of slope instability. Snow avalanches and glacial lake outburst floods predominate at very high elevations, debris flows and flash floods in the middle elevations, and floods in the plains. In the east, the likelihood of natural hazards of this type is highest in the summer because of the south-east monsoon, whereas in the west they are more frequent in winter.

Hundreds of lives and billions of dollars' worth of property and infrastructure are lost every year as a result of landslides, debris flows, and floods. A poor understanding of natural and man-made processes and a paucity of relevant hydrometeorological data have perpetuated uncertainties in dealing with natural hazards. It is necessary to fill these gaps and to develop appropriate methods and techniques to deal with mountain hazards within the overall context of integrated watershed management. Hazard control and management techniques should be simple and affordable. ICIMOD has accorded high priority to the problems of natural hazards in the HKH region, focusing on capacity building through training programmes and the dissemination of information.

Introduction to the HKH Region

General features

Extending about 3,500 km from Afghanistan in the west to Myanmar in the east, the Hindu Kush-Himalaya (HKH) is home to approximately 140 million people and influences the lives of more than three times as many living in the downstream basins and plains. As the largest global storehouse of fresh water in the lower latitudes, this greatest of mountain ranges, together with the associated Tibetan Plateau, is the source of such mighty rivers as the Indus, Ganges, Yarlung-Tsangpo, Brahmaputra, Nu-Salween, Mekong, Yangtze, and Yellow. The population of the HKH region, extending over an area of 3.4 million sq.km, is growing rapidly, with an estimated population of 140 million in 1993, expected to double by 2030 (Sharma 1993). The consequences of such population growth will be enormous.

The environment of the HKH is inherently fragile, and the land is highly susceptible to natural hazards due to a combination of weak geology, intense seasonal precipitation, and rugged topography. Hydrological factors further contribute to landslide hazards in the region, while the potential impacts of climate change, although largely unknown, are likely to further exacerbate such hazards.

Climatic features

The HKH acts as a physical and climatic barrier between regions to the north and south. The south-west monsoon, which is only 5,000m thick, cannot penetrate the much higher Himalaya, and must make a virtual U-turn toward the north-west from the Bay of Bengal (Boucher 1979). Similarly, the northern continental airmass cannot easily cross the range towards the south. Thus the HKH acts as an effective barrier between the lower- and middle-latitude climatic systems and can be looked upon as an 'air-shade' between the two.

The range's abrupt rise from the plains further complicates the climate of the region (see, for example, Figure 4.1). It is therefore not possible to speak of a single HKH climate. Although there is a broad monsoonal influence over the southern slopes, a great number of meso and micro climates exist influenced by topographical variations. The different Himalayan climates can be broadly classified as follows.

Macro scale: dominated by the monsoon

The climate of the HKH is, like other parts of South Asia, dominated by the monsoon; but the monsoon is generally weaker here than in the plains as it is further from its source of moisture. Rainfall from the south-west monsoon, which originates in the Bay of Bengal, generally decreases from east to west. Thus while the 'summer' rainy season in the Eastern Himalaya (Assam) lasts about eight months (March-October), it only lasts four months (June-September) in the Central Himalaya (Sikkim, Nepal, and Kumaon) and two months(July-August) in the Western Himalaya of Kashmir. In the Western Himalaya, summer monsoon rains are no longer the most dominant feature, while orography (the terrestrial relief form) becomes extremely important for rainfall (Domroes 1979).

Table 4.1 shows the variation of rainfall patterns from east to west as well as between the Trans Himalayan and Siwalik (Outer Himalaya) Zones. Rainfall in eastern locations such as Pasighat (Assam) and Darjeeling is not only higher but also highly concentrated in the summer months; summer rainfall gradually drops off, and winter precipitation becomes relatively more important, as

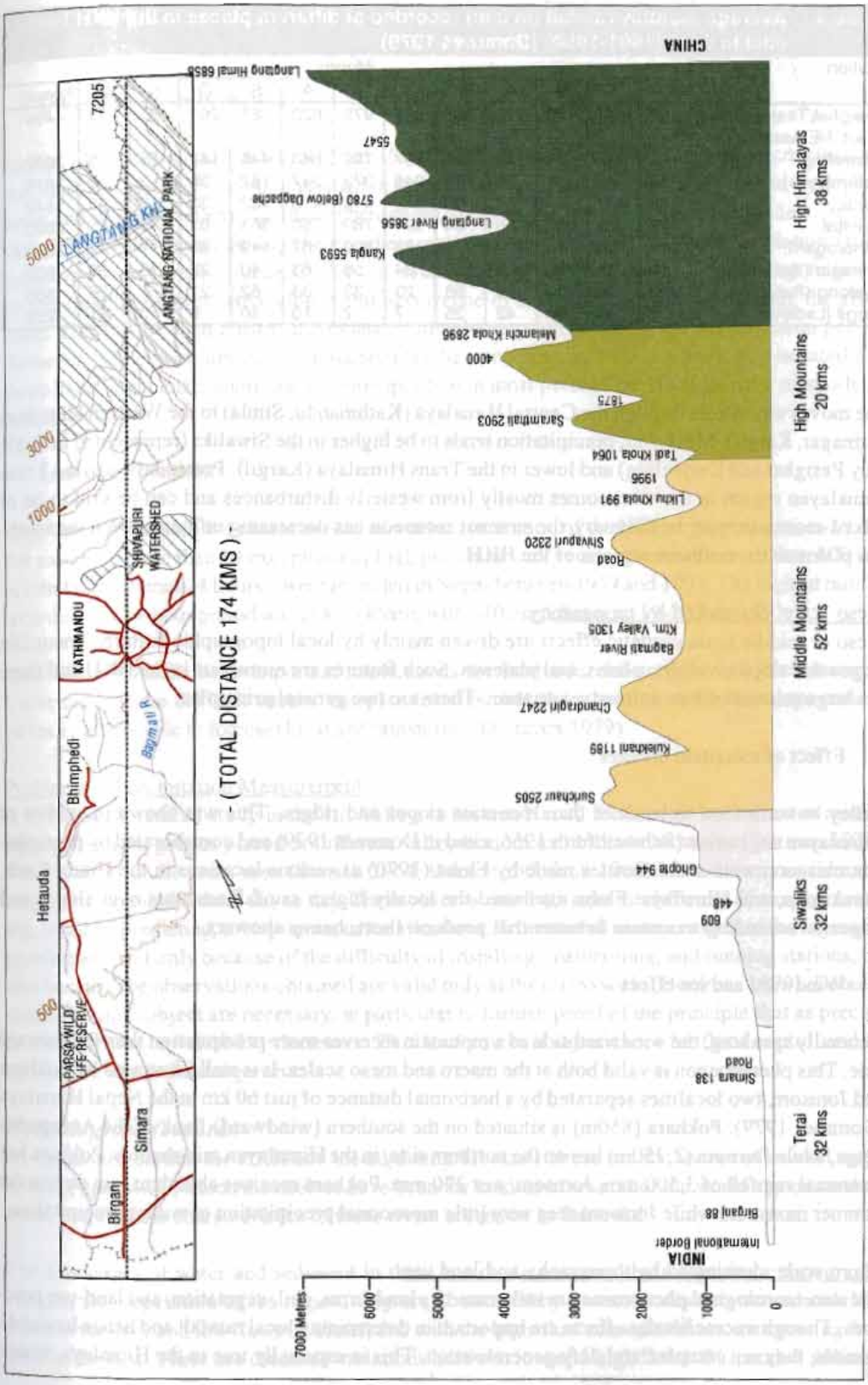

Figure 4.1: Cross-section of central Nepal (Chalise 1994)

Table 4.1: **Average monthly rainfall (in mm) recorded at different places in the HKH from east to west (1901-1950) (Domroes 1979)**

Station	Month												
	J	F	M	A	M	J	J	A	S	O	N	D	Annual
Pasighat/Tirap Frontier Tract, NE Assam	55	97	138	273	466	967	975	622	585	261	33	24	4494
Darjeeling	11	32	54	113	231	597	792	643	446	142	25	6	3092
Kathmandu	10	42	15	26	129	246	373	347	182	36	2	8	1416
Simla	65	70	64	46	60	149	416	419	182	33	10	28	1542
Nainital	70	73	53	38	84	391	769	750	363	61	13	25	2690
Pithoragarh	44	56	40	28	73	183	300	287	149	33	7	22	1223
Srinagar (Kashmir)	70	74	94	90	60	34	56	63	40	28	13	37	659
Kyelong (Punjab)	59	64	102	79	56	23	33	33	52	21	7	26	555
Kargil (Ladakh)	37	38	60	42	25	7	7	10	10	6	3	21	265

one moves westwards through the Central Himalaya (Kathmandu, Simla) to the Western Himalaya (Srinagar, Kargil). Moreover, precipitation tends to be higher in the Siwaliks (represented in Table 1 by Pasighat and Darjeeling) and lower in the Trans Himalaya (Kargil). Precipitation in the Trans Himalayan region in the west comes mostly from westerly disturbances and can be said to be of mixed-monsoon type. In summary, the summer monsoon has decreasing influence from the southern plains to the northern regions of the HKH.

Meso scale: dominated by topography

Meso or middle scale climatic effects are driven mainly by local topographic features: mountain ridges and slopes, valleys, plains, and plateaux. Such features are numerous in the HKH and there is a large amount of meso-climatic variation. There are two general principles.

- Effect of mountain breezes

Valley bottoms tend to be drier than mountain slopes and ridges. This was shown in studies of Himalayan vegetation (Schweinfurth 1956, cited in Domroes 1979) and corroborated by precipitation measurements and estimates made by Flohn (1970) at various locations in the Hindu Kush, Karakoram, and Himalaya. Flohn attributed the locally higher rainfall amounts over slopes and ridges to ascending mountain breezes that produce short, heavy showers.

- Windward and lee effect

Generally speaking, the windward side of a mountain receives more precipitation than the leeward side. This phenomenon is valid both at the macro and meso scales. It is well illustrated by Pokhara and Jomsom, two localities separated by a horizontal distance of just 60 km in the Nepal Himalaya (Domroes 1979). Pokhara (850m) is situated on the southern (windward) flank of the Annapurna range, while Jomsom (2,750m) lies on the northern side, in the Himalayan rain shadow. Pokhara has an annual rainfall of 3,500 mm; Jomsom, just 270 mm. Pokhara receives abundant rain during the summer monsoon, while Jomsom sees very little monsoonal precipitation or winter precipitation.

Micro scale: dominated by topography and land use

Micrometeorological phenomena are influenced by landforms, soil, vegetation, and land-use practices. Though microclimatic effects are important in determining local rainfall and hence landslide hazards, they are complex and defy generalisation. This is especially true in the Himalaya, where

extreme topographical variations occur within a short distance. In terms of rainfall, two microclimatic features are of special significance.

- Diurnal variation of rainfall

Studies of diurnal rainfall in Nepal (Dhar 1960) and India (Prasad 1970) have shown conclusively that diurnal variations in rainfall is small in places where precipitation is mainly caused by depressions and cyclonic storms, as these phenomena act irrespective of the time of the day. Diurnal variation can, however, be significant where precipitation is caused by strong insolation (solar radiation per unit area), with heating up and evaporation of moisture during the morning, followed by the creation of convective clouds and occurrence of isolated heavy showers during the afternoon. This can be seen outside the monsoon months, especially during the pre-monsoon period. However, while such diurnal cloudbursts may be very intense, they are generally isolated and short-lived, and hence contribute less precipitation in most parts of the HKH than the macro-level monsoon.

- Intensity of rainfall

High-intensity rainfall is a characteristic microclimatic feature of the HKH region (Domroes 1979). For example, more than 19 exceptionally high precipitation events – those with more than 400 mm of rain falling within 24 hours – were recorded in Nepal between 1959 and 1993. The highest rainfall recorded in a 24-hour period was at Kulekhani, with 540 mm of rain on 19-20 July 1993.

Such heavy rainfalls have important implications for landslide, debris flow, and flood hazards. Unfortunately, the difficult terrain, complex features, and sheer heights of the Himalaya make it virtually impossible to forecast localised rainstorms (Domroes 1979).

Problems of Precipitation Measurement

A micro-scale rainfall study in the Jiri Valley, in eastern Nepal, found wide variations in rainfall among five rain gauges placed at different valley-bottom and hillside locations (Dittman 1970). Other studies in the same area (Boesch 1964; Boesch and Groh 1966) have shown considerable irregularity in rainfall from day to day. These observations highlight the difficulty of simply recording, let alone predicting, precipitation in the Himalaya. True rainfall measurements in the region are problematic, not only because of the difficulty of installing, maintaining, and running stations, but also because the observations obtained are valid only at the micro scale (Domroes 1979). Detailed studies on this subject are necessary, in particular to furnish proof of the principle that as precipitation increases its variability decreases. This is of practical significance for flood control and for agriculture and soil management.

Hydrological features

As mentioned earlier, the HKH and the adjoining Tibetan Plateau are the source of several major rivers (Figure 4.2) , which themselves have been the cradles of several of the world's great civilisations. Some of the characteristics of these rivers are given in Table 4.2.

The discharges of water and sediment in these rivers are governed by the geology, topography, climate, and vegetation of the region; they are dominated by monsoon characteristics, with high flows in summer and low flows in winter, and with the high-flow season's duration increasing from west to the east. There are dramatic variations between low and high flows. Suspended sediment

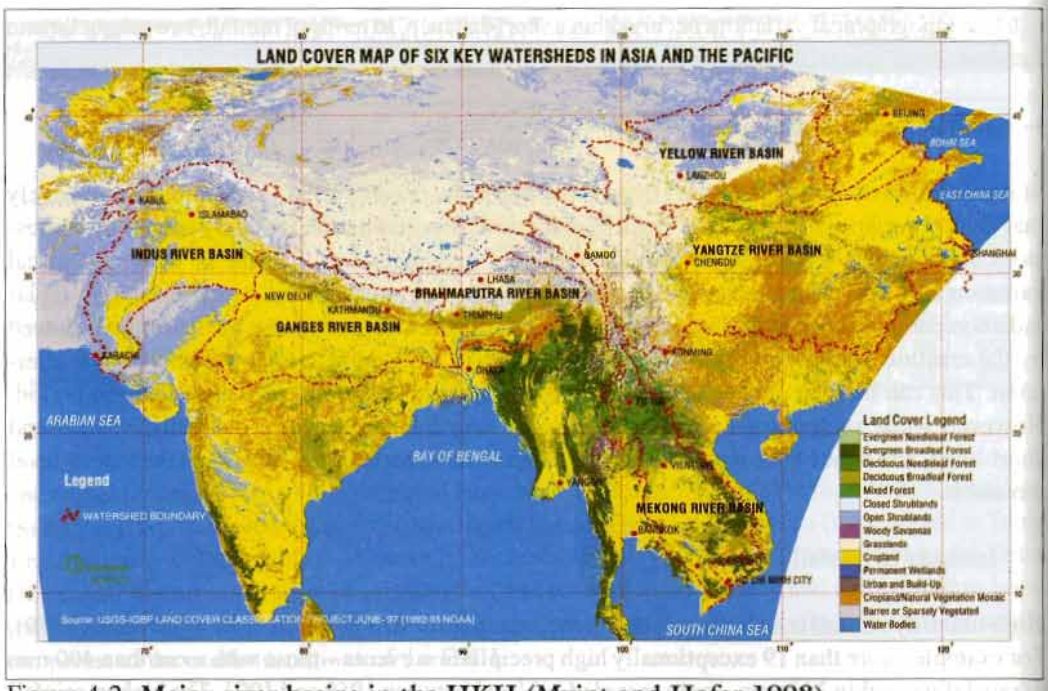

Figure 4.2: **Major river basins in the HKH (Myint and Hofer 1998)**

Table 4.2: **Major rivers draining the HKH region (Myint and Hofer 1998; Alford 1992)**

River	Indus	Ganges	Brahmaputra	Mekong	Yangtze	Yellow
Basin area (sq. km.)	945,000	1,050,000	580,000	795,000	1,808,500	752,443
Length (km)	3,200	2,950	2,880	4,800	6,290	5,464
Average annual discharge (million cumec)	115,000 (upstream from Tarbela)	460,000	600,000 (at Bahadurbad)	NA	NA	NA
Total suspended sediment (million tons per year)	250	520	540	150	480	1100
Suspended sediment load (world rank)	9	5	4	12	7	2

Note: NA = data not available; cumec= cubic metres per second

discharge in these rivers is very high. Discharge in the Indus river in the west is highest in summer as a result of increased ice melt, almost all its tributaries are fed by glaciers. In the central area the contribution of glacier melt is less significant. In the east, the Brahmaputra's seasonal variation in discharge correlates with the temporary storage of early precipitation as snow and subsequent melting.

The rivers of the Central Himalaya are of three distinct types: comparatively dry rivers originating from the Tibetan Plateau, perennial rivers originating from the Higher Himalaya, and flashy rivers (i.e., rivers with flash flows) originating from the Mahabharat and Siwalik ranges.

From time to time river flows may be affected by mud flows or landslide blockages. Flood waves as high as 9m have been attributed to glacial lake outburst floods and the failure of landslide-dams (Alford 1992). The bedloads (the solid material like sand, gravel, and sometimes boulders pushed

down by rivers rather than being carried in suspension) in these rivers at the time of the failure is extremely high but difficult to measure.

The region's rivers have witnessed major climate-induced disasters in recent years such as the consecutive catastrophic monsoon floods in Bangladesh during 1987 and 1988 (Rogers et al. 1989), the Indus Basin floods in Pakistan in September 1992, and floods and debris flows in south-central Nepal in July 1993 (Dhital et al. 1993).

Landslide Hazards in the HKH

Terminology

The term **landslide** is commonly used to denote the downward and outward movements of slope-forming materials along surfaces of separation by falling, sliding, or flowing at a faster rate. **Falls** are abrupt movements of materials that become detached from steep slopes or cliffs and drop down by free fall or a series of leaps and bounds. **Slides** (often called landslides) refer to mass movements with a distinct surface of rupture separating the slide material from more stable underlying material (**slope failure**). The downward sliding material is usually relatively dry. A **debris slide** is a slide of coarse-grained soil usually containing angular rock fragments, typically made up of debris from glaciers or from colluvium resulting from the disintegration of rocks in situ. A **debris flow** is a rapid mass movement of loose soil, rocks, and organic material along with entrained air and water to form a slurry that flows downslope. A **debris avalanche** is a very to extremely rapid debris flow. An **earth flow** has a characteristic bowl-like depression at the head where the slope material becomes liquefied and flows out; the flow is usually channelised on the slope and spreads out at the toe. The flow generally occurs in fine-grained materials or clayey rocks under saturated conditions. A **mud flow** is a type of earth flow containing about 50% of sand, silt, and clay-sized particles that are well saturated and flow rapidly. (Deoja et al. 1991)

A **landslide-dam** is a natural river dam formed by the rock, earth, debris, and or mud transported by a landslide. They are easily formed in the steep, narrow valleys of high rugged mountains, and can fail catastrophically, causing major downstream flooding and loss of life. A **glacial lake outburst flood (GLOF)** is a debris torrent resulting from the sudden and catastrophic release of water from a lake of glacial origin. Such lakes are usually impounded by glacial ice or a moraine. (Deoja et al. 1991)

Factors affecting landslide hazards

Mountain slopes are only conditionally stable, as they are continually subject to the downward pull of gravity. There is therefore a general tendency for mountain slopes to slide down, making them inherently hazardous. The causative and triggering factors for landslide hazards and slope instability are briefly discussed here in the context of the HKH.

Natural factors

These include inherent local factors such as:

- geology (including tectonics, seismicity, and soil type);
- topography (slope inclination, elevation, relief, and aspect);
- hydrology (including groundwater);
- vegetation cover;
- climate[1] (radiation, temperature, precipitation).

[1]Although climate is generally considered to be an external factor, it determines the characteristics of local ecosystems and hence can be considered as an inherently local factor too.

In addition, there are external (uncertain) factors such as:

- abnormal/extreme weather events;
- impacts of climate change (at present essentially unknown).

Human factors

These include:

- changes in (or inappropriate) land use and poor watershed management practices (deforestation, extension of agriculture on steep slopes, unplanned settlement, rural and urban growth);
- intensive agriculture/unsuitable crops;
- poor water management.

Principal triggering factors

The principal triggering factors for landslides, debris flows, slope failures, and other associated natural hazards in the HKH are:

- intense precipitation;
- earthquakes.

As it is difficult to predict or control earthquakes, disasters triggered by them cannot be avoided (although their potential effects can be mitigated by appropriate planning and construction). However, landslides, debris flows, and slope failures triggered by intense precipitation can be predicted, controlled, mitigated, and to a large extent managed.

Natural hazards in different elevation zones

The HKH is tectonically very active and hence inherently vulnerable to hazards. In addition, these mountains – particularly in their eastern parts – are exposed to intense seasonal precipitation during the summer monsoon. This acts as a trigger for various types of natural hazards in different elevation zones. Snow avalanches and glacial lake outburst floods predominate at high elevations (above 3,500m), while landslides, debris flows, and flash floods are common in the middle elevations (500-3,500m). Floods are the principal hazard in the lower valleys and plains. Figure 4.3 shows a generalised view of natural hazards at different altitudes; the relative seasonal susceptibility to hazards from west to east is schematically represented in Figure 4.4.

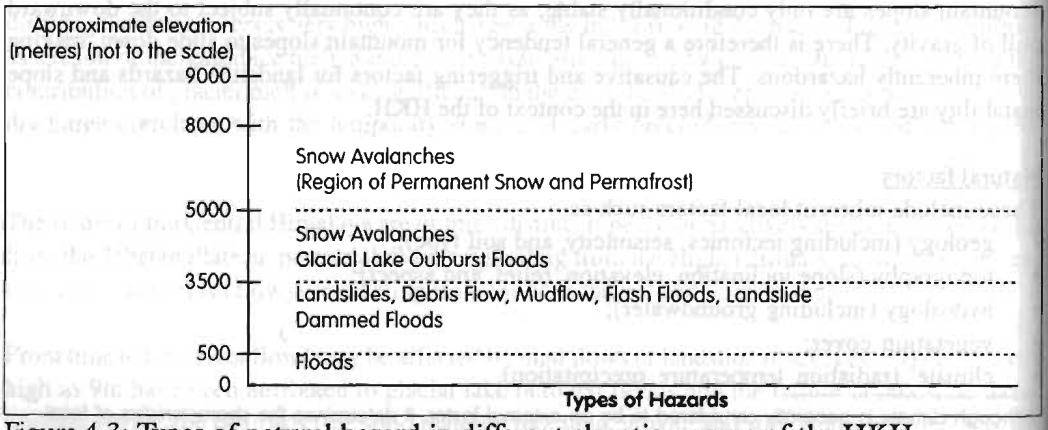

Figure 4.3: Types of natural hazard in different elevation zones of the HKH

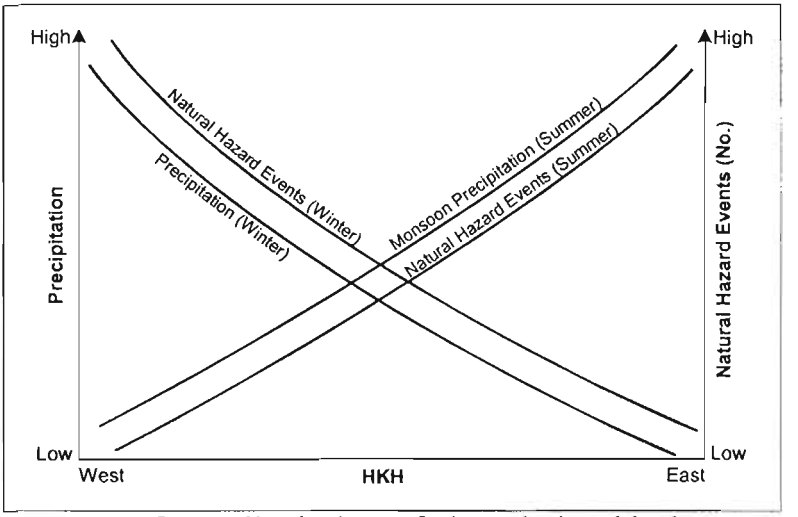

Figure 4.4: **Generalised view of the relationship between precipitation, natural hazards, and seasonality across the HKH**

Loss and damage from natural hazards

The consequences of extreme weather events are grave. Hundreds of lives and billion of dollars' worth of property and infrastructure are lost in the region every year as a result of landslides, debris flows, and floods, along with the permanent or temporary destruction of scarce agricultural lands. In China, for example, landslides alone are estimated to cost US$15 billion and cause 150 deaths annually (Li 1996). In the Indian Himalaya, average annual economic losses resulting from landslides are estimated to be about US$60 million (Thakur 1996). In Nepal, landslides and floods take approximately 400 lives and cause nearly US$ 20 million worth of infrastructure damage annually (Khanal 1996). Across the globe, the total loss of life and property resulting from landslides is far greater than that resulting from any other potentially predictable geological hazard (Leighton 1976).

Natural hazards: lack of information and understanding

Much of the discussion about environmental degradation in the HKH that started in the mid-1970s (Eckholm 1975 and 1976) focused on ecological concerns, particularly on deforestation caused by a fast-growing human and animal population and its impact on erosion and sedimentation. Since then the bulk of research work has attempted to quantify the relative roles, impacts, and contributions of human and natural processes in the region's environmental degradation. A recent study has shown that human processes are more influential in the degradation of micro-basins (the area drained by a stream or small river) whereas natural processes predominate in macro-basins (the area drained by a river and all its tributaries) (Grosjean et al. 1995).

The continued preoccupation with differentiating the roles of humankind and/or nature has somewhat overshadowed the fact that the HKH environment is not only inherently fragile but also subject to two powerful triggering factors: earthquakes and climate. Earthquakes are occasional occurrences; although their effects can be devastating they are difficult if not impossible to predict. In contrast, climate affects the environment regularly, and overall there is a better chance of predicting and avoiding climate-caused hazards. The effects are more intense during extreme weather

events — which have occurred with increasing frequency in recent years (Chalise and Khanal this volume).

Though still uncertain, the effects of climate change on the HKH region could include increased monsoon rainfall, enhanced precipitation outside the monsoon period, and shrinking of areas under snow and permafrost (Chalise 1994). These carry the risk of an increase in hazardous events associated with water flows, since both accumulation and melting of snow occur primarily in the summer in most parts of the HKH, and could increase the summer discharge and thus the risk of floods.

There has been insufficient research into climate and hydrology in the HKH. This is primarily because it is difficult and expensive to establish reliable monitoring systems. In addition, hydrometeorological services and research have a short history in many countries of the region. Although hydrological and climatic data for operational and forecasting purposes are regularly collected in many countries, the data are rarely shared. These difficulties are serious stumbling blocks for dealing with known or new uncertainties.

More attention should be focused on understanding, predicting and avoiding climate-based hazards so that increased loss of life, property, and infrastructure can be avoided.

Control and Management of Slope Instability

Although much progress has been made, new methods and techniques are still needed to deal with the problems of slope instability and associated hazards. The concerns of mountain people about slope instability or landslides on their own farmlands are no less important than those associated with infrastructural development. This aspect tends to be neglected, however, and priority is normally given to devising new methods and techniques to stabilise slopes or control landslides in areas of major infrastructural development projects. It is extremely important to consider the problems of slope instability within the overall context of integrated watershed management, including local communities perceptions of hazards, and their socioeconomic imperatives and cultural practices. It is equally important that any new method should not only be well tested for its suitability but should also be

- simple – easily understood, assimilated, and adopted by the community, and
- affordable – within the means of the community.

If they are not simple and affordable, new methods and techniques, however technically sound, are unlikely to be used widely.

Another important consideration in the development of methods to control and manage slope instability and landslides is the chronic lack of data for the HKH, and the continuing difficulty in obtaining them, in particular:

- long-term climatological, hydrological, ecological, and spatial data;
- short-term data for parameters such as precipitation intensity and infiltration;
- detailed information on local geology, land use; and land cover; and
- critical threshold values of rainfall for slope stability.

Considering these limitations, both simple methods such as direct measurements of rainfall and runoff, and innovative approaches such as remote sensing (RS) data and geographic information

systems (GIS), will need to be used in developing measures to stabilise slopes and landslides and for the mitigation of natural hazards in the HKH.

It is equally important to remember that a unique combination of 'extremes' (high population pressure, active geology, high elevations, very steep slopes, and intense seasonal rainfall) makes the HKH extremely vulnerable to natural hazards. Methods should be devised that help to mitigate and avoid disasters through better preparedness. An improved understanding of natural processes, their impacts on natural hazards, and their interrelationships with human processes on mountain slopes are the important elements to be considered while devising methods for the control and management of mass movements and slope instability in the HKH watersheds. It should also be remembered that although individual slopes can be stabilised in isolation, it is best to look at slope instability within the context of a watershed.

ICIMOD's Programme Activities in the Management of Natural Hazards

ICIMOD has accorded high priority to the problems of natural hazards, including slope instability, in the HKH within the overall context of its concern for sustainable development and improved living conditions for the region's inhabitants. From ICIMOD's very inception, its programme activities have focused on the problems of environmental degradation due to both natural and human processes. Programme activities relating to the management and control of natural hazards and slope instability are essentially geared towards building regional countries' capacities to deal with these problems. They are implemented in partnership with national institutions (GOs, NGOs, and academic bodies) and are developed through regional consultation and the integration of available knowledge, methods, and skills with new and sophisticated technologies and analytical systems. These programmes are mainly focused on training at various levels and raising awareness to create better preparedness for, and avoidance and mitigation of, disasters. Considering the challenges of natural hazards in the region and the lack of pertinent data, much work still needs to be done. However, the training organised by ICIMOD under its various programmes is expected to contribute significantly to enhancing human capacity to deal with these problems in the HKH countries at all levels.

References

Alford, D. (1992) *Hydrological Aspects of the Himalayan Region,* Occasional Paper No. 18. Kathmandu: International Centre for Integrated Mountain Development (ICIMOD)

Boesch, H. (1964) 'Zwei Jahre Wetterbeobachtungen in Nepal (1961-1963)'. In *Geographica Helvetica* 19:170-178

Boesch, H.; Groh, A. (1966) 'Wetterbeobachtungen 1963-1965 in Jiri, Nepal East No. 2'. In *Geographica Helvetica*, 21:69-74

Boucher, S. B. K. (1979) *Global Climate.* London: The English Universities Press Ltd

Chalise, S. R., (1994) 'Mountain Environments and Climate Change in the Hindu Kush-Himalayas'. In Benniston, M. (ed) *Mountain Environments in a Changing Climate.* London: Routeledge

Deoja, B; Dhital, M.; Thapa, B.; Wagner, A. (eds) (1991) *Mountain Risk Engineering Handbook, Vol 1.* Kathmandu: ICIMOD

Dhar, O.N. (1960) 'The Diurnal Varieties of Rainfall at Barahkshetra and Kathmandu During Monsoon Months'. In *Indian J. Meteorol. Geophys.* 11:153-156

Dhital, M. R.; Khanal, N.; Thapa, K.B. (1993) *The Role of Extreme Weather Events, Mass Movements and Land Use Changes in Increasing Natural Hazards*. Kathmandu: International Centre for Integrated Mountain Development (ICIMOD)

Dittmann, E. (1970) 'Statistische Untersuchungen zur Struktur der Niederschlaege in Nepal'. In Hellmich, W. (ed) *Khumbu Himal,* 17(2):47-60

Domroes, M.; (1979) 'Temporal and Spatial Variations of Rainfall'. In *Journal of the Nepal Research Centre*, 2(3):49-67

Eckholm, E. (1975) 'The Deterioration of the Mountain Environment'. In *Science,* 189:764-70

Eckholm, E. (1976) *Losing Ground*. New York: World Watch Institute and W.W. Norton & Co

Flohn , H. (1970) 'Beitraege zur Meteorologie des Himalaya'. In Hellmic, W. (ed) *Khumbu Himal,* 7(2): 25-45

Grosjean, M.; Hofer, T.; Liechti, R.; Messerli, B.; Weingartner, R.; Zumstein, S. (1995) 'Sediment and Soils in the Flood Plains of Bangladesh: Looking up to the Himalaya'. Paper Submitted to ICIMOD-IDRC Workshop on Resource Dynamics in the Middle Mountain Watersheds, Kathmandu, 10-12 April (unpublished)

Khanal, N.R. (1996) 'Assessment of Natural Hazards in Nepal'. A Report Submitted to the Research Division, Tribhuvan University, Kathmandu

Leighton, F.B. (1976) 'Urban Landslides: Targets for Landuse Planning in California' In Coates, D.R (ed) *Urban Geomorphology,* Special Papers, vol. 174, pp 37-60. Colorado: Geological Society of America

Li, T. (1996) *Landslide Hazard Mapping and Management in China*. Kathmandu: International Centre for Integrated Mountain Development (ICIMOD).

Myint, A. K.; Hofer, T. (1998) *Forestry and Key Asian Watersheds*. Kathmandu: International Centre for Integrated Mountain Development (ICIMOD)

Prasad, B. (1970) 'Diurnal Variation of Rainfall in India'. In *Ind. J. Meteorol. Geophys,* 21: 443-450

Rogers, P.; Lydon, P.; Seckler, D. (1989) *Eastern Waters Study.* Arlington (Virginia): ISPAN

Thakur, V.C. (1996) *Landslide Hazard Management and Control in India.* Kathmandu: International Centre for Integrated Mountain Development (ICIMOD)

Sharma, P. (1993) 'Population and Employment Challenges in the Mountains'. In Verghees, B.G. (ed) *Waters of Hope*. New Delhi: Oxford and IBH

5 Rainfall and Related Natural Disasters in Nepal

S.R. Chalise[1] and N.R. Khanal[2]
[1]As in Chapter 4
[2]Central Department of Geography
Tribhuvan University, Kirtipur
Kathmandu, Nepal

Water-induced disasters are common in Nepal, and are usually triggered by extreme weather events associated with heavy rainfall during the monsoon. Floods due to excessive rain, outbursts of glacial lakes and landslide dams, and the failure of dams and other man-made structures are directly or indirectly triggered by extreme weather events. Rainfall events exceeding 300 mm within a 24-hour period, which disturb both slope and channel equilibria on a regional scale, occur frequently in the country. The increasing frequency of such extreme precipitation events, together with changes in snow and ice cover due to global warming and other factors, have led to an increase in the number of natural disasters in the country.

The specific characteristics of slope and channel instabilities depend on the volume and intensity of the precipitation events that cause them. Experience shows that landslides, debris flows, and flood disasters can be accurately predicted based on rainfall characteristics and known thresholds for slope instabilities and floods, which can eventually help reduce damage to life and property. However, the hydrometeorological systems of mountain areas are very complex and poorly understood. Nepal's hydrometeorological network is still poor; the existing observational network is not capable of capturing the diversity of the mountain landscape, and there are difficulties in the generalisation of weather and climate because there is little or no long-term data. Methodological problems in generating data and a poor understanding of flow-path dynamics, water balance, and highland-lowland interaction have created problems in accurately predicting the magnitude of natural hazards. Special efforts are therefore required to improve the understanding of hydrometeorological processes and the thresholds for different types of natural hazards.

Introduction

Mountain environments in Nepal, as in other mountainous regions of the Hindu Kush-Himalaya, are fragile and extremely vulnerable to hazards and disasters, whether natural or man-made. Of the natural disasters occurring in Nepal, those induced by water are the most common. These are usually triggered by extreme weather events associated with heavy rainfall, which cause floods, landslides, debris flows, and widespread damage almost every monsoon. Between 1970 and 1995, an average of 186 people were killed annually and property worth more than US$ 7.25 million was lost as a result of landslides, and 230 people killed, 5,000 houses destroyed, and property worth US$12 million lost as a result of floods in the Terai and Inner Terai districts (Khanal 1996). In 1993, a record year, landslides and floods killed 1,336 people and caused more than US$ 70 million in damage (Khanal 1997).

The different types of landslides that occur in Nepal in the country have been described briefly in the previous chapter (Chalise, this volume). The common types of flood hazard can be described as follows:

- glacial lake outburst floods (GLOFs), such as those that occurred in the Sun Koshi River in 1935, 1964, and 1981, and in the Dudh Kosi in 1977 and 1985;

- floods due to the failure of landslide-dams, such as in the Burhi Gandaki in 1967 and 1968 and in the Tadi river in 1986;
- floods due to excessive rainfall, such as in Lele watershed (Lalitpur District) in 1981, Kulekhani in 1993, and Syangja in 1998; and
- floods triggered by the failure of man-made infrastructure, as in the case of the Bagmati barrage in 1993, the check dams and embankments along the Tinau river in Butwal in 1981, and the check dams along the Rapti river in Chitwan in 1990 and 1993 (Khanal 1996, 1999).

Spatial and Temporal Variation in Precipitation

The average area-weighted annual precipitation for Nepal is about 1,630 mm, with half of the country lying within the 1,500-2,000 mm precipitation zone (Chyurlia 1984). Both the temporal and spatial variations in precipitation are highly pronounced. Nearly 80% of all precipitation occurs during the monsoon (June-September), with 8% falling during the post-monsoon (October-January) and 12% during the pre-monsoon periods (Chalise et al. 1996; Chyurlia 1984).

Spatial variations in precipitation are strongly influenced by elevation and terrain. In Nepal, average annual precipitation ranges from only 163 mm at Lomangthang (Mustang) to 5,244 mm at Lumle (near Pokhara). The Trans Himalayan region, which includes Mustang and Manang, receives annual precipitation of less than 500 mm; the valleys of the Fore-Himalaya 500-1,000 mm; the Terai, Siwalik (Churia) Hills, lower Midlands valleys, and Dun valleys between 1,000 and 2,000 mm; and most slopes in the Midlands, Mahabharat Range, and Higher Himalaya between 2,000 and 3,000 mm (Khanal et al. 1998, and see Figure 3.8 in Upreti, this volume). A few pockets, such as Pokhara (Kaski) and Kanyam Tea Estate (Ilam) receive more than 3,000 mm of annual rainfall. Rainfall events exceeding 300 mm within a 24-hour period, which disturb both slope and channel equilibria on a regional scale, occur frequently (Khanal 1995a, 1995b). Precipitation as high as 540 mm in 24 hours, with a peak intensity of 70 mm per hour, has been recorded (Dhital et al. 1993; Chalise et al. 1996).

Extreme precipitation events and trends

Although the main triggering factor for floods and landslides is the rainfall associated with extreme weather events, a combination of both natural and anthropogenic factors and processes determine the extent and magnitude of such disasters for any affected area.

Table 5.1 summarises data for 24-hour events with rainfall amounts exceeding 100 mm in Nepal for the months from June to October during 1971-80 and 1981-90. Most of these events are confined to the June-September monsoon period, although heavy pre-monsoon showers can also occur in May.

In all four categories of 24-hour rainfall events, the number of events were higher in 1981-90 than in 1971-80 (Chalise 1998) indicating that the number of extreme precipitation events is increasing. Although considerable further work needs to be done to show that this is a real trend, and not

Table 5.1: Number of 24-hour rainfall events (June to October) between 1971-80 and 1981-90 in different categories of total rainfall

	Categories of total 24-hour rainfall amount (mm)			
	100-199	200-299	300-399	>400 mm
Number of events in 1971 to 1980	802	130	22	4
Number of events in 1981 to 1990	938	210	29	8

simply a reflection of improved observation, the impact of an extreme year, or other factors, it indicates the possibility that water-induced hazards and disasters may be increasing.

This trend is in agreement with a recent review of the potential impacts of climate change in the Hindu Kush-Himalaya: "increased monsoon rainfall, increase in rainfall intensity, and melting of snow, ice and permafrost with a consequent decrease in their surface areas" (Chalise 1994).

Studies of Rainfall/Event Relationships

Precipitation thresholds

A 'precipitation threshold' is the level of precipitation (rainfall duration and intensity) needed to initiate a landslide, debris flow, or similar event. The threshold is specific for a particular slope and hazard as it depends on a large number of factors like slope angle, soil type, vegetation cover, and soil saturation, not just on rainfall. However, generalisations can be made for different types of slope in different areas.

There have been no systematic studies on precipitation thresholds for the initiation of landslides and debris flows in the Himalaya that take into consideration all relevant parameters such as slope angle, geology, soil type, vegetation, and soil saturation. However, a number of simple studies have been made of the relationship between rainfall amount or intensity and number and size of landslides and debris flows. The results of some of these in different regions of the Himalaya are summarised below.

According to a Chinese study (Li and Wang 1992), cumulative precipitation of 50-100 mm in one to two days and daily precipitation of about 50 mm was enough to precipitate small-scale shallow landslides in their region of study; two-day cumulative precipitation of 150-200 mm and daily precipitation of 100 mm, was enough to precipitate medium-scale landslides, and two-day cumulative precipitation of more than 250 mm led to an abrupt increase in the number of large landslides of debris and rock. Intense rainfall, even of short duration, caused shallow and quick landslides, whereas prolonged rainfall precipitated deep-seated and slow landslides. Li and Wang used measurements of rainfall intensity over 10-minute intervals (to identify short bursts of intense rainfall), of rainfall on the day before, and of rainfall immediately before an event, to predict the occurrence of landslides and debris flows. Of the 27 landslides and debris flows predicted, 25 actually occurred (Li and Wang 1992). This indicates that with sufficient information and knowledge of the effects of intense and prolonged rainfall it may be possible to predict landslide and debris flow events.

In another study in the Darjeeling area, shallow landslides and slumps on steep slope segments were observed when 24-hour rainfall exceeded 130-150 mm or three-day rainfall 200-240 mm. Slumps, landslides, and debris flows on a larger scale were observed after 24-hour rainfall exceeding 250 mm or three-day rainfall 350 mm. Extensive and simultaneous debris flows were observed after 24-hour rainfall of more than 300 mm or three-day rainfall of more than 600 mm (Froehlich and Starkel 1987; Froehlich et al. 1990).

In a study in the Kolpu Khola area of central Nepal, the precipitation threshold was found to be 100mm of rain within 24 hours. The frequency of landslides was observed to increase later in the monsoon, presumably as a result of increased groundwater levels and soil saturation (Caine and Mool 1982).

Number, area and volume of mass-movements

During a normal year, the erosion rate in the Nepal Himalaya is estimated to be less than 2 mm, in the Darjeeling Himalaya 0.5-5 mm. However, catastrophic occurrences can have a marked impact. During one three-day period in 1968 (3-5 October) between 600 mm and 1,200 mm of rain fell in Darjeeling precipitating some 20,000 landslides. It is estimated that more than 2% of the surface area covered by forest and 20-25% of the surface area under cultivation was transformed by mass-movements, and an average of 20 mm of soil was removed across the region by that single catastrophic event. River channels and valley floors were totally changed, and there were material deposits, of up to 10 metres (Agrawal and Chak 1991; Froehlich et al. 1990).

In 1993 (19-20 July), more than 2,000 small and large landslides occurred along Nepal's Tribhuvan Highway and between 23 and 40% of the total surface area in the vicinity of Okhar Bazaar and Daman villages in the Kulekhani basin was affected by the landslides (Dhital et al. 1993). Similarly, a cloudburst on 30 September 1981 triggered 46 landslides per sq.km in the Lele watershed, south of Kathmandu (Manandhar and Khanal 1988).

On 30 August 1998, a 24-hour rainfall of 238 mm in Syangja triggered many landslides, debris flows, and floods, killing 55 persons and destroying 640 houses. A total of 1,137 landslides was counted within an area of 28 sq.km; 65% were small (average width 12m, length 17m) and the rest were large (average width 30m, length 40m). Thus 2.25% of the total land area was occupied by the landslides initiated by this event. The estimated average depletion-zone depth was 1m, giving an average denudation rate of more than 22.5 mm, with a total estimated weight of 40,500 tonnes per sq. km or 405 tonnes per ha (based on the average soil density of silty gravel of 1.8 mg per cu.m) (Khanal 1999).

Issues

While losses due to natural disasters can be minimised by the better understanding and forecasting of weather, climate, and hydrological behaviour, there are a number of obstacles to doing so in the HKH in general and Nepal in particular. These include the lack of well-developed observational networks and thus of data, and the complexity of and variability within the region.

The region's inaccessibility, remoteness, and hazards pose serious difficulties in maintaining and expanding the observation network. At the same time, lack of funds means that many of the stations that have been established have been abandoned and that others are not operating for a significant portion of the year (Kundzewicz and Kraemer 1998; Chalise and Khanal 1996; Hossain 1998). In Nepal, only 264 pluviometric (precipitation measurement) stations have kept records for more than five years, whereas 600 to 1,500 stations would be required for good representation of the country as a whole (Chalise et al. 1996). This limited pluviometric network is a serious weakness when it comes to estimating the total precipitation (input) for the study of hydroecological behaviour in the river basins of the country. Remote sensing has tremendous potential as an alternative for studying the hydrology in the HKH area. However, the lack of baseline data has made it difficult to calibrate and verify the available remotely-sensed data, while the high cost of such data has inhibited the expansion of the network.

Not only is there insufficient data, the highly variable nature of the region also complicates understanding of the various components and processes of its hydrological systems (Rodda 1994; Lang 1998; Jodha et al. 1992; Chalise 1994, 1998). The region's climate and hydrology are very complex and vary highly within short distances as a result of differences in altitude, and slope steepness

and aspect. Moreover, the frequent occurrence of water-related natural hazards such as glacial lake outburst floods (GLOFs), avalanches, landslides, debris flows, and landslide-dam failures have made it difficult to estimate discharges accurately (Lang 1998; Kundzewicz and Kraemer 1998; Khanal et al. 1998; Shah et al. 1998). Systematic wind-induced errors also affect estimates of precipitation input in mountain areas (Lang 1998). It is an unfortunate paradox that the physical difficulties and costs of developing and maintaining an observational network are greatest in mountainous areas – the very place where a dense network is most needed to capture the diversity of the landscape. At present the density of hydrometeorological stations in the whole HKH region is much less than that recommended by WMO (Chalise et al. 1996).

The absence of long-term data and the extremely limited number of meteorological stations – particularly at elevations above 2,500m – have seriously hindered a better understanding of climates in the HKH (Barry 1981; Mani 1981; Das 1983; Chalise 1986; Hofer and Messerli 1997). Reliable data on precipitation is probably the most critical need for proper planning and management of water resources in the region. However, true measurements of precipitation are problematic and of limited value, not only because of the difficulty in installation, maintenance, and running of stations but also because of the only local-scale validity of the observations obtained (Domroes 1979). Little attention has been paid so far to daily rainfall in the Himalaya. In the absence of data, and given the very low density of hydrometeorological stations, it is very difficult to investigate water balance (the input/output/storage relationship of water in a given area) for any watershed. Similarly, lack of adequate reliable data also inhibits systematic assessment of the impact of upland activities and events on lowland areas (highland-lowland interactions) or the base-flow contribution of highland areas (flow from groundwater sources rather than from precipitation events) (Khanal et al. 1998; Hofer and Messerli 1997

The rivers of the HKH are also characterised by very high sediment loads and high bedloads (the solid material like sand, gravel, and sometimes boulders pushed down by rivers rather than being carried in suspension) resulting from landslides, debris flows, and GLOFs. Information on sediment loads, and particularly on bedloads, is very scanty, especially for headwater regions where the measurement of bedloads remains a major challenge (Khanal et al. 1998; Kattlemann 1987).

There are no good models of the climatic and hydrological systems of the HKH mountain basins, partly because the hydrology of high mountain areas is itself not very well developed, and partly because the peculiar combination of extremely high altitudes, steep slopes, and intense seasonal monsoonal rainfall limits and even precludes the application of the hydrological techniques, principles, and models developed in temperate regions. Special efforts are required to develop models specific to this region that can be combined with global models.

Even if we had sufficient data from the past to enable understanding and prediction of the events associated with rainfall, and models of the climatic and hydrological systems, we still couldn't be sure if they would hold true in the future because the potential impacts of climate change remain unknown. Lack of long-term climatological data has hindered the assessment of climate change impacts on the region — a subject that has only recently started to receive some attention (Gupta and Pachauri 1989; Chalise 1994). Most of the information available comes from glacier studies, which have received a lot of attention in the HKH (Higuchi 1978; Mayewski and Jeschke 1979; Miller 1989; Miller and Marston 1989; Zhang 1984; Wang et al. 1984, Chen et al. 1989; Zheng et al. 1990, Young and Hewitt 1993). But further work is necessary to ascertain the relationship between glacial fluctuations and climate change.

The importance of hydrological research has not been well understood at the policy level in the region. This is mainly the result of the inability of regional institutions to influence decision-makers at the policy level, and also partly due to the fact that scientific research in general is not considered a priority by the countries of the region.

References

Agrawal, A.; Chak, A. (eds) (1991) *State of India's Environment, A Citizen's Report 3: Flood Plains and Environmental Myths*. New Delhi: Centre for Science and Environment

Barry, R.G. (1981) *Mountain Weather and Climate*. London: Methuen

Caine, N.; Mool, P. K. (1982) 'Landslides in Kolpu Khola Drainage, Middle Mountains, Nepal'. In *Mountain Research and Development*, 2(2):157-173

Chalise, S. R. (1986) 'Ecology and Climate in the Mountain System: A Review'. ICMOD Working paper No. 12, Kathmandu: ICIMOD (unpublished)

Chalise, S. R. (1994) 'Mountain Environments and Climate Change in the Hindu Kush- Himalayas'. In Beniston, M. (ed) *Mountain Environments in a Changing Climate*, pp 382-404. London: Routledge

Chalise, S. R. (1998) 'Headwaters in Changing Climates: A Review of Hydrological and Related Issues in the Hindu Kush-Himalaya'. In: Singh, R.B. (ed) *Ecological Techniques and Approaches to Vulnerable Environment: Hydrosphere-Geosphere Interaction*, pp 177-197. New Delhi: Oxford and IBH Publishing Co.Pvt. Ltd

Chalise, S. R.; Khanal, N. R. (1996) *Hydrology of the Hindu Kush-Himalayas*, A Report of the Regional Workshop, March 23-24. Kathmandu: ICIMOD

Chalise, S.R. (1997) 'High Mountain Hydrology in Changing Climates: Perspectives from the Hindu Kush-Himalaya'. In Molnar, L.; Miklanek, P. and Meszaros, L. (eds) *Developments in Hydrology of Mountainous Areas*. Paris: UNESCO IHP-IV Projects H-5-5/H-5-6, 23-31

Chyurlia, J.P. (1984) 'Water Resources' Report'. Kathmandu: Land Resource Mapping Project

Das, P.K. (1983) 'The Climate of the Himalaya'. In Singh and Kaur (eds) *Studies in Eco Development Himalayas Mountains and Men*. Lucknow (India): Print House

Dhital, M.; Khanal, N.; Thapa, K. B. (1993) 'The Role of Extreme Weather Events, Mass Movements, and Land Use Changes in Increasing Natural Hazards', A Report of the Preliminary Field Assessment and Workshop on Causes of the Recent Damage Incurred in South-central Nepal (July 19-20, 1993). Kathmandu: ICIMOD

Domroes, M. (1979) 'Temporal and Spatial Variations of Rainfall'. In *Journal of the Nepal Research Centre*, 2(3): 49-67

Froehlich, W.; Gill, E.; Kasza, I.; Starkel, L. (1990) 'Thresholds in the Transformation of Slopes and River Channels in the Darjeeling Himalaya, India'. In *Mountain Research and Development*, 10(4): 301-312

Froehlich, W.; Starkel, L. (1987) 'Normal and Etreme Monsoon Rains - Their Role in the Shaping of the Darjeeling Himalaya'. In *Studia Geomorhologica Carpatho – Balcanica*, 21(Karkow): 129-156

Gupta, S.; Pachauri, R.K. (1989) *Global Warming and Climate Change Perspectives from Developing Countries*. New Delhi: Tata Energy Research Institute (TERI)

Higuchi, K. (1978) 'Outline of Glaciological Expedition of Nepal'. In *Seppyo* 3:1-3

Hofer, T.; Messerli, B. (1997) 'Floods in Bangladesh: Process Understanding and Development Strategies'. A Synthesis Paper Prepared for the Swiss Agency for Development Cooperation, Institute of Geography, University of Berne

Hossain, M.M. (1998) 'Present Status of Studies on Hydrological Aspects in Bangladesh'. In Chalise, S. R.; Hermann, A.; Khanal, N.R.; Lang, H.; Molnar, L. and Pokharel, A.P (eds) *Proceedings of the International Conference on Ecohydrology of the Mountain Areas*, pp 35-47. Kathmandu: ICIMOD

IPCC, (1996) *Climate Change 1995: Impacts, Adaptations and Mitigation of Climate Change, Scientific-Technical Analyses.* New York: Cambridge University Press

Jodha, N.S.; Banskota, M.; Pratap, T. (eds) (1992) *Sustainable Mountain Agriculture: Perspectives and Issues,* (2 vols). New Delhi: Oxford and IBH Publication Co. Pvt. Ltd

Kattelmann, R. (1987) 'Uncertainty in Assessing Himalayan Water Resources'. In *Mountain Research and Development,* 7(3), 279-286

Khanal, N.R. (1996) 'Assessment of Natural Hazards in Nepal'. Report Submitted to the Research Division, Tribhuvan University, Kirtipur, Kathmandu, Nepal (unpublished)

Khanal, N. R. (1995a) 'Mass Movements in Nepal Himalaya'. Paper Presented at the Regional Workshop on Landslide Hazard Management and Control in the Hindu Kush-Himalayas, July 12-14, ICIMOD, Kathmandu (unpublished)

Khanal, N.R. (1995b) 'The 1993 Extreme Event in Nepal and Its Consequences'. Unpublished paper presented at the International Himalayan/Tibetan Plateau Paleoclimate Workshop, 2-7 April 1995, Kathmandu

Khanal, N.R., (1997) 'Floods in Nepal'. In *River Flood Disaster a Report of ICSU SC/IDNDR Workshop, 1996,* pp 33-46. Koblenz: Deutsches IHP/OHP – National Komitee

Khanal, N.R. (1999) 'Study of Landslides and Flood Affected Areas in Syangja and Rupandehi Districts of Nepal'. Report Submitted to the Mountain Natural Resources Division, ICIMOD, Kathmandu (unpublished)

Khanal, N.R.; Chalise, S. R.; Pokhrel, A. P. (1998) 'Ecohydrology of River Basins of Nepal'. In Chalise, S. R.; Hermann, A.; Khanal, N.R.; Lang, H.; Molnar, L. and Pokharel, A.P (eds) *Proceedings of the International Conference on Ecohydrology of High Mountain Areas,* pp 49-61. Kathmandu: ICIMOD

Kundzewicz, Z. W.; Kraemer, D. (1998) 'Striving Towards Assessment of Mountain Water Resources'. In Chalise, S. R.; Hermann, A.; Khanal, N.R.; Lang, H.; Molnar, L. and Pokharel, A.P (eds) *Proceedings of the International Conference on Ecohydrology of High Mountain Areas,* pp 175-186. Kathmandu: ICIMOD

Lang, H. (1998) 'Mountain Ecohydrology: Issues and Challenges'. In Chalise, S. R.; Hermann, A.; Khanal, N.R.; Lang, H.; Molnar, L. and Pokharel, A.P (eds) *Proceedings of the International Conference on Ecohydrology of High Mountain Areas,* pp 3-6. Kathmandu: ICIMOD

Li, T.; Wang, S. (1992) *Landslide Hazards and Their Mitigation in China.* Beijing: Science Press

Manandhar, I.N.; Khanal N.R. (1988) 'Study on Landscape Processes with Special Reference to Landslides in Lele Watershed, Central Nepal'. Report Submitted to the Research Division, Tribhuvan University, Kathmandu (unpublished)

Mani, A. (1981) 'The Climate of the Himalaya'. In Lall, J. and Moddie, S. (eds) *The Himalaya, Aspects of Change*, pp 2-15. Delhi: Oxford University Press

Mayewski, P.A.; Jeschke, P.A. (1979) 'Himalayan and Trans-Himalayan Glacier Fluctuations since AD 1812'. In *Arctic and Alpine Research,* 11(3): 267-287

Miller, M.M. (1989) *Comparative Accumulation Regimes of Himalayan and Alaskan Neves and the Issue of Global Warming, Environment and Society in the Manaslu-Ganesh Region of the Central Nepal Himalaya.* Idaho: Foundation for Glacier and Environmental Research and University of Idaho

Miller, M.M.; Marston, R.A. (1989) *Glacial Response to Climate Change and Epeirogency in the Nepalese Himalaya, Environment and Society in the Manaslu-Ganesh Region of the Central Nepal Himalaya.* Idaho: Foundation for Glacier Research and University of Idaho

Rodda, J. C. (1994) 'Mountains – A Hydrological Paradox or Paradise?' In *Hydrologie Kleiner Enzugsgebiete Gedenkschrift Hans M. Keller Beitrage zur Hydrologie der Schweiz,* 35: 41-51

Shah, S. M.S.; Khan, A.A.; Khan M.T. (1998) 'Present Status and Problems of the Hydrology of Mountainous Areas of Pakistan'. In Chalise, S. R.; Hermann, A.; Khanal, N.R.; Lang, H.; Molnar, L. and Pokharel, A.P (eds) *Proceedings of the International Conference on Ecohydrology of High Mountain Areas,* pp 89-101. Kathmandu: ICIMOD

Wang, W.; Huang, M.; Cheng, J. (1984) 'A Surging Advance of Balt Bare Glacier, Karakoram Mountains'. In Miller, K.J. (ed) *The International Karakoram Project,* 76-83. Cambridge: Cambridge University Press

Zhang, Y. (1984) 'Recent Variations of Some Glaciers in the Karakoram Mountains'. In Miller, K. J (ed), *The International Karakoram Project,* pp 39-50. Cambridge: Cambridge University Press

Zheng, B.; Jiao, K., Q.; Li, G.; Fushimi, H. (1990) 'The Evolution of Quaternary Glaciers and Environmental Change in the West Kunlun Mountains, Western China'. In *Bulletin of Glacier Research,* 8: 61-72

6 Water-Induced Disasters in the Himalaya: Case Study of an Extreme Weather Event in Central Nepal

K.B. Thapa
Central Department of Hydrology and Meteorology
Tribhuvan University, Kirtipur Campus, Kathmandu, Nepal

A cloudburst over the central region of the Bagmati catchment on 19-20 July 1993 caused catastrophic landslides and debris flows. The flood, estimated to be about 16,000 cumec, damaged the Bagmati barrage and flooded Sarlahi and Rautahat districts in the Terai. Tistung and Hariharpur Garhi recorded the highest point values for 24-hour rainfalls, of 540 mm and 483 mm respectively. Mountainous catchments are vulnerable to such events, which are quite frequent but still unpredictable.

This paper provides information about water-induced disasters in Nepal in general and the 1993 Bagmati event in particular, and discusses the contributing factors and implications for future planning.

Introduction

The rivers in Nepal are categorised into three grades, based on their sources and dry season flow. The first-grade rivers – namely the Karnali, Narayani, and Sapta Kosi – originate north of the Himalayan range and have substantial dry-season flow. Second-grade rivers, such as the Bagmati, originate further south (mostly in the Mahabharat range) below the snowline and are fed by groundwater and springs in the dry season. Third-grade rivers, originating in the lower Siwalik (Churia) Range, have very low annual discharges and can even dry up in the dry season. The annual mean streamflow in Nepal is about 200 x 10^9 cu.m, of which about 72% is contributed by the first-grade rivers. About 75-80% of the total annual surface water flow out of the country occurs during the monsoon season.

The present case study pertains to the extreme weather event of 19-20 July 1993 over the Bagmati River watershed in central Nepal (Figure 6.1).

Floods, Debris Flows, and Landslides Triggered by the Extreme Weather Event of 19-20 July 1993

The rainfall event that occurred over the Kulekhani portion of the Bagmati watershed on 19-20 July 1993 produced Nepal's highest-ever recorded 24-hour rainfall. During the 1993 monsoon period in Nepal, more than 1,300 people lost their lives and 60,000 hectares of arable lands were damaged. About 67 small and large irrigation projects, 337 km of highways, and many bridges were also destroyed (DPTC 1994).

Some observations and conclusions made from a reconnaissance study fielded by ICIMOD (Dhital et al. 1993) in the worst-affected regions are important. Table 6.1 summarises past landslides and floods in some of the study areas. Such disasters are clearly quite frequent but occur irregularly.

Meteorological Aspects of the Event

A monsoon trough which developed over the foothills of central Nepal on 19-20 July 1993 brought record-setting rainfall to the upper regions of the Mahabharat Range of Makawanpur and Dhading

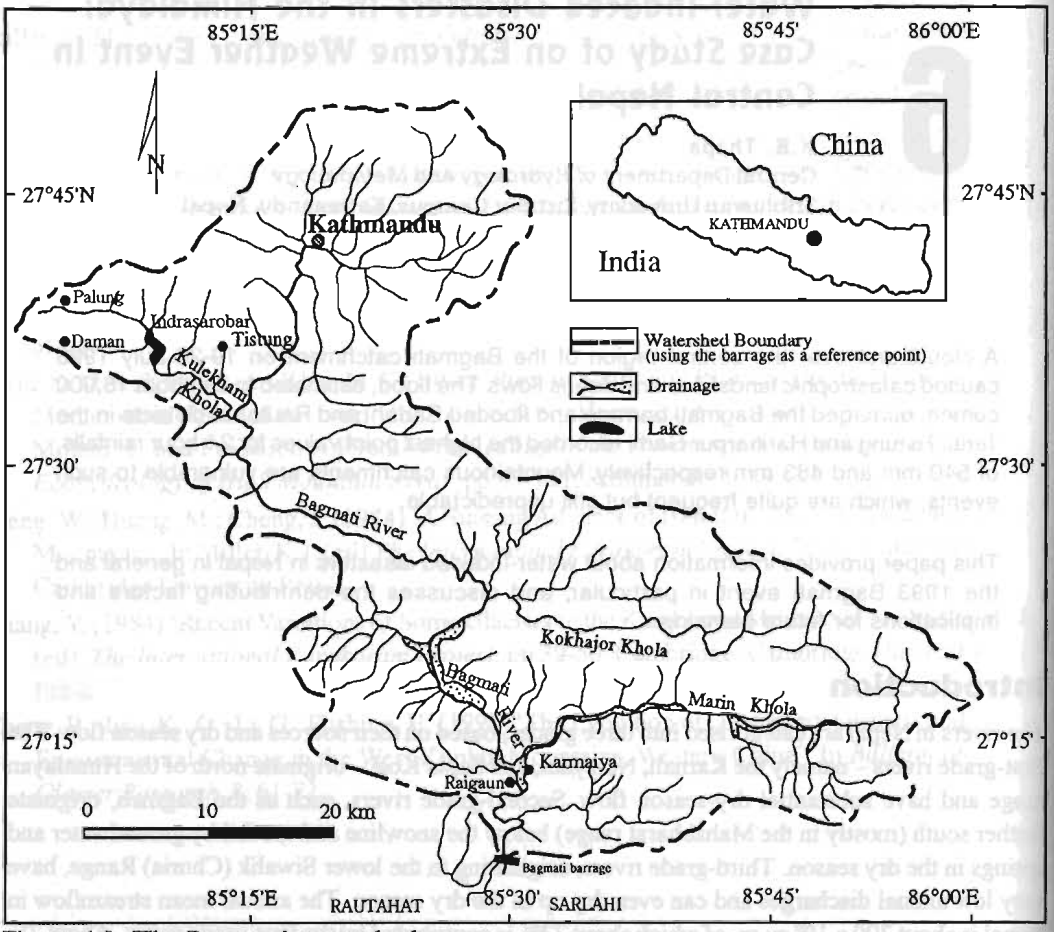

Figure 6.1: **The Bagmati watershed**

Table 6.1: Major landslides and floods associated with high-intensity rain in the study area (Dhital et al. 1993)

Place	Major events
Daman- Palung	1915 (more or less equal to 1993 event), 1954, 1979, and 1993
Phedigaun-Agra	1954, 1970, 1971, 1974, 1985, and 1993
Milche	1954 (bigger than the 1993 flood) 1970, 1971, and 1981 (more sediment and logs observed than in 1993 event)
Saldhara	1954 and 1970 (many landslides on the upper slopes of the Mahabharat Range)
Baldeu	1970 local rain (a bigger flood than the 1993 event)
Raigaun	1954 (more or less equal to the 1993 event), 1970 (no local rain but large flood), 1984, and 1993 (heavy local rainfall with thunderstorms and landslides)
Bhimphedi	1915, 1954 (Dhorsing Bazaar and Pati Bazaar swept away), 1973, 1984, 1986, 1990, and 1993
Manahari	1954, 1961, 1970, and 1984 (slightly smaller than the 1993 event)
Bhandara-Khumroj	1970, 1979, 1990, and 1993

districts. Disastrous floods, debris flows, and landslides were observed all over the Bagmati, Trisuli, and Rapti watersheds.

In the 24 hours from 8:00 am on July 19 to 8:00 am on July 20 1993 400-450 mm of rain (average isohyetal values) fell in the northern regions of the Kulekhani watershed and the central region

of the Bagmati catchment (Figure 6.2). During the evening of July 19 incredible rainfall of 540 mm at Tistung and 483 mm at Hariharpur Garhi (single point measurements) were recorded, which are respectively the highest and the fourth highest rainfalls ever recorded in Nepal. Tistung and Simlang received 65 mm and 73 mm of rainfall respectively in just one hour. The Bagmati catchment as a whole (2,720 sq.km upstream of the barrage) received intense rainfall.

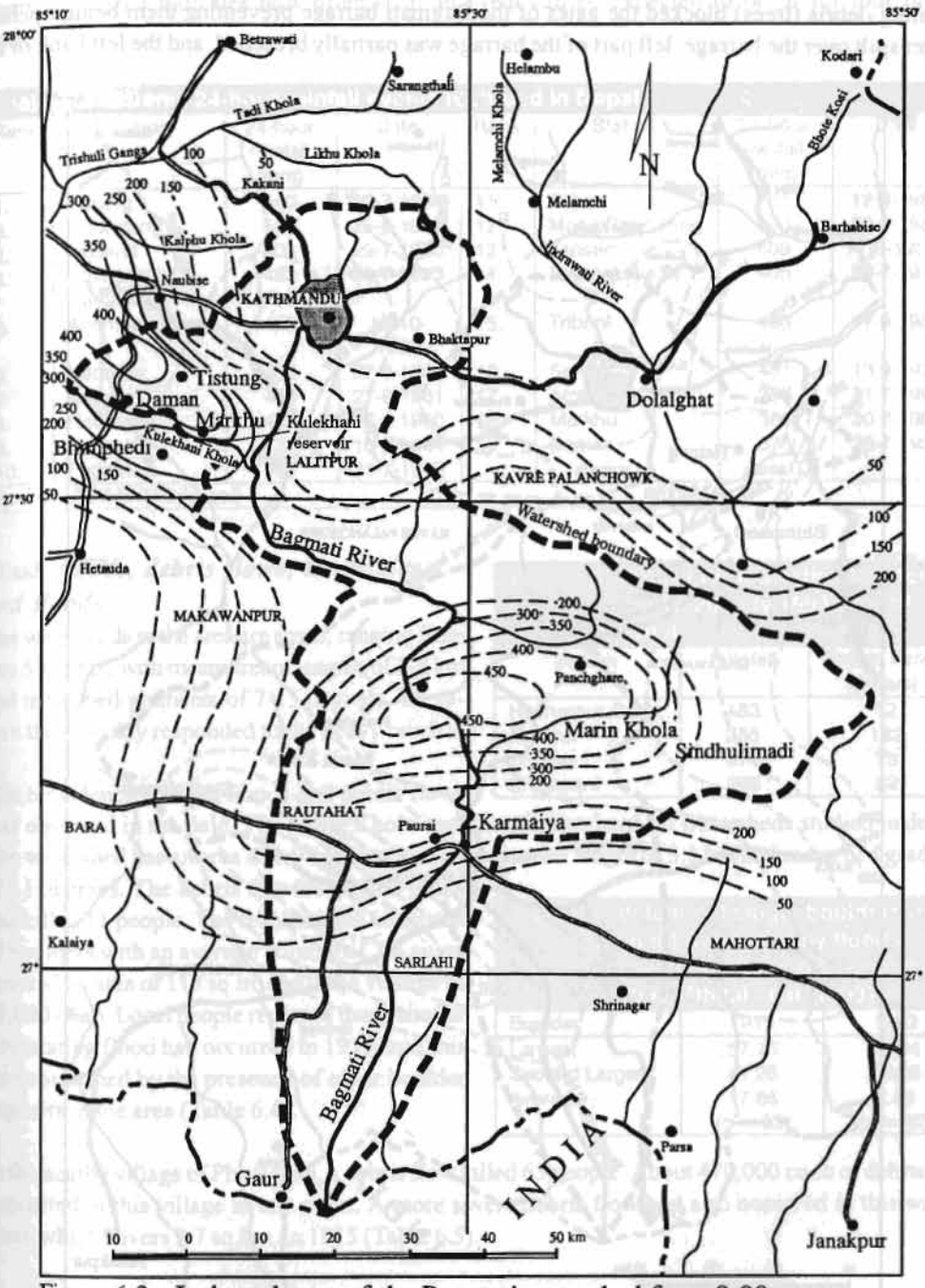

Figure 6.2: **Isohyetal map of the Bagmati watershed from 8:00 am on July 19 to 8:00 am on July 20 1993 (isohytes in mm)**

The following day (8:00 am on July 20 to 8:00 am on July 21 1993) this intense pocket of rainfall shifted over to a region about 25 km to the east of the Bagmati Barrage (Figure 6.3) (Shakya 1995). It appears that that as the flood swept downstream the intense rainfall pocket also shifted downstream towards the south, resulting in coincident arrivals of various tributary floods with the main stream flood course.

Floating debris (trees) blocked the gates of the Bagmati barrage preventing them being opened. Water spilt over the barrage, left part of the barrage was partially breached, and the left bank of the

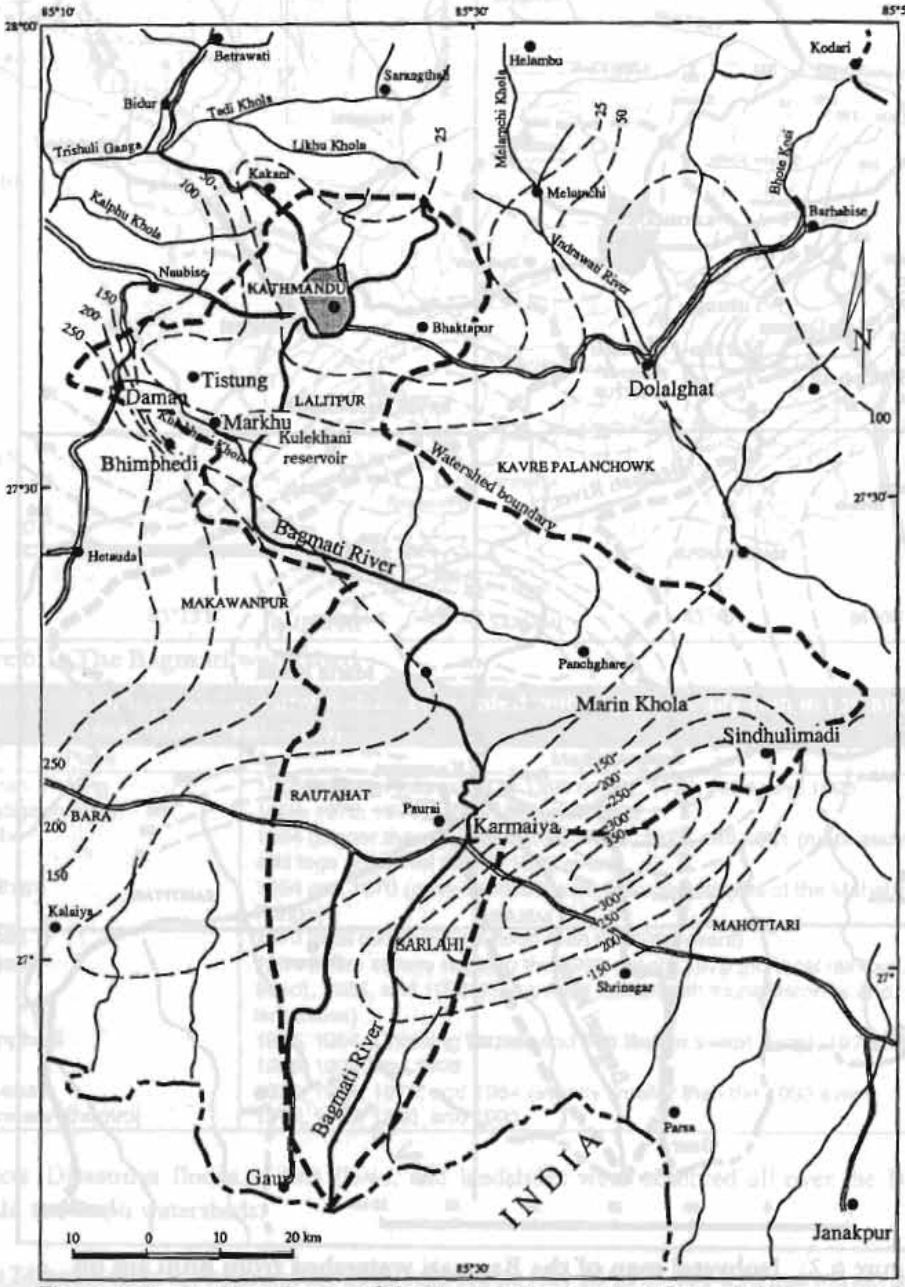

Figure 6.3: Isohyetal map of the Bagmati watershed from 8:00 am on July 20 to 8:00 am on July 21 1993 (isohytes in mm)

river and was disrupted at midnight on the 20 July – which resulted in major flooding in Sarlahi and Rautahat districts to the south in the Terai.

Table 6.2 puts the 1993 Bagmati event in context: of the 19 24-hour rainfalls registering 375 mm or greater that have been recorded by meteorological stations in Nepal, six occurred during this one event. Table 6.3 indicates how often such an event can be expected to occur for four of the stations.

Table 6.2: Extreme 24-hour rainfall events recorded in Nepal

Rank	Station	24-hour rainfall (mm)	Date	Rank	Station	24-hour rainfall (mm)	Date
1.	Tistung	540	20-7-1993	11.	Bajura	431	12-9-1980
2.	Ghumtang	505	25-8-1968	12.	Mane Bhanjyang	420	30-9-1981
3.	Musikot	503	29-7-1960	13.	Tansen	409	7-9-1959
4.	Hariharpur Garhi	483	20-7-1993	14.	Barahakshetra	405	28-7-1974
5.	Anarmani Berta	473	10-10-1959	15.	Tribeni	403	17-9-1984
6.	Hetauda	453	27-8-1990	16.	Semari	401	13-9-1982
7	Batuwa	446	27-8-1981	17.	Amlekhganj	399	21-7-1993
8.	Hetauda	438	27-8-1990	18.	Markhu	385	20-7-1993
9.	Kankai	437	16-9-1984	19.	Daman	375	20-7-1993
10.	Patharkot	437	21-7-1993				

Source: (DHM/HMG/Nepal)

Flash floods, debris flows, landslides and floods

The watersheds in the area are small, ranging from 2 to 50 sq.km, with mean stream lengths of 3-8 km and mean bed gradients of 7-15 degrees. Therefore they quickly responded to the heavy rainfall.

Table 6.3: Return-period estimation for the 19-20 July 1993 rainfall event

Station	Rainfall	Return Period (Years)
Hariharpur Garhi	483	52
Markhu	385	132
Daman	375	78
Chisapani	295	52

Much evidence of flash floods and debris flows was observed in the field. The Kitini Khola was one of a few hard-hit watersheds studied in detail. The watershed has an area of 1.9 sq.km with a mean stream length of 3.1 km and mean bed gradient of 11 degrees. The debris flow destroyed farms and killed 11 people. The resulting fan consisted of boulders with an average volume of 7.6 cu.m, covered an area of 118 sq.m, and had a volume of 59,000 cu.m. Local people reported that a similar devastating flood had occurred in 1915, and this was confirmed by the presence of older boulder deposits in the area (Table 6.4).

Table 6.4: Volume of single boulders (in cu.m) deposited by floods on the Kitini Khola in 1915 and 1993 (Dhital et al. 1993)

Boulder	1915	1993
Largest	57.75	17.64
Second Largest	41.26	16.60
Average	17.86 (n = 33)	7.56 (n = 32)

In the nearby village of Phedigaun, a debris flow killed 65 people. About 470,000 cu.m of debris was deposited in this village in one night. A more severe debris flow had also occurred in this watershed, which covers 3.7 sq.km, in 1915 (Table 6.5).

A debris flow along the Agra Khola, in an adjacent watershed, washed away four piers of a bridge on the Prithvi Highway. The peak discharge was estimated to be about 1,800 cumec. A field survey

Table 6.5: **Volume of single boulders (in cu.m) deposited by floods on the Phedigaun Khola in 1915 and 1993** (Dhital et al. 1993)

Boulder	1915	1993
Largest	109.8	52.5
Second Largest	57.98	20.4
Third Largest	46.62	11.9
Fourth Largest	5.07	11.8

indicated that debris had raised the bed by 5m along a reach of 17 km (average width 40m).

The debris flow on the Jurikhet Khola, with a 9 sq.km catchment area, destroyed the Kulekhani penstock pipe (the water conduit from the intake to the turbines in a hydroelectric plant). Large boulders, 5-10m in diameter, filled the channel. Further downstream, a tributary of the Mandu Khola destroyed a village and the intake of a second Kulekhani hydropower project.

Many regions of the Bagmati catchment were more or less saturated with antecedent rain from May and June, and the intense rain of 19-20 July triggered uncountable landslides. There were more than 2,000 landslides along the Tribhuvan Highway alone. Landslides, rockslides, bank collapses, and gully erosion created sources for debris flows. Undercutting of steep bank slopes triggered more landslides.

The Kulekhani reservoir received a very large amount of sediment from the nearby watersheds that received the cloudburst. Many landslides and remnants of debris flows were observed all along the field route from Palung to Raigaun. Flood marks 10m above the normal river level were observed near Raigaun. The Kokhajar and Marin Kholas, tributaries of the Bagmati river (Figure 6.1), contributed substantially to the flood event. The peak flood estimated at Pandhero Dobhan, about 1.5 km upstream of the Bagmati barrage, was 16,000 cumec; the barrage was designed for a maximum flood of 8,000 cumec.

Discussion

Although the major factor that precipitated the 1993 disaster was climatic – exceptional rainfall of high intensity – there were many other contributory factors, some unavoidable, some that could have been influenced or foreseen. The major factors that together contributed directly or indirectly to the occurrence of the disaster, and its extent and impact, (and could play a role in the development of other similar disasters in the region) can be summarised as follow.

Natural causative factors

Geological

- The tectonically active mountain system – the mountains are rising, thus they have very steep slopes and intense down-cutting activities, and there is much reworking of materials previously deposited along streams. Most large, deep landslides are located along streams; recently formed fans are more vulnerable.
- Weak geological structure – joint systems of rocks produce large boulders.

Climatic

- Seasonal and daily temperature variation
- Monsoon rainfall

Hydrological

- Sharp bends in river courses causing partial damming and deposition of bed materials (areas where tributaries merge more or less at right angles are much more vulnerable to flooding)

Past events

- Earthquakes, precipitation, and landslide activities (reinitiating landslides)

Other factors

Population pressures

- Encroachment on marginal and forest lands as a result of rapid population growth (cultivation on very steep slopes – up to 45° – and maize-based subsistence agriculture, both of which increase slope instability)
- Free access to common lands (no need to grow trees on farmland)
- Deforestation and frequent forest fires
- Lack of long-term understanding of the environment in recently inhabited areas, particularly in the Siwaliks (Churia), Bhabar, and Inner Terai
- Construction of private and public buildings on unsuitable land, particularly in accessible areas, without regard for potential risks
- Extraction of sand and gravel along streams (building materials)

Development activities

- Horticultural farms in previously forested areas
- Kulekhani hydro project (forced people to encroach on marginal land)
- Road construction (pressure on forests)
- Quarrying on steep slopes and on steep stream banks (causing a rise in bed levels and lateral erosion)

Technical shortcomings

- Lack of historical records and their application in designing major construction works like the Bagmati barrage, penstock pipes, the check dam on the Rapti, and many bridges
- Lack of communication systems (information exchange and warning)

Lessons Learnt

To avoid disasters on this scale in the future, it is important that steps are taken to ensure that constructions are less vulnerable and that people can be warned of the situation. It is essential for the proper design of infrastructure such as bridges, dams, and barrages that rainfall frequency analyses are made and that there is a sufficiently good network of hydrometeorological stations to enable rainfall-runoff studies. Warning stations should be installed so that people can be warned about approaching floods, and debris lying idle in channels upstream of the infrastructure mapped so that potential debris flows during flash floods can be predicted.

References

Baidya, S. (1996) 'Rainfall Analysis for Bagmati Catchment'. M. Sc. Dissertation, Central Department of Meteorology, Tribhuvan University, Kathmandu, Nepal

Chalise, S.R.; Shrestha, M.L.; Thapa, K.B.; Shrestha, B.R.; Bajracharya, B. (1996) *Climatic and Hydrological Atlas of Nepal.* Kathmandu: ICIMOD

Dhital, M.; Khanal, N.; Thapa, K.B. (1993) *The Role of Extreme Weather Events, Mass Movements, and Land-use Changes in Increasing Natural Hazards.* Kathmandu: ICIMOD

DPTC (Water Induced Disaster Prevention Technical Centre) (1994) *Annual Disaster Review.* Kathmandu: DPTC

Shakya, B. (1996) 'Hydrometeorological Study of Bagmati Catchment with Special Reference to the Flood of 19-20 July, 1993'. M.Sc. Dissertation Central Department of Meteorology, Tribhuvan University, Kathmandu, Nepal

7 Landslide Study Using Aerial Photographs

H. Yagi
Department of Geography, Faculty of Education
Yamagata University
Kojirakawa, Yamagata 990, Japan
E-mail yagi@kescriv.kj.yamagata-u.ac.jp

Stereoscopic aerial photography allows one to obtain an overall view of the terrain as a three-dimensional image. Interpretation of such photographs gives a wide range of information on landforms, as the land's geomorphological features are visible on a larger scale than is generally possible from a ground survey. Landforms directly reflect the ongoing and past evolutionary processes related to geomorphological change. One such evolutionary process is gravitational mass movement. Aerial photographs are commonly used to detect areas of potential landslides, identifying surface expressions of present or past mass movements of slope material like main scarps, depressions, cracks, bulges, and pressure ridges.

Identifying landslide-susceptible slopes from stereoscopic interpretation of aerial photographs is usually quicker, and sometimes more effective, than field survey. However, adequate experience in the complex techniques of geomorphologic interpretation is required in order to produce good results.

Introduction

Present-day landslides originate as a result of the same geological, especially geomorphological, and hydrological conditions that led to past landslides. Old landslides often reactivate when they are disturbed by human activities such as the construction of roads and canals. The past is the key to predicting future landslide risks. The first step in reducing human and economic losses due to landslides is to prepare landslide maps that inventory past and potential landslide distribution by locating existing and potential landslide areas (Figure 7.1). Such maps can help planners and decision-makers in planning development activities in hilly and mountainous countries, and are particularly helpful in developing countries, where it can be difficult to carry out large-scale mitigation works.

Landslide Survey Using Aerial Photographs

Landforms directly reflect the processes related to their geomorphological evolution, i.e., the physical and chemical interactions between the earth's surface and the natural forces acting upon it which have made them the way they are. These evolutionary processes include tectonic movement; volcanic, fluvial, and colluvial processes; and gravitational mass movement, including falls, slides, flows, creep, spread and others. Stereoscopic aerial photography allows one to obtain an overall view of the terrain in a three-dimensional image. It facilitates the extraction of detailed qualitative and quantitative information about the terrain, such as slope systems, microtopography (surface features with dimensions from a few centimetres to metres), drainage systems, land use, and vegetative land cover, all of which offer clues to understanding the geology, soils, and hydrology of the area. Interpreting aerial photographs, in turn, helps the observer understand the processes occurring on the mountain slopes. Some examples of stereo aerial photographs of landslides from Japan and Nepal are presented in the Annex.

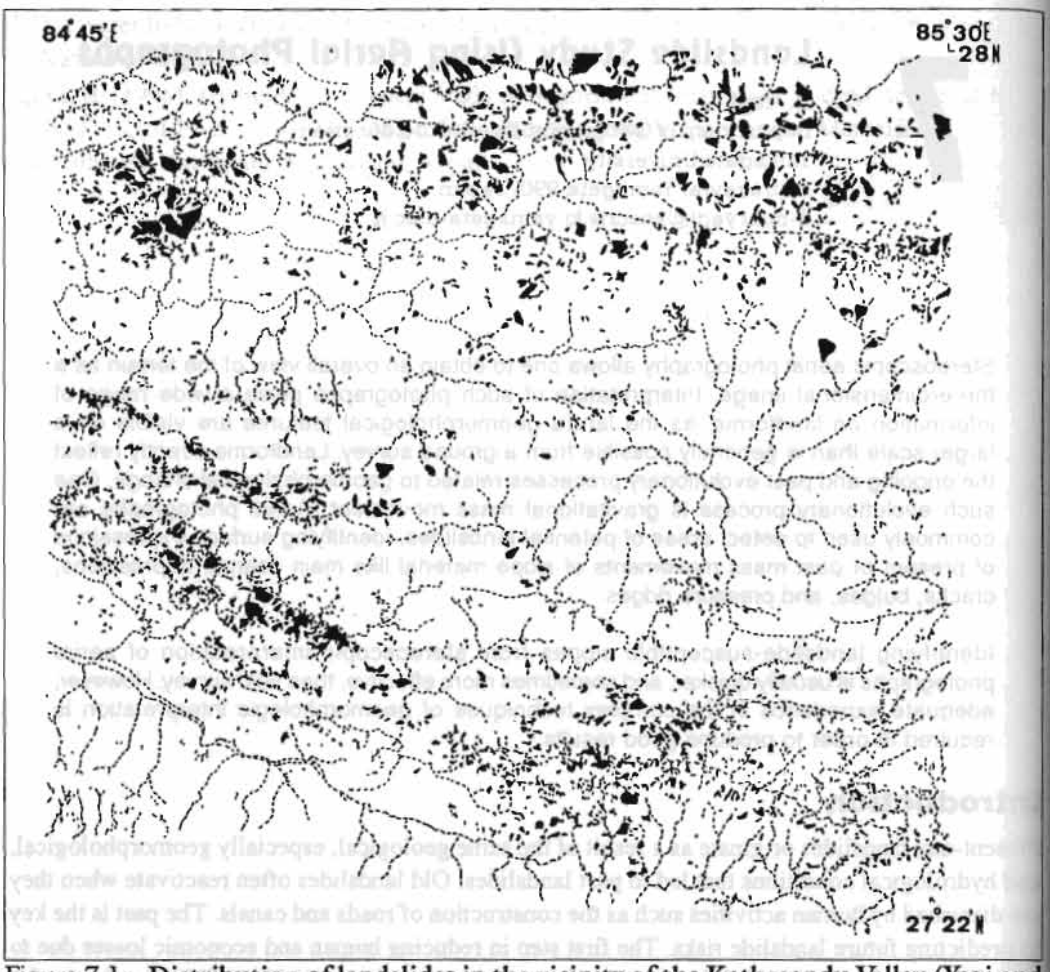

Figure 7.1: **Distribution of landslides in the vicinity of the Kathmandu Valley (Yagi and Oi 1993)**

Aerial photographs are commonly used to map existing landslides, detect the locations of potential landslides, and identify the surface expressions of present or past mass movements of slope material. Mapping landslides and identifying landslide-susceptible slopes from stereoscopic interpretation of aerial photographs is quicker, and sometimes more effective, than field survey. However, adequate experience in the complex techniques of geomorphologic interpretation is required in order to produce good results.

Stereoscopic Aerial Photography

When conducting stereoscopic aerial photography, the aeroplane must fly in such a way that there is a 60% forward overlap between successive frames of photographs along a straight flight line and a 20% lateral overlap between adjacent flight lines (Figure 7.2). Overlapping pairs of aerial photographs create an apparent image displacement for the same object

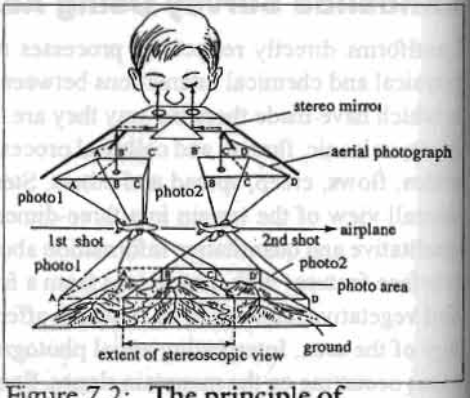

Figure 7.2: **The principle of stereoscopic viewing**

along the flight course because the projected images on the pair of aerial photographs are taken from two slightly different positions (Figure 7.3); viewed stereoscopically, this displacement produces a three-dimensional view. Relief displacement increases radially from the centre of the aerial photographs because of the central perspective projection. Hence, the image displacement of a high-relief point on two successive exposures changes; this is defined as the parallax intensity. When the two images are fused (using a stereo viewer, or by a practised observer using eye control) this parallax can provide the observer with a three-dimensional image (Figure 7.4). Interpretation and mapping of terrain features is considerably facilitated by the three-dimensional effect.

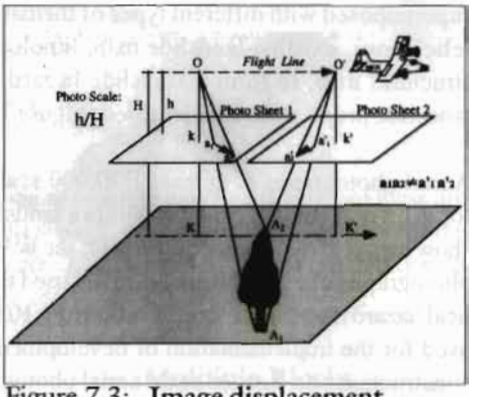

Figure 7.3: **Image displacement projected on successive aerial photo sheets** (after Ikeda et al. 1996)

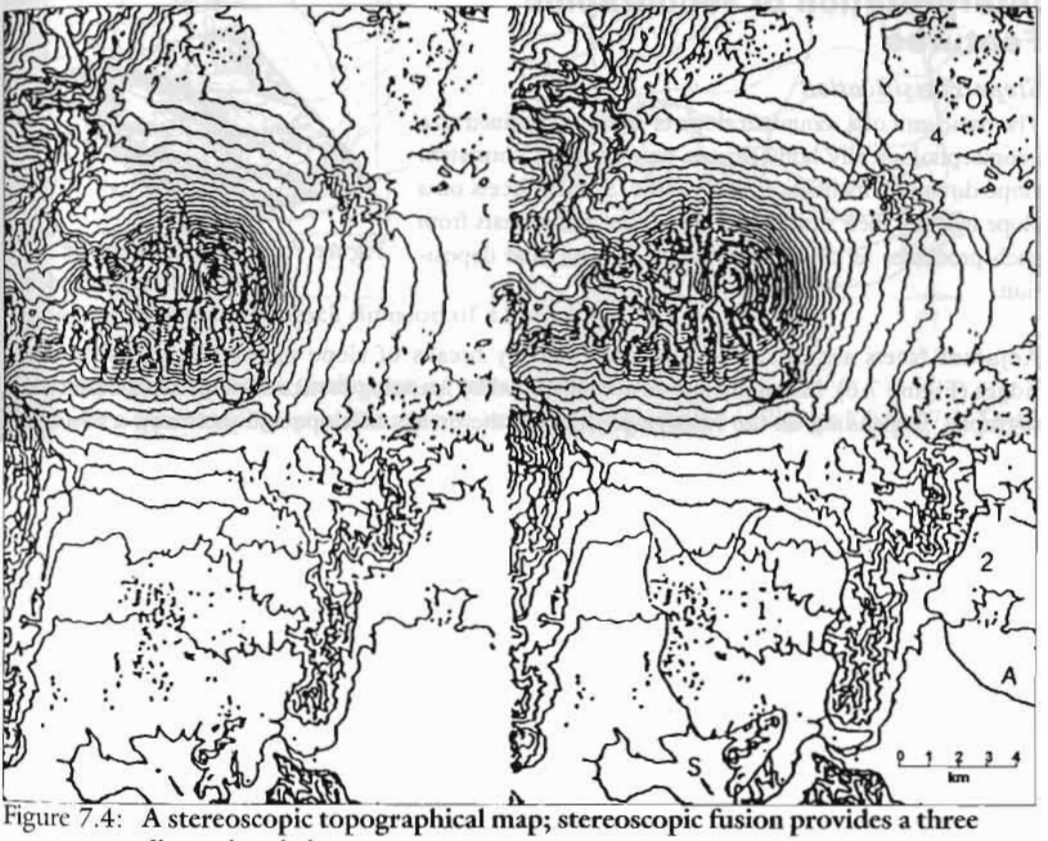

Figure 7.4: **A stereoscopic topographical map; stereoscopic fusion provides a three dimensional view**

Scales of photographs

Aerial photographs at a scale of 1:20,000-1:50,000 are sufficient to detect landslide topography and to prepare a landslide distribution map covering a large area. The aerial photo interpretation map is prepared as a base map or facet map (with grouping of land elements of similar genesis). This is

superimposed with different types of thematic map such as relief maps, existing landslide map, lithological map, and structural map, to form a landslide hazard map in which landslide prone areas are identified (Figure 7.5).

Aerial photographs of at least 1:20,000 scale are required for detecting landslide blocks within a landslide (areas that show separate, secondary movement, see below). Similarly, photographs of 1:20,000 are normally used to prepare practical hazard maps at a scale of 1:5,000 to 1:10,000 that can be used for the implementation of development projects at a construction site. Larger-scale aerial photographs are used for alignment surveys of new roads or other large project sites. Vertical photographs are normally used, although oblique photographs can be helpful for detailed topographic survey of specific slopes.

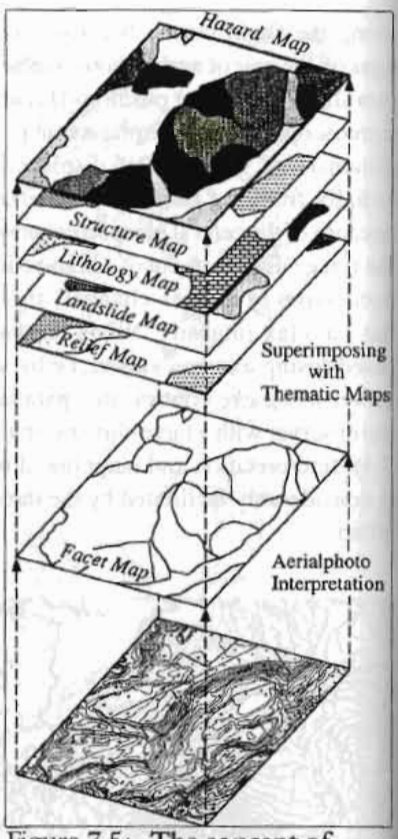

Figure 7.5: **The concept of landslide hazard mapping**

Interpretation of Topographic Features

Slope classification

The basic unit of a mountain slope is the facet, defined as a geomorphologically homogenous unit showing consistent slope direction, inclination, and profile. Similar facets on a slope indicate their similar formative ages and genesis from such processes as denudation, transportation, and deposition.

Adjacent facets are discontinuous, separated by breaks of slope marked by spurs or small ridges (Figure 7.6). Mountain slopes are classified by mapping breaks of slope from aerial photographs. Depending on the relative position of the breaks of slope and the facet, a mountain slope can be classified as a

- crest slope,

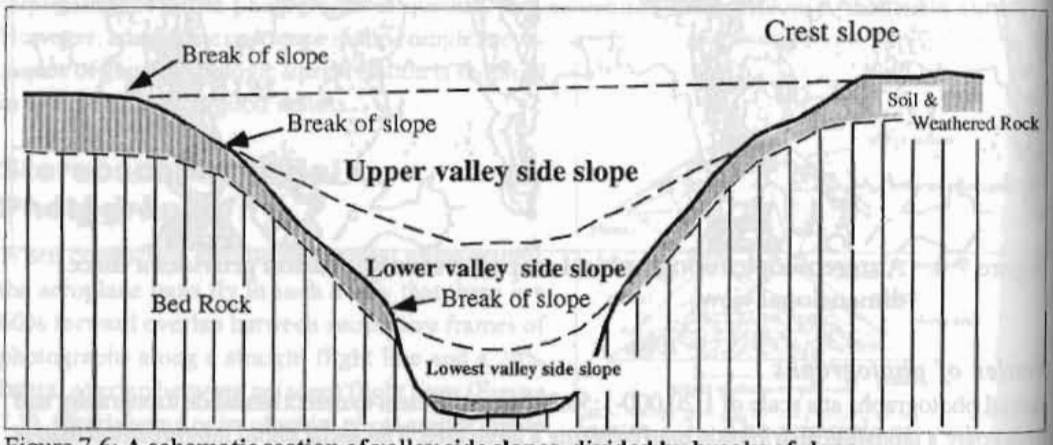

Figure 7.6: **A schematic section of valley side slopes, divided by breaks of slope**

- upper valley side slope,
- lower valley side slope, or
- lowest valley side slope (side of the valley bottom).

Landslide blocks

A landslide area may consists of several blocks, each showing separate movement. Some of these are usually active (Figure 7.7). Prevention work on an active block may be sufficient to restrain the movement of a landslide area as a whole. Active blocks are characterised by microtopography with cracks, pressure ridges, breaks of slopes, and scarplets.

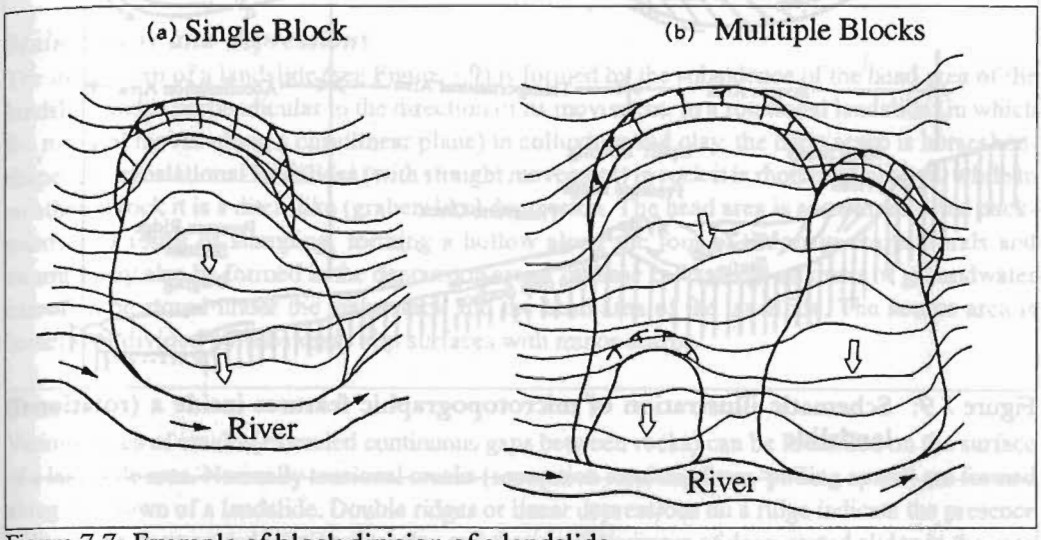

Figure 7.7: **Example of block division of a landslide**

Microtopography as an indicator of mass movement

Some of the typical topographic features of a landslide are illustrated in Figures 7.8 and 7.9. These features are generally depicted on topographic maps using the symbols shown in Figure 7.10. Slope deformations related to landslides like scarps, hollows, linear depressions, cracks, bulges, and pressure ridges are detected through aerial photography and can be used to gain an understanding of past and future mass slope movement. Microtopography, i.e., ruptures or deformation of slope surfaces with dimensions of a few centimetres to a metre or more, can be examined from aerial photographs at larger scale. These micro-topographic features are convincing signs for identifying moving blocks, their direction of movement and precursors of landsliding (Figure 7.9). The larger geographical features (or homogeneous

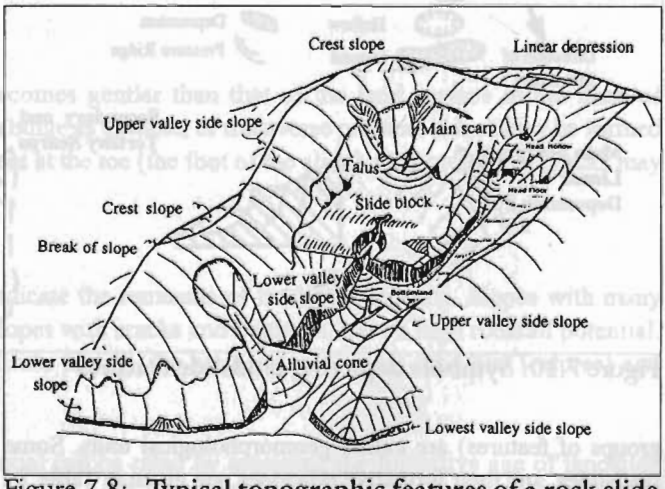

Figure 7.8: **Typical topographic features of a rock slide**

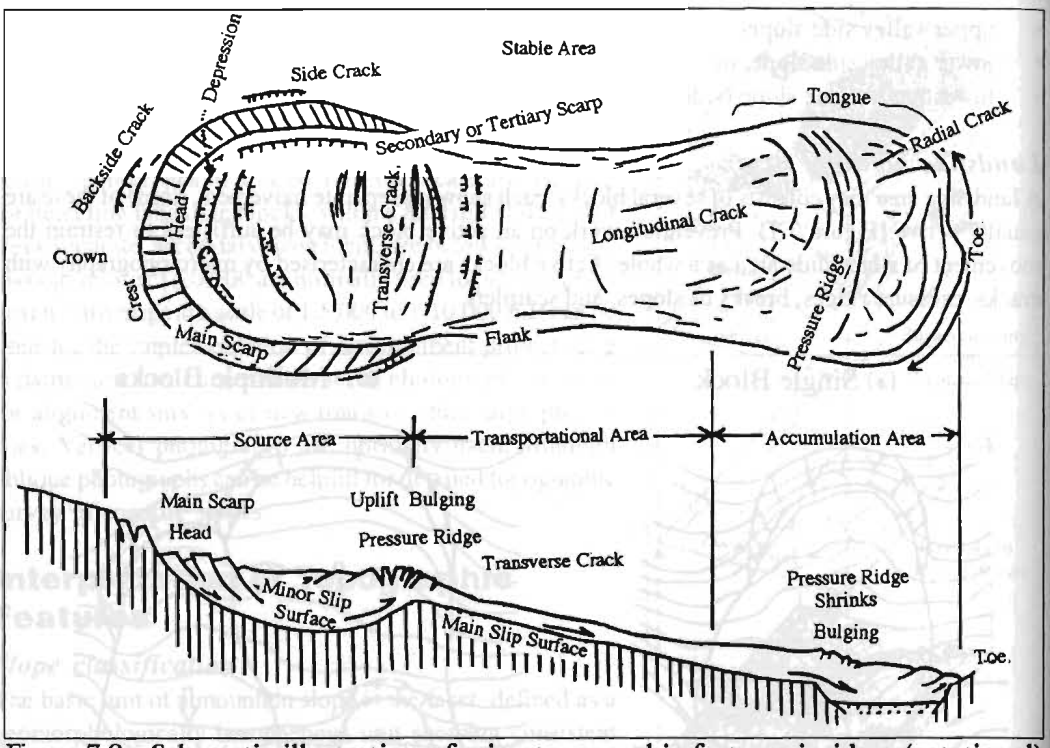

Figure 7.9: **Schematic illustration of microtopographic features inside a (rotational) landslide**

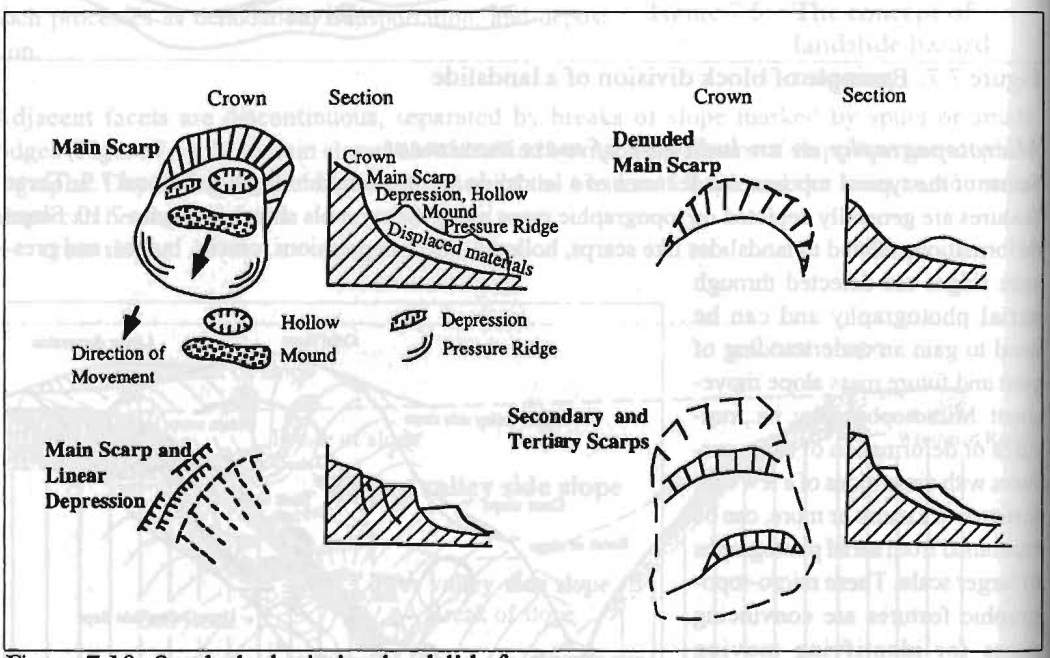

Figure 7.10: **Symbols depicting landslide features**

groups of features) are called geomorphological units. Some geomorphological units relating to landslides, and their formative processes, are given in Table 7.1.

Table 7.1: Origins of some geomorphological units relating to landslides

Geomorphological unit	Formative process	
	Type of movement	Type of stress
Tensional crack	Slide	Tension
Compressional crack	Bulge, thrust	Compression
Main scarp	Slump, glide	Tension
Detached scarp	Glide	Tension
Rhomboid depression	Glide	Tension
Block	Slide	Tension
Pressure ridge	Slump, glide, or bulge	Compression
Debris-flow ridge	Flow	Tension
Debris-flow cone	Flow	Compression

Main scarps and depressions

The main scarp of a landslide (see Figure 7.9) is formed by the subsidence of the head area of the landslide and is perpendicular to the direction of its movement. In a rotational landslide (in which the material moves along a curvilinear plane) in colluvium and clay, the main scarp is horseshoe-shaped; in translational landslides (with straight movement) in rock it is rhomboid-shaped, while in weathered rock it is a ditch-like (graben-like) depression. The head area is sometimes tilted backwards as a result of slumping, forming a hollow along the foot of the main scarp. Ponds and swamps may also be formed in the depression areas; in these cases, large amounts of groundwater can often be stored under the main crack and the head area of the landslide. The source area is sometimes divided by subsidiary slip surfaces with minor scarps.

Cracks

Various types of cracks (extended continuous gaps between rocks) can be identified on the surface of a landslide area. Normally tensional cracks (separation resulting from 'pulling apart') are formed along the crown of a landslide. Double ridges or linear depressions on a ridge indicate the presence of large and deep-seated tensional cracks, and they are precursors of deep-seated slides in the case of rock slide or creep. Transverse tension cracks with vertical displacements will appear in a source area. Transverse open cracks will develop on an upwarping sliding mass in a transition zone between the source and transportational areas. (At the local scale upwarping is the uplifting of a tract of land as a result of the impact of one of several possible effects like cryostatic processes or seismic uplift.) Radial cracks may occur in an accumulation area as a result of the lateral spreading of transported materials. Diagonal tension shear cracks may be observed along the flanks.

Bulges and pressure ridges

If the slope of the slip surface becomes gentler than that of the land surface in the zone of accumulation, the sliding mass may bulge as a whole, or transverse pressure ridges may be formed as a result of the compressional stress at the toe (the foot of the slide). Compressional cracks may form in the bulge.

Other features

Slopes with an irregular surface indicate the remnants of landslide deposits. Slopes with many boulders or overhangs, and steep slopes with cracks and boulders, have a high rockfall potential. Slopes with leaking water can indicate piping (the presence of sloping tube-like features) and erosion inside the material.

The relative landslide hazard potential can be rated by assessing the formative age of landslide slopes from the extent of dissection. Older landslides tend to have lower potential hazard ratings

than newer ones, since they have clearly already successfully withstood earthquakes, heavy rains, and other natural phenomena.

Reference

Ikeda, Y., Shimazaki, K.; Yamazaki, H. (1996) *A Primer on Active Faults in Japan.* Tokyo: University of Tokyo Press

Yagi, H.; Oi, H. (1993) 'Hazard Mapping on Large-scale Landslides in Lower Nepal Himalaya', Proc. 7th International Conference and Field Workshop on Landslides, Bratislava

Appendix

Aerial Photographs

Pairs of six aerial photographs are presented in Figures 7.A1 to 7.A6. When viewed stereoscopically these photographs show some examples of landslides as seen in aerial photographs. Figures 7.A1-7.A3 show typical landslides in Japan, the remainder are from Nepal. Landslide areas and divisions of landslide blocks are delineated in Figures 7.A4 and 7.A5.

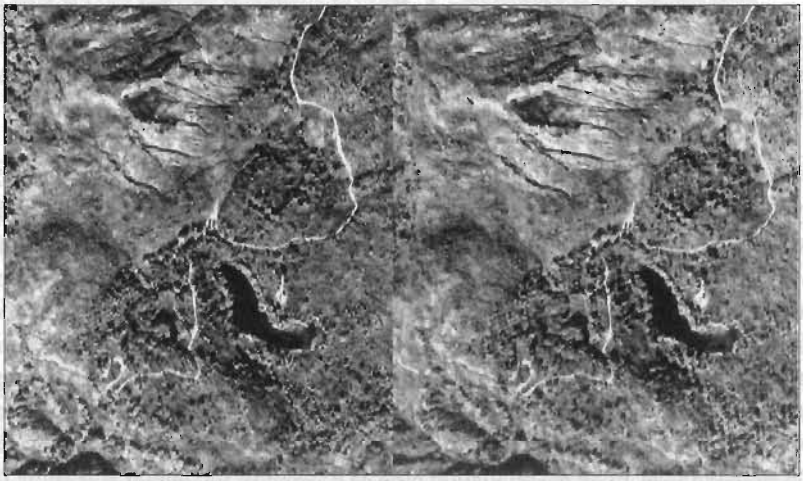

Figure 7.A1: **A large-scale rockslide (Mt. Amagazariyama, Japan)**

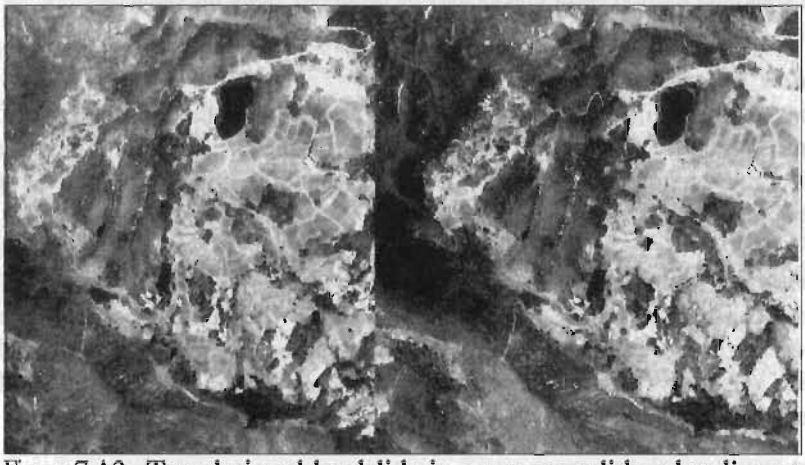

Figure 7.A2: **Translational landslide in an unconsolidated sediment zone (Matsunoyama Hot Spring, Japan)**

Figure 7.A3: **Multiple landslide in an unconsolidated sediment zone (Saikawa Hill, Japan)**

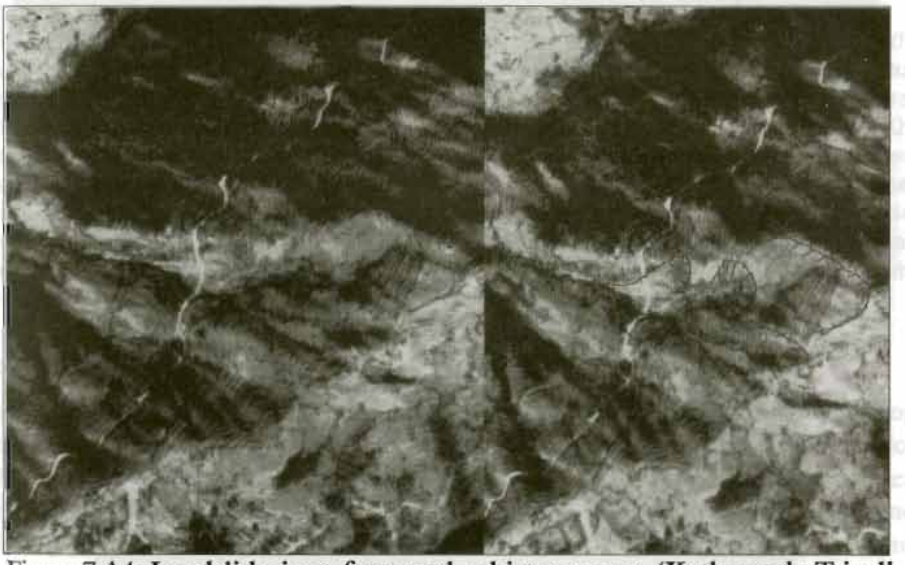

Figure 7.A4: **Landslide in a fractured schistose zone (Kathmandu-Trisuli Road, 19-km, central Nepal)**

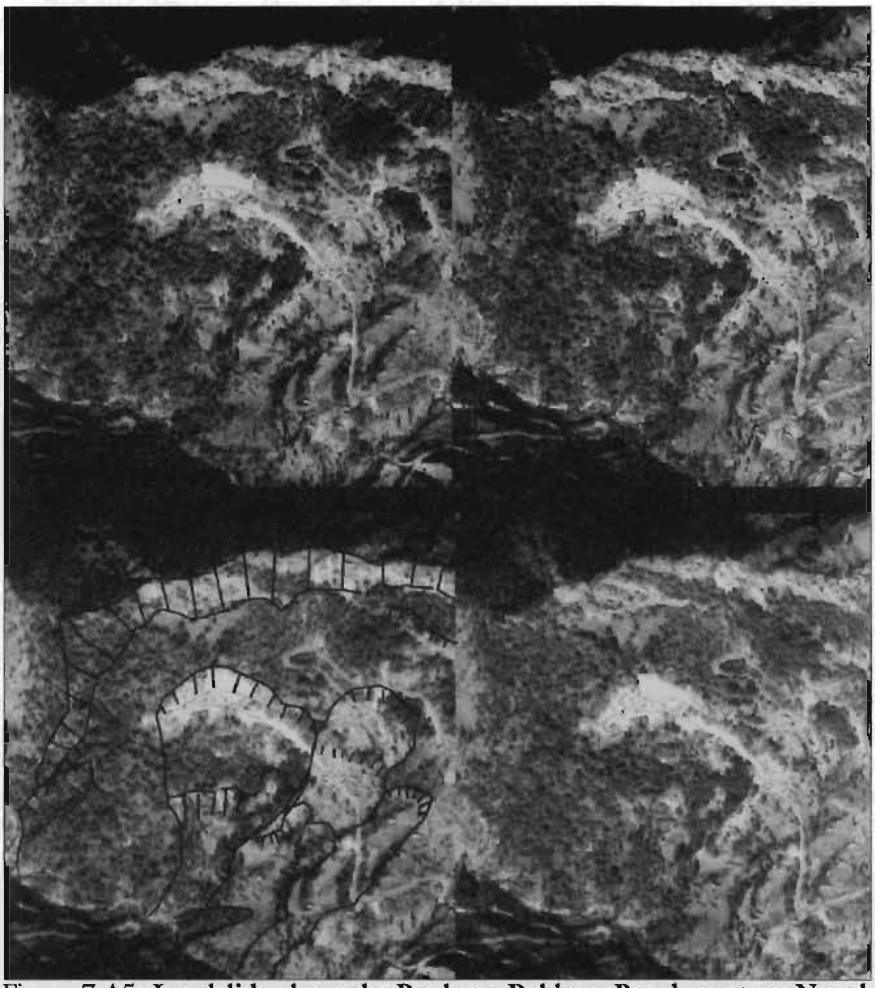

Figure 7.A5: **Landslide along the Baglung-Pokhara Road, western Nepal**

Figure 7.A6: **Landslide south of Charikot, central Nepal**

8 Study of the Subsurface of a Landslide by Geophysical Methods

S.R. Pant
Department of Geography, Tribhuvan University
Kiritipur, Kathmandu, Nepal

The geophysical methods commonly used in site investigations are equally applicable for the study of landslides. These methods can furnish subsurface information regarding types of material, depth to water table and bedrock, slip surfaces, and displaced and intact masses. In order to obtain this information, however, it is necessary to design the survey in an appropriate way, and to use the appropriate data acquisition and data processing techniques.

This paper provides an overview of the geophysical methods that are commonly used in the investigation of landslides. Seismic refraction and electrical resistivity methods have been widely applied; seismic reflection and ground-penetrating radar methods, though not used routinely at present, may be useful for the study of morphology and material-type distribution within the subsurfaces of landslides. The electrokinetic (filtration) potential method is also useful for studying the intensity and direction of groundwater movement.

Data acquisition and processing techniques for seismic refraction and electrical resistivity methods are described in detail. Usually geophysical data are collected under less than ideal circumstances, and processing and interpretation based on theoretically simplified earth models can yield erroneous results. New techniques described in this paper are more likely to accommodate actual subsurface geological conditions.

The paper includes a description of selected case studies acquired, processed, and interpreted by the author. A landslide in Sichuan, China provides a comparative study of conventional and generalised reciprocal method (GRM) processing of seismic refraction data. Studies of landslides and critical slopes along the Arniko Highway and at the Khimti I hydropower project in Nepal illustrate the use of 2-D electrical profiling (also called electrical resistivity tomography (ERT) or subsurface imaging (SSI)), a recent development in geophysics that has received wide application in environmental, groundwater, glaciology, and engineering investigations. The results obtained by these data processing techniques and seismic refraction and geoelectrical methods demonstrate their use in producing images of real subsurface geology.

Introduction

Geophysical methods of investigation involve the measurement of fields associated with changes in physical properties (density, magnetic susceptibility, electrical conductivity, elasticity, and radioactivity) in the near-surface and subsurface of the earth. Changes in physical properties, both in vertical and lateral directions, may indicate discontinuities, or anomalies (i.e., an inhomogeneous distribution) in subsurface materials. (The physical source of an anomaly is termed the geophysical target.) By processing the data observed on the surface, parameters related to the physical properties, depth, and size, of the subsurface layers and/or bodies that are creating the fields may be estimated. This process of estimating parameters of objects from observed fields is known as inverse solution. Data received from geophysical surveys can convey useful information about subsurface features such as geology, water table levels, buried cultural structures, and contaminant plumes, quickly and relatively inexpensively.

Geophysical methods have been widely applied in hydrocarbon, mineral, and groundwater exploration, glacier, permafrost, and landslide studies, engineering site investigations, the mapping of archaeological remains, and the location of buried pipes and cables. Hydrocarbon exploration remains by far the most common application of geophysical methods, but their use in environmental studies – for example, mapping variations in pore-fluid conductivity to indicate pollution plumes within groundwater – appears to be expanding significantly (Reynolds 1997). The same geophysical principles can be used in investigations ranging from a few metres to tens of kilometres in depth.

Applied geophysics provides a wide range of very useful and powerful tools when used correctly and in the right situations. Large areas can be surveyed quickly and in detail at relatively low cost. Moreover, geophysical methods are for the most part environmentally benign: there is no disturbance of subsurface materials. This is especially useful for the study of hazard areas.

Both the engineering and environmental aspects of landslides may be studied and monitored by geophysical methods. Site investigations usually entail the study of such engineering concerns as material types, depths to water table and bedrock, and locations of possible slip surfaces. By using time-series observations of different geophysical fields (such as geomagnetic, geoelectrical, electrokinetic (filtration) potential, and seismic velocity), the subsurface condition of a landslide can be assessed and the information can be used for risk analysis.

Methods of Investigation

Periodic saturation and dewatering of clayey and silty materials leads to changes in volume. This disturbs the structural relationships between materials in a slope and decreases the friction and cohesive forces that hold them together. Consequently the geophysical characteristics of a sliding area are likely to be different from those of a stable area (Novitskii 1974).

The study of landslides requires information on slopes, material types, and the thickness, physical properties, and water saturation of different layers. Geophysical methods can be used to detect different material types with different physical properties and/or for the differentiation of physical properties between sliding and intact masses within the same material type (Bogoslovsky et al. 1977).

Several of the available geophysical methods – based on seismic refraction, seismic reflection, electrical resistivity, filtration potential, and others – can be used to investigate landslides. Seismic refraction and electrical resistivity methods are widely used at all stages of landslide and other critical-slope investigations. These methods were already used in the late 1950s to study material types, slip surfaces, and water tables in the Alps and Caucasus (Klushin 1968) and their use has grown steadily since then, thanks to substantial improvements in the quality of equipment and data interpretation techniques. Since the late 1980s, the electrical resistivity method has evolved from 1-D to 2-D and even 3-D, while the interpretation of seismic refraction data has incorporated high-resolution processing. Mauritsch et al. (2000) have described a combined approach based on the interpretation of results from several different geophysical methods.

Seismic methods

In seismic methods, a signal is generated by vibrating to test the extent to which earth materials can be stretched or squeezed, somewhat like a sponge. Propagation of the vibration (seismic wave) causes the particles of a material to be stretched temporarily out of their position. The capacity of

a material to be temporarily deformed by seismic waves – its properties of elasticity – can be used to distinguish different types of materials. As these waves pass through subsurface media they are reflected and refracted back to the surface, where the returning signals are detected. The elapsed time between the source being triggered and the arrival of various waves is then analysed to determine the nature and dimensions of the subsurface layers.

The usual seismic sources are impulsive in nature. Seismic waves can be initiated by a dynamite blast, a shot from a shotgun using a blank cartridge, or the impact of a sledgehammer or dropped weight.

Physical and geological basis for seismic methods

When an external force (F) is applied across an area (A) of a surface of a body, forces inside the body are established in proportion to the external force. The ratio of the force to area (F/A) is known as stress. The stress applied to any surface can be resolved into two components, one at right angles to the surface (normal or dilatational stress) and the other parallel to the surface (shear stress). The stressed body undergoes strain, which is the amount of deformation expressed as the ratio of the change in length (or volume) to the original length (or volume). According to Hooke's Law, stress and strain are linearly dependent, and a body behaves elastically until the yield point is reached, i.e., the body reverts to its pre-stressed shape and size following relaxation of the stress. At stresses beyond the yield point, the body behaves in a plastic or ductile manner, and permanent damage results. If further stress is applied, the body is strained until it fractures.

Seismic waves, which consists of tiny packets of elastic strain energy, travel away from any seismic source at speeds determined by the elastic moduli (the constants that specify the relationship between stress and strain) and the densities of the media through which they pass. There are two main types of seismic waves: those that pass through the bulk of the medium are called body waves, while those that are confined to the interfaces between media with contrasting elastic properties, particularly the ground/air surface, are called surface waves.

There are two types of body waves that travel through elastic media: P-waves (also known as longitudinal, primary, push, or compressional waves) and S-waves (also known as transverse, secondary, or shear waves). The P- wave 'pushes and pulls' the rock it moves through in the same way that sound waves push and pull the air; in other words it radiates in the form of zones of compression separated by zones of dilation. The particle motion for P-waves is in the direction of the propagation (Figure 1a). In contrast S-waves move the rock up and down or side-to-side, i.e., the particle motion is at right angles to the direction of propagation (Figure 1b).

The velocity of the propagation of a seismic wave is given by the expression

$$V=(K/\rho)^{1/2} \qquad (1)$$

where V is the P- or S-wave velocity, K is the effective elastic parameter, and ρ is the density of the medium. K is a function of Lame's constants, λ and μ, which are related to how a material responds to normal and shearing stresses. The effective elastic parameter for P-waves is

$$K=\lambda+2\mu \qquad (2)$$

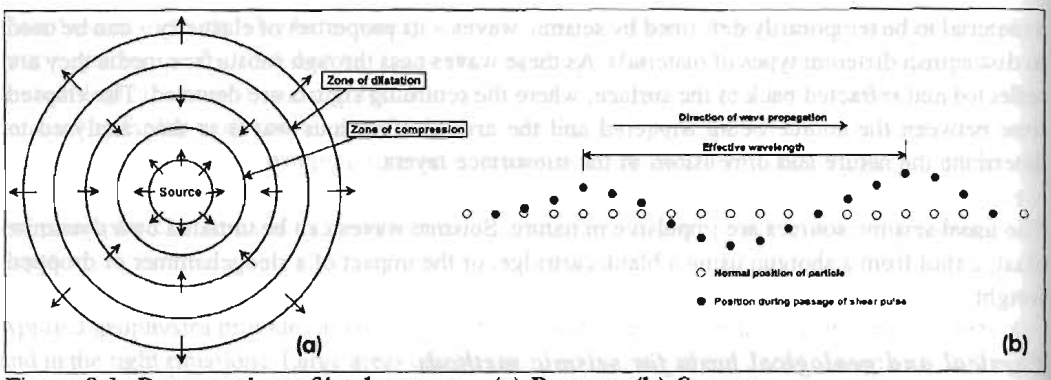

Figure 8.1: Propagation of body waves – (a) P-wave, (b) S-wave

and for S-waves

$$K = \mu \tag{3}$$

One of the most important parameters in seismic work is Poisson's ratio σ. If a cube of isotropic material (i.e., with the same properties in all directions) is stretched along one of its axes, the dimensions of the other two axes will decrease. Poisson's ratio is the ratio between the fractional lateral contraction and the fractional longitudinal extension of such a cube under tensile stress caused by a force from one direction.

Poisson's ratio can be expressed in terms of Lame's constants by

$$\sigma = \frac{\lambda}{2(\lambda + \mu)} \tag{4}$$

Or it can be expressed in terms of the P- and S-wave velocities, V_p and V_s, by

$$\left(\frac{V_p}{V_s}\right)^2 = \frac{(0.5 - \sigma)}{(1 - \sigma)} \tag{5}$$

For most consolidated rock material, V_p/V_s is between 1.5 and 2.0. By measuring the P- and S-wave velocities, Poisson's ratio can be calculated from equation (5). It can vary between the theoretical limits of 0 (a hard, rigid medium) and 0.5 (a fluid). Earth materials exhibit values for Poisson's ratio from about 0.05 for very hard rock to 0.45 for water-bearing unconsolidated materials (Sheriff and Geldart 1987). By measuring P- and S-wave velocities in a landslide, parameters and information needed for the stabilisation of the landslide can be deduced.

Equation (1) suggests that seismic velocity varies inversely with the square root of the density of the medium. However, P-wave velocity is higher for denser rock. An empirical relationship given in Gardner et al. (1974) shows the increase in P-wave velocity with density,

$$\rho = 0.31\ V^{1/4} \tag{6}$$

where ρ is density in g/cm³ and V is P-wave velocity in m/s. P-wave velocity also depends on the porosity and on the material filling the pores. The velocity generally increases as the porosity decreases. The relationship given by Wyllie et al. (1958) is

$$\frac{1}{V} = \frac{\varphi}{V_f} + \frac{1-\varphi}{V_m} \quad (7)$$

where V_f and V_m are acoustic velocities in the pore fluid and the rock matrix, and φ is fractional porosity.

The P-wave velocities for some materials commonly encountered in landslides are given in Table 8.1. These values are approximate and may overlap with the nearby ranges. It is essential to consider the geology and hydrogeology of a landslide area before interpreting the seismic data for material type. However, P-wave seismic velocity has a direct relationship with the strength and quality of a rock: the higher the velocity, the stronger the rock. This is true for materials below the water table (if the P-wave only is considered).

Table 8.1: **Approximate P-wave velocities for different materials commonly encountered in landslides or slopes**

Velocity (m/s)	Materials
200-400	very loose material above the water table
400-1500	unconsolidated clays and silts; unsaturated sands and gravels
1500-2000	saturated sands and gravel; compacted clays and silts; completely weathered rocks
2000-2500	partially consolidated sediments, probably water saturated; highly weathered and/or fractured metamorphic and igneous rocks; weathered and/or jointed sandstones and shales
2500-3700	partially weathered to fresh shales and sandstones; weathered and/or sheared metamorphic or igneous rocks or limestones
3700-4500	slightly weathered and/or fractured metamorphic or igneous rocks or limestones; some very hard or indurated sandstones and shales
4500-6000	unweathered metamorphic and igneous rocks; some limestones and dolomites

In addition to body waves, there are two types of **surface waves**, Rayleigh waves and Love waves (Figure 8.2). Rayleigh waves travel along the free surface of the earth in the same way that a wave rolls across a lake or an ocean, moving the ground up and down or side-to-side in the same direction that the wave is moving with amplitudes that decrease with depth. The particle motion is actually a retrograde ellipse in a vertical plane with respect to the direction of propagation. Love waves occur only where a medium with a low S-wave velocity overlies a layer with a higher S-wave velocity. Love waves move the ground from side-to-side, i.e., the particle motion is parallel to the surface, at right angles to the direction of wave propagation. Surface waves can be used to determine ground stiffness in situ. These waves somewhat mask the arrival of body waves; this masking effect can be filtered out in subsequent processing of seismic data. The velocity of surface waves is less than or equal to that of shear waves.

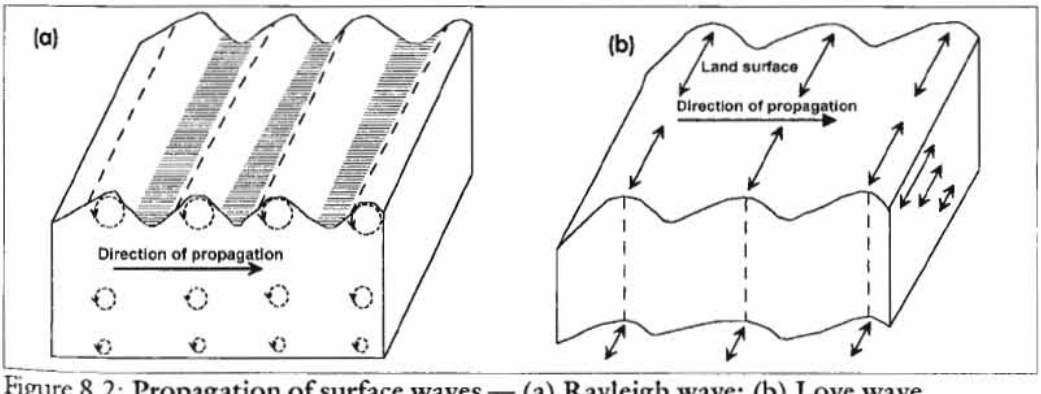

Figure 8.2: **Propagation of surface waves — (a) Rayleigh wave; (b) Love wave**

The amplitude of a seismic wave decreases as it travels away from the source – called **attenuation**. Attenuation results from the spherical spreading of the wave and from loss from absorption due to frictional dissipation of elastic energy into heat. Both mechanisms of attenuation for a homogeneous material are combined in the equation

$$I = I_0 \frac{r_0}{r} e^{-\alpha(r-r_0)} \tag{8}$$

where I and I_0 are the amplitudes at distances r and r_0 from the source, and α is the absorption coefficient (Dobrin and Savit 1988). Experiments with different rock types show that higher-frequency energy has a greater absorption rate than does lower-frequency energy. This property of rocks causes a progressive lowering of the apparent frequency of seismic waves with increasing distance of travel through the earth.

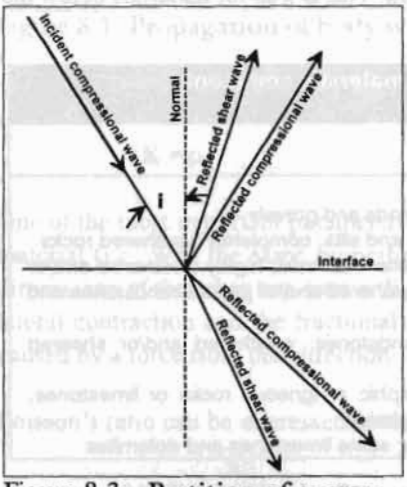

Figure 8.3: **Partition of energy of an incident compressional wave at an interface**

Whenever a wave impinges upon an interface across which there is a contrast in elastic properties, some of the wave's energy is reflected back off the interface – **reflection**, and the remainder passes through the boundary and is refracted on entering the second medium — **refraction** (Figure 8.3). The relative amplitudes of reflected and transmitted (refracted) seismic waves depend on the seismic velocities and densities of the two layers (Sheriff and Geldart 1987). The product of density (ρ) and velocity (V) for a given layer is its acoustic impedance. The reflection coefficient R gives the relative amplitudes of reflected waves. This can be expressed for a P-wave when the wave impinges at a right angle (normal) to the interface (Dobrin and Savit 1988) as

$$R = \frac{A_r}{A_i} = \frac{(\rho_2 V_{p2} - \rho_1 V_{p1})}{(\rho_2 V_{p2} + \rho_1 V_{p1})} \tag{9}$$

When a P-wave impinges at an oblique angle to an interface it produces both reflected and refracted P- and S-waves. The angles made by the incident, reflected, and refracted waves with the perpendicular to the interface are called the angles of incidence, reflection, and refraction. The angles of incidence and reflection for P-waves are equal. However, the velocity of S-waves is smaller than for P-waves, which causes the angles of reflection and refraction for S-waves to be smaller than the angles of incidence and refraction for P-waves.

Seismic reflection method

Seismic reflection is the most commonly used method in hydrocarbon exploration. However, this method has not been applied as much as it could be in engineering and environmental investigations. Since around 1980 seismic reflection has been widely used for mapping Quaternary deposits, buried rock valleys, and shallow faults (Reynolds 1997). It can also be useful in the study of major landslides, since it has the capability of providing detailed subsurface images.

The essence of the seismic reflection technique is to measure the time taken for a seismic wave to travel from a source down to the interface and back to the surface, where it is detected by a receiver or detector. Such a receiver, called a geophone, converts ground motion into electrical energy. The output of a geophone is further filtered, amplified, and recorded on a seismograph. The record of each geophone is called a trace. A group of traces make a seismogram. The directions of wave propagation of the seismic waves can be shown schematically in the form of a 'raypath' diagram (Figure 8.4a).

The time a seismic wave takes to travel from source to detector, known as two-way travel time, can be calculated as follows:

$$(SO)^2 = 4h^2 + x^2$$

$$(Vt)^2 = 4h^2 + x^2$$

$$\frac{V^2t^2}{4h^2} - \frac{x^2}{4h^2} = 1 \qquad (10)$$

where S is the position of the source, O is the position of the reflector (reflecting surface), t is the two-way travel time, h is the depth to the reflector, V is the velocity of the seismic wave, and x is the distance from source to detector.

As the distance between the source and detector (x) is increased, the wave's two-way travel time (t) increases at twice the rate: thus the plot of t against x is a hyperbola (Figure 8.4b). Several hyperbolic forms of waves reflected from different interfaces can be observed on a seismogram.

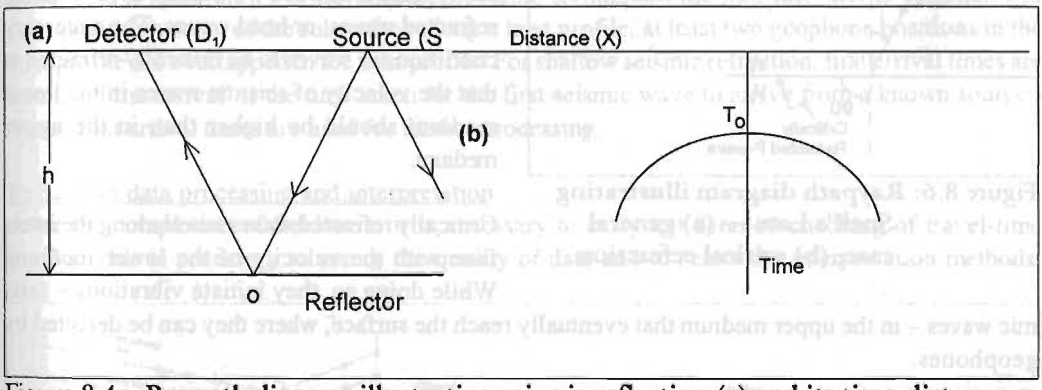

Figure 8.4: **Raypath diagram illustrating seismic reflection (a) and its time-distance graph (b)**

One of the principal reasons for the increased use of shallow seismic reflection is the improvement in equipment capabilities and the availability of microcomputers for processing. The equipment produced recently is portable and can be carried by one person. New equipment for shallow-depth studies can be used for both seismic reflection and refraction, and can record both P- and S-waves. The reflection method has been applied in groundwater investigations and in glaciology and palaeontology (Reynolds 1997; Geissler 1989).

Nowadays almost all reflection data are acquired and processed by the common midpoint (CMP) technique, which helps to enhance the signal/noise ratio. In this technique, a signal is emitted from

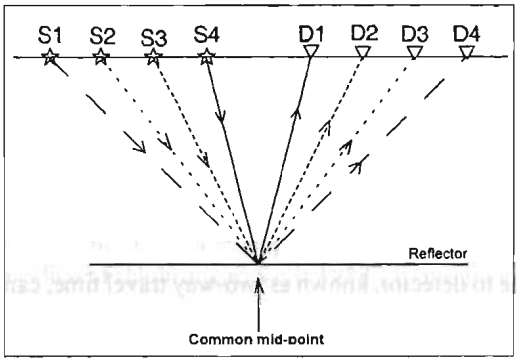

Figure 8.5: **The principle of the common midpoint (CMP) technique**

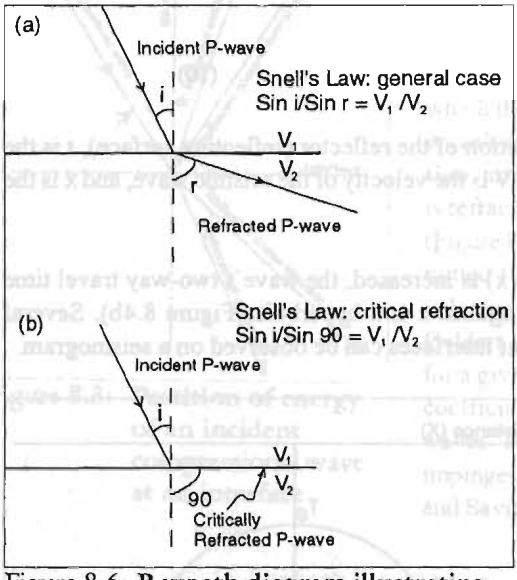

Figure 8.6: **Raypath diagram illustrating Snell's Law — (a) general case, (b) critical refraction**

multiple sources, and reflections arising from the same point on the interface – known as the common midpoint (CMP), common depth point (CDP), or common reflection point (CRP) – are detected by different geophones placed at the surface (Figure 8.5). The waves reflected from this point are summed after necessary corrections have been made to each trace signal; this summing tends to strengthen the coherent signals and reduce incoherent noise (for more details see Reynolds 1997; Robinson and Coruh 1988). Seismic reflection results are usually presented in the form of a time section. Depth sections are produced if needed and if the distribution of seismic velocities is known.

Seismic refraction method

When a seismic wave impinges on an interface, a portion of it is refracted – transmitted at a different angle – through the interface. According to Snell's law, which defines the relationship between a wave's incident and refracted angles, there is a certain critical angle of incidence that produces an angle of refraction of 90° (Figure 8.6). Such waves are called critically refracted waves, or head waves. The necessary condition for waves to be critically refracted is that the velocity of seismic waves in the lower medium should be higher than in the upper medium.

Critically refracted waves travel along the interface with the velocity of the lower medium. While doing so, they initiate vibrations – seismic waves – in the upper medium that eventually reach the surface, where they can be detected by geophones.

The time-distance relationship for an ideal two-layer case is given by the equation

$$t_x = \frac{x}{V_2} + \frac{2h_1 \cos i}{V_1} \qquad (11)$$

where t is time, x is distance, V_1 and V_2 are the velocities of seismic waves in the first and second (refractor) layer, and h is the depth of the refractor. Equation (11) is in the form of a straight line. The second term on the right hand side of the equation is the intercept of the refracted line with the time axis; this is called the intercept time.

Similarly the time-distance relationship for a multi-layered (n-layered) case can be calculated by the formula

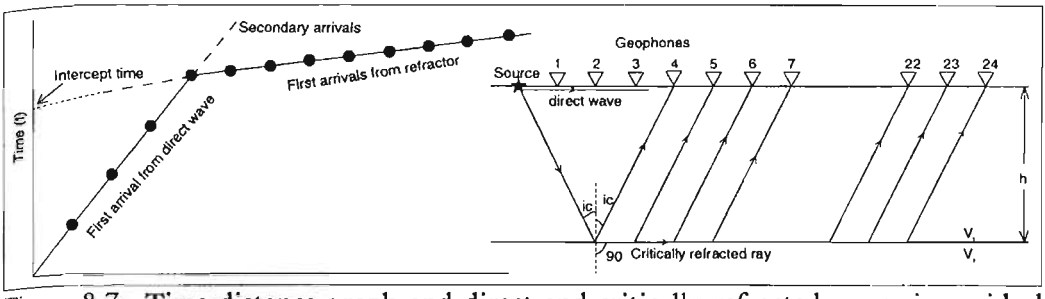

Figure 8.7: **Time-distance graph and direct and critically refracted waves in an ideal two-layer case**

$$t_x = \frac{x}{V_n} + \sum_{j-1}^{n-1} 2h_j \frac{\cos i_j}{V_j} \qquad (12)$$

Refraction data acquisition

In conventional methods of data interpretation, the subsurface is considered to be made up of horizontal or dipping planar interfaces. For the gross estimation of velocities and depths below each shot point (the gunshot or wave source), only two shots per spread are required: forward shot and reverse shot (Figure 8.8). However, this is not appropriate in a landslide investigation, as it tends to oversimplify the geological settings of the site.

For non-planar interfaces, a data acquisition procedure that is able to provide full coverage of the refractor is necessary. The processing and interpretation methods also make demands on the field operation. Three additional shots – off-end forward, off-end reverse, and mid-line – should be conducted (Figure 8.8). For advanced processing techniques, the mid-line shot is optional. For continuous coverage of the subsurface along a long profile, at least two geophone positions in the first profile are overlapped in the next profile. For shallow seismic refraction, first arrival times are noted. ('First arrival' is the time taken for the first seismic wave to arrive from a known source.) These first arrival times are used for further processing.

Refraction data processing and interpretation

After the completion of fieldwork, it is necessary to carry out detailed checking of travel-time graphs. This is necessary to assure the quality of data and to select the interpretation methods,

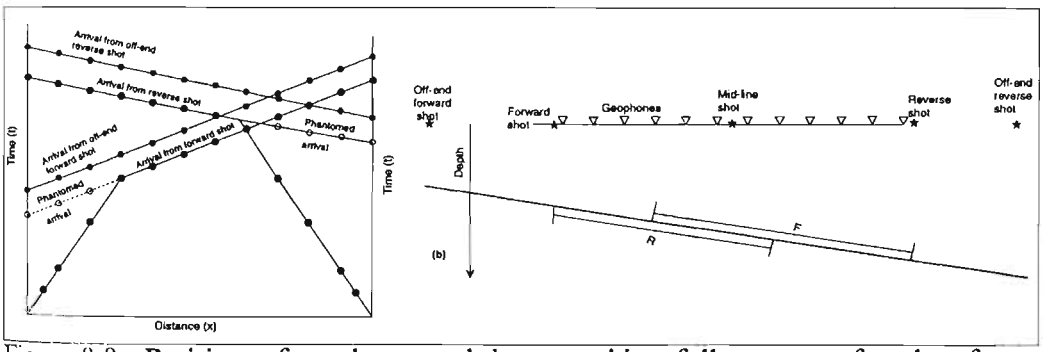

Figure 8.8: **Positions of geophones and shots to achieve full coverage of a subsurface (a), and time-distance graphs for a subsurface model (b). The segments of the refractor labelled 'R' and 'F' are those covered by the reverse and forward shots.**

and it may also help to optimise time and cost. During the selection of interpretation methods, the geological setting, morphology of the refractor, and probable thickness of the layer above the refractor (the overburden) of the landslide should all be considered. Among several methods of data processing and interpretation, only two are considered to be useful for landslide investigations. They are method t_0 and the generalised reciprocal method (GRM).

The first step in arranging time-distance graphs is **phantoming**. For the forward and reverse shots, there may be segments in the refractor where there is no overlap of the sort shown in Figure 8.8 (Lankston 1990). The travel times recorded for the off-end forward and off-end reverse shots are parallel to the travel times from the forward and reverse shots respectively. By shifting the travel-time curves of the off-end shots down in a parallel fashion, the first-break type arrival time for the section before the crossover distance can be reconstructed. Though not true arrival times, these so-called phantomed arrivals correspond to true arrival times. Determination of reciprocal time – the time taken for a wave to travel from the forward shot to the reverse shot or vice versa – is crucial for the interpretation of refraction data.

Method t_0 is a modification of the plus-minus method of interpretation originally proposed by Hagedoorn (1959) and helps determine the position of an undulating refractor. It is based on the following assumptions (Gurvich 1972):

- the refracted waves travel along the interface – that is, there is no effect of penetration in the refractor;
- the radius of curvature of the refractor's undulation is very high compared to the refractor's depth; and
- the refractor velocity does not have any sharp change.

After identifying the first breaks from the target refractor and performing the necessary phantoming calculations, the difference curve q(x) is calculated from the relationship

$$\theta(x) = t(x) - t'(x) + T \qquad (13)$$

where t(x) is the time reading at distance x in the forward phantomed curve; t'(x) is the time reading at distance x in the reverse phantomed curve; and T is the reciprocal time. The reciprocal times for the forward shot and reverse shot should be in good agreement. The target refractor velocity (V_b) is then calculated by taking the inverse of the slope of the curve θ(x)

$$V_b = 2\frac{\Delta x}{\Delta \theta} \qquad (14)$$

The change in the alignment of the points in the difference curve indicates the change in the velocity of the target refractor. The curve of the target refractor $t_0(x)$ and its depth h(x) are calculated for every x value using the following equations

$$t_0(x) = t(x) + t'(x) - T \qquad (15)$$

$$h(x) = K\, t_0(x) \qquad (16)$$

where $K = \dfrac{V_{av} V_b}{2\sqrt{V_b^2 - V_{av}^2}}$,

V_{av} is the average velocity of the overburden (above the target refractor) and V_b is the target refractor velocity.

The average velocity of the overburden is derived from the effective velocities, which are calculated by joining the lines from O to A and taking the inverse of the slope, where A is the start of the first break of the target refractor (Figure 8.9). The average velocity can be estimated from the effective velocities for forward and reverse profiles using

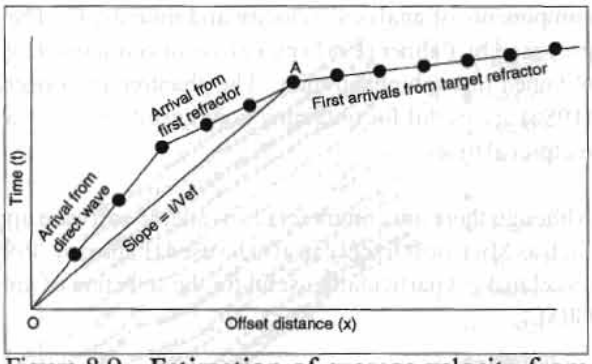

Figure 8.9: **Estimation of average velocity from effective velocity**

$$\frac{1}{V_{av}} = 0.5\left(\frac{1}{V_{ef1}} + \frac{1}{V_{ef2}}\right) \qquad (17)$$

where V_{ef1} and V_{ef2} are the effective velocities measured for the forward and reverse shots.

The estimation of average velocity from effective velocity works well for shallow depth investigations, and usually gives satisfactory results in cases where refracted waves are observed from all layers in the overburden. As the depth increases, however, the error in the average velocity determination also increases as a result of layering of the overburden, curvature of the refractor, and lithological change along the layer (Gurvich 1972). In a landslide, estimated average velocity will also be inaccurate if the layers are so thin that the arrival from these layers cannot be recorded.

An example of interpretation by method t_0 is presented in Figure 8.10. In this example, the t_0 (x) curve has a negative correlation with the refractor topography; θ(x) shows the possibility of several velocity changes along the target refractor. The depth calculation shows that the overburden is very thick. In general, the probability of layering within the overburden increases with its thickness. Furthermore, undulations in the refractor's topography may produce fictitious velocity changes in the target refractor. The reliability of the interpretation in such cases is discussed in more detail in the case studies.

The more sophisticated method called the **generalised reciprocal method (GRM)** should be used in an area where the overburden above the target refractor is relatively thick (probably more than 10m). When the overburden is thick, the assumptions used during an interpretation using the t_0 method may not reflect the real situation. Hidden layers and velocity inversions in the overburden are apt to distort the calculated depth. GRM is used for delineating an undulating refractor at any depth from in-line seismic refraction data consisting of forward and reverse travel times (Palmer 1981). GRM has two

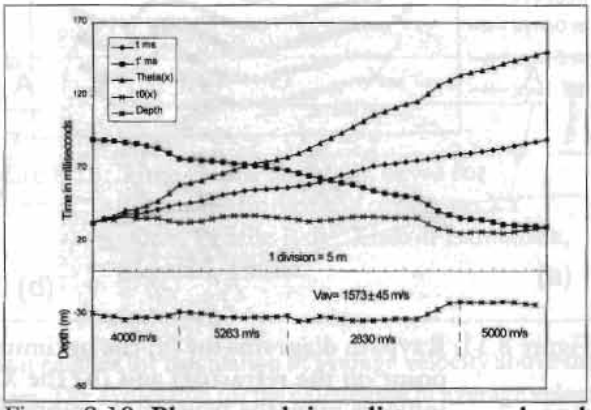

Figure 8.10: **Phantomed time-distance graph and its interpretation by method t_0, profile B-B', Xiakou Landslide, Sichuan, China (see also Figure 8.24)**

components of analysis: velocity and time-depth. The velocity and time-depth analysis function proposed by Palmer (1981) makes use of continuous forward and reverse direction profiles that are obtained through phantoming. The phantoming procedures described by Lankston and Lankston (1986) are useful for obtaining good results even in cases where it is difficult to find out reliable reciprocal times.

Although there are commercially available software applications for GRM, spreadsheet programs such as Microsoft Excel can also be used (Pant et al. 1999). The graphic presentation capabilities of Excel make it particularly useful for the selection of optimum velocity and time-depth functions in GRM.

Velocity analysis is the initial step in GRM processing. The velocity analysis function t_v is defined by the equation

$$t_V = \frac{t_{AY} - t_{Bx} + T}{2} \qquad (18)$$

where t_{AY} and t_{BX} are the arrival times for head waves from the forward and reverse shots that have emerged from the same point in the refractor and arrived at locations Y and X at the surface; and T is the reciprocal time (Palmer 1981). The value of the velocity analysis function is referred to G, which lies midway between X and Y (Figure 8.11a). With method t_0, XY is zero, which means the waves that emerge from the same point in the refractor arrive at the same point G on the surface (Figure 8.11b). In GRM, however, the velocity analysis is conducted using Palmer's minimum detail criterion (Palmer 1981) according to which the t_v curve that exhibits the least amount of irregularity is deemed to be the optimum one. The optimum XY is used in the later stages of GRM processing.

An example of velocity analysis is presented in Figure 8.12. To remove the overlapping of the curves, time has been added for each XY value. In Figure 8.12, the curves that exhibit the least amount of detail are for XY=45, 50, and 55m. The selection of any of these values is subjective. However, results will not be that much different. Each linear section in a velocity-analysis curve denotes one velocity zone in the target refractor. The inverse of the slope of each linear segment of the velocity curve is the velocity of the target refractor.

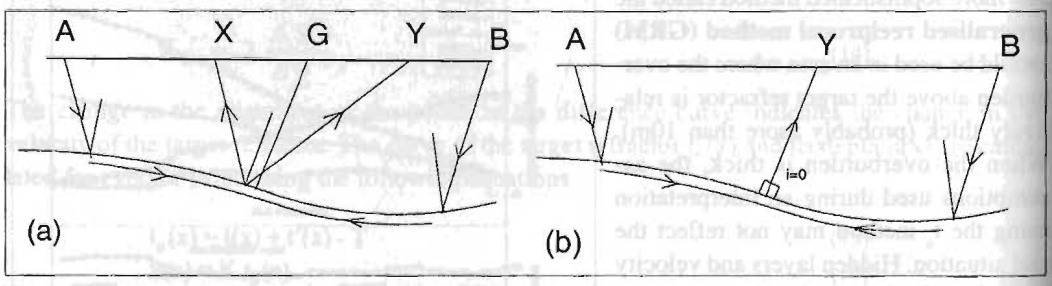

Figure 8.11: **Raypath diagrams for (a) the optimum XY case (rays emerge from the same point on the refractor) and (b) the XY = 0m case. Lines with arrowheads indicate raypaths from shot points A and B to geophone points Y and X, respectively. The time to follow the path from A to B is the reciprocal time. X and Y represent one pair of geophone positions. Numerous pairs are used in GRM processing (Lankston 1990)**

The process of restoring depth information from time information is called **migration**. It is important for the interpretation of both seismic refraction and reflection data. Time-to-depth migration is performed in two stages. The first is calculation and interpretation of the time-depth function t_G using the following formula

$$t_G = \frac{t_{AY} + t_{Bx} - \left(t_{Ab} + \frac{XY}{V_n}\right)}{2} \qquad (19)$$

where V_n is the refractor velocity determined from the velocity analysis function (Palmer 1981).

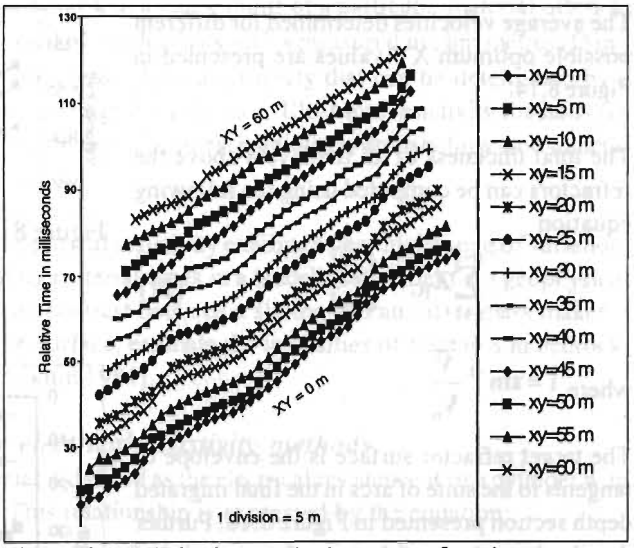

Figure 8.12: Velocity analysis curves for the determination of the optimum XY value, profile B-B', Xiakou Landslide, Sichuan, China

Time-depth analysis shows more detail in the target refractor's topography than do other conventional methods, including method t_0. In time-depth analysis, the optimum curve – the one that best approximates the shape of the refractor – is the one with maximum displacement in bedrock topography. Note that both velocity and time-depth analysis should yield the same optimum XY values; in the case of a discrepancy, reanalysis can be conducted.

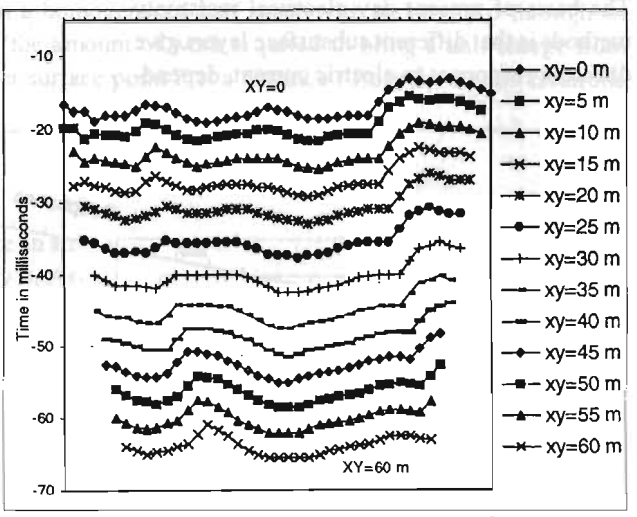

Figure 8.13: Time-depth analysis curves for determination of the optimum XY value, Profile B-B', Xiakou Landslide, Sichuan, China

An example of time-depth analysis curves is presented in Figure 8.13. Again, the time values have been shifted relative to each other so that they do not overlap. In this example, the optimum XY value for the time-depth analysis function can be chosen as 45, 50, or 55m. Thus the optimum XY values as determined by velocity analysis and time-depth analysis are the same.

One of the main advantages of GRM is that it enables the calculation of average velocity above the target refractor without defining all the layers. The expression for the calculation of average velocity is

$$\overline{V} = \left(\frac{V_n'^2 XY}{XY + 2t_G V_n'}\right)^{1/2} \qquad (20)$$

The average velocities determined for different possible optimum XY values are presented in Figure 8.14.

The total thickness of all the layers above the refractors can be computed using the following equation

$$\sum_{j=1}^{n-1} Z_{jG} = \frac{t_G \overline{V}}{\cos \bar{i}} \qquad (21)$$

where $\bar{i} = \sin^{-1} \frac{\overline{V}}{V'_n}$

The target refractor surface is the envelope of tangents to the suite of arcs in the final migrated depth section presented in Figure 8.16. Further details about the usefulness and superiority of GRM is presented in the case studies.

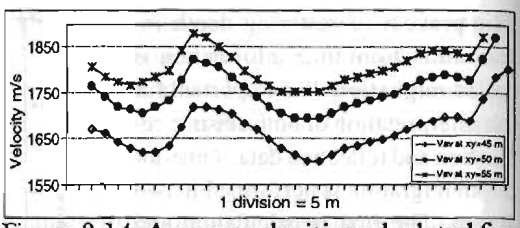

Figure 8.14: Average velocities calculated for different possible optimum XY values, profile B-B', Xiakou Landslide, Sichuan, China

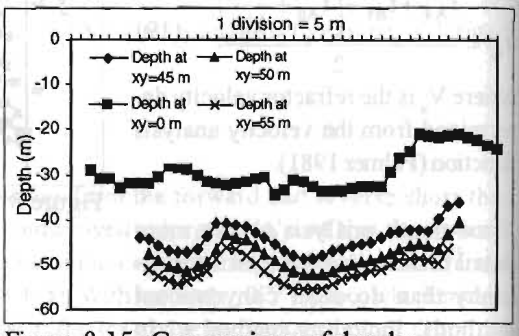

Figure 8.15: Comparison of depths calculated for different optimum XY values, profile B-B', Xiakou Landslide, Sichuan, China

Electrical Resistivity Methods

The basis of present day electrical resistivity methods is that different subsurface layers give different responses to electric current, depending mainly on their conductivity. The serious application of electrical resistivity methods dates back to before the First World War. At the beginning, two poles were used to send a current into the subsurface and conclusions were reached about the ground conductivity by measuring the amount of current; this provided information only about the conductivity of the surface near the grounding electrode. Later the four-pole system was developed in which two current electrodes were used to feed current to the subsurface and two potential electrodes measured the potential difference.

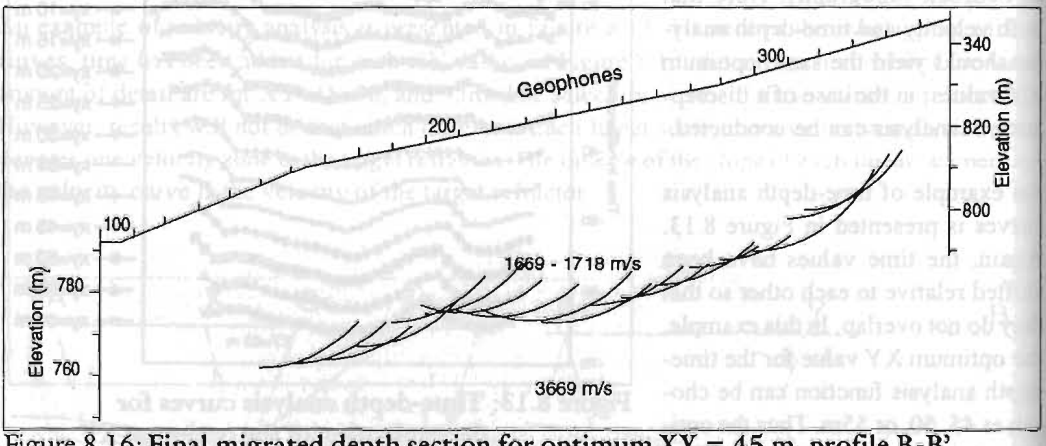

Figure 8.16: Final migrated depth section for optimum XY = 45 m, profile B-B', Xiakou Landslide, Sichuan, China

Electrical resistivity is the electrical resistance that a unit volume of a particular material offers to the flow of current at 0°C. It is the reciprocal of conductivity and is measured in ohm metres (Ω m). Electrical resistivity is a fundamental diagnostic physical property that can be determined by a wide variety of techniques, including electromagnetic induction. Electrical resistivity methods are widely used today in engineering and environmental studies, glaciology, archaeology, and mineral and groundwater exploration.

Compared to other physical properties, electrical resistivity exhibits a very high range of variation. This gives the possibility of differentiating material types in a landslide by other than geophysical methods (Novitskii 1974). The resistivity contrast between a sliding and an intact mass makes it possible to map the sliding mass and slip surface, estimate the intensities of fractures in bedrock, and forecast landslides (Brodovoe and Nikitin 1984).

Physical and geological basis for electrical resistivity methods

The electrical resistivity (ρ) of any material is defined as the electrical resistance R of a cylinder with a cross-section of area A and length l. This relationship is expressed by the equation:

$$\rho = R\frac{A}{l} \qquad (22)$$

Resistivity calculations are based on the following concepts.

A half-space is a model formed by only one plane surface; one example is a model with an air-earth interface. If a current I is injected into a homogeneous half space with resistivity ρ through an electrode at the surface, the potential (the amount of work required to bring a unit charge from infinity to the given point) V_p at another surface point P at a distance r from the source electrode will be

$$V_p = \frac{I\rho}{2\pi r} \qquad (23)$$

Let us consider a semi-infinite solid (like an air-earth interface) with uniform resistivity ρ. Assume that the current I is introduced into the ground through electrodes A and B and the potential difference is picked up between electrodes M and N (Figure 8. 17).

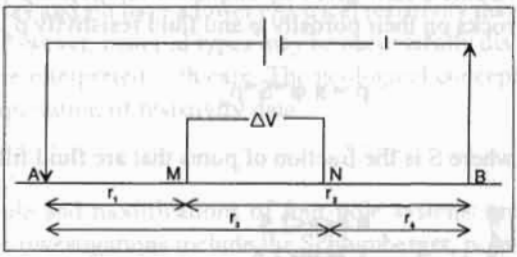

Figure 8.17: Arrangement of current electrodes (A and B) and potential electrodes (M and N)

The potential at M will be

$$V_M = \frac{I\rho}{2\pi}\left(\frac{1}{r_1} - \frac{1}{r_2}\right)$$

The potential at N will be

$$V_N = \frac{I\rho}{2\pi}\left(\frac{1}{r_3} - \frac{1}{r_4}\right)$$

The potential difference between M and N will be

$$\Delta V = V_M - V_N = \frac{I\rho}{2\pi}\left[\left(\frac{1}{r_1} - \frac{1}{r_2}\right) - \left(\frac{1}{r_3} - \frac{1}{r_4}\right)\right]$$

$$\rho = \frac{2\pi}{\frac{1}{r_1} - \frac{1}{r_2} - \frac{1}{r_3} + \frac{1}{r_4}} \cdot \frac{\Delta V}{I} \tag{24}$$

$$\rho = K\frac{\Delta V}{I} \tag{25}$$

where K is called the geometrical coefficient. If the resistivity is measured for inhomogeneous and anisotropic ground (i.e., without the same properties in all directions), the resistivity calculated by the above equation is called apparent resistivity and is denoted by ρ_a.

In electrical resistivity methods, DC or AC current of very low frequency (usually ≤10 Hz) is injected into the subsurface. Different geological formations, such as clay, silt, sand, gravel, boulders, and bedrock, will all respond differently. Bedrock, if it is weathered and fractured and saturated with water, will have lower electrical resistivity than fresh rock. In addition the different material types will usually have different degrees of porosity and permeability; for porous formations, electrical resistivity depends on the amount of water present and the salinity of the water.

Dry and unconsolidated, granular, and loose formations normally exhibit high resistivity values ranging from a few hundred to a few thousand Ohm metres. When saturated with water, the same formation will produce a much lower resistivity value due to the free conduction of electric current through water-filled pores. Thus an electrical resistivity of a saturated rock or sediment is a function of porosity, the electrical resistivity of the saturating fluid, the resistivity of the solid rock or sediment, the surface conduction of the rock or sediment, and the turtuosity of the fluid and electrical path. (Surface conduction is a form of ionic transport that takes place at solid-liquid interfaces by means of exchange mechanisms. Turtuosity is the length of the pore channel in which fluid migrates per unit length of the sample.)

Archie's Law gives an empirical relationship for the dependence of the resistivity of saturated rocks on their porosity φ and fluid resistivity ρ_w.

$$\rho = a\,\varphi^{-m} S^{-n} \rho_w \tag{26}$$

where S is the fraction of pores that are fluid filled; n=2; and a and m are constants with

$0.6 < a < 2.5$
$1.3 < m < 2.5$

For a saturated material equation (26) takes the form

$$\rho = a\,\varphi^{-m}\,\rho_w$$

The formation factor (F) is defined as the ratio of the electrical resistivity of the saturated formation to the electrical resistivity of the saturating water.

$$F = \rho/\rho_w = a\,\varphi^{-m}$$

In general for consolidated rocks

$$F = 1/\varphi^2 \quad (27)$$

For granular materials the relation is given by Humble's Formula

$$F = 0.81/\varphi^2 \quad (28)$$

The high formation factor for granular materials is an indication of their higher hydraulic conductivity (the measure of the relative ease of water flow under unequal pressure).

The resistivities of some rocks and other materials commonly encountered in landslides are given in Table 8.2. More extensive lists are given in Telford et al. (1976), Keller and Frischknecht (1966), and Reynolds (1997).

Table 8.2: Resistivities of granular materials and rocks commonly encountered in landslides

Material	Resistivity (Ωm)		
Marls	3 - 70	Granite	300 - 1,000,000
Clays	1-100	Schists (calcarious and mica)	20 – 10,000
Alluvium and sand	10 - 800	Schist (graphite)	10 - 100
Moraine	10 - 5000	Slates	10 - 100
Laterite	800 - 1500	Marble	600 – 40,000,000
Lateritic soil	120 - 750	Conglomerates	200 – 10,000
Quartz	300 – 1,000,000	Sandstones	1 – 740,000,000
Anthracite	0.001 – 200,000	Limestones	50 - 10,000,000
Lignite	9 - 200	Dolomite	350 - 5000

Table 8.2 shows that electrical resistivity varies considerably both within and between different types of material. Moreover, the resistivity ranges for different types of material overlap. In general rocks and formations made of fine materials like clay and silt have a lower electrical resistivity than do formations made of coarse-grained material. However, material types may be successfully distinguished using resistivity methods if the data are interpreted with care. The geological concept of landslides is important for the successful interpretation of resistivity data.

Electrode configurations

In modern electrical resistivity methods, four-pole and modifications of four-pole systems are used. Those that are or may be useful in landslide investigations include the Schlumberger, pole-pole, half-Schlumberger, Wenner (Wenner 1912), and dipole-dipole configurations (Figure 8.18). The Schlumberger and half-Schlumberger are the most commonly applied conventional configurations. The value of the apparent resistivity measured depends on the geometry of the electrode configuration. Different types of electrode configurations have certain advantages and disadvantages. It is up to the user to determine the suitability of a particular electrode configuration in a particular situation.

- **Schlumberger configuration.** In this configuration, the relationship between potential electrode distance (MN) and current electrode distance (AB) is MN £ (1/5) AB and the apparent resistivity is calculated as

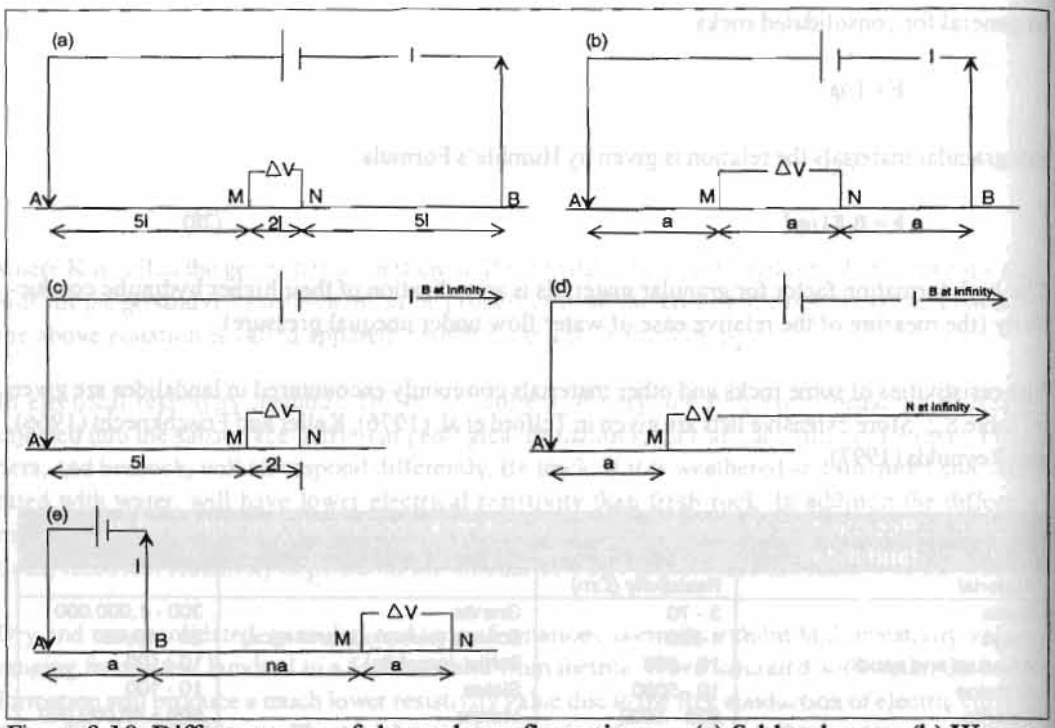

Figure 8.18: **Different types of electrode configurations — (a) Schlumberger, (b) Wenner, (c) half-Schlumberger, (d) pole-pole, and (e) dipole-dipole**

$$\rho_a = \pi \frac{AM\ AN}{MN} \frac{\Delta V}{I} \qquad (29)$$

- **Wenner configuration.** The inter-electrode distances are equal. The geometrical coefficient for this configuration is $2\pi a$, where a is the inter-electrode distance.
- **Half-Schlumberger configuration,** also called the three-point electrode configuration. One of the current electrodes, the remote electrode, is grounded at a remote position - at least 3.5 times the maximum distance between the centre and the current electrode), at right angles to the expanding profile. The geometrical coefficient is double that of the normal Schlumberger configuration.
- **Pole-pole configuration,** sometimes called the half-Wenner array. One current and one potential electrode are kept at the remote position. The potential difference measured between M, the measuring electrode, and N, the remote electrode, will be equivalent to the potential created by current electrode A. The geometrical coefficient is equal to $2\pi a$, where a is the distance between electrodes A and M.
- **Dipole-dipole configuration.** Two current electrodes, a positive electrode A and a negative electrode B, and two potential electrodes M and N, form dipoles if they are separated by a very large distance; the current dipole AB must be separated from the measuring dipole MN by a distance more than five times the dipole length (A to B or M to N, they are the same). The geometrical factor for the dipole-dipole method is $n(n+1)(n+2)\pi a$, where a is the dipole length and n is any integer.

A wide range of equipment is available to suit various purposes. Some setups are for shallow-depth investigations, others are for deep investigations. Because the grounding conditions in a landslide may not be favourable, the receiver of the equipment should have very high input

impedance (at least 10 MΩ). The basic requirement on a transmitter is that it can provide a constant-current source while this current is introduced into the ground. The use of very low AC current will help to minimise the polarisation effect (layering of electrical charge at the contact between an electrode and the ground). A microprocessor-controlled resistivity meter with a multi-electrode switching system is helpful for the detailed investigation of landslides in a short time.

In general the term 'depth of investigation' refers to the depth below which surface devices are insensitive to the value of the physical properties of the earth (Oldenburg and Li 1999). This depth depends on the distance between the current and potential electrodes and/or on the total length of the array (Edwards 1977). It also depends on the geology. By increasing the distance between the current and potential electrodes, information from a greater depth can be obtained. This can be achieved in different ways: by increasing the distance between the current electrodes and keeping the distance between the potential electrodes fixed, or by increasing the distance between the current and the potential electrodes.

Measurement procedures

There are three main procedures used in resistivity measurement: electrical profiling, vertical electrical sounding, and 2-D profiling (also called electrical resistivity tomography (ERT) or subsurface imaging (SSI)). Any of the electrode configurations can be used for electrical profiling and sounding measurements; pole-pole and Wenner configurations are usually used for 2-D profiling.

In **electrical profiling (EP)** profiling, inter-electrode distances are kept fixed, and the array of the electrodes is moved laterally along a profile, the apparent resistivity being plotted at midpoints. This is called continuous profiling or simple profiling. In profiling, the search depth remains the same throughout the profile. Profiling is used to find out lateral variations in resistivity. This method is useful for mapping loose, sliding, and intact masses in the slope, fracture zones in rocks, or steeply dipping contacts between different types of earth materials.

Vertical electrical sounding (VES) is conducted to find out resistivity variations with depth. This is done by increasing the distance between the outer current electrodes or by increasing the relative distance between the current and potential electrodes. The centre of the measurement is kept fixed. The curve is plotted on bi-logarithmic paper with electrode spacing versus apparent resistivity (Figure 8.19). This curve, known as a sounding curve, implies variations in electrical resistivity with depth.

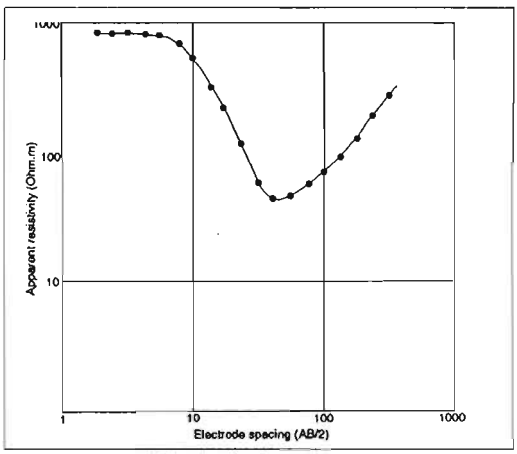

Figure 8.19: **Vertical electrical sounding curve, showing apparent resistivity as a function of electrode spacing (AB/2)**

The method of **2-D electrical profiling** is used to measure both vertical and lateral change in electrical resistivity. This can be considered as a combination of profiling and sounding. Increasing the distance between the current and potential electrodes produces the effect of sounding while shifting the current electrode along the measurement line produces the effect of conventional profiling (Figure 8.20). This method is useful for preparing electrical resistivity

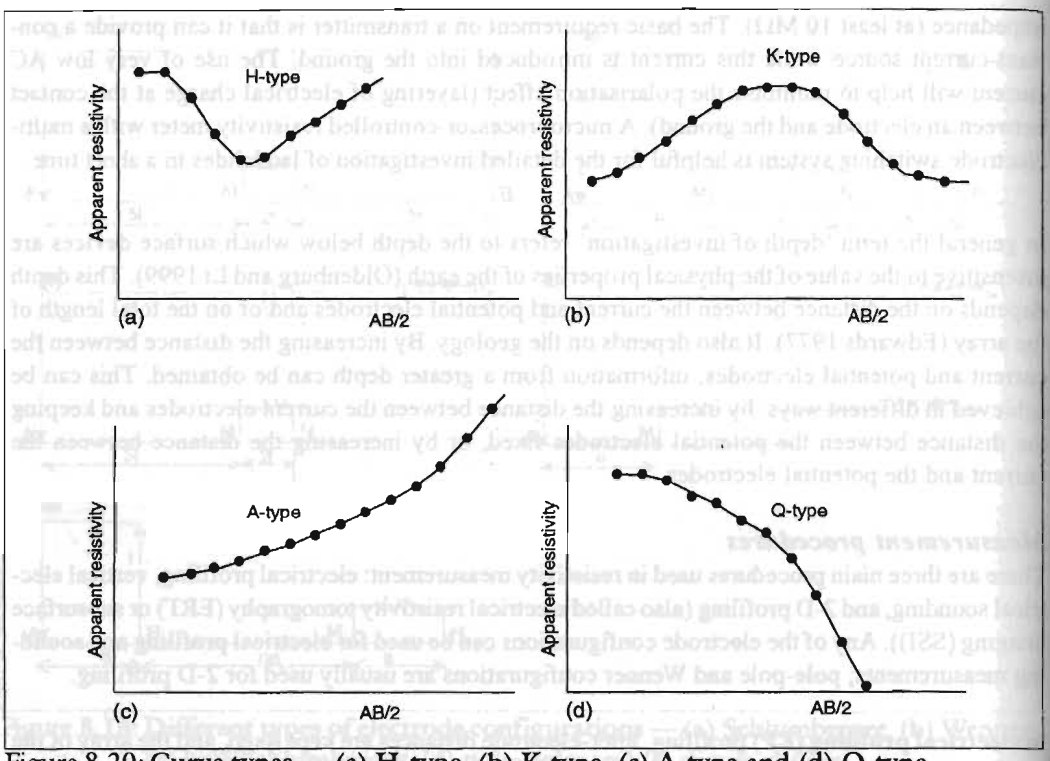

Figure 8.20: **Curve types — (a) H-type, (b) K-type, (c) A-type and (d) Q-type.**

tomograms (showing the variation in electrical resistivity across a 2-D section) of the subsurface of a landslide.

Interpretation of Data

The first stage in the interpretation of electrical resistivity data is **qualitative interpretation**.

Conventional electrical profiling data undergo only qualitative interpretation and the end products are apparent resistivity maps and profiles.

The subsurface under investigation may include a number of layers of a geological formation. Each layer of the formation will show certain values of electrical resistivity. VES curves are separated during qualitative interpretation according to curve types. Separating the curves by type and analysing them helps in the formation of a geoelectrical and geological concept of the study area; VES curves roughly show the geoelectrical characteristics of a site. Depending on the relative distribution of resistivity along a depth section, there may be different types of curves. For a three-layered section there are four different types of curves: H (bowl) type, K (bell) type, A (ascending) type, and Q (descending) type (Figure 8.21).

H-type	$\rho_1 > \rho_2 < \rho_3$
K-type	$\rho_1 < \rho_2 > \rho_3$
A-type	$\rho_1 < \rho_2 < \rho_3$
Q-type	$\rho_1 > \rho_2 > \rho_3$

where ρ_1, ρ_2, ρ_3 are the resistivities of the first, second, and third layers.

A combination of these types of curves can be obtained for sections with more than three layers.

During qualitative interpretation, VES data are usually presented as maps of curve types and apparent resistivity maps at different electrode spacings and sections. Maps at different electrode spacings are useful for the analysis of resistivity distributions at different depth levels. This information can be further used to estimate material type distributions.

Quantitative interpretation is based on mathematical analysis. Quantitative analysis is highly developed for VES data for depth probing. Interpretation of VES data is carried out by matching field curves against curves theoretically calculated by computer. Suitable parameters of the layers (true resistivity and thickness) that fit with geological concepts are chosen. The matching is made based on the assumption that the layers are horizontal. In the case of landslides, layers are assumed to be parallel to the surface of the slide. The final results are presented as geoelectric sections.

Recent developments in finite element processing techniques applied in electrical resistivity methods also make it possible to invert 2-D profiling data. Commercial 2-D resistivity imaging inversion packages are available from a number of sources. One such is RES2DINV. This program automatically determines a two-dimensional resistivity model for the subsurface using the data obtained from electrical imaging surveys. The 2-D model used by the inversion program consists of a number of rectangular blocks. The distribution of the block sizes is automatically generated by the program so that the number of blocks do not exceed the number of data points. The depth of the bottom row of blocks is set to be approximately equal to the equivalent depth of investigation of the data points with the largest electrode spacing (Edwards 1977). A finite-difference forward modelling subroutine is used to calculate the apparent resistivity values, and a non-linear least-squares optimisation technique is used for the inversion routine. The optimisation method basically tries to reduce the difference between calculated and measured apparent resistivity values by adjusting the resistivity of the model blocks. The software has different options that help to modify processing parameters to suit the nature of the data and the geological problems to be solved. The end product of such processing is an image of the true resistivity distribution of the subsurface. A subsurface that consists of bodies or layers can be produced by finite-element forward modelling. In this modelling, the resistivity response for a 2-D model is calculated and displayed as a pseudo-section for comparison with the original field data. This approach is useful for generating realistic subsurface geometries. The end products of the processing are called electrical resistivity tomograms.

Elektrokinetic (Filtration) Potential Method

The electrokinetic (filtration) potential method is a passive method: there is no need to create an artificial source as in the seismic and resistivity methods. The method measures the naturally occurring electrokinetic potential (also called zeta potential or filtration potential, the electric potential that exists across the interface of all solids and liquids). Electrokinetic potentials are related to the movement of groundwater in porous rocks. Favourable conditions for the formation of strong electrokinetic potentials are: a large pressure gradient on the filtering horizon, high resistivity (low mineralisation) of water, a shallow filtering horizon, high resistivity of the overburden overlying the filtering layer, and a narrow pore structure with high permeability (Semenov 1974). These conditions are fully satisfied in a landslide and other critical slopes. Although there are no publications related to the application of this method to landslides, there are reports of its successful use to detect leakage from a water reservoir (Bogoslovsky and Ogilvy 1970), leakage of contaminant plumes from a waste disposal site, and groundwater contamination (Corwin 1986; Schiavone

and Quarto 1984; Hughes et al. 1986). The method's application in other fields related to groundwater movements suggests that it could also be used to investigate shallow landslides.

Since electrokinetic potential measurement does not require an external source, only two electrodes are needed (to receive the signal). The receiving electrodes consist of a porous pot made of ceramic or wood that leaks a concentrated salt solution, usually copper sulphate, into the ground through which contact with the ground is maintained; the metal electrode is immersed in the solution. For the acquisition of data in a landslide, one of the potential electrodes is kept fixed outside the landslide and the other is moved to measure along a profile. The end products are presented as maps or profiles. The groundwater recharge area will be indicated as negative and the discharge area as positive potential areas. The area with predominant movement of groundwater will be indicated by relatively high-intensity potential areas.

Other methods

There are other methods that can be applied to the investigation of landslides, including the ground conductivity, electromagnetic, and ground penetrating radar (GPR) methods (Parasnis 1997; Reynolds 1997). All these methods may be useful for shallow depth investigations, usually ranging from a few metres to a few tens of metres.

Applications and Case Studies

The following case studies were carried out in landslides along the Arniko Highway and near the desilting basin of a hydropower project in Nepal, and near Yaan in Sichuan, southwest-central China. The location maps for these sites are presented in Figures 21 and 22.

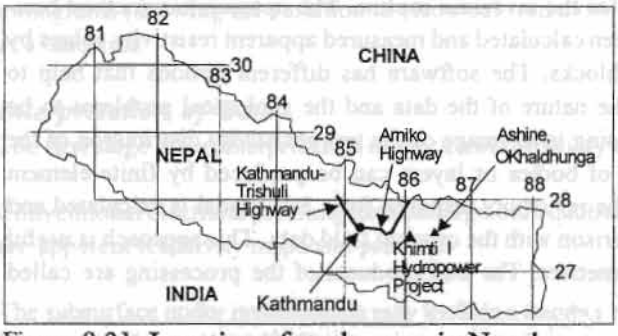

Figure 8.21: Location of study areas in Nepal

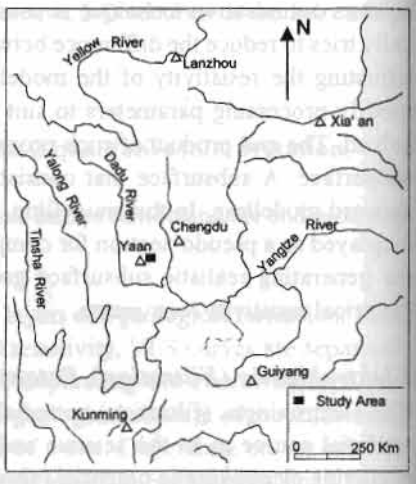

Figure 8.22: Location of study areas in south-west central China

Investigation of a landslide using Seismic Refraction and VES: Xiakou Landslide, Sichuan, China

Yaan, a small city in Sichuan, has been inundated by floods several times in the past, mainly due to the blocking of the Longxi River by a landslide. This landslide, known as the Xiakou Landslide, was identified as one of the study sites of the Mountain Risk Engineering, China Project (Figure 8.22). The slide is 9 km upstream of Yaan City.

Two methods were proposed for the investigation: seismic refraction and vertical electrical sounding (VES). The objectives of VES and seismic refraction were to decipher the overburden and

discover the depth to bedrock. During the interpretation and processing of field data, findings of both seismic refraction and VES were compared. The fieldwork was conducted during November 1995.

Previously the area had been studied by drilling a single borehole. The borehole showed a multi-layer sequence of gravel and boulders, and boulders mixed with clay. The bedrock consists of series of sandstone, claystone, and silty-claystone. As part of the geophysical investigation, the subsurface of the landslide was explored by five seismic profiles and 28 VESs. Due to the constraints in the available number of channels, the geophones were spaced at 10m intervals. With this spacing, it was only possible to obtain average information for the overburden. Most of the VESs were conducted using the Schlumberger configuration, and a few using the half-Schlumberger. The electrodes were expanded along the slope. The locations of the VES and seismic profiles are shown in Figure 8.23.

The VES curves were interpreted both qualitatively and quantitatively. They indicated that the water table was at a shallow depth (1-3m), and that a very low resistivity layer overlay the bedrock everywhere. One of the representative sounding curves is shown in Figure 8.24 together with the qualitative interpretation. The apparent resistivity map at electrode spacings (AB/2) of 8m is shown in in Figure 8.25. The idea behind the selection of this particular electrode spacing for mapping was to acquire information about the very shallow sliding layer. At very short electrode spacings (<5m), measurements may be highly affected by surface inhomogeneities. The apparent resistivity values can be roughly correlated with the material-type distribution in the near-subsurface. From the map, a coarse-grain-dominated material would be expected at a shallow depth in the north-east part of the area. The proportion of clay increases toward the south, south-east, and south-west parts of the area. The area dominated by low resistivity is more prone to mudslide than the others.

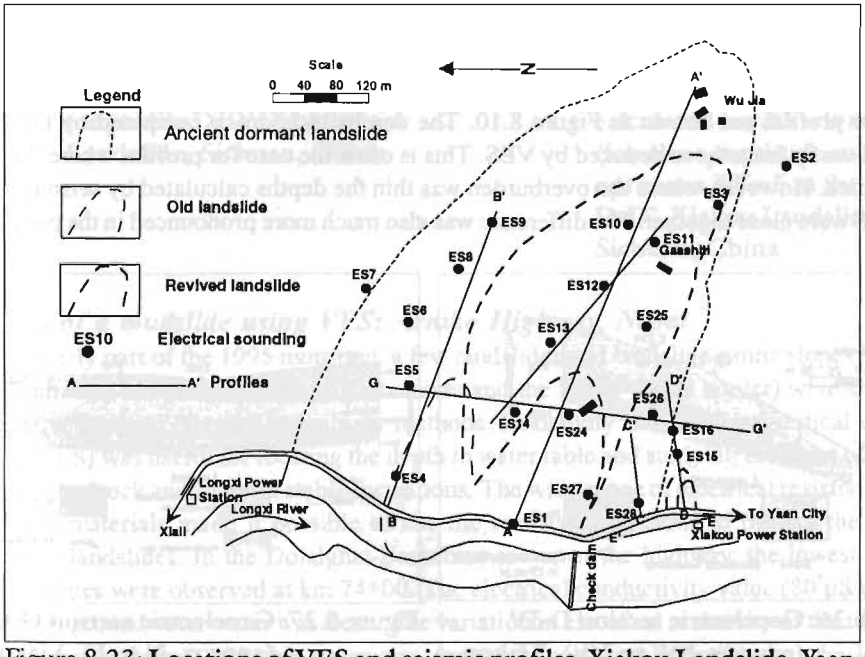

Figure 8.23: **Locations of VES and seismic profiles, Xiakou Landslide, Yaan, Sichuan, China.**

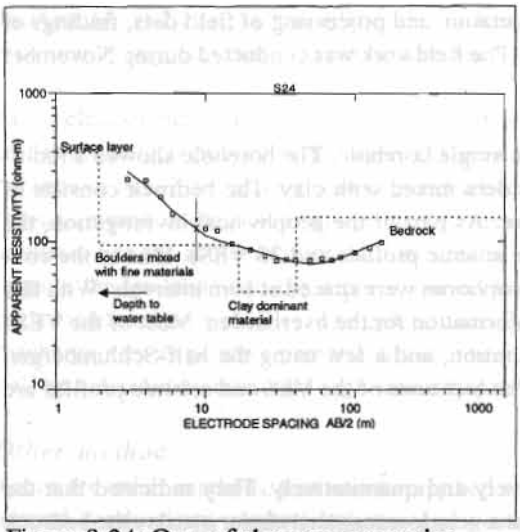

Figure 8.24: One of the representative sounding curves and its curve matching results, Xiakou Landslide, Sichuan, China

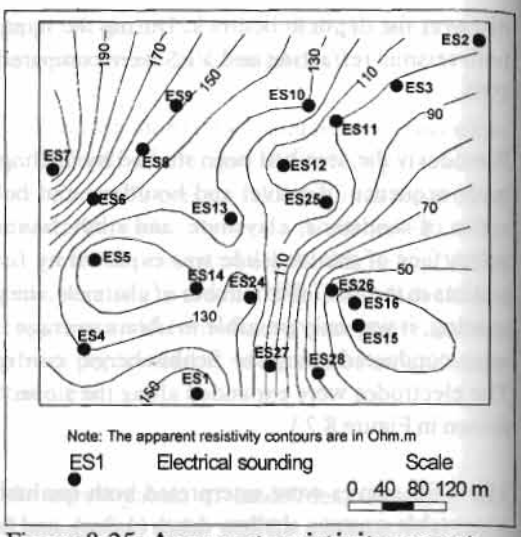

Figure 8.25: Apparent resistivity map at electrode spacing (AB/2) of 8 m, Xiakou Landslide, Sichuan, China

The results of the quantitative interpretation of the VES curves are presented as geoelectric sections D-D' and G-G' in Figures 8.26 and 8.27. Figure 8.27 shows a very thick overburden. The northern part of this profile reveals four electric layers, reducing to three in the south. The first layer is a very loose surface layer above the water table; the second is a cumulative effect from an accumulation of different layers of clay and boulders or clay and boulders mixed together; and the third is a clay-dominant material. The fourth electric layer effect is from bedrock. Geoelectric section D-D' (Figure 8.26) indicates only two layered media: the bedrock is overlain by a clay-dominant layer.

Seismic refraction profiles were interpreted using the t_0 method. The results for one of the representative profiles are shown in Figure 8.10. The depths to bedrock computed by the t_0 method differed vastly from those deduced by VES. This is often the case for profiles where the overburden is thick. However, where the overburden was thin the depths calculated by seismic refraction and VES were close together. The difference was also much more pronounced in the profiles where

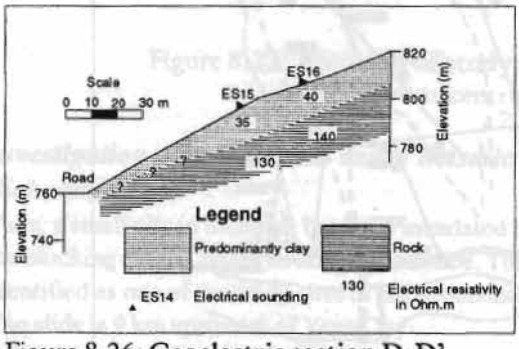

Figure 8.26: Geoelectric section D-D' (approx. SW to NE), Xiakou Landslide, Sichuan, China

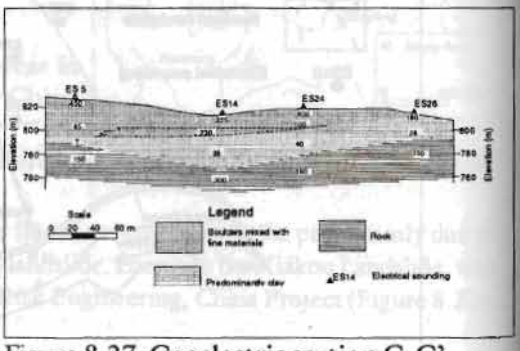

Figure 8.27: Geoelectric section G-G' (approx. N to S), Xiakou Landslide, Sichuan, China

more clay was expected. The velocity of the refractor deduced from the t_0 method is highly affected by bedrock topography. Due to the bedrock topography, several fictitious velocity changes were identified that were not compatible with the actual bedrock geology in the landslide (see Figure 8.10 for details).

To overcome this problem, all seismic profiles were processed using the generalised reciprocal method (GRM). Since there was no micro-seismic survey, it was not possible to make a detailed study of the overburden. Hence the objectives of the GRM processing were to determine depth to bedrock (target refractor) and to estimate the true refractor velocity. An average velocity of the overburden (above the target refractor) was calculated for optimum XY values. The final migrated sections of representative profiles B-B' and D-D' are presented in Figures 16, and 28 respectively; in these figures, the interface between the refractor and the overburden is tangent to the arcs. The results produced by GRM and the t_0 method were similar for profile D-D' but differed considerably for profile B-B'. The results of the GRM processing show again that the conventional method of interpretation can only be justified for shallow-depth investigations (less than 10-15 m; see Figure 8.29). When the results obtained by the t_0 method (Figure 8.10) and GRM (Figure 8.16) for profile B-B' are taken together, they indicate that the velocity changes along the bedrock indicated by the t_0 method result from the bedrock topography.

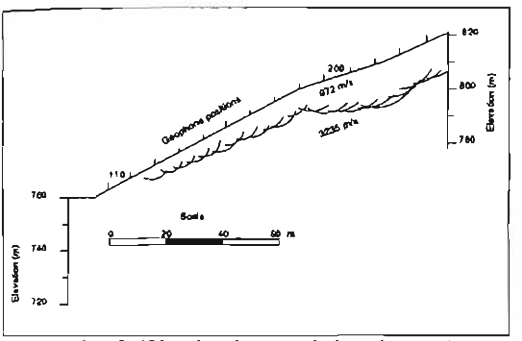

Figure 8.28: **Final migrated depth section for profile D-D', Xiakou Landslide, Sichuan, China**

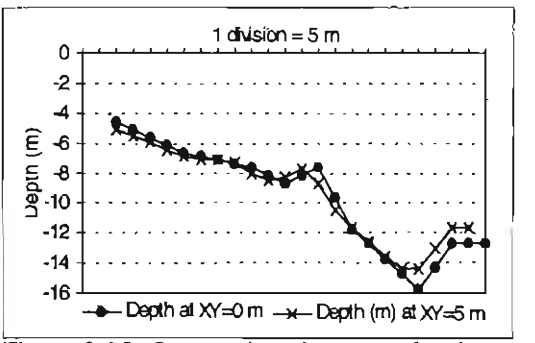

Figure 8.29: **Comparison between depths calculated for XY=0 metres (for the t_0 method) and optimum XY=5 m for profile D-D', Xiakou Landslide, Sichuan, China**

Prediction of a mudslide using VES: Arniko Highway, Nepal

During the early part of the 1995 monsoon, a few landslides and landslide-prone slopes along the Arniko Highway (which runs between Kathmandu and the Nepal-China border) were studied by seismic refraction and electrical resistivity methods. Resistivity measured by vertical electrical sounding (VES) was useful for locating the depth to water table and studying the types of material and depth to bedrock and/or more stable formations. The wide range of electrical resistivity values for different materials made it possible to use the resistivity methods to predict the possible activation of landslides. In the Dolalghat-Barhabise sector of the highway, the lowest apparent resistivity values were observed at km 74+00. The electrical conductivity value (80 µS/cm) indicated that the groundwater water was fresh. The variation in electrical resistivity of the material in the overburden saturated with this water was due to the variation in grain size: the lower the electrical resistivity, the finer the grain size.

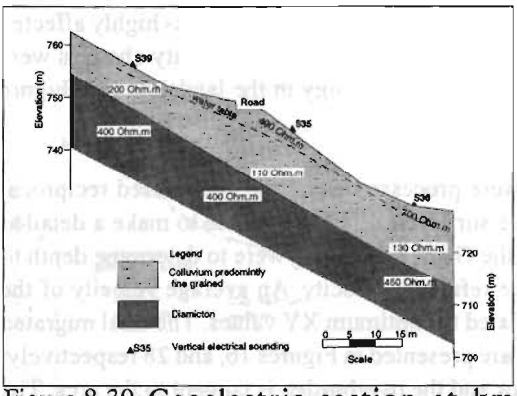

Figure 8.30: **Geoelectric section at km 74+00, Arniko Highway, Nepal**

Several vertical electric soundings were conducted on the slope to the mountain and valley-side of the highway at km 74+00 (Figure 8.30). The VES measurements showed that the water table was at a depth of 2-3.5m. The electrical resistivity was 110-130 Ω m in the lower part of the profile (valley side), and 200 Ωm and more on the mountain side. The low electrical resistivity on the valley side indicated that the overburden consisted of a predominantly finer matrix, with higher porosity and lower permeability. Since there was the possibility of a further rise in the water table during the monsoon, occurrence of a mudslide was predicted. The road slid a week after completion of the fieldwork.

Study of landslides using 2-D profiling: Arniko Highway, Nepal

In February 1997, a proposal was made to study in detail the subsurface of two landslides at km 85+280 and km 87+700 of the Arniko Highway using electrical resistivity methods. The objectives of the study were not only to investigate the subsurfaces of these landslides but also to work out appropriate methodologies for continuous coverage to enable estimation of types of material in the subsurface. The types of material and the nature of the slides observed at these sites were similar to those observed in other sections of the Barhabise-Kodari section (km 87-114). Thus it was hoped that the findings and methodologies worked out for these landslides could be used in future investigations along the Barhabise-Kodari section as well as other parts of the Arniko Highway.

The landslide surface material was dominated by silt at km 87+700, and by mostly coarse-grained material at km 85+280. There are reports that in 1955 a mudflow from the Sandhi Kholsa (km 87+700) dammed the Bhote Kosi River for a few hours. A shallow mudslide has been reactivated at the Sandhi Kholsa since 1990, and there is a possibility that the Bhote Kosi could again be dammed in the future.

The landslides were studied using 2-D profiling (electrical resistance tomography or ERT) and by conventional vertical electrical sounding (VES). The 2-D profiling was conducted using a pole-pole configuration with a unit electrode spacing of 4m together with some additional measurements at 1, 2, and 3m to get the effect of microsounding. Conventional VES's were conducted using the Schlumberger configuration. The Schlumberger and pole-pole results were compared and the results showed that the pole-pole configuration was less affected by near-surface inhomogeneities and had greater depth penetration. Thus the pole-pole configuration was recommended for future shallow-depth investigations (Pant 1998), especially for mapping shallow landslides. Figures 31-33 show three of the tomogram profiles: one at km 85+280 and two at the Sandhi Kholsa (km 87+700).

The sliding area at km 85+280 seems to be a part of a larger unstable area. Figure 8.31 shows the 2-D profile along the downslope (below road level) at an angle of 32 degrees. The very high electrical resistivity (more than 5000 Ωm) in the model section is indicates a dry, loose, and displaced mass. The maximum thickness of the image (high resistivity zone) is 10-12m. This zone is prone to sliding

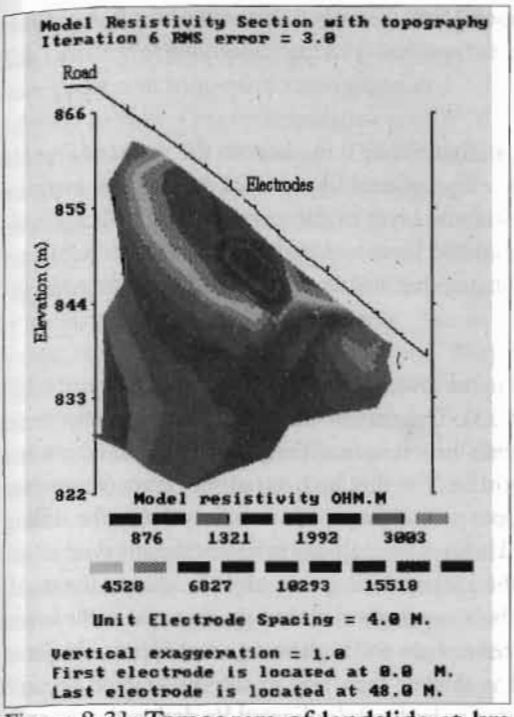

Figure 8.31: Tomogram of landslide at km 85+280, Arniko Highway, Nepal

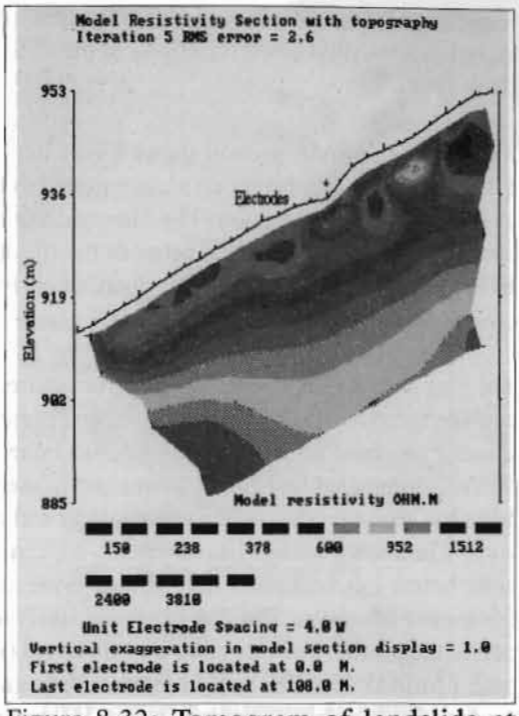

Figure 8.32: Tomogram of landslide at Sandhi Kholsa, Profile One, Arniko Highway, Nepal

during the monsoon. Below this zone the resistivity decreases slowly. From the resistivity distribution pattern at depth it can be inferred that there is no effect from fresh rock. However the low resistivity formation at depth indicated by the tomogram might indicate the presence of fractured and weathered rock.

The 2-D profiles shown for the Sandhi Kholsa (km 87+700) were made at an angle of 45° to each other and in a slope of 20°. The first profile (Figure 8.32) trends north-east to south-west, and the second (Figure 8.33) south-east to north-west; they cross each other at the point denoted by the asterisk. The unit electrode spacings for the first and second profiles were 4 and 5m respectively. Micro-VES measurements using a pole-pole configuration showed the ratio of the resistivity of the slide to the resistivity of the underlying layer to be 3:10. This was interpreted as reflecting differences in rock (lithological) characteristics between the sliding material and the underlying material that serves as the slip surface. The lower part of the slide (silt-domi-

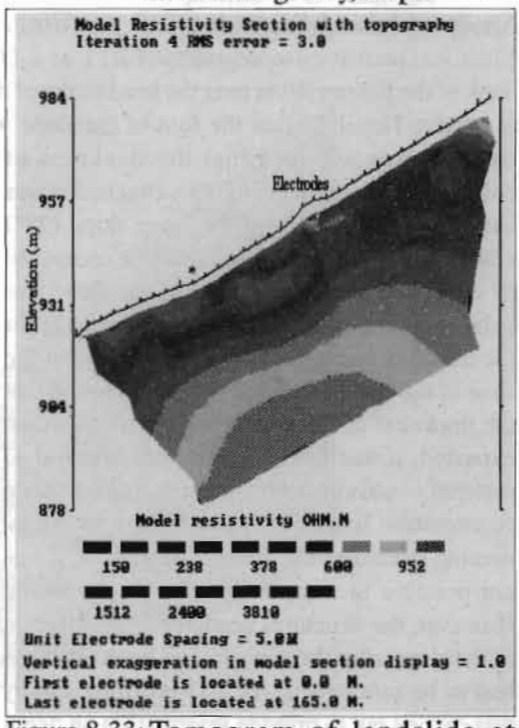

Figure 8.33: Tomogram of landslide at Sandhi Kholsa, Profile Two, Arniko Highway, Nepal

nated material) was developed within the same material type (usually only the case for fine-grained materials); the ratio of the resistivity of the slide to the resistivity of the underlying layer was 1.3:2 (Pant 1998).

The model resistivity section shows a very low-resistivity layer quite near to the surface (Figures 8.32 and 8.33). This layer can be interpreted as the effect of a silt-dominated deposit that is prone to flow during the monsoon. The intermediate-resistivity layer is interpreted as the effect of collapsed rock mass sandwiched between the silt-dominated layer and high-resistivity bedrock (Pant 1998). The pattern of resistivity distribution indicates that the thickness of the overburden increases toward the upslope.

The near-subsurface low-resistivity layer apparent in the lower part of the first profile (Figure 8.32) can't be seen clearly in the second profile (Figure 8.33). This may be because a larger unit electrode spacing was used for the second profile (5 rather than 4m). It seems likely, however, that there is a thin silt-dominated layer at the lower part of the profile. The thin high-resistivity layer (more than 500 Ωm) seen near the surface in the middle and upper part of the profile is mainly due to the sliding layer. The sliding surface lies on the silt-dominated layer. The inability to detect the silt-dominated layer below this high-resistivity sliding layer in the second tomogram might be due to the small thickness of the layer. The sliding layer is likely to be coarser-grained than the material in the lower part of the profile. The other two electric layers (intermediate and high-resistivity) appear similar in both profiles. The overburden at the upper end is thicker than that at the lower end. In both profiles, the high-resistivity substratum is interpreted as bedrock (indicated by dark red colours in the figures).

Study of a landslide using 2-D profiling: Khimti I Hydropower Project, Nepal

Electrical resistivity tomography (ERT), or 2-D profiling, was used to study a slope on the right bank of the Khimti River near the headworks of the Khimti I hydropower project being constructed in eastern Nepal. Before the foot of the slope was excavated during preparations for a desilting basin, it was assumed that the thickness of colluvium was less than 5m. This conclusion was based on the evidence of the steep slope (38°) and the proximity of exposed bedrock composed of schist and gneiss. The base of the slope was to be cut for about 10-15m to prepare the site for the desilting basin. As the loose material at the base of the slope was removed, it was found that the thickness of the colluvium was greater than expected; it was feared that further removal of material would affect the slope stabilisation. Since construction had already started on the engineering structures for the desilting basin, it was not possible to completely relocate the basin. However, the structures needed for stabilisation of the slope after the material had been removed had to be redesigned. An 2-D profiling survey was carried out to provide information on depth to bedrock, type of material in the overburden, and depth to water table in the slope.

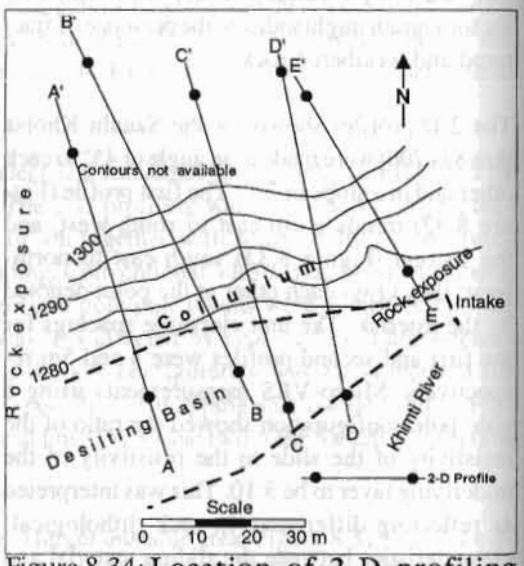

Figure 8.34: Location of 2-D profiling profiles, Khimti I hydropower project, Nepal

Measurements were conducted along five profiles laid along the slope (Figure 8.34). The data were processed to prepare tomograms and 2-D polygon models. One representative profile (C-C') is taken here for discussion. The tomogram is shown in Figure 8.35. It contains an image of very high electrical resistivity (>5000 Ωm) extending from the surface to a depth of about 12-15m. The image below the yellow colour is produced by rock that is below the water table. The expected bedrock is jointed and weathered. Very high electrical resistivity values (probably more than 9000 Ωm) indicate the presence of very loose and dry material within the overburden in the lower and central part of the profile.

The data used to prepare the tomogram were also processed to prepare a polygon model, and these results used to prepare geoelectric sections. The geoelectric section for profile C-C' is shown in Figure 8.36. The very high electrical resistivity layer indicates mainly loose and dry overburden. The VES results indicated the presence of a saturated alluvial deposit in the lower part of the profile. Bedrock is represented by relatively low resistivity. The body in the section with a resis-

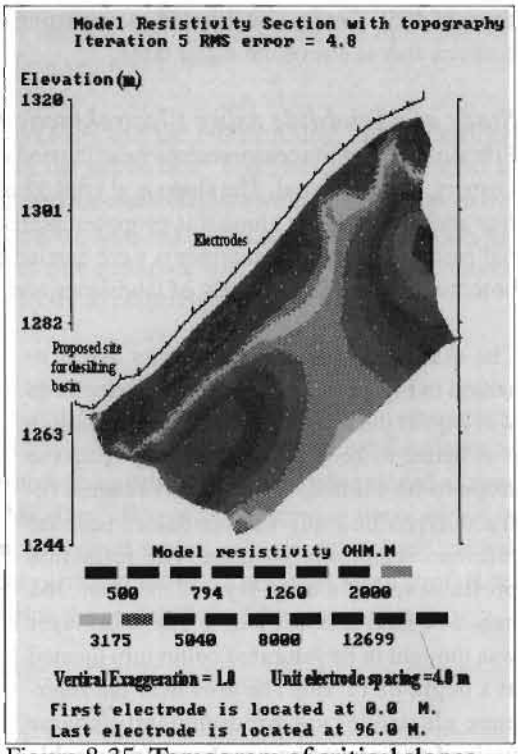

Figure 8.35: Tomogram of critical slopes for profile C-C' near the Khimti I hydropower project, eastern Nepal

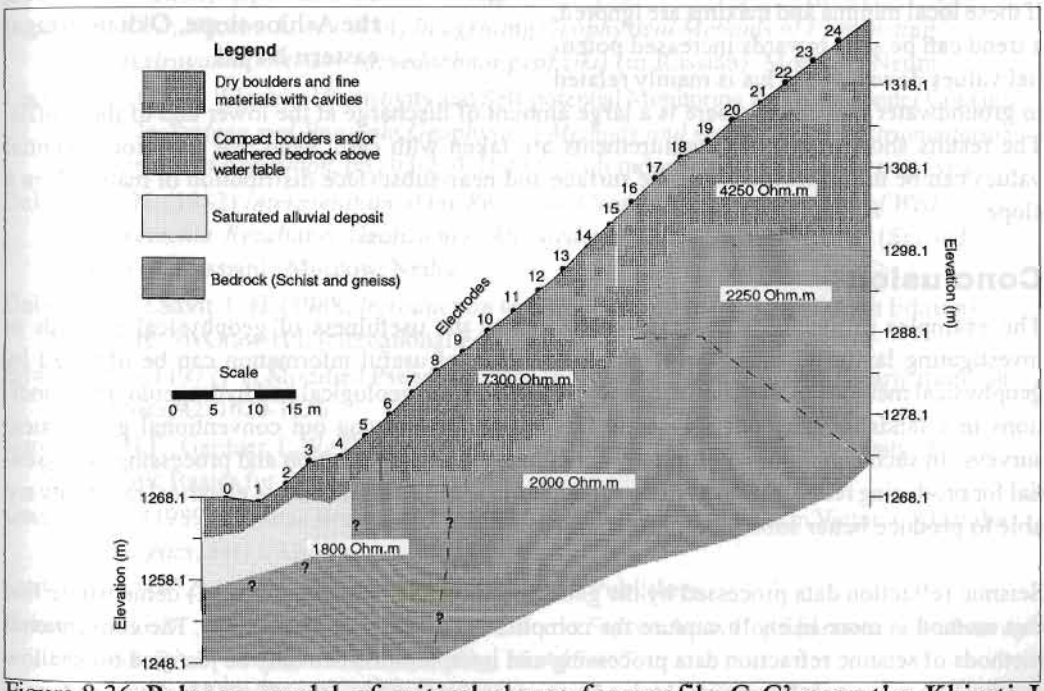

Figure 8.36: Polygon model of critical slopes for profile C-C' near the Khimti I hydropower project, eastern Nepal.

tivity of 4250 Ωm was interpreted as consisting of compact boulders and fine material, and may be bedrock that is above the water table.

Study of a landslide using Electrokinetic (Filtration) potential: Okhaldhunga, Nepal

Filtration potential measurements were carried out on the slope of Ashine village in Okhaldhunga District, eastern Nepal. The slope is at km 157 of the proposed Gaighat-Okhaldhunga Highway. A few additional slopes along this proposed highway were also investigated by the filtration potential method. These measurements were carried out to demonstrate the usefulness of the filtration potential method in the study of landslides and critical slopes.

The Ashine slope measurements are presented in Figure 8.37. The reference electrode was kept at the middle of the profile, although it is better to keep electrodes away from the slope to be studied. A very short seismic refraction profile study was conducted near the reference electrode position. The refraction profile revealed a three-layered medium: 365 m/s, 674 m/s, and 1561 m/s. The third layer was thought to be saturated colluvium located at a depth of 11.5m. The area near the reference electrode was predominantly coarse grained and served as a recharge (permeable zone). The upper and lower parts of the slope had several permeable and impermeable beds indicated in the figure as local lows and highs. If these local minima and maxima are ignored, a trend can be seen towards increased potential values downslope. This is mainly related to groundwater movement; there is a large amount of discharge at the lower end of the profile. The results show that if the measurements are taken with care, even low filtration potential values can be useful for mapping the surface and near-subsurface distribution of materials in a slope.

Figure 8.37: **Filtration potential observed on the Ashine slope, Okhaldhunga, eastern Nepal**

Conclusion

The examples presented in the case studies show the usefulness of geophysical methods in investigating landslide subsurfaces. A large amount of useful information can be obtained by geophysical methods in a cost-effective way. However, the geological and hydrogeological conditions in a landslide may not always be favourable for carrying out conventional geophysical surveys. In such situations, appropriate techniques for data acquisition and processing are essential for producing reliable results. New techniques in seismic refraction and electrical resistivity are able to produce better subsurface information.

Seismic refraction data processed by the generalised reciprocal method (GRM) demonstrate that this method is more likely to capture the complicated geology of a landslide. The conventional methods of seismic refraction data processing and interpretation can only be justified for shallow depths. The velocity information obtained by conventional methods is affected by bedrock topography and near-surface lateral inhomogeneities – situations often met in landslide areas. In con-

trast, the velocity information obtained by GRM is reliable, and the velocities and optimum XY values can be used to generate a migrated subsurface section.

The electrical resistivity tomograms of the landslides show that the 2-D profiling, or ERT, method is capable of producing detailed information about the subsurface. The method can be used to separate sliding masses from intact masses and slip surface materials by virtue of the high resistivity contrasts. However, if there is fine material in the near-subsurface that is prone to mudslide, the resistivity difference between the sliding and intact fine materials will not be very high. Good-quality bedrock is always indicated by very high electrical resistivity values.

Acknowledgements

The author is thankful to Dr. John M. Reynolds for his reading and comments during the preparation of this paper. The author is grateful to the Arniko Highway Project and the owner and developer of the Khimti I Hydropower Project for granting permission to publish the materials enlisted as case studies in this paper. I extend my sincere thanks to Mr. Alexis Wagner for reviewing the materials in the case studies; he has always emphasised the importance of investigating landslides and critical slopes along the highways of Nepal by geophysical methods. Finally, I am thankful to Prof. B.N. Upreti and Prof. Li Tianchi for their suggestions during the preparation of the manuscript.

References

Bogoslovsky, V.A.; Ogilvy, A.A.; Strakhova, N.A. (1977) 'Magnetometric and Electrometric Methods for the Investigation of the Dynamics of the Landslide Processes'. In *Geophysics Prospect,* 25: 280-291

Bogoslovsky, V.A.; Ogilvy, A.A. (1970) 'Natural Potential Anomalies as a Quantitative Index of the Rate of Seepage from Water Reservoirs'. In *Geophysical Prospecting*, 18(2): 261-268

Brodovoe, V. V.; Nikitin, A. A. (1984) *Integrating Geophysical Methods of Prospecting (Complexirovania metodov razvedochnoi geofiziki)* (in Russian). Moscow: Nedra

Corwin, F.R. (1986) 'Electrical Resistivity and Self-potential Monitoring for Groundwater Contamination'. In *Surface and Borehole Geophysical Methods and Groundwater Instrumentation Conference and Exposition,* pp 203-214. Denver, Colorado: Name of Publisher not given

Dakhnov, V.N. (1982) *Interpretation of the Results of Geophysical Investigation of Wells (Interpretachia Rezultatov Geofizicheskikh Isledovanii Razrezov Skvajhin)* (Second edition) (in Russian). Moscow: Nedra

Dobrin, M.B.; Savit, C.H. (1988) *Introduction to Geophysical Prospecting* (Fourth Edition). Singapore: McGraw-Hill International Editions

Edwards, L.S. (1977) 'A Modified Pseudo-Section for Resistivity and Induced Polarization'. In *Geophysics*, 42: 1020-1036

Gardner, G.H.F.; Gardner, L.W.; Gregory, A.R. (1974) 'Formation Velocity and Density- The Diagnostic Basics for Stratigraphic Traps' In *Geophysics*, 39: 770-780

Geissler, P.E. (1989) 'Seismic Reflection Profiling for Groundwater Studies in Victoria, Australia'. In *Geophysics*, 54(1): 31-37

Gurvich, I.I. (1972) *Seismic Prospecting*. Moscow: Mir Publishers

Habberjam, G. M.; Watkins, G. E. (1967) 'The Use of a Square Array Configuration in Resistivity Prospecting'. In *Geophysical Prospecting*, 15: 445-467

Hagedoorn, J.G. (1959) 'The Plus-Minus Method of Interpreting Seismic Refraction Sections'. In *Geophysical Prospecting* , 7(2):158-182

Keller, G. V.; Frischknecht, F. C. (1966) *Electrical Methods in Geophysical Prospecting*. London: Pergamon

Klushin, I.G. (1968) *Integrated Application of Geophysical Methods for Solving Geological Problems (Complexirovannoe primenenia geofizicheskikh metodov dlya reshenia geologicheskikh zadach)* (in Russian). Leningrad: Nedra

Lankston, R.W. (1990). 'High-resolution Refraction Data Acquisition and Interpretation'. In Ward, S.H. (ed) *Geotechnical and Environmental Geophysics. Vol. I: Review and Tutorial*, pp 45-73. Tulsa: Society of Exploration Geophysicists

Lankston, R.W., Lankston, M.M. (1986) 'Obtaining Multilayer Reciprocal Times Through Phantoming'. In *Geophysics*, 51: 45-49

Mauritsch, J.H.; Seiberl, W.; Arndt, R.; Romer, A.; Schneiderbauer, K.; Sendlhofer, G.P. (2000) 'Geophysical Investigations of Large Landslides in the Carnic Region of Southern Austria'. In *Engineering Geology*, 56:373-388

Novitskii, G. P. (1974) *Integrating Geophysical Methods of Investigation* (*Complexirovannia geofizicheskikh metodov razvedki)* (in Russian). Leningrad: Nedra

Oldenburg, D.W.; Li, Y. (1999) 'Estimating Depth of Investigation in DC Resistivity and IP Surveys'. In *Geophysics*, 64(2):403-416

Palmer, D. (1981) 'An Introduction to Generalized Reciprocal Method of Seismic Refraction Interpretation'. In *Geophysics*, 46:1508-1518

Pant, S.R. (1998) 'Use of Pole-Pole and Schlumberger Electrode Arrangements of Electrical Resistivity Survey of Landslides along Arniko Highway'. In *Bull. Dept. Geology, Tribhuvan Univ.*, 6:31-42

Pant, S.R.; Li, T.; Wagner, A.; Wei, F.; Jiaman, C. (1999). 'High Resolution Seismic Refraction Data Interpretation: An Example from Xiakou Landslide, Sichuwan, China'. In *Jour.Nepal Geol.Soc.*, 19:31-40

Parasnis, D.S. (1997) *Principles of Applied Geophysics*, Fifth Edition, London: Chapman & Hall

Reynolds, J.M. (1997) *An Introduction to Applied and Environmental Geophysics*. England: John Wiley & Sons

Robinson, S. E.; Coruh, C. (1988) *Basic Exploration Geophysics*. USA: John Wiley & Sons

Schiavone, D.; Quarto, R. (1984) 'Self Potential Prospecting in the Study of Water Movements. In *Geoexploration*, 22: 47-58

Semenov, A.S. (1974) *Electrical Methods of Natural Electrical Fields (Elektropazbedka metodom estectvennogo elektricheskogo polya),* (in Russian). Leningrad: Nedra

Sheriff, R.E.; Geldart, L.P. (1982) *Exploration Seismology (Seismorazvedka), Vol.1* (Translated into Russian). Moscow: Mir

Telford, W.M.; Geldart, L.P.; Sheriff, R.E.; Keys, D.A. (1976) *Applied Geophysics*, 2nd edn. Cambridge: Cambridge University Press

Wenner, F. (1912) 'A Method of Measuring Earth Resistivity'. In *US Bureau of Standards Bulletin*, 12:469-478

Wyllie, M.R.; Gregory, A.R; Gardner, G.H.F. (1958) 'An Experimental Investigation of Factors Affecting Elastic Wave Velocities in Porous Media'. In *Geophysics*, 23(3) 459-493

9 Stability Analysis: Practical Problems in Rock Slopes

A.B. Singh
Institute of Engineering, Tribhuvan University,
Pulchowk Campus, Lalitpur, Nepal

The first part of this paper attempts to assess rock mass qualitatively and as far as possible quantitatively in the light of recent developments in the field of rock mechanics. It also provides the basic theoretical background needed for the analysis of the most common types of rock slope failure. The second part discusses examples of the stability analysis of rock slopes at the dam sites of the Upper Arun and Kali Gandaki A hydroelectric projects in Nepal. The analyses are based on information provided by field geologists. The geological and geotechnical conditions in the Upper Arun were not complex so the stability analysis of the rock slopes at this site was more definitive. The geological and geotechnical conditions for the Kali Gandaki A Project were more difficult to interpret, for example the contact between dolomite and phyllites inside the slope could not be ascertained unequivocally even after the conclusion of the design phase. It is likely that problems will be encountered during construction at Kali Gandaki A.

Introduction

In certain situations, stability problems in rocks and soils may appear similar. However, there are a number of characteristics of rock mass that can lead to modes of slope failure that are quite different to those for soils. The first part of this paper deals with the stability problems related to rock or rock slopes, including the structural features related to stability, assessment of rock characteristics, and types of rock slope failure.

Rock or **rock mass**, invariably contains geological weakness planes such as joints, fractures, faults, bedding planes, and foliation planes. From the engineering point of view, rock or rock mass is the total in situ medium including all these discontinuities; **rock material, rock matrix,** or **intact rock** refers to the intact material between discontinuities, for example a hard piece of rock taken from a drill core.

Rock mass may contain various geological discontinuities oriented or distributed in various ways. It is the nature and distribution of these features within a rock mass that mainly governs its behaviour. The rock material is generally stronger than the rock mass and in most cases, except with soft sedimentary rocks, it is not the failure of intact rock but of weaker material and along planes of separation that leads to failure. However, failure will also pass through the intact material and hence, for the same type of rock structure, rock masses that contain stronger intact rock matrices are usually stronger.

It is important to emphasise that rock mass behaviour cannot be described easily in the way possible for materials such as concrete, steel, and some soils. Many variables govern the behaviour of rock masses. These usually vary so widely that scientists must often satisfy themselves with only approximate indications. The most important thing is to make as best an assessment as is possible. Very sophisticated patterns may be mapped out for a rock matrix but failure might take

place along a pre-existing geological discontinuity. This is where a competent engineer needs field experience coupled with a theoretical knowledge of the principles of rock mechanics in order to be able to make sound judgements. Furthermore, practicality demands that geological and rock mechanics data be interpreted in both physical and mechanical terms. Over the years, rock mechanics has made considerable progress and methods have been developed. For example, quantitative methods have now been developed to assess the mechanical behaviour of some geological discontinuities.

In what follows, an attempt will be made to summarise briefly the ways in which rock mass can be characterised and to give examples of how the knowledge so gained is used in practice.

Part A: Geotechnical Background For Rock Slope Analysis

Major Types of Structural Features

There are a number of excellent publications which describe the structural features of rock masses (Price 1966). The most common rock structures — bedding planes, folds, faults, joints, and, shear zones — are described below.

Bedding planes are characteristic of sedimentary rocks and serve to divide these kinds of rocks into a number of beds or strata. Bedding planes are usually very persistent particularly if their deposition has taken place in a wide-open sea in calm water conditions. However, if the sediments are laid down rapidly from heavily laden winds or water currents, bedding planes may have cross or discordant features. In each case bedding planes represent planes of weakness; these planes of weakness may be parallel to the bedding planes if there was no other preferred orientation of particles during deposition. Usually, the strength parameters of the bedding planes will have both cohesion and friction components, but they will be considerably smaller than those in an orthogonal direction.

Folds are formed when the orientation of beds is changed by flexing following the application of post-depositional tectonic forces. Folds range from major structures extending up to several kilometres long to very small localised features. During the folding process, shear stresses are set up between the beds which may reduce the bedding plane shear strength. Large-scale folds, when considered on a regional scale, may be thought of as a rough excrescence which increases the shear strength due to increased frictional resistance. The prominent features generally associated with folds are well-defined sets of joints that are formed in the crest, trough, and limbs of the fold and which divide the rock into discrete elements (Figure 9.1). The higher the number of discontinuities associated with folding, the weaker a rock mass will be. Further information can be found in Price (1966).

Faults are basically fractures on which relative displacement has taken place on opposite sides of a fault plane due to shear. Faults may be pervasive and may extend to several hundred kilometres long, as with the 1,500 km long San Andreas Fault in California, USA. On the other hand they may be of local extent and only metres or centimetres long. The fault zone thickness can also vary from millimetres in the case of local faults to metres and even hundreds of metres in the case of regional faults. A fault zone may contain weak material such as fault gouge (clay), fault breccia (cemented angular rock fragments), rock flour, or granular material. The walls may be coated with minerals such as graphite and chlorite and as a result will have low shear strength. In addition, the fault zone or the area adjacent to the fault may be crushed and disturbed by drag folds or secondary faults or

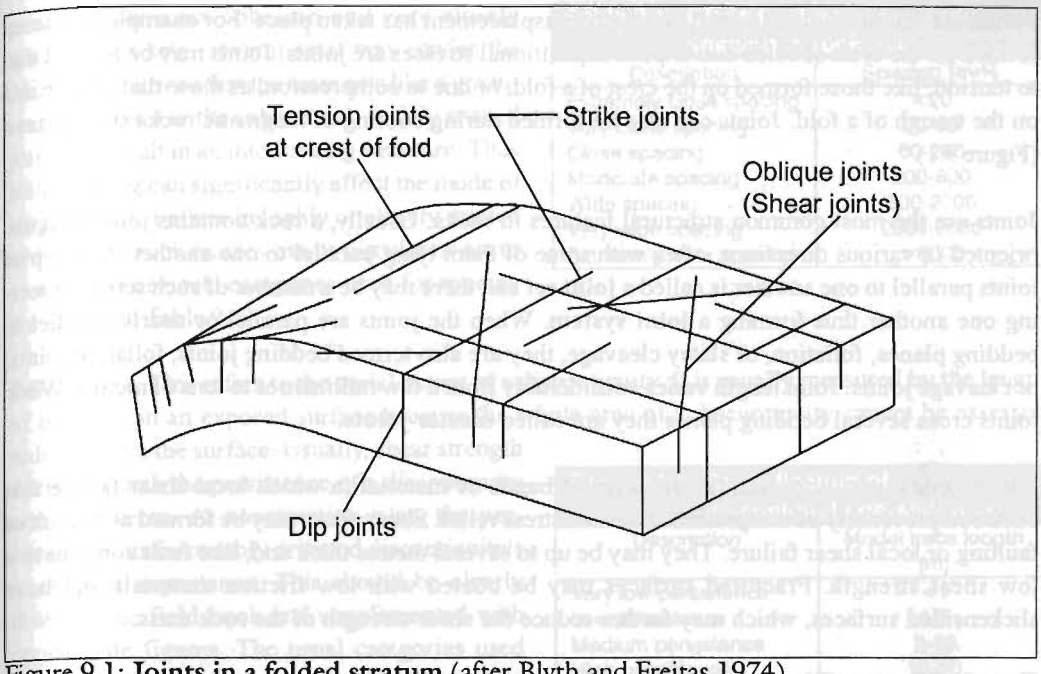

Figure 9.1: **Joints in a folded stratum** (after Blyth and Freitas 1974)

joints (Figure 9.2). The combined effect of all these factors is to reduce the shear strength of the fault zone and increase the instability of the rock containing the fault.

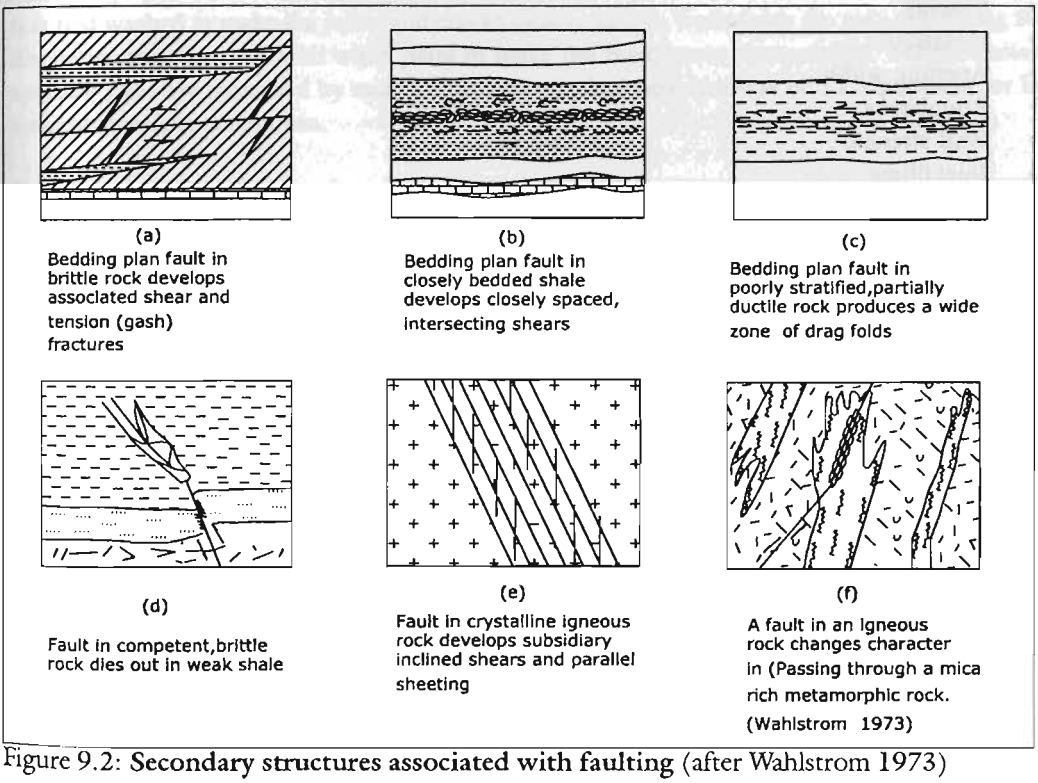

Figure 9.2: **Secondary structures associated with faulting** (after Wahlstrom 1973)

Joints are fractures along which no relative displacement has taken place. For example, fractures formed on the crest of folds due to post-depositional stresses are joints. Joints may be formed due to tension, like those formed on the crest of a fold, or due to compression, as those that are formed on the trough of a fold. Joints can also be formed during cooling of magmatic rocks such as lava (Figure 9.1).

Joints are the most common structural features in rocks. Usually, a rock contains joints that are oriented in various directions, often with some of them lying parallel to one another. A group of joints parallel to one another is called a **joint set** and there may be a number of such sets intersecting one another thus forming a **joint system**. When the joints are parallel or nearly parallel to bedding planes, foliation, or slatey cleavage, they are also termed bedding joints, foliation joints, or cleavage joints. Joint length varies considerably from a few millimetres to tens of metres. When joints cross several bedding planes they are called **master joints**.

Shear zones usually present in the form of bands of material in which local shear failure that occurred previously now represents zones of stress relief. Shear zones may be formed as a result of faulting or local shear failure. They may be up to several metres thick and, like fault zones have a low shear strength. Fractured surfaces may be coated with low friction materials and have slickensided surfaces, which may further reduce the shear strength of the rock mass.

Rock Mass Characterisation

In order to assess the in situ behaviour of rock mass, the following parameters related to geological discontinuities and rock structure should be investigated and mapped in the field.

- Orientation
- Spacing
- Persistence
- Aperture width
- Roughness
- Wall strength
- Joint filling
- Seepage conditions
- Joint set number
- Block size

Orientation – The orientation of a discontinuity denotes its three-dimensional position in space and is described by the dip direction (the direction perpendicular to the strike of the rock strata) and dip amount or inclination (the angle it makes with a horizontal plane, measured in the dip direction). The orientation of discontinuities relative to an engineering structure has an extremely important effect on the stability of that structure. For example, a rock bed dipping with a slope increases the instability of the slope, while one dipping into the slope may increase stability. The importance of the orientation of a discontinuity increases when other conditions are present that can lead to deformation and instability. For example, weathering along the bedding plane will render slopes more unstable, if this is coupled with weathering along another set of joints the slope will be even more unstable. Water seepage usually adds to slope instability.

Spacing usually refers to the mean distance between adjacent discontinuities measured in a direction perpendicular to them. In general, it is also related to rock mass qualities such as cohesion and shear strength which increase with the increase in spacing. Closely spaced joint sets tend to

produce low mass cohesion and very closely spaced joint sets (several sets) may render the cohesion so low so that the mass acts like a granular soil mass. On the other hand, widely spaced joint sets result in an interlocking structure. Thus joint spacing can significantly affect the mode of slope failure. Failure in highly or closely jointed or fractured rock masses can be circular or occur as a flow. The usual categories used for spacing are shown in Table 9.1.

Table 9.1: Classification of discontinuity spacing in rock masses

Description	Spacing (mm)
Extremely close spacing	<20
Very close spacing	20-60
Close spacing	60-200
Moderate spacing	200-600
Wide spacing	600-2000
Very wide spacing	2000-6000
Extremely wide spacing	>6000

Persistence. This refers to the aerial extent of a discontinuity. It is usually measured by the length of its trace on an exposed surface because the whole area of a discontinuity cannot be assessed unless it is on the surface. Usually, shear strength decreases with the persistence of a discontinuity and vice versa. At construction sites, the persistence of unfavourably oriented discontinuities is of great importance. This should be clearly noted in the field book and supplemented with appropriate figures. The usual categories used for levels of persistence are shown in Table 9.2.

Table 9.2: Classification of discontinuity persistence

Description	Model trace length (m)
Very low persistence	<1
Low persistence	1-3
Medium persistence	3-10
High persistence	10-20
Very high persistence	>20

Aperture – The aperture is the perpendicular distance between adjacent rock walls filled either by air or water. Aperture sizes are measured using measuring tapes calibrated in mm. If the exposed surface containing the discontinuity trace is dirty, it is first washed to make the joints and cracks clearly visible. Sometimes the area containing the discontinuity is sprayed with white paint to make the finer traces more visible. For boreholes, aperture sizes are measured by means of periscopes, borehole cameras or TV equipment, or by integral sampling techniques.

Roughness is caused by surface irregularities and can consist of small-scale surface roughness or larger scale roughness, which is expressed by waviness. In the latter case, individual parts of the 'waves' may themselves be characterised by surface roughness. The higher the level of roughness, the higher the shear strength. Roughness is described in qualitative terms (Table 9.3).

Table 9.3: Classification of discontinuity roughness

Class	Description
I	Rough or irregular and stepped
II	Smooth and stepped
III	Slickensided and stepped
IV	Rough or irregular and undulating
V	Smooth and undulating
VI	Slickensided and undulating
VII	Rough or irregular and planar
VIII	Smooth and planar
IX	Slickensided and planar

Since roughness is associated with the angle of internal friction, it directly affects the shear strength of rock. Barton (1973) has carried out extensive model test studies to evaluate the effect of joint roughness on shear strength. He divided roughness into a number of qualitative categories such as stepped, undulating, and planar and suggested how to calculate the shear strength of rock by increasing the angle of internal friction due to roughness as follows.

$$\tau' = \sigma'_n \tan(\Phi' + I)$$

where

τ' is the shear strength (peak or residual),
Φ' the angle of friction (peak or residual),
σ'_n the normal stress, and
I the roughness angle or waviness.

Wall strength. Wall strength is an assessment of the compressive strength of adjacent rock walls. It is an important parameter of rock shear strength but may be considerably reduced due to weathering or alteration of the walls. However, if the rock walls are not in contact, the shear strength of the filling material may play the governing role.

Wall strength very much depends on whether adjacent walls are weathered or not. The degree of weathering is assessed following the well-known weathering classification scheme, which divides rock into 6 grades ranging from fresh rock to residual soil. Wall strength is usually determined either by manual index tests such, as the uniaxial compression test, or by the Schmidt hammer test.

Filling material – Filling material may change the shear strength of a rock mass considerably. The filling material may consist of sand, silt, clay, or breccia and include the thin coating material. When the filling material is thick, the design shear strength will be reduced to that of the filling material. In this case, the mineralogy, grading, over consolidation ratio (OCR), and moisture content of the filling material are also determined. When required, sampling needs to be done very carefully.

Seepage – Water may percolate through a discontinuity and may have free-flow conditions or it may just be free moisture. Free-flow conditions not only reduce the shear strength of rocks but often cause difficulties on construction sites. The seepage of water into rock masses and joints may keep filling material moist or it may seep out along the dip of the planes. However, water flow can also be large and wash out the filling material. It then becomes a serious problem particularly in tunnelling work as recently happened at Khimti Khola Hydel Project in eastern Nepal.

Number of Joint Sets – Joints that lie approximately parallel to one another constitute a joint set. The higher the number of such joint sets intersecting each other, the lower will be the shear strength.

Block Size – Block size refers to the dimensions of the individual rock blocks and pieces which result from the mutual orientation of intersecting joint sets as well as from the spacing of individual sets. Large block sizes usually indicate better interlocking; as the block size goes down, the rock mass tends to become more like a granular mass.

Geological Data Collection

Ultimately the above-mentioned parameters will have to be evaluated for a specific project site. In order that the geological data collected represent the site in question as reliably as possible, measurements should be done with a full knowledge of the scope and limits of geological field investigation and data collection. The extent of field investigations and the type of geological data to be collected depend on the scope of the particular project. However, whatever the scope of a study it is always good practice to start by reviewing the available information on regional geology. For example, stereoscopic examination of pairs of aerial photographs can reveal linear surface features that indicate underlying geological structures such as faults.

Field mapping, or structural data collection, involves investigating all of the ten parameters listed above in the area related to the project area. Mapping of the exposed rock outcrops and other

geological features is usually sufficient to analyse rock slope stability. Geological compasses and hammers and measuring tapes are usually required. What is most important in collecting data is that it should be representative and sufficient. Clearly it is not possible to map every point in a project area so the area must be sampled. The experience and judgement of the field geologist will indicate to him or her which portion of the rock mass should be sampled to obtain satisfactory results. Sampling is carried out either by line sampling or area sampling.

Line sampling involves stretching a long measuring tape along the face of an outcrop or excavation and recording every structural feature that intersects the tape. In **area sampling** the area is divided into an appropriately sized grid and all the structural features inside the selected grids are recorded. It is often difficult to assess the number of field measurements needed to represent a project area adequately. The suggested number of field measurements ranges from 300 to 2000 for a single site depending on the site conditions and the priorities.

One of the most important points related to field mapping is to ensure uniform data entry. The dates, times, location, and sketches of the discontinuities must be entered every day in the data book. Field geologists should not rely on their memories to record details later on.

Types of Rock Slope Failure

Rock slopes usually fail as a result of the presence of structural weaknesses such as weakness planes. Sometimes, one set of weakness planes may play the dominant role leading to plane failure, while in another case failures may be induced by two joint sets leading to wedge failure. When a rock mass is intensively fractured so that it is more like an assemblage of coarse-grained material its behaviour is more like that of a soil slope and the slope may fail in a circular fashion. Rock slope failures can be categorised as one of the following.

- Plane failure
- Wedge failure
- Circular failure
- Toppling failure
- Rock falls

In reality, particularly where failure involves a large volume of material, rock slope failure is more likely to be a combination of these types. The mechanics of different types of failure is described in considerable detail in Hoek and Bray 1981. In the following, a brief description is given of the most important points related to plane failure and wedge failure, the only two modes that can be treated with some mathematical accuracy.

Plane Failure

Plane failure usually takes place in rock slopes composed of sedimentary or stratified rocks when the strata dips towards the slope and the daylight in the slope. Plane failure comprises sliding on a single plane and is effectively two-dimensional; in many ways it can be considered as a special case of the more common, three-dimensional, wedge mode of failure. In practice plane failure is relatively rare in rock slopes, as it is rare for all the necessary geometrical conditions to be met. However, many valuable lessons can be learnt from a consideration of the mechanics of this simple mode of failure. In general, the geometrical conditions shown in Figures 9.3 a, b, c, and d and listed below are necessary for plane failure to occur.

- The plane on which sliding occurs must strike parallel or nearly parallel (within approximately $\pm 20^0$) to the slope face.

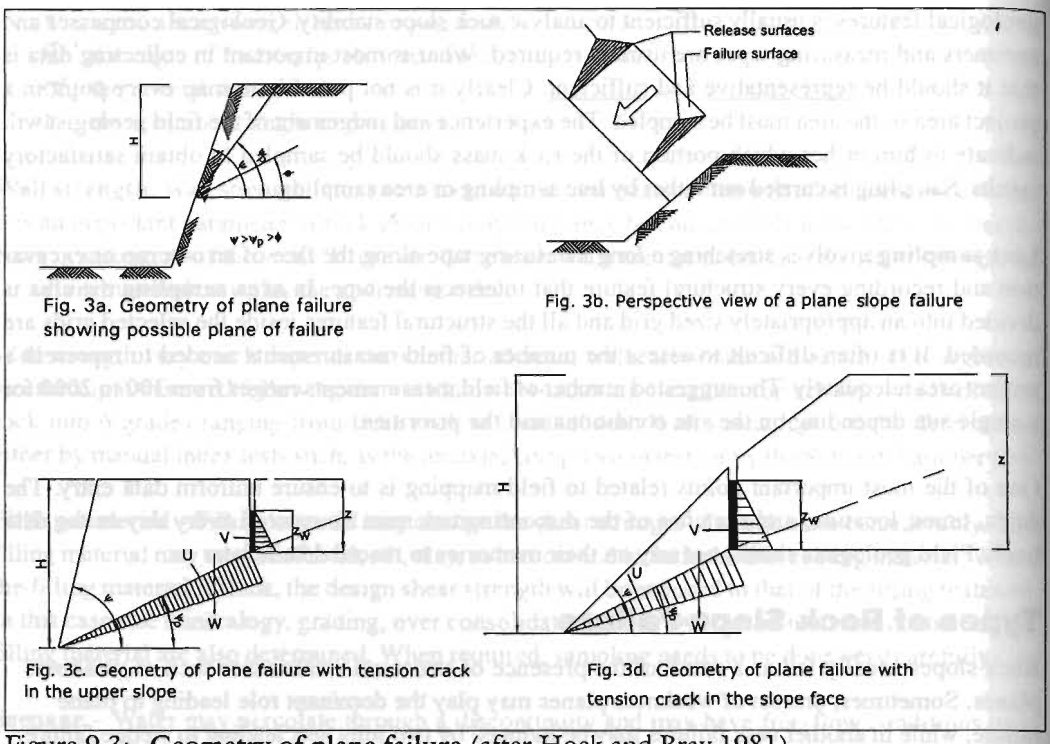

Fig. 3a. Geometry of plane failure showing possible plane of failure

Fig. 3b. Perspective view of a plane slope failure

Fig. 3c. Geometry of plane failure with tension crack in the upper slope

Fig. 3d. Geometry of plane failure with tension crack in the slope face

Figure 9.3: **Geometry of plane failure** (after Hoek and Bray 1981)

- The failure plane must 'daylight' on the slope. In other words its dip (Ψ_p) must be smaller than the dip of the slope face so that $\Psi > \Psi_p$, and the trace of the failure plane with the slope must be above the toe of the slope.
- The dip of the failure plane must be greater than the angle of friction (ϕ) of this plane so that $\Psi_p > \phi$
- The release surfaces on either side of the failed mass must provide negligible resistance to sliding.

Plane failures happen in two dimensions and so for the sake of analysis a slice measured in the direction perpendicular to the dip direction is usually taken. Once the dip angles corresponding to the slope and the failure surface are known, the surface area on which failure takes place as well as the volume of rock involved in the downward movement can be calculated easily. These parameters will, however, also depend on the geometry of the tension crack that may exist either on the slope itself or on its upper surface. Water may have access into the tension crack; the hydrostatic pressure will vary depending on whether the tension crack is dry or contains water.

Barton (1997) carried out very detailed studies on the failure of jointed rock slopes and concluded that tension cracks are formed as a result of very small shear movements within the rock mass. Hence, when a tension crack becomes visible on the surface it means that shear failure may well have started within the rock mass. It is therefore reasonable to assess the stability of a slope based on the condition of its limit state equilibrium.

Cohesion and friction parameters are either assumed, estimated, or calculated from field and/or laboratory tests or back calculations based on actual slope failures. In fact, the importance of the

field investigation and rock mass characterisation mentioned earlier lies exactly in assessing cohesion, friction angle, shear strength, and other design parameters. Once a reasonable assessment of these parameters has been made, the analysis becomes a simple matter of solving the following equation for the safety factor F, the ratio of the total force resisting sliding to the total force tending to induce sliding.

$$F = \frac{cA + (W\cos\psi_p - U - V\sin\psi_p)\tan\phi}{(W\sin\psi_p + V\cos\psi_p)} \quad (1)$$

Further

$$A = (H-z)\,\mathrm{cosec}\psi_p \quad (2)$$

$$U = \tfrac{1}{2}\gamma_w z_w (H-z)\,\mathrm{cosec}\psi_p \quad (3)$$

$$V = \tfrac{1}{2}\gamma_w z^2_w \quad (4)$$

and for a tension crack in the upper surface

$$W = \frac{1}{2}\gamma H^2\left[\left\{1-\left(\frac{z}{H}\right)^2\right\}\cot\psi_p - \cot\psi_f\right] \quad (5)$$

and for a tension crack in the slope face

$$W = \frac{1}{2}\gamma H^2\left\{\left(1-\frac{z}{H}\right)^2 \cot\psi_p(\cot\psi_p \tan\psi_f - 1)\right\} \quad (6)$$

where z is the depth of the tension crack measured from the top of the slope, z_w is the depth of water in the crack, W is the weight of the sliding block, U is the uplift force due to water pressure on the sliding surface, V is the force due to water pressure in the crack, c the cohesion, and ϕ the friction angle define the shear strength of the sliding surface, and ψ and ψ_p are the angles of dip of the slope face and the fault plane as shown in Figure 10.3.

Transformation from the first case (tension crack in the upper surface) to the second case (tension crack in the slope) occurs when the tension crack coincides with the crest so that:

$$z/H = (1-\cot\psi.\tan\psi_p) \quad (7)$$

Hoek and Bray (1981) have presented the same relationship in a more versatile form, which can accommodate a range of slope geometry, water depths, and variation in shear strength parameters. This is very useful for comparative analysis. The dimensionless relationship has the following form:

$$F = \left[\frac{2c}{\gamma H}p + \{Q\cot\psi_p - R(P+S)\}\tan\varphi\right] \Big/ \{Q + R.S\cot\psi_p\} \quad (8)$$

where,

$$P = (1-z/H)\,\mathrm{cosec}\psi_p \quad (9)$$

$$Q = [\{1-(z/H)^2\}\cot\psi_p - \cot\psi_f]\sin\psi_p \quad (10)$$

when the tension crack is in the upper surface

$$Q = [(1-z/H)^2\cos\psi_p(\cot\psi_p \tan\psi_f - 1)] \quad (11)$$

when the tension crack is in the slope face

$$R = (\gamma_w/\gamma).(z_w/z).(z/H) \quad (12)$$
$$S = (z_w/z).(z/H)\sin\psi_p \quad (13)$$

The ratios P, Q, R, and S are all dimensionless and depend on the geometry of the slope but not on its size. Note, however, that the depth of the tension crack z is always measured from the top of the slope. Hoek and Bray (1981) have presented the ratios P, Q, R, and S in graphical form for a range of slope geometries and these can be used directly to analyse the stability of rock slopes that are likely to fail by plane failure.

Depth and position of the critical tension crack

The analysis presented above assumes that all the parameters needed to calculate the safety factor F are known. In particular it assumes that the position of the tension crack is known from its visible trace and that its depth can be established by constructing an accurate cross-section of the slope. However, sometimes it becomes necessary to estimate some of the figures; for example, the tension crack may not be visible due to thick growth or other masking effects. As the influence of a tension crack on the safety factor is considerable, particularly when filled with water, it is necessary to estimate the most probable position of the tension crack and the critical tension crack depth. This will vary depending on the extent to which the crack is filled with water.

When the slope is dry or measures are taken to drain the slope, the water forces U and V are zero and equation (1) becomes

$$F = \frac{cA}{W\sin\psi_p} + \cot\psi_p \tan\phi \quad (14)$$

The critical tension crack depth z_c for a dry slope can be derived by partial differentiation of this equation with respect to z/H and equating the result to zero which gives:

$$z_c/H = 1 - (\cot\psi_f \tan\psi_p)^{1/2} \quad (15)$$

The corresponding position of the crack is

$$b_c/H = (\cot\psi \cot\psi_p)^{1/2} - \cot\psi_f \quad (16)$$

Similar calculations can be made for conditions when the crack is not dry or is filled with water to various heights. The safety factor starts to go down once a crack is filled to more than approximately one quarter of its depth, and reaches a minimum when the crack is water-filled. The minimum factor of safety is given by a water-filled tension crack that coincides with the crest of the slope, i.e., b = 0. An example of the effect of tension crack depth and the depth of water in it on the safety factor is given in Figure 9.4 (Hoek and Bray 1981).

Estimation of critical failure plane inclination

Slopes are more likely to fail where there is a well-defined failure plane such as with a through-going discontinuity surface. However, in many cases this does not exist and the failure surface can only be determined by minor geological features. This might be the case where the rock is highly fractured or when the discontinuity density is high.

Usually with soft rock slopes or soil slopes that have rather flat surfaces ($\psi < 45°$), the failure surface is circular, whereas in steep slopes the failure surface is nearly planar. The angle of inclina-

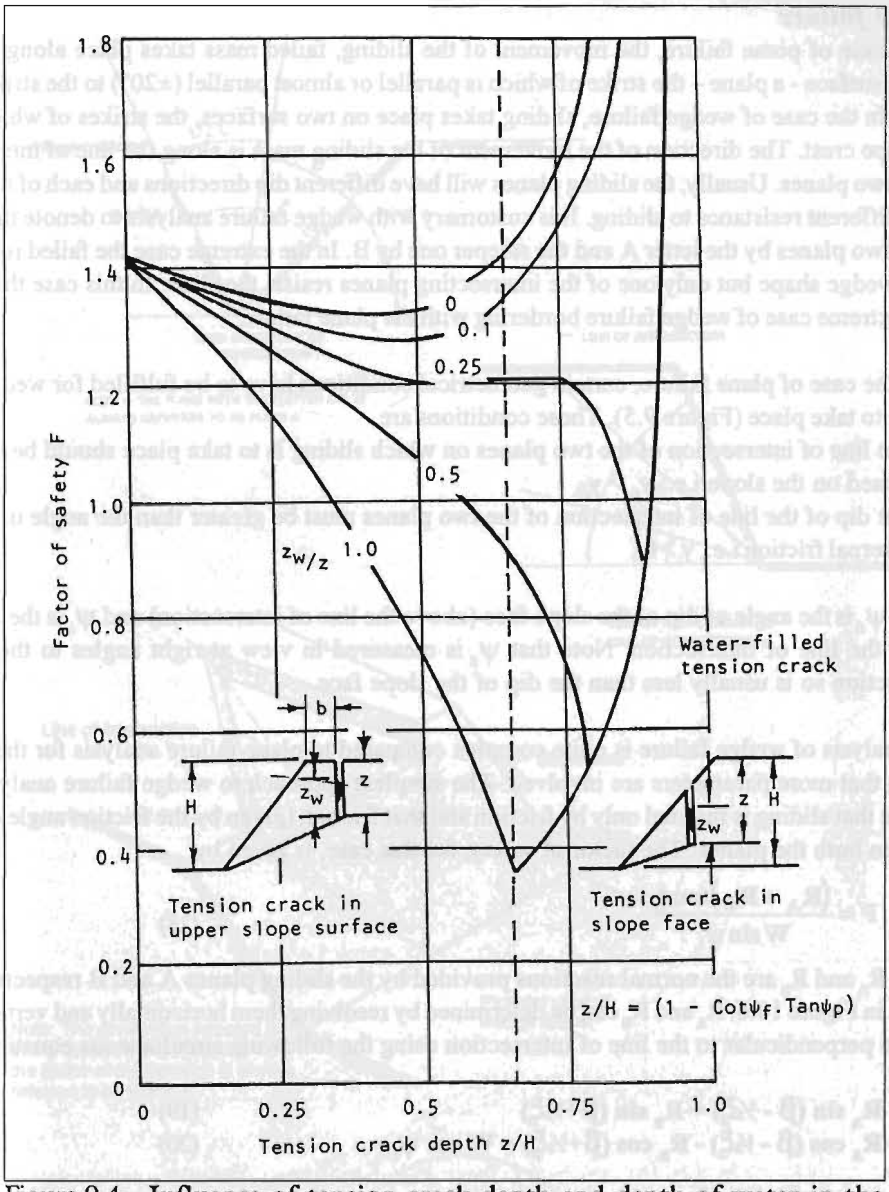

Figure 9.4: **Influence of tension crack depth and depth of water in the tension crack upon the safety factor of a typical slope (Hoek and Bray 1981)**

tion of the slope can be estimated by differentiating equation (1) with respect to ψ_p and equating the differential to zero. For dry slopes this gives a critical failure plane inclination ψ_{pc} of

$$\psi_{pc} = \tfrac{1}{2}(\psi + \phi) \qquad (17)$$

Hoek and Bray (1981) mention that the presence of water in cracks may reduce the failure plane inclination by about 10%. But they recommended the use of the above relationship for wet slopes on the grounds that this type of estimation is approximate and it is not justified to include the added complication of the influence of groundwater.

Wedge failure

In the case of plane failure, the movement of the sliding, failed mass takes place along a single failure surface - a plane – the strike of which is parallel or almost parallel (±20°) to the strike of the slope. In the case of wedge failure, sliding takes place on two surfaces, the strikes of which cross the slope crest. The direction of the movement of the sliding mass is along the line of intersection of the two planes. Usually, the sliding planes will have different dip directions and each of them will offer different resistance to sliding. It is customary with wedge failure analysis to denote the flatter of the two planes by the letter A and the steeper one by B. In the extreme case the failed rock mass has a wedge shape but only one of the intersecting planes resists the slide. In this case the failure is an extreme case of wedge failure bordering with the plane failure.

As in the case of plane failure, certain geometrical conditions have to be fulfilled for wedge failure to take place (Figure 9.5). These conditions are

- the line of intersection of the two planes on which sliding is to take place should be exposed on the slope i.e., $y_{fi} > y_i$
- the dip of the line of intersection of the two planes must be greater than the angle of internal friction i.e., $y_i > f$

where ψ_{fi} is the angle of dip of the slope face (above the line of intersection) and ψ_i is the angle of dip of the line of intersection. Note that ψ_{fi} is measured in view at right angles to the line of intersection so is usually less than the dip of the slope face.

The analysis of wedge failure is quite complex compared to plane failure analysis for the simple reason that more parameters are involved. The simplest approach to wedge failure analysis is to assume that sliding is resisted only by friction and that friction (given by the friction angle ϕ) is the same on both the planes. The factor of safety, for this case, is given by:

$$F = \frac{(R_A + R_B)\tan\phi}{W\sin\psi_i} \qquad (18)$$

where R_A and R_B are the normal reactions provided by the sliding planes A and B respectively as shown in Figure 10.6. R_A and R_B can be determined by resolving them horizontally and vertically on a plane perpendicular to the line of intersection using the following simultaneous equations.

$$R_A \sin(\beta - \tfrac{1}{2}\xi) = R_B \sin(\beta + \tfrac{1}{2}\xi) \qquad (19)$$

$$R_A \cos(\beta - \tfrac{1}{2}\xi) - R_B \cos(\beta + \tfrac{1}{2}\xi) = W\cos\psi_i \qquad (20)$$

where ξ is the included angle of the wedge and β the angle of tilt of the wedge (Figure 10.5).

Solving these equations and adding the values of R_A and R_B gives

$$R_A + R_B = \frac{W\cos\psi_i \sin\beta}{\sin\tfrac{1}{2}\xi} \qquad (21)$$

hence

$$F = \frac{\sin\beta}{\sin\tfrac{1}{2}\xi}\,\frac{\tan\phi}{\tan\psi_i} \qquad (22)$$

When only friction is considered, $(\tan\phi/\tan\psi_i)$ is the factor of safety for plane failure. Hence the above equation can be expressed as follows

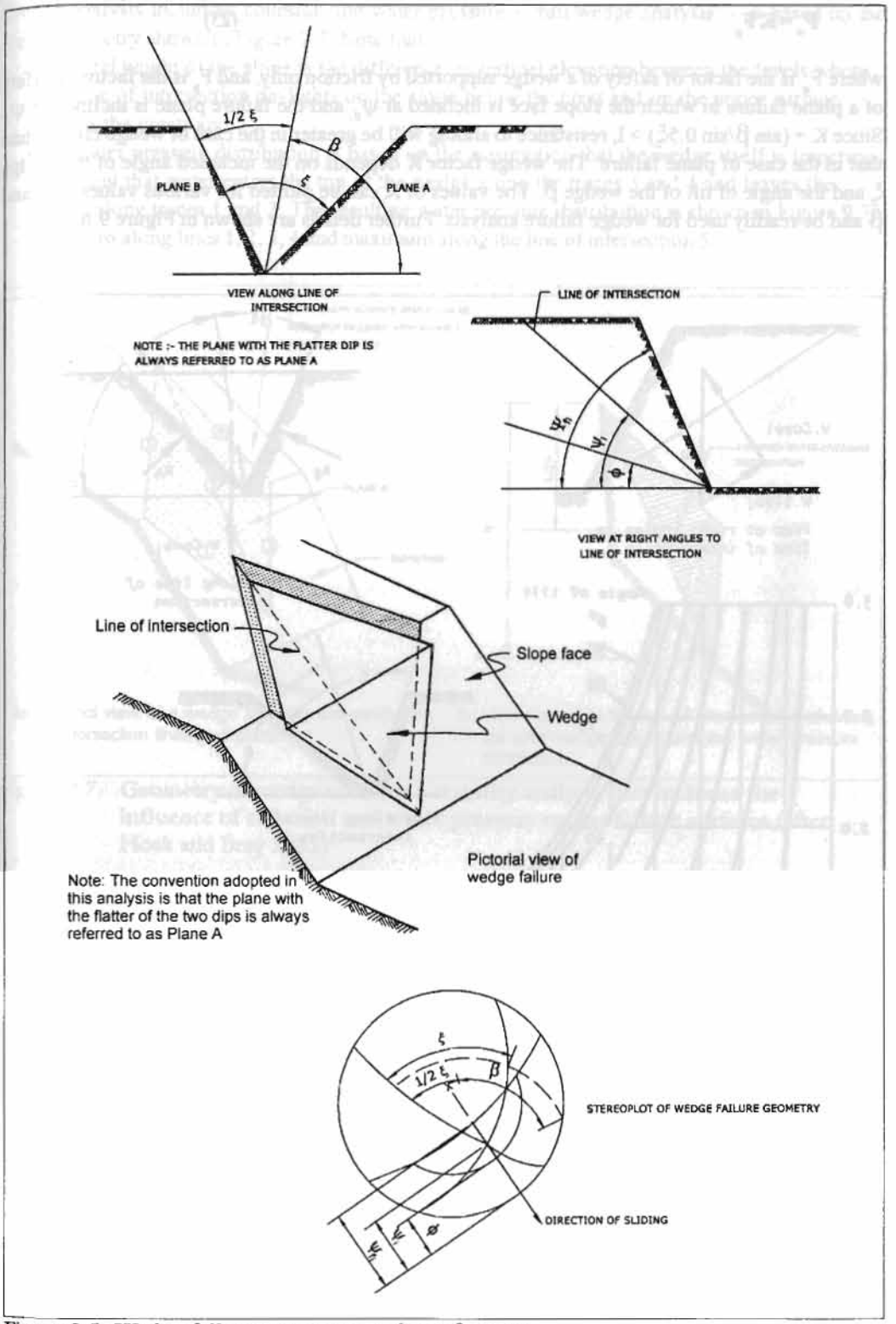

Figure 9.5: **Wedge failure geometry replaces former**

$$F_w = K F_p \qquad (23)$$

where F_w is the factor of safety of a wedge supported by friction only, and F_p is the factor of safety of a plane failure in which the slope face is inclined at ψ_f, and the failure plane is inclined at ψ_i. Since $K = (\sin\beta/\sin 0.5\xi) > 1$, resistance to sliding will be greater in the case of wedge failure than that in the case of plane failure. The wedge factor K depends on the included angle of the wedge ξ and the angle of tilt of the wedge β. The values of K can be plotted for various values of ξ and β and be readily used for wedge failure analysis. Further details are shown in Figure 9.6.

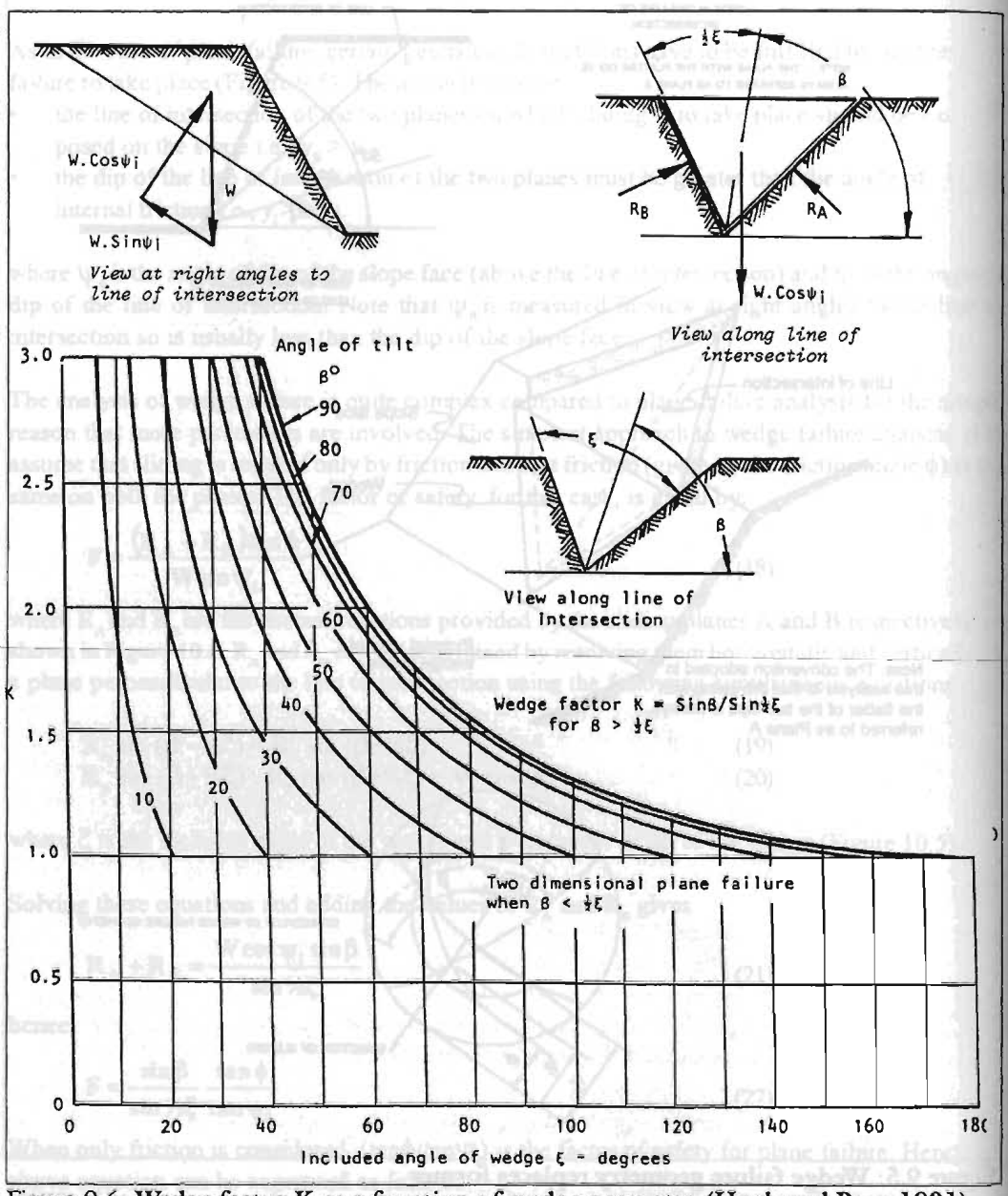

Figure 9.6: Wedge factor K as a function of wedge geometry (Hoek and Bray 1981)

Wedge analysis including cohesion and water pressure – 'full wedge analysis' – is based on the slope geometry shown in Figure 9.7. Note that

- the total height of the slope is the difference in vertical elevation between the levels where the line of intersection daylights on the slope below the crest and on the upper surface above the crest; and
- the water pressure distribution is based on the assumption that the wedge itself is impermeable and that water enters the top of the wedge along the traces 3 and 4 and leaves the slope along traces 1 and 2. The resulting water pressure distribution is shown in Figure 9.7; it is zero along lines 1, 2, 3, 4 and maximum along the line of intersection 5.

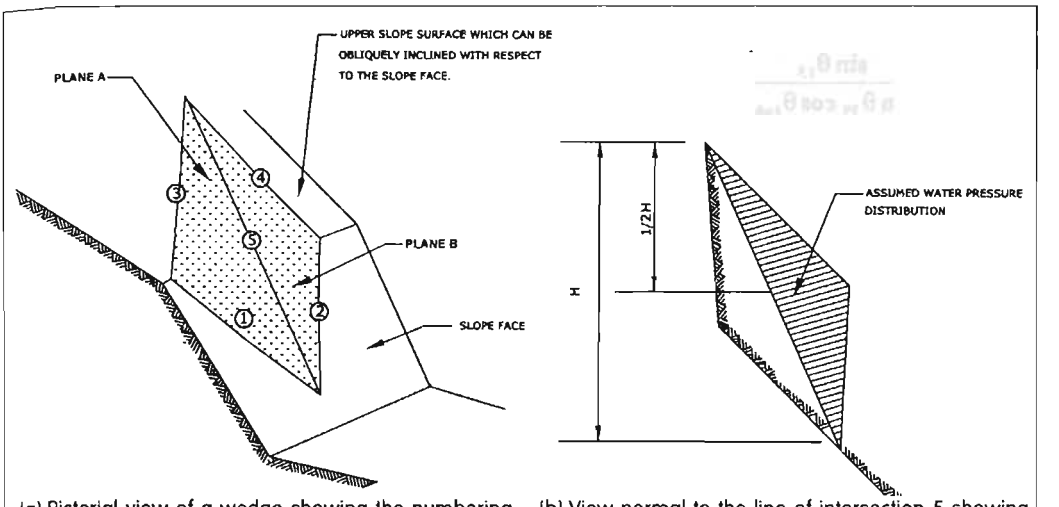

(a) Pictorial view of a wedge showing the numbering of intersection lines and planes

(b) View normal to the line of intersection 5 showing the total wedge height and the water pressure distribution

Figure 9.7: **Geometry of wedge used for a stability analysis that includes the influence of cohesion and water pressure on the failure surfaces** (after Hoek and Bray 1981)

Since these sorts of analyses are most effectively carried out using computers, it is of utmost importance to number the lines of intersection in the same sequence throughout. Following Hoek and Bray (1981) the numbering of the lines of intersection of various planes involved in wedge failure analysis (Figure 9.7a) is as follows:

1 - intersection of plane A with the slope face
2 - intersection of plane B with the slope face
3 - intersection of plane A with the upper slope surface
4 - intersection of plane B with the upper slope surface
5 - intersection of planes A and B

Now assuming that sliding always takes place along the line of intersection of the sliding surface numbered 5 above, the factor of safety is given by the following equation (Hoek and Bray 1981)

$$F = \frac{3}{\gamma H}\left(c_A X + c_B Y\right) + \left(A - \frac{\gamma_w}{2\gamma} X\right)\tan\phi_A + \left(B + \frac{\gamma_w}{2\gamma} Y\right)\tan\phi_B$$

where

c_A and c_B are the cohesive strengths of planes A and B

ϕ_A and ϕ_B are the angles of friction on planes A and B

γ and γ_w are the densities of rock and water

H is the total height of the wedge

X, Y, A and B are dimensionless factors which depend on the geometry of the wedge.

Thus

$$X = \frac{\sin\theta_{24}}{\sin\theta_{45}\cos\theta_{2na}}$$

$$Y = \frac{\sin\theta_{13}}{\sin\theta_{35}\cos\theta_{1nb}}$$

$$A = \frac{\cos\psi_a - \cos\psi_b\cos\theta_{na\,nb}}{\sin\psi_5\sin^2\theta_{na\,nb}}$$

$$B = \frac{\cos\psi_b - \cos\psi_a\cos\theta_{na\,nb}}{\sin\psi_5\sin^2\theta_{na\,nb}}$$

where ψ_a and ψ_b are the dips of planes A and B respectively and ψ_5 is the dip of the line of intersection 5.

Examples of the practical application of these analysis techniques are given in Part B.

Part B: Practical Examples of Rock Slope Stability Analysis

Example 1: Stability Analysis of Rock Slopes at the Dam Site of the Upper Arun Hydel Project

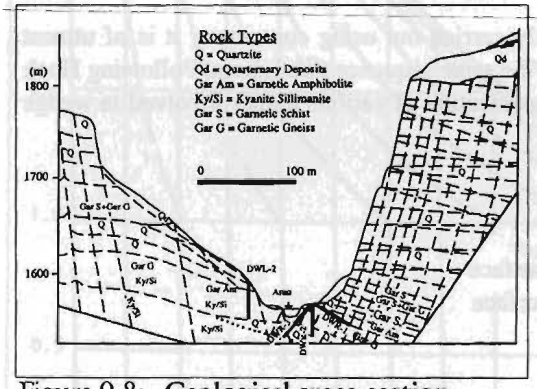

Figure 9.8: Geological cross-section 300m downstream of proposed Upper Arun dam site

Geological and geotechnical conditions at the dam site

The dam site of the Upper Arun Hydel Project is located in Sankhuwasabha in eastern Nepal. Stability analysis of the rock slope was carried out by the author. The site is underlain mainly by gneiss and quartzite rock. The right bank is very steep, it runs approximately parallel to the Arun river for about 380m and reaches a height of up to 240m above the river bed (Figure 9.8). The average slope of the cliff is approximately 70° to the horizontal at its lower levels up to 1700m elevation and 80° above this. The average strike of the cliff is N75E. The slope is intersected by a number of joints, bedding planes, foliation planes, and shear planes, al of which could affect the stability of the cliff and endanger the diversion structure. The discontinuities that are likely to govern the failure of the cliff are of four types.

Sub-vertical joints striking approximately NS (Joint set A) at orientations of

$270° \pm 10°/60 \pm 10°$ and $90° \pm 5°/80° \pm 10°$

Sub-vertical joints striking approximately EW (Joint set B) at orientations of

$180° \pm 10°/80 \pm 10°$ and $000° \pm 10°/85° \pm 5°$

Sub-horizontal foliation planes (Joint set C)

At the dam axis — lower part: 030° /20°; upper part: 180°/15°
Downstream of the dam: — lower part: 355°/ 20°; upper part: 040°/15°

Sub-horizontal shear planes (Joint set D)

320°/15°

The A-set joints are rather systematic. Some of the master joints, spaced at about 10 to 20m from each other, extend all along the cliff and beyond, with some up as far as Chepuwa village. In between there are a number of major joints spaced at about 5m, some of which extend up to the cliff top. Their depth into the cliff is estimated to be less than 3 to 5m, and they mostly terminate at the surface of the B-set joints.

The B-set joints are either stress relief or tension joints – mostly minor. It was not possible to measure their spacing; the estimated separation is about 10m.

The sub-horizontal C-set joints are either the bedding plane or foliation plane joints. Spacing between foliation planes in intact rock varies from 10 cm to a few metres; however, spacing between planes of weakness due to foliation or schistosity is estimated to be 10-20m. At this site, the foliation planes show greater scatter in terms of their dip direction and dip angle. The dipping is, in all cases, into the cliff. Figure 9.9 shows a stereographic plot of the various discontinuities.

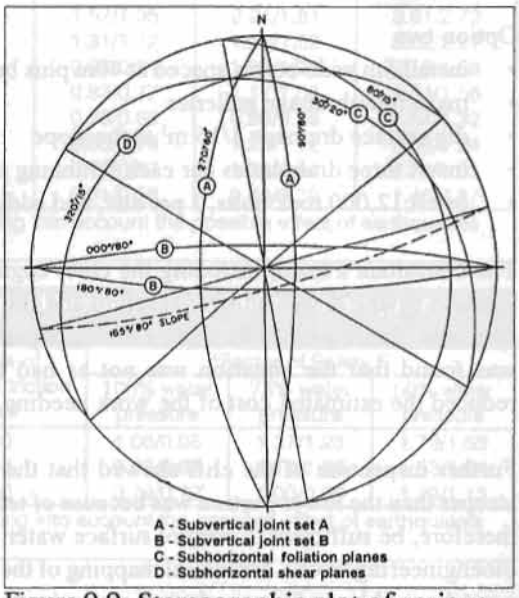

Figure 9.9: Stereographic plot of various discontinuities at the proposed Upper Arun dam site area

The upper surface of the slope is composed of quite thick residual/colluvial material that has a number of circular failures. A large one has been observed about 200m upslope. Seepage water emerges on the surface and there is a waterfall a few metres downstream of the dam site. This seepage water is, however, mainly in the middle portion of the slope; the two other ends of the slope (approximately northern and southern ends) are relatively well drained.

The left bank is also composed mainly of quartzite and gneiss but is comparatively massive. The lower part of the slope is flatter but the upper part is almost vertical and has, at places, slikensided

surfaces most probably due to fault movement. The portion above the flatter slope has a dense tree cover.

Stability analysis of the right cliff at the dam site of the Upper Arun Hydel Project

The left bank at the dam site was thought to be stable, but the World Bank Panel of Experts invited to assess the overall design of the project questioned the stability of the right bank. A consultant who had not visited the site previously carried out the analysis. To cover the worst case geological scenario for the engineering of the dam, the consultant postulated

- shear planes or planes of discontinuity may exist somewhere around the point where the cliffs become steeper at 1,700m where presumably the bedding planes also change their attitudes; and
- the reason for the upper portion of the slope being steeper than its lower portion may be that it is being pushed, albeit imperceptibly, by the overburden and other earth pressures.

The consultant suggested removing the overburden on the upper surface of the slope in addition to carrying out one of the following two options.

Option one

- install 5m wide berms spaced at 20m plus berm sealing and protection work
- dig surface drainage 1/50 m^2
- make 1900 drain holes

Option two

- install 5m wide berms spaced at 40m plus berm sealing and protection work
- make four drainage galleries
- dig surface drainage 1/15 m^2 at the slope
- insert three drain holes per each 5 running metres of gallery
- insert 12,000 rock bolts, 1 per 8m^2, and additional shotcrete

The consultant's team, including the chief engineer of the project, expressed concern about the solution saying it was an over-reaction and the previous field geologist had not expressed such concerns. Subsequently the author of this paper carried out a stability analysis of the slope and it was found that the situation was not as bad as postulated (see below). This finding greatly reduced the estimated cost of the work needing to be done.

Further inspection of the cliff showed that the reason for the upper portion of the slope being steeper than the lower portion was because of tectonic movement and not earth pressure. It would, therefore, be sufficient to control surface water on the upper surface of the slope by carrying out bioengineering works. Structural mapping of the slope showed that the rock mass was divided into a number of blocks by a number of approximately orthogonal joint sets. The cross-section shown in Figure 10.8 suggests that the most likely modes of failure are planar block sliding or planar block overturning.

Analysis of **planar block sliding** is equivalent to checking the safety of a retaining wall against base shear failure. The extent and spacing of various joints indicated that blocks of various sizes could be involved, with probable block sizes of 20m x 10m; 20m x 8m; 20m x 5m; 40m x m; and 40 m x 10 m. However, the size of the design block depends on its location on the slope face as shown in Tables 9.4, 9.5, 9.6, and 9.7.

Table 9.4: Stability analysis of dam abutment area, upper half of the cliff (planar block sliding)

Block size	Base angle a°	Back-face angle b°	Angle of internal friction (in degrees)	[a]Factor of safety F		
				100% water pressure	75% water pressure	50% water pressure
20 m x 10 m	0°	90°	40	2.09/1.80	2.93/2.41	4.61/3.48
			35	1.79/1.54	2.50/2.06	3.93/2.54
			30	1.52/1.32	2.13/1.75	3.33/1.82
	0°	80°	40	1.98/1.70	2.09/1.71	4.53/3.41
			35	1.69/1.45	1.78/1.47	3.87/2.91
			30	1.44/1.23	1.51/1.24	3.27/2.46
20 m x 8 m	0°	90°	40	1.68/1.48	2.35/2.00	3.69/2.93
			35	1.43/1.27	2.00/1.70	3.14/2.49
			30	1.21/1.07	1.70/1.44	2.66/2.11
	0°	80°	40	1.48/1.03	2.13/1.81	3.44/2.73
			35	1.25/1.11	1.87/1.54	2.91/2.30
			30	1.05/0.93	1.52/1.29	2.45/1.93
20 m x 5 m	0°	90°	40	1.05/0.98	1.47/1.32	2.30/1.98
			35	0.89/0.83	1.25/1.13	1.96/1.69
			30	0.76/0.70	1.06/0.96	1.66/1.43
	0°	80°	40	0.92/0.84	1.34/1.20	2.19/1.85
			35	0.78/0.72	1.15/1.04	1.87/1.58
			30	0.67/0.62	0.97/0.87	1.58/1.34
40 m x 20 m	0°	90°	40	1.97/1.69	2.76/2.27	4.36/3.29
			35	1.66/1.43	2.34/1.92	3.68/2.78
			30	1.39/1.19	1.95/1.60	3.08/2.33
	0°	80°	40	1.85/1.59	2.62/2.15	4.21/3.17
			35	1.57/1.35	2.21/1.81	3.61/2.72
			30	1.31/1.12	1.25/1.52	3.02/2.27
40 m x 10 m	0°	90°	40	0.98/0.91	1.38/1.24	2.18/1.88
			35	0.83/0.77	1.17/1.06	1.84/1.58
			30	0.70/0.65	0.98/0.88	1.54/1.32
	0°	80°	40	0.85/0.79	1.24/1.12	2.06/1.24
			35	0.72/0.67	1.04/0.94	1.74/1.05
			30	0.61/0.56	0.88/0.79	1.46/0.87

Note: [a]the second figure shows the factor of safety taking into account the possible effect of earthquakes (seismic coefficient)

Table 9.5: Stability analysis of the eastern edge of the cliff facing Chepu Khola (planar block sliding)

Block size	Base angle a°	Back-face angle b°	Angle of internal friction 0°	[a]Factor of Safety F		
				100% water pressure	75% water pressure	50% water pressure
20m x 10m	15° (away from the cliff)	90°	40	1.08/0.98	1.37/1.23	1.79/1.53
			35	0.93/0.84	1.18/1.06	1.53/1.34
			30	0.79/0.72	1.00/0.90	1.29/1.13

Note: [a]the second figure shows the factor of safety taking into account the possible effect of earthquakes (seismic coefficient)

Table 9.6: Stability analysis of the slope downstream of diversion structure (planar block sliding)

Block size	Base angle a°	Back-face angle b°	Angle of internal friction 0°	Factor of safely F		
				100% water pressure	75% water pressure	50% water pressure
20m x 10m	10° (into the cliff)	80°	40	2.53	3.51	5.48
			35	2.23	3.09	4.81
			30	1.97	2.71	4.22
		70°	40	2.43		5.42
			35	2.14		4.76
			30	1.89		4.18

Table 9.7: **Stability analysis of dam abutment area, upper half of the cliff (planar block overturning)**

Block size	Base angle a°	Slope angle b°	[a]Factor of safety F		
			100% water pressure	75% water pressure	50% water pressure
20m x 10m	0°	80°	1.54/1.35	2.03/1.73	3.08/2.42
	0°	70°	1.68/1.44	2.25/1.84	3.37/2.53
20m x 5m	0°	80°	0.67/0.61	1.15/.99	1.54/1.26
	0°	70°	0.93/0.85	1.24/1.10	1.86/1.57

Note: [a]the second figure shows the factor of safety taking into account the possible effect of earthquakes (seismic coefficient)

Calculations were performed for various block sizes and for 100%, 75%, and 50% hydrostatic water pressure. The results are presented in Tables 9.4, 9.5, 9.6, and 9.7. Note that the factors of safety as presented in these tables are smaller for smaller back face angles, which are also the slope angles. This is because friction along the back face of the block has not been considered.

The average dip angles were 20° and 15° respectively at the lower and higher elevations of the cliff. However, since the strike of the foliation plane was not parallel to that of the cliff, the base angle of the block will be smaller than the dip angle. In this analysis, the dip angles have been reduced conservatively by 40%. Other parameters assumed were

Density of rock: 2.7 t/m³
Angle of internal friction: 40°/35°/30° to represent various possibilities.
Cohesion: c = 5 t/m²

Analysis using **planar block overturning** sliding is equivalent to checking the safety of a retaining wall against overturning about its toe. The block dimensions and other parameters used here were the same as those assumed for planar block sliding.

Except for block sizes 20m x 5 m and 40m x 10m, for which the factor of safety was as low as 0.6 after considering the seismic coefficient suggested by the underground structure experts (0.06g), the slope was found to be stable. The factor of safety varied from about 1.30 for 100% saturation of rock having an angle of internal friction of 30° to over 3.0 for 50% saturated rocks. A few blocks at the upstream and downstream ends of the slope were found to be unstable; these will have to be removed as a part of the face trimming works.

Conclusions

The most probable block size has a base to height ratio of 1:2, but for the purpose of comparison blocks of base to height ratio of 1:2 to 1:4 were analysed. The angle of friction for this rock is likely to be more than 30° and the analysis shows that the cliff, except near its upstream and downstream faces, is probably stable. However, taking into consideration the magnitude and cost of the dam the following cliff stabilisation measures were suggested.

- Remove overhanging and/or loose rock pieces from the cliff
- Construct three rows of 2m x 2m, 200m long drainage galleries spaced at 50m vertical to 75m horizontal intervals
- Dig further drainage borings to connect these drainage galleries, some extending up to 50-75m into the rock; this should be done based on the observations of the drainage galleries
- Control surface water above the cliff and monitor the movement of the overburden and the cliff; the work associated with monitoring the movement of the overburden and the cliff should commence at least a year before the project starts

The analysis suggested that rock anchoring may not be required, but this can only be decided once the drainage galleries have been constructed and the deformation behaviour of the overburden above the cliff has been monitored.

If rock failure did occur it would start first at the northern and southern ends of the cliff where there is no confinement. It was therefore suggested that rock anchors be installed to tie at least two blocks at these ends at elevations of between 1,650m and 1,800m. Individual rock blocks along the top of the cliff may also need rock bolting.

Example 2: Stability Analysis of Rock Slopes at the Dam Site of the Kali Gandaki 'A' Hydel Project

Geological and geo-technical conditions at the dam site

The dam site of the Kali Gandaki 'A' Hydel Project is less than one kilometre downstream from the confluence of the Kali Gandaki River and the Andhi Khola. The desander basins of this project are planned to be placed on the left bank in highly fractured and crushed dolomite rock. This rock is also folded as shown by large variations in the dip direction of the bedding planes, which are intersected by closely spaced vertical to sub-vertical joints. The geological cross-section along the dam axis is shown in Figure 9.10.

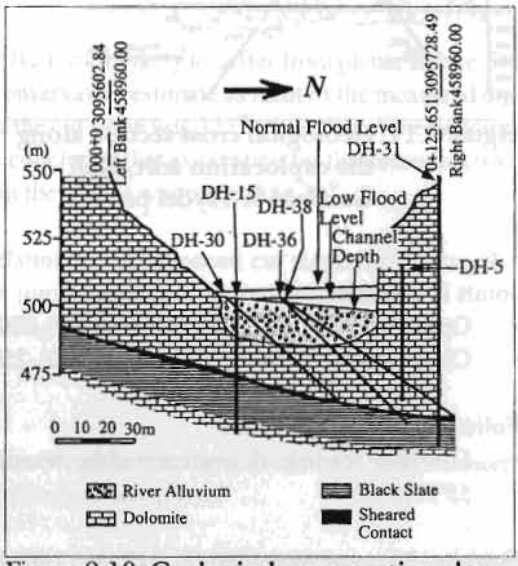

Figure 9.10: Geological cross-section along the dam axis of the Kali Gandaki 'A' hydel project (Kafle 1996)

The site is underlain by a 15-25m thick layer of black slate which is inclined at approximately 15° towards the river. A sub-vertical fault separates dolomite on the riverside from phyllites that extend deep into the slope. Contact between the two rock types was observed downstream of the desander basins and another about 200m upstream of the existing suspension bridge. The contact between the dolomite and overlying phyllite is not exposed on the surface. However, Kafle (1996) mentioned that the sheared, shattered, slickensided, closely jointed, and tightly folded carbonaceous phyllites found inside the adit (exploration tunnel) as well as in trenches and sections of core from different boreholes, provides evidence of some tectonic contact between the two rock types. Although it was not possible to exactly locate the position of the above-mentioned tectonic contact/fault inside the rock mass, its tentative position has been worked out extrapolated from the dip angle measured inside the adit (Figure 9.11).

The right bank of the Kali Gandaki just downstream of the dam site is less fractured than the left bank. It is vertical to overhanging and has stood stable for many years.

A considerable volume of excavation will have to be carried out for the construction of the intake structures and the desander basins. The height of excavation will reach to about 140m. The design proposes to line the lower portion of the cut slope adjacent to the desanders with concrete and

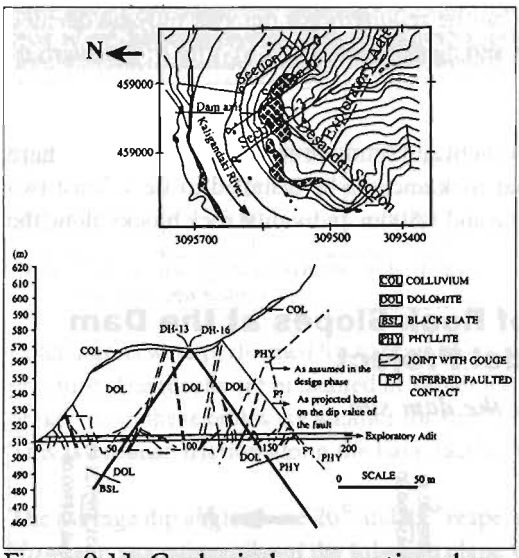

Figure 9.11: **Geological cross section along the exploration adit, Kali Gandaki 'A' Hydel project**

leave the remaining portion exposed. The upper portion of the slope is composed of highly and closely folded phyllites and schists and a cut slope could be designed as for soils. Since the desanders are to be placed in highly fractured and crushed dolomites, it is very important to analyse the stability of the cut slopes. Detailed structural mapping of the site has been carried out. The prominent structural features were found to be bedding planes, joints, and foliation planes.

Bedding planes (B1, B2 etc.) in dolomite

- B1 Series – low-level readings near the suspension bridge: 310°/15°, 305°/15°, 300°/10°
- B2 Series – mid-level readings on the exposed steep slope: 180°/10°, 185°/20°, 134°/50°, 195/30
- B3 Series – top-level readings near the top of the exposed slope in dolomite: 000°/45°.

Joints in dolomite

- Open joints - 020°/80°, 045°/35°, 090°/70°, 050°/65°
- Closed joints - 350°/60°, 350°/65°,237°/70°, 250°/85°, 274°/35°, 042°/65°

Foliation planes in phyllites

- Low level readings downstream of the desanders: 130°/60°, 120°/35°, 295°/45°, 169°/60°, 162°/55°, 118°/35°/

Damsite - Mirmitar spur: 180°/45°, 312°/35°, 180°/40°, 168°/40°, 210°/20°

Cut slope: Approximately 322° (dip angle varies)

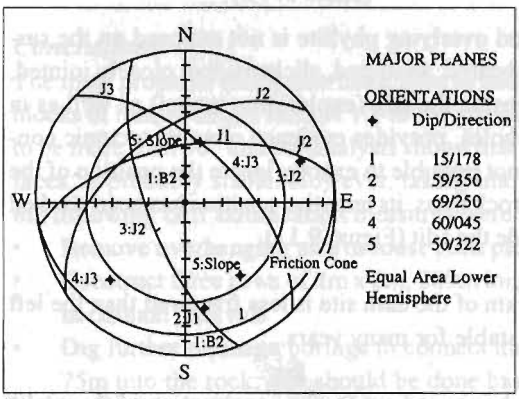

Figure: 9.12: **Stereo-plot of discontinuities at the left bank of the Kali Gandaki 'A' dam site**

Figure 9.12 shows a stereographic projection of the discontinuities and the cut slope. One field geologist suggested that data represented by the B1 series are of a local nature and that their attitudes (position relative to the horizontal) may have been changed by the combined effect of erosion, riverbank cutting, and the impact of large riverbed loads. Similarly, discontinuities represented by B3 series data are also thought to be of a local nature and they may not extend up to the excavation line. Hence this data was not considered for the analysis. The data selected as relevant for the stability analysis of rock slope and/or cut slopes in dolomite were

- joint sets J1, J2, and J3, and
- bedding plane B2

Stability analysis of cut slopes

In the initial design phase it was recognised that the cut slope at the upper part of the slope was composed of highly and closely folded phyllites and schists and so would be flatter. The upper part could be treated as if it was composed of soils. The lower part composed of dolomites could be cut at much steeper angles, depending of course on the measures to be taken to stabilise the cut slope. In the initial design phase, it was proposed bench the lower part of the slope with an average bench slope angle of 60°. Since this part of the slope was going to adjoin the desanding basins directly, however, the stability was more important. Although the slope was highly fractured, field observations indicated that the probable modes of failure were wedge failure and planar failure.

Of all the discontinuity surfaces, the bedding plane B2 is most likely to suffer from planar failure. Its average dip value is assumed to be 30°. This is a conservative estimate as most of the measured dip angle values are less than this. The dip direction of the cut slope was 322° while that of the bedding plane B2 varied between 134 and 195. Thus it was concluded that excavation for the desanders was unlikely to lead to plane failure as the difference in the strikes was more than 30°.

The three dimensional position of joint sets in relation to the proposed cut slope for placing the desanders showed that the following combination joints might lead to wedge failure

- Case A combination of joint set J1 and bedding plane
- Case B combination of joint sets J1 and J2
- Case C combination of joint sets J2 and J3.

Case A. The plunge of the line of intersection of the two planes is about 6° whereas the minimum friction angle is 30°. Therefore, wedge failure is unlikely to take place.

Case B. The dip value of the cut slope is greater than the plunge of the line of intersection of the two joint surfaces and the plunge is greater than the friction angle. Hence wedge failure is possible with the movement along the line of intersection. A detailed analysis is given in Table 10.8. The joint set J4 shown in the stereonet is not likely to be a problem as only a few of them were noted and they were not sufficiently persistent.

Case C. The two joint sets J2 and J3 are again likely to lead to wedge failure with sliding on both the surfaces. However, if the friction angle is assumed to be 35°, wedge failure is unlikely, thus case B is more critical.

Design of cut slopes in dolomite

Judging from a few boreholes and other visible surfacial lineations, the rock slope does not contain large through-going discontinuity surfaces but is highly jointed or fractured, thus wedge failures are most likely to be in the form of localised surface ravellings (rock breaking into small pieces). Analysis using stereographic projection suggested that such localised failures might take place if the slope were cut at angles steeper than about 50°.

Based on previous experience, the chief designer of the project chose a slope of 1:1 for the upper part which was composed of closely jointed and tightly folded carbonaceous phyllites, and an

average slope of 65° for the lower slopes, which are composed of dolomitic rocks with individual benches sloping at about 70°-73°.

The plan is to drain the slope by sub-surface drainage galleries so analysis was made assuming a dry state. The factor of safety was calculated to be 1.17 for a friction angle of 30° and 1.42 for a friction angle of 35°. Analysis using stereographic projection, however, showed that small scale localised ravellings could take place if the slope were cut at angles steeper than about 50°. Therefore localised patches will have to be stabilised by shotcreting, nailing, or bolting or a combination of these.

In view of the crucial importance of the stability of the cut slope, the initial design proposed was to line the lower part of the slope with concrete in addition to the treatments mentioned above. However, it was recognised that the actual position of the contact between dolomite and phyllite inside the slope as well as the position of the 15-25m thick layer of black slate below the riverbed would have to be taken into consideration. At the time of writing excavation of the desander basins was in progress and the tectonic contact between dolomite and the overlying phyllite had been found to be very complex. The design of the cut slope is therefore being revised.

The stereo plot of the relevant data with all the four planes and all the angles required are given in Figure 10.13. This figure also shows the stereographic method for calculating the angles required for wedge analysis. Computer software is also available to carry out such types of stability analysis.

Table 9.8: Worked out example of wedge stability analysis of the cut slope behind the desander basins at Kali Gandaki 'A' Hydroelectric Project

Discontinuity planes	dip°	dip direction°	properties
A (J1)	59	350	ϕ_A=35°,c_A=200kN/m²
B(J2)	69	250	ϕ_B=30°,c_B=200kN/m²
Slope surface	60	322	c= 200kN/m²
Upper surface	45	322	c=100kN/m²
Height H = 125m			

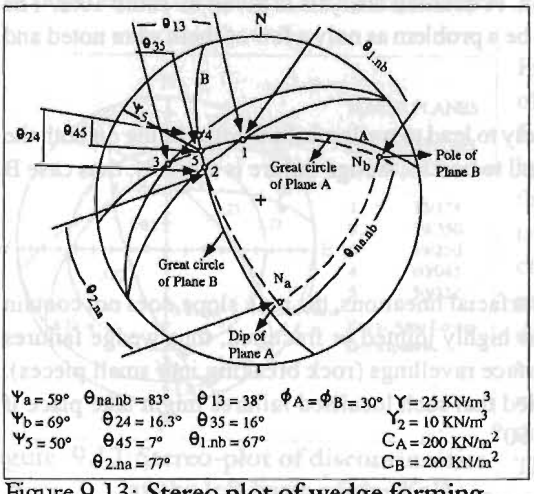

Figure 9.13: Stereo plot of wedge forming joints, Kali Gandaki 'A' Hydel project

Wedge stability calculation sheet

Of the various discontinuities mapped at the location of the desanding basins, joints J1 and J2 are those most likely to experience wedge failure. The input data related to these joints together with the assumed values of cohesion and friction are given above. Figure 10.13 shows a stereo plot of the wedge forming joints. The other details required for wedge stability analysis of the cut slope at the desanding basins are given in Table 9.9.

Note that the discontinuity parameters used for this example are only averaged values so localised failures may still occur. In rock slope stability analysis, it is not easy to make a reliable assessment of cohesion although this might affect the stability of the slope considerably. For example, if cohesion in the above example is reduced by 10%, the safety factor would be reduced to 1.5, generally considered to be the minimum acceptable, and if the cohesion were reduced by 17%, the corresponding safety factor would be only 1.3, the minimum value suggested by Hoek and Bray (1980).

Table 9.9: Wedge stability calculation sheet for the cut-slope of the desanding basins, Kali Gandaki 'A' hydel project

Input data	Function value	Calculation
$\psi_a = 59$ $\psi_b = 69°$ $\theta\psi_5 = 50°$ $\theta na.\ Nb = 83°$	$\cos \psi a = 0.515$ $\cos \psi b = 0.358$ $\sin \psi 5 = 0.766$ $\cos \theta na.\ Nb = 0.122$ $\sin \theta na.\ Nb = 0.992$	$A = \frac{\cos\psi_a - \cos\psi_b . \cos \theta na \times nb}{\sin\psi_5 - \sin 2\theta_{na} \times nb} = \frac{0.515 - 0.358 \times 0.122}{0.766 \times 0.984} = 0.625$ $B = \frac{\cos\psi_b - \cos\psi_a . \cos \theta_{na} \times nb}{\sin\psi_5 - \sin 2n_{na} - nb} = \frac{0.358 - 0.515 \times 0.12}{0.766 \times 0.584} = 0.391$
$\theta\ 24 = 16.3°$ $\theta\ 45 = 7°$ $\theta\ 2.na = 77°$	$\sin \theta\ 24 = 0.281$ $\sin \theta 45 = 0.122$ $\cos \theta 2.na = 0.225$	$X = \frac{\sin \theta_{24}}{\sin \theta_{45} . \cos \theta_2 . na} = \frac{0.281}{0.122 \times 0.225} = 10.237$
$\theta\ 13 = 38°$ $\theta\ 35 = 16°$ $\theta\ 1.nb = 67°$	$\sin \theta\ 13 = 0.616$ $\sin \theta\ 35 = 0.276$ $\cos \theta\ 1.nb = 0.391$	$Y = \frac{\sin \theta_{13}}{\sin \theta_{35} . \cos \theta_1 . nb} = \frac{0.616}{0.276 \times 0.391} = 5.708$
$\theta_A = 30°$ $\theta_B = 30°$ $\gamma = 25 KN/m^3$ $\gamma_w = 10\ KN/m^3$ $CA = 200 KN/m^3$ $CB = 200 KN/m^2$ $H = 125m$	$\tan \theta_A = 0.577$ $\tan \theta_B = 0.577$ $\frac{3\ C_A}{\gamma_H} = 0.192$ $\frac{3C_B}{\gamma_H} = 0.192$ $\frac{\gamma_w}{2\gamma} = 0.2$	$F = \frac{3}{\gamma_H}(CA.X + CB.Y) + (A - \frac{\gamma_w}{2\gamma} X) \tan\theta_A + (B - \frac{\gamma_w}{2\gamma} Y) \tan \theta_B$ $F = 0.192 \times 10.237 + 0.192 \times 5.708 - .820 - 0.433 = 1.81$
Note: Since the draft of this paper was written some time back, construction work at the dam site has progressed considerably. Excavation and/or stabilisation of the left bank adjacent to the desanders is almost complete.		

The lower part of the slope in dolomite has been cut at a slope of V:H 1:0.3, almost the same as proposed in the design phase. The final cut slope has been treated with 30 cm thick fibre reinforced shotcrete and up to 7 metre long rock bolts placed along a grid of 2m x 2m. The upper part of the slope composed of highly microfolded, thinly bedded, and foliated phyllites, however, proved very problematic. Initially this part of the slope was cut at a slope of 1:1, but was later flattened to a slope of 1.5:1 H:V due to its failure. It was shotcreted and further strengthened by up to 6m long rock dowels. However, it failed again, and as suggested by the World Bank Panel of Experts has now been flattened to a constant slope of 1.8:1. The final cut slope has been shotcreted, but no other reinforcing elements have been used.

Acknowledgements

I am thankful to The Institution of Mining and Metallurgy for giving permission to reproduce Figures 9.3, 9.4, 9.5, 9.6, 9.7 from the book Rock Slope Engineering by E. Hoek and J. Bray.

References

Barton, N.R. (1973) 'Review of A New Shear Strength Criterion for Rock Joints'. In *Eng. Geology*, 8, pp.287-332

Barton, N.R. (1997) 'The Shear Strength of Rock and Rock Joints'. In *Intl. J. Mech. Min. Sci. & Geomech. Abstr.* 13(10): 1-24

Blyth, F.G.H.; De Freitas, M.H. (1974) *Geology for Engineers* (6th Edition). London: Edward Arnold

Brown, E. T. (ed) (1981) *Rock Characterization Testing and Monitoring*, Oxford: Pergamon Press

Hoek, E.; Bray J. (1981) *Rock Slope Engineering.* London: Institute of Mining and Metallurgy

Hoek, E.; Kaiser, T.K.; Bawden, W.F. (1995) *Support of Underground Excavation in Hard Rock.* Netherlands: A. A. Balkema Rotterdam Brookfield

Kafle, K.N. (1996) 'Engineering Geological Study of the Kali Gandaki "A" Hydroelectric Project Area, Western Nepal Lesser Himalaya'. In *Jour. Nepal Geol. Soc.*, 13: 65-71

Price, N. J. (1966) *Fault and Joint Development in Brittle and Semi-brittle Rock.* Oxford: Pergamon Press

Wahlstrom, E.E. (1973) *Tunnelling in Rocks*. Amsterdam: Elsevier

10 Application of Bio-Engineering in Slope Stabilisation: Experience From Nepal

J.H. Howell
Living Resources Limited, Durston's Field, Heath House
Wedmore, BS28 4UJ, United Kingdom

This paper gives an introduction to the use of bio-engineering for slope stabilisation and erosion control in Nepal. It describes the scope of the subject, including both the basic principles and practice. These are applied specifically to the prevailing conditions in Nepal. It is based on the author's experience of the development of bio-engineering in the Nepal road building programme over about twelve years.

Introduction

Bio-engineering is the use of live plants or plant parts to control soil erosion and the mass movement of land, in order to fulfil engineering functions. Other terms that have been used to describe this process include: vegetation structures, bio-technical engineering, vegetative soil conservation, and engineering biology. Bio-engineering does not replace standard civil engineering procedures, nor does it offer magic solutions. It does, however, increase the number of available ways to address roadside slope stability problems.

Bio-engineering is especially useful in developing countries such as Nepal where it is relatively cheap to apply. The materials are locally available and cost little and the main input is labour - a low cost resource in Nepal.

Bio-engineering is not a new subject with the first recorded use in the Fifth Century AD in ancient China. There is evidence of it being used in Europe during the Dark Ages and Medieval times (between about 500 and 1500 AD). It has also been practised widely in other parts of the world for many years. It may have been used in Nepal in the past but what we know of as bio-engineering today has been brought into Nepal and adapted for local conditions only over the last 25 years. Shrestha (1991) and Clark (1992) give more details of the development of bio-engineering in Nepal.

The Himalayas present major environmental difficulties for the development of infrastructure. The most notable are:

- young and active geology, giving weak materials and steep slopes (Plate 10.1);
- a harsh climate, giving long periods of drought and intense rainstorms.

These combine to give unstable mountains and extremely high rates of erosion. Even in plain areas the harsh climate can create extreme conditions on steep embankment slopes. On the micro scale, there is little difference between the hills and the Terai.

There are many publications that deal with the evolving geology and geomorphology of the Nepal Himalaya. Most are academic publications and are of little direct practical help in bio-engineering practice. They do however give a good introduction to the subject and include: Brunsden et al

Plate 10.1: **The Trisuli-Somdang road above Syabrubesi (central Nepal)**

(1981), Carson (1985), Fookes et al (1985), Deoja et al (1991), and Transport Research Laboratory (1997).

In the mountains of Nepal there is a large variety of forms of erosion and instability (Table 10.1). Resolving slope problems depends on a clear understanding of exactly what is happening on the site. This does not just mean the major landslide or gully features, but also the micro-sites in every part of the main site. Careful site assessment is the key to the successful resolution of any instability. The engineer's design must be based on the results of this site survey. Kappeler (1984), Schaffner (1987) and Deoja (1994) give descriptions of construction methods specifically adapted for these environmental conditions.

Basic Principles and Techniques of Bio-Engineering

There are different methods of using vegetation to protect and stabilise slopes. The main categories are:

- simple planting (e.g. grass seeding; planting trees, shrubs and bamboos);
- structures using vegetation (e.g. lines of grasses or of shrub cuttings, in the form of brush layering); and
- composite systems (e.g. planted jute netting or vegetated stone pitching).

The author's long experience suggests that bio-engineering should always be used as part of an overall design when resolving any particular slope problem. It must always be integrated in such a way that it complements and enhances any other measures. In this way, bio-engineering is often used as part of a broad design, in conjunction with a number of standard civil engineering measures such as check dams, prop walls, toe walls, wire bolsters, and jute netting.

Table 10.1: **The most common forms of erosion and slope instability**

Mechanism	Description
Erosion on the surface	Rills and gullies form in weak, unprotected surfaces. Erosion should also be expected on bare or freshly prepared slopes.
Planar sliding (translational landslide or debris slide)	Mass slope failure on a shallow slip plane parallel to the surface. This is the most common type of landslide, slip or debris fall. The plane of failure is usually visible but, depending on site conditions, may not be straight. It may occur on any scale.
Shear failure (rotational landslide)	Mass slope failure on a deep, curved slip plane. Many small, deep landslides are the result of this process. Large areas of subsidence may also be due to these.
Slumping or flow of material when very wet	Slumping or flow of material that is poorly drained or has low cohesion between particles. Often occurs where liquefaction is reached. These sometimes appear afterwards like planar slides, but are due to flow rather than sliding. The resulting debris normally has a rounded profile.
Debris fall or collapse	Collapse due to failure of the supporting material. This normally takes the form of a rock fall where a weaker band of material has eroded to undermine a harder band above. These are very common in mixed Churia strata.

Information on commonly used bio-engineering techniques may be found in Schiechtl, 1980; Gray and Lieser, 1982; Coppin and Richards, 1990; Morgan and Rickson, 1995; and Schiechtl and Stern, 1996). Methods specifically relevant to Nepal are described in manuals by Meyer (1987), ITECO (1990 and 1991), Howell et al (1991), Nepal SPWP (1992), Eastern Region Road Maintenance Project (1993), and Geo-Environmental Unit (DOR) publications (1997a and 1997c).

Bio-engineering measures can contribute by achieving the following.

- Preventing scour erosion: by strengthening the surface so that gullies cannot be formed. Also, roots will strengthen the surface layers of soil.
- Reducing the incidence of shallow planar landsliding: as the roots add strength to the surface soil layers and increase the shear strength. Vegetation also reduces the extent of shallow failures by binding the surface together laterally.
- Channelling runoff to alter slope hydrology: Lines of grass or cuttings can channel water into gullies or down the slope, so that infiltration is reduced. At the same time, the plants strengthen the surface and prevent erosion from starting.
- Providing support to the base of the slope and trapping material moving downwards: Vegetation can be used in this way to form a kind of flexible, growing retaining structure.
- The provision of social, economic and environmental benefits.

Table 10.2 gives more detail on the physical and hydrological effects of vegetation on slopes. Not all vegetation effects are good for engineering purposes. The thesis by Clark (1992) and the manual by Clark and Hellin (1996) cover this topic well.

In Nepal most erosion and slope failures take place towards the end of extreme rainfall events. These usually occur during the monsoon season when the soil is already near saturation. With more intense rainfall slopes becomes super-saturated. Slopes are most likely to fail at this point, when the material is at its lowest level of cohesion and has maximum weight. Under these conditions, the interception of rain by vegetation and the contribution to moisture reduction by plant transpiration is negligible making this type of bio-engineering benefit inapplicable in Nepal during the monsoon.

Table 10.2: The main effects of vegetation on slope stability

Hydrological mechanisms		Mechanical mechanisms	
1. Foliage intercepts rainfall causing absorptive and evaporative losses that reduce rainfall available for infiltration.	NA	1. Roots reinforce the soil and increase soil shear strength.	B
2. Roots and stems increase roughness of the ground surface and the permeability of the soil, leading to an increased infiltration capacity.	A/B	2. Tree roots may anchor into firm strata providing support to the upslope soil mantle through buttressing and arching.	B
3. Roots extract moisture from the soil, which is lost to the atmosphere via transpiration, leading to lower water pressures.	NA	3. Weight of trees surcharges the slope, increasing normal and downhill force components.	A/B
4. Depletion of soil moisture may accentuate desiccation cracking in the soil, resulting in higher infiltration capacity.	A	4. Vegetation exposed to wind transmits dynamic forces into the slope.	A
5. Lines of vegetation affect runoff and infiltration, depending on the surface micro-topography.	A/B	5. Roots bind soil particles to the ground surface and reduce their susceptibility to erosion.	B

A = adverse effect B = beneficial effect NA = not applicable in Nepal

A single plant gives a point of strength on a slope. The depth of its effectiveness depends on the size of the plant. A structure gives a line or area of strength, rather than just a point. For different purposes, it is necessary to use different levels and sizes of vegetation to cover the same area (Table 10.3).

While the properties of single plants can be valuable to stabilise certain areas of slopes, often more can be achieved by using plants as part of a structure. This may take the form of a simple line of planted grass, or may be more intricate, such as a fascine (a bundle of live cuttings buried in a trench) or a live check dam (an inter-woven construction of cuttings from different types of plant). Table 10.4 lists the main bio-engineering options available in Nepal, and what they contribute to strengthening slopes. Of all of these, the planting of grass lines is by far the most cost-effective and robust method of protecting slopes, and is recommended in the majority of situations.

Table 10.3: **The effective rooting depths of different plant types**

Plant type	Examples	Effective rooting depth (m)
Small grasses	Dubo (*Cynodon dactylon*) Kikiyu (*Pennisetum clandestinum*)	0.1
Large grasses	Kans (*Saccharum spontaneum*) Amliso (*Thysanolaena maxima*) Khar (*Cymbopogon microtheca*)	1
Large bamboo	Choya bans (*Dendrocalamus hamiltonii*) Mal bans (*Bambusa nutans*)	1.5
Shrubs	Bhujetro (*Butea minor*) Dhanyero (*Woodfordia fruticosa*)	1.5
Trees	Bakaino (*Melia azedarach*) Khayer (*Acacia catechu*) Utis (*Alnus nepalensis*)	2

Table 10.4: **Common bio-engineering techniques appropriate to Nepal and their contribution**

Class	Technique	Contribution to the slope
Simple planting	Grass seeding	Surface protection against erosion
	Tree and shrub seeding	Anchoring of the surface layers; reinforcement
	Grass planting	Surface protection against erosion
	Tree and shrub planting	Anchoring of the surface layers
	Big bamboo planting	Support to the slope; trapping of debris
	Turfing with grass	Surface protection against erosion
Structures using vegetation	Lines of grasses	Protection against erosion; trapping of debris; channelling of runoff
	Lines of shrub cuttings (brush layering and palisades)	Protection against erosion; trapping of debris
	Bundles of cuttings (fascines)	Protection against erosion; trapping of debris; channelling of runoff; drainage
Composite	Planted jute netting	Protection against erosion on very steep slopes
	Vegetated rip-rap	Protection against erosion in areas where there is a lot of running water
	Other inert structures with vegetation added	Numerous: these often need to be designed specifically for individual sites.

Practical Application of Bio-Engineering

Detailed appraisal of bio-engineering methods

The range of bio-engineering techniques adopted for use on the steep slopes in Nepal's road programme are versatile and robust, and can be recommended for use throughout the country. These are described in Howell et al (1991), Geo-Environmental Unit (1997a and 1997c) and Shrestha

et al (1998). Table 10.5 gives details of the various methods in some detail. Some of these techniques are illustrated in Plates 10.2, 10.3 and 10.4.

In most situations it is best to use a combination of techniques (Plate 10.3). This can be done in two ways.

- Where a site needs several different techniques used in the same place to give the optimum effect. Examples might be:
  - wire bolster cylinders and grass slip planting;
  - grass seeding, mulching and wide mesh jute netting; and
  - standard mesh jute netting and grass slip planting.
- Where a site consists of a number of different components such as different slope segments, each of which require different techniques to be applied. Examples might be:
  - a steep head slope requiring standard mesh jute netting and grass slip planting;
  - a moderate, middle slope portion requiring contour grass lines; and
  - a gentle slope toe requiring bamboo planting.

The basic rules of bio-engineering design are:

- make a thorough site investigation;
- always consider each site independently;
- break the site down into manageable sections; and
- use any combinations of techniques, depending on what is appropriate.

As with any civil engineering work the use of bio-engineering techniques must be based on sound site investigation. Designs should be site-specific rather than "typical", and must be carefully created to resolve the specific problems on each site.

Selection of the Right Technique

To select the right technique for stabilising a slope first it is necessary to look at a site and its surroundings and make a number of investigations.

Plate 10.2: **A steep cut slope in a weak sand deposit on the Naubise-Mugling road (central Nepal), stabilised with jute netting and grass planting**

Plate 10.3: **A typical cut slope in deep colluvium on the Dharan-Dhankuta road (eastern Nepal), stabilised using a combination of a gabion toe wall and bio-engineering**

Plate 10.4: **Large scale civil and bio-engineering works on the Dharan-Dhankuta road (eastern Nepal)**

Table 10.5: **Bio-engineering techniques appropriate to Nepal and their structural contribution (adapted from Shrestha et al, 1998)**

System	Design and function
Planted grass lines: contour (horizontal)	Grass slips (rooted cuttings), rooted stem cuttings or clumps grown from seed are planted in lines across the slope. They protect the slope with their roots and, by providing a surface cover, reduce the speed of runoff and catch debris, and 'armour' the slope.
Planted grass lines: downslope (vertical)	Grass slips (rooted cuttings), rooted stem cuttings or seedlings are planted in lines running down the slope. They protect the slope with their roots, provide a surface cover and help to drain surface water. They do not catch debris. Using this technique, a slope is allowed to develop a semi-natural drainage system, with gullying happening in a controlled way.
Planted grass lines: diagonal	Grass slips (rooted cuttings), rooted stem cuttings or seedlings are planted in lines running diagonally across the slope. They armour the slope with their roots and by providing a surface cover. They have limited functions of catching debris and draining surface water. This technique offers the best compromise of the grass line planting systems in many situations.
Planted grasses: random planting	Grass slips (rooted cuttings), rooted stem cuttings or seedlings are planted at random on a slope, to an approximate specified density. They armour and reinforce the slope with their roots and by providing a surface cover. They also have a limited function of catching debris. This technique is most commonly used in conjunction with standard mesh jute netting, where complete surface protection is needed on very steep, harsh slopes. In most other cases, however, the advantages of one of the grass line planting systems (contour, downslope or diagonal) offer better protection to the slope.
Grass seeding	Grass is sown direct on to the site. It allows easy vegetation coverage of large areas. This technique is often used in conjunction with mulching and jute netting to aid establishment.
Turfing	Turf, consisting of a shallow rooting grass and the soil it is growing in, is placed on the slope. This technique is commonly used on gentle embankment slopes. Its only function is armouring.
Shrub and tree planting	Shrubs or trees are planted at regular intervals on the slope. As they grow, they create a dense network of roots in the soil. The main engineering functions are to reinforce and, later, to anchor the slope. In the long term, large trees can also be used for slope support.
Shrub and tree seeding	Shrub (or tree) seeds are applied directly to the site. This technique allows very steep, rocky and unstable slopes to be revegetated where cuttings and seedlings cannot be planted. There are two methods: (1) direct sowing and (2) broadcasting. In the first method, seeds are placed individually, whereas the second involves scattering the seed all over the site. The main engineering functions are to reinforce and, later, to anchor the slope.
Large bamboo planting	Large bamboos can reduce the movement of material and stabilise slopes. Large bamboos are usually planted by one of two methods: (1) the traditional planting method or (2) planting rooted culm cuttings from a nursery. Large clumps of the larger stature bamboos are one of the most substantial vegetation structures available to reinforce and support slopes. However, they do not have deeply penetrating roots and so do not have an anchoring function; also, they can add weight (surcharge) high up on the slope.
Brush layering	Woody (or hardwood) cuttings are laid in lines across the slope, usually following the contour. These form a strong barrier, preventing the development of rills, and trap material moving down the slope. In the long term, a small terrace will develop. The main engineering functions are to catch debris, and to armour and reinforce the slope. In certain locations, brush layers can be angled to provide a drainage function.
Palisades	Woody (or hardwood) cuttings are planted in lines across the slope, usually following the contour. These form a strong barrier and trap material moving down the slope. In the long term, a small terrace will develop. The main engineering functions are to catch debris, and to armour and reinforce the slope. In certain locations, palisades can be angled to give a drainage function.

Table 10.5: Bio-engineering techniques appropriate to Nepal and their structural contribution (adapted from Shrestha et al, 1998)	
System	Design and function
Live check dams	Large woody (or hardwood) cuttings are planted across a gully, usually following the contour. These form a strong barrier and trap material moving downwards. In the longer term, a small step will develop in the floor of the gully. The main engineering functions are to catch debris, and to armour and reinforce the gully floor.
Fascines	The word "fascine" means a bundle of sticks. In this technique, bundles of live branches are laid in shallow trenches. After burial in the trenches, they put out roots and shoots, forming a strong line of vegetation. This technique is sometimes called live contour wattling. The main engineering functions are to catch debris, and to armour and reinforce the slope. In certain locations, fascines can be angled to provide drainage. Where time is at a premium, brush layers may be more appropriate as these are quicker to establish than fascines.
Vegetated stone pitching	Slopes are strengthened by a combination of dry stone walling or cobbling, and vegetation planted in the gaps between the stones. There are two distinct uses: (1) reinforced toe walls; and (2) protected gully beds. This technique provides a very strong form of armouring. Because it specifically uses vegetation to strengthen a simple civil engineering technique, it represents a stronger form of normal stone pitching.
Jute netting* (standard mesh)	A locally made geotextile of woven jute netting is placed on the slope. The four main functions of standard mesh jute netting (mesh size about 40 × 40 mm) are to: protect the surface by armouring it against erosion and by catching small debris; enable seeds to hold and germinate; improve the microclimate on the slope surface by holding moisture and increasing infiltration; and as it decays to act as a mulch once the vegetation is established.
Jute netting* (wide mesh)	A locally made geotextile of woven jute netting (mesh size about 150 × 450 mm) is placed on the slope. It is used to hold mulch on slopes that have been seeded.
*Any use of jute netting is a temporary measure designed to enhance vegetation establishment. It does not protect a surface in itself for more than one or two seasons of monsoon rains.	

There is no such thing as a simple 'text book' landslide. They all have a variety of processes at work and it is essential to identify them before remedial work is started.

What erosion processes are active on the site?

A site may contain one or more types of erosion. Examples of the processes of erosion which may be found are as given in Table 10.1.

- *surface erosion*, such as rilling and gullying;
- *planar sliding*, on a shallow slip plane parallel to the surface;
- *rotational sliding*, on a deep, curved slip plane;
- *slumping* of material when very wet, through low particle cohesion; and
- *debris falling* due to failure of the supporting material.

Secondly, there will be both "internal" and "external" factors affecting the site. Internal factors will include:

- small fault lines causing differential erosion in parts of the site;
- seasonal springs within the site; and
- small slip planes additional to the main failure mechanism.

External factors will include:

- gullies which may discharge on to the site;
- landslides which may supply debris on to the site; and
- rivers that may undercut the toe.

Initial assessment of treatment needs

A further series of questions helps to delineate the problems.

- *Is the site very long, steep and in danger of a massive failing below the surface?*
  If the answer is "yes", retaining walls should be used to break the slope into smaller, more stable lengths.
- *Is the foot of the slope undermined, threatening the whole slope above?*
  If the answer is "yes", toe walls should be considered.
- *Is there a distinct overhang or are there large boulders supported by a soft, eroding band?*
  If the answer is "yes", prop walls should be considered.
- *Is the slope made up mostly of hard rock, so that the planting of nursery stock would be impossible?*
  If the answer is "yes", direct seeding may be an option.
- *Is the slope rough, covered in loose debris or does it have any locally very steep or overhanging sections, however small?*
  If the answer is "yes", then it must be trimmed.

Once these questions have been answered, it is possible to move on to a more detailed examination of the slope segments.

Slope segments

A slope segment can be defined as a length of slope with a uniform angle and homogeneous material that is likely to erode in a uniform manner. The most straightforward way to approach the choice of stabilisation technique is by splitting sites into segments of slopes. The assumption is that each segment can be treated using the same technique or combination of techniques. But first, there are two important considerations which must be addressed:

- Is the slope segment longer than 15 metres?
  If it is, there may be a danger of surface scour. Therefore some kind of physical scour check should be used, such as wire bolsters.
- Is the slope made up of poorly drained material, with a relatively high clay content?
  If it is, there is a danger of shallow slumping. Techniques used on this sort of material must be designed to drain rather than accumulate moisture.

Drainage is the most critical consideration in many locations. This is shown by experience throughout Nepal, and is particularly highlighted by Kappeler (1984) and Schaffner (1987).

Guidelines for applying bio-engineering techniques for slopes

In Table 10.6, I have attempted to define which bio-engineering technique is most suitable for each of a range of site conditions. There are many different factors which determine the optimum technique or combination of techniques, but only the most important ones have been included here for the sake of simplicity. The following text examines the five columns of Table 10.6 one by one.

Slope angle: This is the primary distinction. Slopes of less than 30° usually need only mild soil conservation treatment whereas those with a slope steeper than 45° usually demand more attention as they will have greater erosion problems.

Table 10.6: Choice of bio-engineering technique (adapted from Howell *et al*, 1991 and Howell, 1999)

Slope angle	Slope length	Material drainage	Site moisture	Technique(s)
> 45º	> 15 Metres	Good	Damp	**Diagonal grass lines**
			Dry	**Contour grass lines**
		Poor	Damp	1 **Downslope grass lines and vegetated stone pitched rills**, or 2 Chevron grass lines and vegetated stone pitched rills
			Dry	**Diagonal grass lines**
	< 15 metres	Good	Any	1 **Diagonal grass lines**, or 2 Jute netting and randomly planted grass
			Damp	1 **Downslope grass lines**, or 2 Diagonal grass lines
		Poor	Dry	1 **Jute netting and randomly planted grass**, or 2 Contour grass lines, or 3 Diagonal grass lines
30º - 45º	> 15 metres	Good	Any	1 **Horizontal bolster cylinders and shrub/tree planting**, or 2 Downslope grass lines and vegetated stone pitched rills, or 3 Site grass seeding, mulch and wide mesh jute netting
		Poor	Any	1 **Herringbone bolster cylinders & shrub/tree planting**, or 2 Another drainage system and shrub/tree planting
	< 15 Metres	Good	Any	1 **Brush layers of woody cuttings** or 2 Contour grass lines, or 3 Contour fascines, or 4 Palisades of woody cuttings, or 5 Site grass seeding, mulch and wide mesh jute netting
		Poor	Any	1 **Diagonal grass lines**, or 2 Diagonal brush layers, or 3 Herringbone fascines and shrub/tree planting, or 4 Herringbone bolster cylinders & shrub/tree planting, or 5 Another drainage system and shrub/tree planting
< 30º	Any	Good	Any	1 Site seeding of grass and shrub/tree planting, or 2 Shrub/tree planting
		Poor	Any	1 **Diagonal lines of grass and shrubs/trees or** 2 Shrub/tree planting
	< 15 metres	Any	Any	**Turfing and shrub/tree planting**
	Base of any slope			1 **Large bamboo planting**, or 2 Large tree planting
Special conditions				
Any *	Any *	Any *	Any *	**Site seeding of shrubs/small trees †**
> 30º	Any	**Any rocky material**		**Site seeding of shrubs/small trees**
Any loose sand		Good	Any	**Jute netting and randomly planted grass**
Any rato mato (red clay)		Poor	Any	**Diagonal lines of grass and shrubs/trees**
Gullies ≤ 45º	**Any gully**			1 **Large bamboo planting**, or 2 Live check dams, or 3 Vegetated stone pitching

Notes for Table 10.6:

* Possible overlap with parameters described in the rows above.

† May be required in combination with other techniques listed on the rows above.

Any rocky material is defined as material into which rooted plants cannot be planted, but seeds can be inserted in holes made with a steel bar.

Any loose sand is defined as any slope in a weak, unconsolidated sandy material. Such materials are normally river deposits of recent geological origin.

Any rato mato (Nepali for red soil) is defined as a red soil with a high clay content. It is normally of clay loam texture, and formed from prolonged weathering. It can be considered semi-lateritic.

Techniques in **bold type** are preferred.

Chevron pattern: <<<<< (like a sergeant's stripes).

Herringbone pattern: ←←←← (like the bones of a fish).

Slope length: The partly arbitrary length of 15 metres is usually taken as representing a good dividing figure between 'big' and 'small' sites. Slope segments longer than 15 metres are usually open to greater risks in terms of both gullying and deep-seated failures.

Material drainage: This is related to the internal porosity of soils and the likelihood of their reaching saturation and losing cohesion, thereby starting to flow. Those materials which have a high content of clay relative to sand and silt in the fine fraction tend to have poor internal drainage. They tend to be prone to shallow slumping if too much moisture accumulates. In this case stabilisation will require some kind of drainage in addition to protection.

Site moisture: The level of moisture across the entire site must be considered. Although aspect is usually the dominant factor in determining the moisture levels at a site the environmental dryness of each site also needs to be assessed. These include:

- altitude; topographical location; rain shadow effect; and
- stoniness; soil moisture holding capacity; winds and ex-monsoon rains.

To distinguish between one and the other of these factors usually involves a subjective judgement which a bio-engineer will develop as they become more experienced.

Technique(s): Table 10.6 recommends one or more technique for each of the given site types which are known to have been successful on similar sites in the field. Due to the large variation in site conditions the recommendations should only be viewed as general guidelines and are by no means comprehensive. Variations from these general given prescriptions will often be needed, and this is for the engineer to determine on site.

Table 10.6 gives guidelines for choosing bio-engineering techniques in Nepal. An example of a site on which these guidelines were successfully was at the Manohari River in central Nepal (Plates 10.5 and 10.6.

Selection of Plant Species: Principles and Practice

Physical features are usually the factors which dominate the selection of species for bio-engineering. It is necessary to choose plants which can grow in the prevailing conditions which often

Plate 10.5: **The Manohari River (central Nepal) embankment in May 1994, during construction**

Plate 10.6: **The Manohari River (central Nepal) embankment in Sept. 1995, two growing seasons after being planted with kans (*Saccharum spontaneum*)**

involve dryness, stoniness and extremes of temperature. Soil fertility is not usually a problem if local plants are used, as they will be naturally adapted to poor soils. Most forest soils in Nepal are infertile due to the young, unstable terrain and the weathering and leaching properties of the monsoon. As a result, it is hardly ever necessary to add topsoil to slope surfaces.

Principles of species selection

The main principles of selecting plants for inclusion in a bio-engineering programme are that they must be:

- known to grow well on similar sites;
- locally available in plentiful supply; and
- serve the right purpose technically and in socio-economics terms.

In general, species introduced from outside Nepal (exotics) should be avoided because they may become weeds, as happened with the highly invasive ban mara, or they may be prone to insect attack, as with ipil ipil.

Species need to be found which:

- have a good root system;
- show an ability to grow well on harsh, stony sites;
- are common in the locality; and
- can be easily propagated.

A number of species have been identified which have been successfully established on bio-engineering programmes in Nepal (Table 10.7). However, the identification of suitable species is not complete and many local species have still to be tried out.

In some areas there is a risk of damage to plantings from domestic animals. If this can be controlled, multipurpose plant species may be planted which not aid slope stabilisation but also yield useful products as well as. The best way to control damage from domestic animals is to get the people themselves to manage the plants. If it is not possible to manage the plants carefully, then it is usually best to select plants with few or no economic uses such as kans grass and bhujetro.

Preferred species for bio-engineering

Table 10.7 gives a list of the preferred species for bio-engineering in the road sector. The Geo-Environmental Unit publication (1997c) gives comprehensive lists of species, running to hundreds of potential bio-engineering plants. Table 10.7 gives only the plants found to be the best for use in bio-engineering on difficult sites throughout Nepal.

The species to avoid in bio-engineering include those that:

- are annual, not perennial (*e.g.* maize);
- have a poor, weak root system (*e.g.* ban mara, tite pate); and
- have a shallow root system (*e.g.* dubo grass).

Bio-Engineering Maintenance

Even though bio-engineered slopes get stronger over time they still need regular maintenance (Geo-Environmental Unit 1997b). Maintenance interventions of vegetation on slopes are either:

- routine, which means that action must be taken continuously or on a frequent or seasonal basis; or

Table 10.7: Preferred species for bio-engineering (adapted from Geo-Environmental Unit, 1997c)

Local name	Botanical name	Altitude	Sites	Best propagation
Grasses				
Amliso	*Thysanolaena maxima*	Terai-2000m	Varied	Slip cuttings
Babiyo	*Eulaliopsis binata*	Terai-1500m	Hot and dry	Slip cuttings/seeds
Dhonde	*Neyraudia reynaudiana*	Terai-1500m	Hot and dry	Stem/slip cuttings/seeds
Kans	*Saccharum spontaneum*	Terai-2000m	Hot and dry to moist	Slip cuttings
Katara khar	*Themeda* species	Terai-2000m	Varied	Slip cuttings/seeds
Khar	*Cymbopogon microtheca*	500-2000m	Hot and dry; varied	Slip cuttings/seeds
Khus	*Vetiver zizanioides*	Terai-1500m	Varied	Slip cuttings
Narkat	*Arundo clonax*	Terai-1500m	Hot and dry; varied	Stem/slip cuttings
Padang bans	*Himalayacalamus hookerianus*	1500-2500 m	Moist	Large slip cuttings
Phurke	*Arunduella nepalensis*	700-2000 m	Varied; stony	Slip cuttings/seeds
Sito	*Neyraudia arundinacea*	Terai-1500m	Varied	Slip cuttings/seeds
Tite nigalo bans	*Drepanostachyum intermedium*	1000-2500 m	Varied	Large slip cuttings
Shrubs and small trees				
Areri	*Acacia pennata*	500-1500 m	Hot and dry; harsh	Seeds/polypots
Assuro	*Adhatoda vasica*	Terai-1000m	Varied	Hardwood cuttings
Bainsh	*Salix tetrasperma*	Terai-2700m	Moist	Hardwood cuttings
Bhujetro	*Butea minor*	500-1500 m	Hot and dry; harsh	Direct seeding
Dhanyero	*Woodfordia fruticosa*	Terai-1500m	Hot and dry; harsh	Seeds/polypots
Dhusun	*Colebrookea oppositifolia*	Terai-1000m	Hot and dry; harsh	Seeds/polypots
Kanda phul	*Lantana camara*	Terai-1750m	Hot and dry	Hardwood cuttings
Kettuke	*Agave americana*	Terai-2400m	Hot and dry	Root suckers
Keraukose	*Indigofera atrotpurpurea*	Terai-2000m	Hot and dry; harsh	Seeds/polypots
Namdi phul	*Colquhounia coccinea*	1000-2000 m	Varied	Hardwood cuttings
Saruwa/ bihaya	*Ipomoea fistulosa*	Terai-1500m	Varied; sunny sites; stands waterlogging	Hardwood cuttings
Simali	*Vitex negundo*	Terai-1750m	Hot and dry; varied	Hardwood cuttings
Tilka	*Wendlandia puberula*	Terai-1500m	Hot and dry; harsh	Seeds/polypots
Large clumping bamboos				
Choya/tama bans	*Dendrocalamus hamiltonii*	300-2000 m	Moist	Culm cuttings
Dhanu bans	*Bambusa balcooa*	Terai-1600 m	Varied	Culm cuttings
Kalo bans	*Dendrocalamus hookeri*	1200-2500 m	Varied	Culm cuttings
Mal bans	*Bambusa nutans*	Terai-1500 m	Dry/varied	Traditional method
Nibha/ghopi/ lyas bans	*Ampelocalamus patellaris*	1200-2000 m	Varied	Traditional method
Tharu bans	*Bambusa nutans*	Terai-1500 m	Varied	Traditional method
Large trees				
Bakaino	*Melia azedarach*	Terai-1800m	Hot and dry; harsh	Seeds/ polypots
Chilaune	*Schima wallichii*	900-2000 m	Varied; dry to moist	Seeds/ polypots
Dabdabe	*Garuga pinnata*	Terai-1300m	Varied and dry	Seed/ hardwood cuttings up to 2m
Gobre salla	*Pinus wallichiana*	1800-3000 m	Dry; varied	Seeds/ polypots
Kalo siris	*Albizia lebbeck*	Terai-1200m	Hot and dry; harsh	Seeds/ polypots
Khanyu (khosro)	*Ficus semicordata*	Terai-2000m	Hot and dry; varied	Seeds/ polypots
Khayer	*Acacia catechu*	Terai-1000m	Hot and dry; harsh	Seeds/ polypots
Lankuri	*Fraxinus floribunda*	1200-2700 m	Varied; best in moist sites	Seeds/ polypots
Painyu	*Prunus cerasoides*	500-2400 m	Varied and dry; stony	Seeds/ polypots
Phaledo	*Erythrina* species	900-3000 m	Varied	Seeds/ hardwood cuttings up to 2m
Rani (khote) salla	*Pinus roxburghii*	500-1950 m	Hot and dry; varied	Seeds/ polypots
Rato siris	*Albizia julibrissin*	800-3000 m	Varied and moist	Seeds/ polypots
Seto siris	*Albizia procera*	Terai-1350m	Moist	Seeds/ polypots
Sisau	*Dalbergia sissoo*	Terai-1400m	Varied	Seeds/ polypots / stump cuttings
Utis	*Alnus nepalensis*	900-2700 m	Varied and moist	Seeds/ polypots

- recurrent, where action is required at regular, but less frequent, intervals, such as once per year.

Table 10.8 lists the main bio-engineering maintenance activities. Plate 10.7 shows an example of a maintained mature bio-engineering site.

Table 10.8: **Bio-engineering maintenance activities**

Category	Task description
Routine (continuous, seasonal or regular – such as once per month)	
Protection of sites	Control of access to sites by people and animals to avoid unacceptable damage to the vegetation.
Weeding	Remove unwanted vegetation which is competing with the growth of the desired plants.
Mulching	Place mulch around seedlings to keep the soil cool and moist, thereby enhancing growth. Mulch is made by cutting the stems and leaves of unwanted plants.
Grass cutting	Cut grasses once a year to encourage vigorous growth and the development of new shoots.
Watering (exceptional activity)	Spray water around plants at dry times of the year to improve the growth on harsh, newly planted sites.
Recurrent (such as once per year)	
Thinning of shrubs and trees	Thinning means removing selected shrubs or trees to decrease the density of the plants. Pruning is the removal of lower branches. Both open out the canopy and allow ground cover plants to grow better.
Repair of vegetation structures	The repair of any form of bio-engineering treatment: mainly palisades, fascines and brush layering, and re-turfing.
Vegetation enrichment	Planting more grasses, shrubs or trees within a site area or in gaps within the existing vegetation
Removal of shrubs and trees	The removal of any unwanted large shrub or tree from a site.

Conclusion

Bio-engineering continues to be developed in many parts of the Hindu Kush-Himalayan region. It needs to be adapted to the local conditions and the specific environment of each landslide. Knowledge can be applied from different areas, but must be done so with caution. Local resources and local skills form the basis of the successful use of bio-engineering techniques.

A considerable amount of extended knowledge is required. More needs to be known about the best species for bio-engineering in every ecological zone (of which there are many in these mountains). But perhaps the biggest change that is required is in attitude. In poor rural areas, it is necessary for engineers and others to improve their understanding of the function of vegetation in engineering, so that they can rely on it more. Only then can they avoid using expensive civil engineering structures in inappropriate locations, and begin to use a truly sustainable technology more wisely.

Plate 10.7: **A mature bio-engineering site: utis (*Alnus nepalensis*) forest on the Lamosangu-Jiri road (central Nepal)**

REFERENCES

Brunsden, D.; Jones, D.K.C.; Martin, R.P.; Doornkamp, J.C. (1981) 'The Geomorphological Character of Part of the Low Himalaya of Eastern Nepal'. In *Zeitschrift für Geomorphologie*, 37: 25-72

Carson, B. (1985) *Erosion and Sedimentation Processes in the Nepalese Himalaya*. Occasional Paper No 1. Kathmandu: ICIMOD

Clark, J.E. (1992) 'Principles of Bioengineering with Reference to East Nepal', Ph.D. Thesis, Cranfield University, UK

Clark, J.E.; Hellin, J. (1996) *Bio-engineering for Effective Road Maintenance in the Caribbean*. Chatham: Natural Resources Institute

Coppin, N.J.; Richards, I.G. (1990) *Use of Vegetation in Civil Engineering*. London: CIRIA

Deoja, B.B. (1994) *Sustainable Approaches to the Construction of Roads and Other Infrastructure in the Hindu Kush-Himalaya*, Occasional. Paper No 24. Kathmandu: ICIMOD

Deoja, B.B; Dhital, M.R.; Thapa, B.; Wagner, A. (eds) (1991) *Mountain Risk Engineering Handbook*. Kathmandu: ICIMOD

Eastern Region Road Maintenance Project, (1993) *Bio-engineering for Road Protection in Nepal: Techniques Used on the Jogbani-Basantapur Road*. Dharan (Nepal): Eastern Region Road Maintenance Project.

Fookes, P.G.; Sweeney, M.; Manby, C.N.D.; Martin, R.P. (1985) 'Geological and Geotechnical Engineering Aspects of Low Cost Roads in Mountainous Terrain'. In *Engineering Geology*, 21:1-152.

Geo-Environmental Unit (1997a) *Use of Bio-engineering*. Kathmandu: Department of Roads, Geo-Environmental Unit

Geo-Environmental Unit (1997b). *Maintenance of Roadside Vegetation*. Kathmandu: Department of Roads, Geo-Environmental Unit

Geo-Environmental Unit (1997c). *Bio-engineering Information*. Kathmandu: Department of Roads (2nd Edition), Geo-Environmental Unit

Gray, D.H; and Lieser, A.T. (1982) *Biotechnical Slope Protection and Erosion Control*. New York: Van Nostrand Reinhold Company

Howell, J.H.; Clark, J.E.; Lawrance, C.J.; Sunwar, I. (1991) *Vegetation Structures for Stabilising Highway Slopes*. Kathmandu: Department of Roads, HMG/Nepal and Overseas Development Administration (UK)

Howell, J.H. (1999) *Roadside Bio-engineering, Site Handbook*. Kathmandu: Department of Roads (Nepal) and Department for International Development (UK)

ITECO (1990) *Handbook for Bio-Engineering Methods in Gully and Landslide Stabilization Works. Lamosangu-Jiri Road, Charnawati Rehabilitation Programme Phase III*. Affoltern: ITECO/SDC/HMGN

ITECO (1991) *Small Scale Engineering Techniques in Gully and Landslide Stabilization Works, Lamosangu-Jiri Road, Charnawati Rehabilitation Programme Phase III*, Affoltern: ITECO/SDC/HMGN

Kappeler, W. (1984) *Rural Road Construction in Nepal: Evaluation of Experiences from the Lamosangu-Jiri Road Project*. Kathmandu: His Majesty's Government of Nepal with the Swiss Association for Technical Assistance

Meyer, W.P. (1987) *Vegetative Soil Conservation Measures: A Field Manual*. Tansen (Nepal): Tinau Watershed Project, GTZ/Helvetas

Morgan, R.P.C.; Rickson, R.J. (1995) *Slope Stabilization and Erosion Control: A Bioengineering Approach.* London: E & F N Spon

Nepal SPWP (Special Public Works Programme) (1992) *Environmental Protection Measures for Hill Irrigation Schemes in Nepal.* SPWP Manual No 1. Kathmandu: ILO

Schaffner, U. (1987) *Road Construction in the Nepal Himalaya: The Experience from the Lamosangu-Jiri Road Project,* Occasional. Paper No 8. Kathmandu: ICIMOD

Schiechtl, H.M. (1980) *Bioengineering for Land Reclamation and Conservation.* Edmonton: The University of Alberta Press

Schiechtl, H.M.; Stern, R. (1996) *Ground Bioengineering Techniques.* Oxford: Blackwell Science

Shrestha, J.B.; Howell, J.H; Rajbhandari, S.P.; Mull, A.K.; Maskey, D.R. (1998) 'Landslides and Road Development in Nepal'. In *DPTC Proceedings of the International Seminar on Water-Induced Disaster*, pp 1-10. Kathmandu: DPTC

Shrestha, V.P. (1991) 'Biotechnical Slope Stabilisation in Mountain Roads'. PhD Thesis, University of Strathclyde, UK.

Transport Research Laboratory, (1997) *Principles of Low Cost Road Engineering in Mountainous Regions.* Overseas Road Note No 16. Crowthorne: Transport Research Laboratory

11 Landslide Hazard and Risk Mapping in the Himalaya

R. Anbalagan[1] and B. Singh[2]
[1]University of Asmara, P.O.Box 9582, Asmara, Eritrea
E-mail: anba@earth.uoa.edu.er
[2]University of Roorkee, Roorkee 247667, India

The building of new infrastructure in the Hindu-Kush Himalaya has greatly increased in recent times. Due to the lack of systematic investigations, these schemes are often faced with landslide problems. Sustainable development planning should guide the design and implementation of construction projects in the hills. This paper presents methods of assessing landslide hazards and risks in the Himalaya.

Introduction

Landslides are the most common natural hazards in the Hindu Kush-Himalaya region. The Himalaya is a geologically and ecologically fragile mountain ecosystem that has been the target of intense development activities over the past few decades. The planning, design and execution of development schemes, such as road and building construction are often carried out in an unplanned way due to financial, time and other constraints. As a result, many projects pay insufficient attention to the necessary geological and geo-technical situation. The resulting unstable slopes and the increased incidence of landslides results in rapid environmental degradation.

Sustainable development in a mountainous region refers in part to the implementation of development schemes taking into consideration the existing instabilities of the terrain so that the resultant geo-environmental hazards are minimised. Sustainable development has to be integral in the planning and implementation of projects in hilly areas. Systematic investigations need to be carried out that move from the regional to the local perspective. Initially areas should be studied on a regional scale (1:25,000 to 50,000) and a landslide hazard zonation (LHZ) map prepared to indicate the distribution of hazard prone slopes. While planning infrastructure projects, different site and alignment options should be considered and the one with the minimum hazard should be chosen for implementation. Where hazard prone slopes are unavoidable for construction, their recognition early on will help engineers to adopt suitable preventive measures.

Once the landslide hazard potential of an area has been assessed by the appropriate specialists, the next step is to formulate a risk assessment. The risk depends on both the hazard probability and the damage potential. Landslide management should be based on risk assessment; priority areas should be identified by estimating where most damage to human structures will occur. For example, an active landslide in a remote area will have a lower priority for intervention than a moderate hazard slope adjoining a densely populated area.

Methods of Landslide Investigations

The investigation of landslides has undergone significant developments in the past few decades. Several new techniques have been developed which have contributed to understanding the behaviour of landslides. Recently developed techniques for investigations on a regional scale have contributed significantly to the systematic planning of infrastructure development in hilly areas.

These methods further the understanding of landslides and help in designing control measures. The choice of any method is dependent on the objectives of the investigations in terms of the required accuracy and other details. The methods of analysis can be classified as empirical, detailed, and observational (Figure 11.1).

Empirical methods

The empirical approach relates experiences gained from previous field investigations of landslides to the existing slope conditions. On the basis of field experience, causative factors are identified and their influence in bringing about instabilities is studied. The qualitative nature of field conditions is quantified on the basis of a relative rating scheme.

The empirical approach is the most recent approach and has become the usual way of assessing rock slopes. Landslide hazard zonation (LHZ) mapping and landslide risk assessment (LRA) mapping fall into this category. These methods are economical as large areas can be covered in relatively short periods. Landslide hazard zonation (LHZ) is a macro-zonation approach that categorises an area into very stable, stable, moderately stable, unstable, and very unstable zones. It is useful for the preliminary planning stages of infrastructure schemes to steer them away from unstable areas. LRA mapping is particularly useful for landslide hazard management. Although many methods are available for LHZ mapping, there is a need to rationalise all these approaches. The mapping techniques based on the basic causative factors provide the more realistic results, since these factors are global and maps made in this way can be used effectively in different terrains. Empirical studies are usually done between scales of 1:25,000 and 50,000 to provide rapid assessments covering larger areas.

Detailed methods

Detailed methods include detailed studies of unstable slopes on scales of 1:1,000 to 1:5,000. They require knowledge of soil and rock properties, which can be obtained by a carefully planned and executed field and laboratory investigation. They can also be estimated by 'back analysis' whereby a known slope is analysed by assigning a suitable factor of safety, which gives various combinations of strength parameters from which realistic values are chosen. Detailed studies are also used to analyse different slope segments using the following parameters:

- nature of slope materials;
- attitude of geological discontinuities with reference to the slope;
- strength properties of the slope materials such as c (the cohesion) and ϕ (the friction angle);
- strength along the planes of discontinuities;
- section and height of the slope; and
- possible seepage water pressures.

These studies calculate the status of stability of slopes in terms of the factor of safety (FOS) by taking into consideration the total shear stresses acting on the planes of failure and the shear strength of the discontinuities. If a slope indicates a FOS of less than 1, then it is unstable and may require remedial measures. The nature of the remedial measures required for stabilisation can be identified on the basis of the FOS. This is also called a micro-zonation approach. It also includes the computer modelling of landslides by the discrete element method (DEM). Several computer programs have been developed to study failed or high hazard slopes.

Observational methods

Observational methods refer to instrumental monitoring of slopes. The surface monitoring of movements through pegs located on the slope is one popular technique. Extensometers or incli-

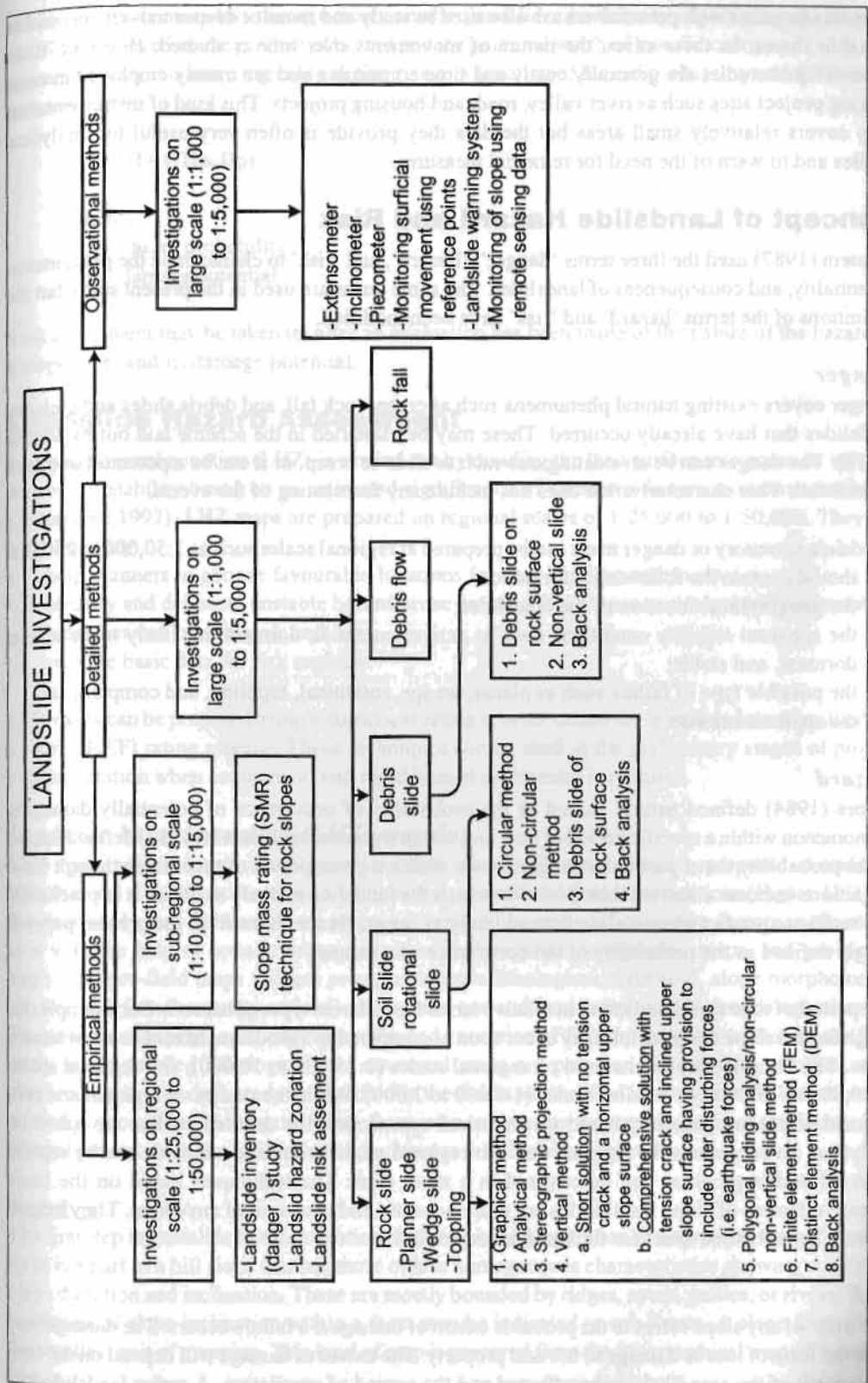

Figure 11.1: General methods of landslide investigations

nometers together with piezometers are also used to study and monitor deeper movements within unstable slopes. In these cases, the nature of movements over time is studied. However, these observational studies are generally costly and time consuming and are mainly employed in engineering project sites such as river valley, road, and housing projects. This kind of instrumentation only covers relatively small areas but the data they provide is often very useful for analytical studies and to warn of the need for remedial measures.

Concept of Landslide Hazard and Risk

Einstein (1987) used the three terms 'danger', 'hazard', and 'risk' to characterise the phenomena, potentiality, and consequences of landslides. The same terms are used in the present study but the definitions of the terms 'hazard' and 'risk' have been modified.

Danger

Danger covers existing natural phenomena such as creep, rock fall, and debris slides and includes landslides that have already occurred. These may be classified in the scheme laid out by Varnes (1978). The danger can be an existing one such as slide or creep, or it can be a potential one such as rock fall. This characterisation does not include any forecasting of the events.

Landslide inventory or danger maps can be prepared at regional scales such as 1:50,000 to 250,000 and should contain the following information:

- the geographical location of the landslides;
- the apparent stability conditions such as active, potential, dormant but likely to be active, dormant, and stable;
- the possible type of failure such as planar, wedge, rotational, toppling, and complex; and
- the approximate size.

Hazard

Varnes (1984) defined natural hazard as the probability of occurrence of potentially damaging phenomenon within a specific period of time and within a given area. Einstein (1987) defined hazard as the probability that a particular danger occurs within a given period of time. Even though these definitions indicate a limited time period in which the landslide is likely to occur, it is practically impossible to predict when a slide is most likely to occur. Hence 'hazard' in the present paper is simply defined as the probability of the occurrence of a danger.

The period of time can be indicated in relative terms for different types of hazards. For example, for a high hazard slope the landslide may occur soon as compared to a moderate hazard or a low hazard slope. The hazards may be analysed on regional scales (1:25,000 to 50,000), sub-regional scales (1:10,000 to 15,000), or detailed scales (1:1,000 to 2,000). While the studies on regional and sub-regional scales are generally based on empirical approaches, the detailed studies are based on analytical investigations. In regional and sub-regional studies, landslide hazards can be rapidly assessed and large areas can be covered in a short time. The techniques based on the basic causative factors of slope instabilities are more accurate and can be used anywhere. They help to identify hazard prone areas for further detailed studies.

Risk

The 'risk' of any slope refers to the probable extent of damage if a failure occurs. The damage may be in the form of loss or damage to life and property. The extent of damage will depend on the land use pattern of the area likely to be affected and the spread of population. A major landslide in a

remote area will cause less damage than a smaller landslide in a densely populated area. Einstein (1987) defined risk as the product of hazard and the potential worth of loss. Since loss will vary with space and time, it is more logical to define risk as a function of hazard probability and the damage potential.

$$R = f(Hp, Dp)$$

where,
Hp = hazard probability
Dp = damage potential

Risk assessment may be taken up after an evaluation has been made of the nature of the hazard of a slope facet and its damage potential.

Landslide Hazard Assessment

Landslide hazard zonation (LHZ) is carried out by dividing the land surface into zones of varying degrees of stability based on an estimated significance of causative factors to induce instability (Anbalagan 1992). LHZ maps are prepared on regional scales of 1:25,000 to 1:50,000. They are useful as they

- help planners to choose favourable locations for new building and roads;
- identify and delineate unstable hazard prone areas so that proper environmental regeneration measures can be initiated; and
- provide basic data for risk analysis.

LHZ maps can be prepared using a numerical rating scheme called the landslide hazard evaluation factor (LHEF) rating scheme. These techniques can be used in the preliminary stages of project implementation when economical and rapid hazard assessment is required.

Landslide hazard zonation (LHZ) mapping

LHZ maps indicate the probabilities of landslide hazards. They are generally prepared on scales of 1:25,000 to 1:50,000 and based on a combination of desk and field investigations (Figure 11.2). In the desk study, pre-field maps are prepared to show the status of causative factors in the study area with the help of aerial photographs, satellite imageries, topographic maps, and geological maps. The pre-field maps that are prepared include lithological, structural, slope morphometry, relative relief, rock outcrop and soil cover, land use and land cover, and hydrogeological maps. This information helps systematic planning and execution of field investigations. During the field study, more detailed lithological and structural maps are prepared. The details of other maps prepared during the desk study are verified in the field and modified if necessary. Field studies are carried out to collect the required data facet wise to estimate the total hazards of the facets. The general procedure of the LHZ mapping technique is outlined in Figure 11.2.

Procedure

The first step in landslide hazard zonation mapping is the preparation of a **slope facet** map. A slope facet is a part of a hill slope that has more or less homogeneous characteristics showing consistent slope direction and inclination. These are mostly bounded by ridges, spurs, gullies, or rivers. Local variations of slope inclination within a facet may be indicated as sub-facets. A slope facet forms the smallest unit of mapping. This kind of map is prepared from the topographical map of the study area.

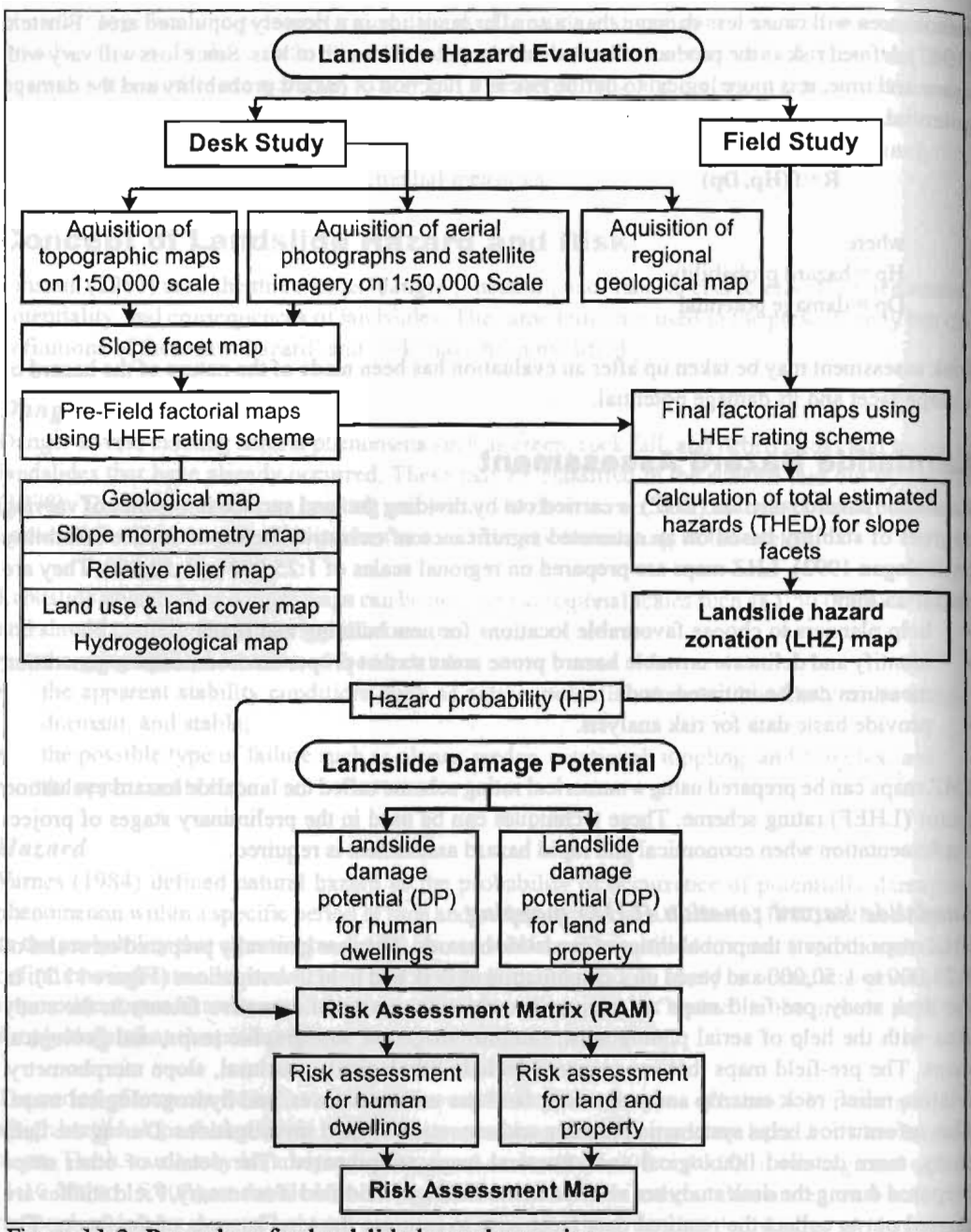

Figure 11.2: **Procedure for landslide hazard mapping**

The **landslide hazard evaluation factor** (LHEF) rating scheme is based on an empirical approach that combines the background knowledge of the causative factors of landslides with a study of those prevailing. The qualitative nature of field conditions can be quantified by relative rating schemes. Similar approaches have been adopted in the well-known rock mass classifications such as the rock mass rating (RMR) and Q systems (Barton et al. 1974; Bieniawski 1979).

The LHEF rating scheme is a numerical system based on the major inherent causative factors of slope instability such as geology, slope morphometry, relative relief, land use and land cover, and

hydrogeological conditions. External factors such as rainfall and seismicity are not included in LHZ mapping as they are not part of the slope character and cannot be evaluated for assessing the landslide hazard of a slope facet. Such external factors are erratic and regional in nature and act over large areas. However when heavy rain or earthquakes occur, a high hazard facet is more likely to be triggered off than a low hazard one (Gupta and Anbalagan 1995). The maximum LHEF ratings for different categories are determined on the basis of their estimated significance in causing instability (Table 11.1). The maximum LHEF ratings value for the total estimated hazard (TEHD) is 10. A score of 10 describes a slope that is most likely to slide. Table 11.1 shows a detailed LHEF rating scheme with the maximum ratings related to individual causative factors.

Table 11.1: **Maximum landslide hazard evaluation factor (LHEF) ratings**

Contributory factor	Maximum LHEF ratings
Lithology	2.0
Relationship of structural discontinuities with slope	2.0
Slope morphometry	2.0
Relative relief	1.0
Land use and land cover	2.0
Groundwater conditions	1.0
Total	**10.0**

Geological maps provide information on the lithology and structure of the area. Lithological and structural maps are prepared separately where better representation is needed.

The erodibility, or the response of rocks to the processes of weathering and erosion, is the main criterion for judging the **lithology** of a slope and designating LHEF ratings. For example, quartzite, limestone, and igneous rocks are generally hard, massive, and resistant to erosion, and form steep slopes. In comparison, terrigenous sedimentary rocks are much more vulnerable to erosion and hence are more susceptible to landslides. Similarly, phyllites and schists are characterised by flaky minerals, which weather quickly and promote instability. A correction factor to allow for the extent of weathering of the rocks has been incorporated in the rating system. In the case of soil, genesis and age are the main consideration in awarding the ratings. Older alluvium is generally well compacted and has a high shear resistance. Recent materials such as slide debris are loose and have a low shearing resistance.

Structure includes primary and secondary discontinuities in the rocks such as bedding, joints, foliations, faults, and thrusts. The attitude of structural discontinuities in relation to slope inclination and direction has a great influence on the stability of slopes (see also Singh in this volume). Three types of relationships are considered important (Romana 1985):

- the extent of parallelism between the directions of the discontinuity, or the line of intersection of two discontinuities and the slope;
- the steepness of the dip of the discontinuity, or the plunge (dip) of the line of intersection of two discontinuities; and
- the difference in the dip of the discontinuity, or the plunge of the line of intersection of the two discontinuities to the inclination of the slope

The more discontinuities tend to be parallel to a slope, the greater is the risk of slope failure. When the dip of the discontinuity or plunge of the line of intersection of two discontinuities increases, the probability of failure also increases, because this angle may exceed the angle of friction for the discontinuity surfaces. The failure potential remains high, until the point where the dip of the discontinuity plane or the plunge of the line of intersection of the two discontinuities does not exceed the inclination of the slope. LHEF ratings have been assigned accordingly for various stability conditions (Table 11.2). If the problem is one of potential movement of soil rather than rock, the inferred depth of the soil cover is used as a basis for the ratings.

Table 11.2: **Landslide hazard evaluation (LHEF) rating scheme**

Contributory Factor	Category	LHEF rating	Remarks
Lithology			
Rock Type	Type-I		*Correction factors for weathering*
	Quartzite and limestone	0.2	Correction factor C_1: Highly weathered - rock discoloured joints open with weathering products, rock fabric altered to a large extent
	Granite and gabbro	0.3	
	Gneiss	0.4	
	Type-II		Correction factor C_2: Moderately weathered - rock discoloured with fresh rock patches, weathering more around joint planes, but rock intact
	Well-cemented terrigenous sedimentary rocks, dominantly sandstone with minor beds of claystone	1.0	
	Poorly cemented terrigenous sedimentary rocks, dominantly sandstone with minor clay shale beds	1.3	Correction factor C_3: Slightly weathered - rock slightly discoloured along joint planes, which may be moderately tight to open, intact rock
			The correction factor for the observed degree of weathering should be multiplied by the fresh rock rating to get the corrected rating
	Type-III		
	Slate and phyllite	1.2	For rock type I
	Schist	1.3	$C_1 = 4, C_2 = 3, C_3 = 2$
	Shale with inter-bedded clayey and non-clayey rocks	1.8	For rock type II
	Highly weathered shale, phyllite & schist	2.0	$C_1 = 1.5, C_2 = 1.25, C_3 = 1.0$
Soil Type	Older well-compacted fluvial fill material (alluvial)	0.8	
	Clayey soil with naturally formed surface (eluvial)	1.0	
	Sandy soil with naturally formed surface (alluvial)	1.4	
	Debris comprising mostly rock pieces mixed with clayey/sandy soil (colluvial)		
	I. Older well compacted	1.2	
	II. Younger loose material	2.0	
Structure			
Relationship of structural discontinuity with slope			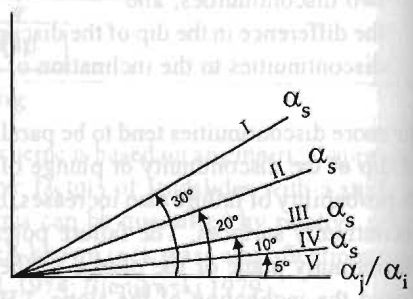
Relationship of parallelism between the slope and the discontinuity*	I < 30°	0.20	
	II 21° - 30°	0.25	
	III 11° - 20°	0.30	
	IV 6° - 10°	0.40	
	V ≤ 5°	0.50	
Planar (α_j, α_s) Wedge (α_i, α_s)			Parallelism between the slope and the discontinuity ($\alpha_j/\alpha_i, \alpha_s$)

Table 11.2 (cont'd)

Contributory Factor	Category	LHEF rating	Remarks
Relationship of dip of discontinuity* and inclination Planar - (β_j - β_s) Wedge - (β_i - β_s)	I > 15° II 0° - 10° III 0° IV 0° -(-10°) V -10°	0.65 0.85 1.30 2.00 1.20	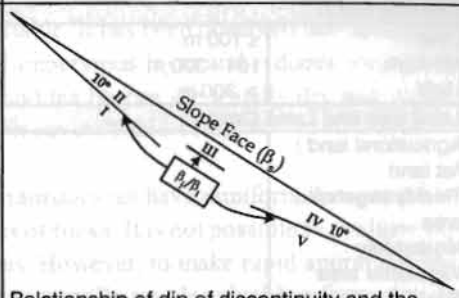 Relationship of dip of discontinuity and the inclination (dip) of slope (β_j - β_r- β_s)
Dip of discontinuity* Planar - β_j Wedge - β_i	I ≤ 15° II 16° - 25° III 26° - 35° IV 36° - 45° V > 45°	0.65 0.85 0.30 0.40 0.50	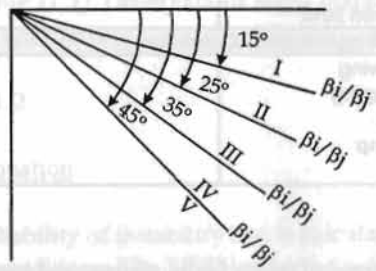 Dip of discontinuity (β_r- β_j) α_j = dip direction of joint α_i = direction of line of intersection of two discontinuities α_s = direction of slope inclination β_j = dip of joint β_i = plunge of line of intersection β_s = inclination of slope Category I = Very favourable II = Favourable III = Fair IV = Unfavourable V = Very unfavourable *Discontinuity refers to the planar discontinuity in the case of planar failure or the line of intersection of two planar discontinuities in the case of wedge failure, or whichever more is important
Depth of soil cover			
	≤5 m 6-10 m 11-15 m 16-20 m >20 m	0.65 0.85 1.30 2.00 1.20	
Slope morphometry			
Escarpment/cliff Steep slope Moderately steep slope Gentle slope Very gentle slope	45° 36°-45° 26°-35° 16°-25° ≤15°	2.00 1.70 1.20 0.80 0.50	

Table 11.2 (cont'd)

Contributory Factor	Category	LHEF rating	Remarks
Relative Relief			
Low	≤ 100 m	0.3	
Medium	101 - 300 m	0.6	
High	> 300 m	1.0	
Land Use and Land Cover			
Agricultural land / flat land		0.65	
Thickly vegetated area		0.85	
Moderately Vegetated area		1.20	
Sparsely vegetated area with lesser ground cover		1.50	
Barren land		2.00	
Hydrogeological Condition			
Flowing		1.00	
Dripping		0.80	
Wet		0.50	
Damp		0.20	
Dry		0.00	

In areas of major faults, thrusts, and intra-thrust zones, an extra rating of 0.5 may be awarded to take into account the higher susceptibility depending upon the intensity of fracturing.

Slope morphometry refers to the general slope angle with the horizontal. Slope morphometry maps define slope categories on the basis of the frequency of occurrence of different slope angles. The distribution of slope categories in any area is a result of the geomorphological history of an area. The angle of slope of each unit is a reflection of a series of micro-morphological processes and controls imposed on that facet. Slope morphometry maps are prepared by dividing the larger topographical map into smaller units defined by the slope facets. Five slope categories are used for slope morphometry study; different LHEF ratings are assigned for each (Table 11.2): escarpment/ cliff (>45^0); steep slope (35^0-45^0); moderately steep slope (25^0-35^0); gentle slope (15^0-25^0); very gentle slope (< 15^0).

On a topographical map of known scale, the number of contour lines per km of horizontal distance can be calculated for each category of slope morphometry. Thus the slope morphometry can be determined from a topographical map by counting the number of contour lines per unit distance for the slope.

Relative relief maps show the local relief, that is the maximum height between ridge tops and the valley floor within an individual facet. Thus they show the major breaks in the slopes of the study area. Three slope categories of relative relief have been chosen for hazard evaluation purposes and assigned different LHEF ratings: low (<100m), medium (101-300m) and high (>300m).

The type of **land cover** that a slope has is an indirect indicator of the stability of that slope. Barren and sparsely vegetated areas have faster rates of erosion and greater instability than areas that are thickly vegetated (as often found in reserves or protected forests). Forest cover, in general, hinders the negative action of climatic agents on slopes and protects them from the effects of weathering and

erosion. A well-spread root system increases the shearing resistance of slope material. Agriculture (the **land use**) is generally practised on gentle to very gentle slopes; though moderately steep slopes are also cultivated where land is in short supply. The water levels of irrigated agricultural land are frequently recharged which makes them more stable. It has been observed that the humus produced by grass on slope surfaces provides a natural impervious layer and reduces seepage of run-off water into the slope. Slopes turfed with grass and tea bushes are usually dry and stable. Ratings are awarded based on the intensity of vegetation cover (Table 11.2).

Hydrogeological conditions — Groundwater in hilly terrain does not have a uniform flow pattern as it is generally channelled along structural discontinuities of rocks. It is not possible to evaluate the behaviour of groundwater on hill slopes over large areas. However, to make rapid appraisals, the nature of surface indications of the behaviour of groundwater will provide valuable information on the stability of hill slopes for hazard mapping. The presence of surface water such as damp, wet, dripping, or flowing areas are used for rating purposes (Table 11.2). Observations taken immediately after the monsoon will show the worst groundwater conditions.

The **LHEF ratings** for all these factors are given in Table 11.2.

Calculation of total estimated hazard (TEHD) and hazard zonation

The **total estimated hazard** (TEHD) indicates the net probability of instability and is calculated facet-wise, as adjoining facets may have different stability conditions. The TEHD of an individual slope facet is obtained by adding the ratings of the individual causative factors obtained from the LHEF rating scheme.

TEHD value = ratings of lithology + structure + slope morphometry + relative relief + land use and land cover + hydrogeological conditions

The TEHD scores allow slopes to be assigned to one of five categories of landslide hazard: very low hazard (VLH), low hazard (LH), moderate hazard (MH), high hazard (HH) and very high hazard (VHH), (Table 11.3).

Table 11.3: **Landslide hazard zonation on the basis of total estimated hazard (TEHD)**

Zone	TEHD value	Description of zone
I	<3.5	very low hazard (VLH) zone
II	3.5 - 5.0	low hazard (LH) zone
III	5.1 - 6.0	moderate hazard (MH) zone
IV	6.1 - 7.5	high hazard (HH) zone
V	>7.5	very high hazard (VHH) zone

Case study of landslide hazard zonation from the Kumaun Himalaya, India

A landslide hazard zonation map was made for the Tanakpur-Sukhidhang area in the south-eastern part of the Kumaun Himalaya in Uttar Pradesh, India. This area covers about 70 sq.km and includes two well-defined physiographic regions: the Siwalik hill range (Outer Himalaya) in the south, which extends to Balkholi, and the Lesser Himalaya region further north (Figures 11.3 and 11.5). The Tanakpur-Ghat-Pithoragarh road, a strategically important road, passes through the centre of the area. A slope facet map (Figure 11.4) was prepared for the purposes of LHZ mapping,. Using this as a base map, other thematic maps were prepared including a lithological map (Figure 11.5), structural map (Figure 11.6), slope morphometry map (Figure 11.7), relative relief map (Figure 11.8), land use and land cover map (Figure 11.9), and hydrogeological map (Figure 11.10). From these maps, the total estimated hazard (TEHD) was calculated facet-wise and presented as a landslide hazard zonation (LHZ) map (Figure 11.11).

Figure 11.3: Location map of Sukhidhang area

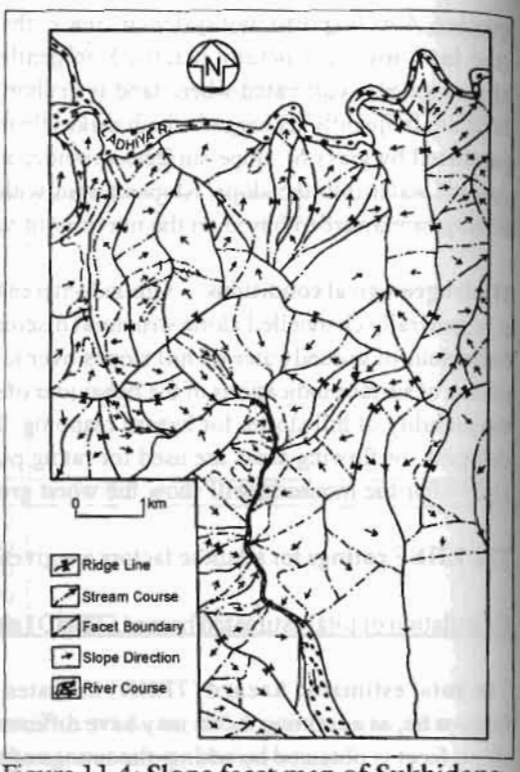

Figure 11.4: Slope facet map of Sukhidang area

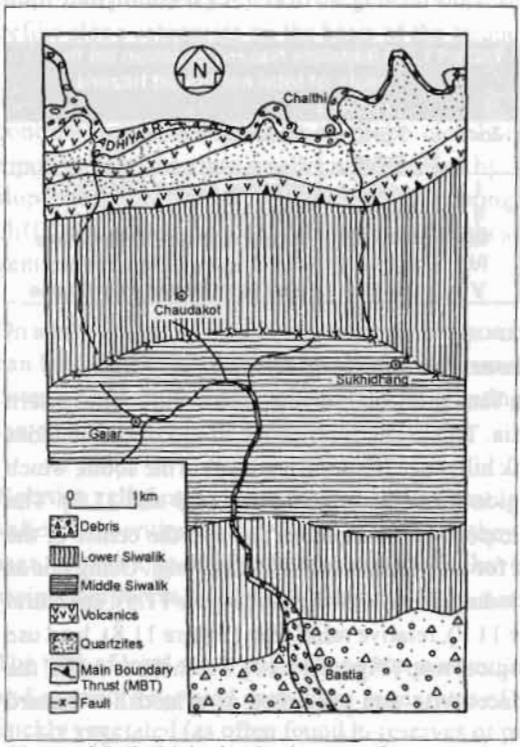

Figure 11.5: Lithological map of Sukhidang area

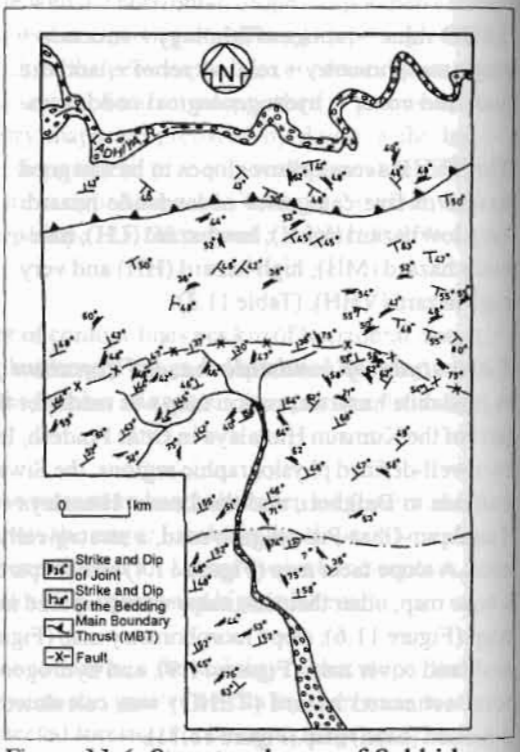

Figure 11.6: Structural map of Sukhidang area

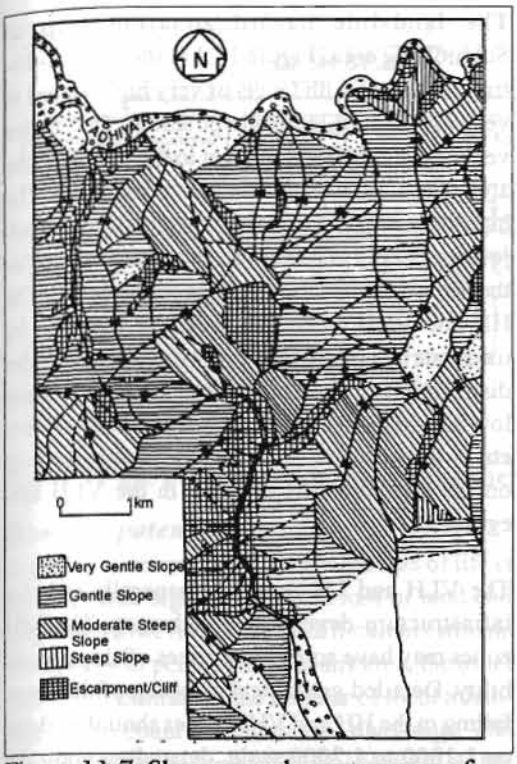

Figure 11.7: Slope morphometry map of Sukhidang area

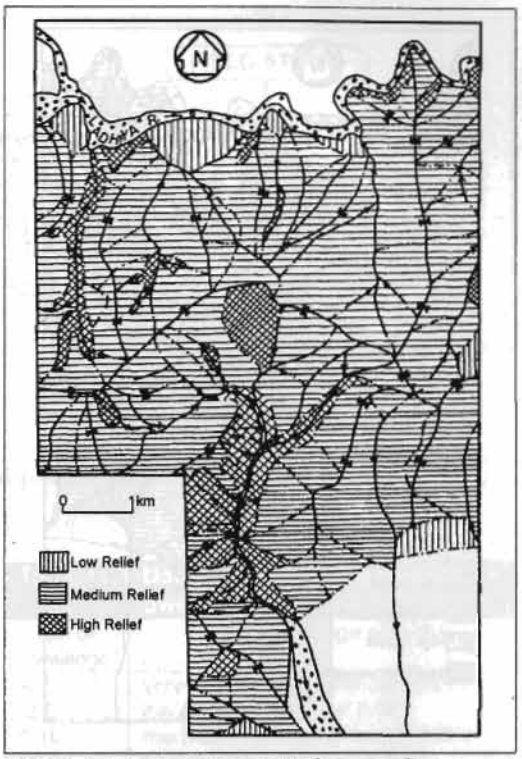

Figure 11.8: Relative relief map of Sukhidang area

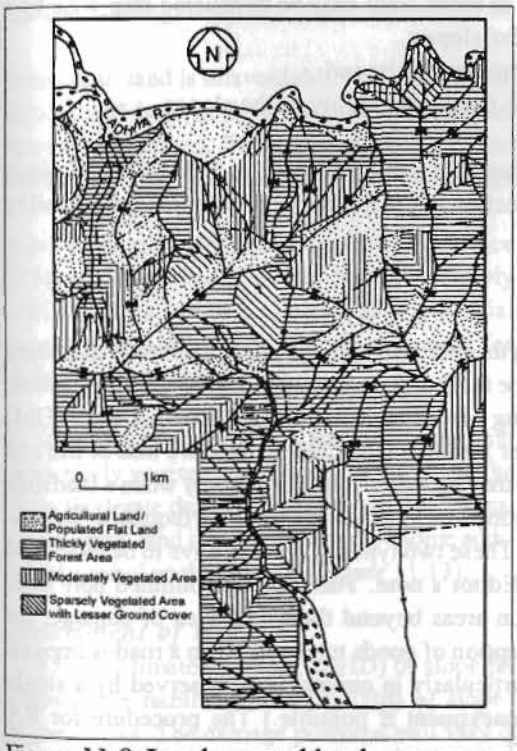

Figure 11.9: Land use and land cover map of Sukhidang area

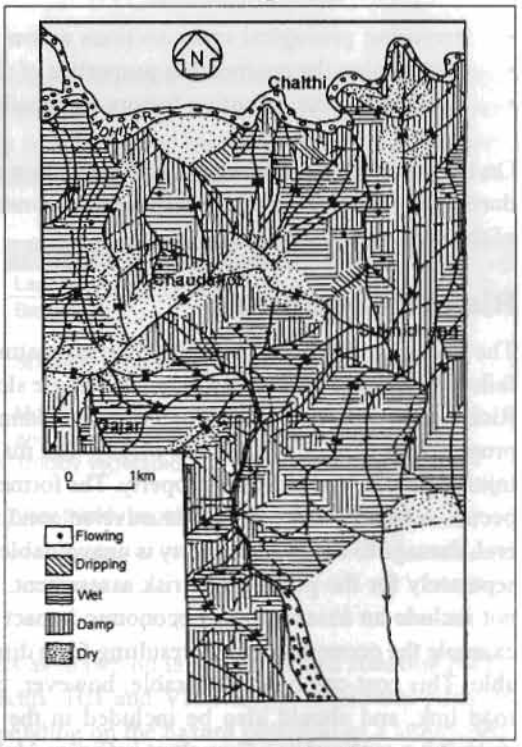

Figure 11.10: Hydrogeological map of Sukhidang area

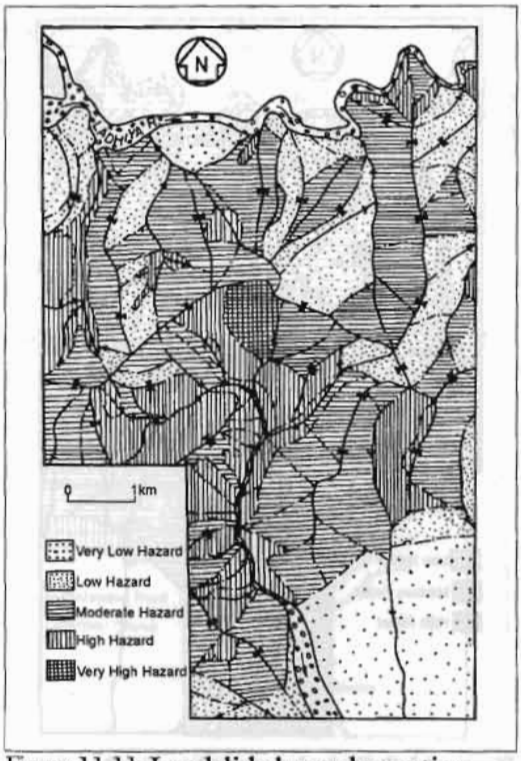

Figure 11.11: **Landslide hazard zonation map of Sukhidang area**

The landslide hazard zonation map of Sukhidhang area (Figure 11.11) shows well-distributed zones with facets of very high hazard to very low hazard landslide potential. One major very high hazard (VHH) facet in the middle of the area near Chaudakot is an active landslide. The high hazard (HH) facets are generally seen adjoining deeply dissected stream courses such as the Rela-Ka Khola and Khagota streams. The HH and VHH facets are generally bounded by moderate hazard (MH) facets, which have a wider distribution in the study area. There are many low hazard (LH) and very low hazard (VLH) facets in the northern part. The loose fan deposits on the southern part also fall in the VLH category.

The VLH and LH zones are generally safe for infrastructure development schemes. The MH zones may have some local zones of slope instability. Detailed geological mapping of the areas falling in the HH and VHH zones should be done on 1:1000 to 1:2000 scale, depending upon the total area of the facet. The factor of safety (FOS) of these areas may be calculated step-wise by

- preparing geological cross-sections across the slopes;
- determining the engineering properties of slope materials; and
- determining the causative factors responsible for the instability of the slopes.

On the basis of this, preventive and mitigation measures can be adopted in HH and VHH zones during implementation of any engineering construction to protect the geo-environmental stability of the area.

Risk Assessment

The risk assessment of a slope involves estimating the extent of damage likely to result if that slope fails. The damage may be restricted to a single slope facet or it may extend into the adjoining facets. Risk assessment (RA) maps are useful for planning proper landslide hazard management (LHM) programmes (Figures 11.12 and 11.13). The major forms of landslide damage are loss of life and injuries, and loss of land and property. The former may be significant, particularly when a landslide occurs suddenly – usually under adverse conditions of cloudbursts and/or earthquakes. In general, damage to land and property is unavoidable. These two types of damage have to be evaluated separately for the purposes of risk assessment. [Editor's note. The approach outlined here does not include an assessment of economic impact on areas beyond the actual area of damage, for example the economic impact resulting from disruption of goods transport when a road is impassable. This cost can be considerable, however, particularly in mountain areas served by a single road link, and should also be included in the assessment if possible.] The procedure for RA mapping is outlined as a flow chart in Figure 11.12.

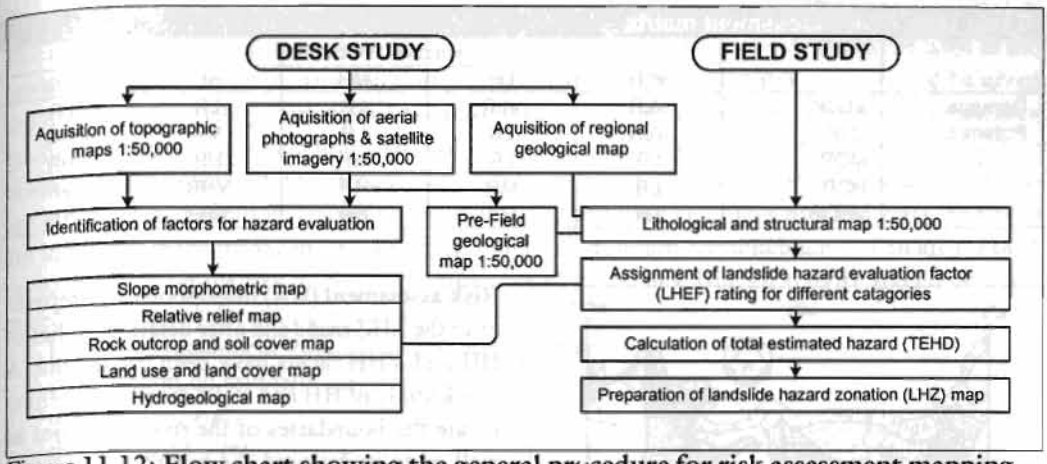

Figure 11.12: **Flow chart showing the general procedure for risk assessment mapping**

Damage potential

In risk assessment, the potential for loss of life is given greater significance than loss of land and property. However, it may be difficult to estimate the number of people living in any area; the usual method of estimating the number of local inhabitants is to count the number of dwellings. The history of damage may also be assessed on the basis of experience. The damage potential to human dwellings is rated as shown in Table 11.4.

Table 11.4: **Damage potential for human dwellings**

No. of dwellings	Status of damage potential
<2	very low damage potential (VLDP)
2-5	low damage potential (LDP)
5-10	moderate damage potential (MDP)
10-50	high damage potential (HDP)
>50	very high damage potential (VHDP)

Damage to land is unavoidable when a landslide occurs. Affected areas may include barren land, agricultural land, and forest land. Forested land may be thickly, moderately, sparsely, or very sparsely vegetated. The types of property likely to be affected by landslides include houses, roads, mines, offices, factories, schools, playgrounds, parks, and other (engineering) structures.

Since properties are located on the land surface likely to be affected, they can be shown simply with different symbols. The damage potential status scheme shown in Table 11.5 is used for different land types.

Table 11.5: **Damage potential for land types**

Land category	Status of damage potential
Barren	very low damage potential (VLDP)
Sparsely vegetated	low damage potential (LDP)
Moderately vegetated and agricultural land	moderate damage potential (MDP)
Thickly vegetated	high damage potential (HDP)
Very thickly vegetated	very high damage potential (VHDP)

In Table 11.5 agricultural land has been joined with moderately vegetated land because they have the same moderate damage potential characteristics. Agricultural land is often indicated by some additional symbol on the risk map (Figure 11.13).

Assessment of risk

The total estimated hazard (TEHD) of slope facets as drawn on landslide hazard zonation (LHZ) maps is the hazard probability (Hp) of slope facets. HH and VHH slopes obviously pose the highest risks. The damage potential will vary depending on the hazard potential of a slope facet; the relationship is indicated in a risk assessment matrix (RAM) (Table 11.6). The calculations are performed twice, once for risk to human dwellings and once for risk to land and property.

Table 11.6: Risk assessment matrix

		Hazard Probability →				
		VLH	LH	MH	HH	VHH
Damage Potential ↓	VLDP	VLR	VLR	LR	LR	LR
	LDP	VLR	LR	LR	MR	MR
	MDP	LR	LR	MR	HR	HR
	HDP	LR	MR	HR	VHR	VHR
	VHDP	LR	MR	HR	VHR	VHR

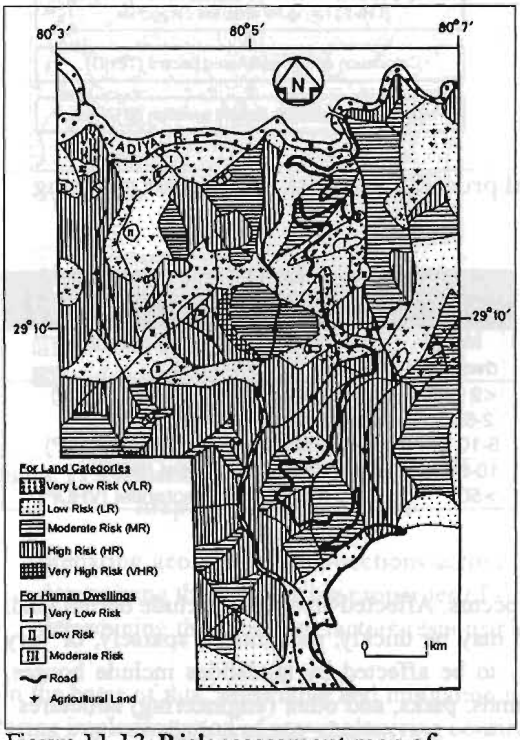

Figure 11.13: Risk assessment map of Sukhidang area

Risk assessment (RA) maps should be prepared after the LHZ maps and after detailed studies of HH and VHH facets have been carried out. A quick study of HH and VHH facets will help to locate the boundaries of the risk categories as well as to understand the nature of causative factors and the likely types of failure. Moreover the land use and land cover map prepared during the LHZ mapping and data on the distribution of human dwellings and other structures will help inform the risk assessment.

The boundaries of the risk categories may lie within the same slope facets as the hazard, entirely outside the facet, or partly within and partly outside. For example, if a human settlement is located on a stable slope adjoining a steep cliff, the risk from the unstable cliff face may lie entirely outside the facet containing the cliff. Hence, risk assessment maps may have different zone boundaries to LHZ maps.

The following factors are considered, when deciding on the boundaries of the risk categories.

- **Topography of the area** – Both the slope facet in which the hazard exists and the adjoining facets are important. If the hazard containing slopes are steeper, the risk may encroach onto adjoining slope facets, particularly at lower levels. Tension cracks likely to be caused by a landslide may affect adjoining slopes at higher levels.
- **Nature of failure** - Debris flow along gullies can penetrating far into adjoining slopes at lower levels. Rock falls may be only occasionally active, but are more likely to affect slopes further down. Planar, wedge, and rotational failures may affect the peripheral regions of adjoining facets. Before the actual failure, the effects of distressing may be seen on the slopes.
- **Geological factors** – For rock slides, the type of rock, the extent of fractionation, the attitude of critical discontinuities, and the nature of weathering are important in deciding how far the risk from a particular slope failing will spread.

The boundaries of the zones of risk to human dwellings are usually shown with specific symbols. The risk to other engineering structures and properties may also be indicated by different symbols. The risk assessment map for Sukhidang area is shown in Figure 11.13.

Landslide hazard management and the use of risk assessment (RA) maps

The risk assessment map indicating the threats to people, land, and property should be used as the basis for planning a risk management programme. High and very high risk areas should be given top priority for initiating remedial and control measures. Immediate short-term measures include grading of slopes, improving drainage, and building retaining walls. Long-term measures include biotechnical stabilisation, maintenance of existing drainage, and provision of sub-surface drainage, anchors, and additional catch water drains. Afforestation and other precautionary measures are important in the management of high-risk areas. In addition, the inhabitants of an area should be educated about the risk, and the consequences of landslides. Human activity should be minimised in risk prone areas by preventing

- human encroachment into the natural water courses;
- urbanisation on critically stable slopes;
- overgrazing; and
- the cutting of trees.

Since the damage potential is a variable parameter, risk assessments may need to be modified over time. In the case of progressive failures, the risk zone boundaries will expand unless long-term stabilisation measures are implemented.

Specific risks due to landslide hazards in the Hindu-Kush Himalaya

The fragile mountain ecosystems of the Hindu-Kush Himalaya are characterised by complicated geology, steep slopes, and extreme climatic conditions. They are very susceptible to landslides, and catastrophic slides often occur. Some particularly important hazards in the Himalayan region are described below.

Landslide dams

Major deep-seated landslides in the Himalaya may result in the transportation of huge amounts of debris along long steep gullies to form dams behind which reservoirs of water can build up. Such dams are usually unstable and will often burst within a few hours or days or after longer times. The resultant surging floodwater can destroy riverbanks, constructed dams, roads, buildings, and bridges. Major examples of this phenomenon include the Gohna landslide dam along the Alaknanda River, the Kanauldhia Gad landslide dam on the Bhagirathi River, and the Diexi landslide dam in China.

Debris flow

Long, steep gullies often witness sudden flows of debris (mixtures of rock, earth, and other inorganic material) from upper levels that can engulf everything in their path. During continuous periods of rain (>one week), groundwater levels may rise steeply to above the effectively impervious bedrock. At places where the debris cover is thin (<5m), water levels may rise to close to the surface. The high water pressure and resultant loss of grain-to-grain contact may induce a landslide which then becomes a debris flow. The resultant fast flowing viscous liquid charged with debris may cause large-scale toe erosion leading to more landslides further down.

Rock jumping

The steep rocky slopes of the Himalayan terrain are traversed by joints and may often release loose rock blocks as a result of loosening caused by freezing and thawing action along the joints or

during earthquakes. The random unpredictable release of rock blocks may cause devastation in the areas below. The steep Naina peak of Nainital, Kumaun is a classic example of rock jumping problems, which have continued for more than a century. During major earthquakes (>6 magnitude), the rock-jumping problem is serious and causes severe damage.

Surface erosion

The Himalayan mountain range is the youngest in the world and is highly erosion prone. The rocks are weak and erodible with steep slopes. There is a wide range of estimates of denudation rates of the mountains (0.5 to 20 mm/year), but the overall average rate of about 7 mm/year indicates a high rate of erosion (Ives and Messerli 1987).

Forest fires

Forest fires often occur in the Himalaya during periods of hot weather and can contribute to the development of landslides. These fires burn away the vegetation cover exposing the soil to atmospheric hazards, in particular accelerated erosion and excessive infiltration of water into the slope during times of heavy rain. This can trigger a landslide.

A case study of risk assessment in the Sukhidang area

A risk assessment map was prepared as described above to show the landslide hazard and damage potential in the Sukhidang area. First a landslide hazard zonation (LHZ) map was prepared from six factorial maps using the LHEF rating scheme (Figures 11.5 to 11.10). The total estimated hazard (TEHD) was calculated facet-wise for the landslide hazard zonation map (Figure 11.11).

The damage potentials were evaluated using the ratings shown in Tables 11.4 and 11.5. The damage potential and landslide hazard were combined to give a risk assessment map for land categories and human dwellings (Figure 11.13). The main role of these maps is to help field engineers and engineering geologists to identify the highest risk zones so that they can prioritise remedial measures.

The risk assessment map of the Sukhidang area (Figure 11.13) shows that the high and very high risk slopes are mostly located along the sides of the south-flowing Rola-ka Khola stream and the north-flowing Khagota stream, both of which lie in steep valleys, apart from a few isolated high-risk slopes in the north-eastern and eastern parts of the area. Low to moderate risk slopes are found throughout the area. Human dwellings and agricultural lands are mostly located on the low risk slopes with some on the medium risk slopes. The highest risks to human dwellings are found on the medium risk slopes. The Tanakpur-Sukhidang-Champawat road runs mostly along low to moderate risk slopes, except in a few locations where the road passes high-risk slopes. At such points the road has been built close to the ridge tops to avoid major stability problems. A detailed risk map was prepared for the road using the damage potential indicators and the modified slope mass rating (SMR) technique of Anbalagan et al. (1992) on a 1:10,000 scale to evaluate the hazard. The method is described below.

Risk assessment of slopes for roads

Hazard assessment

Romana (1985) developed a Slope Mass Rating (SMR) technique as a special application of Bieniawski's (1979) rock mass rating (RMR) classification, which was developed to measure the

stability of rock slopes. The SMR is a useful tool for the preliminary assessment of cut slopes in rocks. It helps engineers to assess the relative hazard of rock slopes without actually calculating the factor of safety. It follows some simple rules about instability modes and the required support measures.

The SMR technique uses the rock mass rating (RMR) classification to evaluate the rock mass quality. The relative hazards of instability are indicated on the basis of studies and experience with attitudes of discontinuity and slope, failure mode, and slope excavation methods.

The following parameters are measured to give the Rock Mass Rating (RMR).

- uniaxial compressive strength of rock material
- rock quality designation (RQD)
- spacing of discontinuities
- condition of discontinuities
- ground water condition

These are all measured either in the field or from boreholes. These five parameters are classified into various sub-categories that have been assigned different relative values (Table 11.8). The sum of the weighted ratings of individual parameters indicates the overall rock mass quality.

Bieniawski (1979) defines the RMR_{basic} as the basic parameter of rock mass quality. Romana (1985) calculates the SMR from the following formula.

$$SMR = RMR_{basic} + (F1*F2*F3) + F4$$

Table 11.8: **Rock mass rating calculation matrix (Bieniawski 1979)**

Parameter	Range of values						
1. Strength of intact rock material							
Point load strength index (MPa)	>10	4-10	2-4	1-2	For these low ranges the uniaxial compressive test is preferred		
Uniaxial compressive strength (MPa)	>250	100-250	50-100	25-50	5-25	1-5	<1
Rating	*15*	*12*	*7*	*4*	*2*	*1*	*0*
2. Drill Core Quality RQD%							
	90-100		75-90	50-75	25-50	<25	
Rating	*20*		*17*	*13*	*8*	*3*	
3. Spacing of discontinuities							
	>2 m	0.6-2 m	200-600 mm		60-200 mm		<60 mm
Rating	*20*	*15*	*10*		*8*		*5*
4.Condition of discontinuities							
	Very rough surfaces, not continuous; no separation; unweathered wall rock		Slightly rough surface; separation <1 mm; Slightly weathered walls	Slightly rough surface; separation <1 mm; highly weathered walls	Slickensided surfaces; gouge <5 mm; separation 1-5 mm; continuous		Soft gouge >5 mm; separation >5 mm; continuous
Rating	*30*		*25*	*20*	*10*		*0*
5. Groundwater in joints							
	Completely Dry		Damp	Wet	Dripping		Flowing
Rating	*15*		*10*	*7*	*4*		*0*
(high value is favourable, low is unfavourable)							

The parameters F1, F2, F3 are empirically established adjustment values for joints and F4 an adjustment factor for the method of excavation.

- F1 is a measure of the relative parallelism between a discontinuity and the slope face. It ranges from 1.00, when both sides are nearly parallel, to 0.15 when the angle between them is more than 30° and the failure probability is very low.
- F2 is a measure of the dip of discontinuity. It ranges from 1 for joints dipping more than 45°, to 0.15 for joints dipping less than 20°. In the toppling mode of failure, F2 remains 1.00.
- F3 is a measure of the relationship between the dip of discontinuity and the inclination of the slope. The conditions are fair when the slope face and the discontinuity are parallel. Unfavourable conditions occur when the slope dips 10° more than the discontinuity.
- F4 is an empirical adjustment factor for the method of excavation.

Here, the term discontinuity refers to the planar discontinuity in the case of potential plane failure or the line of intersection of two planar discontinuities in the case of potential wedge failure, whichever is more important. The values for F1 to F3 are given in Table 11.9, those for F4 in Table 11.10.

Table 11.9: Adjustment rating for joints (Romana 1985)

Case	Very favourable	Favourable	Fair	Unfavourable	Very unfavourable
P $\alpha_j - \alpha_s$	>30°	30°-20°	20°-10°	10°-5°	<5°
T $\alpha_j - \alpha_s - 180°$					
P/T F1	0.15	0.40	0.70	0.85	1.00
P β_j	<20°	20°-30°	30°-35°	35°-45°	>45°
P F2	0.15	0.40	0.70	0.85	1.00
T F2	1	1	1	1	1
P $\beta_j - \beta_s$	>10°	10°-0°	0°	0°- (-10°)	<-10°
T $\beta_j + \beta_s$	<110°	110°-120°	>120°	-------	--------
P/T F3	0	-6	-25	-50	-60

P plane failure — α_s slope dip direction — β_s slope dip

T toppling failure — α_j joint dip direction — β_j joint dip

Romana (1985) used plane and toppling failure modes for his analysis. The wedge failures were considered as special cases of plane failures and were analysed in terms of individual planes. The minimum value of SMR was taken to assess the rock slopes. However, this analysis is limited because where a wedge is unstable the instability results from the combined effect of the intersection of two joints. This can be shown by looking at a typical example (Figure 11.14). Supposing, there are two joint sets with dips of 45° and 35° towards the dip directions of N66°E and N35°W respectively. The inclination of the slope is 55° towards N10°E. The plunge and trend of the line of intersection of these wedge-forming joints are 28° and N4°E respectively. According to the SMR approach suggested by Romana (1985), the SMR value for the above two joints should be worked out separately and the critical value of SMR should be used for the classification. The adjustment factor (F1*F2*F3) calculated from Table 9 is -6.4 for the first joint and -6.3 for the second joint; but it is -20.4 for the plunge and the trend of the line of intersection of the joints. Thus it is better to estimate wedge failure on the basis of the plunge and trend of the line of intersection.

Table 11.10: Adjustment rating for methods of excavation (Romana 1985)

Method	F4
Natural slope	+15
Pre-splitting	+10
Smooth blasting	+8
Mechanical blasting	0
Deficient blasting	-8

Anbalagan et al. (1992) recommended a modified SMR technique in which plane and wedge failures are treated as different cases. The method of Romana (1985) is followed to estimate SMR in cases of potential plane failure, but the plunge and direction of the line of intersection are used for potential wedge failure. This technique has been accepted as an Indian Standard by the Bureau of Indian Standards (BIS).

The SMR values are used to classify the slopes into stability classes (Table 11).

The critical slope facets need to be identified and the RMR_{basic} assessed in the field. In rock masses, movement leading to slope failure will occur along the surfaces formed by one or more sets of the geological discontinuities. The likely failure mode is determined by stereographic analysis of the geological discontinuities as they present on the slope face. Depending upon the size and structural complexity of the slope, 10 to 100 readings of the geological discontinuities will need to be made. These observations are plotted in an equal area stereo-net and contoured to show the maxima of pole concentrations. The most likely mode of failure can be identified from the pattern of maxima of pole concentrations.

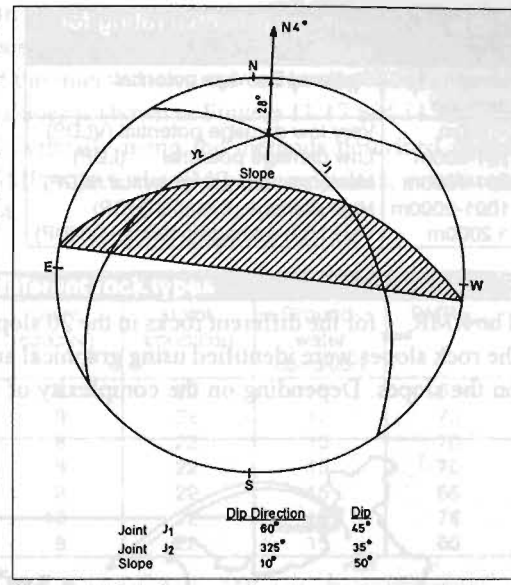

Figure 11.14: **Stereo-plot for wedge analysis**

Table 11.11: **Slope mass rating (SMR) classes and hazard probability** (modified from Romana 1985)

Class no.	I	II	III	IV	V
SMR	81-100	61-80	41-60	21-40	0 – 20
Description	Very good	Good	Normal	Bad	Very bad
Stability	Completely stable	Stable	Partially stable	Unstable	Completely unstable
Failures	None	Some blocks	Some joints, or many wedges	Planar, big wedges	Big planar, or soil like
Support	None	Occasional	Systematic	Important, corrective	Re-excavation
Hazard Probability	VLH	LH	MH	HH	VHH

Remedial measures to stabilise hazard-prone slopes can be recommended based on the SMR ratings. Very unstable slopes may require re-excavation and modification of their geometry. Unstable slopes may need extensive corrective measures including partial slope modification, rock anchors, and shotcreting in addition to drainage measures. Partially stable slopes may have to be supported with systematic supports such as rock bolts and rock anchors. The safe cut for slopes of less than 20m height can be determined from Table 9 by varying the slope angle ($ß_s$) until the SMR of the cut slope comes to more than 60 or any other determined value.

Risk assessment

Risk is the product of hazard probability (Hp) and damage potential (Dp). For a road, the hazard probability is obtained using the modified SMR approach (Table 11.11) and the damage potential is determined from Table 11.12. The risk assessment is then made from these using the risk assessment matrix (Table 11.7). An example is given below.

Table 11.12: **Damage potential rating for roads**	
Length of damage	Status of Damage potential
<100m	Very low damage potential (VLDP)
101-500m	Low damage potential (LDP)
501-1000m	Moderate damage potential (MDP)
1001-2000m	High damage potential (HDP)
>2000m	Very high damage potential (VHDP)

Case study of stability analysis for a road

The Lakshmanjhula-Shivpuri road lies in the Garhwal Himalaya (Figure 11.15). It passes through the Lesser Himalaya along slopes of varying stability. Twenty excavated hill slopes with different rock types, were selected for stability analysis using the modified SMR approach. The geology of the area is shown in Figure 11.16.

The RMR_{basic} for the different rocks in the 20 slopes are given in Table 11.13. The failure modes in the rock slopes were identified using graphical analysis of the geological discontinuities observed on the slopes. Depending on the complexity of a slope, 50-100 readings were taken of the geo-

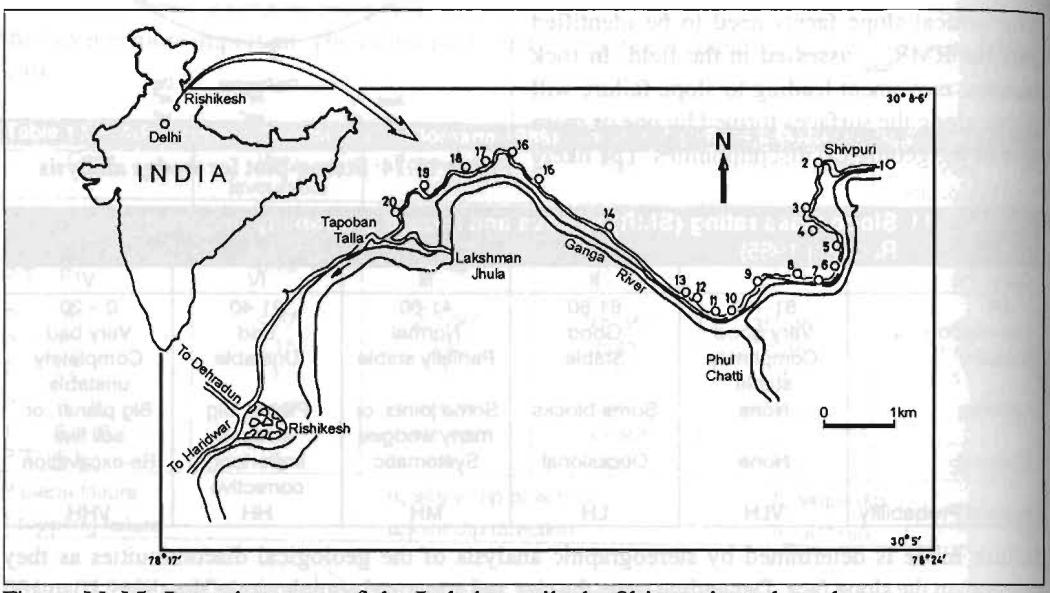

Figure 11.15: **Location map of the Lakshmanjhula-Shivpuri road study area**

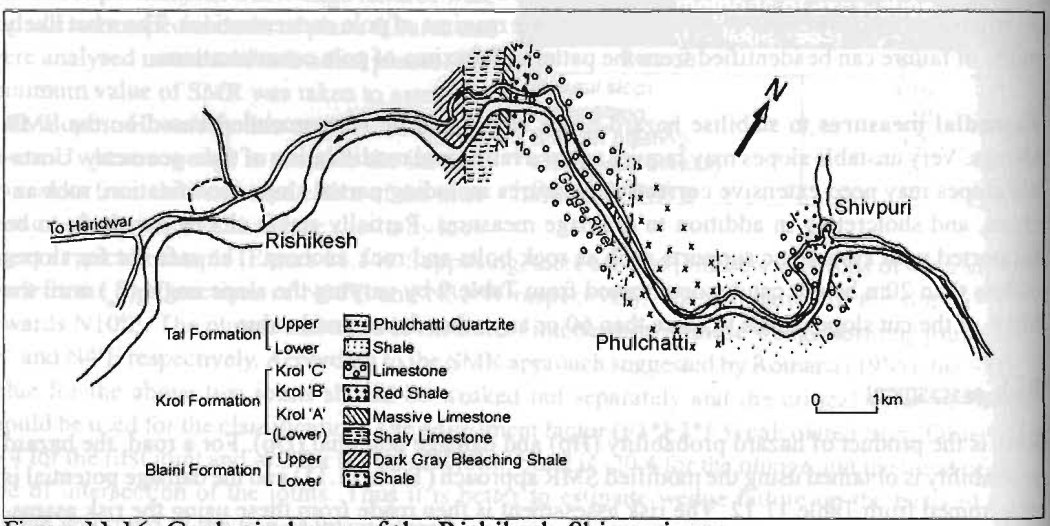

Figure 11.16: **Geological map of the Rishikesh-Shivpuri area**

logical discontinuities and the poles plotted on an equal area stereo-net which was contoured to show the maxima of pole concentrations. The most likely modes of failure were determined by studying the orientation of the various joints and the intersections and comparing them with the slope. The stereographical analysis of individual slopes is shown in Figures 11.17 and 11.18. The SMR classes were calculated for each slope individually using the methods described above (Tables 11.9, 11.10, and 11.11). The calculated SMR values, the SMR (hazard) class, and the required support measures are shown in Table 11.14.

Table 11.13: Rock mass rating (RMR) for the different rock types

Rock Type	Uniaxial compressive strength	RQD	Joint spacing	Joint condition	Ground-water condition	RMR_{basic}
Infra Krol Shale	7	13	8	22	15	65
Krol 'A' Shali Limestone	12	13	8	22	15	70
Krol 'B' Shale	12	13	8	22	15	70
Krol 'C' Limestone	12	13	8	22	15	70
Lower Tal Shale	7	13	8	22	15	65
Upper Tal Quartzite	12	17	10	22	15	76
Blaini Shale	7	13	8	22	15	65

Table 11.14: Slope Mass Rating (SMR) classes of 20 sample sites on the Lakshmanjhula-Shivpuri road

Location No	SMR value	Class No.	Slope description	Stability	Failures	Support
1	44.2	III	Normal	Partially stable	Wedge failure	Systematic
2	47.8	III	Normal	Partially stable	Wedge failure	Systematic
3	36.25	IV	Bad	Unstable	Planar failure	Important/ corrective
4	32.4	IV	Bad	Unstable	Planar failure	Important/ corrective
5	18	V	Very bad	Completely unstable	Big wedge failure	Re-excavation
6	24	IV	Bad	Unstable	Planar or big wedge failure	Important/ corrective
7	26	IV	Bad	Unstable	Wedge failure	Important/ corrective
8	40	III	Normal	Partially stable	Planar failure	Systematic
9	56.8	III	Normal	Partially stable	Planar failure	Systematic
10	30	IV	Bad	Unstable	Planar failure	Important/ corrective
11	69.6	II	Good	Stable	Block failure	Occasional
12	55.2	III	Normal	Partially stable	Planar failure	Systematic
13	51.6	III	Normal	Partially stable	Planar failure	Systematic
14	36.6	IV	Bad	Unstable	Wedge failure	Important/ corrective
15	60.9	II	Good	Stable	Block failure	Occasional
16	24	IV	Bad	Unstable	Planar failure	Important/ corrective
17	61.8	II	Good	Stable	Block failure	Occasional
18	57	III	Normal	Partially stable	Wedge failure	Systematic
19	22.65	IV	Bad	Unstable	Planar failure	Important
20	18.5	V	Very bad	Completely unstable	Big planar failure	Re-excavation

Conclusions

Infrastructure development programmes are being widely implemented across the Himalayas. If these programmes fail to take into account the inherent instabilities in the landscape, the new constructions could be severely damaged or even destroyed. Equally, sustainable development planning in hill areas must try and minimise damage to the environment and reduce the threats to people and property from natural hazards.

The first step is to prepare regional landslide hazard zonation maps. The VLH and LH zones are generally safe for development schemes. The MH zones may have some local zones of instability

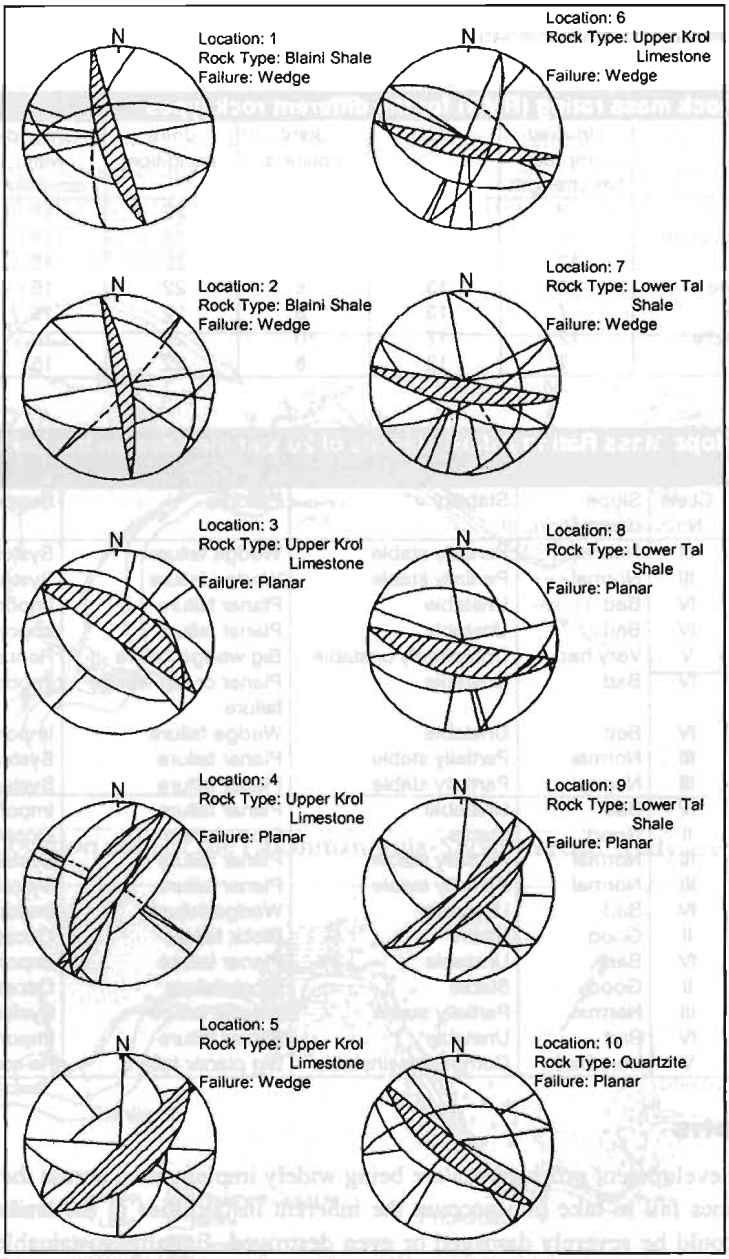

Figure 11.17: **Stereo-plots of stability analysis for locations 1-10** (Anbalagan et al. 1992) **on the Lakshmanjhula-Shivpuri road**

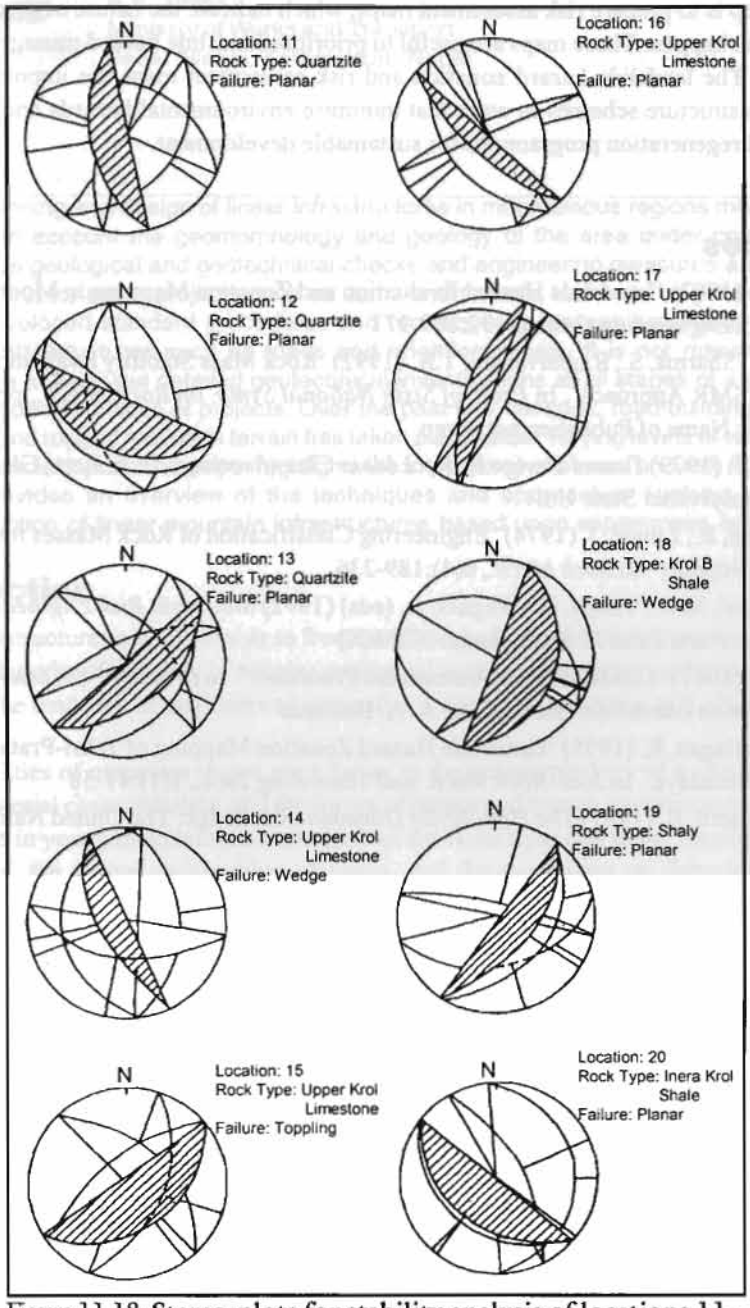

Figure 11.18: **Stereo-plots for stability analysis of locations 11-20** (Anbalagan et al. 1992)

that can be avoided. The HH and VHH zones should be avoided as far as possible. If it is not possible to avoid these areas, their initial recognition will help planners to adopt suitable preventive measures.

The second step is to prepare **risk assessment** maps, which indicate the nature of damage likely to occur if failures happen. These maps are useful to prioritise landslide hazard management (LHM) interventions. The landslide hazard zonation and risk assessment maps are important tools for designing infrastructure schemes in ways that minimise environmental hazards and for planning environmental regeneration programmes for sustainable development.

References

Anbalagan, R. (1992) 'Landslide Hazard Evaluation and Zonation Mapping in Mountainous Terrain'. In *Engineering Geology*, 32:269-277

Anbalagan, R.; Sharma, S.; Raghuvanshi, T.K. (1992) 'Rock Mass Stability Evaluation Using Modified SMR Approach'. In *Proc. of Sixth National Symp. on Rock. Mech.*, pp 258-268. Bangalore: Name of Publisher not given

Bieniawski, Z.T. (1979) *Tunnel Design by Rock Mass Classifications*, Tech. Rep., GL-79-19. USA: Pennsylvania State Univ

Barton, N.; Lien, R.; Lunde, J. (1974) 'Engineering Classification of Rock Masses for the Design of Tunnel Support'. In *Rock Mech.*, 6(4):189-236

Deoja, B.; Dhital, M.R.; Thapa, B.; Wagner, A. (eds) (1992) *Mountain Risk Engineering Handbook, Parts I and II*. Kathmandu: ICIMOD

Einstein, H.H. (1987) 'Landslide Risk Assessment Procedure'. In *Proc. of Fifth International Symposium on Landslides*. Rotterdam: A. A. Balkema

Gupta, P.; Anbalagan, R. (1995) 'Landslide Hazard Zonation Mapping of Tehri-Pratapnagar Area, Garhwal Himalaya'. In *Jour. Rock Mech. and Tunnelling Tech.*, 1(1):41-58

Ives, J.D.; Messerli, B. (1987) *The Himalayan Dilemma*. Rontledge: The United Nations University

Romana, M. (1985) 'New Adjustment Rating for Application of Bieniawski's Classification to Slopes'. In *Proceedings of Int. Symp. on Role of Rock Mechanics*, pp 49-53. Zacatecas: ISRM

Varnes, D.J. (1978) 'Slope Movement Types and Processes'. In Schuster, R.L. and Krizek, R.J. (eds) *Landslide Analysis and Control*. Special Report, Vol. 176. Washington, D.C.: National Academy of Sciences, Transportation Research Board, NRC

Varnes, D.J. (1984) *Landslide Hazard Zonation: A Review of Principles and Practice*, IAEG Monograph. Paris: UNESCO

12 Hazards and Risks to and from Linear Infrastructures in Mountainous Regions

B.B. Deoja
Ministry of Works and Transport
Babar Mahal, Kathmandu, Nepal

The planning and design of linear infrastructures in mountainous regions must carefully take into account the geomorphology and geology of the area under consideration. Rigorous geological and geotechnical checks and engineering measures are generally carried out for major projects such as dams and tunnels. However, as yet there are no fully developed standard procedures and techniques to assess hazards and risks for linear infrastructures such as roads and irrigation canals. It is not relevant or cost-effective to carry out detailed geotechnical investigations at all stages of a project and for all types and sizes of projects. Over the past four decades, road building in Nepal's young and rugged mountain terrain has taken place under varying levels of technological and financial inputs. This paper highlights the importance of hazard and risk assessments and provides an overview of the techniques and approaches evolved to plan the construction of linear mountain infrastructures based upon experiences in Nepal.

Introduction

Linear infrastructures are vulnerable to frequent damage from ground failures due to their spread along long lengths of a variety of terrain, geological profile, and surface and ground water conditions; and the tendency of engineers to generalise a design to save time and effort.

The instabilities of mountain slopes are a factor in the geomorphology of a site; they include the inherent material characteristics, and the forces of nature and human interventions. The problem is more severe in young mountainous areas such as the Himalayas due to the fragility caused by the steep slopes, the severe undercutting of rivers, and the continuous up thrusting from tectonic movements. The beauty and grandeur of the high Himalaya and the rich biodiversity of its lower mountain ranges, where a growing human population is increasingly exerting pressure, is a matter of pride and challenge not only for the people of this area but also for the whole world. Most of the mountain slopes in this region are only marginally stable and so any change or disturbance in the surface or subsurface drainage of slopes or the material structure may destabilise them; rainfall is the main trigger of erosion, gullying, undercutting, and landslides. The natural processes of vegetation and forest-controlled runoff, infiltration, and evapotranspiration maintain a cycle of instability and stability. Human interference can accelerate this process and pose threats to the topsoil, the fertile land, and the rich plant diversity. The indiscriminate development of infrastructures in fragile areas is inadvisable as the associated hazards pose a big risk not only to the investment but also to the precious ecology and environment.

From time to time the geomorphological processes of mountain slopes may change and so structures that were considered secure under the conditions prevailing at the time of construction may not be secure later. The potential threat of ground failure is the **hazard**, whilst the potential loss of life and property is the **risk**. Hazards and ground failures are normally of little concern unless they threaten life and property. Scientists and engineers need to understand the geological processes in

order to be able to estimate the extent of temporal and spatial instabilities; they must also assess the extent of damage that can be tolerated. When planning a construction, the hazards must be identified and their extent assessed as must possible alternatives, applicable technology, the amount of money available, the benefits, and the initial and recurring costs. This is called risk management. Minor hazards may be modified within the small area of influence of any structure after it has been built, but it is not possible to counteract major natural hazards. It is not the hazard but the risk that we have to try and manage.

Engineering is essentially an exercise dictated by the level of investments and the recovery of costs or the return on investment, normally over a 15 to 20-year period (the design life). Therefore most risk management has to be viewed over this time period, although potential damage to the environment from a structures should be considered over a longer time frame to ensure that irreversible impacts are avoided. Cost cutting measures should not increase the levels of erosion or the hazards. From an economic standpoint, the accuracy of costing is crucial. The accuracy of pre-feasibility and feasibility costing depends upon the accuracy of the hazard and risk assessments. Geologists need to be able to understand the needs of the engineers in order to assess the temporal and spatial hazards, and in turn the engineer must try and understand the natural processes and use this information to assess and manage the risk. This requires an ability to link the hazard with the potential damage to the proposed structure over the design life. An affordable level of risk can be allowed for in the design and can be built into the cost.

Until recently engineers and geologists only looked at the hazards and risks from their own subjective perspective. In many instances, their recommendations have been more academic than practical. Though many methods have been developed by geologists to assess and map landslide susceptibility and natural hazards, very few have linked the hazards to the risks and the overall impact on the cost and life of engineering structures. This has been particularly so for linear infrastructures such as roads and canals.

It is crucial that geologists and engineers co-operate in their work to facilitate a common understanding of geological and geomorphological processes and how they act upon structures. This will indicate how best to design a structure to enable it to resist these forces over its economic life by using the appropriate strength of material and adequate foundations.

Need to Assess Hazards and Risks

Structures built in mountainous terrain are subject to instabilities from various natural forces, both sudden and gradual, that cause ground movement. Structures built on slopes, are subject to considerable forces from lateral earth pressure and slope movements over time due to disturbances up slope or down slope from the structure. Structures in mountainous terrain have to be designed to allow for changing conditions in the forces acting on and around them – in contrast to level terrain where both the forces and the strength of underlying materials are constant.

Assessment of hazards to a structure means trying to understand and quantify, in simple terms, the effects of geomorphic processes and thus enable designers to allow for the maximum natural forces that a structure is likely to be subjected to over its lifetime. Such assessments aren't simple, but the priority is to minimise the risk to human life and the investment (the structure) from unexpected frequent failures. The mountain environment is in many ways a fragile environment and structures that are built on it without a reasonable understanding of the impacts to and from the environment are likely to be subject to serious problems.

To summarise, hazards and risks need to be assessed and used as a decision making tool. It is important to

- understand instabilities from geomorphic processes;
- quantify and communicate uncertainties; and
- assess the probable damage from existing or potential events;

in order to

- increase the accuracy of project cost estimates;
- optimise investment efficiency;
- understand total costs over a period of time;
- develop reliable designs; and
- understand impacts on and from the environment.

Definitions of Hazard and Risk

British Standard (BS) 4778 defines hazard as "a set of conditions in the operation of a product or system with the potential for initiating an accident sequence". Varnes (1984) says, "Natural hazard is the probability of occurrence within a specified period of time and within a given area of a potentially damaging phenomenon". Einstein (1988) defines hazard as the "Probability that a particular danger occurs within a given period of time." Dangers include existing or potential phenomena such as landslide, creep, rock fall, debris flow, mudflow, and slope undercutting.

BS 4778 defines risk as "The probability that a potential hazard will be realised and the probability of the harm itself. ...(risk is) the combined effect of the probability of occurrence of an undesirable event and the magnitude of the event". Varnes defines risk in terms of specific risk and total risk. Specific risk (Rs) is the expected degree of loss due to a particular natural phenomenon and may be expressed as:

$$R_s = \text{hazard} \times \text{vulnerability}$$

He defines the **vulnerability** as "the degree of loss to a given element or a set of elements at risk resulting from the occurrence of a natural phenomenon of a given magnitude". It is expressed on a scale of 0 (no damage) to 1 (total loss).

"Total risk (R_t) means the number of lives that could be lost, persons injured, damage to property, or disruption of economic activity due to a particular natural phenomenon. It is therefore the product of specific risk (R_s) and element at risk (E)". It is expressed as:

$$R_t = R_s \times E = H \times V \times E$$

where, V= vulnerability and H = hazard

Einstein (1988) expresses risk as:

hazard x potential worth of loss, and
R= P[danger] . u(x)

In other words, risk is the "probability of an event multiplied by the consequences if the event occurs". The danger can be any event that may cause damage; whilst hazard assesses the prob-

ability that this danger may occur. The probability of an event occurring can be worked out either by collecting data, or through a subjective estimation.

In many instances, the hazards and risks at any site are taken as the same, as risks are taken to be implicit and are assumed to be proportional to the hazards. The relative levels are adequate for comparisons, and it is often not necessary to quantify the physical and monetary value

Types of Hazard and Risk

Hazards can be classified in relative, empirical, absolute, or monitoring terms.

- The relativity of a hazard is expressed as high, medium, or low with reference to a pre-determined measure of hazard attributes.
- The empirical nature of a hazard is expressed in terms of the height and the slope angle.
- The absolute nature of a hazard is expressed in terms of the factor of safety and the probability of the event happening.
- Observations from monitoring hazards are expressed in terms of changes over time including, deformation and rate of movement.

Risks may be classified in terms of physical, economic, or monetary risk, as in the following examples.

- *Physical risk:* "There would be a loss of 50% of the road in a slope area B if a large deep seated rotational soil slide occurred at B."
- *Economic risk:* "There is a 90% probability that the economic rate of return in a road project through hazardous terrain is less than 15%".
- *Monetary risk* "If a landslide resulted in the failure of the bridge, repair costs would amount to about 100,000 dollars."

Stages in Hazard and Risk Assessment

National and regional level preliminary planning stage

Before attempting to assess the hazards of ground failure, the purpose of any assessment and its practical value to the end-user must be clearly understood. Small-scale maps are useful for preliminary planning at the macro-level. For example, a 1:1,000,000 hazard map is useful to indicate the risks of locating major projects at different locations. Such hazard maps can be prepared by overlaying and picking out the relevant information from separate hazard maps of tectonic/seismic hazards, rainfall hazards, and slope hazards. For regional level planning for a mountainous country such as Nepal a 1:50,000 scale map is appropriate.

Project level and pre-feasibility level planning stage

Existing hazard maps of 1:50,000 scale or larger should be used to make preliminary comparisons of alternatives and to determine the extent of further investigations of proposed sites. If such maps are not available, they need to be prepared by overlaying 1:50,000 scale seismicity, rainfall, landslide, land use, geological, and terrain maps. Alternatively, strip maps can be made for the proposed paths of linear infrastructure projects from walk over surveys. Such maps will indicate the geomorphologic, land use, and engineering geological features within the watershed areas that will influence the structure. Relative hazards can be assessed by rating the characteristics such as slope, soil type and depth, lithology, structure, relief, land use, and drainage, and calculating the total rating and predicting landslides, gullying, and erosion.

A simple approach for directly assessing hazards and risks along road alignments is by doing field surveys and marking hazards onto topographical maps. The first step is to mark the proposed alignment of the road on 1:50,000 or 1:25,000 scale topographical maps and divide into one kilometre sections. Next the following should be marked on in a field survey: rock or soil types; existing dangers such as landslides, debris flow, major gullying, major erosion, and river undercutting; and potential dangers. Probabilities may be assigned to each type of potential failure on the basis of the subjective judgement of the survey geologists and engineers. The extent of damage to the proposed structure if the danger occurred once the structure was built should also be rated based on judgement.

Project level feasibility, hazard assessment, stage

At the project feasibility stage, indicative designs need to be prepared to allow cost estimates of about ±10% accuracy to be prepared. This means assessing both hazards and risks to the proposed structure. All the maps and any aerial photographs need to be at a scale of 1:25,000 or larger. Available maps and aerial photos may suffice for rapid assessment of the extent of hazards, otherwise new engineering geological and geomorphologic maps need to be prepared from field walk-over surveys. It is crucial to understand the effect of the type and magnitude of the hazard on the type and size of the structure proposed in order to assess the risks from the hazards. The frequency and magnitude of the hazards and their relationship to the risk can be determined from subjective assessments.

Detailed design stage

The map scale has to be much larger at the detailed design stage. Feasibility stage assessments may be adequate in low hazard and no hazard areas; in high hazard areas, a 1:2,000 to 1:10,000 survey is necessary to indicate engineering geological and geotechnical details. These allow slope stability analysis and the determination of the factors of safety with or without any proposed countermeasures. Hazards can often be modified by countermeasures.

Hazard and Risk Assessment Methods

A number of methods have been developed to assess hazards for project feasibility studies. These methods are not normally justified in pre-feasibility studies because of the amount of work involved.

Slope mass rating method (Romana 1988)

(For a detailed description of this method see also Anbalagan and Singh, this volume). The Slope Mass Rating (SMR) index for measuring the stability of rock slopes was developed by Romana (1998). It is based on Bieniawski's (1979) rock mass rating index, which uses adjustment factors for dip direction, dip amount, and method of blasting. It is expressed numerically as:

$$\mathbf{SMR = RMR - (F1xF2xF3) + F4} \text{ or}$$
$$\mathbf{SMR = RMR + (F1xF2xF3) + F4,} \text{ if the factor F3 is itself expressed as negative}$$

where RMR is the rock mass rating. The RMR is indicated by values within a range of 0 to 100 (the higher ratings indicate lower hazard) and is computed by adding together rating values for the five parameters:

- strength of intact rock;
- RQD or rock quality designation (measured or estimated);

- spacing of discontinuities;
- condition of discontinuities; and
- water flow through discontinuities.

F1, F2, and F3 are adjustments for joints and F4 is an adjustment factor for the method of excavation. The likely extent of different types of failure can be predicted from the limits of SMR values (Table 12.1). A rock slope hazard map can be prepared to show the relative values assigned to the type and extent of failures.

Soil slope movement hazard rating method *(Deoja and Thapa 1989)*

The soil slope movement hazard rating developed by Deoja and Thapa (1989) is expressed numerically as:

$$H = D[(R + H_w)(S + C) + (I + L)]$$

where, H = hazard value, D, R, H_w, S, C, I, L are weightages for depth of soil, rainfall, depth of water table, soil characteristics, complexity, slope, and land use respectively. The level of hazard is low where H lies between 0 and 30, medium for an H of 31 to 50, and high for an H of more than 50. The weightages for the different factors are given in Table 12. 2.

The extent of damage depends upon the hazard level and the type of instability. Instabilities such as debris flows, deep-seated slides, GLOFs, landslide dams, major undercutting by rivers, and high seismicity are regarded as high hazards. Soil hazard maps can be prepared based upon the relative hazard values calculated by this method.

Table 12.1: Prediction of types and extent of failure from Slope Mass Rating (SMR) values

Plane failure		Wedge failure		Toppling failure		Soil-like failure	
SMR values	Failure	SMR values	Failure	SMR values	Failure	SMR values	Failure
>60	None	>75	None	>65	None	>30	None
40-55	Big	60-75	Some	50-65	Minor	10-30	Possible
15-40	Major	40-55	Many	20-35	Major		
		15-40	None				

Table 12.2: Weightages for different factors

Depth of soil (m)		Annual Rainfall (m)		Depth of water table		Soil characteristics[1]		Complexity		Slope angle (degrees)	
Range	Weightage, D	Range	Weightage, R	Range	Weightage, H_w	Range	Weightage, S	Range	Weightage, C	Range	Weightage, I
0-0.9	0	0-0.4	0.5	0-5	0.5	GW, GP, SW,SP	0.5	Strong dissection	1.5	0-14	1
1-5	1.5	0.5-2	1	6-10	2	GM, SM	1	moderate dissection	0.75	15-24	3
6-10	2	2-3.5	1.2	11-20	1.5	GL, SL	2	simple dissection	0.25	25-34	5
11-15	3	>3.5	1.5	>20	0	ML, CL, OL	2.5			35-54	7
15-20	2.5									45-54	7
>20	2									55-60	8
										60	8

[1]soils classified according to the Unified Classification System.
Basic symbols G – gravel; S – sand; C – clay, M – silt, O – organic; modifying symbols W – well-graded, P – poorly-graded, M – with silt fines, L – low liquid limit

Map overlay method *(Gupta and Anbalagan 1997)*
(For a detailed description of this method see also Anbalagan and Singh, this volume). The area to be mapped is divided into facets; then structural, land use and land cover, relative relief, lithological, slope morphometry, and hydrogeologic condition maps are prepared from existing maps and field surveys. Ratings are then assigned for each facet of these various maps based upon a predetermined rating scheme. The total estimated hazard is the sum total of these ratings for each facet. The hazard map is then prepared using five categories of hazard on a scale of 0 to 10: very low hazard (rating <3.5); low hazard (3.5-5); moderate hazard (5.1-6); high hazard (6.1-7.5); and very high hazard (>7.5).

Landslide hazard mapping method *(TRL Overseas Road Note 16 1997)*
The relative hazards of different sites can be assessed by landslide hazard mapping (LHM). Maps are prepared based upon a series of factor maps that are derived from 1:25,000 scale aerial photos, 1:50,000 scale topographical maps, and 1:200,000 scale geological maps. The factor maps are landslide distribution and underlying geology maps, slope physiographic classification maps, slope angle distribution maps, slope aspect distribution maps, land use distribution maps, and summary of landslide hazard zones map. These records are then set against the actual density of landslides and compared with those expected had there been no control of the distribution of slope failure.

Landslide risk assessment procedure *(Einstein 1988)*
The Landslide Risk Assessment Procedure as developed by Einstein is a formal procedure for hazard and risk assessment. It involves the preparation of separate state-of-nature, danger, hazard, and risk maps. The first-level state-of-nature map, is prepared by combining information from topographic, geological, vegetation, hydrological, and geotechnical maps, with test results, displacement measurements, water level observations, and visual observations. The second-level danger map, is prepared by making an inventory of existing and potential slope instabilities. The third-level hazard map maps the dangers and the probability of 'dangerous events' occurring. The fourth-level risk map shows the hazards and their potential consequences. The fifth step in this method is to calculate the hazard by working through probability calculations from the data shown on the state of nature and danger maps.

Hazard and risk assessment by pre-assigned ratings *(Deoja et al. 1991)*
The mountain risk engineering (MRE) handbook prepared by ICIMOD in 1991 (Deoja et al. 1991) suggests quantification of hazards and risks. It describes the assessment of hazard by preparing maps showing various attributes of a slope such as slope angle, soil and rock type, sub-surface and surface drainage conditions, rock discontinuities, faults, and land use, and rating these attributes on a scale of 0-1 using a rating table suggested on the basis of experienced judgement. The total rating, called the state-of-nature, is an indication of the probability of slope failure assuming that the ratings are valid for the threshold rainfall that is considered to be the main trigger of slope failure. Rainfall factors are also suggested so that this probability can be modified for other threshold rainfall values. At present these are indicative values based on judgement rather than research and detailed analysis. The MRE handbook suggests a simplified method of hazard assessment using charts and tables rather than detailed mapping for the pre-feasibility stage of a project. For the feasibility stage, detailed mapping and detailed ratings are suggested.

Risks are quantified by multiplying the hazard with the value of the potential loss expressed in monetary or physical terms. For example, assume that a deep-seated rock slide in the influence area of a road section could wash out the entire 1 km of road costing Rs 10 million per km. Let the hazard

be 0.70 for the particular influence area of the road. This means that the probability of a deep-seated rock slide occurring once during the design period (the analysis period) is 70%. The risk is therefore 0.7 km (i.e., 0.7 x 1 km) of road washout or 7 million rupees (i.e., 0.7 x 10 million rupees) worth of loss during the analysis period (taking into account the loss of the structure only).

Examples of hazard and risk assessment in road projects in Nepal

Alexis Wagner carried out hazard mapping for the feasibility studies for the Rapti integrated roads in 1986 and the rehabilitation of the Lamosangu-Jiri road in 1988-1990. The hazard maps (called risk maps by Wagner) were prepared on the basis of slope maps, geological engineering maps, and morphostructural maps by assigning tentative weights on a scale of 0 to 100 for structures (number of wedges, orientation of slope, bedding, and dip), lithology, hydrogeological condition, and tectonic condition. Risks and levels of risk of plane failure and wedge failure in rock structures were predicted on the basis of the structure and the total weight. The calculated 'risks' were in fact what are more commonly called 'hazards' because the extent of damage to and from the road in terms of loss of life or property was not calculated. The information was therefore of little value for comparison of alternatives or economic appraisals.

ITECO, Nepal carried out a feasibility study for the Baitadi-Darchula road for the Department of Roads of HMG Nepal in 1990 using a combination of Wagner's rock slope hazard rating and Deoja's soil slope hazard rating techniques to assess the hazards and the risks in terms of the expected loss of road length, and thus facilitate comparison of the alternatives.

A simplified approach to risk management for linear infrastructures in mountainous regions

Engineers prefer to assess hazards and risks quantitatively by using tables and charts rather than by preparing rigorous maps at various levels and overlaying the maps to calculate the total hazard. Risk management for linear infrastructures like roads or canals normally means the development of designs that ensure both the safety of the proposed structures and non-alteration of the natural hazards during the design life of the structure. A rather simplified approach can be taken in such a case. The approach suggested here uses a clear distinction between hazards and risks. It employs ratings or weights similar to the probabilities assigned subjectively. The approach is described briefly.

Step 1 Evaluation of the 'state-of-nature'

The area which could influence the proposed road or canal or any structure is divided into slope facets (or watershed areas) with distinct characteristics in terms of slope, land use, soil and rock types, and geological structures. Various attributes of the facet are assigned ratings as shown in Table 12.3, the description of the attributes, and their ratings recorded in a table similar to the example shown in Table 12.4. The total value of the state-of-nature (SN) is an indication of the degree of instability of the slope, that is the probability of slope failure. The ratings suggested in Table 3 may be changed if the evaluator's experience so dictates (e.g., to suit local conditions).

Step 2: Assessment of danger

This stage involves making an inventory of existing, potential, and imminent dangers such as erosion, gullying, debris and mudflows, undercutting, and landslides. The geometry and impact area of each feature is noted on the facet or watershed area. Table 12.5 shows a suggested format for collecting the data. A danger map showing all of these features should be prepared on the same

Table 12.3: Rating for the parameters used to determine the state of nature (SN)

Topography				Drainage			
Slope Deg.	Rating	Relative Relief (m)	Rating	Surface drainage type	Rating	Ground water depth (m)	Rating
Soil Slope		0-50	0	Simple	0	Dry	0
0-5	0	51-100	0.03	Active	0.04	Wet	0.04
15-25	0.05	101-150	0.06	Very		Flowing	0.09
16-25	0.1	150-200	0.09	Active	0.08		
26-35	0.14	>200	0.12				
36-45	0.12						
>45	0.1						
Rock Slope							
<45	0						
46-60	0.03						
>60	0.14						
Landuse		**Fault**		**Soil**			
Type	Rating	Distance from Road (m)	Rating	Soil Type	Rating	Soil depth (m)	Rating
Thick vegetation	0	>50	0.16	Compact alluvium	0- 0.04	<1	0
Mod Vgtn	0.03	51 – 100	0.08	Loose alluvium	0.07 - 0.12	1-3	0.04
Sparse	0.06	>100	0.04	Colluvium	0.06 - 0.08	4-6	0.06
Barren	0.09			Eluvium	0.04 - 0.06	7-10	0.10
Cultivated	0.09			Talus	0.08 - 0.12	11-15	0.12
				Till	0.06 - 0.12	16-20	0.08
				Debris	0.06 - 0.12	>20	0.05
Lithology/Structure							
Rock	Rating	Weathering Grade	Rating	Joint spacing	Rating	Orientation of discontinuity	Rating
Massive, Resistant Limestone quartzite	0	Fresh	0	Wide, >1m	0	Slope oblique to joint/beding> 30°	0
Highly cemented, conglomerate	0.01	Moderate	0.02	Medium 51-100cm	0.03	Dip slope of joint+15°	0.04
Soft rock	0.02	High	0.04	Close, 50-10 cm	0.04	Dip slope of beding+15°	0.08
*Alternative phylite quartzite	0.04	Complete	0.06	Tight. <10cm	0.06		
Weak rock crushed	0.06						

scale as the state-of-nature map. Imminent danger can be predicted by looking at site conditions but predictions are not made at this stage. This map will assist in predicting future dangers.

Where a shallow soil slide exists in a particular facet or unit in the watershed and influences the proposed structure then the probability of occurrence of a shallow slide is rated as '1'. Since the area of the potential landslide may only be a fraction of the total area of the facet, the probability that a shallow soil slide will cover the entire area of the facet is less than one. This allows for adjustments to be made for the possible non-homogeneity of the state of nature on the facet.

Step 3: Assessments of hazards

A hazard assessment is a determination of the probability of a certain danger occurring in a certain area within a certain period of time. The hazard can be assessed by comparing the value of the state-of-nature with the existing and imminent dangers and their types, sizes, and geometry. Table 12.6 shows a suggested format for such records and assessments. The conventional low cost and

Table 12.4: **Format for recording the state-of-nature (SN) and type of instabilities**

Chainage	Facet				State of Nature, SN											Total SN	Type of Probable Instability
	No	Length of Facet/ road L	Size of facet sqm LxBxH	Area of Facet sqm A	Slope Degree	Relative Relief	Drain-age	Ground Water	Land Use.	Fault	Rock/ Soil Type	Soil Depth	Weath-ering Grade	Joint Spacing	Orienta-tion of Discon-tinuity		
1	2	3	4	5	6	7	9	10	11	12	13	14	15	16	17	18	19

Note: Record the description or actual value on top and assign the rating value from the chart for the particular case on bottom

Table 12.5: **Format for an inventory of existing dangers within a facet or block**

Chainage	Facet				Existing Danger							Describe Imminent Danger and likely Impacts	Remarks
	No	Length of facet/ road L	Size of facet sqm LxBxH	Area of facet sq m A	Type	Size LXBxH	History	Area		Length along Proposed road			
								area (a) sqm	% 100xa/A	L m	% 100xl/L		
1	2	3	4	6	7	8		9	10	11	12	13	14

SSS = shallow soil slide; DSS(R/T) = Deep seated soil slide (rotational/translational); DF = Debris flow; MF = Mud flow; MRS(P/W) = Minor rock slide (planar/wedge); MjRS(p/w) = Major rock slide (planar/wedge)

least-disturbance method of road construction does not normally involve modification of the natural hazard by the road construction.

Step 4: Risk assessments

In road building, the risk is expressed in terms of the potential type and extent of damage to the road and the area of the facet. There may be triggers such as heavy rainfall and improper road cuts or landslide removals more than once during the 15 to 20 year analysis period, but for simplification only one failure is usually considered. It is up to the experience of the evaluator to estimate the values of minor and major failures. Minor soil slides or rockslides above the road cut may only cause minor damage to side drains and pavement layers. Major slides above the road cut or slides with a failure surface encompassing the entire road may cause full damage to the road section. For example, a minor failure over one metre of the road may only incur costs of 10% of the total cost of completely replacing one metre length of the road, whereas major danger may entail a 100% replacement cost. There may also be other risks such as the loss of land, damage to houses, and injury to people and animals. Obviously there will be very serious risks in highly populated areas. Table 12.7 shows the format suggested for assessing the risks.

Step 5: Risk Mitigation

Once the level of risk has been determined in terms of the monetary value of the damage to the structure, life, and property, there are several ways to proceed. Risk can be managed by

- living with the risk;
- avoiding the risk, for example by moving the alignment away from hazardous sections;
- reducing the risk by only building a minimum of standard stretches of road in hazardous sections;
- removing the hazards, for example by removing unstable material; and
- reducing the hazard or modifying the state-of-nature by providing active countermeasures, for example by building retaining walls or buttresses, adding vegetation and/or plantations, and by other soil and rock reinforcement measures.

Conclusions

In mountainous regions, assessment of the hazards and risks to new infrastructures from erosion, gullying, and landslides, and in turn the effect of new infrastructures on the environment and the infrastructure itself, is crucial during the feasibility stage and project appraisal and feasibility studies. It is necessary so that the best use can be made of resources and the environment protected from irreversible impacts. Due to the dynamic nature of mountain environments and the complex of variables involved, it is difficult to determine and quantify these uncertainties and convert them into potential economic impacts. Nevertheless, experience and judgement can be applied to make a reasonable assessment.

There is a strong tendency among engineers to avoid hazard and risk assessments because of the need to collect a considerable amount of geological data and the difficulties in the assessments of probabilities. No matter whether a probability is assessed or not, the assessments of geological, geomorphic, topographical, lithological, and land use attributes will definitely contribute to an engineer's understanding of a site and will make clear to him the innumerable uncertainties already hidden in assumptions about the material strengths and external forces that act upon a structure over a period of time. Uncertainties exist, but it is better to know their extent and try to design the

Table 12.6: **Format for prediction of instabilities**

Chainage	Facet				State of nature		Existing danger			Predicted danger without influence of road				Remarks
	No	Length road along facet, L	Size of facet sqm LxBxH	Area of facet Sqm A	SN	Imminent danger type	Type	% area covered	% Length of road affected	Danger type	Probability of occurrence	Prob. of full area under danger	Combined prob. (hazards) P 12x13	Describe dangers with or without road, to indicate the effect of road technologyproposed, if significant.
1	2	3	4	5	6	7	8	9	10	11	12[1]	13	14	15

[1]This is to be based on judgement on the basis of the values in Columne 6, 9, and 10 and other site conditions use values within zero to one. Assume one time occurrence during the design life

Table 12.7: **Format for Reading Hazards and Risks**

Chainage	Facet				Hazard			Risks					Other Risks			Total Risks	Remarks
													Land		Others		
	No	Length of Facet /road L	Size of facet sqm LxBxH	Area of Facet sqm	Type of Danger	Size	Proba-bility p	Type of Danger	Probability of full damage to road	Road length fully damaged 8x10x3	% of facet length 11x100/3	Value of road dmgd	Area 8x5	Value		13+15+16	
1	2	3	4	5	6	7	8	9	10[1]	11	12	13	14	15	16	17	

[1]This is to be estimated on a zero to one scale on the basis of judgment/degree of belief. A shallow slide may damage 10 to 20 per cent of structure whole a deep seated slide or major under cutting or debris flow may washable the complete structure.

project and its structures around them than to have false confidence through overlooking them. The frequent failure of high cost roads; the alarming environmental damage from inappropriate techniques used in road construction; the scarcity of funds for maintenance; and the insufficient impact that roads have had on Nepal's mountain economies are sufficient reason to justify the need for hazard and risk assessments in the early stages of a project cycle.

Risk management using the simplified approach discussed in this paper will also be helpful in generating data for research and analysis, and thus contribute to the development and refining of probability ratings and formal approaches to the risk management of linear infrastructures in mountainous terrain.

References

Bieniawski, Z.T. (1979) '*The Geomechanics Classification of Rock Masses and Its Application in Tunnelling*'. In *Proc., Third International Congress on Rock Mechanics*, Vol 2, Part 2, pp 27-32 Washington D.C.: National Academy of Sciences

Deoja B.B.; Thapa, B. (1989) 'Manual on Mountain Risk Engineering, Volume 2a - Application Guide'. Kathmandu: International Centre for Integrated Mountain Development (ICIMOD) (unpublished)

Deoja, B.; Dhital, M.; Thapa, B.; Wagner, A. (1991) *Mountain Risk Engineering Handbook, Part I: Subject Background, Part II: Applications*. Kathmandu: International Centre for Integrated Mountain Development (ICIMOD)

Einstein, H.H. 1988) 'Landslide Risk Assessment Procedure'. In *Proceedings of the Fifth International Symposium on Landslides*, Vol. 2, pp 1075-1050. Rotterdam: A. A. Balkema

Gupta, P.; Anbalagan R. (1997) 'Slope Stability of Tehri Dam Reservoir Area, India, Using Landslide Hazard Zonation Mapping'. In *Quarterly Journal of Engineering Geology*, 30:27-36

ITECO (1990) *Feasibility Study of Baitadi-Darchula Road Project,* Vol 1 and 2, Prepared for HMG Nepal, Department of Road. Kathmandu: ITECO

TRRL (Transport and Road Research Laboratory) (1997) *Principles of Low Cost Road Engineering in Mountainous Regions,* Road Note 16. Crowthorne (UK): TRRL

Romana, M. (1988) 'Practice of SMR Classification for Slope Appraisal'. In *Proceedings of the Fifth International Symposium on Landslides*, Vol. 2, pp 1227-1233. Rotterdam: A. A. Balkema

Varnes, D. J. (1984) 'Landslide Hazard Zonation:. A Review of Principles and Practice'. In *Natural Hazards,* An IAEG Monograph. Rome: UNESCO

Wagner, A.; Leite, E.; Olivier, R. (1988) 'Rock and Debris Slides Mapping in Nepal – A User Friendly PC System for Risk Mapping'. In Proceeding of the Fifth International Symposium on Landslides, Vol. 2, pp 1251-1258. Rotterdam: A. A. Balkema

13 Behaviour and Characteristics of Debris Flows

Wu Jishan[1] and Li Tianchi[2]
[1]Institute of Mountain Hazards and Environment
CAS, Chengdu, China
[2]International Centre for Integrated Mountain Development
Kathmandu, Nepal

A debris flow is a rapid mass movement of loose soil, rocks, and organic material along with entrained air and water forming a slurry that flows downhill. Debris flows are one of the major causes of natural disasters in mountain areas; they claim many lives and cause extensive damage to property. Debris flows usually occur unexpectedly. Their sudden breakout, rapid scouring, and filling in may cause serious damage in downstream areas. The prevention and control of debris flows is an important task to safeguard economic development and human lives in mountainous areas.

Debris flows have widely varying characteristics depending on the nature of a basin or watershed and the rainfall conditions. Understanding the fundamental mechanics of debris flows is the key to mitigating their hazards. Mitigation is achieved by designing structural control measures or setting up non-structural systems.

This paper, based on studies done in China, describes the types, characteristics, dynamics, and fundamental mechanics of debris flows, as well as the type of damage they cause to roads and other structures, settlements, and farmland. Five different ways of classifying debris flows are described based on the viscosity, composition, triggering factors, origin, and scale. The differences between debris flows and other similar phenomena such as landslides and floods are summarised.

Definitions and Classification

Debris flows are a rapid mass movement of loose soil, rocks, and organic material (earthen material) along with entrained air and water to form a slurry that flows down ravines and other slopes in mountainous areas. Essentially it is a two-phase flow: the liquid phase contains a mixture of water and fine-grained sediments, whereas the solid phase contains coarse sediments (Qian and Wang 1983, Wu 1992). A debris flow is an intermediate phenomenon between a sediment-laden water-flow (flood) and a landslide, but there are significant differences between these and debris flows.

Debris flows and sediment-laden water flows have different structural characteristics. Debris flows have the structural characteristics of mixed loose solid materials. They have an initial static shear strength τ_0, whereas sediment-laden water flows have no structure, i.e., $\tau_0 \approx 0$. Generally if the unit weight of a flow is more than 1.3 t/m^3 it is classified as a debris flow, if the value is below 1.3 t/m^3 it is classified as a flood. Another difference is that debris flows occur in mountainous areas so the bed gradient (or flow gradient) is usually more than 1%. A flow with a large amount of suspended material along a gradient of less than 1% is usually classified as a water flow with a hyper-concentration of sediment.

Debris flows and landslides have different flow characteristics. A debris flow flows with the characteristics of water. It has a velocity gradient of $d_{\mu c}/d_y$. A landslide has a sliding plane between the slide mass and the underlying ground mass but it has no velocity gradient. Debris flows can also

be distinguished from landslides according to their saturation levels. If a solid flow is saturated or over-saturated then it is classified as a debris flow, if unsaturated it is classified as a landslide.

There are many different types of debris flow. They can be classified in various ways using such factors as viscosity, composition, triggering factor, origin, scale, location, or source of solid materials.

Figure 13.1: **Low viscous debris flow in the Jangjia Ravine, Dongchuan, Yunnan**

Figure 13.2: **Viscous debris flow in Xiaojiang River valley, Dongchuan, Yunnan**

Figure 13.3: **Deposit from a slowly moving plastic debris flow that originated in the upper part of the Jangjia Ravine, Dongchuan, Yunnan (deposit located where the person is standing)**

Classification based on viscosity

Low-viscous debris flow — Water plays the main role in low-viscous debris flows, their characteristics are similar to those of floods. The ratio of solids to water C_v ranges from 0.18-0.55; the unit weight γ_c from 1.30-1.90 t/m^3; and the initial static shear τ_0 should be less than 1.0 Pa. In this kind of debris flow, the mass is free flowing and mostly turbulent. Coarse-grained sediments and blocks of rocks move as bed load, and silting occurs when the velocity suddenly decreases or the flow becomes static (Figure 13.1).

Viscous debris flow — In viscous debris flows, water and solid materials play a more or less equal role. The ratio of solids to water C_v ranges from 0.50-0.78; the unit weight γ_c from 1.80 to 2.30 t/m^3, and the initial static shear τ_0 from 1.0-20.0 Pa. The mass is free flowing and has turbulent, laminar, sliding, and creep flow characteristics. Except for a few larger boulders, solid particles are mostly found as suspended load. Earth and water are not separated when the flow stops. This is also a two-phase flow but, except for a few big stones, should be regarded as a pseudo one-phase flow (Figure 13.2).

Plastic debris flow — In plastic debris flows, the solid material plays the main role. The characteristics are similar to those of a landslide. The ratio of solids to water C_v is >0.75, the unit weight γ_c is >2.25 t/m^3, and the initial static shear τ_0 is >20.0 Pa. The flow is difficult and arrested; most are sliding flows or creep flows. All solid material is in the form of suspended load and earth and water are not separated when the flow stops. This should also be regarded as a pseudo-one-phase flow (Figure 13.3).

Classification based on composition

Water-and-rock flow — Water-and-rock flows are mainly made up of large rock fragments and fine

sediments. Less than 5%, and generally less than 2%, of the total mass is made up of cohesive grains (Figure 4, curve D). These are all low-viscous or fluid debris flows with a unit weight of 1.3-1.8 t/m^3.

Mud-and-rock flow — In mud-and-rock flows, the grain size in the debris flow mass ranges from colloids of less than 0.001 mm to boulders more than 20m in diameter. More than 5% of the total mass is made up of cohesive grains (<0.005 mm) (Figure 13.1, curves B and C). Most of these kinds of flows are viscous or plastic debris flows.

Mud flows — In mud flows, the debris flow mass is mainly made up of cohesive grains and sediment with a few rock fragments (Figure 13.4, curve A). Most mud flows are low viscous to viscous debris flows with a unit weight of 1.5 to 1.8 t/m^3.

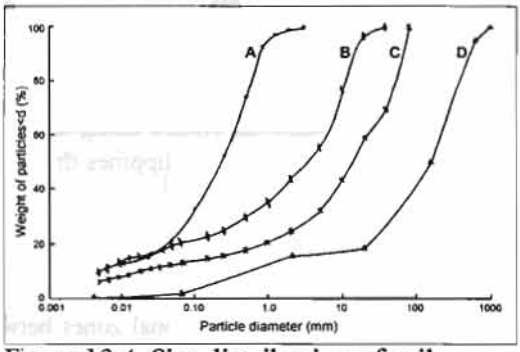

Figure 13.4: **Size distribution of soil particles in debris flows: A - mud flow; B & C - mud and rock flow; D - water and rock flow**

Classification by triggering factor

Rainstorm-induced debris flows — Eighty per cent of debris flows in the world are rainstorm induced.

Ice-and-snow-melt debris flows — Debris flows caused by melting of ice and snow are mainly found in high and very high mountain areas. Debris flows caused by melting glaciers are called glacial debris flows.

Dam-failure debris flows — This kind of debris flow is caused by the failure of natural or man-made dams and includes debris flows caused by glacial lake outbursts and by the failure of landslide and debris flow dams.

Classification based on origin

There are three main types in terms of origin.

Runoff-erosion type — Strong runoff caused by rainstorms can mobilise loose earth on slopes to form debris flows. These are called hydraulic debris flows; most are low viscous.

Gravity-sliding type — This type is mainly caused by landslides and other mass movements. Loose solid materials on a slope saturated with water slide down into ravines as debris flows (Li et al. 1984). These are called sliding debris flows and are mostly plastic or viscous.

Mixed type — Mixed debris flows can occur as a result of a combination of the processes mentioned above. Such flows are usually viscous or low viscous depending on the water content. Some begin as the runoff-erosion type (low-viscous flow) but become gravity-sliding type when large quantities of sliding material join in. Some start as gravity-sliding type (viscous) and become low viscous debris flows after being joined by a lot of low-viscous flow or rainstorm runoff.

Classification by scale

For engineering purposes, debris flows can be classified according to their scale as shown in the table on page 206.

Table 13.1: **Classification of debris flows according to scale**

	Mini-scale	Small-scale	Medium-scale	Large-scale	Very large scale
Peak discharge (Q_c)	<1 m³/s	1-10 m³/s	10-10² m³/s	10²-10³ m³/s	$>10^3$ m³/s
One time outflow (W_c)	$<10^2$ m³	10²-10⁴ m³	10⁴-10⁵ m³	10⁵-10⁶ m³	$>10^6$ m³

Geographical Distribution

More than 60 countries are affected by debris flows. They mainly occur in mountainous areas that have steep topography, active tectonic movement, and heavy rainstorms, and are particularly prone to occur in areas where there has been recent seismic or volcanic activity. Debris flows occur across the semi-humid and semi-dry temperate areas of the Alps, the Caucasus, the Tianshan Mountains, the Qiliashan-Qingling Mountains, and the Himalayas (including the Gangdisi, Kunlun, and other mountains); in the areas of high humidity and rainstorms of the Rocky Mountains, the Madri Mountains and the Andes along the Pacific coast; and in the mountains of Japan, the islands to its south, and the Philippines through to the Indonesian islands.

Two-thirds of China is mountainous and debris flow activities have been recorded in 28 of China's 33 provinces. The distribution of debris flows in China is mainly influenced by topography, geological structure, lithology, climate, and human activities. There are a number of debris flow ravines distributed along the deep-cut transitional zones between the three major topographical steps, i.e., the Qing-Tibet Plateau in the west; the Yungui, Chuanxi, and Huangtu Plateaux, and Sichuan and Chaidamu basins in the centre; and the low mountains, hills, and plains in the east. Eighty per cent of debris flow ravines are concentrated in the two transitional zones between these three steps. Within these areas, the main active and catastrophic debris flow ravines are concentrated along the large rivers that flow along the major fault lines, i.e., the Boduzangbu River fault in Tibet, the Daying River and Xiaojian faults in Yunnan, the Xiangshu River and Anning River faults in Sichuan, and the Bailong River fault in Gansu. These fault regions are also associated with strong earthquake activities.

High-frequency viscous debris flows occur most often in the soft rock outcrops along fault zones. The soft rocks most prone to debris flows are:

- mudstone, shale and coalstone, slate, and schist;
- volcanic rocks such as andesite, rhyolite, and volcanic ash;
- semi-cemented rocks such as gravel, sand, silt, and sub-clay;
- loose Quaternary deposits; and
- granite with thick weathered shells.

The most famous high-frequency viscous debris flow ravines are the Guxiang ravine in Tibet, Jiangjia ravine in Yunnan, Huoshao ravine in Gansu, and Heishahe and Majing ravines in Sichuan. All occur in areas underlain by soft rocks.

In the last half-century, the incidence of debris flows has greatly increased in regions where the environment is being seriously degraded. For example, the Xiaojing catchment area in Yunnan has lost more than half of its forest area, and the vegetation has been reduced to between 2.5 and 8% cover. As a result, the number of debris flow ravines has increased from 38 at the beginning of the 1950s to 101 at present.

Types of Damage

Because of their sudden outbursts, debris flows usually cause great economic loss and heavy casualties. In China, it is estimated that debris flows cause economic losses of 1-1.5 billion Yuan

(US $120-180 million) and kill 300-500 persons every year. The main forms of damage are described below.

Filling — Debris flows carry a large amount of coarse particles and dense silt and clay slurry. After reaching gentler gradients, the solid mass in viscous debris flows is deposited in the debris flow channel and surrounding areas. The depth of deposition can vary from as little as 10 cm to more than 10m. Structures, farmland, and water conservancy structures may be buried (Figure 13.5).

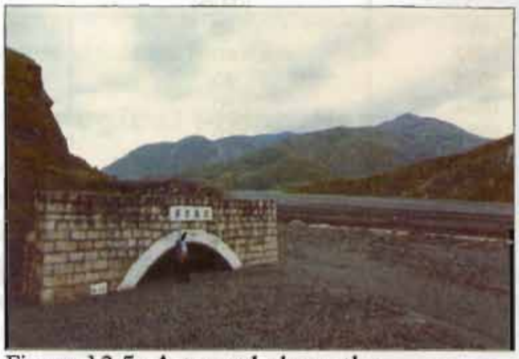

Figure 13.5: **A tunnel along the Dongchuan railway line was silted up by debris flow in**

Impact — The solid mass in debris flows, which often contains big rocks, exerts a strong dynamic pressure and impact force when moving at high speeds. The dynamic pressure can reach as high as 50 t/m^2 and the impact force up to 15,000 t/m^2. Bridge piers or other structures lying along the course of debris flows are often sheared and broken.

Erosion — Debris flows have a great potential to erode narrow ravine sections that have a slope gradient of more than 3%. A single event could deepen such a channel by 5 to 20m, breaking the foundations of bridge piers, houses, and other constructions in the ravine or on the banks (Figure 13.6). The great eroding power of the flow can burst river dykes, check dams, and sediment-trapping dams.

Figure 13.6: **Central pier of a railway bridge damaged by a debris flow, Dongchuan, Yunnan**

Up-rushing and overtopping at a bend — When the mainstream line of a debris flow reaches a bend or meets a bank at an angle, the fast flowing inertia of the flow can cause it to up-rush as high as 10m or more. A few stones may up-rush to 20m or more, filling or bursting constructions on the bank or slopes (Figure 13.7).

Figure 13.7: **Splash and up-rush of debris flow at the Debris Flow Research and Observation Station in the valley of the Jiangjia Ravine, Dongchuan**

Blocking, filling, or extruding of the mainstream line — When a large-scale debris flow enters a main watercourse, the water flow is unable to carry the debris, and the mainstream becomes filled up, extruded, or blocked. This can often cause serious damage to water navigation and diversion works. When the mainstream is dammed, the area immediately upstream will form a lake, submerging villages, farmland, and com-

Table 13.2: **Damming of the Xiaojiang River by debris flows from Jiangjia Ravine (1919-present)** (Kang et al., 1980)

Year	Period of damming (days)	Height of dam (m)	Length of impoundment (km)
1919	48	10-11	>10
1937	40	NK	>10
1949	30	NK	NK
1954	>20	10	9
1961	10	9.5	NK
1964	10	NK	NK
1968	180	10	>10

NK = not known

munication lines. When these dams fail, the large outburst discharge usually causes catastrophic damage downstream (Table 13.2).

Increase in mainstream sediment — Large quantities of debris flow mass entering a mainstream will rapidly increase the sediment budget of the stream and widen and fill up riverbeds. The capability of water to transport sediment is decreased as is the capacity for flow-relief. Surface runoff will give way to underground flow below the sediments, causing streams to dry up in the dry season. The sediment deposits lead to an increase in flood hazards during the wet season and water scarcity in the dry season.

In steep middle and high mountain valleys there may be some areas with gentler slopes. Debris flow fans sometimes form in such areas. During the dormant periods of debris flow, local people regard these areas as suitable sites for settlement. There are many towns, villages, and factories located on such sites. Two-thirds of the towns in the western mountainous areas of Sichuan Province are built on the fans of ancient debris flows. Most of the roads and railway lines pass along debris flow fans. If debris flows reactivate, these towns, villages, farmlands, and communication lines will be threatened. More than ten towns built on ancient debris flow fans in the western mountainous areas of Sichuan have been seriously damaged in this way during the last 50 years. During the rainy season, half of all cases of interruption of roads in the mountainous areas of China are caused by debris flows. Many mines, and especially open mines, located in unsuitable places also create harm to villages through mine debris flows.

Conditions for Formation

Specific geomorphic, geological, meteorological, and environmental conditions lead to the formation of debris flows; variation in these factors leads to differences in the actual processes involved. The three main conditions for the formation of debris flows are steep topography, the availability of large quantities of loose solid material, and adequate water.

Steep topography — This provides the required potential energy and can be considered as the 'starting motor' for a debris flow. The specific factors that control the initiation and nature of a flow are the slope gradient, the ravine gradient, and the relief. The larger the values, the more readily a debris flow will occur. Debris flows begin most easily when the slope angle is more than 35^0, the gradient of the ravine bed is more than 18^0, and the height difference of relief is more than 400m.

Loose solid materials — Earth and water are the two main components of a debris flow mass. In plastic and viscous debris flows, solid material is the main component. The lithology and tectonic

activities in an area essentially control the nature and amount of loose solid materials. In most debris flow ravines, landslides are the main source of loose solid material.

Abundant water — Water is an important component of a debris flow. Abundant quantities of water from heavy rainfall or ice and snowmelt are needed for their formation.

Composition, Structure and Rheological Properties

Composition of debris flows — The mass of a debris flow is made up of solid matter (sometimes called simply 'earth') and water. The solid matter includes boulders, sand, silt, and clay in varying proportions. Plastic and viscous debris flows have a similar composition of solid matter in the debris flow forming area. However, as a debris flow passes down a ravine, the proportion of large fragments often decreases and the amount of fine sediment increases, often quite rapidly so that the fluid properties change from plastic to low viscous flow.

Structure of debris flows — The structure of a debris flow mass refers to the nature of the interlocking arrangements between the earth grains; whether they are cohesive grains, sandy grains, or boulders and water. This determines the characteristics and rheological properties of the debris flow mass. There are three basic kinds of structure (Wu 1981):

- a network structure in a fine grained slurry mass formed by the fine cohesive grains and electrolytic water;
- a net-grained slurry with a network structure and sandy grains; and
- a frame structure made up of coarse slurry and large fragments.

Frame structure is the word used to describe the arrangement of large fragments (rocks, stones) in a viscous debris flow. There are four subtypes based on the proportion of large fragments: suspended, bared (propped), superimposed, and interlocked (Figure 13.8). In the suspended type, each fragment is surrounded by slurry. In the beared and superimposed types, bulky fragments restrain and support each other to some degree. There may be collisions as well as friction resistance among fragments, which can result in turbulent flow. In the interlocked type, individual large fragments are in contact while flowing. Although the collision effects between fragments may not be strong, the friction resistance is very large. When the ravine-bed has a steep gradient and/or a lubricating layer of slurry is formed on the ravine bed, incomplete sliding flow or creeping flow may occur.

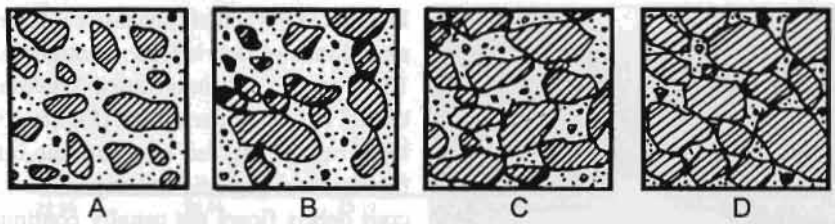

Figure 13.8: **Frame structure of a debris flow containing coarse slurry and large fragments: A - suspended type; B - bared type; C - superimposed type; D - interlocked type**

Flow patterns

The characteristic flow pattern of a debris flow lies halfway between those of a sediment-laden water flow and a landslide. The flow can be classified as turbulent (Figures 13.9, 13.10), laminar

(Figure 13.11), creeping (Figure 13.12), or sliding (Figure 13.13). Low-viscous debris flows have mainly turbulent and laminar flow patterns; plastic debris flows mainly creeping and sliding patterns; and viscous debris flows all four flow patterns. Different flow patterns have different rheological and movement equations.

Figure 13.9: **A viscous turbulent debris flow in the Jiangjia Ravine, Dongchuan Yunnan**

Figure 13.10: **Front of a viscous turbulent debris flow surge, August 13, 1991**

Figure 13.11: **A highly viscous laminar debris flow in the Jangjia Ravine, Dongchuan, Yunnan**

Figure 13.12: **A creeping debris flow in the Jiangjia Ravine, Dongchuan, Yunnan**

Figure 13.13: **A sliding debris flow with interruption between two surges**

In terms of the actual flow process there are three main kinds of debris flow: continuous (Figures 13.14 and 13.15), intermittent/continuous (Figure 13.16), and intermittent (Figure 13.17). The latter can be divided into periodic intermittent flow and non-periodic intermittent flow. Low-viscous debris flows are usually continuous (Figure 13.14). Most viscous debris flows are periodic intermittent flows, but if the supply of saturated earth materials from the upper reaches is large they can become continuous flows (Figure 13.15). A typical example was recorded in the Jangjia Ravine where at around 23.25 hours on the 14th June 1984 the flow changed from inter-

mittent to continuous (Figure 13.18). Plastic debris flows are usually non-periodic intermittent flows with one or more intermittences. The transitional types of debris flows are classified between low-viscous and viscous and are mostly intermittent.

Figure 13.14: **A continuous low viscous (fluid) debris flow**

Figure 13.15: **A continuous viscous debris flow**

Figure 13.16: **Intermittent/continuous flow with a 'head', 'body' and 'tail'**

Figure 13.17: **Intermittent flow**

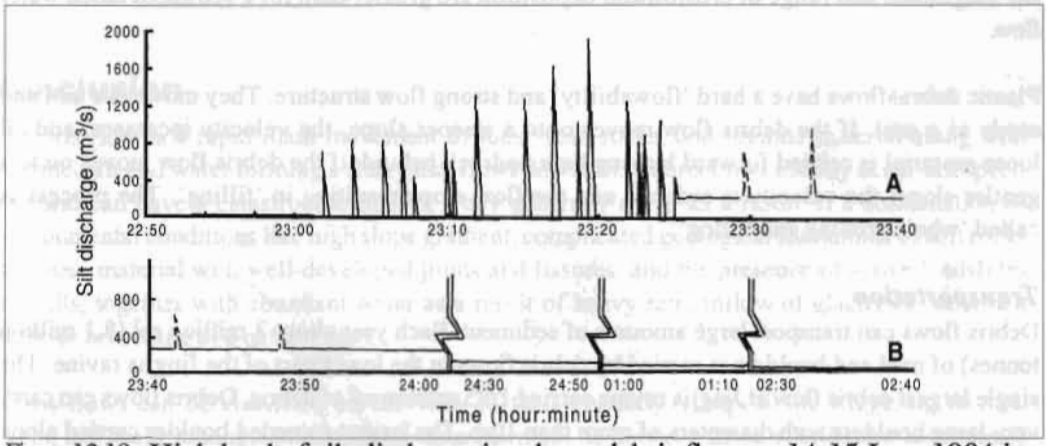

Figure 13.18: **High level of silt discharge in a large debris flow on 14-15 June 1984 in the Jangjia Ravine, Dongchuan, Yunnan**

Dynamics

Because of their high unit weight and high velocity, the magnitude and dynamics of debris flows are different from those of sediment-laden water flows. Debris flows have large impact forces that can erode, fill, up-rush, and overtop at channel bends. Debris flows also have vibrating and abrasive effects. These dynamic actions can transform landscapes within a few hours or even minutes in a way that sediment-laden water flow can only do over periods of several years. Some of the major effects are described in the following.

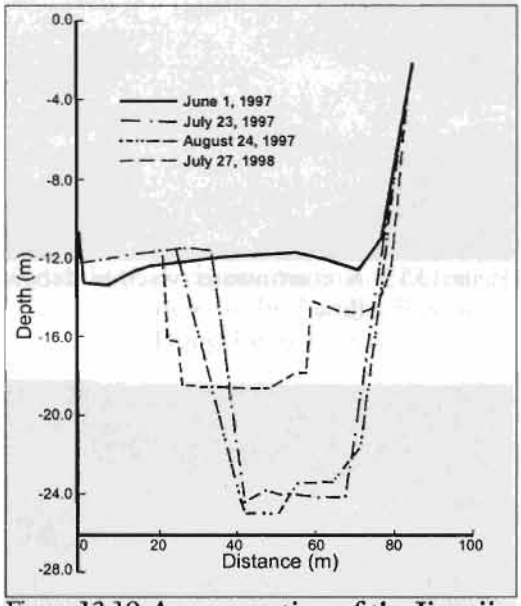

Figure 13.19: A cross section of the Jiangjia Ravine showing topographical changes caused by debris flows on four occasions between June 1997 and July 1998

Erosion

Scouring and deposition by debris flows is often extensive; for example, between June 1997 and July 1998, a debris flow in Jingjia ravine eroded the ravine by more than 20m (Figure 13.19) then filled the depositional area to a depth of more than 3m. This debris flow has deposited about 38m on the debris flow fan during the last 40 years. Debris flows, especially viscous and plastic ones, have two special forms of erosion and depositional features: one-single-grain up and down, and eroding and filling.

The one-single-grain up and down type of erosion process is similar to that produced by a sediment-laden water flow. With the change of velocity, grains move up and down in the flow eroding anything they come into contact with. In contrast to a flood, the medium of flow is fine-grained slurry not water. A debris flow has a higher unit weight, higher rigidity coefficient, and higher yield strength than a sediment-laden water flow, and the sediment transport ability is also higher. Thus the magnitude and range of erosion and deposition are greater than for a sediment laden water flow.

Plastic debris flows have a hard 'flowability' and strong flow structure. They move as a unit and erode as a unit. If the debris flow moves onto a steeper slope, the velocity increases, and all loose material is carried forward leaving bare bedrock behind; if the debris flow moves on to a gentler slope, the velocity is reduced and the flow stops resulting in 'filling'. The process is called 'whole eroding and filling'.

Transportation

Debris flows can transport large amounts of sediment. Each year about 3 million m^3 (8.1 million tonnes) of mud and boulders is carried by debris flows in the lower part of the Jingjia ravine. The single largest debris flow at Jingjia ravine carried 1.95 million m^3 of debris. Debris flows can carry very large boulders with diameters of more than 10m. The largest recorded boulder carried along the Jingjia ravine was 22m in diameter.

As with the flow process itself, there are three types of sediment transport: continuous; intermittent/continuous; and intermittent. There are also two main types of transport flow: two-phase and pseudo-one-phase.

In two-phase flow transport, the medium of transport is a uniform slurry composed of material with grain sizes of less than 0.2 mm diameter and electrolytic water. Particles larger than 0.02 mm, and pebbles and boulders are transported as suspended load or bed load. All low-viscous debris flows have two-phase flow transport.

In pseudo-one-phase flow transport, all solid material regardless of size is mixed with and moves with the same velocity as water. All plastic debris flows are pseudo-one-phase flows because all the particles are suspended.

Deposition

Debris flows have three main modes of deposition: gradational deposition; integral bulk deposition; and bedded deposition

In gradational deposition, the particles in the flow settle out gradually from large size to small size as the velocity of the flow decreases. This is the main depositional pattern of low-viscous debris flows. In a low-viscous debris flow, all of the sediments larger than 10 cm will settle out when the bed gradient is less than 1%; the debris flow changes into a hyper-concentrated sediment flow.

Integral bulk deposition occurs when a debris flow moves down a slope and then comes to rest as a result of a decreasing gradient in the gully bed or increasing resistance. The composition of the deposited material is the same as that of the debris flow body. This is the typical deposition pattern for a plastic debris flow. Generally, integral bulk deposition occurs when the initial static shear strength of the debris flow body (τ_o) is larger than the drag force (τ_c) or when the gradient of the gully bed is less than 3%.

Bedded deposition is a transitional mode between gradational and integral bulk deposition. It is similar to gradational except that a few isolated big boulders are also deposited. When the drag force of the flow (τ_c) is smaller than the resistance of the bed surface (τ_f), the debris flow settles down layer by layer on the valley bed. This is the major depositional pattern of viscous debris flows.

Conclusion

A debris flow is a rapid mass movement of loose soil, rocks, and organic material along with entrained air and water forming a slurry that flows downhill. Debris flows usually occur unexpectedly and can have a catastrophic impact. They generally occur as a result of a combination of environmental conditions like high slope gradient, complicated geological formations of soft rocks and loose material with well-developed joints and fissures, and the presence of active landslides and falls, together with abundant water as a result of heavy rain, inflow of glacier or snowmelt water, or breaching of a natural dam.

Debris flows can be classified on the basis of their viscosity, composition, triggering factors, origin, and scale, amongst others. Their characteristics lie between those of sediment-laden flows (or floods) and landslides. The movement patterns include both intermittent and continuous flow and their action can be classified as turbulent, laminar, creeping, or sliding. Because of their high

unit weight and velocity, the magnitude and dynamics of debris flows are different from those of common sediment-laden water flows. Debris flows have large impact forces and vibrating and abrasive effects. These dynamic actions can transform landscapes within a few hours or even minutes in a way that sediment-laden water flows can only do over periods of several years. All larger debris flow catastrophes are due to the dynamic effects of such phenomena. Understanding the behaviour and characteristics of debris flows will help in the proper design of control measures to mitigate the hazards posed by debris flows to roads, settlements, farmland, and other structures.

References

Kang, Zicheng; Zhang, Shucheng; Chen, Jinwn (1980) 'A General Description of Debris Flows in the Jiangjia Ravine. Dongchuan, Yunnan'. Chengdu: Chengdu Institute of Geography (unpublished)

Li, Tianchi; Zhang, Shucheng; Kang, Zicheng, (1984) 'Sliding debris flow'. In *Memoirs of Lanzhou Institute of Glaciology and Cryopedology,* Vol. 4, pp 171-177. Beijing: Science Press

Qian, Ning; Wang, Zhaohui, (1983) *Sediment Dynamics.* Beijing: Science Press

Wu, Jishan, (1981) *Structure of Debris Flow,* Collected Papers on Debris Flow (No. 1). Chongqing: Chongqing Branch of Literature Press of Science and Technology

Wu, Jishan, (1992) 'Characteristics of Erosion and Deposition from Debris Flow'. In *Erosion, Debris Flow and Environment in Mountain Regions,* pp 355-359. Oxfordshire: IAHS Press

Wu, Jishan; Tian, Lianquan, (1993) *Debris Flows and Their Integrated Control.* Beijing: Science Press

14 Debris Flow Studies in Japan

S. Miyajima
River Planning Division
Hokkaido Development Bureau
N8-W2 Kita-ku Sappora City 060 0808
Japan

Debris flows are a mixture of loose soil, rocks, organic material, and water that moves rapidly downhill destroying everything in its path. Debris flow disasters are common and cause severe damage to life and property in most parts of Japan where they are often called 'mountain tsunami' (or tidal waves). In order to try and mitigate the damage caused by debris flows it is necessary to have a good understanding of their mechanisms. The study of these mechanisms was greatly facilitated when video cameras became available to record the movement. During the last 30 years a great deal of research on debris flows has been carried out in Japan and their characteristics are considerably better known than before. However, investigation is still difficult as the flows generally occur during or just after periods of heavy and concentrated rainfall.

Introduction

The term 'debris flow' is used to describe flows that contain much larger amounts of sediment, principally clay, sand, gravel, and boulders, than an ordinary water flow, and more water than a landslide. They are flows of mixed sediment and water in which the volume of sediment is greater than that of water. A debris flow does not flow as a result of the traction force of running water but because of the effect of gravity on the sediment load. The sediment does not move as individual grains, there is collective transportation in which fine sediments like clay and sand, and larger fragments like pebbles and boulders flow together as a single mass. The evidence for this is the fact that when such flows stop, sediments accumulate with large boulders in front. Very large boulders that could not be transported by water alone are sometimes transported by a debris flow. In 1934 a debris flow in Japan was able to move a 3,000 tonne boulder. Figure 14.1 shows a diagram of debris flow moving through a channel with large boulders at the head.

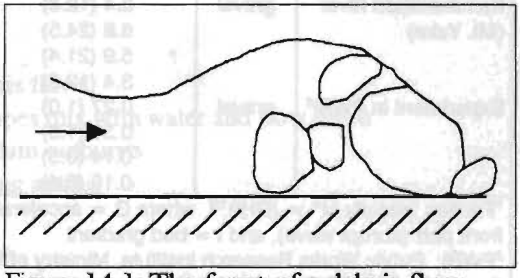

Figure 14.1: **The front of a debris flow showing the large boulders at its head**

One of the characteristic features of a debris flow is the great power with which they flow. This is the reason why they often cause fatalities and serious damage to infrastructure, houses, and other property. As debris flows have a high density and excessive power, they normally flow straight downwards – even at the bends of river courses where they will sometimes run up onto the opposite slope. However, although the damage they cause can be quite intense and serious, the actual area affected is limited compared to the area affected by a flood.

The characteristic features that differentiate a debris flow from a landslide or a collapse are

- the distance the flow travels — typically much further than a landslide (100 to 1,000m or more);
- the velocity — the flow is faster than a landslide (usually several metres to tens of metres per second); and
- that the sediment and water flow down together as a cohesive body, sometimes containing large boulders.

Velocity and Unit Weight of Debris Flows

The velocities of some actual and experimental debris flows in Japan are given in Table 14.1 and the unit weights of different types of debris flow materials in Table 14.2. The velocity and velocity coefficients and unit weight of mud flows are generally higher than those of gravel-type flows.

Sediment volume

Takei (1980) investigated the relationship between the size of a catchment area and the volume of deposited sediment (Figure 14.2). This type of data has been found very useful in planning to help mitigate debris flow disasters in Japan.

Table 14.1: **The velocity of some debris flows in Japan**

Place	Type	Velocity at front U_f m/sec (km/hr)	Coefficient of velocity U_f/U^*[1]	Remarks
Nojiri River (Sakura Island)	mud	11.5 (41.4)	11.9	8 April 1975
		13.6 (49.0)	11.1	17 April 1975
		10.0 (36.0)	8.8	4 April 1975
		9.8 (35.3)	7.4	29 April 1975
Experiment in PWRI[2]	mud	10.1 (36.4)	13.1	Sediment concentration 10%
		18.5 (66.6)	19.7	Sediment concentration 10%
		14.8 (53.3)	16.7	Sediment concentration 20%
		14.7 (52.1)	19.2	Sediment concentration 20%
Kamikamihori River (Mt. Yake)	gravel	3.4 (12.3)	1.5	
		6.8 (24.5)	3.3	
		5.9 (21.4)	2.1	
		3.4 (12.2)	1.5	
Experiment in PWRI[2]	gravel	0.27 (1.0)	0.7	
		0.37 (1.3)	1.3	
		0.14 (0.5)	0.4	
		0.10 (0.4)	0.4	

[1]Friction velocity $U^* = (GHI)^{1/2}$ where G = acceleration of gravity, H = water depth/height of debris flow at front part (abrupt wave), and I = bed gradient
[2]PWRI: Public Works Research Institute, Ministry of Construction, Japan
Source: Ikeya (1980)

Table 14.2: **Unit weight of debris flow materials**

Place	Type	Unit weight (kg/m³)
Mt. Yake, Japan	Gravel	1300
Ura River, Japan	Gravel	1610
Sakura Island, Japan	Mud	1800-1900
Wrightwood, CA, USA	Mud	1720-2230
Wrightwood, CA, USA	Mud	2400
Ten Mile Range, Colorado, USA	Mud	2530

Note: The recorded values depend to some extent on the size of the sediment sampler
Source: Ikeya (1980)

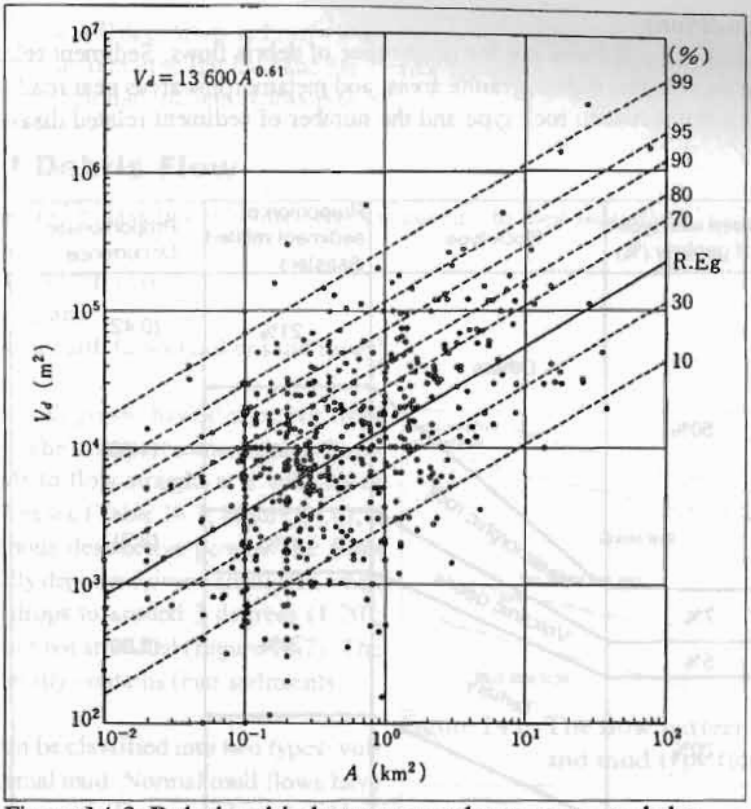

Figure 14.3: Relationship between catchment area and the sediment volume of debris flows

Causes

Ikeya (1974) described three main reasons for debris flows.

- Sediments produced by breaking up of hill slopes mix with water and flow down
- Collapsed sediments dam up a river and the dam outbursts
- A riverbed deposit experiences strong scouring action

Takei (1980) provided a more detailed list of causes.

- High rainfall intensity in a short period of time after a period of continuous rainfall
- High rainfall intensity in a short period of time in an area with new volcanic sediments
- Unstable sediments on steep torrent beds (>20°) become saturated; liquefaction occurs as a result of the impact of surface runoff
- Collapsed materials flow down carrying water and sediment from the torrent bed
- Collapsed sediments block a torrent stream and this natural dam then breaks; the collapsed sediments and water form a debris flow
- Landslide materials turn into a debris flow as a result of liquefaction
- Earthquakes or vibrations from volcanic eruptions cause parts of slopes to break off and the flowing torrent bed sediment liquefies
- Other causes like pyroclastic flow (volcanic eruption), and rapid melting of snow

Geological conditions

Geology is a major factor influencing the occurrence of debris flows. Sediment related disasters frequently occur on volcanic debris, granite areas, and metamorphic areas near roads. Figure 14.4 shows the relationship between rock type and the number of sediment related disasters.

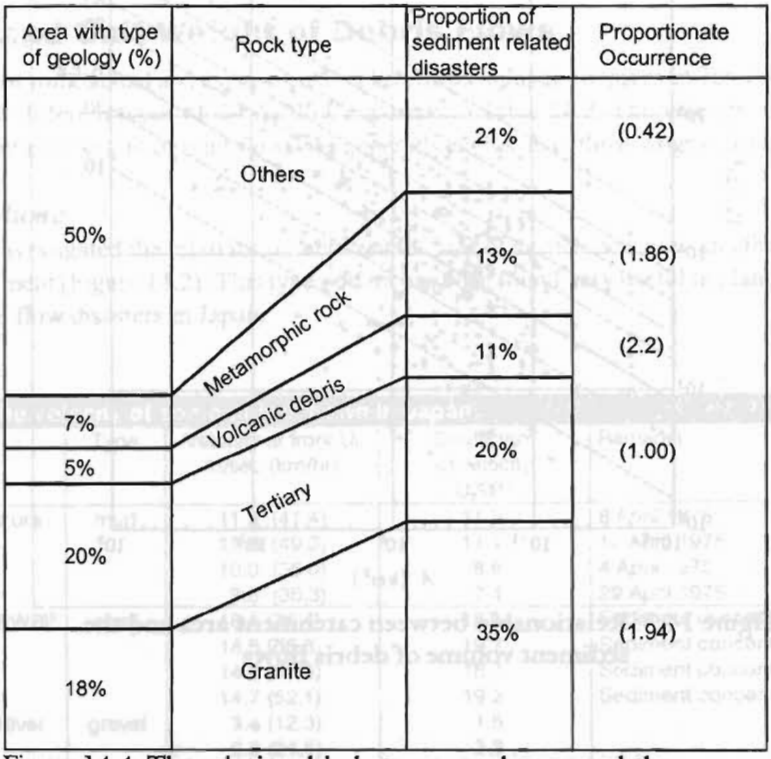

Figure 14.4: **The relationship between rock type and the number of sediment related disasters in Japan**

Generally the following conditions cause a debris flow to come to rest.

- Change in the riverbed slope or width. According to a study by the Public Works Research Institute, Ministry of Construction, Japan, debris flows will come to a virtual halt when the riverbed gradient decreases to less than 10° or is less than half of the preceding gradient, or when the width of the river suddenly increases to 2-3 times the preceding width (Figure 14.5).

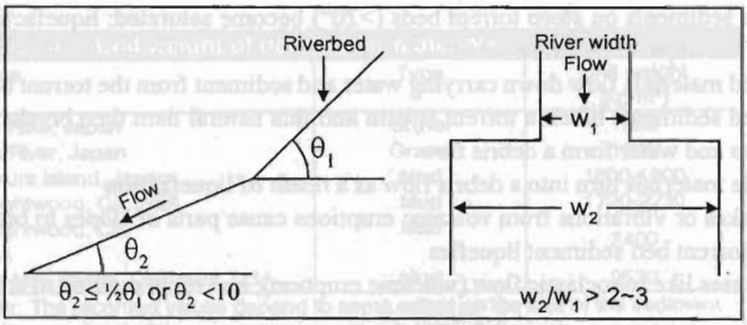

Figure 14.5: **Stop conditions for debris flows** (Ikeya 1980)

- A debris flow will deposit its sediment at the mouth of a valley where a river flows down from a mountainous area onto flat land and the riverbed gradient is around 10° or less. Most debris flows stop when the gradient is less than 4°.

Types of Debris Flow

Debris flows can be classified into three types according to their flow characteristics and type of damage:

- debris flows with gravel;
- mud flows; and
- sediment or earth flows (soil or sand flows).

Debris flows with gravel have distinctive front and rear parts. The front part contains many boulders and tends to flow straight at a velocity of around 3 to 7 m/sec (Table 14.1, Figure 14.6); it has an enormous destructive power. The front part is generally deposited over a small area when the gradient drops to around 3 degrees (1:20); the deposits are not stratified (Figure 14.7). The rear part generally contains finer sediments.

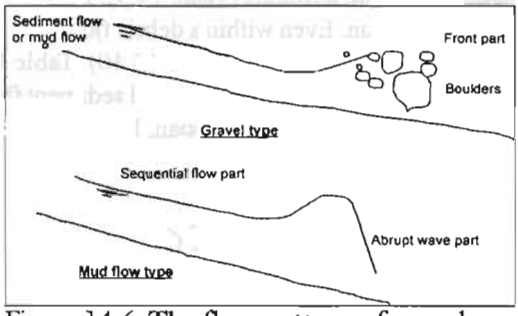

Figure 14.6: **The flow pattern of gravel and mud type flows**

Mud flows can be classified into two types: volcanic and normal mud. Normal mud flows have an abrupt wave — and may not have boulders — at the front (Figure 14.6). The velocity coefficient is several times higher than that of gravel-type debris flows (Table 14.1). The structure of the accumulated material ranges from random to layered depending upon the sediment concentration, discharge, bed materials, and bed gradient (Figures 14.7 and 14.8). The front part has a large striking energy whereas the rear flow has a big abrasive power. In general, mud flows can flow down gentler slopes than gravel-type debris flows, and even on nearly level slopes. Volcanic mud flows occur in active volcanic areas and contain fresh volcanic ash. The infiltration rate tends to be lower in places covered with fresh volcanic ash so that surface run-off is higher. The surface runoff together with the huge amounts of loose fresh ash on a steep slope mean that even rainfall of less than 10 mm in an hour can be sufficient to trigger a flow. Volcanic mud flows are frequent and because of their special characteristics should be considered as a separate category for the sake of disaster mitigation or warning.

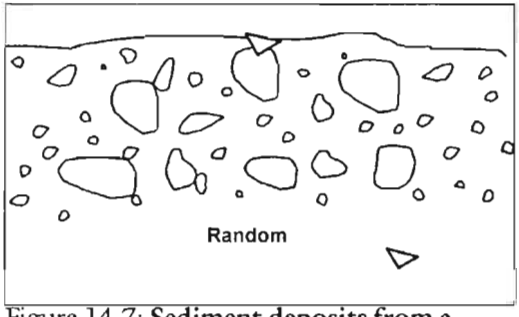

Figure 14.7: **Sediment deposits from a debris flow with gravel showing a random structure**

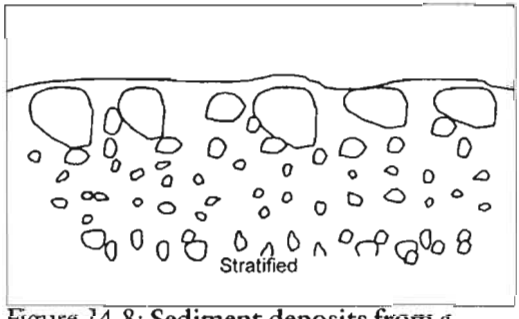

Figure 14.8: **Sediment deposits from a mud flow showing a stratified structure**

Sediment or earth flows (also known as soil or sand flows) are an intermediate type of flow between a mud flow and a debris flow with gravel. They do not flow in the form of mass transport; the individual grains of sand and gravel travel independently. Because of the independent flow, the velocity ranges can be calculated using Manning's formula. Flow surges indicate high velocity and high sediment concentrations (Figure 14.6). The deposits formed by this type of flow are usually stratified.

Figure 14.9 shows an example of comparative particle size accumulation curves for a gravel-type debris flow and a mud flow. There is a big difference in the distribution of grain sizes between the two types of flow.

In general, a debris flow can be differentiated from a sediment flow by the presence of boulders deposited at the terminus (Table 14.3). Further, the deposits have a random structure and there is no stratification. Even within a debris flow, there are different zones, however, with different sedimentation characteristics (Figure 14.10). Table 14.4 shows the accumulation characteristics of the transport zone, debris flow zone, and sediment flow zone in a debris flow that took place in September 1976 at Shoudo Island, Japan. Debris flow deposits are distinguished from colluvium on the basis of the transport distance: if the transport distance is at least five times longer than the length of the deposit the deposit is classified as debris flow, if less then as colluvium.

Debris Flow Surveys

In order to forecast, and try and prevent, debris flow disasters it is important to understand the transport mechanisms and contributing factors. Collection, compilation, and assembly into databases

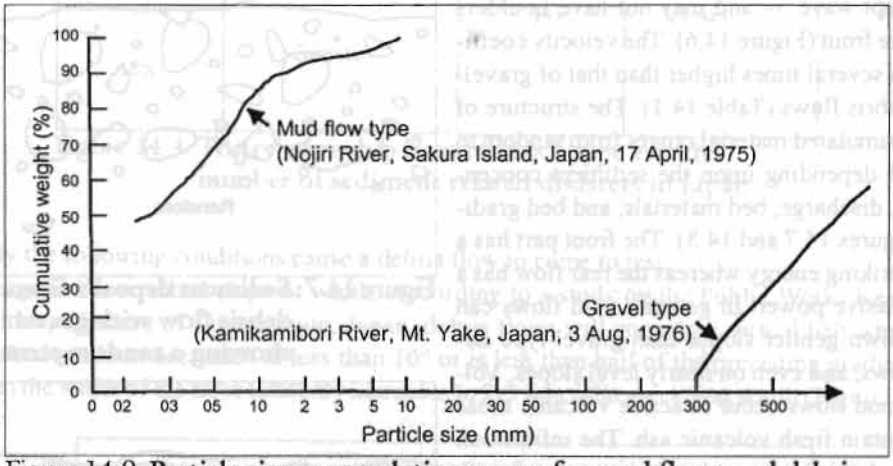

Figure 14.9: **Particle size accumulation curves for mud flows and debris flows with gravel**

Table 14.3: **Accumulation characteristics of debris flows and sediment flows**

Type	Characteristics of accumulation
Debris flow	• big boulders at the front • convex cross section (see Figure 14.9) • lays down a thick deposit
Sediment flow	• stratified accumulation common • maximum particle size 1.0 to 1.5m, fine-grained soil dominant • accumulation range wide
Flood flow	• distribution of grain size quite uniform; accumulation slope gentle • deposit thin and wide

Table 14.4: **Accumulation characteristics of transport zone, debris flow zone, and sediment flow zone, Shoudo Island, Japan, September 1976**

Description	Transport zone	Debris flow zone	Sediment flow zone	Flood flow zone
Grain size (diameter φ)	bedrock dominant, some gravel	most 1.5m max: 3-4m av: 2m	max: 1m av: 5 cm	max: 10-20 cm av: 0.5 cm
Thickness of accumulation		max: 4m av: 2m	max: 1.5m av: 0.5m	max: 1m av: 0.3m
Surface of accumulation		rough	rough/smooth depending upon landscape and material	smooth
Structure		random	almost stratified	clearly stratified

Source: Ikeya (1980)

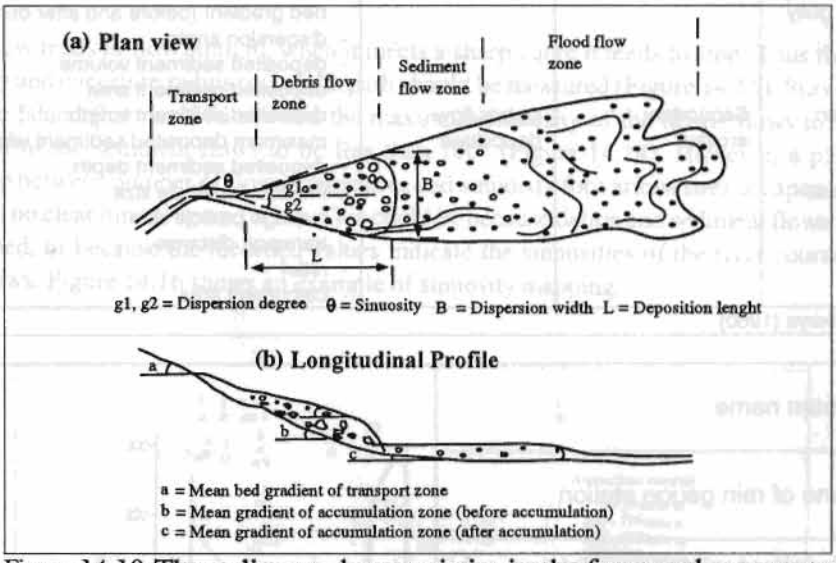

Figure 14.10: **The sediment characteristics in the front and rear parts of a typical debris flow (a) plan view (b) longitudinal profile**

of data related to observed debris flows is an important step towards disaster prevention activities. Engineering structures to prevent (further) debris flows, or mitigate their effects, in an area of risk can be planned using this information. Table 14.5 lists the observations that need to be made after a debris flow has occurred.

Debris flows often occur repeatedly along the same channels. Information about such periodic occurrences should be collected from interviews with local people and by consulting records.

The great majority of debris flows are triggered by rainfall. Rainfall patterns vary depending upon the weather pattern; for example a summer thunderstorm, a typhoon, or monsoon conditions. It is important that as much rainfall data as possible is collected in areas prone to debris flows. These can then be analysed after a debris flow occurs to discover the rainfall conditions that triggered the flow. The data needed are antecedent rainfall (total rainfall during the two weeks preceding the rainfall event that triggered the flow), and total continuous rainfall and maximum rainfall per hour and per ten minutes at the time of debris flow occurrence. The antecedent rainfall affects the moisture in the soil mass and thus determines the likelihood of saturation and liquefaction occur-

ring during a rainfall event. Figure 14.11 shows a typical format for collecting (and plotting) rainfall data related to a debris flow.

Table 14.5: Survey data sheet for debris flows

Place	Phenomenon	Sediment	Necessary data
Hill slope (head of gully)	Landslide or collapse	Collapsed sediment	- slope condition, including geology, gradient, vegetation, soil depth, and so on (preferably before and after collapse) - collapsed sediment volume
Stream bed	Sliding or heavy erosion Flowage (transport)	Bed materials	- bed gradient - deposited sediment volume - bed material - tortuosity - bed width - bed gradient
Mouth of valley or gully	Sedimentation		- bed width (before and after debris flow) - bed gradient (before and after debris flow) - dispersion angle - deposited sediment volume - deposited sediment area
Alluvial fan	Secondary erosion	Debris flow deposition	- deposited sediment length - maximum deposited sediment width - deposited sediment depth
Whole area			- maximum particle size - average particle size - transport distance - relief - catchment area

Source: Ikeya (1980)

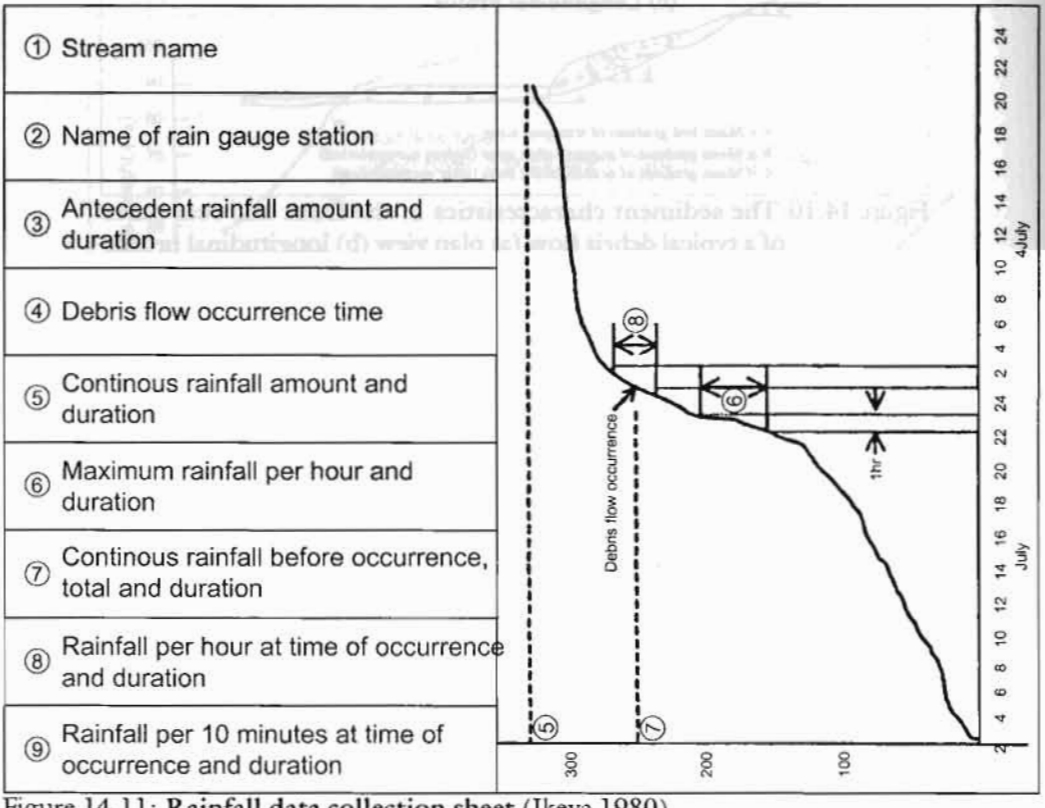

Figure 14.11: **Rainfall data collection sheet** (Ikeya 1980)

The cumulative rainfall is plotted against time (Figure 14.12). This plot can be used to derive the values for continuous rainfall prior to occurrence (CR), initial rainfall (FR), effective rainfall (ER), time of effective rainfall (t), and intensity of effective rainfall (I). The boundary marking the change from initial to effective rainfall is called the inflectional point. Recognising this point can be very useful for forecasting. The relationship between intensity of effective rainfall and effective rainfall, and severity of associated disasters, at various places in Japan is shown in Figure 14.13. The majority of debris flows occur at the time of maximum rainfall intensity.

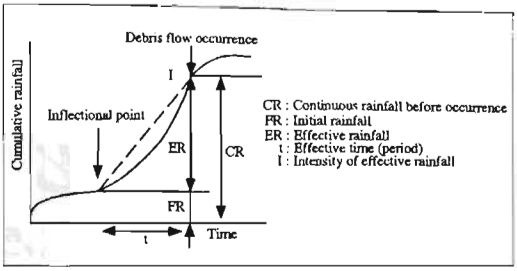

Figure 14.12: **The relationship between time and cumulative rainfall, and debris flow occurrence** (Ikeya 1980)

A debris flow tends to flow straight, when it meets a sharp curve it tends to stop. Thus the degree of sinuosity and curvature radius (m) of the path should be measured (Figure 14.15). Surveys from the Shoudo Island flow in 1976 showed the maximum sinuosity of the debris flows to be about 40°and that of the sediment flows to be less than 100° (Figure 14.14). However, a plot of the relationship between number of flow occurrences and sinuosity for various sites in Japan indicates that there is no clear limit (Figure 14.15). This could be because debris and sediment flows were not differentiated, or because the recorded values indicate the sinuosities of the river courses rather than the flows. Figure 14.16 shows an example of sinuosity mapping.

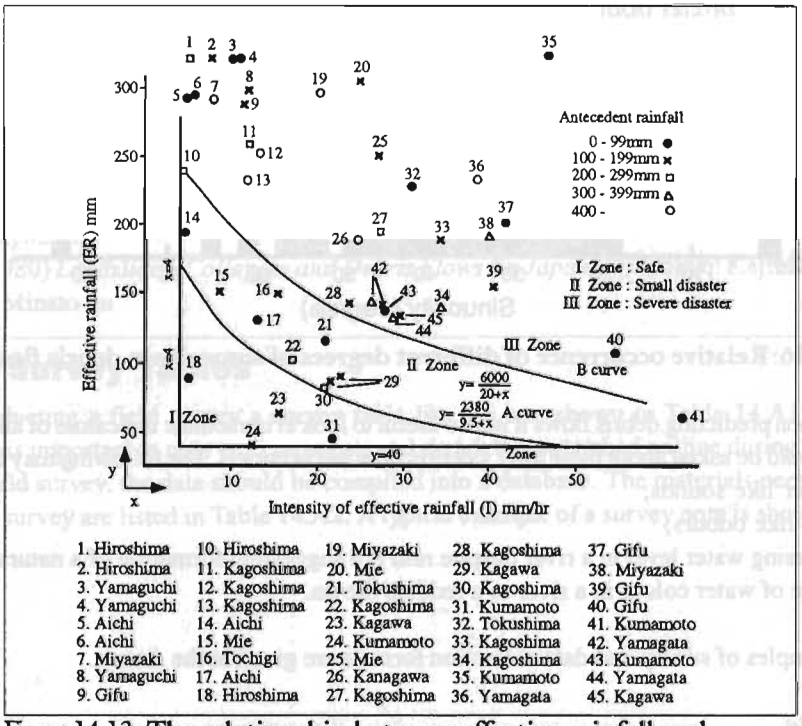

Figure 14.13: **The relationship between effective rainfall and intensity of effective rainfall, and severity of disaster – data from 45 sample sites** (Ikeya 1980)

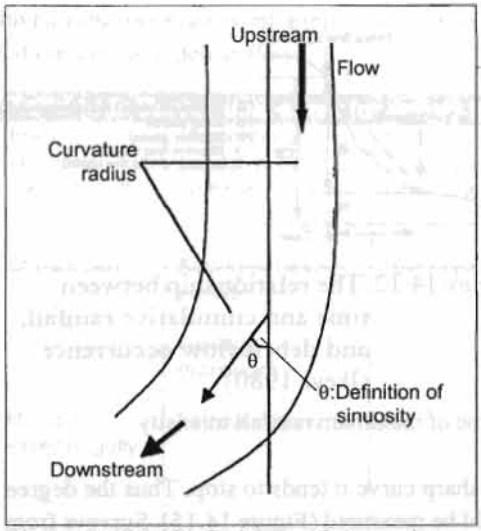

Figure 14.14: **Definition of sinuosity**

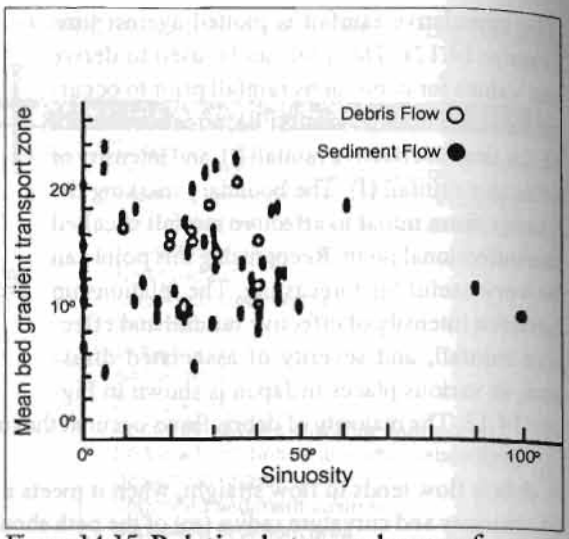

Figure 14.15: **Relation between degree of sinuosity and mean bed gradient in the 1976 Shoudo Island flow disaster**

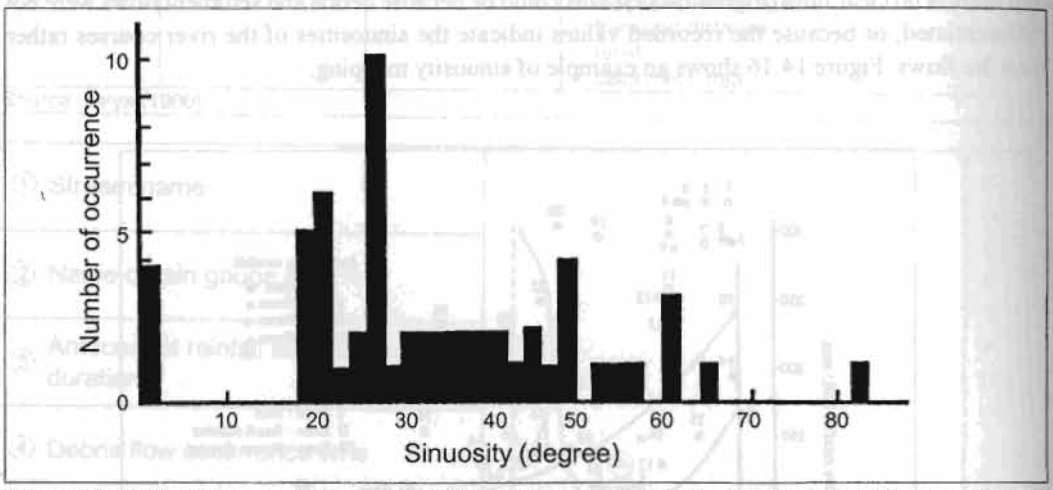

Figure 14.16: **Relative occurrence of different degrees of sinuosity in debris flows in Japan**

Finally, when predicting debris flows it is also useful to look at immediate indicators of an occurrence. People should be asked about these after a debris flow has occurred. The following may be observed:

- thunder like sounds;
- decay-like odours;
- decreasing water level in a river despite rain fall suggesting formation of a natural dam; and
- change of water colour in a river to a reddish brown.

Some examples of survey and data collection formats are given in the Annex.

Final note

Debris flow surveys are best carried out immediately after an event has occurred when the results are still clearly visible. At this time local people are likely to remember the details of the disaster

clearly. However, they will also be feeling disturbed and under stress due to the loss of relatives, friends, and property. Investigators must take care to take into account the sensitivities and feelings of those affected when carrying out such surveys.

Conclusion

Debris flows cause serious disasters in many mountain areas in the world, but they are still not fully understood and predicting is difficult. Detailed studies are still required in different places and under different conditions. Data collection is an important first step. This paper describes some characteristics of debris flows and outlines the type of data that need to be collected.

Acknowledgement

This paper is based heavily on the published work of Hiroshi Ikeya of the Public Work Research Institute, Ministry of Construction, Japan. I am thankful to him and the Public Works Research Institute for allowing me to make use of their materials in this paper.

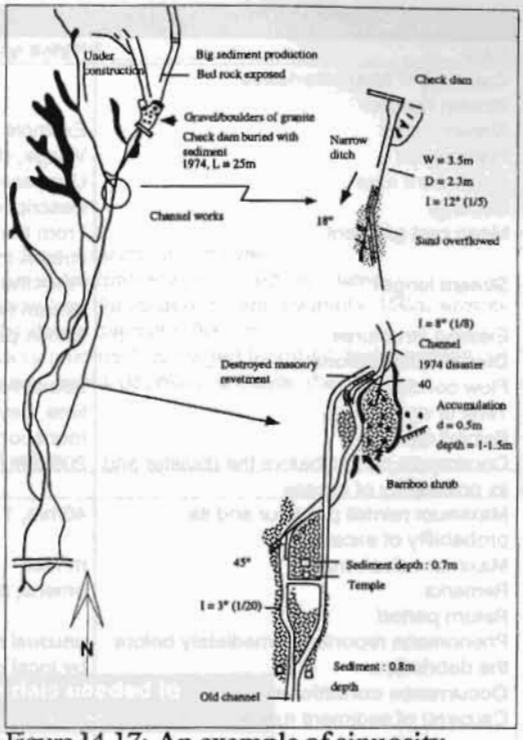

Figure 14.17: An example of sinuosity mapping of a debris flow (Shoudo Island)

References

Ikeya, H. (1974) *Introduction for Sabo Works*. Tokyo: Bunkyou-ku

Ikeya, H. (1980) *How to Investigate Debris Flow Disasters (in Japanese)*. Tokyo: Sankaidou, Bunkyou-ku

Takei, A. (1980) *Landslides, Collapses and Debris Flows (in Japanese)*. Tokyo: Kajima Syuppann Kai, Minato-ku

Annex: Survey Tables

Before conducting a field survey a survey table like the one shown in Table 14.A1 should be prepared. It is important to note any comments and sketch the watershed outline during the survey. After the field survey, the data should be compiled into a database. The materials needed to do a debris flow survey are listed in Table 14.A2. A typical example of a survey note is shown in Table 14.A3.

Table A1: Survey table

Data	Notes and examples
Catchment characteristics	
Stream number	
Stream name	Example: Nallu Khola, upstream of Nakhu Khola
Place name	Village, district, zone and region
Catchment area	Upstream of the confluence with main stream (km^2)
Geology	Description
Mean bed gradient	From the head of first degree gully to the confluence with main stream (degrees)
Stream length	From the head of first degree gully to the confluence with main stream (m)
Existing structures	Check dam (CD), bank protection (BP), bridge
Disaster conditions	
Flow condition	debris flow (D), mud flow (M), sediment flow (S), flood flow (F)
Time of occurrence	time, day, month, year
Rainfall type	monsoon, thunder storm, typhoon, frontal rain, other
Continuous rainfall before the disaster and its probability of excess	200 mm, 1:100
Maximum rainfall per hour and its probability of excess	40mm, 1:100
Maximum discharge	m^3/sec
Remarks	omens, past disasters
Return period	
Phenomena reported immediately before the debris flow	unusual sounds, sudden changes in water level (observations by local people)
Occurrence conditions	
Cause(s) of sediment runoff	landslide collapse, breaking of natural dam, scouring of bank/bed, etc or gathered two or three causes
Bed gradient before disaster	degrees
Bed gradient after disaster	degrees
Area of landslide/collapse	m^2
Volume of landslide/collapse	m^3
Slope of landslide/collapse	degrees
Transport conditions	
Mean bed gradient	degrees
Flow width	m
Bed width	m
Scoured depth and volume	depth: maximum and average volume: total (depth x width x length)
Bending, meandering, and sinuosity	Place of bending (distance from a base point), degree of sinuosity, right or left direction from upstream. Example: 500m from B/P1 30° R
Deposition conditions on stream bed	Example: unstable sediments such as boulders and sand between points 5 and 10, bed rock between points 10 and 12 and deposition on L and R banks between points 10 and 11
Vegetation conditions near stream	Example: both banks dense pine forest, both banks thin shrub
Particle size (maximum and average diameter)	cm
Water level of both banks	Use distinctive marks on banks at the bending point
Deposition conditions	
Topography of deposition zone	Oark alluvial fan, valley plain
Beginning point of the deposition (bed gradient and conditions	Example: bed gradient 8°, valley mouth, alluvial fan, change point of bed gradient
Bed gradient before disaster	degrees
Bed gradient after disaster	degrees
Bed width before disaster	m
Maximum deposition width	m
Dispersion angle	degrees ($Ø_1 + Ø_2$)
Deposition length, L	m
Deposition depth, D (maximum and average)	m

Table A1: **Survey table (cont'd)**	
Data	Notes and examples
Deposition area	m^2
Deposition volume	m^3
Maximum particle size (diameter) (front, middle, and end part)	cm
Average particle size (diameter) (front, middle, and end part)	cm
Damage Conditions	
Human	Number of dead, missing, and injured
Buildings	Number completely/partially destroyed/inundated
Roads	Washed away (m), debris deposit (m) Example: 100m washed away, 150m debris deposit (1000 m^3)
Bridges	Washed away (number), damaged (number) and condition
Cultivated land and forest	Washed away, debris deposit/inundation (ha)
Period of transportation blockage	days
Other	
Total damage	Estimated value
Source: Ikeya (1980)	

Table A2: **Equipment and materials needed to perform a debris flow survey**
Background information
Topographic maps (1/25,000-1/10,000 for location map, 1/5,000-1/2,500 for field survey)
Aerial photographs
Geological maps
Disaster records
Materials for field survey
Camera and film
Field note, pen
Clinometer (clinocompass) to measure strike and dip
Hammer for geological survey
Hand level for bed gradient survey
Range pole
50m measuring tape
3-5m convex rule to measure boulder size and deposition depth
Binoculars
Plastic bags to collect bed materials
Altimeter
Climbing rope
Spade, scoop, etc.

Table A3: **Example of Survey Notes**[1]			
Profile at X- section			
1. Survey point (no.)	1	2	3
2. Distance from the base point	100m	120m	150m
3. Confluence of branch	left branch (L4)	right branch (L4-1)	
Geology of both banks			
4 Geology (rock type)	LR sandstone	LR limestone	LR granite
5. Weathering	strong	Little	little
6. Faults, cracks	not known	50cm intervals	1m intervals
7. Depth of surface soil	3-4m	2-3m	1m
Landslide/collapse			
8. Scale of landslide (width, length, depth, strike and dip)	L. B20*l20*d1m NE30°, N70°	No	No
9. Remaining sediment volume	100 m^3	No	No
10. Possibility of expansion	Yes; if heavy rain	No	No
11. Width	45m	20m	15m
12. Gradient	9°	20°	
13. Scouring/accumulation	balance	small S/A	extreme S.
Stream bed			
14. Bending/meandering (sinuosity : degree)		30°, right	
Bed material			
15. Depth av. (max.)	5-6m (8m)	6-7 (8m)	0-0.5m (1.0m)
16. Gradation (maximum size)	sand	gravel (dia. 10cm)	boulder (dia 1.5m)
17. Accumulation structure	random	lamellar	random
18. Stability	rather stable	unstable	very unstable
19. Debris flow zone or bed load transport zone	BL	BL / DF	DF
20. Occurrence, transport, deposition zone of debris flow	dep.	tran.	occ.
Other			
21. Surface water (change)	yes (yes)	yes (yes when rain)	no (yes when rain)
22. Spring water (change)	no ( )	no ()	a little
23. Vegetation (density)	medium/high trees (dense)	medium/high trees (dense)	shrub (thin)
24. Existing structures	Check dam	No	No
25. Land use	bench, terrace	L forest, R grazing	L/R shrub
26. Remarks			

[1]Note: sketches and/or photographs of occurrence, transport, and deposition zones and any other relevant features should be attached.

Case Studies: Monitoring and Management

Section 2

15 Geotechnical Study of Unstable Slopes: A Case Study at Sunkoshi Power-house Site, Central Nepal

G.S.Pokharel
Soil, Rock and Concrete Laboratory, Nepal Electricity Authority
Bhagwan Pau, Swayambhu, Kathmandu, Nepal

Nepal is a mountainous country with enormous hydropower potential. However, to construct the necessary infrastructure many geological problems need to be overcome, in particular problems of slope instability. Nowadays, these issues are addressed during the feasibility and design phases of a hydropower project. In the past, however, due attention was not given to geological issues when planning projects. This has led to problems that affect the smooth operation of many of the early hydropower projects, problems that now have to be faced by the Nepal Electricity Authority (NEA). A case study of such a project from central Nepal – the Sunkoshi power station – is presented here. The project, completed in 1971, suffers from problems caused by an unstable slope.

This paper considers the following aspects of the Sunkoshi project: the major natural hazards in the area; the geological conditions; geological investigations and studies carried out since 1977; Interpretation of the data acquired during monitoring; additional investigations and studies carried out since 1990; and conclusions about the condition of the unstable slope and recommendations for its long term stabilisation.

Introduction

Nepal is a mountainous country located in the central Himalayas and has an enormous potential for hydropower development. A number of hydropower projects have been constructed to harness this resource and many new hydropower projects are at various levels of planning or construction.

Every hydropower project in Nepal has to be located on sloping mountain terrain. Only the power-houses may be located on gentler slopes or in plains areas. Because of this, slope stability studies and studies of erosion processes in the slopes adjoining hydropower stations are a major consideration during the feasibility and engineering design stages of implementation. After the construction of a hydropower project in Nepal, a major part of the annual maintenance budget is spent on civil works to repair damage done by slope failures caused by natural disasters. The most common types of natural hazards are mass wasting processes such as landslides, mud and debris flows, and mud avalanches, debris torrents, and glacial lake outburst floods (GLOF).

Various natural disasters have already hydropower projects in Nepal. Larger ones include the following (those affecting the Sunkoshi are described in the next section).

- 1993 – landslides, floods, and debris flows caused enormous siltation in the Kulekhani reservoir, Makawanpur district, central Nepal, washed out the penstock over the Jurikhet Khola, destroyed the Kulekhani-II headworks, and increased the bed level of the Kali Khola at the tail water end of the Kulekhani-II powerhouse.
- 1985 – the Namche small hydropower station in Solu Khumbu district, eastern Nepal, was completely washed out by a GLOF before it was put into commission.

- 1994 – The headworks of the Achham small hydropower project were completely washed out by a large flood just before its completion.
- deposition of erosion sediment, although a less dramatic natural process, has had a significant impact on various hydropower schemes by silting up, and thus reducing the economic life, of the reservoirs.

The Sunkoshi Power Station

The Sunkoshi Power Station is a run of the river type of power plant located on the Sunkoshi River in Sindhupalchowk district (Figure 15.1). The plant was completed in 1971and handed over to the Nepal Electricity Corporation. It lies four hours drive east of Nepal's capital, Kathmandu. This power station has been damaged by natural hazards several times. Even before it was built it was known that the area was prone to such events. In 1935 an outburst of the Taraco glacial lake in Tibet destroyed a large area of cultivated land in the Bhotekoshi basin (the Bhotekoshi is a major tributary of the Sunkhoshi which it joins about 700m downstream of the Bhotekoshi bridge at Barhabishe). In 1964 an outburst of the Zhanzangho glacial lake in Tibet caused an 8m rise in the water level in the Bhotekoshi.

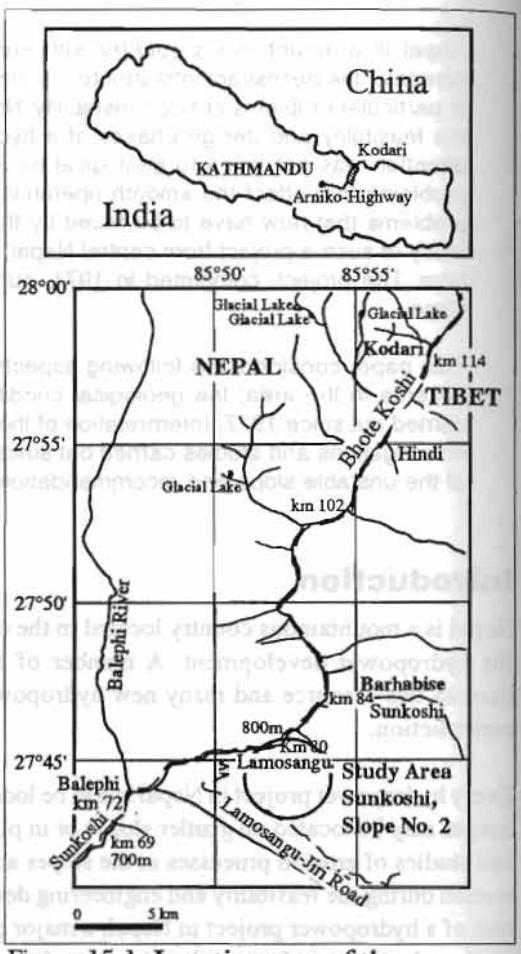

Figure 15.1: Location map of the Bhotekoshi catchment and the Sunkoshi hydropower

The major natural disasters that have affected the Sunkoshi Power Station area since the utility was completed in 1971 are listed below.

- 1976 – a debris flow at Slope No. 2 of the Sunkoshi powerhouse, destroyed the power canal at the toe of the slope and disrupted power generation for many months.
- 1981 – a high intensity flood was caused in the Bhotekoshi by the outburst of the Zhanzangho Glacial Lake in Tibet. It destroyed a number of bridges, a large number of houses, and other property along the Bhotekoshi River, killed four people, and partially damaged the Sunkoshi Hydroelectric Project. The river discharge of the Bhotekoshi at the height of the flood was estimated at 3300 cumecs.
- 1982 – the damming of the Balephi Khola near Phalamesangu caused a high flood in the Bhotekoshi which killed 114 people and swept away 15 houses. It also damaged the power station – it tore away the steel lining of the dam and filled the turbine pits of the powerhouse with mud and debris.
- 1986 – a glacial lake outburst flood in the Sunkoshi caused large-scale damage to the power station.

- 1995 – a debris flow occurred on Slope No. 2 of the Sunkoshi powerhouse, causing extensive damage.
- 1996 – an intensive debris flow in the Larcha Khola tributary of the Bhotekoshi near Tatopani killed 54 people, and swept away 18 houses and an RCC bridge on the main highway. A number of very large boulders, some estimated to weigh more than 1,000 tonnes, destroyed the bridge on the highway (Figure 15.2).

Figure 15.2: **The debris deposit brought down by the Larcha Khola in 1996, a tributary of the Bhotekoshi near Tatopani village. Some of the larger boulders seen in the photograph weigh over 1000 tonnes**

The event of July 5 1995

A large failure occurred in Slope No. 2 of the Sunkoshi Power Station area in July 1995, when the slope was already being investigated in detail (see below), which caused extensive damage to the power project and surrounding property. The mass wasting process started early in the afternoon of July 5, when a great amount of debris gushed down-slope together with a torrent of water, breaching the sides of check dam No. 1 which was located underneath the toe of the upper unstable area. This event was probably caused by a great amount of colluvial material being saturated and loosened during three days of intensive rainfall. This created a torrent of water that ran down from the upper mountain face and drained onto the unstable parts of Block C.

The debris torrent buried the ground floor of a two-storey house adjacent to check dam No. 3. Fortunately, the house was not inhabited at the time. Another 14 houses on the slope were affected. The standing crop was destroyed over a few hundred square metres. Check dams 6, 7, and 8 on the lower elevation of the slope were completely filled up; check dams 1 to 8 were breached from both ends; and check dam 6 was also breached in the middle.

This was the second event of this type since the completion of the hydroelectric project in 1971; the first one occurred in 1976. The recurrence of this danger remains a major threat to the project.

Previous investigations

Instabilities in Slope No. 2 are recognised as the most serious local threat to power generation at the Sunkoshi project. The general plan of Slope No. 2 and surroundings is shown in Figure 15.3, and a general view in Figure 15.4. Slope No. 2 is west-facing. It stretches from an elevation of about 790m up to almost 1,100m (Figure 15.3). It is about 630m long and the average slope angle is 25.5 degrees. The slope angle is gentler in the middle and steepest at the top. The middle part of the slope is terraced and is cultivated (Figure 15.4), some parts are covered with natural vegetation. Some of the lower parts of the slope were previously cultivated for rice paddy but this was stopped by the project because of the instability problems. The upper part of the slope was previously used to grow corn and millet but this area is now covered with landslide debris. The groundwater table varies from about 29.5m in the dry season to about 10m in the wet season. The highest water levels are observed in August and September.

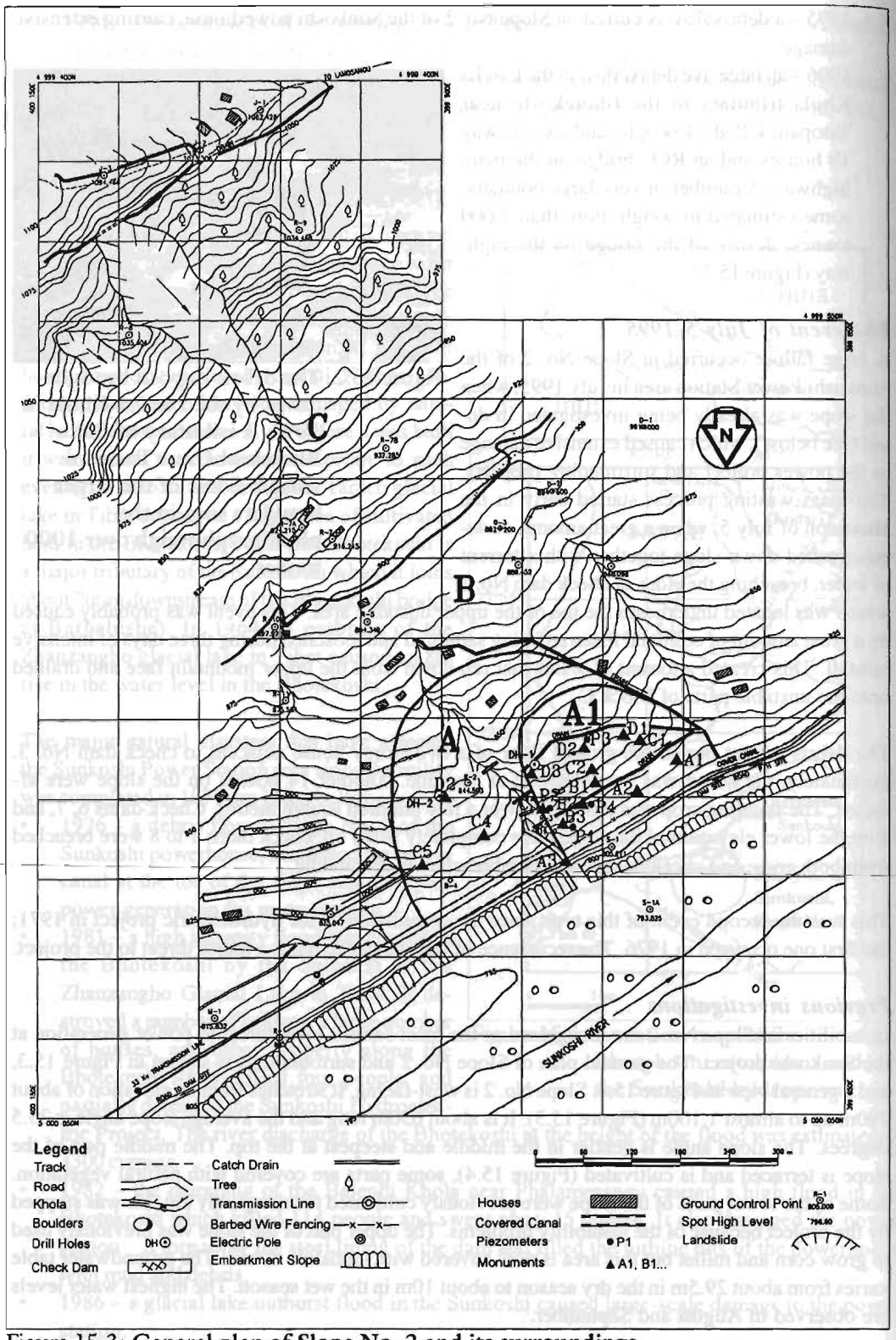

Figure 15.3: **General plan of Slope No. 2 and its surroundings**

Figure 15.4: **General view of Slope No. 2 towards the south**

Figure 15.5: **Debris accumulation at the check dams brought down by the debris torrent of July 1995**

Slope No. 2 was rated as unstable before the project was completed. The first major impact was the 1976 debris torrent, which caused extensive damage to the power project by breaching the power canal around the toe of the slope. The debris flowed along a gully down the middle of Slope No. 2. To try and mitigate this problem, a series of check dams (numbered from the top part of the slope) were constructed across, and stone masonry walls along, this flow channel (Figure 15.5). These walls subsequently moved as much as 25 cm (Figure 15.6) as a result of movement of the slope.

Figure 15.6: **Displacement of the drainage masonry wall at the toe of the slope**

In 1977-78 a team of geologists from the Water and Energy Resources Development Project (WERDP) of the Electricity Department of the Ministry of Water Resources, studied the slope. The team recommended that four piezometers be installed in the lower and middle parts of the slope to monitor the groundwater table. The piezometer standpipes were installed in 1979 in the lower and middle parts of Slope No. 2. The drill holes were terminated in the colluvium. The standpipes were numbered from P1 to P4 (Figure 15.3) and were at the elevations shown in Table 15.1.

Table 15.1: Elevation of piezometer stand pipes

Piezometer No.	Elevation, m	Depth, m
P1	807.850	11.35
P2	817.050	14.20
P3	839.200	16.00
P4	809.000	8.80

Piezometer P2 became clogged at the very beginning, whilst piezometer P3 remained dry for the whole period of monitoring. Piezometers P1 and P4 remained mostly dry and the water table rose above the bottom only during the wet season. Piezometer P1, located at the bottom part of the slope, recorded the highest water table on September 5, at 0.47 m above the bottom of the piezometer at an elevation of 796m. Piezometer P4 recorded the maximum water level at 816.2 m on various dates. The maximum water table was recorded around the beginning of September.

Fifteen reference monuments marked as A1, A2, B1, C1, D1, and so on, were installed to monitor movement at different parts of the slope (Figure 15.3). Monitoring of these monuments over 14 years

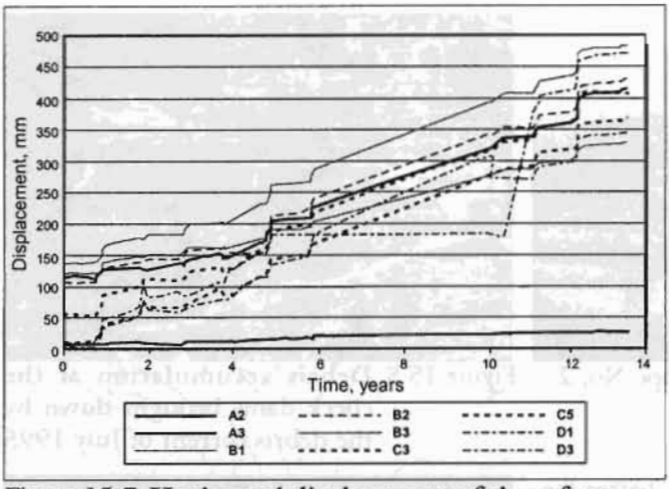

Figure 15.7: **Horizontal displacement of the reference monuments against time No axis labels, still to come**

has shown total displacements varying from 0.09 m at A1 to 1.32 m at B1. The relation between horizontal displacement and time is illustrated in Figure 15.7.

The water level in the piezometers rose in the wet season; horizontal displacement of the slopes took place at the same time. This suggests a close relationship between the rise in the groundwater table and the horizontal displacement of the reference monuments.

The information obtained from these investigations was used to establish a monitoring programme for the slope. However, the core logs from drilling for the piezometers did not provide adequate information on the quality of the slope material and it was difficult to establish the reasons for the instability of the slope from the information provided by the investigations carried out between 1977 and 1990.

Investigations by the Soil, Rock and Concrete Laboratory

In 1990, NEA's Soil Rock and Concrete (SRC) Laboratory, was entrusted with studying Slope No. 2. The laboratory studied the slope with the aim of trying to formulate a permanent solution and devise measures to stabilise the slope. The SRC was assisted by teams from the Japanese International Cooperation Agency (JICA) and HMGN's Water Induced Disaster Prevention Technical Centre (DPTC) who made field visits and offered valuable advice on the sequence of investigation. The team of engineers formed by NEA's Design Department to study the slope started work in 1990. The investigations were designed to answer the following questions.

- Is there just one distinctive instability block or are there a number of smaller blocks?
- What are the causes of the mass erosion processes?
- What immediate and short-term measures are required for their control?
- What is the long-term solution for stabilising the slope?

The results of the various investigations are described in detail in the following.

Geological conditions

Figure 15.8 shows the geological map of the area and Figure 15.9 the structural map. The bedrock under Slope No. 2 is composed of rocks of the Midland meta-sediment group or Kuncha Formation consisting of phyllite, quartzose-phyllite, meta sandstone and grey pellitic quartzite (Maruo et al. 1993). Structurally, the phyllite rocks constitute the core of the Lamosangu anticilinorium (Department of Mines and Geology 1985).

The unstable part of Slope No. 2 is entirely composed of colluvium, which is made up of fragments of phyllites of various sizes and shapes in different states of weathering. The finer material is represented by silt and sand size particles derived from the weathering of phyllites. This soil is

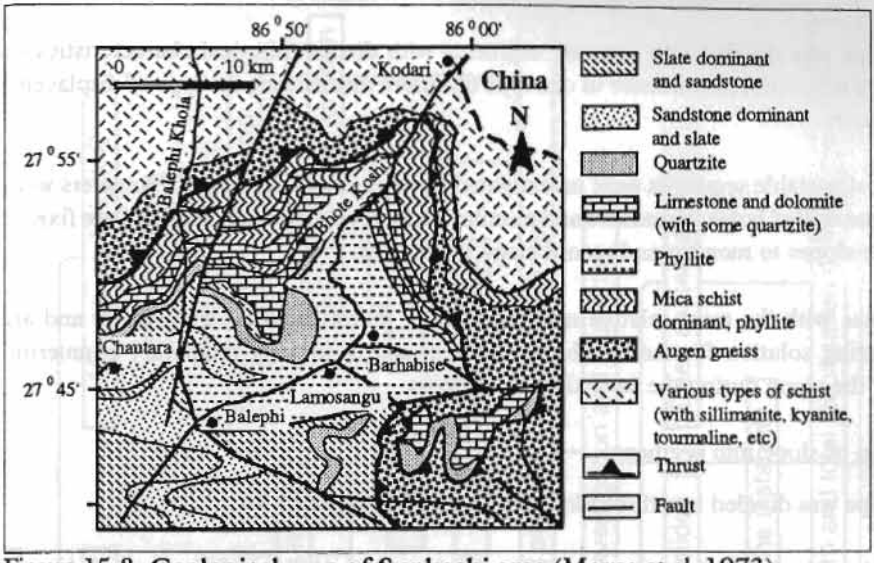

Figure 15.8: **Geological map of Sunkoshi area** (Maruo et al. 1973)

greatly affected by the seasonal rise of the groundwater table in the monsoon. The rise in the water table not only lubricates the slip surface but also causes the shear strength of the soil to decrease resulting in a decrease in slope stability.

The properties of the soil of Slope No. 2 have not been studied because of the problems of soil sampling in non-cohesive (granular) material; using present-day techniques it is difficult to obtain a reasonable quality sample at a reasonable cost. Use of the Standard Penetration Test (SPT) and Dynamic Cone Penetration Test (DCPT) methods to evaluate the strength properties of the soil formation was restricted by the presence of large-size fractions in the colluvium.

Figure 15.9: **Structural map of the Sunkoshi area** (JICA 1985)

Investigations to identify unstable areas

Plan

The investigations were designed to discover whether the instabilities located at the top of the slope and the landslide at the bottom were one interrelated phenomenon or separate unrelated processes on the same slope, and whether they were related to the rise in the water table in the slope. Permanent counter-measures would be designed once the size of the instability was known.

The logical diagram used to identify which areas of Slope 2 were unstable is presented in Figure 15.10. The planned approach for identifying the unstable areas of Slope No. 2 was as follows.

The slope was divided into separate segments with distinct physical characteristics such as the presence of gullies, prominence of one type of failure mechanism, the type of displacement, or the topography.

The most unstable segments were investigated by exploratory drilling. Piezometers were installed inside the drilled holes to measure and monitor water levels. Reference piles were fixed in rows all over the slopes to monitor and record slope movement.

The areas with the most relative movement were investigated in detail to try and arrive at an engineering solution for the instability problem and to identify temporary countermeasures to protect the slope during the investigation process.

Division of slope into segments

The slope was divided into three blocks A, B, and C (Figure 15.3).

Block A – Block A is the area of an old landslide at the lower end of the slope. This area had been stable before work was started on the slope during construction of the power station. Block A was sub-divided into A1, the lower western part, and the remainder, called A minus A1 or A - A1. Block A1 is separated from Block A – A1 by gullies located on either side of the slope. Movements have been observed in Block A1 since 1972, as indicated by the horizontal displacement (by about 25 cm) of the masonry drainage walls located at the northern end of the block (Figure 15.6). Movement has only been observed in Block A - A1 since 1992 in the form of (progressing) cracks along the drainage channel which lies along the toe of the slope between the slope and the power canal. As Block A - A1 started moving long after Block A, it seems likely that it was the movement of Block A1 that caused the whole of Block A to become unstable.

Block B – Block B is the central part of the slope. It is located above Block A and stretches up to the tree line. This block is partially forested and covered by thick vegetation, and partly cultivated. No movement has been recorded from this block. It is relatively stable, even though the slope angle is not significantly less than in the other blocks.

Block C – Block C is the uppermost and steepest part of the slope and is separated from the middle by a line of natural vegetation. In the past, this block comprised a number of small, superficial instabilities (mass wasting processes) and was partly used to grow corn and millet. A large part of this block is under natural vegetation. This part of the slope contributed a large quantity of debris to the 1976 monsoon debris flow and the debris torrent of July 1995. At present, it contains two increasingly unstable areas.

Investigations and Monitoring

A seismic profile of the slope was made in 1991 (Figure 15.11). The first stability analysis was carried out using the results of seismic refraction.

At the end of December 1994 the slope was investigated by exploratory drilling; two holes were drilled to a depth of 36m at the top of blocks A1 and A-A1 as marked on Figure 15.3. Piezometers were installed in each of these holes. Two holes were drilled to a depth of 36m at the top of Block A1. It is planned to drill a third hole in Block B. Then reinforced concrete (RCC) piles were installed in rows

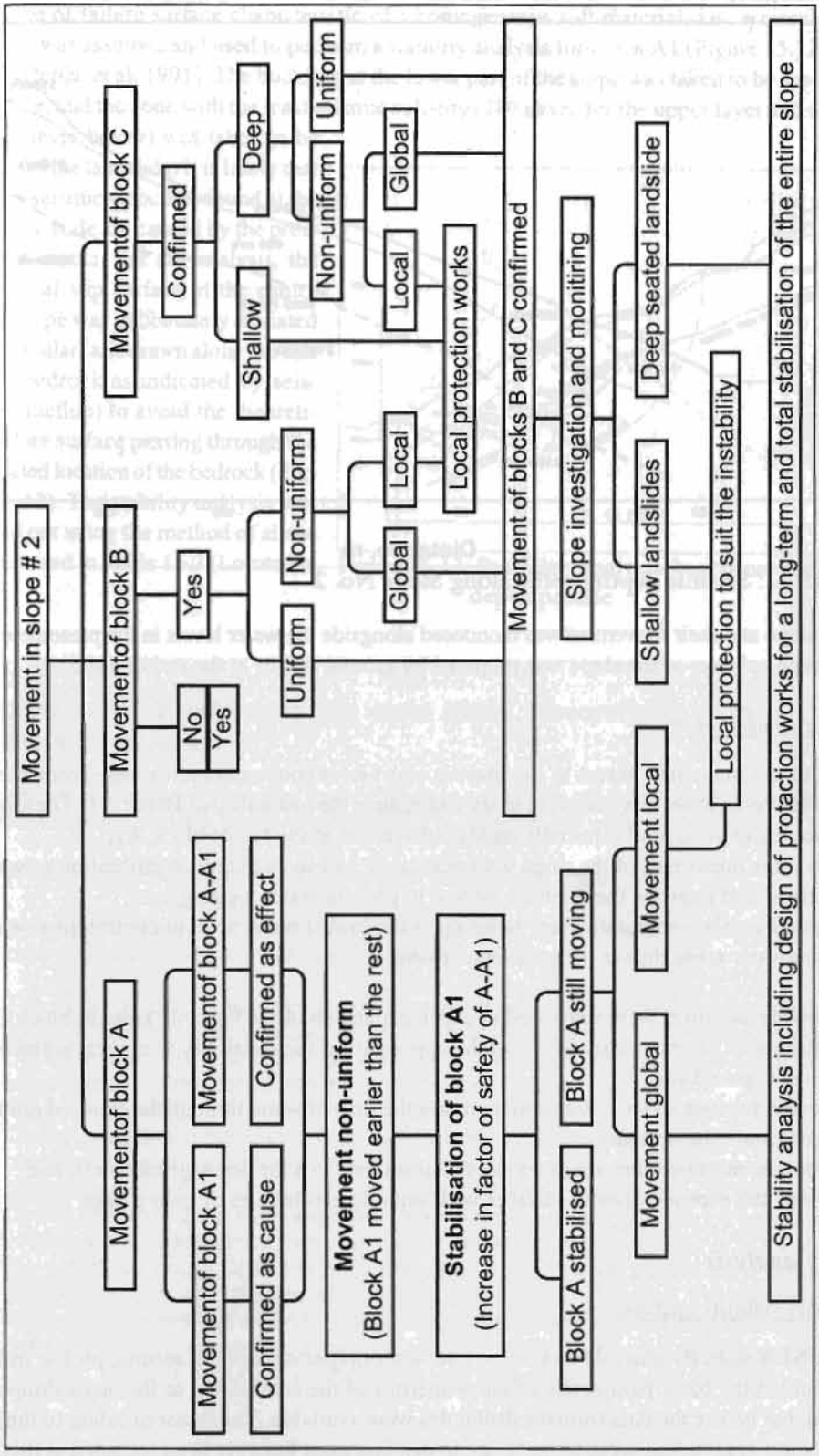

Figure 15.10: **Logical diagram of investigations to identify unstable areas and design countermeasures**

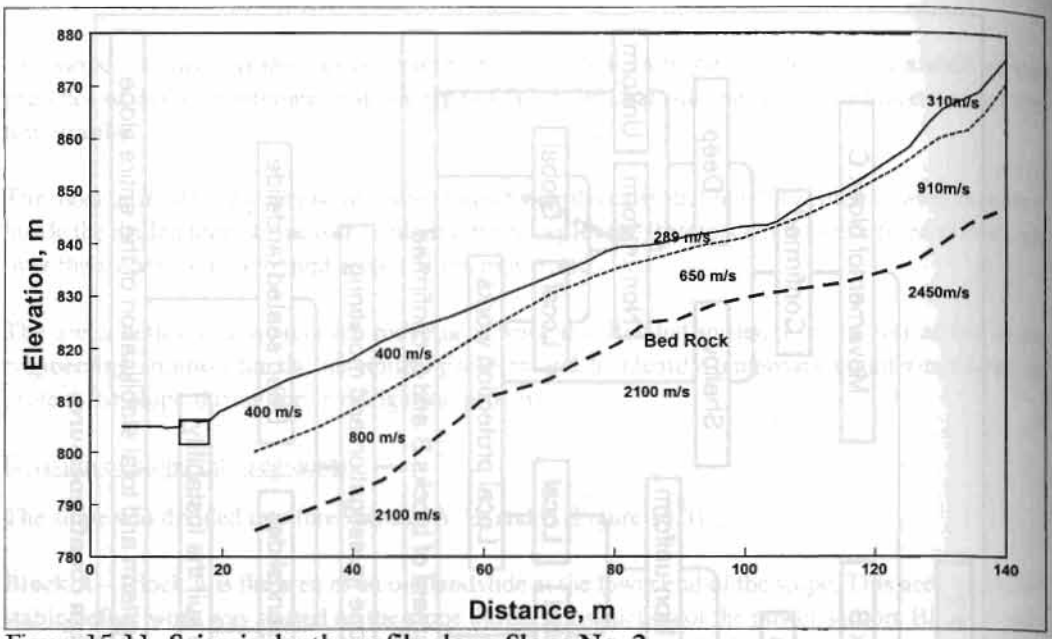

Figure 15.11: **Seismic depth profile along Slope No. 2**

over the slope and their movement was monitored alongside the water levels in the piezometers. A topographical map of the slope was prepared by ground survey at the end of 1995.

Temporary measures

Because of the immediate threat to the project, short-term countermeasures were recommended before the investigation was complete to try and reduce the instability of Block A1. These were

- to stop cultivation, and especially paddy cultivation, at the top of block A1;
- to treat the upper part of the slope with red clayey soil so as to reduce infiltration of water;
- to extend and improve the drainage system to prevent water logging; and
- to install five horizontal drainage holes up to the lowest water level to control the rise in the groundwater table during the monsoon season.

The following measures were suggested to check expansion of the unstable areas in block C:

- to construct a drainage channel along the upper part of the instability to prevent surface flow into the exposed soil;
- to design a system of RCC drains to minimise the flow of water through the exposed ground in order to minimise soil loss;
- to implement bio-engineering measures in areas between the drainage channels; and
- to cover the exposed ground surfaces with suitable geo-textiles or gunny bags.

Stability analysis

Preliminary stability analysis

The first NEA stability analysis was carried out after preparation of the seismic profile in 1991, which enabled the basic parameters of the properties of the soil related to the instabilities to be identified, but before the data from the drill holes were available. The factor of safety of the slope during the dry season was taken to be '1' as no displacement has ever been recorded at this time.

The type of failure surface characteristic of a homogeneous soft material, i.e., a circular failure surface, was assumed and used to perform a stability analysis for block A1 (Figure 15.12 and Box 15.1) (Deoja, et al. 1991). The buckling at the lower part of the slope was taken to be the toe of the landslide, and the zone with the least seismic velocity (280 m/sec for the upper layer and 650 m/sec for the layer below) was taken to be the top of the landslide. It is likely that the low seismic velocities found at the top of the slide are caused by the presence of cracks. For the analysis, the theoretical slip surface at the centre of the slope was deliberately deviated from circular (and drawn along the line of the bedrock as indicated by seismic refraction) to avoid the theoretical failure surface passing through the calculated location of the bedrock (Figure 15.12). The stability analysis was carried out using the method of slices as presented in Table 15.2 (Lomtadze 1977).

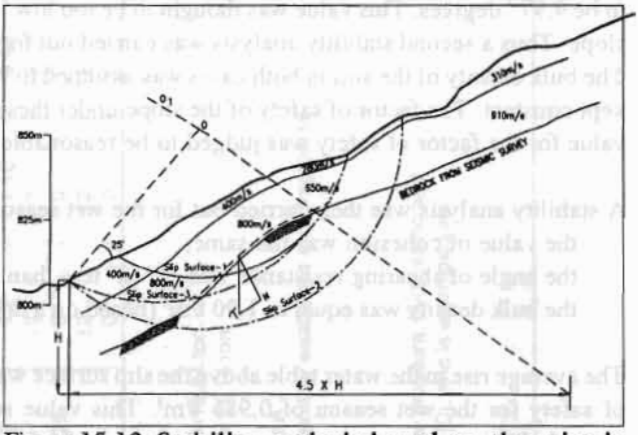

Figure 15.12: Stability analysis based on the seismic depth profile

Box 15.1

Method used to determine the most likely (theoretical) path of the slip surface

The graphical method (Fellenious method) was used to draw the theoretical slip surface. The centre of the slip surface is drawn as follows. The steps are illustrated in Figure 15.12.

- An angle of 25 degrees was added to the slope and a line drawn
- An angle of 35 degrees was added to the upper surface of the slope and a second line drawn (Values taken from tables in Lomtadze (1977))
- The meeting point of these two lines was taken to be one of the centres of the slip surface (marked O).Other probable centres are located along the line 0-01 passing through the point 0 and a second point located one height (of the slope) below and 4.5 height (of the slope) along the horizontal into the slope from the toe
- Circles were drawn from point 0 as well as other centres located along the line 0-01 to obtain a slip surface passing through the toe of the slope, where slope movement is observed, and the top of the slope, characterised by the least velocity of seismic waves. Circles (theoretical slip surfaces) drawn from centres including the point 0 were either cut very deep into the bedrock (not possible) or deviated considerably either at the toe or at the top of the slope. Of all the probable centres, 01 was the best fit for a slip surface passing through both the toe and the top of the slope. However, this theoretical slip surface cut the bedrock within the range of high weathering (about 10m).Thus the circular path of the curve was deliberately changed and drawn 'free hand' along the top of the bedrock. The area included within this arc was subjected to stability analysis.

A stability analysis was carried out for the dry season. The first stability analysis was based on the assumption that the slope has a factor of safety of one during the dry season. The value of cohesion was assumed to be 0.25 t/m² for the lower six slices and zero for the remaining three slices (effect of loosening and loss of fines by piping from the upper part of the slope). From this analysis, the angle of shearing resistance (φ)of the material composing the slope was determined to be 9.97° degrees. This value was thought to be too low for the type of colluvium composing the slope. Thus a second stability analysis was carried out for an angle of shearing resistance of 20°. The bulk density of the soil in both cases was assumed to be 1.75 t/m³. The value of cohesion was kept constant. The factor of safety of the slope under these conditions was found to be 1.48. This value for the factor of safety was judged to be reasonable during the dry season.

A stability analysis was then carried out for the wet season. For this it was further assumed that

- the value of cohesion was the same;
- the angle of shearing resistance was 18° (2° less than in dry conditions); and
- the bulk density was equal to 1.90 t/m³ (based on a dry bulk density of 1.75 t/m³).

The average rise in the water table above the slip surface was equal to 11m giving an average factor of safety for the wet season of 0.985 t/m³. This value seems reasonable as the slope is fairly unstable having shown a maximum displacement of 1.32m (pillar C1) and an average horizontal displacement of 1.056m over 14 years. The rate of horizontal displacement of the slope appears to be constant at about 7-10 cm per year.

Final stability analysis

The final stability analysis was performed in 1996 after the data from the drill holes became available. Drill hole DH 1 was located at almost the same position as the seismic refraction line.

The drill hole data showed that the assumptions made on the basis of the seismic survey were not completely correct. At the drill hole altitude of 804.5m, the bedrock was actually located at a depth of 34.50m and not 15.10m as indicated by the seismic refraction. Furthermore, an accumulation of clay at a depth of 31m indicated the location of the possible slip surface. This level accurately matches with the slip surface originally plotted in the preliminary stability analysis on the basis of the seismic profile, before the erroneous correction was made for the calculated position of the bedrock.

At an elevation of 809.50m, the groundwater table is located at 29.50m (minimum level recorded in the dry season.

Separate stability analyses were performed for blocks A1 and (A-A1). The analysis for A1 was carried out using both the graphical method with a circular slip surface (Figure 15.13) and the Hoek and Bray method. The stability analysis for A-A1 was carried out using the Hoek and Bray method only.

The stability analysis for Block A1 using the graphical method is presented in detail in Table 3; the graphical plot is shown in Figure 15.13. As with the preliminary stability analysis, the soil properties were taken to be : (Φ) = 20 degrees for the lower part of the slope decreasing step by step in the upper sections (Table 15.3) ; cohesion (c)= 0.25 t/m² ; dry density (D_d) = 1.75 t/m³ ; wet density (D_w) = 1.9 t/m³ ; rise in water table during the wet season = 19.5 m ; decrease in the Φ- value of the soil upon wetting = 10%.

The factor of safety was found to be approximately equal to 1.1 in dry conditions, close to a state of equilibrium, and to decrease to 0.89 as the groundwater table rises in the wet season.

Table 15.2: Slope stability analysis on the basis of seismic refraction

Parameter	Slice									Sum
	1	2	3	4	5	6	7	8	9	
Area of slice, m^2	0.63	3.6	5.6	6.8	8	8	7	5.6	2.3	
Thickness of slice, m	1	1	1	1	1	1	1	1	1	
Density (dry) of Slice, t/m^3	1.75	1.75	1.75	1.75	1.75	1.75	1.75	1.75	1.75	
Weight of slice, ton (W)	1.1025	6.3	9.8	11.9	14	14	12.25	9.8	4.025	83.1775
A, deg	-15	-8	0	9.5	18	24	36	47	60	
Sin A	-0.259	-0.139	0	0.165	0.309	0.407	0.588	0.731	0.866	
Cos A	0.966	0.99	1	0.986	0.951	0.913	0.809	0.682	0.5	
W Cos A, ton	1.07	6.24	9.8	11.73	13.31	12.73	9.91	6.68	2.01	73.48
W Sin A, ton	-0.29	-0.88	0	1.96	4.33	5.7	7.2	7.16	3.49	28.67
Φ	?	?	?	?	?	?	?	?	?	
Cohesion (c), t/m^2	0.25	0.25	0.25	0.25	0.25	0.25	0	0	0	1.5
Length of Slip Surface (L), m	3	12	12	12	12	12	12	12	12	99
cL	0.75	3	3	3	3	3	0	0	0	15.75

'A' is the angle between the normal and the resisting component of the force.

In Dry Season
Summation of W Cos A =73.54 ton
Summation of W Sin A = 28.63 ton

In wet season
Summation of W Cos A =79.84 ton
Summation of W Sin A = 31.14 ton

Factor of Safety, F = **[Summation of W Cos A x tan Φ + cL]/Summation of W Sin A**
For the State of Equilibrium for F = **1, Φ = 9.97 deg**, which is low for colluvium composed of moderately weathered rock fragments

Hence, second analysis is carried out for the value of Φ = 20 deg.
For Φ = 20 deg., the Factor of Safety of the Slope = 1.48

The reduction in the Factor of Safety (F) in the wet season is caused mainly by the increase in pore water pressure, hydrostatic and hydrodynamic forces as well as increases in the weight of the material acting against the resisting force (D), and is estimated as:

F = [Summation of W Cos A x tan Φ + cL-D]/Summation of W Sin A
For a Creep, Factor of Safety F = 1, D = 9

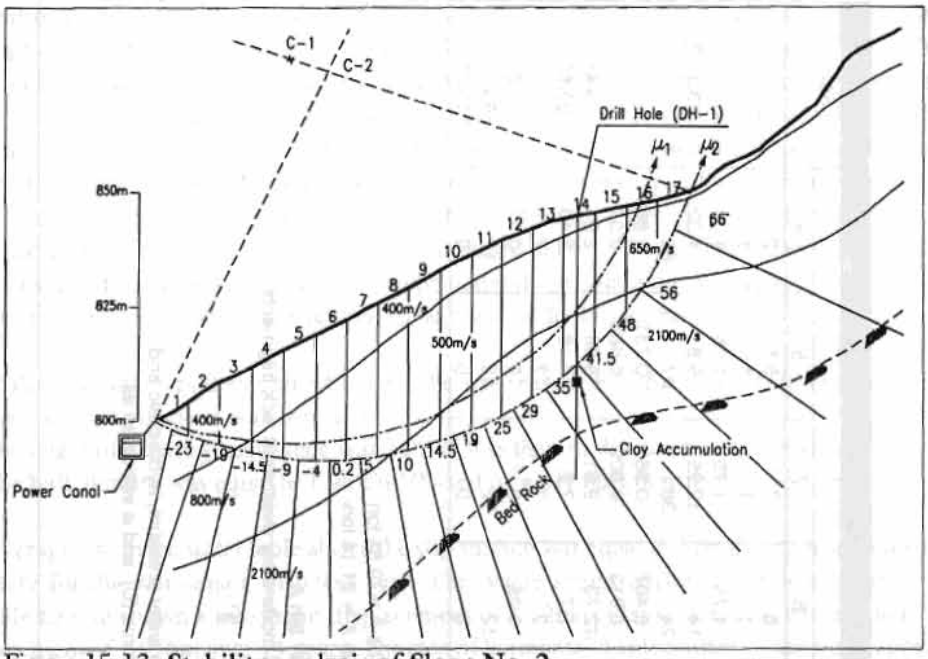

Figure 15.13: **Stability analysis of Slope No. 2**

A second analysis of A1 was carried out using the Hoek and Bray method, which can be used for stability analysis of a slope composed of homogeneous material. The material properties were assumed to be: angle of shearing resistance, Ø = 20°; cohesion c = 0.25 t/m²

Using this method, the factor of safety under dry conditions was calculated to be 1.08.

The factor of safety in the wet season was calculated as follows. The lowering of the factor of safety during the monsoon was assumed to be mainly due to a decrease in the values of cohesion c and the angle of shearing resistance (Ø) as a result of the wetting of the soil mass, and of a decrease in stability due to a rise in the piezometric head. The impact of the increase in weight of soil due to wetting was ignored because of the absence of relevant data.

The factor of safety F in the wet season was calculated using the following.

Dimensionless Factor = c/(DH tan Ø) = 0.25x75/(1.6x35xtan15) = 0.1

where D = bulk density of the soil in t/m³
H = height of the slope, m
Ø = value of the angle of shearing resistance of the soil, degrees

Using this dimensionless factor, the slope angle of 30 degrees and the slope height of 35m, the Factor of Safety (F) is calculated from

c/(DHF)=0.042

giving
F = 0.6 for wet season conditions.

Table 15.3: Final slope stability analysis

Parameter	Slice																	Sum
	1	2	3	4	5	6	7	8	9	10	11	12	13	14	15	16	17	
Area, sq. m.	32	97	151	193	235	270	296	319	329	347	368	355	335	304	251	180	71	4133
Thickness, m	1	1	1	1	1	1	1	1	1	1	1	1	1	1	1	1	1	
Density (dry)	1.75	1.75	1.75	1.75	1.75	1.75	1.75	1.75	1.75	1.75	1.75	1.75	1.75	1.75	1.75	1.75	1.75	
W, ton	56	169.75	264.25	337.75	411.25	472.5	518	558.25	575.75	607.25	644	621.3	586.25	532	439.25	315	124.25	7232.75
A, deg.	-23	-19	-14.5	-9	-4	0.2	5	10	14.5	19	25	29	35	41.5	48	56	66	
Sin A	-0.391	-0.325	-0.25	-0.156	-0.07	0.003	0.087	0.174	0.25	0.325	0.423	0.485	0.574	0.663	0.743	0.829	0.913	
Cos A	0.921	0.945	0.968	0.988	0.998	0.999	0.996	0.985	0.968	0.946	0.906	0.875	0.819	0.749	0.669	0.559	0.407	
W cos A	51.58	160.41	255.79	333.7	410.43	472.03	515.93	549.88	557.33	574.46	583.46	543.6	480.14	398.47	293.86	176.09	50.57	6407.72
W Sin A	-21.9	-56.17	-66.06	-52.69	-28.79	1.42	45.07	97.14	143.94	197.36	272.41	301.3	336.51	352.72	326.36	261.14	113.44	2223.21
	20	20	20	20	20	20	20	20	20	20	18	17	16	15	14	12	10	
Tan Φ	0.364	0.364	0.364	0.364	0.364	0.364	0.364	0.364	0.364	0.364	0.325	0.306	0.287	0.268	0.149	0.212	0.176	
W Cos tan Φ	18.77	58.391	93.109	121.47	149.4	171.82	187.8	200.15	202.87	209.1	189.63	166.3	137.8	106.79	43.785	37.33	8.9003	2103.46
c, t/sq. m	0.25	0.25	0.25	0.25	0.25	0.25	0.25	0.25	0.25	0.25	0.26	0	0	0	0	0	0	
L, m	3	12	12	12	12	12	12	12	12	12	12	12	12	12	12	12	12	195
CL	0.75	3	3	3	3	3	3	3	3	3	3	0	0	0	0	0	0	30.75
D	9	9	9	9	9	9	9	9	9	9	9	9	9	9	9	9	9	

Factor of Safety in dry conditions, Fd = (summation (W Cos A)x tanO +cL)/Summation (W SinA)
or, Fd = (2103.4+30.8)/2224.2 or, Fd= 0.96

Reduction in the Factor of Safety (F) during the wet season is mainly attributed to an increase in the soil density, a decrease in the Φ value, increase in pore water pressure , and hydrodynamic pressure caused by a to rise in the groundwater table.
It is assumed that the value of the angle of shear resistance of the material will decrease by 10% upon wetting.

The factor of safety in the wet season, F_w = 0.83

The same method and values were used to calculate the factor of safety of block A -A1. The factor of safety was calculated to be 1.04 in the dry season. The slip surface corresponding to this factor of safety was the shallowest of all the possible slip surfaces drawn for the stability analysis of this block and was drawn as passing through the middle part of the slope. In reality, the cracks located along the toe of the slop suggest the presence of another slip surface passing through the toe. Hence, another slip surface was plotted passing through the wash out zone (located at a depth of 31m). The factor of safety for this slip surface was calculated to be 0.46 in the wet season.

Conclusions and Recommendations

The studies of Slope No. 2 showed that the movements of Blocks A - A1 and A1 are separate phenomena. They were initiated at different times, their failure mechanisms are different, and they are behaving as separate instabilities. Block B seems to be stable as no movement has been recorded from that slope segment.

Block C contains two progressively increasing superficial instabilities. The upper part of the slope above the larger of the instabilities has numerous tension cracks, which may develop into a circular slip surface.

There is no evidence to suggest that the instability of Slope No. 2 is a single phenomenon affecting the entire slope, rather it seems that the slope is composed of a number of localised instabilities in blocks A and C. The recommendation was made to treat each of these instabilities individually. The individual treatments are listed below. Some were the same as recommended initially, some were new.

- For Block A1
  - Stop cultivation and especially paddy cultivation at the top of Block A1. This has already happened and has resulted in a general decrease in the horizontal displacement rate of the slope.
  - Treat the upper part of the slope with red clayey soil so as to prevent infiltration of water into the slope.
  - Extend the drainage system of this part of the slope to prevent water logging and drill five horizontal drainage holes up to the lowest water level to control the rise in the groundwater table.
  - Apply bio-engineering to prevent or control soil loss.
  - Continue to monitor the movement of each block as stabilisation of block A1 may lead to stabilisation of A-A1.

- For Block C
  - Construct a drainage channel along the upper part of the instability to prevent surface flow into the exposed soil of the instability.
  - Design a system of RCC drains to prevent water flowing through the ground and thus prevent soil loss.
  - Carry out bio-engineering in areas between the drainage channels.
  - Cover the exposed surface of the ground with either a suitable geo-textile or with gunny bags.
  - Cover and fill the tension cracks in the vicinity of the instabilities with red clay to prevent infiltration of water into the cracks.

- Construct a retaining wall with horizontal drains along the upper part of the landslide to control slumping ofsoil mass weakened by moisture during the wet season.

References

Department of Mines and Geology (1985) *Geological Map of Nepal*. Kathmandu: HMG/Nepal

Deoja, B.; Dhital, M.R.; Thapa, A.; Wagner, A. (eds) (1991) *Mountain Risk Engineering Handbook, Parts 1 and 2*. Kathmandu: ICIMOD

ITECO Engineering (1996) *Hazard Mitigation in Northern Sunkoshi and Bhote Koshi Water Catchment areas*. Kathmandu: Department of Roads/HMG

Lomtadze, V.D. (1977) *Engineering Geology*. Nedra: Engineering Geodynamics

Maruo Y.; Ohta, Y.; Akiba, C.; Arita, K. (1993) 'Chautara Region'. In Hashimoto, S., Ohta, Y. and Akiba, C, (eds) *Geology of the Nepal Himalayas*, pp 69-97. Sapporo: Himalayan Committee of University and Saikon Publishing Co. Ltd

JICA (1985) *Master Plan Study on the Koshi River Basin, Water Resources Development*, Final Report, Vol. 2. Kathmandu: Japan International Cooperation Agency (JICA)

16 Landslide Monitoring: A Case Study of the km 19 Landslide along the Kathmandu-Trishuli Road, Central Nepal

M. Poudel[1], D. Bhattarai[2] and B. Tiwari[2]
[1]Department of Irrigation, Jawalakhel, Lalitpur, Nepal
[2]Water Induced Disaster Prevention Technical Centre, Pulchowk, Lalitpur

A landslide at Okharpauwa on the Kathmandu-Trishuli Road was taken as a case study by the Water Induced Disaster Prevention Technical Centre (DPTC) in collaboration with the Department of Roads to study investigation methods and landslide countermeasures. This is one of the first studies from Nepal that has attempted to understand the mechanisms involved in an individual landslide. The main purpose of this exercise was to recommend appropriate countermeasures.

Background

The case study landslide has been observed by the Water Induced Disaster Prevention Technical Centre (DPTC) since July 1993. It is situated at Okharpauwa village in Nuwakot district, 19 km from Kathmandu, along the Kathmandu-Trishuli Road (Figure 16.1). It lies directly adjacent to the main road. The average altitude of the landslide area is 1665m. The study was designed to identify and propose appropriate countermeasures against the landslide to protect the road. It also aimed to acquire data on the nature and movement of the landslide to prepare guidelines for the investigation and prevention of landslides using appropriate low cost methods.

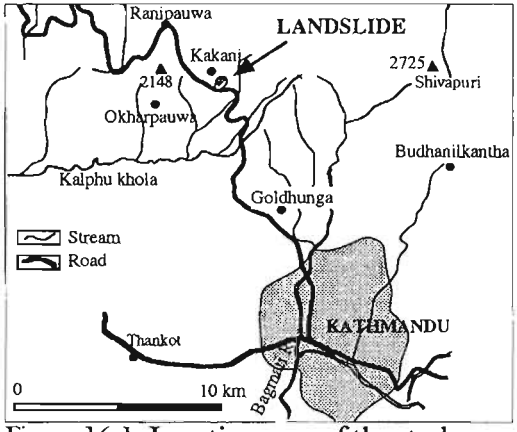

Figure 16.1: Location map of the study area

According to local residents, this landslide was triggered for the first time in 1942 after a long period of intensive rainfall. The landslide was reactivated in 1979 and again by an earthquake in 1989.

The landslide has damaged a section more than 100m long of the Kathmandu-Trishuli road. This road is a 3.5m wide degraded blacktopped road, constructed in 1950 as an access road to the Trishuli Hydropower Project. It is the main link road to the tourist areas of Kakani and the Langtang National Park. This landslide often hinders the smooth flow of traffic, especially during the monsoon season. It affects more than 1.5 ha of land above the road. The landslide area above the road is barren whilst the area below the road is covered by a sparse forest of *Alnus* trees and bushes. Perennial streams bound the landslide on both sides. Gradually more land and hence more people are being threatened as the landslide extends uphill. The landslide directly influences twenty households.

Many tension cracks are apparent on the landslide surface and their number and extent is increasing. Many springs have also developed within the landslide zone. The presence of leaning trees and electric poles indicates the ongoing movement of the landslide. Prominent landslide scars are visible near the crown and sides. The underlying cause of the landslide is the geology of the slope,

whilst it is the strong monsoon rains that trigger it. The influence of the heavy rains is exacerbated by a number of man-made factors including

- seepage of water from farmland and streams into the landslide area, particularly from unlined irrigation canals;
- quarrying of stone at the downstream side of the road at the toe of the landslide;
- choked roadside drains; and
- leakage of a water supply pipeline in the landslide area.

Aerial photos of the area together with geological studies suggest that a fault passes along the landslide area. The landslide is on a colluvial mass resting on a steep slope. Soil samples from boreholes indicate that the sliding mass of the landslide developed in colluvial soil. This soil is a heterogeneous mixture of fine materials and gneissic boulders of various sizes. The extent of displacement of the landslide is gradually increasing and the road level has dropped considerably. At the points where the landslide crosses the road, the drainage channels, retaining walls and road pavement have been almost completely destroyed.

The study shows that this landslide, which has a circular failure surface, is presently active within the ancient debris zone in the slope. Though the first occurrence of the landslide is thought to have been mainly due to geological and meteorological factors, the 1979 reactivation was due to disturbance of the stabilised mass by heavy rainfall and the 1989 event was due to disturbance by an earthquake. Monitoring shows that the rate of movement is increasing. Thus immediate application of countermeasures is vital, otherwise further development of the landslide upslope is inevitable. There is a two metre diameter sinkhole above the topmost crown which has developed as a result of piping seepage. The average slope of the upper zone is about 12^0, whereas the average gradient of the landslide area is 27^0. A number of springs that have developed above the landslide area have increased the amount of water in the landslide zone.

Investigations and Monitoring

In 1992 a 1:500 scale topographic map with 1m contour intervals was prepared for the landslide area (Figure 16.2). Streams, surface cracks, existing infrastructure, and other permanent objects were marked on this map. A cross section of the landslide is shown in Figure 16.3.

Geological survey

As there were no exposed rock outcrops in the landslide area, a 30m deep hole was drilled adjacent to the road to observe the geology of the sliding surface. The core samples gave a good indication of the sub-surface conditions of the landslide. Layers of clay 2.75 and 1m thick were recorded at depths of 3 and 17m. This indicated that the maximum depth of the sliding surface below road level at the boring point is 17m. A soft bedrock of gneiss was encountered 22.05m below the surface, and fresh hard bedrock of gneiss at 23m (Figure 16.4). Experiences from other landslides show that the cohesive strength of clay at landslide slip surfaces is about 1.7 t/m^2. The study was limited to a single drill hole. Other investigations such as geophysical explorations were not conducted.

Monitoring

The landslide was monitored using a range of equipment. The technical aspects are described in detail in the appendix to this paper.

Rain gauge – A manual rain gauge was installed in the area above the road in May 1993. Daily rainfall records have been recorded continuously since then.

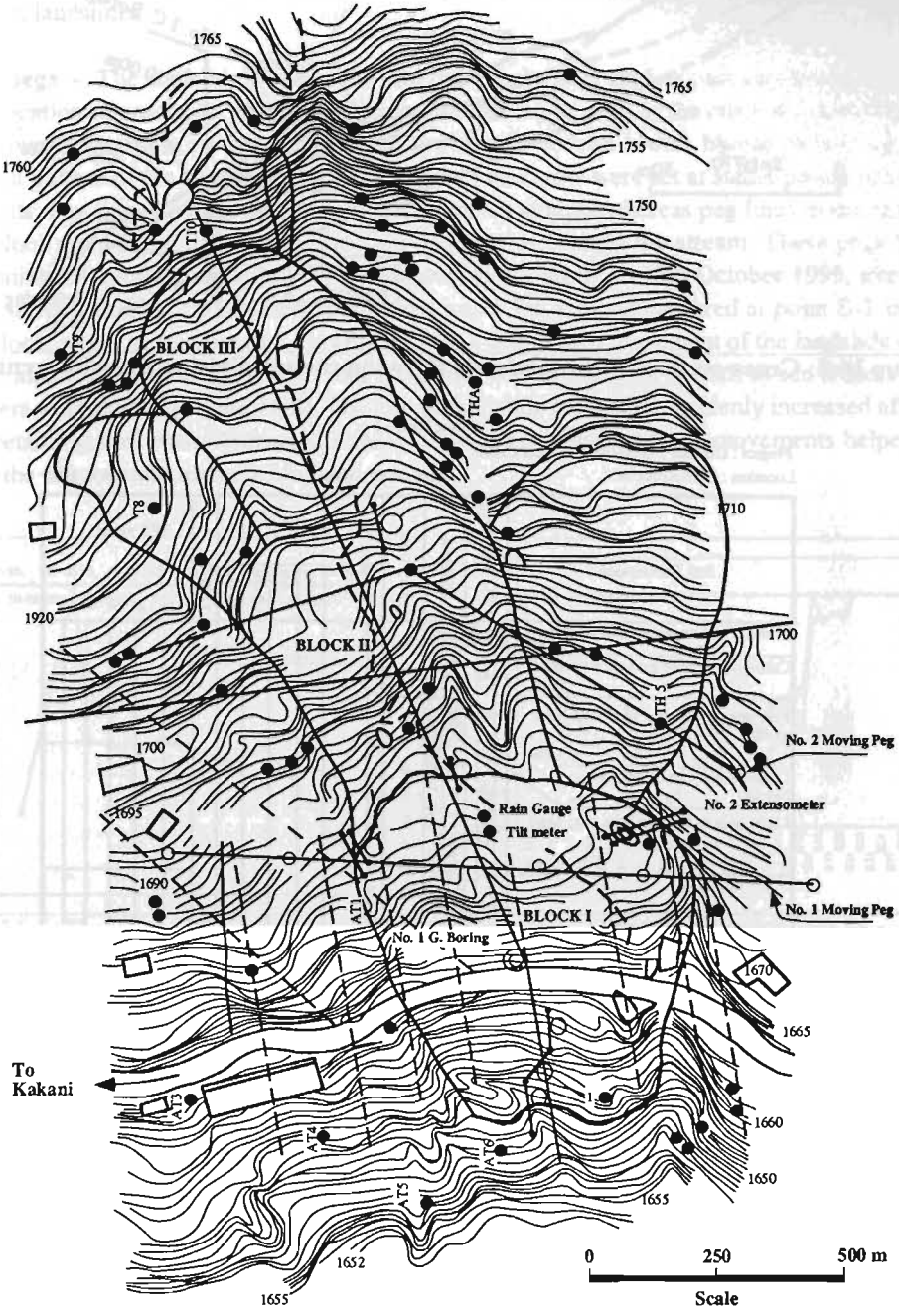

Figure 16.2: **Topographic map of the landslide area and location of monitoring equipment**

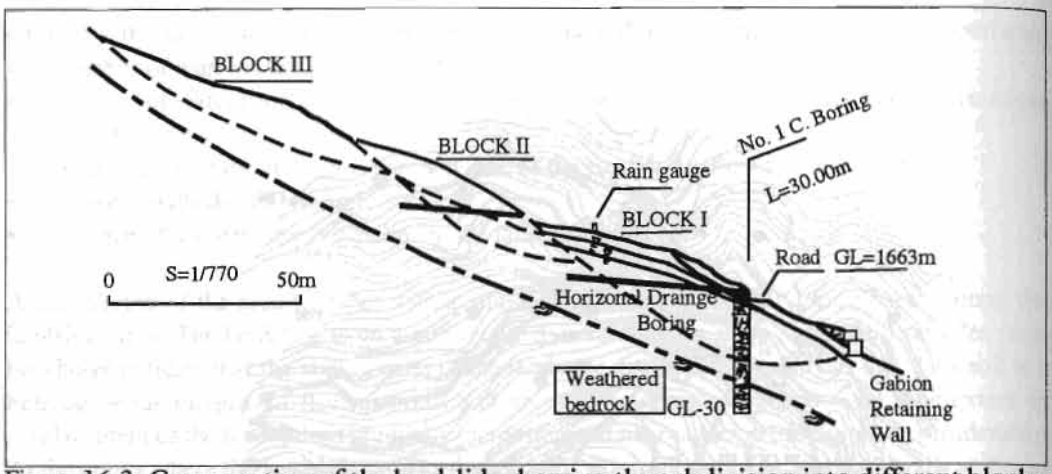

Figure 16.3: Cross-section of the landslide showing the subdivision into different blocks

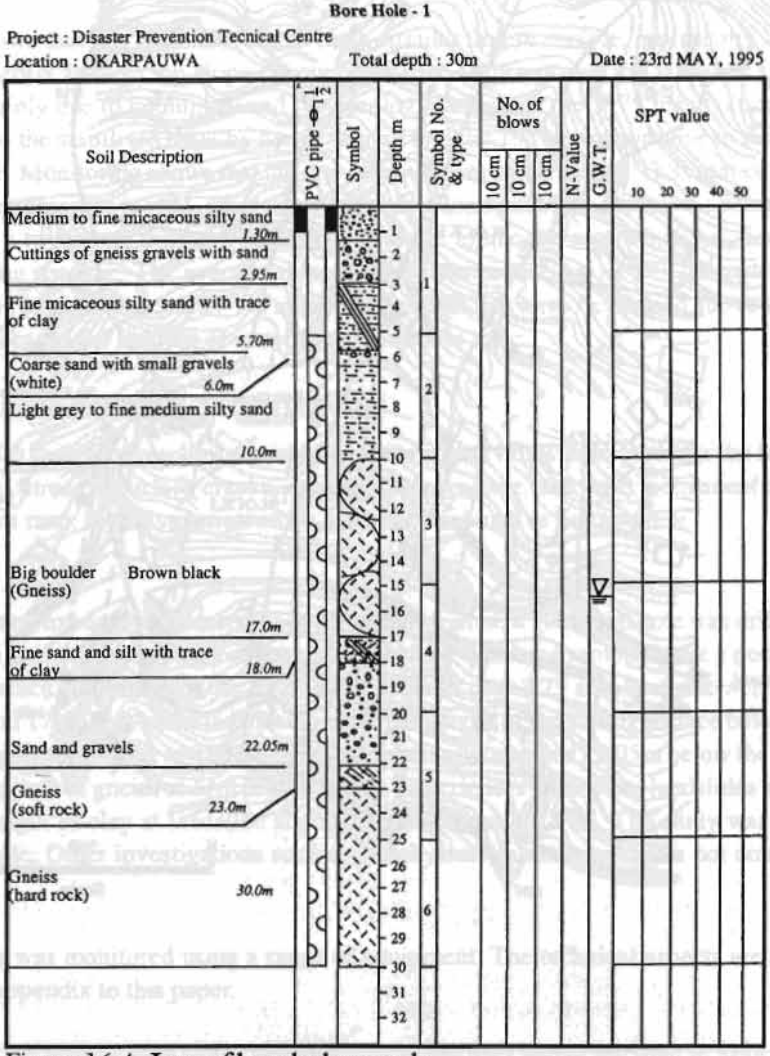

Figure 16.4: Log of borehole sample

Piezometer – One 30m deep piezometer was installed in the roadside bore hole in May 1993. A groundwater logger measures the groundwater level. The variation between May and September, 1995 is shown in Figure 16.5. Fluctuations in the level of groundwater are useful to help analyse the stability of landslides.

Moving pegs — The landslide was divided into five blocks after studying the topographical map and the location of cracks on the surface, three of these can be seen in the cross-section (Figures 2, 3). Rows of pegs were positioned on the lowest and second-lowest blocks to indicate the movement pattern of the landslide. The end points of each row were set at stable points as reference points. Peg lines in the lower-most blocks were set straight whereas peg lines in the second lowest block were set at an oblique direction downwards beyond the stream. These pegs have been monitored regularly since July 1993. Measurements taken on 30th October 1995, after 28 months, showed that the maximum displacement was 5.7m and had occurred at point B-2 in the lowest block, with a settlement of 2.7m (Figure 16.6). The rate of movement of the landslide over time was also calculated (Figure 16.7) and compared with cumulative rainfall to see if these two parameters were related (Figure 16.8). The rate of landslide movement suddenly increased after a gabion retaining wall was constructed in May 1994. The pattern of these movements helped to confirm the existence of separate blocks.

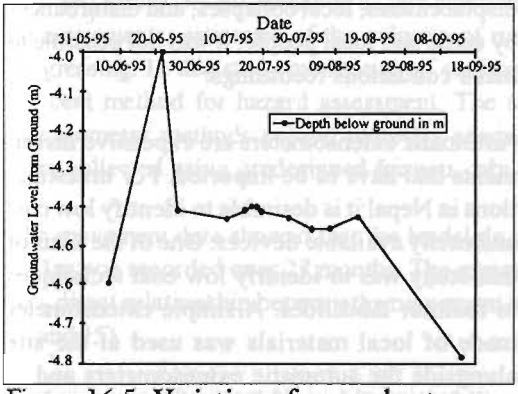

Figure 16.5: Variation of groundwater level in the landslide area as shown by piezometer readings

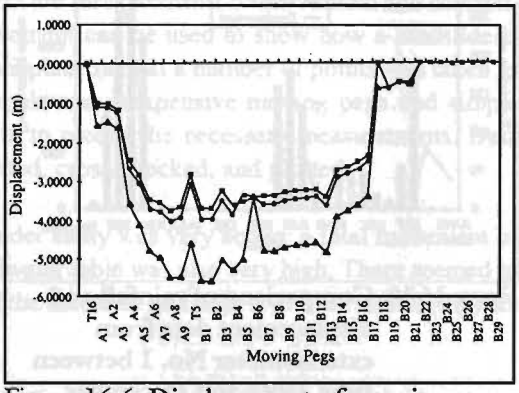

Figure 16.6: Displacement of pegs in a northerly direction in the lowermost block after 28 months

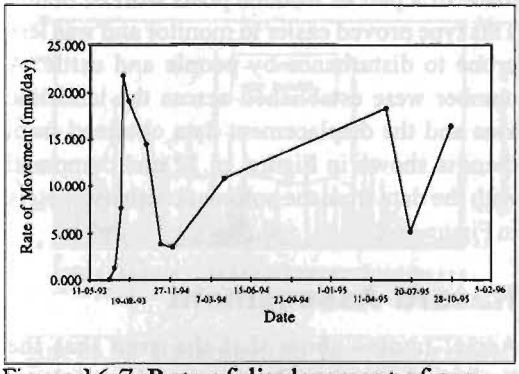

Figure 16.7: Rate of displacement of pegs over time

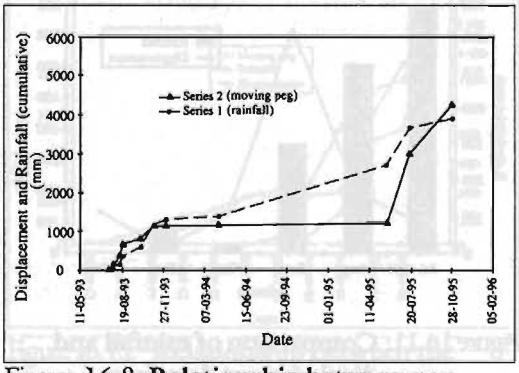

Figure 16.8: Relationship between peg displacement and cumulative rainfall data

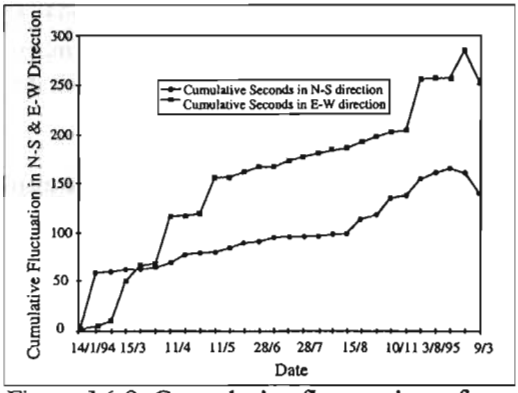

Figure 16.9: **Cumulative fluctuation of ground (in N-S and E-W directions) measured by tiltmeters over time**

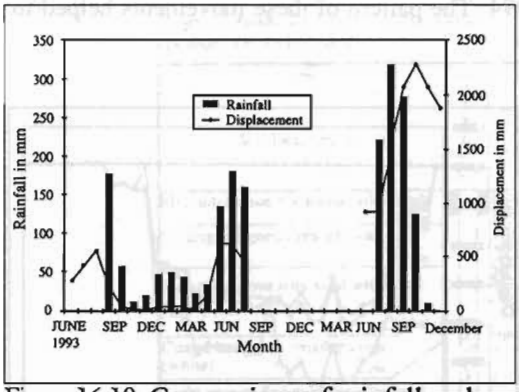

Figure 16.10: **Comparison of rainfall and displacement data from extensometer No. 1 between June 1993 and December 1995**

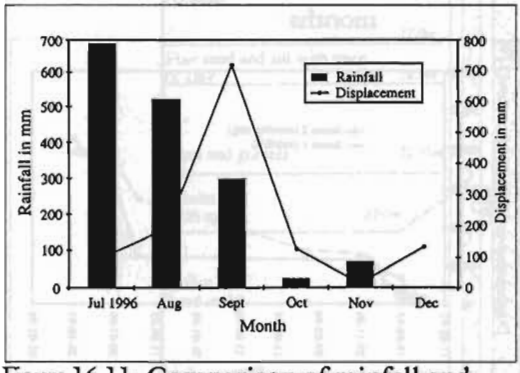

Figure 16.11: **Comparison of rainfall and displacement data from extensometer No.2 between July and December 1996**

Tiltmeter – A tiltmeter observation platform was constructed in June 1993 to study the ground fluctuation over time. Since then the ground fluctuation has been measured at regular intervals in north-south and east-west directions. The results are shown in Figure 16.9. The ground fluctuation in an E-W direction was more than that in a N-S direction.

Extensometers – Two types of extensometers were located to check the surface displacement of the landslide at specific points. One automatic extensometer was positioned in the western part of the lowermost moving peg line in September 1993 and another in the lowest landslide block in the easternmost part. Measurements were recorded regularly. The correlation between rainfall and displacement is shown in Figures 16.10 and 16.11. As a result of the occurrence of large displacements, local collapses, and disturbances by cattle and local people, it was not possible to make continuous recordings.

Automatic extensometers are expensive instruments that have to be imported. For investigations in Nepal it is desirable to identify low cost and easily available devices. One of the aims of this study was to identify low cost techniques to monitor landslides. A simple extensometer made of local materials was used at the site alongside the automatic extensometers and in other areas to monitor crack and block movements. The initial design using wooden posts and planks did not work well. A second design made of a pair of wooden posts worked better. This type proved easier to monitor and was less prone to disturbance by people and cattle. A number were established across the landslide area and the displacement data obtained from them is shown in Figure 16.12 and compared with the data from the automatic extensometers in Figure 16.13.

Hazard Assessment

Aerial photos show that the area that the Kathmandu-Trishuli Road passes through has a moderate distribution of landslides. A comparison of 1978 aerial photographs with ones taken

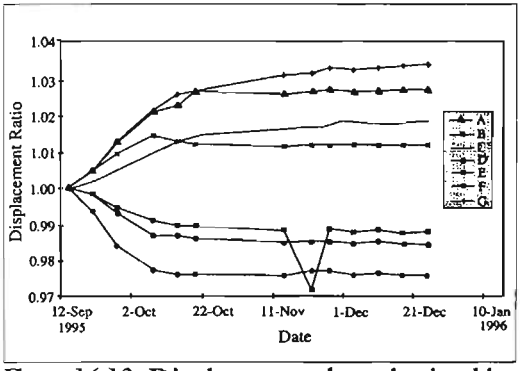

Figure 16.12: **Displacement data obtained by the simple extensometers**

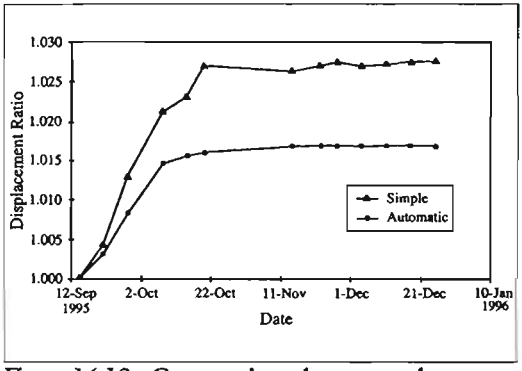

Figure 16.13: **Comparison between the displacements shown by simple and automatic extensometers**

in 1993 showed that a considerable number of landslides had happened in this period along the Kathmandu-Trishuli road.

The best indicators for landslide hazard assessment are measurements of the vertical and horizontal movements; estimates of the velocity of movement can be used to show how a landslide is progressing. In this study monitoring of surface displacement at a number of points was taken as the best method for hazard assessment. The simple and inexpensive moving pegs and simple extensometer methods proved perfectly adequate to record the necessary measurements. Data were collected using predesigned formats, tabulated, cross-checked, and plotted.

The movement data showed that the landslide under study was very active; a total movement of 5.61m was recorded over 27 months. The groundwater table was also very high. There seemed to be a direct relationship between the movement of the landslide and high levels of rainfall (Figures 14 and 15).

In the past nothing had been done to stabilise the landslide except for the construction of one retaining wall. This wall however had not been built at the proper location and had failed to contain

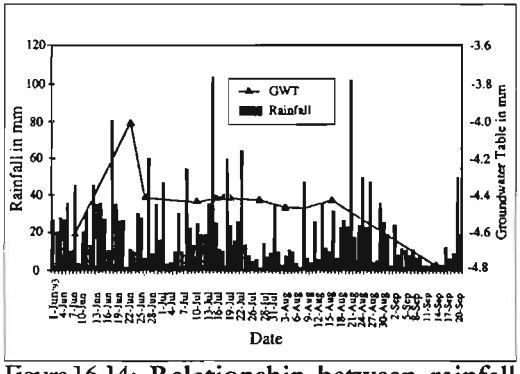

Figure 16.14: **Relationship between rainfall and the groundwater table**

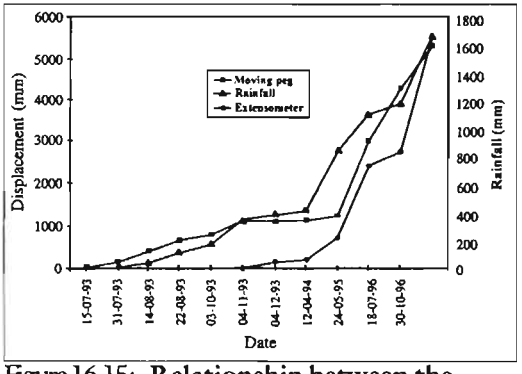

Figure 16.15: **Relationship between the displacement shown by pegs and extensometers and rainfall (cumulative)**

the landslide. Where a landslide is affecting a road, the cost of stabilisation should be compared with the cost of re-routing the road. In this case, although the landslide was very active, it was impractical to re-route the road because of the steep topography. Thus it was essential to stabilise the landslide

Proposed Stabilisation Measures

As mentioned above, the landslide was found to be very active during the investigation and monitoring period. The geological setting of the area is prone to landslides. However, the high groundwater level in the sliding mass and the weight of the sliding mass itself were considered to be the main causes of this particular landslide. The following stabilisation measures were recommended by the investigating team to control the landslide.

Protective measures

The movement data showed that the lowermost block was moving significantly downhill, thus control of this block was the first priority. The priority protective measure was to control water leaking from water supply pipes, irrigation channels, and the landslide surface itself by constructing surface drainage and diverting the stream that ran down the landslide area to outside. Non-structural measures such as planting appropriate species were also recommended. As the toe of the lowermost block was severely disturbed, the possibility of a landslide below the lowermost toe could not be ruled out. However, measures to counteract this were not so urgent

Planning long-term countermeasures

A road can be protected by either preventive or restraining work. Preventive works, which include surface drainage works and shallow sub-surface drainage works, aim to control landslide movement by ameliorating the natural condition. Restraining works such as retaining walls aim to control the landslide by decreasing its movement.

The landslide mass consisted of five major blocks of which the lowermost block was the most unstable and directly threatened the road. As it was the lowermost block that was unstable, it appeared to be crucial to prevent the other blocks from sliding and affecting it. Past experience shows that for a road the safety factor should be at least 1.1 to 1.2.

The protective measures suggested were a combination of drainage works and retaining walls. Groundwater should be drawn away from the landslide area by installing bored horizontal drainage. Improved surface drainage should control the percolation of surface water and divert it to outside the landslide area.

Stability analysis was done to find the safety factor of the lowermost block. As the landslide is very active, the factor of safety was taken to be 0.95. The value of the cohesive strength of the landslide clay was taken to be 1.7t/m^2 and the value for the bulk density of the soil 1.8 t/m^3. Using these values, the estimated value for the angle of internal friction of the soil at the slip zone was 21.2^0. This value was taken as the basis for estimating the effects of various countermeasures proposed for stabilising the landslide in terms of the change in the estimated Factor of Safety. The results are shown in Tables 16.1 and 16.2.

The analysis showed that if the groundwater level in the landslide area could be reduced as expected as a result of the proposed drainage works, the stability of block I would be improved by 17% and that of Block I + Block II by 12%. If a retaining wall could be built at the toe of the

Table 16.1: **Factor of safety for various conditions of the landslide (Block 1)**		
Condition of landslide	Factor of safety	Remarks
Without any countermeasures, when the groundwater level is maximum and the ratio of the resisting force to the overturning force a minimum	0.950	angle of friction 21.2° from back analysis
With surface drainage and horizontal drainage works	1.108	1.0~2.0m reduction in the water level is assumed
With retaining wall with embankment at the toe of the landslide	1.145	
With combination of drainage works and retaining wall with embankment	1.303	

Table 16.2: **Factor of safety for various conditions of the landslide (block I + block II)**		
Condition of landslide	Factor of safety	Remarks
Without any countermeasures, when the groundwater level is maximum and the ratio of the resisting force to the overturning force a minimum	0.980	angle of friction 21.2° from back analysis
With surface drainage and horizontal drainage work	1.098	1.0~2.0m reduction in the water level is assumed
With retaining wall with embankment at the toe of the landslide	1.113	
With combination of surface drainage, horizontal drainage and retaining wall	1.234	

landslide, the stability of block I would be improved by 21% and that of Block I + Block II by 14%. If the combination of retaining wall and drainage works could be built to control the landslide, the stability of block I would be improved by 37% and that of Block I + Block II by 26%. Considering the importance of the road and the construction cost for the countermeasures, the results of the analysis seemed to show that the construction measures would be justified.

The proposed countermeasures are described in detail below and their location shown in Figure 16.16.

Gabion retaining/toe wall with embankment – The location of the toe of the lowermost landslide block was identified by core drilling and regular monitoring with a simple extensometer. The team proposed that a gabion retaining wall be built at the toe to contain landslide movement. A small portion above the toe of the landslide would need filling with soil to form an embankment to act as a counterweight against the landslide. The embankment should be planted with trees and shrubs.

Surface Drainage – Surface drainage should be installed to divert water from the springs, and seeping and leaking water away from the landslide area to reduce groundwater levels. Two types of surface drainage, one along the stream and the other along the landslide area were recommended.

Roadside-drain cum irrigation-channel – Water seeping through from the unlined roadside drain had contributed to movement of the landslide. This roadside drain should be lined.

Horizontal drainage boring – To control the groundwater level, the team proposed that a horizontal drain be bored at two places. This was expected to reduce the water table by about 3m.

Extensive **bioengineering works** were also proposed.

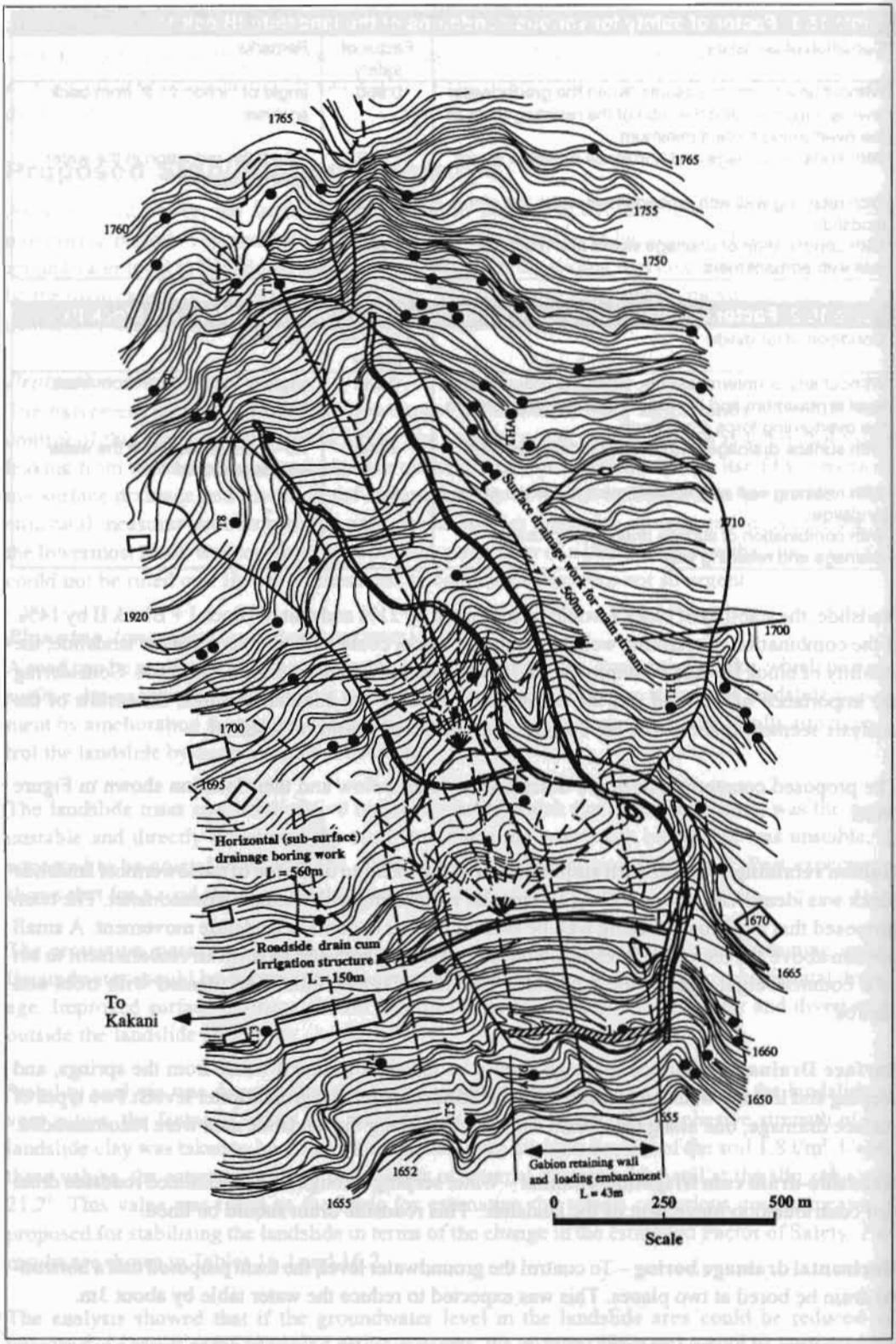

Figure 16.16: Map showing location of countermeasures proposed to stabilise the landslide

ent

The size and priority of the proposed construction works are shown in Table 16.3.

Table 16.3: **Proposed construction work**

Type of prevention work	Size	Priority
Gabion retaining/toe wall	43 m	First
Loading embankment	4000 m^3	First
Surface drainage along stream	560 m	First
Surface drainage along landslide area	150 m	First
Road side drain cum irrigation structure	150 m	First
Horizontal drainage boring works	560 m	Second
Bio-engineering works	1.5 ha	Second

Impact of Countermeasures

All the countermeasures proposed by the DPTC were carried out by the Department of Roads, His Majesty Government of Nepal in the fiscal year 1996/97 (pre-monsoon). Subsequent monitoring data obtained from both simple and automatic extensometers indicated that there was no significant movement of the landslide mass during the 1997 monsoon period. This suggests that the landslide had been stabilised by the countermeasures.

Conclusion

Detailed investigations and hazard assessments are planning tools for the implementation of countermeasures to safeguard a road against destruction by an active landslide. In the case considered here, any delay in installing the countermeasures would have accelerated the development of further landslide blocks and increased the costs of stabilisation.

Moving peg and simple extensometers proved to be effective low cost methods for measuring landslides; the displacement data recorded using simple and automatic extensometers showed similar trends. Moving peg displacement, automatic extensometer displacement, and recorded data of rainfall show that There was a direct relationship between the movement of the landslide and the amount of accumulated rainfall (and consequent rise in groundwater level), as shown by displacement and rainfall measurements. A stability analysis of Block I and a combination of Block I and Block II for the conditions before and after completion of the proposed countermeasures, indicated that the countermeasures would increase the Factor of Safety to 1.303 and 1.234 from 0.95 and 0.98, respectively. These values were considered acceptable, given the budget constraints and the limitations of the investigation.

It is recommended that in future landslide investigations be carried out prior to road construction in Nepal's hills so that necessary stabilisation countermeasures can be planned and constructed at the same time a road is built, and the costs included in the road construction costs.

Appendix: Details of Monitoring Equipment

Moving pegs

'Moving pegs' are square wooden posts with a marker nail in the top embedded in concrete (Figure 16.A1) in a predetermined pattern in an area of potential movement. The outside pegs are fixed in stable ground. The initial coordinate of each peg is surveyed and calculated in terms of distance and the horizontal angle. In this case study, the pegs were located in rows, one row in each of the two unstable blocks.

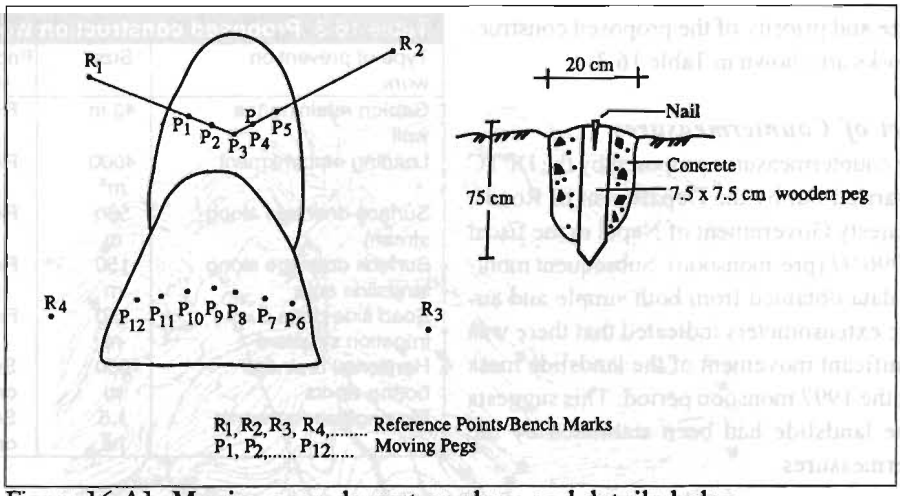

Figure 16.A1: **Moving pegs: layout on slope and detailed plan**

Automatic extensometers

An extensometer is a device for measuring the relative displacement between points on a landslide and a point on stable land. This method is used widely to analyse the speed of sliding masses. Normally a number of extensometers with self-recording systems are installed between the main scarps. They record the motion continuously and these values are used to calculate strain rates. This instrumentation is one way of warning of an impending slide event.

Extensometers are made up of an invar wire, mechanical gears, and a clock driven by a spring (Figure 16.A2). A self-plotting small drum is attached, which rotates as the invar wire stretches. The instrument is relatively simple and a continuous record can be kept. Movements of more than 0.2 mm are recorded together with the time of movement (to within 2.4 hours, or the nearest 1/10th of a day). The instrument is usually set 1m above the ground surface and the invar wire is connected from the pulley of the extensometer to another post. The span between the posts is normally less than 5m. The invar wire and its supports should be protected by vinyl chloride pipe. Rainfall data are often collected in parallel so that the affect of rainfall on surface displacement can be assessed.

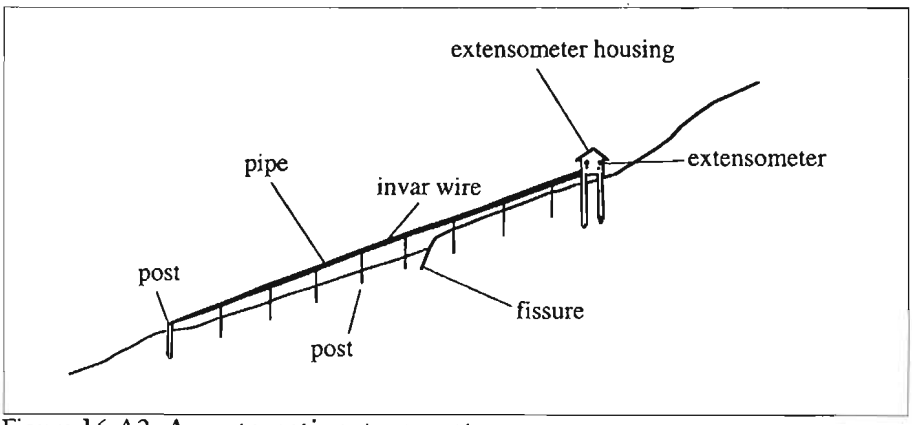

Figure 16.A2: **An automatic extensometer**

Automatic extensometers are widely used in developed countries (Japan, for example) but are difficult to protect in the field.

Simple extensometers

Type A

The type A simple extensometer is made of wooden planks and posts (Figure 16.A3). The basic principle is the same as that of the automatic extensometer. The wooden plank held between fixed posts has a flexible joint. Once the instrument is set up a line is marked at the joint position of the plank. The date of measurement is written on the plank. The difference between new and previous marks indicates the displacement of the landslide block.

Although not as accurate as an automatic extensometer, this instrument gives an idea of landslide movement in relation to time.

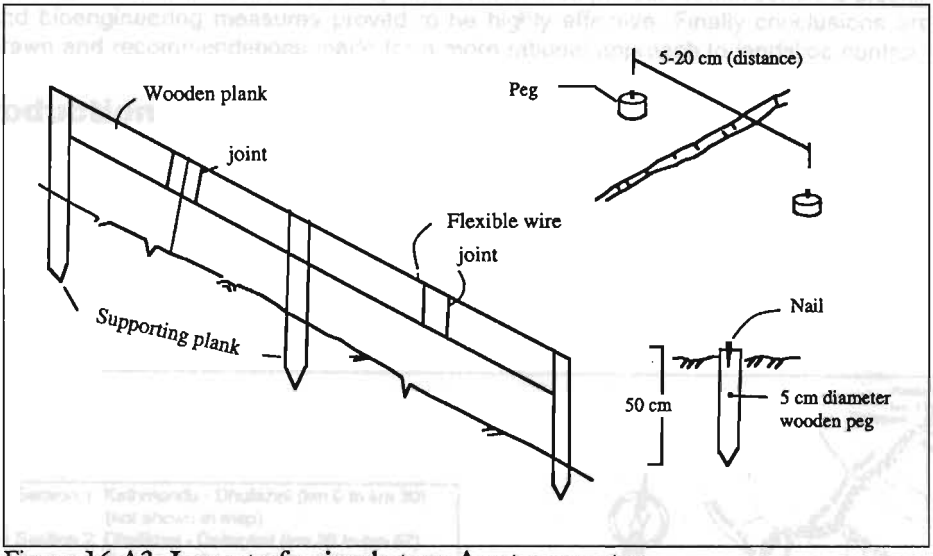

Figure 16.A3: **Layout of a simple type A extensometer**

Type B

This type of extensometer is simpler, cheaper, and more easily maintained than type A. A set of wooden pegs is set up in the unstable part of the slope to measure the extension of the ground. The length of each set is measured weekly and any increase or decrease recorded.

Tiltmeters

Tiltmeters are used to indicate small ground fluctuations. Their main purpose is to judge whether a potential landslide is stable or whether it is moving into a more active or final stage. One common type is a bubble tiltmeter. The basic layout is shown in Figure 16.A4.

Tiltmeters should be installed on the upper slope of a potentially sliding block along the line of extension of the principal measuring line to examine the possibility of landslide enlargement. A tiltmeter may also be installed on the sliding block itself or one slope of the block.

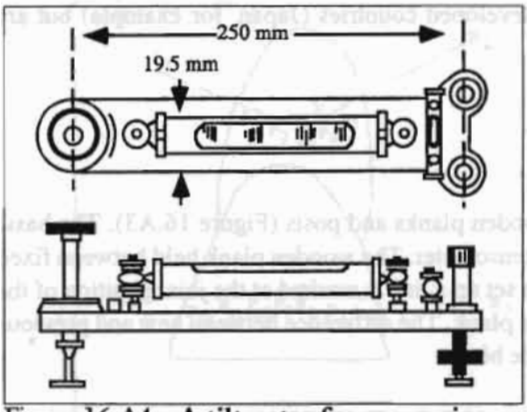

Figure 16.A4: A tiltmeter for measuring ground displacement

Tiltmeter data are used to produce a diagram of tilt variation and the accumulation of tilt over time. This data can be compared with rainfall and groundwater levels to see if there is any correlation.

Groundwater surveys

Groundwater levels can be measured manually. Self-recording float or water pressure type recorders are also available. Perforated PVC pipe wound with geonet is installed inside a borehole and the level of the groundwater is recorded using a manual or automatic water logger (a piezometer).

17 Landslide Control and Stabilisation Measures for Mountain Roads: A Case Study of the Arniko Highway, Central Nepal

T. L. Adhikari
ITECO Nepal (P) Ltd., New Baneswor, Kathmandu Nepal
Email:

This case study is concerned with landslide hazards along the Arniko Highway in central Nepal. Two landslides have been selected for detailed examination. This paper describes their history, their effect on human settlements and infrastructure, investigations and monitoring, the design and construction of hazard mitigation and stabilisation measures, and assessment of the effectiveness of these measures. The integrated approach used in the project for the investigation, design, and construction was found to be successful. The innovative solutions for the landslide stabilisation and river training works such as earth/rock anchors, shallow and deep drains, armoured protection with concrete blocks, and bioengineering measures proved to be highly effective. Finally conclusions are drawn and recommendations made for a more rational approach to landslide control.

Introduction

The present case study is intended as a practical illustration of the landslide-related problems encountered along roads in Nepal using specific examples from the Arniko Highway. The Arniko Highway (Figure 17.1) runs along one of the most fragile river valleys in Nepal. Since its completion in 1967, it has been severely affected by a number of hydrological disasters, including glacial lake outburst floods (GLOFs) in 1964 and 1981, and a flood in 1987. The associated landslide problems are typical of those faced in many Hindu Kush-Himalayan river valleys.

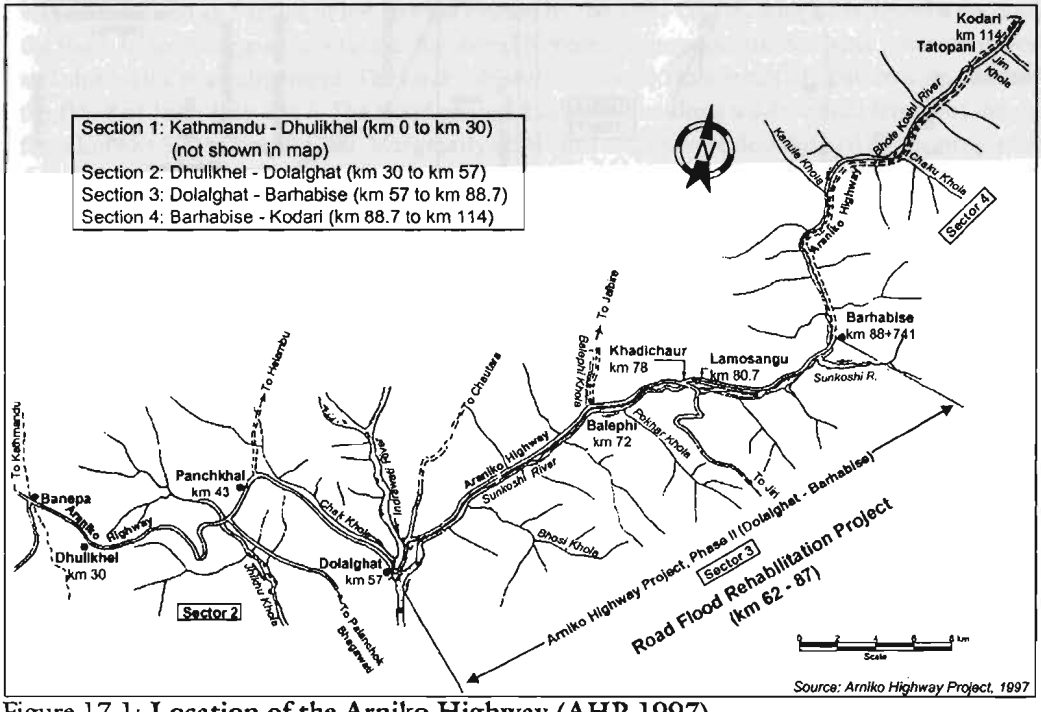

Figure 17.1: Location of the Arniko Highway (AHP 1997)

The Arniko Highway is one of Nepal's most important highways. It is the only road link to China and is classified as ' a strategic national highway linking the capital city to an international border'. In 1990 the traffic volume was about 200 vehicles per day.

The highway is an all-weather metalled road up to Barhabise (km 88 from Kathmandu) and an all-weather gravel road from there to the Chinese border (km 114 from Kathmandu). The Arniko Highway was constructed in the mid 1960s to provide the shortest link between Kathmandu and the border point at Kodari. For this reason, the alignment mostly follows the banks of the Bhotekoshi, Sunkoshi, and Chak Khola watercourses. The alignment runs across a large number of cross drains, fan deposits, landslides, and sharp rock wedges and is susceptible to bank erosion. The road is 114 km long with a width of between 3.75 and 5.5m.

The highway, has experienced a number of major hydrological disasters owing as a result of both glacial lake outbursts and incessant heavy (monsoon) rainfall leading to floods and debris flows. The stretch of highway most affected by these disasters, as indicated by the frequency of landslides and bank erosion, lies between kms 62 and 114 along the banks of the Sunkoshi and Bhotekoshi rivers. Major GLOFs occurred along the Bhotekoshi river in 1964 and 1981. In 1964 the magnitude of devastation was less as the valley was only in the initial stages of infrastructural development. The GLOF incident of 1981 had a source discharge of about 16,000 m^3/s and washed out many sections of the highway and two major bridges. The presence of glacial lakes in the Bhotekoshi catchment area is shown in Figure 17.2. The discharge attenuation along the river from the GLOF in 1981 is shown in Figure 17.3.

The highway experienced another catastrophic flood in July 1987 that resulted in disastrous washouts and major erosion along the Sunkoshi, Charnawati, and Tungbhadra rivers. More than a

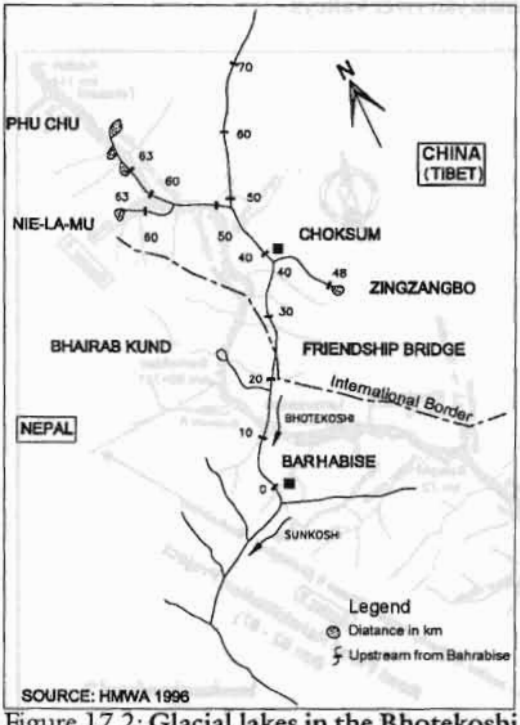

Figure 17.2: **Glacial lakes in the Bhotekoshi catchment (ITECO 1997)**

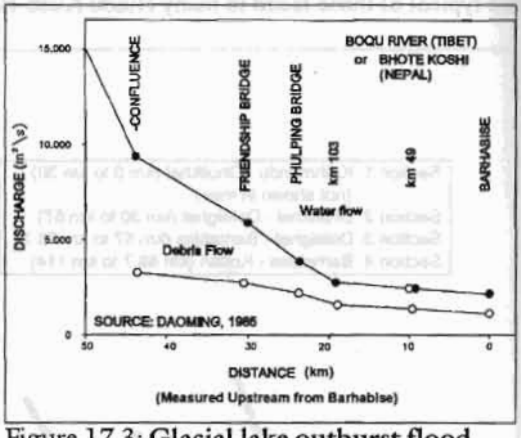

Figure 17.3: **Glacial lake outburst flood (GLOF) discharge attenuation along the Bhotekoshi River (1981)**

hundred human casualties and heavy loss of cattle, houses, and cultivated land were reported. A number of suspension bridges, and a substantial length of the Arniko Highway and Lamosangu-Jiri road were damaged or washed out.

The Landslides

Following the catastrophic cloudburst and subsequent debris flow along the Sunkoshi valley on June 30th to July 1st 1987, the Department of Roads (DoR), with assistance from the Swiss Development Co-operation (SDC), carried out a flood disaster appraisal along the most severely affected sector of the Arniko Highway with ITECO as its consultant. It was found that more than a quarter of the road between kms 62 and 87 had been either totally washed out or partially damaged. HMGN entered into an agreement with the International Development Agency (IDA) in 1989 to rehabilitate the same stretch under the Road Flood Rehabilitation Project (RFRP) in parallel with the Swiss funded DoR investigation of the slope conditions. The landslides were monitored by engineering geological and geophysical surveys, exploratory drilling, geotechnical testing, and piezometric monitoring under the Arniko Highway Rehabilitation Project. In turn RFRP carried out surveys, investigation, and design work in 1990, construction work in 1991 to 1993, and defect liability work in 1994.

Detailed description

Of the ten problematic sites included under the RFRP, seven had landslide problems. The landslides at km 69+000 (AH-1) and km 72+500 (AH-4) were chosen for this case study.

Landslide at km 69+000 (AH-1)

This landslide is located between km 68+900 and km 69+200 of the Arniko Highway. It faces southeast and is bounded by the Sunkoshi River at its toe, by a small torrent to the north, and by settlements on its western and southern sides. Figure 17.4 shows a plan of the landslide and Figure 17.5 an aerial view.

Before 1981, the landslide area was mostly occupied by paddy fields and grazing land. The slope was destabilised as a result of toe erosion caused by the 1981 GLOF, which destroyed a section of the road. In an emergency operation, the Royal Nepalese Army constructed bank protection works and shifted the road alignment. The landslide was reactivated as a result of bank erosion caused by the flood of June/July 1987. The flood caused bank erosion along a substantial length of the road from km 68+500 to km 69+200. Marginally stable hill slopes were destabilised by the progressive development of this landslide.

After the 1987 flood, the landslide was monitored and stabilised through extensive drainage works, bioengineering, and a few structural measures. The initial development of the landslide had been rotational, which was followed by a series of slumps, tension cracks, and translational slips. Though the reactivated depth of the slide was shallow, there was a potential for a deep-seated failure.

The landslide area was made up of colluvial material with a sandy-silty matrix with isolated boulders of up to 4m across. The colluvial slope extended from the Sunkoshi River bank to 600m above it. The landslide involved more than 100,000 m^3 of colluvial material. It covered an area of 300m along and 400m above the road and was destabilising paddy fields, dry crops, and settlements. Minor symptoms of instability and tension cracks extended a further 200m.

The reactivation of the landslide in 1987 created havoc in nearby settlements. People had to abandon valuable cultivation land and started to move their houses to safer locations. A 132 kV electric pylon was destroyed. From 1987-1990 landslide activity, characterised by minor slumps, slips, and creeping of soil mass, was moderate.

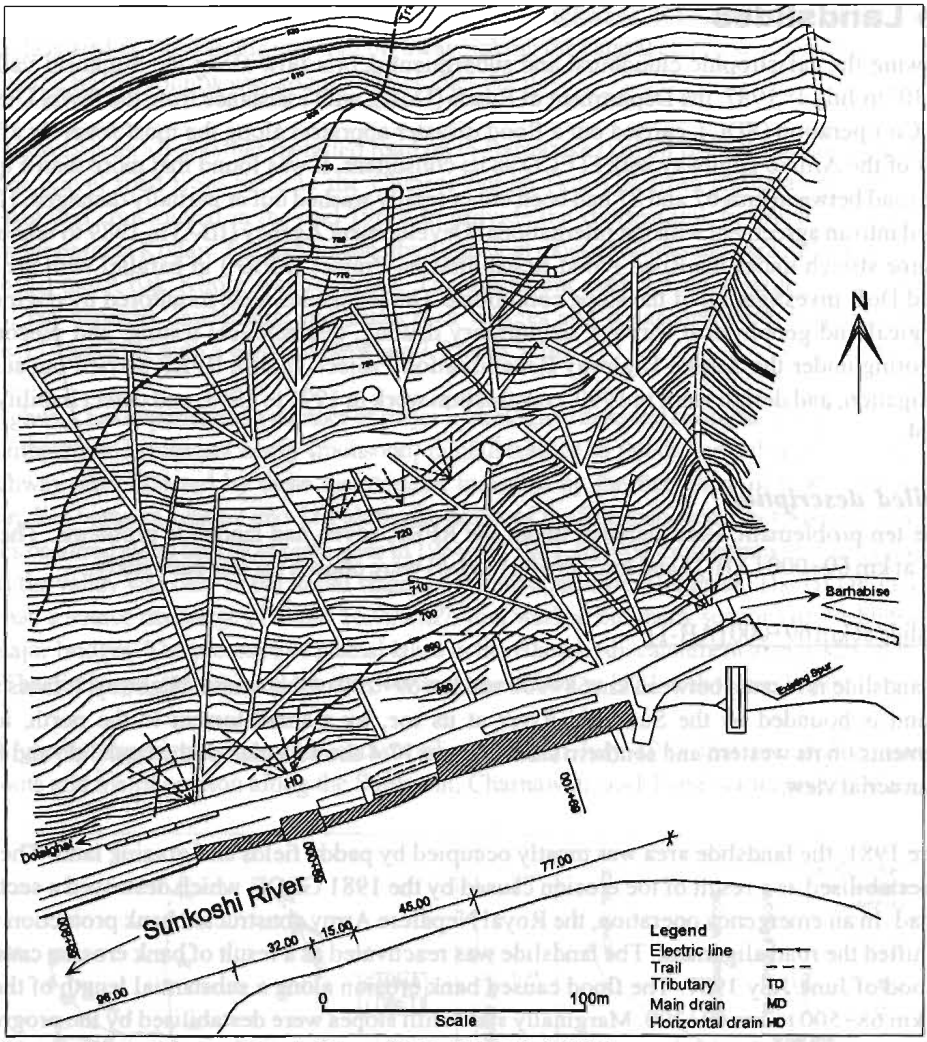

Figure 17.4: **Plan of landslide AH-1 (RFRP 1990)**

The main triggering factor responsible for the sliding was the bank erosion of the Sunkoshi River. The propagation of the landslide from the riverbank to 400m above the road is attributed to the saturation and high ground water table, which was re-charged by the irrigated paddy fields above and within the unstable area. Photographs taken from a helicopter illustrate the extent of the landslide (Figure 17.5).

Landslide at km 72+500 (AH-4)

Landslide AH-4 was located at km 72+600 of the Arniko Highway near Balephi village. The landslide area was bounded by the Sunkoshi River to the east, Balephi village to the west and south, and a small torrent to the north. The landslide faced due south-east. Figure 17.6 shows the plan of the landslide and Figure 17.7 an aerial view taken from a helicopter.

The massive GLOF of 1981 had extensively eroded the Sunkoshi River bank at this site and destroyed a portion of the road. In an attempt to reopen the road, the alignment had been shifted

Figure 17.5: **Aerial photograph of landslide AH-1**

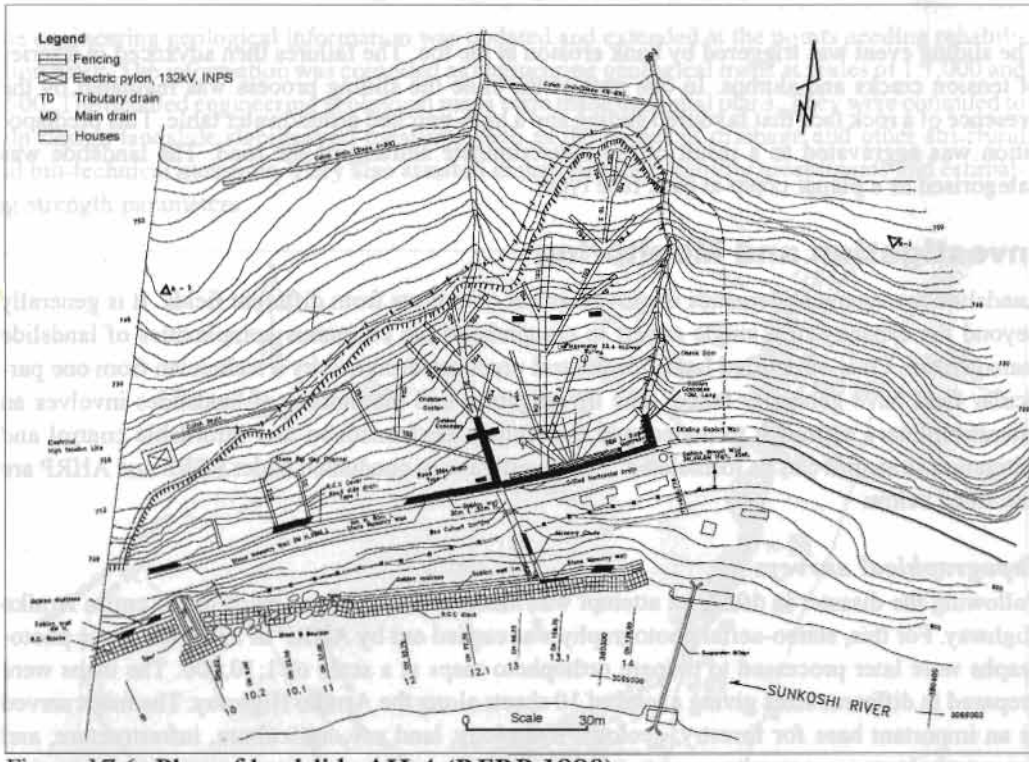

Figure 17.6: **Plan of landslide AH-4 (RFRP 1990)**

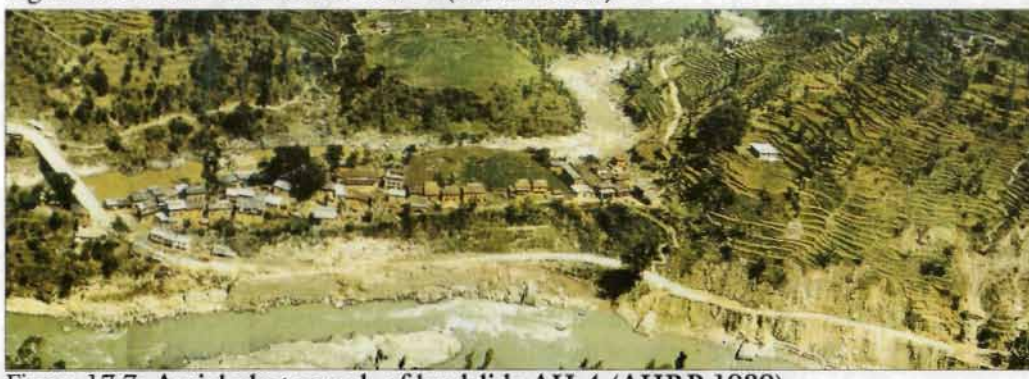

Figure 17.7: **Aerial photograph of landslide AH-4 (AHRP 1989)**

towards the hillside. However, this destabilised the fragile colluvial slope. The flood event of July 1987 further jeopardised the stability of the slope. Emergency measures such as gabion walls and spurs were constructed in 1988. The landslide was studied by AHRP (1989) and during the RFRP design phase (1990). These studies provided the basis for designing and building mitigation measures, which were completed in 1994.

The landslide consisted of colluvial debris and gravels with a silty to clayey matrix. About 30,000 m^3 of material was involved. The landslide affected an area 150m along and 100m above the road and had destroyed a number of cultivated terraces. Some tension cracks were noted above the crest of the active part of the landslide. The growth of the landslide and bank erosion along the Sunkoshi River had led to the loss of at least two hectares of cultivated land and a few houses at Balephi. An electric pylon was also endangered. The landslide remained active from 1987 to 1989 and was still in a moderately active state during the initial stages of RFRP.

The sliding event was triggered by bank erosion at the toe. The failures then advanced in a series of tension cracks and slumps. In one part of the slide the sliding process was regulated by the presence of a rock face that favoured sliding and a high-perched groundwater table. This predisposition was aggravated as a result of the indiscriminate shifting of the road. The landslide was categorised as a planar creep at rock face type.

Investigation and Monitoring

Landslide management demands the involvement of experts from different fields. It is generally beyond the capacity of a single expert to comprehend the enormous complexities of landslide management. Over-simplified landslide control practices designed by a technician from one particular field have generally failed. The investigation and monitoring of landslides involves an interdisciplinary approach to understand the sliding mechanism so that affordable control and mitigation strategies can be formulated. The investigations conducted under RFRP and AHRP are described below.

Topographical surveys

Following the disaster in 1987, an attempt was made to prepare base maps of the entire Arniko Highway. For this, stereo-aerial photography was carried out by AHRP in 1989, and these photographs were later processed to prepare orthophoto maps at a scale of 1:10,000. The maps were prepared in different sizes giving a total of 10 sheets along the Arniko Highway. The maps served as an important base for forestry, geology, hydrology, land use, agriculture, infrastructure, and geomorphology assessments.

Photographs taken from a helicopter were joined together to give a panoramic view of the road. A precise traverse survey was made from Dhulikhel (km 30 from Kathmandu) to Kodari (km 114) with connection to neighbouring geodetic control points along the highway, to serve as a baseline traverse for subsequent road management interventions.

A detailed topographical survey was carried out for the sections of the landslides intended for rehabilitation or mitigation (Figures 17.4 and 17.6). This survey was connected to the baseline traverse. The topographical survey marked tension cracks, big boulders, property lines, springs, creeks, gullies, banks, the road and related structures, prominent trees, electric pylons, houses, drains, and public utilities. The extent of the detailed surveys is shown in Table 17.1.

Table 17.1: **Extent of the surveys for the two case study landslides**				
Landslide	Area covered	Contour interval	Scale of plan	Scale of sections
AH-1	600 x 400	2m	1:1000	1:500 / 1:200
AH-4	600 x 200	2m	1:500	1:500 / 1:200

Engineering geological survey

In 1989, an engineering geological survey of the road corridor between Dhulikhel (km 30) and Kodari (km 114) was conducted as part of the AHRP over the strip out to 50m either side of the road. The survey line was connected to a baseline, which was extended through a compass traverse. The maps included information on rock and soil type, land use, slides, banks, water line, erosion features, exploration pits, bore holes, tension cracks, settlements, slope indicators, and rock structures at a scale of 1:5,000. The engineering geological maps of sites AH-1 and AH-4 are presented in Figures 17.8 and 17.9.

The engineering geological information was updated and extended at the points needing rehabilitation work. The information was compiled as engineering geological maps at scales of 1:1,000 and 1:500. The detailed engineering geological maps were made as spatial plans. They were compiled to help design landslide stabilisation measures such as the layout of drainage and other structural and bio-technical measures. They also assisted in making slope stability assessments and estimating strength parameters.

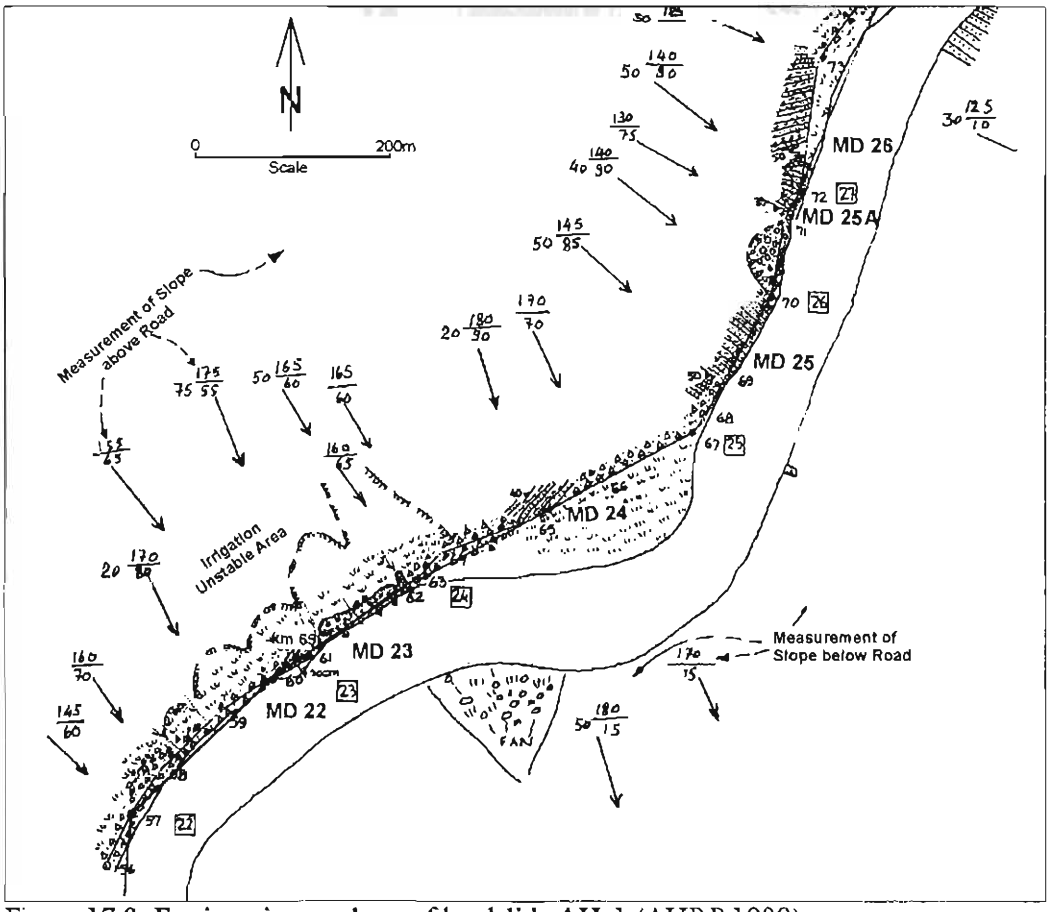

Figure 17.8: **Engineering geology of landslide AH-1** (AHRP 1989)

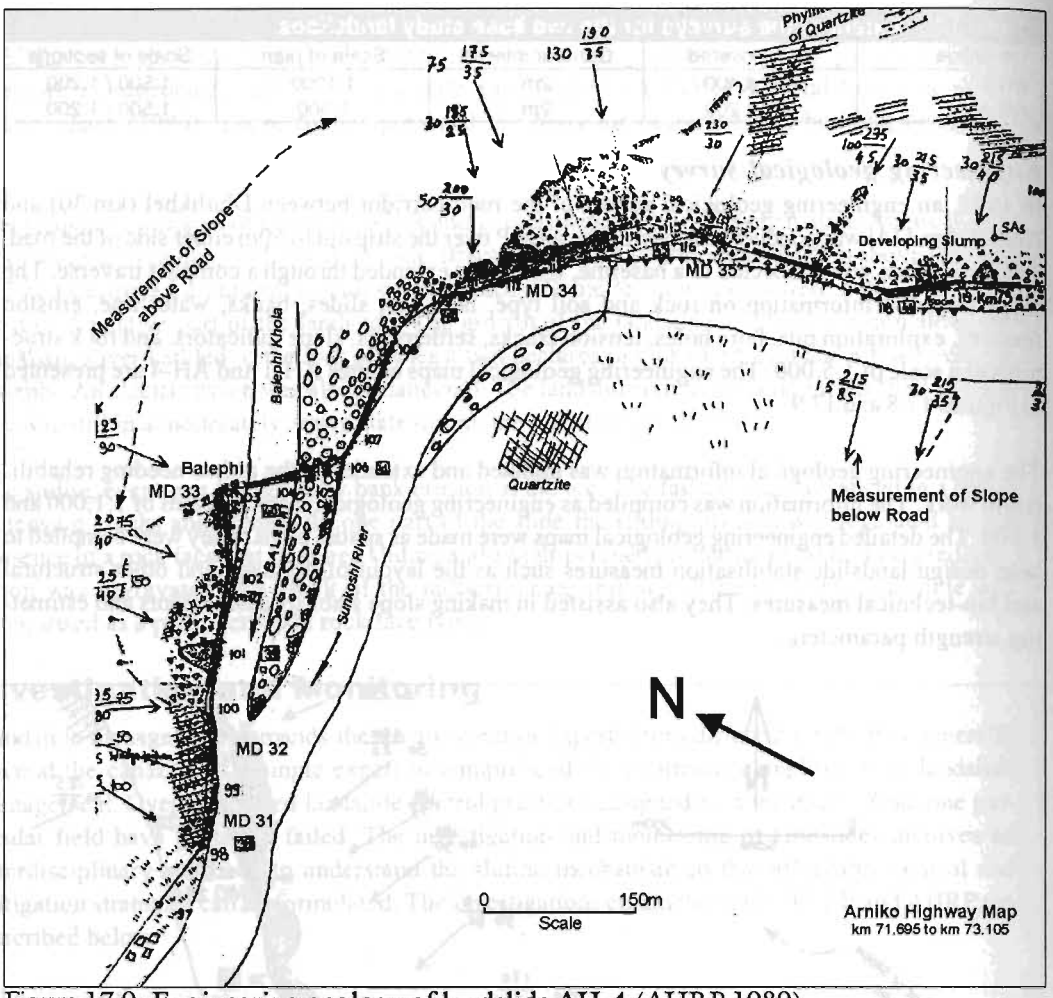

Figure 17.9: Engineering geology of landslide AH-4 (AHRP 1989)

Geophysical investigation

Sub-surface explorations are imperative to understand the mechanism of a landslide. Exploration depths of 20-25m are generally sufficient, but depths of up to 60m are needed for major landslides with deep-seated failures. The geophysical investigation of landslides involves making electrical resistivity profiles and using seismic refraction. A combination of these two approaches has been found to give a reasonable basis for interpretations of sub-surface conditions. The seismic reflection method has been used recently to explore to greater depths with a better level of confidence.

Geophysical investigations were carried out for most of the medium-sized and major landslides along the Arniko Highway. The findings were calibrated using engineering geological and exploratory drillings. The finely interpreted rock and soil strata were used for slope stability analysis. The geophysical sections of landslides AH-1 and AH-4 are presented in Figures 17.10 and Figure 17.11.

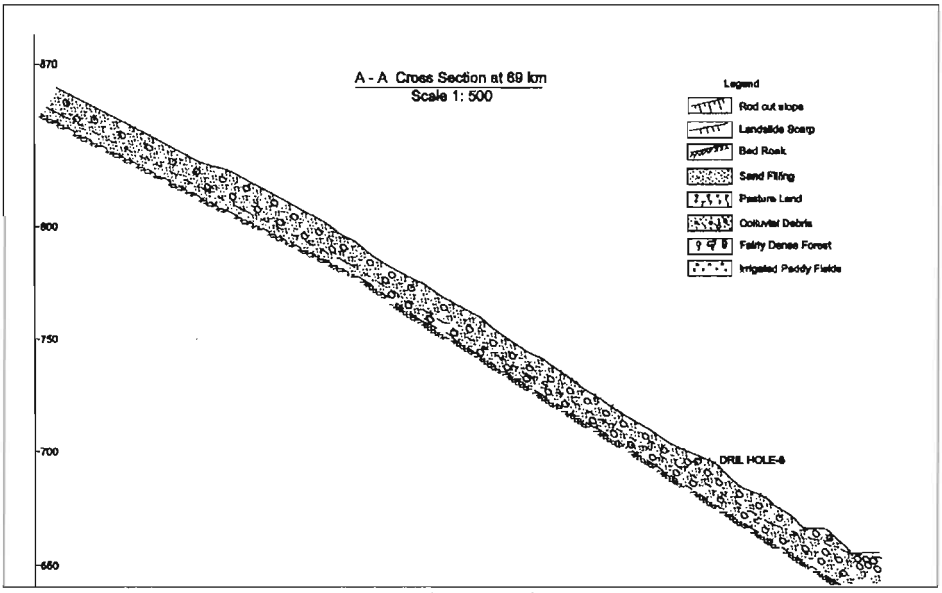

Figure 17.10: **Geophysical section of landslide AH-1** (AHRP 1989)

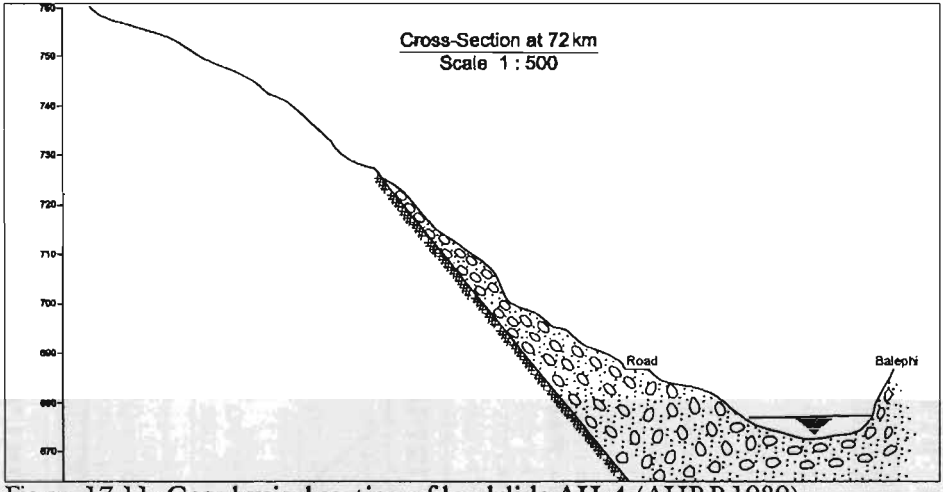

Figure 17.11: **Geophysical section of landslide AH-4** (AHRP 1989)

In 1989 bore holes were drilled at all major landslides along the Arniko highway corridor. The bore logs proved very useful for slope stability assessments to interpret strength parameters, pore pressure ratios, and groundwater table levels. Additional tests, for example for permeability, grain-size analysis, and measurement of groundwater levels, were also undertaken. The bore-hole data for landslides AH-1 and AH-4 are presented in Figures 17.12 and 13.

Geo-technical investigations

Geo-technical investigations are essential to characterise in-situ soil and rock materials. The geotechnical investigations carried out at the landslides included digging test pits on the landslides to a depth of 1.5m. Soil samples were collected for laboratory analysis to determine the bulk density, moisture content, unit weight, and grain size distribution of the soil. Field determinations of permeability, SPT values, surface toughness, weathering grade, and friction angle were also

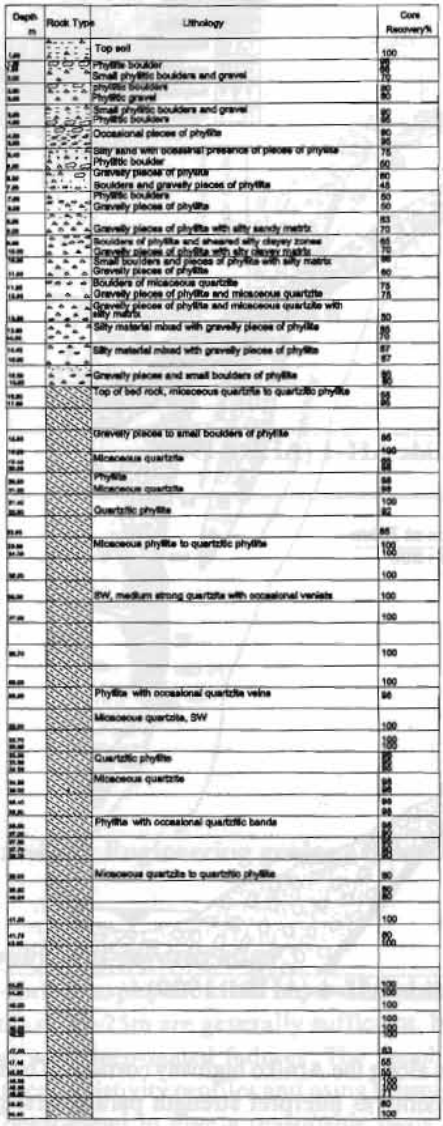

Figure 17.12: **Borehole log for landslide AH-1** (AHRP 1989)

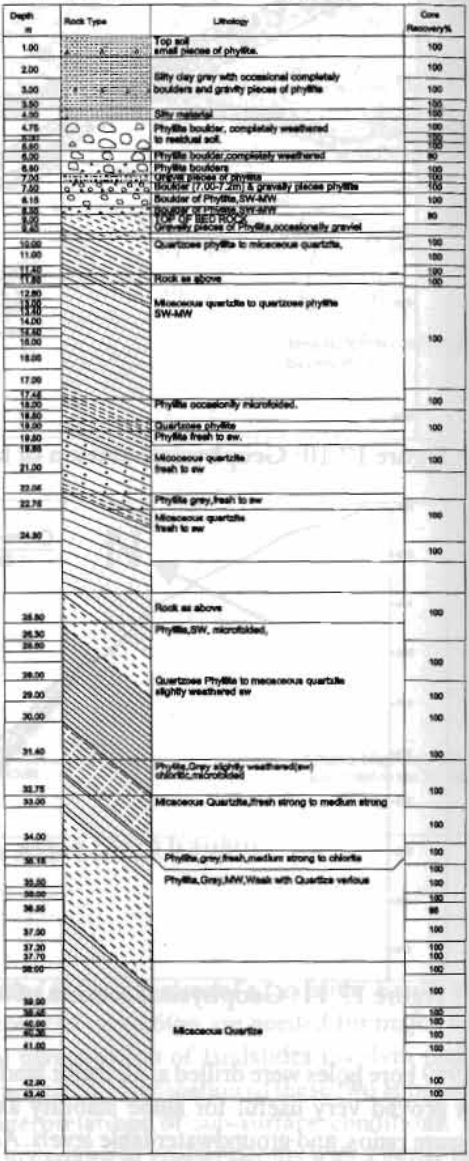

Figure 17.13: **Borehole log for landslide AH-4** (AHRP 1989)

carried out. Material samples were also collected from prospective quarry areas to determine their suitability for construction purposes as backfill.

The findings formed the basis for the computation, analysis, and design of landslide mitigation measures. These investigations were carried out at all major landslides. A summary of the findings is given in Table 17.2.

Table 17.2: **Summary of Geotechnical Test Results**

Position (km)	Natural moisture content (%)	Atterberg limits (%)	Unit weight (gm/cm^3)	Specific gravity and void ratio	Sieve analysis (%)	Hydrometer analysis (%)	Gradation ratios	Strength para-meters (kg/cm^2, deg)	Field Permeability (cm/s)
Landslide materials									
69	ω_n=11.1	LL=19	γ=2.053 γ_d=1.847		G=65 S=27.5 F=7.5	M=98.1 C=1.9	D10=0.07 C_u=200 C_c=1.02		k=0.0066
69	ω_n=17.5		γ=1.707 γ_d=1.452	G_s =2.63 e=0.811	G=58.5 S=35.1 F=6.4	M=96.8 C=3.2	D10=0.08 C_u=102.5 C_c=0.644	ϕ=32.5	k=0.0641
69	ω_n=17.7	LL=26 PL=19 PI=7	γ=1.748 γ_d=1.485 γ_s=2.085					C=0.05 ϕ=28.6	
69	ω_n=15.9		γ=1.943 γ_d=1.676						
70.2	ω_n=21.3	LL=24 PL=18 PI=6	γ=1.707 γ_d=1.407 γ_s=2.054	G_s =2.62 e=0.864	G=24.2 S=50.7 F=25.1	M=88.4 C=11.6	D10=0.03 C_u=10.6 C_c=0.487	ϕ=30.5	k=0.579
72	ω_n=13.1	LL=26 PL=20 PI=6	γ=1.511 γ_d=1.335 γ_s=1.787	G_s =2.61 e=0.954		M=97.7 C=2.3			k=0.239
72	ω_n=22.6	LL=25 PL=19 PI=6	γ=1.699 γ_d=1.385		G=80.0 S=17.8 F=2.2		D10=0.37 C_u=216.2 C_c=1.34		k=0.041
72.3								ϕ=35	k=0.011

Cont't ...

Table 17.2: **Summary of Geotechnical Test Results (cont'd)**

Position (km)	Natural moisture content (%)	Atterberg limits (%)	Unit weight (gm/cm³)	Specific gravity and void ratio	Sieve analysis (%)	Hydrometer analysis (%)	Gradation ratios	Strength para-meters (kg/cm², deg)	Field Permeability (cm/s)
72.3		LL=23 PL=19 PI=4			G=55.0 S=36.6 F=8.4	M=94.1 C=5.9	D10=0.07 C_u=71.4 C_c=0.686		k=0.077
72.3				G_s =2.60	G=74.9 S=20.9 F=4.2		D10=0.14 C_u=72.1 C_c=7.701	ϕ=36.5	
72.3	ω_n=13.2	LL=28 PL=21 PI=7	γ=2.011 γ_d=1.776 γ_s=2.177			M=98.7 C=1.3			
Backfill materials									
62.3			γ_m=2.153 OMC=6.4		G=78.2 S=21.8 F=0		D10=0.25 C_u=96 C_c=5.226	C=0 ϕ=29	
66.3			γ_m=2.153 OMC=6.4		G=68.8 S=21.1 F=10.1		D10=0.06 C_u=301.5 C_c=3.341	C=0 ϕ=33.2	

Legends

ω_n = natural moisture content (%)
LL = liquid limit (%)
PL = plastic limit (%)
PI = plasticity index (%)
γ = field density (gm/cm³)
γ_d = dry unit weight (gm/cm³)
γ_s = saturated unit weight (gm/cm³)

G_s = specific gravity
e = void ratio
G = gravel (%)
S = sand (%)
F = fines (%)
M = silt (%)
C = clay (%)

D10 = sieve passing 10% material
C_u = coefficient of uniformity
C_c = coefficient of convergence
C = cohesion (kg/cm²)
ϕ = friction angle (deg)
k = permeability (cm/s)
γ_m = max. dry unit weight (gm/cm³)
OMC = optimum moisture content (%)

Hydrological investigations

Most of the disasters along the Arniko Highway have occurred as a result of GLOFs or periods of prolonged heavy rainfall. All available meteorological and hydrological data for the Sunkoshi catchment were therefore collected and analysed. The maps showing snow coverage, isohyetals, longitudinal profiles and bed slopes, the catchment area, and the locations of meteorological and hydrological stations are shown in Figures 17.14 to 17.18. The probability of major floods happening over return periods of from two to a hundred years were calculated for landslides AH-1 and AH-4. The probable flows for the project sites were computed by correlation with the gauging stations 610, 620, and 630 (Table 17.3).

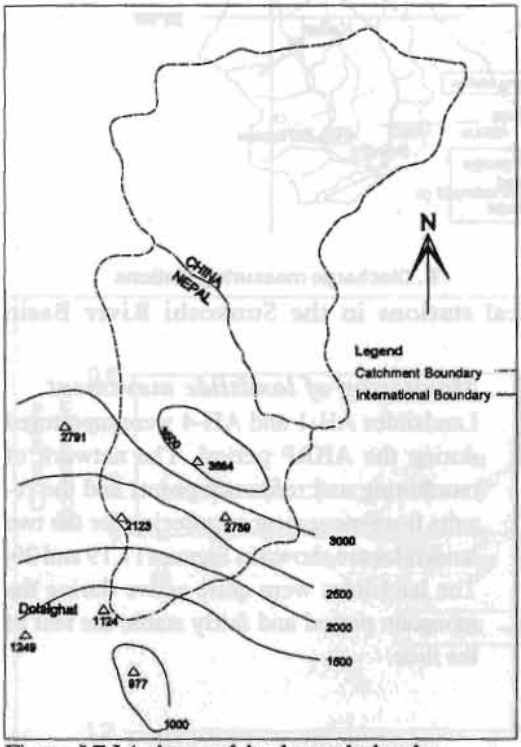

Figure 17.14: Annual isohyetals in the Sunkoshi catchment area (RFRP 1990)

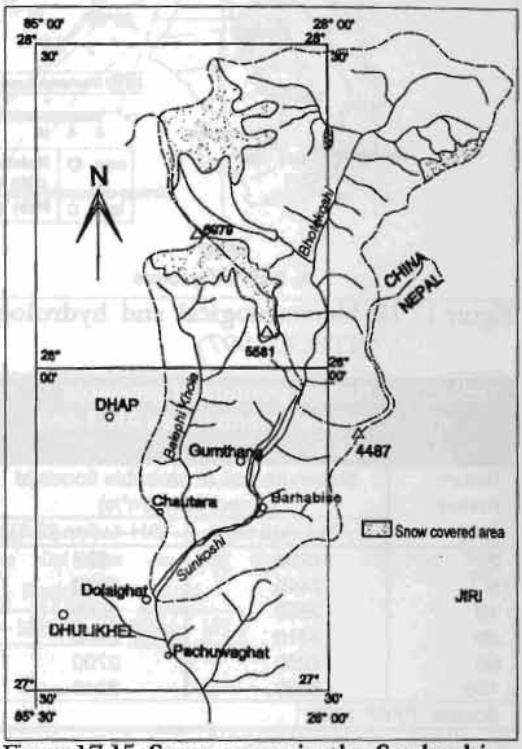

Figure 17.15: Snow cover in the Sunkoshi drainage basin (RFRP 1990)

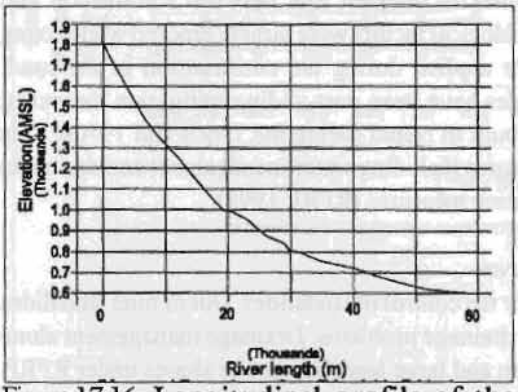

Figure 17.16: Longitudinal profile of the Sunkoshi River (ITECO 1997)

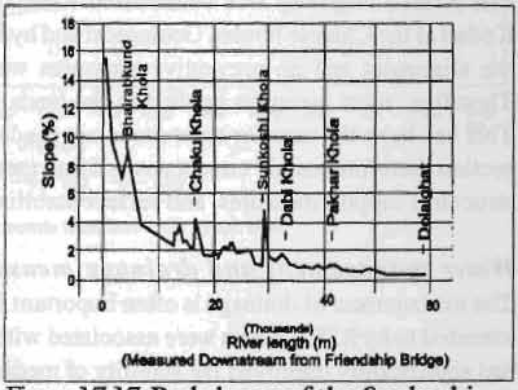

Figure 17.17: Bed slopes of the Sunkoshi River (ITECO 1997)

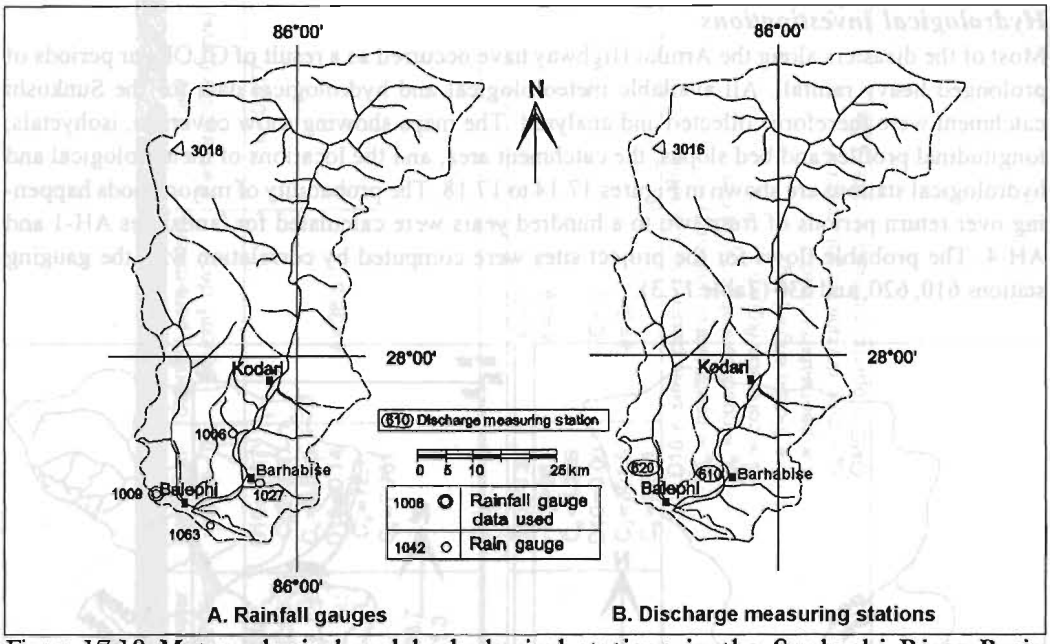

Figure 17.18: Meteorological and hydrological stations in the Sunkoshi River Basin (ITECO 1997)

Table 17.3: **Return periods of probable floods at landslides AH-1 and AH-4**

Return Period (yrs)	Maximum size of probable floods at project sites (m^3/s)	
	AH-1 (km 69)	AH-4 (km 72.5)
2	1250	923
5	2440	1930
10	2850	2260
20	3310	2400
50	4230	2700
100	5000	3340

Source: RFRP 1990

Monitoring of landslide movement

Landslides AH-1 and AH-4 were monitored during the AHRP period. The network of monitoring and reference points and the results from movement monitoring for the two landslides are shown in Figures 17.19 and 20. The landslides were quite active during the monsoon period and fairly stable the rest of the time.

Prevention, Control and Stabilisation Measures

The Arniko Highway was constructed to establish the shortest link between Kathmandu and Kodari at the Chinese border. Geological and hydrological factors were largely ignored while fixing the alignment and no preventive measures were applied during the construction of the road. Therefore, most measures applied to the landslides have been post-sliding mitigation measures. This has been the case for most mountain roads built in Nepal during the 1960s and 1970s. This section therefore mainly covers post-sliding measures including water management and drainage, structural support measures, and surface stabilisation measures (RFRP 1993)

Water management and drainage measures

The management of drainage is often important for the control of landslides. Out of nine landslides attended to by RFRP, seven were associated with drainage problems. Drainage management alone has significantly improved the stability of medium and large landslide-prone slopes under RFRP. Figure 17.21 shows diagrams of some typical drainage measures.

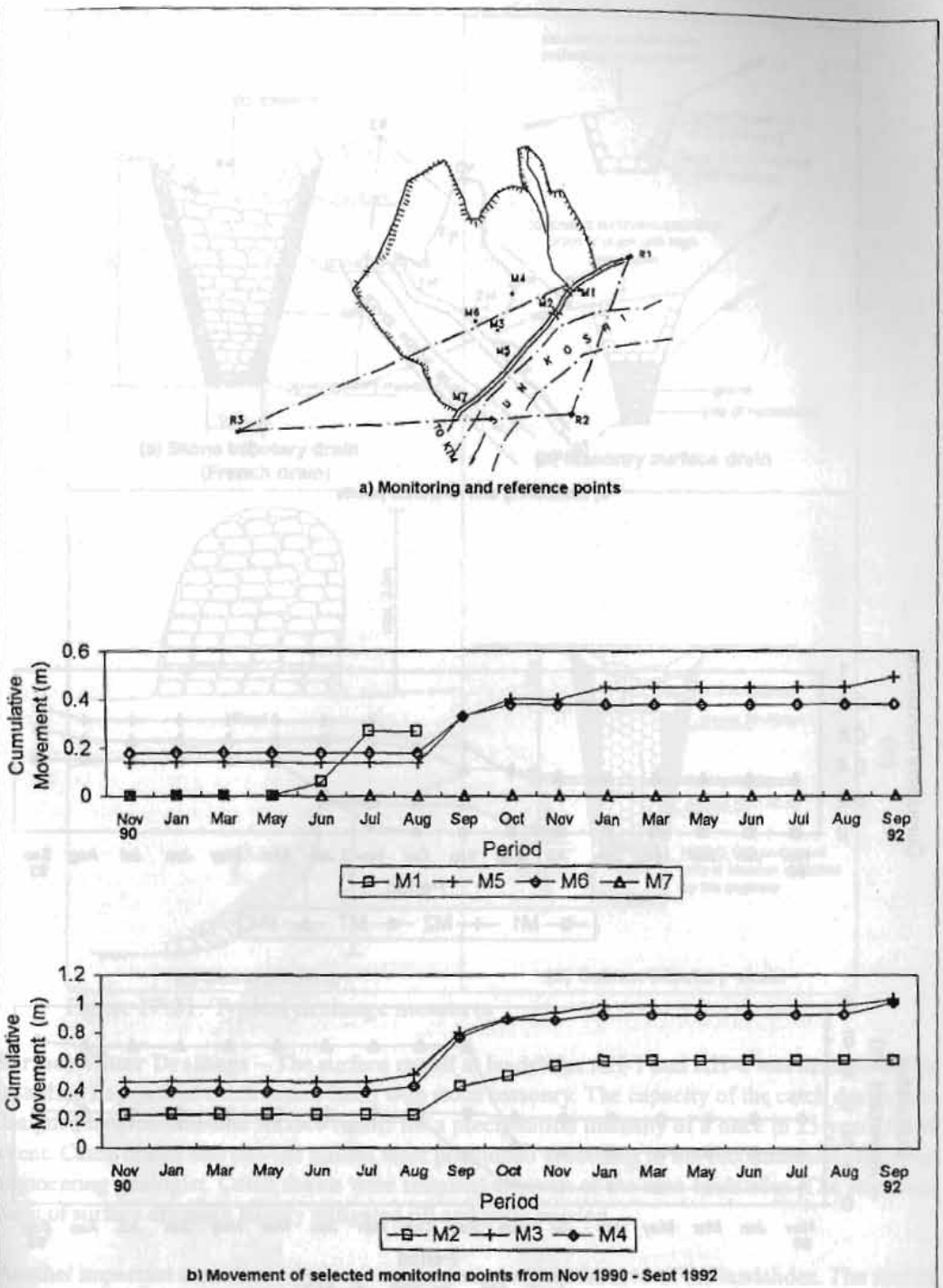

a) Monitoring and reference points

b) Movement of selected monitoring points from Nov 1990 - Sept 1992

Figure 17.19: Landslide movement monitoring at landslide AH-1 (AHRP 1990)

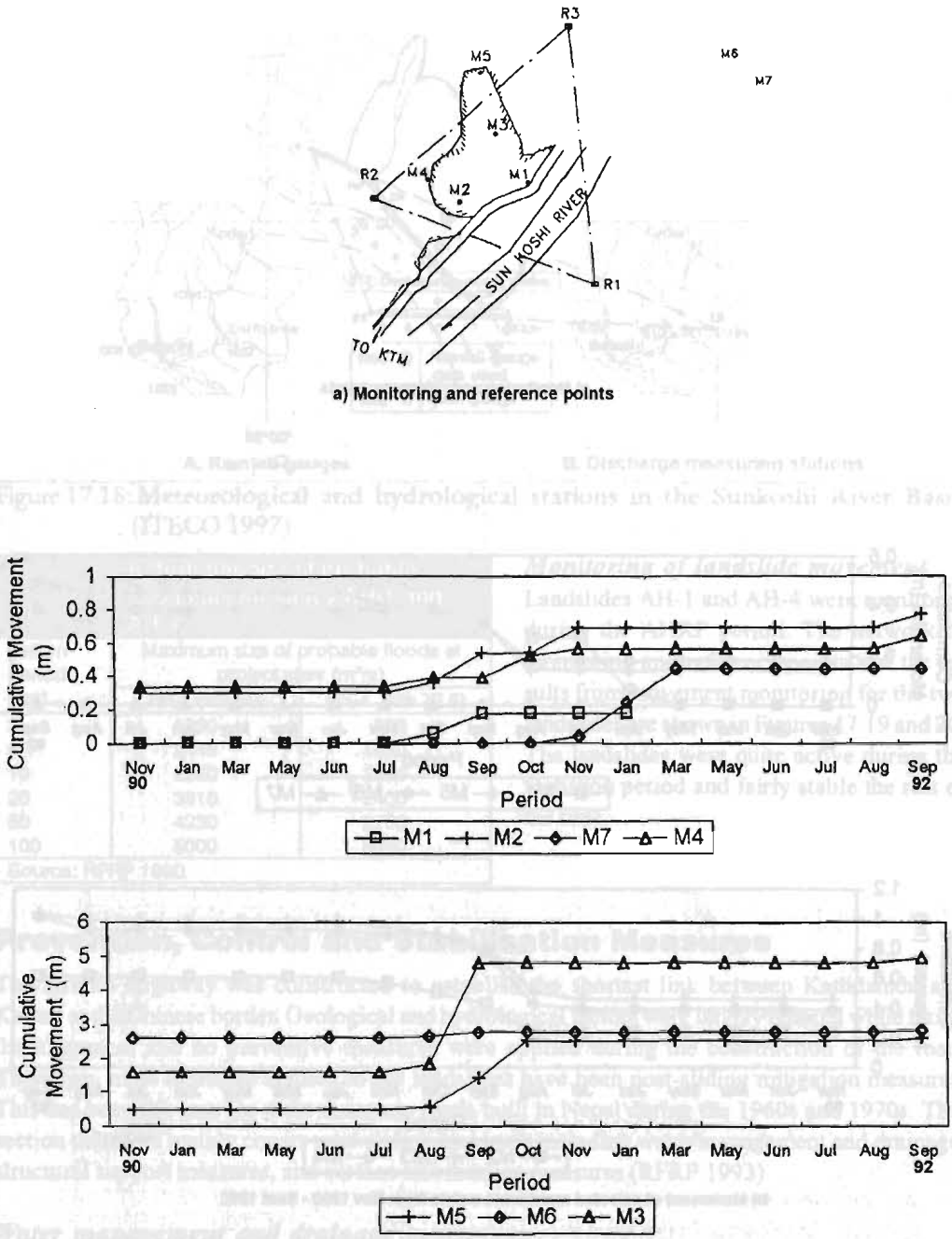

Figure 17.20: **Landslide movement monitoring at landslide AH-4** (AHRP 1990)

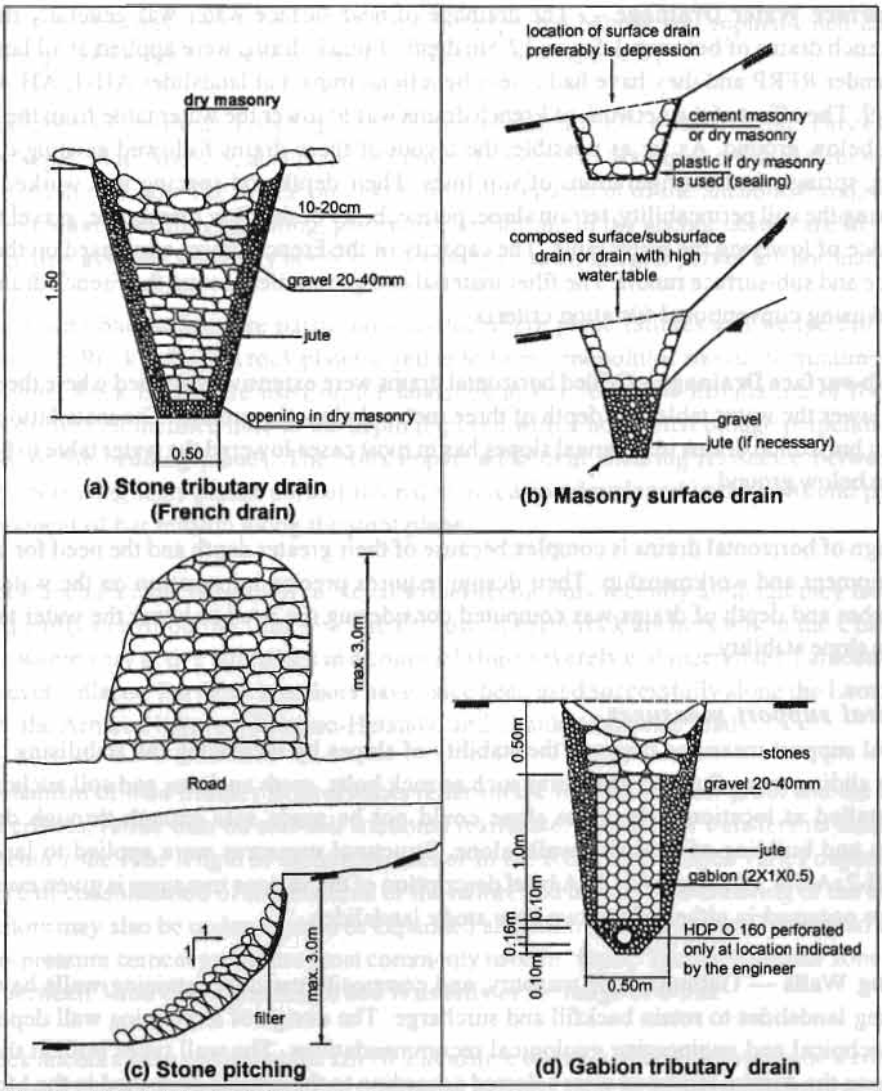

Figure 17.21: Typical drainage measures

Surface Water Drainage – The surface runoff at landslides AH-1 and AH-4 was drained off by installing trapezoidal catch drains lined with stone masonry. The capacity of the catch drains was designed to accommodate surface runoff for a precipitation intensity of a once in 25 years flood event. Catch drains and out-fall gullies were positioned according to the recommendations of an engineering geologist. Catch drains were installed at seven of the nine landslides. The improvement of surface drainage largely mitigated rill and gully erosion.

Another important aspect was drainage management within the area of the landslides. The size of the landslides ranged from between one and ten hectares. The corresponding surface runoff within the landslides was up to 1 m^3/sec. To manage this level of surface runoff safely, a network of riprap channels was constructed. The installation of cascading lined catch drains, to deal with surface runoff was not usually appropriate due to the continued movement within most of the landslides. The riprap channels were aligned and constructed along existing rills, gullies, depressions, and watercourses to harmonise with the micro-hydrology within the landslide.

Near-Surface Water Drainage — The drainage of near surface water was generally managed using French drains of between 1.5m and 2.5m depth. French drains were applied at all landslides treated under RFRP and they have had a very beneficial impact at landslides AH-1, AH-4, AH-8 and AH-9. The effect of the network of French drains was to lower the water table from the surface to 1-2m below ground. As far as possible, the layout of these drains followed existing drainage channels, springs, and configurations of slip lines. Their depth and spacing was worked out by considering the soil permeability, terrain slope, permeability of the filter membrane, gravel fill, and importance of lowering the water table. The capacity of the French drains was based on the levels of surface and sub-surface runoff. The filter material and geotextiles around the French drains were designed using conventional filtration criteria.

Deep Sub-surface Drainage – Drilled horizontal drains were extensively applied where there was a need to lower the water table to a depth of three metres below the ground. The installation of 15-20m long horizontal drains in colluvial slopes has in most cases lowered the water table to between 4 and 6m below ground.

The design of horizontal drains is complex because of their greater depth and the need for specialised equipment and workmanship. Their design requires precise information on the water table. The number and depth of drains was computed considering the need to lower the water table for optimum slope stability.

Structural support measures

Structural support measures improve the stability of slopes by increasing the stabilising component of a sliding mass. Support structures such as rock bolts, earth anchors, and soil anchors have been installed at locations where the slope could not be made safe enough through drainage measures and building of retaining walls alone. Structural measures were applied to landslides AH1, AH-2, AH-4, AH-5 and AH-8. A brief description of the various measures is given even when they were not used in either of the two case study landslides.

Retaining Walls — Gabion, stone masonry, and composite masonry retaining walls have been built along landslides to retain backfill and surcharge. The design of a retaining wall depends on the geotechnical and engineering geological recommendations. The wall types built at the landslides along the Arniko Highway were selected according to the criteria described in the Mountain Risk Engineering Handbook (Deoja et al. 1991). Gabion walls were designed according to the guidelines in Agostini et al. (1989). Most gabion walls used in the project were the rear-stepped type with front batters (inward inclination) of 1:10. Stone masonry was designed with different types of front batters according to site conditions.

Retaining walls were designed and constructed at sites AH-1, AH-4, AH-8, and AH-2 by calculating the selected safety factor against overturning, base sliding, structural adequacy and overall stability. Attention was also paid to providing adequate drainage to ensure the safety and economy of structures. The LARIS-SM and RETAIN computer software were used whilst designing the walls.

Anchored Structures – Some of the instabilities identified by RFRP could not be stabilised using conventional stabilisation measures. Examples were the landslides at km 70.2, 73.5, and 81.8 (but not AH-1 or AH-4). These landslides were stabilised using anchored structures and rock dowels (RCC panels or RCC slices-cum-gabion walls and passive anchors with bar tendons). Stabilisation

of some landslides was deemed too costly for the expected benefit and sophisticated measures were not proposed at such sites (e.g., the Kothe landslide at km 74.4).

The installation of in-situ anchors requires substantial skill and close supervision. This expertise exists in Nepal. With anchors, acceptance of the end product by testing is not sufficient to ensure the safety of the anchor. The whole process from the preparation of the anchors, through equipment preparation to drilling, grouting, placement, and fitting of the anchor needs careful supervision. A quality assurance strategy needs to be developed as an integral part of anchor installation.

Rock bolts with bar tendons are particularly useful where plane failures and wedge failures are likely to occur. Rock bolts join rock plates together to form a monolithic mosaic to minimise future rock failures. Rock bolts were used on the landslide at km 70.2. The installation of rock bolts includes drilling an inclined hole to the depth required with a horizontal plunge perpendicular to the strike of the bedding planes. The bolts impart additional shearing resistance between rock joints by increasing inter-planar normal force due to tension developed in the bolts and partly by the component of bar tension along the joint plane.

Earth/rock anchors have been used in Nepal's road sector only recently although they have been used frequently in hydropower tunnels. The first use of earth/rock anchors was in the Charnawati left bank where very active landslides in a colluvial slope severely endangered the Lamosangu-Jiri road at several places. Earth/rock anchors have since been used successfully along the Lamosangu-Jiri road, the Arniko Highway, Bhainse-Hetauda, and Thankot-Naubise roads.

The mechanism of load transfer from anchors relies on the bond at the soil-grout and the tendon-grout interfaces, rather than on soil-soil frictional resistance. The anchor transfers its tension to a fixed anchor zone. The length of earth/rock anchor in the fixed anchor zone varies depending on the degree of consolidation of soil material or the nature and degree of weathering of the bedrock. The anchors may also be under-reamed or expanded at the fixed anchor zone. Cylindrical anchors with non-pressure cement grouts are most commonly used in Nepal. The fixed anchor zone in rock may be between 3 and 6m, while that in soil is usually in the range of 6-9m.

Earth/rock anchors were applied at the km 70.2 landslide on the Arniko Highway to tie a composite retaining wall to weathered bed rock at a depth of 9-10m. Typical anchorage measures used for stabilisation of the landslide AH-2 are shown in Figure 17.22.

The most commonly used anchor tendons are continuously threaded MACALLOY or DYWIDAG anchor steel 32 mm ϕ with a minimum yield strength of 830–1030 N/mm^2. A working load of 250 kN on each anchor has been found suitable for the geotechnical conditions of landslides in the Sunkoshi Valley.

Surface treatment measures

The Arniko Highway corridor experiences heavy precipitation (>1,500 mm per year), which induces flash runoffs along the fragile slopes, creating rill, gully, splash, and sheet erosion. It was therefore necessary to design and apply surface protection measures on all natural and artificial bare slopes. Such measures consisted of bioengineering and skin protection measures. The long-term stability of the slopes in the landslides depends on the effectiveness of sub-surface drainage and bioengineering measures.

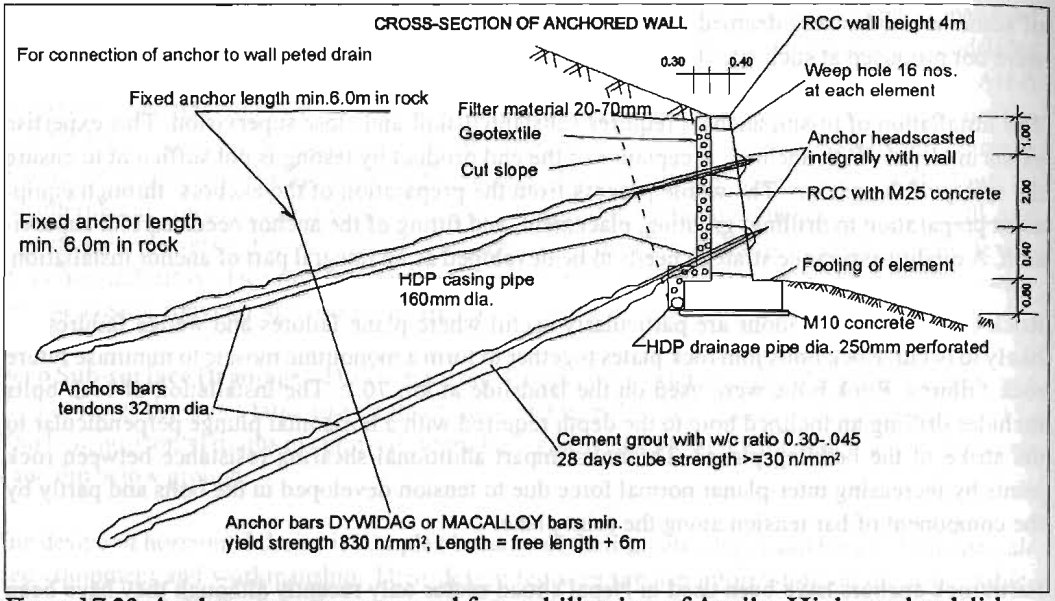

Figure 17.22: **Anchorage measures used for stabilisation of Arniko Highway landslide AH-2 (AHP 1997)**

Bioengineering — Bioengineering was used in RFRP to re-establish vegetation cover on bare landslides and artificial slopes and thus protect them against splash and sheet erosion. Bioengineering reduces rainfall erosion through intercepting rainfall and reducing evapotranspiration. However, these measures usually increase the infiltration rate and thus proper drainage of the root zone is essential. Plants increase the shearing resistance of soils at the root zone, but trees may increase the surcharge load and their presence can be counter-productive. The final choice of species was guided by both the need and the limited time available. The overall project duration was 18 months, which is generally insufficient for the successful application of bioengineering measures. Bioengineering is a long-term solution and relies for its success on repeat inputs and maintenance by the executing agency. The nine most common types of bioengineering measures are illustrated in Figure 17.23.

Both intensive and extensive treatments were applied for surface stabilisation.

Intensive treatment was applied generally on backfill slopes, spoil slopes towards the hillside of the road, and on most of the artificial slopes towards the valley side. The main emphasis was to establish a grass cover rapidly to protect the surface. The combinations of the following were used: terracing; mulching; planting grass; planting trees; stone arching; gabion-netting; edge rounding; spreading top soil; reseeding; and other complementary measures such as palisades, live stakes, and hedge layers.

Extensive measures were applied on less critical and less degraded soil slopes. The measures consisted of planting grass and trees, reseeding grass at lower densities, and making brushwood check dams.

The grass and tree species used for bioengineering were as follow.

- Tree species – utis (*Alnus nepalensis*), salix (*Salix tetrasperma*), poplar, sissoo (*Dalbergia sissoo*), kavro (*Ficus lacor*), khirro (*Sepium insegne*), simali (*Vitex negundo*), badahar (*Artocarpus lakoocha*)

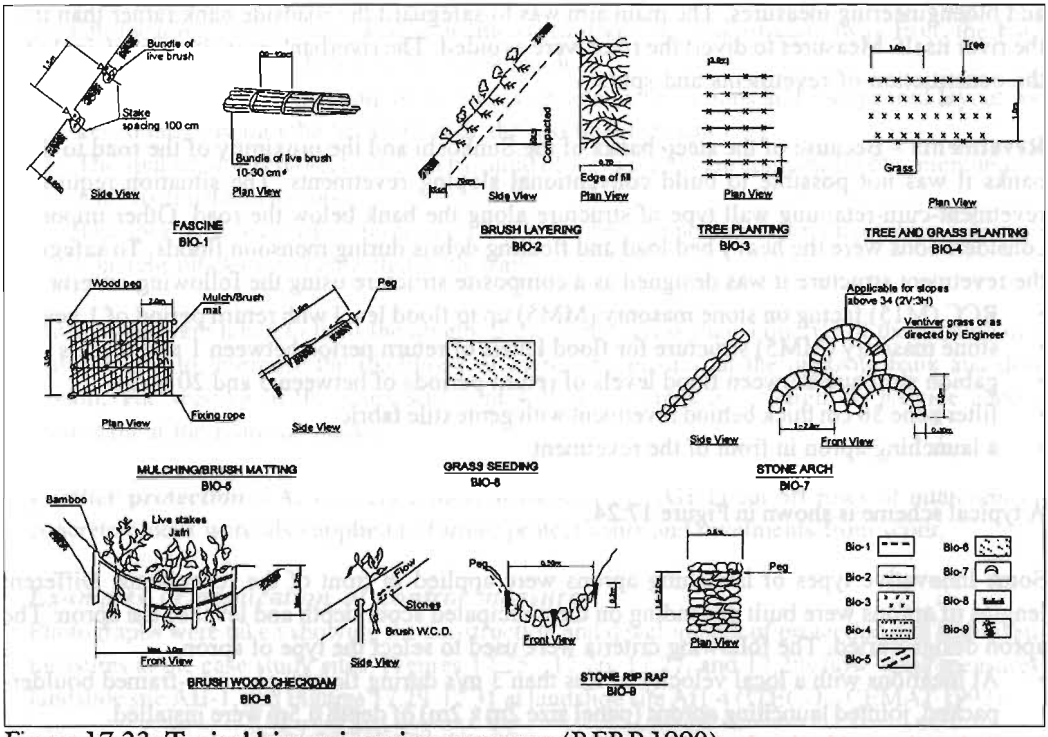

Figure 17.23: **Typical bioengineering measures** (RFRP 1990)

- Grass species – vetiver (*Vetiver zizanioides*), rye grass, paspalum, khar (*Cymbopogon microtheca*), kikiyu (*Pennisetum clandestinum*), kudzu (*Pueraria lobata*), clover (*Trifolium* spp.), Napier grass (*Pennisetum purpureum*)
- Mulch material - straw, banmara (*Eupatorium adenopherum*), titepati (*Artemesia vulgans*), and jute netting

Three nurseries were established along the road to produce tree seedlings, plants, and grass slips. Locally trained labourers were used to apply the bioengineering measures.

These bioengineering measures were the first to be applied along the Arniko highway corridor and there was little experience to build upon. Many of the plants did not establish well, but utis, sissoo, simali, vetiver grass, paspalum, and Napier grass all did well. The grass species kikiyu was highly successful at Charnawati at 1800m altitude but unsuccessful lower down at 600–1000m.

Stone Pitching — In addition to structural, drainage, and bioengineering measures, certain bare soil surfaces within landslides needed immediate surface strengthening to prevent sheet, rill, and gully erosion. In such areas, depending on the availability of supports, light superficial non-structural measures, such as thin gabion mattresses, stone pitching, stone arches, and riprap channels were applied. Such measures are cost effective and often unavoidable because bio-measures take a few years to establish. Such applications provide temporary surface protection, which are then reinforced by the bioengineering measures.

River training measures

The main triggering factor for the landslides was the flooding of the Sunkoshi River. Therefore stabilisation of the landslides required riverbank protection in addition to the drainage, structural,

and bioengineering measures. The main aim was to safeguard the roadside bank rather than train the river itself. Measures to divert the river were avoided. The riverbank protection work included the construction of revetments and spurs.

Revetments – Because of the steep banks of the Sunkoshi and the proximity of the road to these banks it was not possible to build conventional sloping revetments. The situation required a revetment-cum-retaining wall type of structure along the bank below the road. Other important considerations were the heavy bed load and floating debris during monsoon floods. To safeguard the revetment structure it was designed as a composite structure using the following criteria.

- RCC (M15) facing on stone masonry (MM5) up to flood level with return period of 1 year
- stone masonry (MM5) structure for flood levels of return period between 1 and 5 years
- gabion structure between flood levels of return periods of between 5 and 20 years
- filter zone 30 cm thick behind revetment with geotextile fabric
- a launching apron in front of the revetment

A typical scheme is shown in Figure 17.24.

Some innovative types of launching aprons were applied in front of the revetments. Different lengths of aprons were built depending on the anticipated scour depth and level of the apron. The apron design varied. The following criteria were used to select the type of apron.

- At locations with a local velocity of less than 3 m/s during floods, concrete-framed boulder-packed, jointed launching aprons (panel size 2m x 2m) of depth 0.5m were installed.
- At locations with a local speed between 3 and 6 m/s during floods, interconnected 1.5 x 1.5 x 1m concrete blocks tied both ways with 16 mm cable were used.
- At locations with an abundance of boulders and a local speed between 3 and 6 m/s during floods, interconnected armoured boulders (size >1m) were used.

Spurs – Along certain stretches of the banks of the Sunkoshi, such as at AH-1 and AH-4, the banks were highly vulnerable and revetments alone could not ensure safety of the roadside bank.

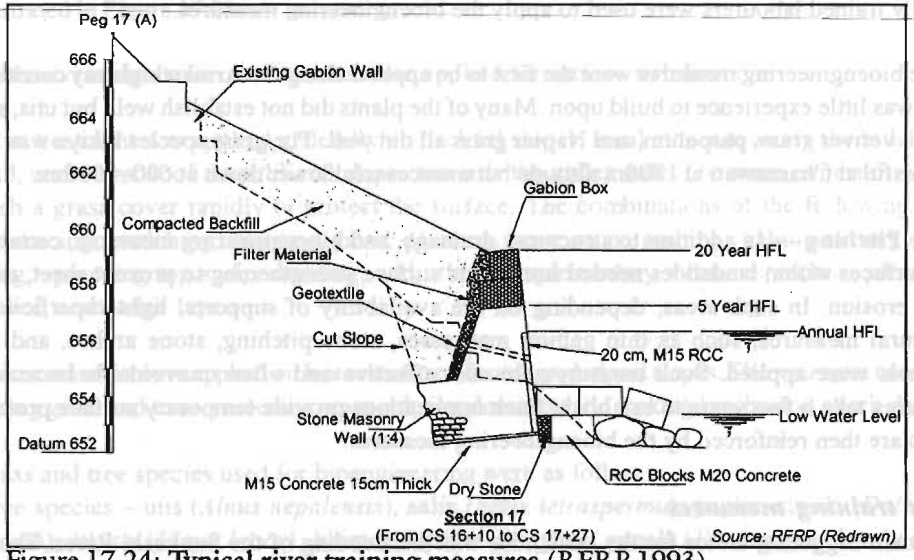

Figure 17.24: Typical river training measures (RFRP 1993)

In such locations, short spurs were constructed to divert the mainstream away from the banks. Composite spurs were installed as described below.

- The main body was made up of gabions with adequate sections and a staggered layout well-keyed laterally into the bank or inside the revetment structure.
- The spur head was protected with a pyramid of 1.5m x 1.5 x 1m concrete blocks interconnected with 16 mm diameter rope.
- The spur head was further protected from scour by a launching apron on all three sides using concrete blocks interconnected both ways.

Precautions were taken to limit the length of the spurs to less than a quarter of the breadth of the water course to minimise the likelihood of increasing erosion at the opposite bank and downstream. The spacing of the spurs was kept within 2.5 times their length to provide adequate protection at the roadside banks.

Further protection – At severely critical stretches (e.g., AH-1) cut off rows of interconnected concrete blocks were also applied to further protect spurs and revetments from scour.

Examples of application of control measures

Photographs were taken showing the construction and development of protection and stabilisation measures at the case study sites. Figures 17.25, 17.26, 17.27, and 17.28s how some measures at landslide site AH-1, and Figures 17.29-17.31 at landslide site AH-4 (ITECO – CEMAT 1992).

Figure 17.25: **Landslide AH-1: a complex network of landslide drainage**

Figure 17.26: **Landslide AH-1: an anchored gabion-retaining structure**

Figure 17.27: **Landslide AH-1: a revetment wall is being constructed with a concrete framed apron**

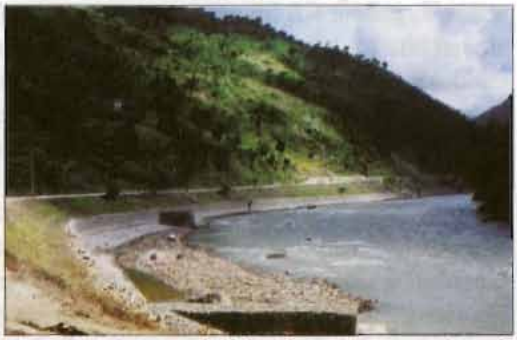

Figure 17.28: **Landslide AH-1: completed bank protection works**

Figure 17.29: **Landslide AH-4: landslide drainage and bank protection upstream from the landslide**

Figure 17.30: **Landslide AH-4: construction of revetment wall**

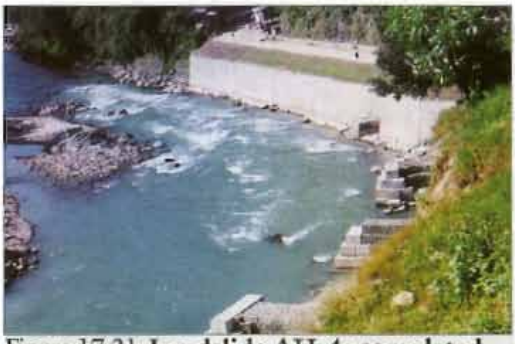

Figure 17.31: **Landslide AH-4: completed revetment wall**

Summary and Conclusions

Road planners, consultants and contractors in Nepal now realise the need for an interdisciplinary approach to investigating, designing, and building stabilisation and mitigation measures for landslides along highways. The necessary expertise includes engineering geology, hydrology, geophysics, geotechnics, highway engineering, bioengineering, river engineering, and soil engineering.

The drainage of landslides, through installing networks of surface, near surface, and deep horizontal drains, was used most in the RFRP. Structural measures were given second priority and only applied where drainage alone was considered insufficient to improve slope stability to an acceptable level of safety. Bioengineering measures were considered as essential components of all stabilisation systems and were applied to all landslides. These measures were highly successful on active and moderately active landslides. The performance of French drains and deep-drilled drains was satisfactory as shown by monitoring with piezometers.

The total cost of stabilisation and mitigation of the nine medium-size and medium complex landslides was about NR 37 million (approx. US$ 0.55 million). The average cost per landslide was around NR 4 million (US$ 60,000). This cost is comparable to the cost of maintaining a standby bulldozer for five years for emergency reopening of the road during the monsoon period. Proper stabilisation means improved serviceability of the road with far fewer blockages during the monsoon and alone justifies this expenditure. The methods of stabilisation described here appear to be practical and affordable.

The efficient management of these sites now relies on carrying out routine maintenance, but as yet no efficient and appropriate system for this has been developed. Efforts are being made by the Geo-environmental Unit of the DoR to prepare guidelines for installation of further bioengineering measures and maintenance of that already in place through community participation. In the absence of maintenance, the works at the landslides along the Arniko Highway have already started to degrade.

Lessons learned

Technical and other lessons learned from the planning, investigation, design, implementation, and maintenance of the mitigation measures under RFRP (ITECO –CEMAT, 1993) are summarised below.

- The project had to complete the design of rehabilitation measures along a 25 km stretch of road, including survey and all investigations, within four months. However, certain types of investigation require dry months while others must take place in the monsoon period. A period of six to eight months is needed to enable consultants to plan for and implement works during the most appropriate season.
- A large number of gabion structures lacking foundations and lateral embedment had been applied at most of the sites during the pre-project period (1987-1992). The inclusion of these would have weakened new structures. It is recommended that short-term measures should be limited to reopening roads by clearing the blockage. The use of massive spurs and revetments as emergency measures should be discouraged.
- Using Lacey's general scour equation and scour factors (Z-factors), the scour depth along several stretches of the Sunkoshi was found to be in the range of 6-8m. However, the practical limit for dewatering was found to be only 1.5m below low water level. The founding of structures below the scour depth is not viable in mountain rivers and the safety of bank structures depends on the construction of launching aprons.
- The specifications and items of bioengineering measures should be precisely given to allow contractors to carry out such work. Bioengineering measures are usually started after the completion of structures and drains. Unlike conventional structures, bioengineering measures need intensive maintenance over at least three years. One way of carrying this out is through the participation of local communities.
- The innovative idea of using inter-connected concrete blocks was unsuccessful at the most vulnerable location at Balephi (AH-4), where the blocks from the upper three layers of spur were washed out by a moderate flood of about a 10-year return period. This experience should be taken into account when building such structures at vulnerable locations.
- The deflection of gabion walls was excessive due to high flexibility. For future projects it is recommended that the front batters for rear stepped gabion walls should be in the range of 1:6 to 1:4 instead of 1:10.
- The main reason for the instability and damage at sites AH-1, AH-2, AH-5, AH-8, and AH-10 was insufficient drainage. This emphasises the importance of drainage for slope stability.
- Most of the landslides along the Arniko Highway are triggered by toe erosion and propagate a couple of hundred metres above the Sunkoshi riverbed. The Hazard Mitigation in Sunkoshi/ Bhotekoshi Water Catchment Areas (HMWA) project has substantiated this finding. Had the alignment of the Arniko Highway been at least 200m above the riverbed, most of the hazards related to the river would have been eliminated. This emphasises the need for proper selection of highway alignment along hazardous river valleys such as the Sunkoshi.

Mitigation planning

The experience of planning and implementing rehabilitation works for landslides along the Arniko Highway emphasises the need for an integrated approach to landslide hazard management and control. The problems encountered in the Sunkoshi valley are typical of those likely to be encountered in other areas of Nepal and the lessons learnt here can be applied overall. In addition to engineering approaches, social and environmental factors must be considered to make the work socially acceptable and long lasting. Landslide management should be a continuous process in geologically fragile and hazardous mountain regions like the Himalayas. Over-

simplified approaches to landslide control and management can lead to conflicts of interest with the local population.

Most of the landslides along the Arniko corridor were caused by hydrological, geo-hydrological and land use factors. More than two-thirds of the landslides were activated due to a lack of drainage. Pressure on marginal lands due to population explosion has further deteriorated slope stability.

The main recommendations for a more rational approach to landslide hazard management and control are as follow.

- Prepare an inventory of all glacial lakes within a catchment area and assess and monitor their condition
- Prepare 1:10,000 scale topographical, hazard and land use maps for all important river valleys that are susceptible to hydrological disasters
- Monitor landslides and potentially unstable areas to warn of impending dangers
- Incorporate risk engineering in civil engineering and geology courses
- Train engineers and geologists how to investigate landslides, and design stabilisation works
- Encourage participation of the local population in landslide stabilisation and bioengineering works
- Introduce legislation to limit the use of high hazard condition areas
- Carry out further research on landslide management
- Improve the level of disaster preparedness in sensitive corridors; emergency measures should be limited to the bare minimum necessary to reopen the infrastructure and should not be applied indiscriminately where long term definitive solutions are envisaged.
- Establish an institution to deal with landslide hazards management and mitigation works
- Equip executing agencies with modern and efficient techniques for slope stabilisation
- Establish regional information networks for landslide hazard management

It may be difficult for planners to implement this long list of activities; but, as suggested from the efficient operation of the Lamosangu-Jiri road where the above measures were largely taken, the extra costs can nearly always be justified.

References

Agostini, R.; Bissarri, A.; Masetti, M.; Papetti, A. (1989) *Flexible Gabions for River Training and Canalised Water Courses.* Bologna (Italy): Officine Maccaferri.

Arniko Highway Rehabilitation Project (AHRP) (1989) 'Engineering Report'. Kathmandu (Nepal): ITECO-Losinger JV (unpublished)

Arniko Highway Rehabilitation Project (AHRP) (1990) 'Landslide Movement Monitoring Report, Final Report'. Kathmandu (Nepal): ITECO Engineering Ltd. (unpublished)

Arniko Highway Rehabilitation Project (AHP), (1997) 'Phase II - Design Report, Main Report'. Kathmandu (Nepal): ITECO, CEMAT and GEOCE (unpublished)

Deoja, B.; Dhital, M.R.; Thapa, A.; Wagner, A. (eds) (1991) *Mountain Risk Engineering Handbook, Parts 1 and 2.* Kathmandu: ICIMOD

Nepal Switzerland Cooperation Project (1997) 'Hazard Mitigation in Northern Sunkoshi and Bhotekoshi Water Catchment Areas (HMWA), Final Report'. Kathmandu (Nepal): ITECO and ICIMOD (unpublished)

Road Flood Rehabilitation Project (RFRP) (1990) 'Design Report, Main Report'. Kathmandu (Nepal): ITECO Nepal and CEMAT Consultants (unpublished)

Road Flood Rehabilitation Project (RFRP) (1992) 'RFRP Progress Report 7'. Kathmandu (Nepal): ITECO Nepal and CEMAT Consultants (unpublished)

Road Flood Rehabilitation Project (RFRP), (1993) 'RFRP Project Completion Report'. Kathmandu (Nepal): ITECO Nepal and CEMAT Consultants (unpublished)

18 Debris Flow Control and Management: Case Studies from the Sichuan and Yunnan Provinces of China

Wu Jishan[1], Li Tianchi[2] and Yin Chongquing[3]
[1]Institute of Mountain Hazards and Environment, CAS, Chengdu, China
[2]ICIMOD, Kathmandu, Nepal
[3]Institute of Debris Flow Protection, Dongchuan, Yunnan, China

Debris flow hazards are quite common in the mountain areas of China. They often cause catastrophic destruction of infrastructure and personal property. Following 30 years' research and practical experience, debris flow control works have now been installed in many ravines. These have provided good economic, environmental, and social benefits.

This paper discusses two successful examples where the debris flow hazard to mountain roads and land has been reduced, the first in Heisha River, Xichang, Sichuan province and the second in Laogan Ravine, Dongchuan, Yunnan province, both in China. The debris flow control project along the Heisha River was successfully completed in 1978 with an investment of US$ 0.5 million. The Laogan Ravine project was completed in 1994 at a cost of US$ 0.17 million. There have been no debris flows in these ravines since the projects were completed.

These case studies show that measures to mitigate debris flow damage to linear infrastructures located in the deposition zone of debris flows should pay attention to controlling slope instabilities in the middle and upper reaches as well as to improving the environmental conditions in the catchment.

Introduction

Mountain areas cover two-thirds of China's land area. One-third of its population and about two-fifths of total cultivated land is found in these regions. The complex geological structure, intense ongoing tectonic and earthquake activities, and high monsoon precipitation make China one of the countries most susceptible to mountain hazards. Debris flows are one of the main types of hazard, and often have catastrophic consequences for mountain infrastructure and personal property. Due to their sudden occurrence, short duration, and strong destructive power, debris flows are a serious barrier to development and construction in mountain regions. There are more than 50,000 ravines in China's mountains that are prone to debris flows, and more than 8,500 of them pose severe risks to infrastructure.

Debris flow hazards are widespread over 31 provinces, autonomous regions, and municipalities. More than 900 counties and 150 cities, hundreds of factories and mine sites, 800 township sites, 36 railways, and half of all mountain highways are affected by debris flows. Every year, the direct economic losses due to debris flows amount to $US 18-25 million. Annually 250-500 people are killed and thousands injured. In addition, debris flows endanger farmlands, water conservation facilities, and rivers. Research on the origin of debris flows and hazard mitigation are of vital significance to China. Through over 30 years of research and practice, comprehensive mitigation measures have been successfully implemented in many ravines with serious debris flow problems. Debris flow control works along the Heisha River in Sichuan Province and the Laogan ravine in Yunnan Province (Figure 18.1) are two successful examples of using a multi-disciplinary integrated approach to mitigate hazards to mountain roads and farmland.

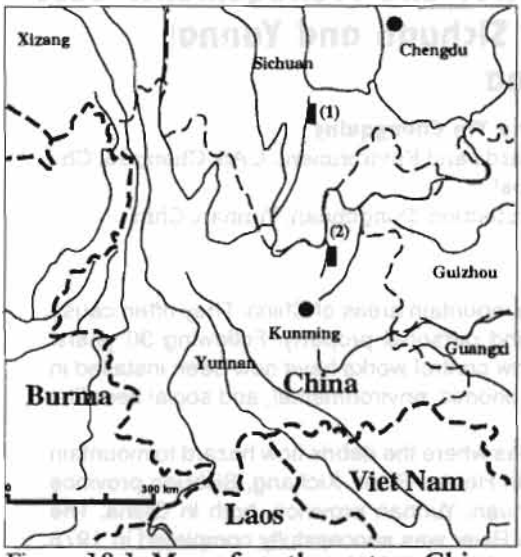

Figure 18.1: Map of south-western China showing location of (1) the Heisha River watershed and (2) the Laogan ravine watershed

Case Study 1: Heisha River Debris Flow Control

The Heisha River in Xichang, southwest Sichuan, China is well known for its hazardous debris flow. The bare mountains, broken rock strata, and many landslides favour frequent debris flows. Between the 1950s and 1960s, five villages were destroyed one after another, 200 ha of cultivated land became wasteland, the Chengdu-Kunming Railway, and the Sichuan-Yunnan Western highway, and three main canals of Xichang city were seriously damaged. Twelve villages, one power plant, and more than 400 ha of cultivated land were threatened.

The Heisha River debris flow seriously threatened the Chengdu-Kunming Railway, which passed through its depositional fan. In 1967, to safeguard the railway and other infrastructures from debris flows, the Chinese Academy of Sciences organized a research team with members mainly from the Chengdu Institute of Mountain Hazards and Environment (IMHE). The team investigated and observed the Heisha River debris flow during 1967 and 1968. In 1970, in collaboration with ex-Xichang district and Xichang Railway Branch, the team made an integrated plan to control the Heisha River debris flow. In March 1971, the Government of Sichuan Province ratified the plan. The Chengdu IMHE was responsible for the technology while ex-Xichang district was responsible for construction and administration in cooperation with Liangsha Prefecture. The construction started in 1971 and was finished in 1978. Civil engineering works consisted of one flood-regulating reservoir, seven sediment-trapping dams, four check dams, seven division dams, a 5.8 km long division dyke and one flood-relief channel.

Bio-engineering works consisted of planting water-source holding forests over 800 ha, water and soil conservation forests on 400 ha, seven lines of debris flow preventing forests, and thirty-one windbreaks. Measures to improve farmland included terracing fields over more than 210 ha. Ex-Xichang County met the labour cost, and Sichuan Province Government invested US$ 0.5 million to implement the project.

Physical setting of the Heisha river catchment

The Heisha River is a tributary of the Anning River located about 28 km north of Xichang City. It originates from Lujihou Mountain in Xide County and joins with the Anning River at Lizhou Town, Xichang City. The river is located on the western slope of Daliangshan Mountain adjacent to southern Hengduan Mountain and the plateaus of Yunnan and Guizhou. The main stream is 12.6 km long and has a goldfish-like shaped catchment area of 22.7 sq.km. Geomorphologically it is stratified vertically and can be divided into the following four regions (Figure 18.2).

Lujihou Mountain — The mountain is the highest part of the catchment with an area of 5 sq.km. The highest point is at 2,920masl. The slopes are steep and there are two main ravines: the Ludong and Ongzu.

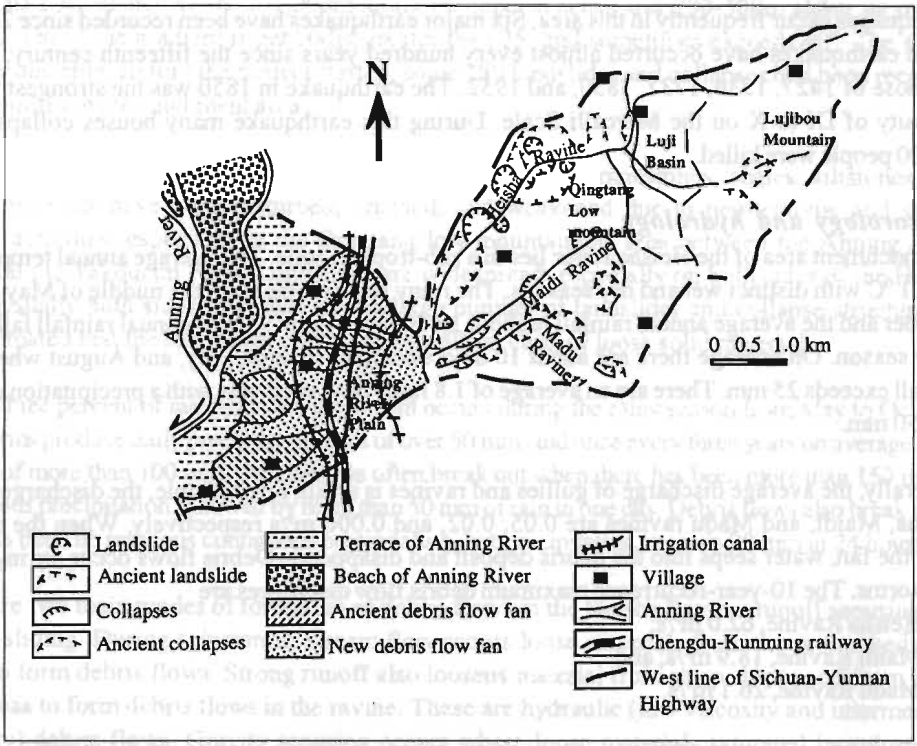

Figure 18.2: **Map of the Heisha River showing geomorphological characteristics and infrastructures lying on the fan**

Luji Basin — This is a fault bound basin lying in the middle of the Lujihou and Xitangli mountains. The basin is covered by alluvium deposited from the Ludong and Ongzu ravines. The basin covers 1.5 sq.km with altitudes ranging from 1,950 to 1,960m.

Qingtang Low Mountain — This includes the four ridges of Qinglongpo, Tangluopo, Hepupo, and Laripo with altitudes of 1,640 to 2,100m. The Heisha, Maidi, and Madu ravines lie between the ridges. The slopes are steep with a gradient of more than 25^0. There are many landslides and ravine erosions on both sides of the ridges that form debris flows. The area covered by this mountain is about 8.18 sq.km.

Anning River Plain and the Fan — The plain is about 3 km wide along the left bank of the Anning River and represents the lowest terrace of the river. The fan produced by the Heisha River debris flows lies above it. The fan covers an area of 5.33 sq.km, and has an average gradient of 2.0^0 and maximum elevation of 1,640m.

Tectonics and stratigraphy

The catchment is located in a major fault zone of the Anning River which passes through the Kang-Dian fold axis. The Anning River Fault and the Yakoucun Fault run through the catchment in a N-S direction. The former runs through the mountain pass under the Quaternary deposits and the latter runs along the southern fringes of Luji Basin. The Heisha Ravine anticline occurs on the west side of the fault.

Stratigraphically the catchment area is underlain by soft rock groups of Upper Triassic and Jurassic mudstone, siltsone, shale, and sandstone, as well as siltstone and sandstone with pebbles of the Lower Pleistocene, and young sediments from the Holocene.

Earthquakes occur frequently in this area. Six major earthquakes have been recorded since 208 AD. Large earthquakes have occurred almost every hundred years since the fifteenth century, including those of 1427, 1536, 1732, 1850, and 1952. The earthquake in 1850 was the strongest with an intensity of IX to X on the Mercalli Scale. During this earthquake many houses collapsed and 26,000 people were killed.

Meteorology and hydrology

The catchment area of the Heisha River lies in a sub-tropical zone. The average annual temperature is 17.1 °C with distinct wet and dry seasons. The rainy season runs from the middle of May to mid-October and the average annual rainfall is about 1,000 mm. About 93% of annual rainfall falls in the rainy season. On average there are about 10 days occurring in June, July, and August when daily rainfall exceeds 25 mm. There are an average of 1.8 rainy days each year with a precipitation of more than 50 mm.

Generally, the average discharge of gullies and ravines is small. For example, the discharges of the Heisha, Maidi, and Madu ravines are 0.05, 0.02, and 0.006 m^3/s respectively. When the streams enter the fan, water seeps into the debris deposit and disappears. Debris flows occur during heavy rainstorms. The 10-year-recurrence maximum debris flow discharges are

- Heisha Ravine, 62.0 m^3/s;
- Maidi Ravine, 18.9 m^3/s; and
- Madu Ravine, 26.1 m^3/s.

Where the Heisha River is joined by the above-mentioned ravines, the 10 year maximum discharge is 89.0 m^3/s. The debris flows travel downstream through the fan in seven branches which flow into the Anning River. The mainstream flow often changes its course between the seven branches.

Soil and vegetation

The catchment has acidic soil in the south-west mountainous area and the soil depth is mostly more than 1m. There are three sub-soil types in the catchment:

- mountainous red earth in the Qingtang low mountain area under 2,100m and in old fan deposits;
- mountainous red soil in the middle and lower part of Lujihou Mountain (above 2,100m); and
- mountainous yellowish-red soil in the upper part of the Lujihou mountain area. Brown, purple and black soils have developed in strongly eroded ravines and slopes.

Vegetation cover in the catchment is mainly composed of sub-tropical evergreen broadleaved trees and pines. The natural vegetation has been destroyed by human activities and only scattered shrubs and grasses remain. Forest cover was only 2.8% in the 1960s. A century ago, there were only a few inhabitants in the lower, middle, and upper reaches of the Heisha River and a dense forest grew in the catchment. Cultivated lands were few and far between. The ravine is narrow and debris flows occurred only rarely. With the coming of settlers, the population increased rapidly and forest cover was destroyed. Steep slopes of up to 35° were cultivated in the middle and upper reaches. Refuse from coal-mines was piled up everywhere. All these activities contributed to the development of frequent debris flows.

Formation of debris flows

The conditions which make the Heisha River catchment area prone to the formation of debris flows are summarised below.

The Heisha River lies at about 1,000m along its upper reaches and 200-300m along its middle reaches. The slope gradient is generally greater than 25° and sometimes exceeds 40°. The slopes are very unstable. Before the project started, some 180 landslides and collapses had been recorded in 135 gullies in the catchment area.

The lithology in the catchment is mostly soft rocks such as mudstones, shales, siltstones, and coal. The rocks have been disturbed, crushed, and weakened due to neo-tectonic and strong seismic activities, especially in the Qingtang low mountainous area between the Anning River Fault and the Yakoucun Fault. Landslides are widespread, especially on both sides of the Heisha River. Usually both sides of gullies have a large number of landslides and collapse structures. It was estimated that the catchment contained 26 million cu.m of loose solid material.

Ninety-three percent of rainfall in the catchment occurs during the rainy season from May to October. Rainstorms produce daily precipitation rates of over 50 mm, and once every three years on average daily rainfall of more than 100 mm. Debris flows often break out when there has been more than 150 mm of continuous precipitation followed by more than 50 mm of rain in one day. Debris flows also break when there has been no previous continuous precipitation, but precipitation exceeds 90 mm in 24 hours.

There are two main modes of formation of debris flows in the Heisha Ravine: runoff scouring and gravity sliding. During rainstorms, stream flow scours loose materials from the ravine beds and banks to form debris flows. Strong runoff also loosens material from steep slopes and from landslide areas to form debris flows in the ravine. These are hydraulic (low viscosity and intermediate viscosity) debris flows. Gravity scouring occurs where loose materials saturated by rainstorms have a decreased internal angle of friction. Earthslides move down the slope and enter the ravine to form debris flows. These are called sliding or viscous debris flows.

Debris flow processes in the mainstream of the river

The rainstorm runoff from the upper reaches of the Lujihou mountainous region collects in the Luji Basin, enters the middle reaches of the Heisha River where it scours loose deposits from the bed and banks, then receives additional debris flow from the sides, and finally forms a strong viscous debris flow in the mainstream of the Heisha River.

Various different types of rainstorm-triggered debris flows have occurred in the Heisha River catchment, but it is seen as a typical low viscosity type debris flow ravine. The average density of debris flows has been about 1.5 t/m^3. The Maidi Ravine has also had mainly low viscosity debris flows, although intermediate viscosity flows with densities of about 1.70 t/m^3 have also occurred. The Madu Ravine has had mainly low viscosity flows, but also occasional viscous debris flows with densities of 2.1 t/m^3. Low viscosity, intermediate viscosity, viscous, and plastic debris flows have occurred in small side branches.

The estimated peak discharge of the very large debris flow that occurred in 1874 was about 1,000 m^3/s. This flow damaged a four kilometre wide zone along its course. At Yuehua Village, debris deposits reached up to the eaves of houses. The 1964 debris flow had a discharge of 200 m^3/s. The largest debris flow in recent years was on June 30, 1971 with a peak discharge of 105 m^3/s (equal to the 10 year recurrence value). The peak discharge of the flow in Madu Ravine, on September 11 1972, was 36.5 m^3/s. If the reservoir had not been built in the upper reaches, the scale of debris flow would have exceeded that of 1964. The calculated peak discharge of a 100-year recurrence in Heisha River is 640 m^3/s.

The frequency of low viscosity debris flows is different to that of viscous debris flows. In some ravines there can be as many as100 viscous debris flows in a year, but low viscosity debris flows generally occur only once in several years or even decades. There are more than 20 viscous debris flows each year in the Majing Ravine. In the Heisha River, low viscosity debris flows occur once or twice a year. Hazardous debris flows, with a peak discharge of more than 100 m^3/s, occur about once every eight years and destructive debris flows about once every 50 years (as in 1874, 1927, and 1972). In 1972, the flow did not burst out in to the Heisha River mainstream because the reservoir had been built in the upper reaches.

The single largest quantity of solid materials carried down by a debris flow in this area was 0.308 million m^3 at Corfe at the confluence of the Heisha, Maidi, and Madu ravines. The average rate of deposition of debris in the fan is 5 cm/year with a maximum of 63 cm/year. More than 6m of debris flow deposits have accumulated since 1874 at the mouth of the ravine and more than 2m on the fan.

The area threatened by debris flow lies between Sankuaishi in the north and Guanzhangcun in the south. The maximum width of this area is 5 km over an area of 5.2 sq.km. There are seven radial branches of debris flows on the fan before they enter the Anning River. However, most debris flows end on farmland without reaching the Anning River. The mainstream keeps shifting. In 1958 it ran through Zhaojia Ravine but in 1968 it shifted to Miaokang Ravine.

Damage

The Heisha River debris flows are characterised by high discharge value, high-frequency, large volume of deposits, and channel shifting. These flows have caused repeated damage in the lower reaches.

Since 1874 debris flows have destroyed the five villages of Fujia, Maojia, Landiaofang, Aojia, and Zhangjia. The 1964 debris flow destroyed 74 houses. Over the past 100 years the Heisha debris flows have silted up more than 200 ha of cultivated land. The seven branches of the river on the fan often destroy the fertile fields located there. The flood used to submerge more than seven ha per year; one debris flow event in 1964 silted up and covered 74 ha of land.

Before 1970, the main irrigation canal of ex-Xichang county was blocked every year by debris flow sediments. In 1964, the canal was blocked in 13 places after one debris flow, preventing the irrigation of over 3,000 hectares of land. At present three canals cross the deposit fan in the lower reaches of the Heisha River.

One of the main power plants of ex-Xichang district, the Yuehua Power Plant, is located in the middle of the No. 2 and No. 3 branches of the seven channels. Debris flows have blocked canal inflows many times interrupting electricity generation. There is only 100m distance between No. 2 branch and the generator room so that a large-scale debris flow could destroy the factory houses and engines.

In the 1960s, the Sichuan-Yunnan highway was often damaged during the rainy season and its alignment had to be shifted. Vehicles were carried away by the debris flows. One debris flow destroyed a 1.5 km long road in 1964, and in 1968 a moving car was buried. The section of highway in the lower reaches of the Heisha River is one of the most frequently damaged sections on the Sichuan-Yunnan highway.

Whilst selecting the alignment of the Chengdu-Kunming railway, the Heisha River section was regarded as the most hazardous crossing. To safeguard the railway, seven bridges were built over the seven branches of the Heisha River. Although the railway project involved a large investment little consideration was given to protecting the railway from debris flows. The railway was damaged twice during its first year of operation in 1965. The first large-scale damage occurred on September 18, 1970. The pier protection of one of the bridges was destroyed following a peak discharge of 170 m^3/s after intense rainfall (34 mm in an hour). The second heavy damage was on June 30 1971. This time the railway was destroyed at three places by low viscosity debris flows with peak discharges of 105 m^3/s. Some houses in Miaokan Village were submerged.

Because of the concentration of debris flows at the bridge openings, the potential for disaster in the lower reaches actually increased. The construction of the seven bridges increased the damage to farmland in the lower reaches and did not protect the railway from debris flow hazards. The only way to safeguard the railway and agricultural land was to implement integrated measures to control the Heisha River debris flows.

Integrated control measures

An integrated plan for debris flow control was drawn up that took into consideration both the debris flow characteristics of the Heisha River and other successful examples of debris flow control at home and abroad. Bioengineering and civil engineering measures were combined with comprehensive planning for the upper, middle, and lower reaches and an integrated management plan for mountain, river, forest, and farmland. The integrated measures consisted of

- planting water-holding forests in the clear-water areas of the upper reaches;
- building a flood-regulating reservoir to regulate water discharge;
- planting water and soil-conservation forests in the farm areas of the middle reaches and building sediment-trapping dams, check dams, and protection dykes to stabilise slopes and fix ravine beds to control debris flow formation; and
- building diversion dykes, excavating flood-refill channels, and planting protection forests in the deposit area to fix the ravine bed.

Bio-engineering

The bio-engineering measures used are summarised in Table 18.1.

Water-holding forests of *Pinus yunnanensis*, *Cyclobalanopsis glauca* and other tree species were planted on more than 667 ha of Lujihou Mountain, Luji Basin, and the surrounding areas.

Water and soil conservation forests, using trees, bushes, and grasses were planted in the low mountain areas of Qingtang, where debris flows originate. The trees included *Pinus yunnanensis*, *Pinus khasya*, *Pinus armandii*, *Quercus glauca*, *Alnus cremastogyne*, and *Robinia pseudoacacia;* bushes like *Coriaria sinica* were planted in areas with poor soil and poor growing conditions. Grasses like *Themeda triandra var. japonica* were planted and protected in the areas with the most hostile growing conditions.

Dyke-protection and windbreak forest belts were planted in the debris flow deposit areas in the lower reaches and around settlements. A 15m wide, 1.5 km long plantation was established in the dyke-protection belt. *Robinia pseudoacacia* was the main species planted, other species included *Alnus cremastogyne*. A 10-20m wide windbreak belt of trees, mainly *Robinia pseudoacacia, Eucalyptus robusta, Paulownia fortunei*, and *Ligustrum fragrans,* was planted on the former fan deposit running parallel to the diversion flume of the Heisha River.

Table 18.1: **Bio-engineering measures used in the Heisha River catchment**

Afforestation zones		Plantation types		Soil types	Soil-vegetation types	Afforestation methods
Zone	Sub-zone					
Mountainous area	Middle hills	Soil and water conservation	Water source protection	Red soil and yellow-red soil	Medium-deep soil with humid shrubs	Air-seeding sowing by hand, spreading, sowing by dibbling
	Gentle slopes		Watershed protection	Red soil and red earth	Deep soil with humid grass	
	Steep slopes		Sloping land protection	Purple soil, purple-brown soil	Medium-deep soil with less humid grass	Same as above and afforestation by planting saplings
	Collapses and landslides		Protecting collapses and landslide	Black young stage soil	Landslides and ravines with thin, exposed soils	
	Upper part of ravine		Regulating water flow	Purple-red-brown soil		
	Bottom of ravine		Controlling ravine-bottom erosion	Recent stone and sand layers		
	Exposed land		Controlling exposed land erosion			
Plains	Debris flow deposit fans	Checking wind	Protecting a dam against debris flow	Stony soil in floodland and sandy soil		
	Cultivated land	Protecting channels and fields	Protecting channels and cultivated fields	Rice soil	Deep soil with humid agricultural zone	

Economic trees (i.e., nut, fruit, or other trees grown for cash crops) were planted on previously cultivated land that had been laid waste by debris flows. The main trees planted were *Malus* and *Alba*, with subordinate species including *Malus pumila* and *Pyrus* spp. The total area of these forests was about 66 ha. The area has developed into an important centre in Sichuan Province for the production of silkworm cocoons.

Civil engineering

The civil engineering works used for debris flow control are summarised in Table 18.2.

A 23m high reservoir, the Qiyi reservoir, was built at the exit of the Luji Basin (Figures 18.3 and 18.4). The reservoir has a storage capacity of 656,000 m^3 and collects water from from a 9.2 sq.km catchment area, 72% of the total Heisha Ravine catchment. During the rainy season the reservoir acts as a flood regulator. The 20-year-frequency flood peak discharge of 64.6 m^3/s and 100-year-frequency of 110 m^3/s can be reduced to 13.4 m^3/s and 33.9 m^3/s respectively when a storage capacity of 601,000 m^3 is used to regulate annual floods and hold the water (Table 18.3). Since the completion of the reservoir in 1972, the mainstream of the Heisha Ravine has not produced any substantial debris flows and neither has the Heisha River. The reservoir dam was made of earth using hammer-ball installation. This type of construction can easily be manipulated to drain sediment away. In the event of a 100-year-frequency flood, if in-reservoir discharge is 1 m^3/s, the water level can be reduced to the normal level of 10.2m within 48 hours. Even in the highly unlikely event that a rainstorm of the same strength occurred the next day, the reservoir would still be safe.

Figure 18.3: **The flood regulating Qiyi reservoir constructed in the Luji Basin, in the upper reaches of the Heisha Ravine**

Sediment-trapping dams are mainly used to arrest the earth in debris flows. Seven sediment-trapping dams were constructed. No. 1 was designed to arrest sediment, stabilise landslides, and prevent down-cutting; No. 5 was designed to stabilise landslides; and No. 7 was designed to raise the erosion base. The dams were all cement masonry gravity dams or cement masonry gravity arch dams (Figure 18.5). The dimensions of the dams are shown in Table 18.3. Various foundation structures

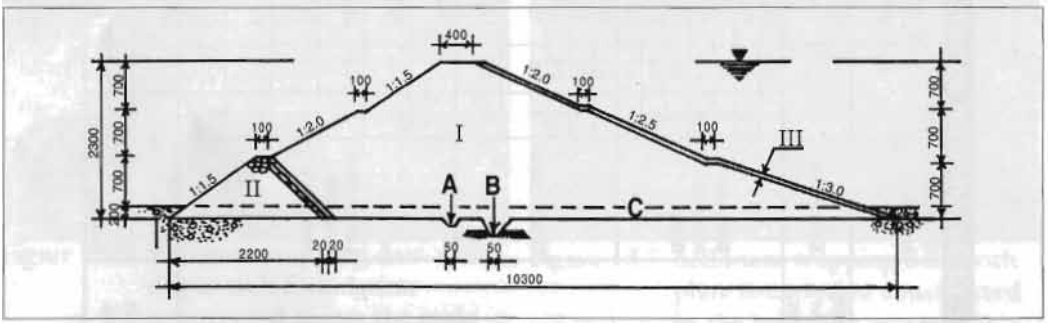

Figure 18.4: **Section through the earth dam of Qiyi Reservoir, I - earth dam; II - water-filter dam; III - slope protection; A - centre groove; B - catch drain; C - old ravine bed**

Table 18.2: **Civil engineering works for debris flow control of the Heisha River**

Engineering location	Engineering project	Symbol		Engineering dimension										Standard		Engineering structures
				Length (m)	Height (m)	Width of top (m)	Width of bottom (m)	Length of spillway (m)	Height of spillway (m)	Width of spillway (m)	Depth of foundation (m)	Gradient of front side	Gradient of back side	Design (p)	Check (p)	
Flood regulating engineering in upper reaches	X-Reservoir			106.6	22.0	4.0	96.0	6.0	17.0	4.0	1.0-2.0	1:2-1:3	1:1.5-1:2	1	0.1	Earth dam with mortar masonry spillway
Small-scale engineering	Sediment-trapping dams	1	A1	70.7	7.1	1.0	7.0	20.0	5.0	20	45	1:0.3-1:0.4	1:0.2	2	0.5	Mortar masonry gravity dam
		2	A2	45.7	5.5	0.7	4.3	16.0	3.5	1.6	3.1	1:0.3-1:0.4	1:0.2	2	0.5	Mortar masonry gravity dam
		3	A3	42.5	5.6	0.8	4.0	10.0	3.5	1.5	3.0	1:0.3-1:0.4	1:0.2	2	0.5	Mortar masonry arch dam
		4	A4	51.6	6.0	0.8	6.2	14.0	4.0	2.0	1.0	1:0.4	1:0.2	2	0.5	Mortar masonry gravity dam
		5	A5	47.0	6.0	1.0	5.8	14.0	4.0	2.0	4.0	1:0.3-1:0.4	1:0.2	2	0.5	Mortar masonry gravity dam
		6	A6	43.5	12.0	1.0	9.2	7.0	9.0	2.5	1.2	1:0.3-1:0.4	1:0.2	2	0.5	Mortar masonry gravity dam
		7	A7	24.0	5.2	0.8	4.3	10.0	3.0	2.0	1.0	1:0.6	1:0.0	2	0.5	Mortar masonry gravity dam
	Check dams	1	B1	11.9	6.0	1.0	4.9	2.0	4.0	2.0	1.0	1:0.3-1:0.4	1:0.2	5	2	Mortar masonry gravity dam
		2	B2	16.1	6.0	1.0	3.6	4.0	4.0	5.0	1.0	1:0.3-1:0.4	1:0.2	5	2	Mortar masonry gravity dam
		3	B3	13.6	6.5	1.0	4.2	3.0	4.5	1.6	1.5	1:0.3-1:0.4	1:0.2	5	2	Mortar masonry gravity dam
		4	B4	12.4	3.5	1.0	1.5	3.0	1.5	1.0	0.3	1:0.0	1:0.0	5	2	Reinforced concrete box-like sub dam
		5	B5	15.5	6.4	1.0	2.5	3.0	4.4	1.5	1.0	1:0.0	1:0.0	5	2	Reinforced concrete box-like main dam
	Longitudinal dyke and revetment	1	C1	70.0	2.0	0.8	1.5-2.5				1.5-2.0			5	2	Mortar masonry dam or revetment
		2	C2	32.0	2.0	0.8	1.5-2.5				1.5-2.0			5	2	Mortar masonry dam or revetment
		3	C3	20.0	2.0	0.8	1.5-2.5				1.5-2.0			5	2	Mortar masonry dam or revetment
		4	C4	14.0	2.0	0.8	1.5-2.5				1.5-2.0			5	2	Mortar masonry dam or revetment
		5	C5	41.0	2.0	0.8	1.5-2.5				1.5-1.2			5	2	Mortar masonry dam or revetment
		6	C6	25.0	2.0	0.8	1.5				2.0	1:0.5	1:0.0	5	2	Mortar masonry dyke
		7	C7	10.0	2.0	0.8	2.0				1.5	1:0.5	1:0.2	10		Mortar masonry dyke
Diversion engineering in lower reaches	Diversion dyke			5800	2.0-2.6	2.0	6.5-8.5				1.0-1.2	1:1.0	1:1.5	5	2	Earth dyke with mortar masonry
	Diversion weir			28.0	1.0			28.0	1.0	15.0	1.7					Mortar masonry
	Drainage canal			1500	1.6-2.0	6.5	4-5									Excavation

Table 18.3: **Peak discharge in and out of the Qiyi reservoir calculated for different rainstorm-frequencies**

Frequency for design (p%)	Relative water level (m)	Peak discharge in into reservoir (m^3/s)	Peak discharge from reservoir m^3/s	Cutting discharge m^3/s
0.1	20.5	181	65.0	116
0.2	20.1	162	54.5	108
0.5	19.6	132	43.9	88.1
1	19.1	110	33.9	76.1
2	18.7	91.2	26.0	65.2
5	17.9	64.4	13.4	51.2

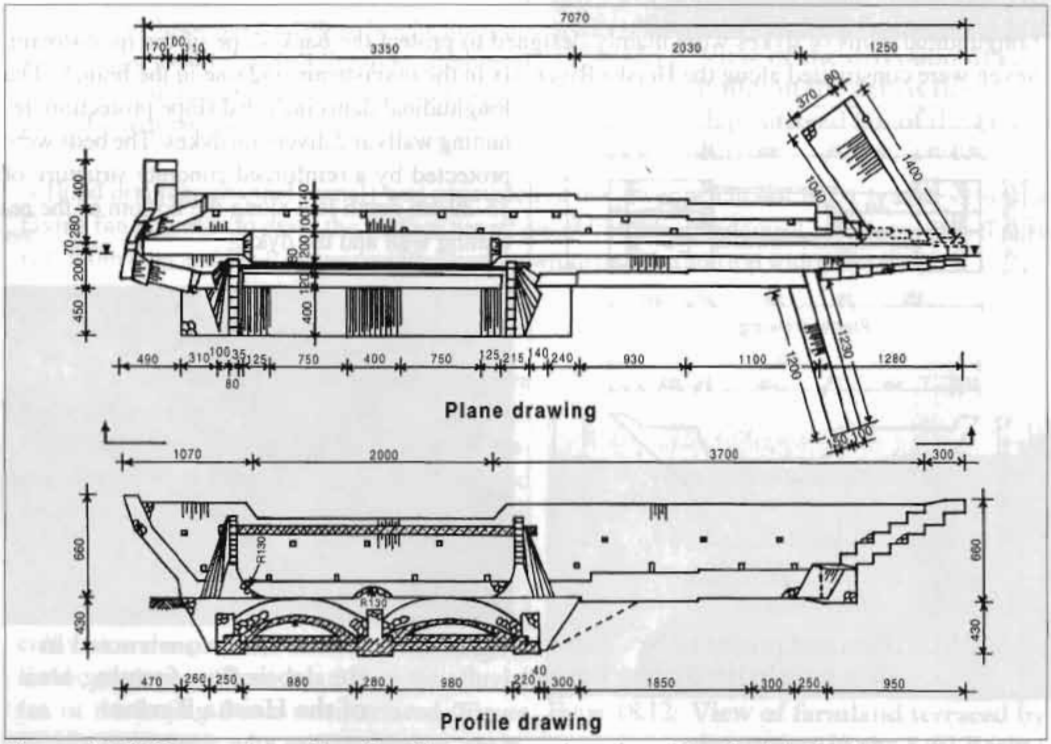

Figure 18.5: **Plan and profile of sediment trapping dam No. 5 with double arch foundation**

Figure 18.6: **Sediment trapping dam with single-arch foundation constructed across the main stream of the Heisha Ravine**

Figure 18.7: **Sediment trapping dam with plate foundation constructed in the landslide area of the mainstream of the Heisha Ravine**

and auxiliary dams were installed to prevent failure due to foundation scouring. Double arches (Figure 18.5), single arches (Figure 18.6), and wedges were used to for the main dam foundations. Arch, beam, plate, and gravity structures were used in the design of the auxiliary dams (Figures 18.6 and 18.7); of these only the gravity type is used regularly outside of China.

Check dams are low volume sediment-trapping dams built in gullies. Five check dams were built; typical plan and profile diagrams are shown in Figure 18.8 (No. 2 check dam built in the middle reach of the Majing Ravine). Figure 18.9 shows a series of check dams built in the debris flow forming area of the Heisha Ravine.

Longitudinal dams or dykes were mainly designed to protect the bank slope of the mainstream. Seven were constructed along the Heisha River: six in the mainstream and one in the branch. The longitudinal dams included slope protection, retaining walls and diversion dykes. The beds were protected by a reinforced concrete structure of 15-20 cm depth laid along the bottom of the retaining wall and the dyke.

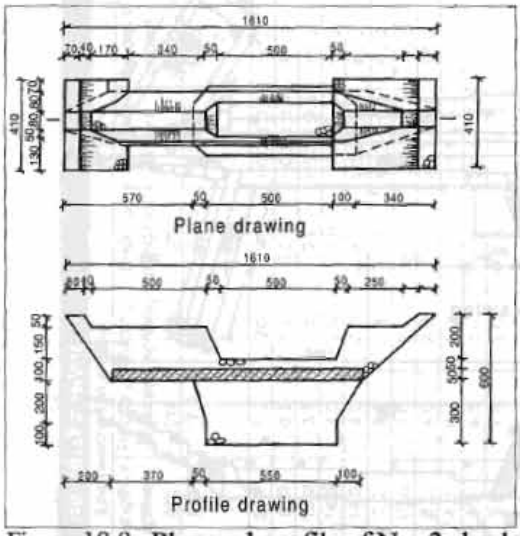

Figure 18.8: **Plan and profile of No. 2 check dam built in the Majing Ravine**

Figure 18.9: **Check dams constructed in the debris flow forming area of the Heisha Ravine**

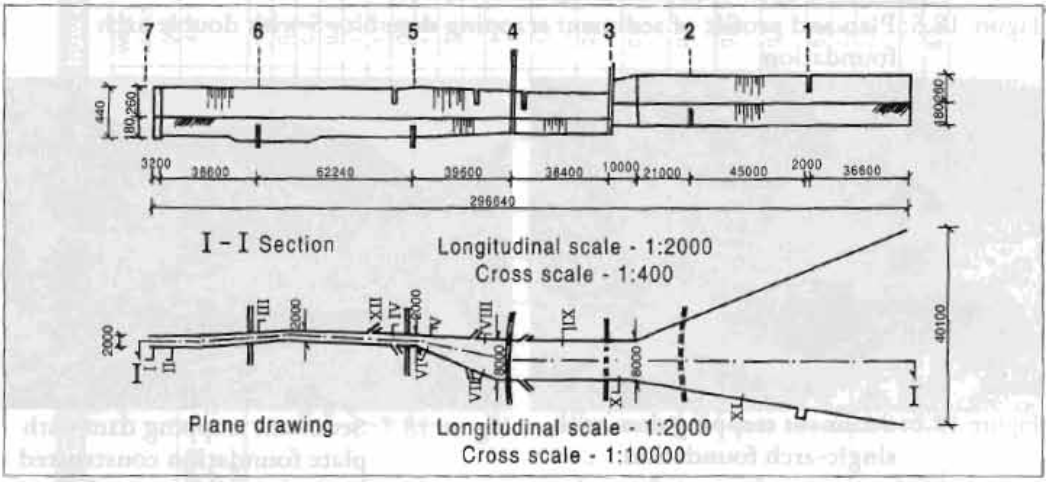

Figure 18.10: **Cross-section of Heisha River diversion flume**
1. Diversion; 2. Lugu canal; 3. Sichuan-Yunnan highway; 4. Chengdu-Kunming railway; 5. Xili canal; 6. Lianghe canal; 7. Anning River

The diversion flume built in the lower reaches of the Heisha River was 2.9 km long. A 2.5 m high diversion dyke was built on both sides of the river (i.e., total length of dyke 5.8 km). The plan of the dyke is shown in Figure 18.10 and the completed dyke in Figure 18.11. Most of the dyke is earthen with the surface protected by cement masonry. There is a spillway in the upper section of the diversion dyke. When debris flows or flood levels in the flume reach a critical height, the spillway can be used to protect the dyke. Sediment exits in the middle and lower reaches are used to push the sediment away.

Figure 18.11: **View of the diversion dyke build on the debris flow depositional fan of the Heisha Ravine**

A flood drainage channel (canal) was excavated in the lower reaches of No. 1 branch - Huoshao ravine fan deposit - to drain the surface runoff away from the fan deposit and slope. The channel is 1,500m long and 1.6-2.0m wide with a bottom width of 4-5m and top width of 6.5m.

Improving agriculture

One very important intervention was to improve the stability and reduce erosion rates in surrounding areas by changing the land use pattern. General erosion was reduced by replacing cultivated areas on steep slopes with forests. Cultivation was forbidden on slopes exceeding 25° and forests were planted in the middle and upper catchments. Fields were terraced, and strip field and cultivation along contour lines was encouraged. Fields on slopes of less than 25° on the alluvial fan of the Lujing Basin were terraced (Figure 18.12). Strip fields with straight ditches, roads, and trees were built on the old fan outside the diversion flume.

Figure 18.12: **View of farmland terraced by the project in the Luji Basin in the upper reaches of the Heisha River**

By 1978, the forest covered 680 ha, 62% of the mountainous area of the middle and upper parts of the Heisha River catchment. Thirty-nine rows of trees had been established in the lower reaches and 1,700,000 trees had been planted around houses. Thirty-one hectares of t mulberry were established. These have since been added to and mulberry trees now cover 63 ha. Figure 18.13 shows a plan of some of the civil engineering works and land use patterns.

Summary

The project was completed in 1978 with an investment of US$ 0.5 million. Since its completion, there has been no debris flow in the mainstream of the Heisha River. With the measures taken, the catchment should be able to withstand the type of rainstorm that occurs once every 50 years. The sediment carried from the upper reaches is now less than a quarter of what it was were before the project started. The flood peak discharge induced by a 10-year recurrent rainstorm is only a fifth of what it was before the project. The peak flood discharge of the mainstream is only a twentieth of

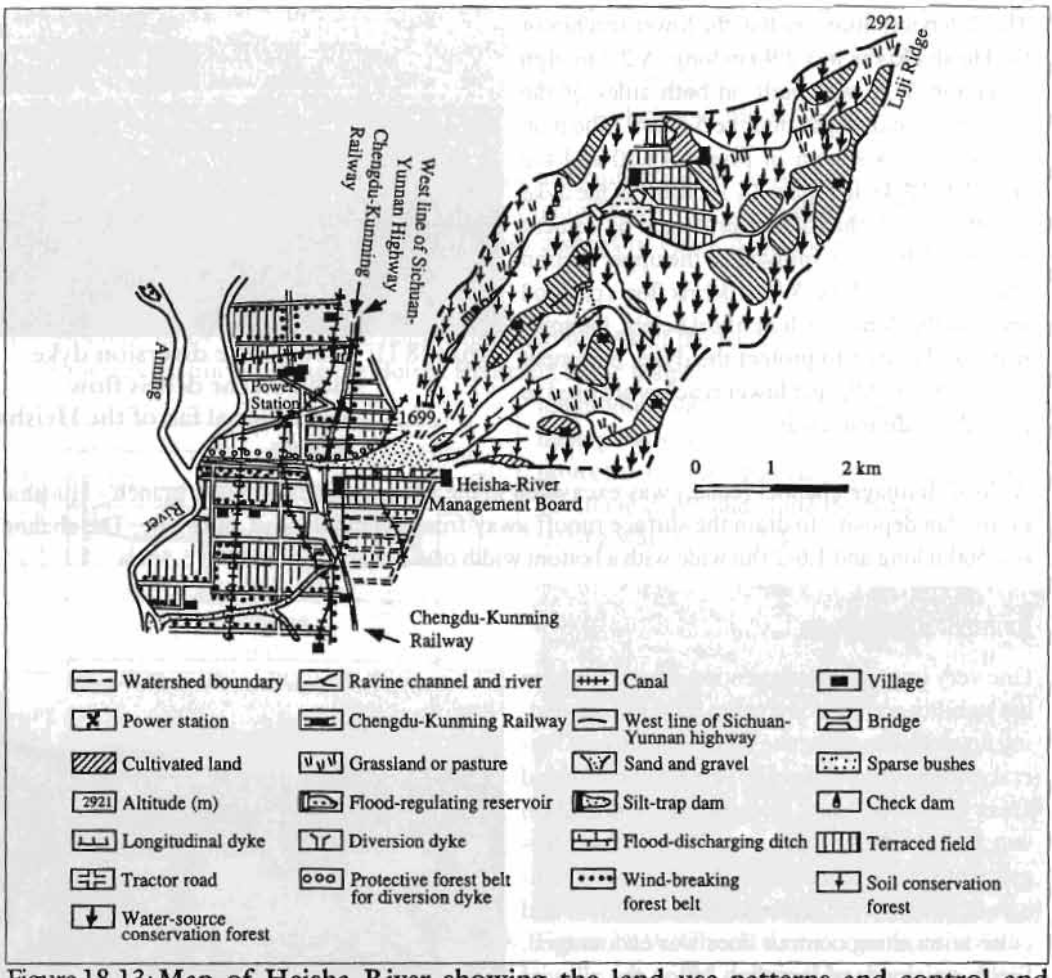

Figure 18.13: **Map of Heisha River showing the land use patterns and control and engineering structures**

what is was in the year the project started. This project has not only mitigated debris flow hazards and protected the railway, highway, power station, villages and farmland, but has also reclaimed 130 ha of farmland, increased the irrigated area by 75 ha, and substantially raised crop yields. Since the completion of the project, a silkworm mulberry farm has been set up on the debris flow fan with an annual production in excess of US$ 1.23 million yielding a net profit of US$ 123,000 to the community. This is impressive when compared to the total investment for the project.

Case Study 2: Debris Flow Control in Laogan Ravine

Laogan Ravine is located 11 km south of Dongchuan city, in Yunnan province, China (Figure 18.1), and is a tributary situated in the middle reaches of the Xiaojiang River. The Xiaojiang River is a tributary of the upper Yangtze River. The catchment area of the Laogan Ravine is 7.7 sq.km and the altitude ranges from 1,300m to 2,600m. The main stream is 5.7 km long with gradients ranging from 10 to 14°. The villages of Zhiga, Heishan, Xiaoxincun, and Xiaomaidi lie in the catchment area. From the 1960s to the 1980s, debris flows from the Laogan Ravine endangered the railway and highway linking Dongchuan and Kunming. A large irrigation canal constructed on the fan deposit of the Laogan Ravine was also threatened. The main features of the area are shown in Figure 18.14.

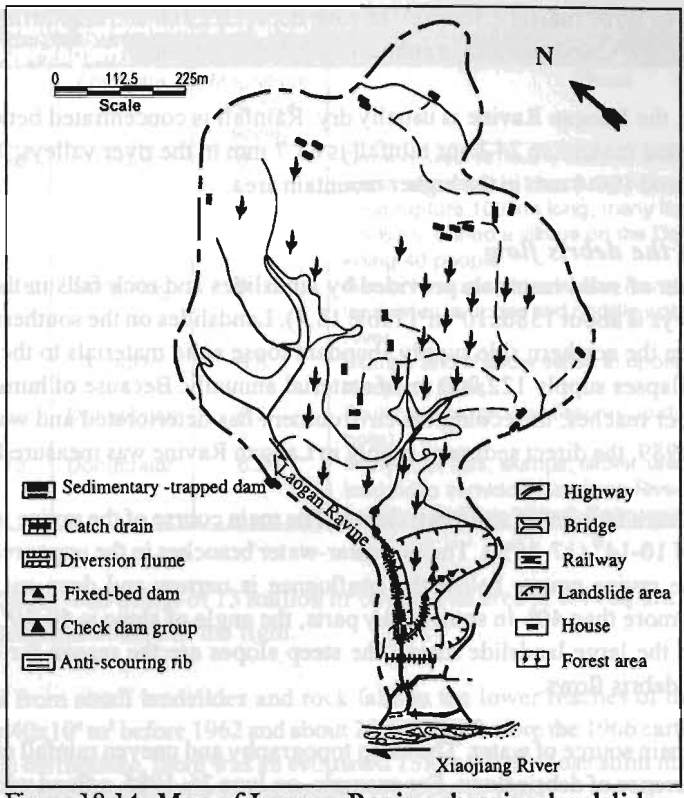

Figure 18.14: Map of Laogan Ravine showing landslides, infrastructure and control measures

Physical setting

The Xiaojiang River catchment is located on the east fringe of the Kang-Dian Axis and on the western fault line of the 'Kunming Hollow'. The project area belongs to the major fault belt of the Xiaojiang River. The north-north-west trending Laogan Ravine Fault runs through the catchment. Tectonic movement causes landslides and collapses along the Xiaojiang River fault belt.

The Laogan Ravine is located in the east of the middle section of the large Xiaojiang Fault. Above an altitude of 1,900m, the outcrops of bedrock are mainly dolomite limestone of Devonian, Carboniferous, and lower Permian age. Below 1,900m, highly-weathered Emeishan basalts of Permian age occur. The outcropping of bedrocks is small as most of the catchment area is covered by landslide and collapse deposits. Semi-weathered basalt can be seen in the middle and lower parts of the mainstream.

The Laogan Ravine catchment has an oak leaf-like topography with very steep slopes below 1,900m. The steep terrain has many deep ravines and gullies. Rapid runoff from the steep slopes is the main contributor to surface solid materials and debris flows.

Meteorology and hydrology

The climatic conditions range from semi-dry to wet-tropical. Below 1,300m, there is a semi-dry river-valley zone with temperatures ranging from 20°to 40°C. The average annual rainfall is 800 mm. The zone between 1,600 and 2,100m has an average temperature of 17.5°C and average rainfall of 900

mm (at 1,600m) to 1,707 mm (at 2,100m). The zone between 2,100 and 2,600m has a mean minimum temperature of -8.32°C and an average annual rainfall of 1,040 mm.

Hydrologically, the Laogan Ravine is usually dry. Rainfall is concentrated between June and August. The recorded maximum 24-hour rainfall is 83.7 mm in the river valleys; 117.2 mm in lower mountain area; and 100.4 mm in the higher mountain area.

Formation of the debris flow

The total amount of solid materials provided by landslides and rock falls in the ravine estimated from field surveys is about 1386×10^4 m³ (Table 18.4). Landslides on the southern side of the ravine and rock falls on the northern side supply abundant loose solid materials to the debris flow. Bank erosion and collapses supply 122,000 m³ of material annually. Because of human activities in the middle and upper reaches, the ecological environment has deteriorated and water and soil loss is worsening. In 1989, the direct sediment supply in Laogan Ravine was measured as 150,000 m³.

The catchment has a high relief and steep slopes. The main course of the ravine is 5.7 km long, with bed gradients of 10-14° (17-25%). The two clear-water branches in the upper reaches join with the mainstream; the ravine course below the confluence is narrow and deep-cut. The slope of the ravine banks is more than 40°. In some rocky parts, the angle of slope is 40-50°. There are several small gullies in the large landslide mass. The steep slopes are the reason for the strong erosion capacity of the debris flows.

Rainfall is the main source of water. The steep topography and uneven rainfall over time and space favour the occurrence of debris flows. For example, on June 26, 1985, a flood with a discharge of 30 m³/s eroded the landslide mass on the left bank setting loose solid materials to form a viscous debris flow with a discharge of 91.5 m³/s and velocity of 6.5 m/s. This one-time deposit amounted to 145,000 m³.

Human activities have contributed to debris flow formation. Studies have shown that the vegetation cover in the Laogan Ravine catchment area was 40% before 1949. The collapsed mass in the ravine remained stable before railway and road building began in 1956. The canal constructed in 1958 ran through the upper parts of an old landslide which was reactivated by the seepage from the canal. Increasing population levels led to the cutting down of trees and cultivation on the steep slopes.

The recorded earthquakes of higher magnitude and their effects in the Xiaojiang River catchment area are summarised in Table 18.5. The strong earthquake of February 5, 1966 at Xiniu Mountain in Dongchuan close to the Laogan Ravine, reactivated a huge landslide in the lower catchment of the

Table: 18.4: **Volume of materials estimated from landslides in the upper reaches of Laogan Ravine in 1989**

	Type	Area (km_2)	Avg. width (m)	Avg. slope (°)	Coefficient of slope	Avg depth (m)	Storage ($x10_4$ m_3)	Note
South of main stream	Landslide	0.444	450	25	0.065	29.3	1302	
North of main stream	Collapse	0.0612	108	36.5	0.126	83.3	83.3	
Upper and middle reaches	Surface & groove erosion	7.1984					2.8	Medium level of erosion assumed
Total							1386.3	

Table 18.5: **Historic earthquakes of great magnitude and their effects in the Xiaojiang River region**

	Epicentre	Magnitude (Richter scale)	Effects
1713, February 26	Xundian	6.5	Ground fissures, many slumps and shallow slides in upper watershed of Xiaojiang river
1733, August 2	Dongchuan	6.75	Fault rupture 100 km long, many landslides, one large landslide buried a village on the Daqiao tributary killing 40 people.
1833, September 6	Songming	8	Ground fissures, liquefaction (sand boils), many landslides in upper and middle watershed of Xiaojiang River
1927, March 15	Xundian	5.5	Slumps and shallow slides in upper watershed of Xiaojiang River
1966, February 5	Dongchuan	6.5	Fault rupture, ground fissures, and liquefaction (sand boils)
1966, February 13	Dongchuan	6.2	Many rock falls, slumps, slides; reactivated ancient landslides in middle Xiaojiang River watershed; combined effects of both February, 1966 earthquakes

ravine. The landslide with debris of 13 million m^3 covered an area of 0.44 sq.km. The mass that slid pushed the mainstream course to the right.

The total debris from small landslides and rock falls in the lower reaches of the ravine was estimated to be only $40x10^4$ m^3 before 1962 and about $200x10^4$ m^3 before the 1966 earthquake. By the end of 1989, after the earthquake, there was an estimated $1386x10^4$ m^3 loose solid material and the area of the landslide had increased to 0.5 sq.km from 0.27 sq.km in 1963.

Characteristics of the debris flow

The Laogan Ravine debris flow is turbulent. The density of the debris mass is 1.4 to 1.8 t/$m^3$and the discharge takes place in a single peak. The flows have caused bank undercutting and slope failure. The Dongchuan Institute of Debris Flow Protection and Investigation measured a peak discharge of 91.5 m^3/s and a velocity of 6.5 m/s on June 26, 1985.

Two very large-scale debris flows that occurred in 1985 and 1987 deposited more than 10m of debris and scoured more than 3m out of the main ravine course above the highway. The most recorded material deposited by one flow was 145,000 m^3. The ravine was formerly 250m long and 8-10m wide in the lower reaches. After the June 1985 debris flow, the width of the ravine increased to 30-50m. Figure 18.15 shows the particle sizes of the debris deposited on the fan by a flow in 1989.

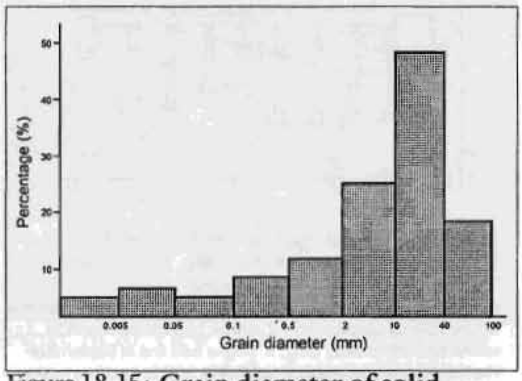

Figure 18.15: **Grain diameter of solid material deposited by a low viscosity debris flow in 1989**

Damage

The railway, highway and irrigation canal pass parallel to each other through the lower reach of the Laogan Ravine (Figure 18.14). As the railway line is at the lower level, it was most exposed to damage from the debris flows.

The railway was constructed across the ravine in the spring of 1959. A debris flow in July of the same year silted up the 60m long bridge and washed away a large section of the railway bed near the bridge. A new ravine canal developed. In 1960, a larger four span bridge was constructed across the ravine. This bridge also gradually silted up between 1961 and 1970. The average rate of deposition was 70 cm per year. In 1971, an open tunnel more than 100m long and a 150m long protection dyke were built above the silted bridge.

Figure 18.16: View of the covered tunnel and fan of the Laogan Ravine. The left outlet of the tunnel was silted up by about 3m as a result of the July 1987 flood

The large debris flow in 1985 buried the open tunnel. After this a covered tunnel was built over which debris flows could pass down into the Xiaojiang river. In July 1987, this tunnel was submerged by a flood and the left outlet of the tunnel was silted up to a height of about 3m (Figure 18.16).

The railway department spent about US$ 3.25 million between 1959 and 1989 to try and prevent damage to the railway,. During the same period, the ravine course bed silted up by about 30m rising from 1,305m to 1,335m altitude with an average rate of deposition of 1m per year (Figure 18.17).

The highway runs 80m upstream of the railway. In the beginning a small bridge was constructed across the ravine course, which was however soon destroyed. A pavement (causeway) was constructed over the destroyed bridge to allow debris to flow down it. A flood in May 1990 also damaged the causeway (Figure 18.18). The annual cost of repairing and maintaining this sec-

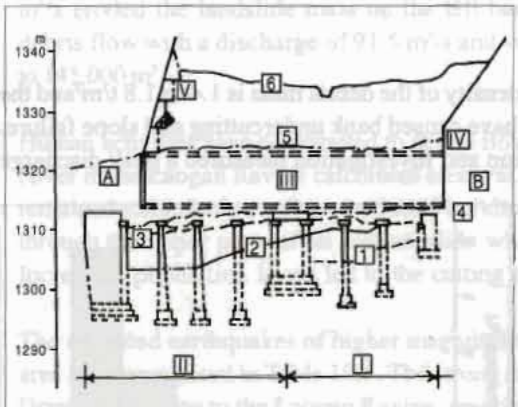

Structures: I-3 span bridge built in 1959; II-4 span bridge built in 1960; III-100m long open tunnel built in 1971; IV-Tunnel built in 1985; V-Slope protection of tunnel outlet
Orientation: A. to Kunming; B. to Dongchuan; 1. ravine bed line before railway construction; 2. ravine bed line in May 1958; 3. ravine bed line in May 1962; 4. ravine bed line in September 1963; 5. ravine bed line in May 1969; 6. ravine bed line in May 1985

Figure 18.17: Cross section of the Laogan Ravine at the level of the railway showing engineering structures and extent of silting

Figure 18.18: The causeway of the highway constructed over the destroyed bridge over the Laogan Ravine. The bridge was damaged by a debris flow in May 1990

tion of the highway has been US$ 25,000. Adding the cost of the new bridge, the total comes to more than US$ 0.67 million.

The Tuanjia irrigation canal is situated 50m upstream of the highway and was constructed in 1958. Very large debris flows in 1985 and 1987 destroyed the canal tunnel, causing losses amounting to more than US$ 50,000. As well as damaging the infrastructure, the disastrous debris flow of 26 June 1985 killed 12 people and injured 3 in a moving bus which was washed away by the flow.

As none of the structures constructed by the Department of Railways and Highways to prevent debris flows in the ravine has been successful, control of this debris flow, and the need to develop a different approach, became an important issue.

Integrated control measures

In 1988 the Dongchuan Institute of Debris Flow Protection was approached by Dongchuan City authorities to conduct detailed investigations of the debris flow ravine and design control measures with assistance from the Chengdu Institute of Mountain Hazards and Environment, Chinese Academy of Sciences (CAS). The detailed investigations indicated that the formation of the debris flow in the ravine was mainly associated with the large landslide on the south slope of the lower reaches of the ravine valley (Figures 18.19 and 18.20). The railway and highway could not be saved without stabilising this large landslide and channelling the ravine's course. An integrated control plan was prepared based on detailed field investigation and analysis, and implemented by the two institutions in collaboration with local communities between 1991 and 1994. The debris flow control measures were designed:

- to improve the natural environment using bio-engineering with an emphasis on planting bushes and trees in the middle and upper reaches of the watershed;
- to combine civil engineering and bio-engineering to obtain the best benefit from the control measures;
- to stabilise the large landslide of the south bank and channel the main stream course in the lower reaches.

Figure 18.19: **View of debris flow forming area in the upper lower reaches of the Laogan Ravine (looking upstream in 1988). In the past, abundant loose solid materials of landslide mass from here contributed to debris flows during heavy rain storms**

Figure 18.20: **View of debris flow forming area of the Laogan Ravine (looking downstream in 1988). Bank erosion and collapses provided abundant loose materials to form debris flows.**

Civil engineering

Landslide stabilisation was one of the major tasks since the large landslide was the main source of loose solid materials. Two 17.5 m high sediment-trapping dams were constructed at the toe of the landslide to control down cutting and toe erosion (Figure 18.14). A 155m long protective dyke and eight small check dams were also constructed in the landslide area to control side and gully erosion.

Figure 18.21: **View of channelised ravine course (diversion flume), with scour-proof ribs and fixed-bed dams, and of bio-engineering structures in the valley of the Laogan Ravine**

Both sides of the mainstream between the altitudes of 1,397m and 1,454m are composed of loose sediments so that it was important to channelling the course of the mainstream to prevent down-cutting and side erosion: 1080m of stream course was engineered into channels. Seventy-eight scour-proof ribs and four small bed-fixings were constructed to strengthen the channels (Figure 18.21). The channelled course had a deep-rectangular cross shape (Figure 18.22) to drain flood and debris flows. The structure of the sediment trapping dam and diversion flume are shown in Figure 18.22.

Catch drains were built to divert the large gully's runoff into the mainstream to prevent fan erosion. Small check dams were built in the small gully to catch sediment and to fix the gully bed.

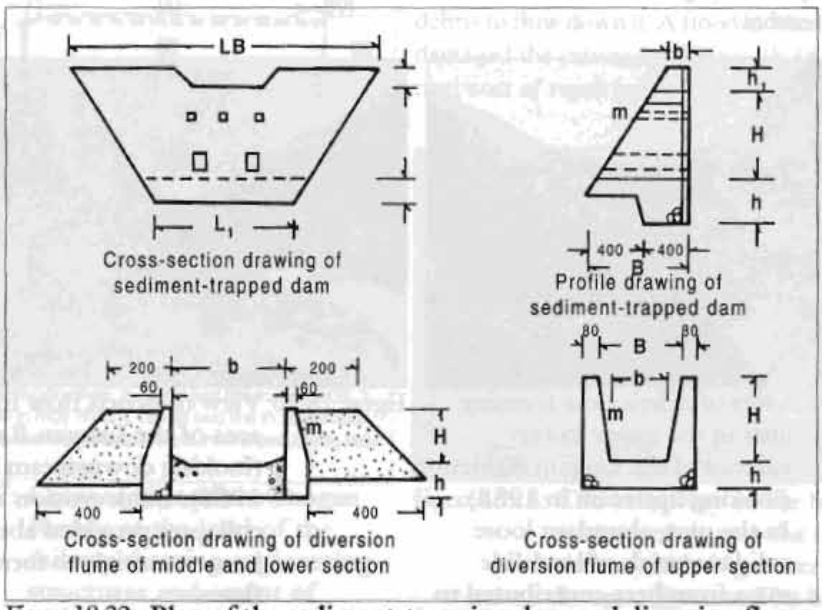

Figure 18.22: **Plan of the sediment-trapping dam and diversion flume (for actual values see Table 18.6)**

Table 18.6: **Technical parameters of civil engineering works** (dimension labels shown in Figure 18.22)

Structure	H (m)	m	B (m)	B (m)	L1 (m)	L2 (m)	h1	Spillway section (m)	Note
Catch dam 1	9.0	1:0.4	1.0	5.0	28.0	36.5	2.0	9 x 2	Small holes for drain 0.6 x 0.8 m
Catch dam 2	8.5	1:0.7	2.0	8.8	15.0	33.0	3	9 x 2	Big holes for drain 1x2m
Steep flume	3.0	1:0.15	2.6	3.0	20		1	2.5 x 3	
One-side flume	3.0		1.0	2.0	610		1.5	8 x 3	
Two-side flume	3.5	1:04	0.6	1.8	476		2.5	8 x 3.5	
Catch drain	3.5	1:0.25	1.5	0.6	60		1.5		
Fix-bed dams (4)	2.5-3.0	1:02	0.8-1.0	1.5-2.5	8-10	8-10	5-5.5	10 x 2.5	height and width varies
Check dams (8)	3-7	1:05	1-1.5	3-4	6.0	10.0	1.5-2.0	6 x 2	height and width varies
Anti-scouring ribs (78)		1:0.25	1.0	1.6	11.6	11.6	2.5	8 x 3.5	height and width varies

In total, the engineering works consisted of two main dams, four bed-fixing dams, eight check dams, a 155m long protection dyke, and a 1080m long diversion flume with seventy-eight scour-proof ribs. The engineering works were completed in 1994 at a cost of US$ 0.16 million. The technical parameters of the engineering works are presented in Table 18.6.

Bio-engineering

Bio-engineering was used to increase vegetation cover and prevent surface erosion. Afforestation was to improve the degraded mountain environment was the main approach used. Tree species were selected for planting on the bare mountain slopes in the middle and upper reaches as well as on the landslide mass in the lower reaches. A 130 ha area was planted in the middle reaches with the tree species *Robinia pseudoacacia*, *Albizia mollis*, *Cupressus funebris*, *Pinus yunnanensis*, and *Pinus armandii*. *Albizia mollis*, *Coris sinica* and other species were planted over an area of 29 ha in the landslide area of the upper and lower reaches (Figure 18.21).

Impact assessment

The sediment-trapping dams arrested about 42,000 m³ sediment and stabilised the main landslide by raising the level of the ravine above the toe of the landslide. The 1,080m long artificial diversion flume confined the flood and prevented side erosion of the ravine, which greatly reduced the sediment released. Before the measures were taken, about 150,000 m³ of loose solid materials were transported in the form of debris flow down to the Xiaojiang River. After completion of the engineering works in 1994, only sediment laden flow and light erosion has been observed in the lower reaches of the ravine.

The tree plantations in the middle and upper reaches covered 130 ha. Thanks to the participation of local people, the rate of survival of the planted trees has been 90.4%. The estimated profit from these trees over 20 years will be US$ 590/ha/yr, i.e., US$ 77,000 – all income for the local people. Twenty-nine hectares of the landslide area was planted with *Albizia mollis* and *Coris sinica*. The estimated profit from these trees over five years is US$ 92/ha per year, a further $2,600. Apart from the economic benefits, this vegetation plays an important role in soil erosion control and shallow landslide stabilisation in the middle and upper reaches of the ravine.

Figure 18.23: New bridge built in 1994 across the Laogan Ravine, the diversion flume can be seen under the bridge

The debris flow in the Laogan Ravine caused US$ 4,875,000 in economic looses between 1958 and 1988. The cost of the control project was only US$ 169,000. There have been no debris flows in the ravine since the completion of the control measures. With the construction of a new bridge across the Laogan Ravine in 1994 (Figure 18.23), the reliability of transport flow has greatly improved.

Conclusions

Debris flows are a common hazard in mountain areas, and sometimes cause catastrophic disasters when they destroy houses, roads, and property. The debris flows in the two drainage areas studied are believed to have been largely caused by deforestation. Following deforestation, other factors such as the weak geologic materials, the high intensity of monsoon rainstorms, and high seismicity undoubtedly also contributed to triggering the landslide-debris flow processes.

In general, debris flow watersheds can be divided into a formation zone, a transportation zone, and a deposition zone. In most cases, landslides in the upper and middle reaches are the formation zone of debris flows.

Debris flow control projects can be successful only when there is a full understanding of the landslide and debris flow processes in the watershed concerned. The key part of the debris control programmes in the two case studies was to build a series of check dams to

- reduce sediment discharge by arresting debris from gully erosion and landslide areas;
- stabilise landslides and potential slope failures by back siltation behind the check dams; and
- prevent down cutting of the ravine by arrested sediment.

Once the dams are filled, the local gradient is also lower and the valleys slightly wider. However, once a group of check dams along a tributary have been filled in, additional retention of material within a ravine is limited unless the heights of the check dams are raised or material is removed. The effectiveness of check dams can be only partial and temporary if a large supply of debris is still entering a channel. Therefore it is necessary to have a comprehensive programme using bio-engineering and reforestation to control the supply of debris, as well as the construction of check dams and other engineering works. Trees and other plants are usually well-established and begin to act effectively to control erosion within five to ten years of planting. The cost of debris flow control is high, but the benefits often justify the investments.

Where possible, the alignment of linear infrastructures such as roads and irrigation canals should avoid the deposition zone of debris flows. Measures to mitigate damage from debris flows to existing highways, railways, and other infrastructures that are located in the deposition zones of debris flows should emphasise controlling slope instabilities in the middle and upper reaches and improving the environmental conditions of the catchment areas. Line agencies such as the Department of Roads need to co-operate with other departments and in particular with the local community and the government for the long-term mitigation of debris flow hazards.

about the editors

Professor Li Tianchi is the Coordinator of the Disaster Management Programme at the International Centre for Integrated Mountain Development (ICIMOD) Kathmandu, Nepal, which he joined in 1995. Before joining ICIMOD, he was a professor at the Institute of Mountain Hazards and Environment, Chinese Academy of Sciences, Chengdu, China. Professor Li received a Master's Degree in Soil Erosion from the postgraduate school of the Chinese Academy of Sciences in 1968 and pursued postgraduate studies and research on mass movement at Goettingen University in Germany from 1980 to 1983. He has been involved in many research activities in the field of landslide and debris flow hazard mitigation in China, the USA, Japan, and various European countries, as well as in the Himalayas, during the past 30 years and has published many articles on hazard mitigation and management, soil erosion and watershed management and environmental conservation. Professor Li has been honoured with five different scientific and technical awards from the State and Provinces of China.

Professor Suresh R. Chalise is the Coordinator of the Water Programme at the International Centre for Integrated Mountain Development (ICIMOD), Kathmandu, Nepal, which he joined in 1984. Before joining ICIMOD he was associated with Tribhuvan University, Kathmandu, where he taught Physics, founded the Department of Meteorology (in 1973), and was at one time Dean of the Institute of Science and Technology. His work and publications have been mainly in the areas of climate, hydrology and water resources, hazard management, and environmental conservation in the Hindu Kush-Himalayas (HKH). At present, he is the Executive Secretary of HKH-FRIEND, a regional network for hydrological research under the global FRIEND (Flow Regimes from International Experimental and Network Data) project of UNESCO's International Hydrological Programme (IHP).

Professor Chalise obtained his MSc. degree in Physics from Calcutta University and pursued postgraduate studies and research at Reading University (U.K.) and the University of Poona (India). He is a Fellow of the Royal Meteorological Society (U.K.) and is also associated with the International Association of Hydrological Sciences (IAHS) and the International Water Resources Association (IWRA) as well as other scientific societies in Nepal and India. He was associated in an honorary capacity with the bi-national (Nepal and UK) Board of Budhanilkantha School, Kathmandu, and was made a Member of the Order of the British Empire (MBE) for his contributions to the school. He received the Gorkha Dakshin Bahu for distinguished service from His Majesty the King of Nepal.

Bishal Nath Upreti is Professor and Head of the Department of Geology, Tri-Chandra Campus, Tribhuvan University, Nepal. He received his MSc. and PhD degrees from India in 1973 and 1980 respectively, and has received further training at various universities and institutions in France, Japan and Switzerland. Prof. Upreti has over 26 years of professional experience with 20 years of university teaching. He has supervised many students for MSc dissertations, and co-supervised doctoral students. In 1999 he was visiting Professor at Hiroshima University. Professor Upreti has done extensive research in the Nepal Himalaya, with the major focus being on the tectonics of the Himalaya and engineering geology. He has published over 40 research papers and abstracts in international and national scientific journals. He is co-editor of the publication 'Geology of the Nepal Himalaya: Recent Advances' published by the Journal of Asian Earth Sciences (Elsevier Science Ltd.) and the author of 'Landslide Studies and Management in Nepal' published by ICIMOD. He has worked as a consultant for engineering geological surveys in more than ten road projects in Nepal and for many years has been involved in training programmes on landslides organised by ICIMOD and the Department of Water Induced Disaster Prevention, Nepal. He was the President of the Nepal Geological Society from 1996 to 1998 and has received the Gorkha Dakshin Bahu and Mahendra Vidhya Bhusan for distinguished service from His Majesty the King of Nepal.

International Centre for
Integrated Mountain Development
4/80 Jawalakhel, GPO Box 3226
Kathmandu, Nepal

Telephone: +977 1 525313
Fax: +977 1 524509/536747
e-mail: distri@icimod.org.np
Web site: http://www.icimod.org
Cable: ICIMOD NEPAL